

**NICKEL-CATALYZED CROSS-COUPPLINGS VIA ACTIVATION OF  
ALKYL CARBON-NITROGEN BONDS**

by

Corey Howard Basch

A dissertation submitted to the Faculty of the University of Delaware in partial fulfillment of the requirements for the degree of Doctor of Philosophy in Chemistry and Biochemistry

Spring 2018

© 2018 Corey Howard Basch  
All Rights Reserved

**NICKEL-CATALYZED CROSS-COUPPLINGS VIA ACTIVATION OF  
ALKYL CARBON-NITROGEN BONDS**

by

Corey Howard Basch

Approved:

\_\_\_\_\_  
Brian J. Bahnson, Ph.D.

Chair of the Department of Chemistry and Biochemistry

Approved:

\_\_\_\_\_  
George H. Watson, Ph.D.

Dean of the College of Arts and Sciences

Approved:

\_\_\_\_\_  
Ann L. Ardis, Ph.D.

Senior Vice Provost for Graduate and Professional Education

I certify that I have read this dissertation and that in my opinion it meets the academic and professional standard required by the University as a dissertation for the degree of Doctor of Philosophy.

Signed:

---

Mary P. Watson, Ph.D.  
Professor in charge of dissertation

I certify that I have read this dissertation and that in my opinion it meets the academic and professional standard required by the University as a dissertation for the degree of Doctor of Philosophy.

Signed:

---

Donald A. Watson, Ph.D.  
Member of dissertation committee

I certify that I have read this dissertation and that in my opinion it meets the academic and professional standard required by the University as a dissertation for the degree of Doctor of Philosophy.

Signed:

---

Catherine L. Grimes, Ph.D.  
Member of dissertation committee

I certify that I have read this dissertation and that in my opinion it meets the academic and professional standard required by the University as a dissertation for the degree of Doctor of Philosophy.

Signed:

---

Gary A. Molander, Ph.D.  
Member of dissertation committee

## ACKNOWLEDGMENTS

I would first like to thank my advisor Professor Mary Watson for her unrelenting scientific and moral support over the past five years. I truly believe that I am most fortunate for having the opportunity to work for you. Your unique approach to solving complex problems with a consistently positive attitude is just one of the many attributes that I will strive to emulate throughout my scientific career.

To my committee members, Professor Donald Watson, Professor Catherine Grimes, and Professor Gary Molander- thank you for your constant encouragement and guidance over the past four years. Your scientific insight has truly shaped me into a better scientist both on and off the bench.

To the members of the incredible MPW group- It has truly been a pleasure to be your friend and colleague. I hope that you all have learned as much from me as I have learned from each of you. To Kelsey Cobb- I cannot thank you enough for your support since the very beginning of this journey. I am honored to have been your coworker and even more so your friend. To Jianyu Xu- within the course of two years, you have transitioned from being a very talented protégé to a brilliant friend. I look forward to working for you someday. Always remember, 100%. To my former undergraduate Jacob Piane- I am extremely proud of the chemist and person you have become. Your ambition and persistence to learn is remarkable and truly the sign of an excellent scientist.

To Rachel- thank you for all of your love and encouragement. Your support has meant so much to me and has been crucial in getting me through to the end. I am so fortunate to have you in my life and truly blessed to call you my best friend.

To my family- Mom, Dad, Ryan, Erin, Ethan, and Emily- you have always believed in me and encouraged me to pursue my dreams and ambitions. Your unconditional love and support has carried me through the best and hardest of times. I love you all beyond words.

## TABLE OF CONTENTS

LIST OF TABLES .....	ix
LIST OF FIGURES .....	x
ABSTRACT .....	xiv
Chapter	
1 STEREOSPECIFIC MIYaura BORYLATION OF ENANTIOENRICHED BENZYLIC AMMONIUM SALTS .....	1
1.1 Introduction .....	1
1.2 Results and Discussion .....	16
1.3 Conclusion .....	24
1.4 Experimental .....	24
1.4.1 General Information .....	24
1.4.2 Stereospecific Borylation of Benzylic Ammonium Salts .....	26
1.4.2.1 General Procedure A: Borylation of Naphthyl-Substituted Benzylic Ammonium Salts .....	26
1.4.2.2 General Procedure B: Borylation of Non-Naphthyl-Substituted Benzylic Ammonium Salts .....	27
1.4.2.3 General Procedure C: Oxidation of Benzylic Boronates to Benzylic Alcohols for Determination of Enantiomeric Excess (ee) .....	27
1.4.2.4 Gram-Scale Synthesis of ( <i>S</i> )-2-(1-(6-Methoxynaphthalen-2-yl)ethyl)-4,4,5,5-tetramethyl-1,3,2-dioxaborolane (1-79) .....	47
1.4.3 Preparation of Benzyl Ammonium Salts .....	48
1.4.3.1 General Procedure D: Preparation of ( <i>S</i> )- <i>N,N,N</i> -Trimethyl-1-(naphthalen-1-yl)ethanaminium trifluoromethanesulfonate (1-99) .....	49
REFERENCES .....	58

2	SUZUKI-MIYaura CROSS-COUPling OF ALKYL PYRIDINIUM SALTS AND ARYL BORONIC ACIDS .....	60
2.1	Introduction .....	60
2.1.1	Non-Photoredox, Metal-Catalyzed Cross-Couplings .....	63
2.1.2	Metallophotoredox Dual-Catalyzed Cross-Couplings .....	66
2.2	Results and Discussion .....	70
2.2.1	Synthesis of Katritzky Pyridinium Salts.....	70
2.2.2	Optimization .....	72
2.2.3	Reaction Scope .....	73
2.3	Mechanistic Studies .....	81
2.4	Conclusion.....	85
2.5	Experimental.....	86
2.5.1	General Information .....	86
2.5.2	Suzuki–Miyaura Cross-Couplings of Alkyl Pyridinium Salts ....	87
2.5.2.1	General Procedure A: Cross-Coupling with Non-Pyridyl Aryl Boronic Acids.....	87
2.5.2.2	General Procedure B: Cross-Coupling with Pyridyl Boronic Acids.....	97
2.5.3	Preparation of Pyridinium Salts.....	102
2.5.3.1	General Procedure C: Conversion of Amines to Pyridinium Salts .....	102
2.5.4	Test for Stereospecificity.....	113
2.5.5	Radical Clock Experiment.....	114
2.5.6	Radical Trap Experiment.....	115
	REFERENCES .....	117
3	NICKEL-CATALYZED NEGISHI CROSS-COUPlingS OF ALKYL PYRIDINIUM SALTS AND ALKYL ZINC HALIDES .....	119
3.1	Introduction .....	119
3.2	Results and Discussion .....	126
3.3	Conclusion.....	134
3.4	Experimental.....	135

3.4.1	Optimization .....	135
3.4.2	Negishi Cross-Coupling of Alkyl Pyridinium Salts .....	135
	REFERENCES .....	137
4	NICKEL-CATALYZED CROSS-ELECTROPHILE COUPLINGS OF ALKYL PYRIDINIUM SALTS AND ARYL HALIDES .....	138
4.1	Introduction .....	138
4.2	Results and Discussion .....	146
4.3	Conclusion .....	153
4.4	Experimental .....	153
4.4.1	General Procedure A: Reaction Optimization .....	153
	REFERENCES .....	155
5	SUZUKI-MIYaura CROSS-COUPLINGS OF $\alpha$ -AMINO ACID- DERIVED PYRIDINIUM SALTS .....	156
5.1	Introduction .....	156
5.2	Results and Discussion .....	163
5.3	Conclusion .....	173
5.4	Experimental .....	174
5.4.1	General Procedure A: Reaction Optimization .....	174
5.4.2	General Procedure B: Suzuki-Miyaura Cross-Coupling of $\alpha$ - Pyridinium Salts .....	174
5.4.3	General Procedure C: Synthesis of $\alpha$ -Pyridinium Salts .....	175
	REFERENCES .....	176
Appendix		
A	SPECTRAL AND CHROMATOGRAPHY DATA FOR CHAPTER 1 .....	177
B	SPECTRAL AND CHROMATOGRAPHY DATA FOR CHAPTER 2 .....	289
C	PERMISSION LETTERS .....	403

## LIST OF TABLES

Table 1.1	Optimization of the stereospecific Miyaura borylation .....	18
Table 2.1	Reaction optimization .....	73
Table 3.1	Ligand optimization .....	126
Table 3.2	Optimization of the Negishi coupling of 1° alkyl pyridinium salts .....	128
Table 3.3	Ligand optimization for secondary alkyl pyridinium salt cross-coupling .....	129
Table 4.1	Optimization of the alkyl pyridinium salt reductive coupling .....	147
Table 4.2	Optimization of salt additives .....	148
Table 4.3	Miscellaneous screens .....	150
Table 4.4	Catalyst optimization .....	151
Table 4.5	Further optimization .....	152
Table 5.1	Investigation into the effect of desiccants on pyridinium formation .....	164
Table 5.2	Optimization of the Suzuki-Miyaura coupling of $\alpha$ -pyridinium salts ...	167

## LIST OF FIGURES

Figure 1.1	Examples of the synthetic utility of enantioenriched organoboronates.....	2
Figure 1.2	Two commonly used 1,2-shift reactions of enantioenriched organoboronates.....	3
Figure 1.3	Bortezomib and ixazomib – boron-containing medications.....	4
Figure 1.4	Enantioselective hydroborations of alkenes .....	5
Figure 1.5	Metal-catalyzed additions of boron nucleophiles to alkenes.....	7
Figure 1.6	Cross couplings of <i>gem</i> -diboronate derivatives.....	8
Figure 1.7	Enantioselective conjugate additions to $\beta$ -boryl- $\alpha,\beta$ -unsaturated esters...9	
Figure 1.8	Morken’s asymmetric hydrogenation of vicinal bis(boronates).....	10
Figure 1.9	Matteson’s stereospecific homologation of alkyl boronates.....	11
Figure 1.10	Hoppe’s chiral-carbenoid-based synthesis of enantioenriched boronates.....	12
Figure 1.11	Aggarwal’s lithiation-borylation strategy.....	13
Figure 1.12	Prior art in stereospecific/stereoselective Miyaura borylations.....	15
Figure 1.13	Suzuki-Miyaura cross-coupling of benzylic ammonium salts and proposed Miyaura borylation.....	16
Figure 1.14	Synthesis of enantioenriched benzylic ammonium salts .....	17
Figure 1.15	Scope in extended $\pi$ -system .....	20
Figure 1.16	Stereospecific Miyaura borylation of phenyl-substituted ammonium salts .....	21
Figure 1.17	Miyaura borylation performed on a one-gram scale on the bench .....	22
Figure 1.18	Effects of 1- and 3-OMe substituents on borylation reaction.....	23

Figure 1.19	Proposed catalytic cycle.....	24
Figure 3.1:	Examples of bioactive natural or synthetic alkyl primary amines.....	60
Figure 2.2	Synthetic precursors to primary alkyl amines.....	61
Figure 2.3	C <sub>sp2</sub> -N electrophiles used in transition metal-catalyzed cross-couplings.....	62
Figure 2.4	C <sub>sp3</sub> -N electrophiles used in transition metal-catalyzed cross-couplings.....	62
Figure 2.5	Reagents used to install unactivated alkyl groups via metal-catalyzed cross-couplings .....	63
Figure 2.6	Fu's nickel-catalyzed Negishi cross-coupling of alkyl halides .....	64
Figure 2.7	Baran's Negishi cross-coupling of redox-active esters.....	65
Figure 2.8	Weix's nickel-catalyzed reductive cross-coupling of RAEs and aryl iodides.....	66
Figure 2.9	Molander's dual metallophotoredox/nickel-catalyzed cross-couplings of alkyl trifluoroborate salts, silicates, and dihydropyridines.....	67
Figure 2.10	MacMillan's dual metallophotoredox/nickel-catalyzed decarboxylative cross-couplings of alkyl oxalates .....	68
Figure 2.11	Potential issues with C-N bond activation using our previous methylation strategy.....	69
Figure 2.12	Synthesis and physical appearance of an alkyl pyridinium salt.....	69
Figure 2.13	Overview of the activation and cross-coupling of alkyl pyridinium salts .....	70
Figure 2.14	Selected examples of alkyl pyridinium salts formed.....	72
Figure 2.15	Scope of non-pyridyl boronic acid.....	75
Figure 2.16	Scope of pyridyl boronic acid.....	76
Figure 2.17	Synthesis and cross-coupling of isoleucine-derived pyridinium salt.....	77
Figure 2.18	Cross coupling of lysine pyridinium salt .....	78

Figure 2.19	Synthesis and cross-coupling of the pyridinium salt derived from Mosapride intermediate .....	79
Figure 2.20	Synthesis and cross-coupling of pyridinium salt derived from atorvastatin intermediate.....	80
Figure 2.21	Comparison of the ring-systems in atorvastatin, rosuvastatin, and <b>2-92</b> ..	81
Figure 2.22	C-alkylation of nitronate anions with alkyl pyridinium salts .....	82
Figure 2.23	Mechanistic studies of the Suzuki-Miyaura cross-coupling.....	83
Figure 2.24	Possible “transmetallation first” catalytic cycle.....	84
Figure 2.25	Alternative catalytic cycle.....	85
Figure 3.1	First, general metal-catalyzed cross-couplings to form alkyl-alkyl bonds.....	121
Figure 3.2	Fu’s seminal publication on the cross-coupling of 2° alkyl bromides... ..	122
Figure 3.3	Negishi alkylation of RAEs .....	123
Figure 3.4	Nickel-catalyzed C–N activation of aziridinyl electrophiles.....	124
Figure 3.5	Gong’s cross-electrophile coupling to form alkyl–alkyl bonds.....	125
Figure 3.6	Competitive side-reaction in the coupling of secondary and tertiary alkyl zinc halides .....	130
Figure 3.7	Preliminary scope of the Negishi alkylation of alkyl pyridinium salts..	132
Figure 3.8	Plausible catalytic cycle of the Negishi cross-coupling.....	134
Figure 4.1	Comparison of aryl nucleophiles and aryl halides as coupling partners	139
Figure 4.2	Radical-chain bimetallic catalytic cycle with stoichiometric metal reductants .....	140
Figure 4.3	Weix’s seminal publication on C <sub>sp3</sub> –C <sub>sp2</sub> cross-electrophile coupling ..	141
Figure 4.4	Recent advances in reductive couplings .....	143
Figure 4.5	Seminal work in Ni/photoredox dual-catalyzed reductive couplings....	145

Figure 4.6	Cobalt- or copper-catalyzed cross-electrophile couplings.....	146
Figure 5.1	Expanding the utility of the amino acid feedstock .....	157
Figure 5.2	Wang's transition metal-free coupling of $\alpha$ -diazo esters and boronic acids .....	158
Figure 5.3	Proposed method of $C_{\alpha}$ -N activation of amino acid derivatives.....	159
Figure 5.4	Bioactive $\alpha$ -aryl propionic acid derivatives .....	160
Figure 5.5	Palladium-catalyzed $\alpha$ -arylations of enolates.....	161
Figure 5.6	Fu's asymmetric Hiyama arylation of $\alpha$ -bromo esters. ....	161
Figure 5.7	Glorius' photoredox-catalyzed, Minisci-type coupling of heteroarenes and $\alpha$ -pyridinium salts.....	162
Figure 5.8	Hydrolysis of intermediate and formation of diketone byproduct.....	163
Figure 5.9	Synthesis of $\alpha$ -pyridinium salts derived from $\alpha$ -amino acids .....	166
Figure 5.10	Preliminary scope in boroxine .....	169
Figure 5.11	Preliminary scope in $\alpha$ -pyridinium salt .....	170
Figure 5.12	Preliminary scope .....	171
Figure 5.13	Radical-clock experiment .....	172
Figure 5.14	Possible catalytic cycle for the cross-coupling with $\alpha$ -pyridinium salts	173

## ABSTRACT

This dissertation focuses on investigations of nickel-catalyzed cross-couplings of alkyl amine electrophiles via carbon-nitrogen bond activation.

Chapter 1 describes a stereospecific nickel-catalyzed Miyaura borylation of enantioenriched benzylic ammonium salts with bis(pinacolato)diboron. Under the mild conditions identified, a variety of electronically and sterically diverse secondary benzylic boronates are obtained in good yields and high enantioenrichment. Ni(cod)<sub>2</sub> in conjunction with a phosphine or *N*-heterocyclic carbene ligand provides borylated products from both naphthyl- and phenyl-substituted ammonium salts. Additionally, the practicality of this transformation was demonstrated by performing the reaction on the bench using air- and moisture-stable Ni(OAc)<sub>2</sub>·4H<sub>2</sub>O. Mechanistic investigations suggest that the oxidative addition step proceeds through an S<sub>N</sub>2' pathway. Importantly, this was the first example of a stereospecific Miyaura borylation of a benzylic electrophile to deliver benzylic boronates in high enantioenrichment.

Chapter 2 describes a nickel-catalyzed Suzuki-Miyaura cross-coupling of alkyl pyridinium salts with aryl boronic acids. This reaction utilizes alkyl amines as sources of unactivated alkyl groups via the intermediacy of redox-active Katritzky pyridinium salts which can be easily obtained in a single step from the primary amine. The optimized conditions, which employ a combination of Ni(OAc)<sub>2</sub>·4H<sub>2</sub>O and bathophenanthroline, deliver both primary and secondary alkyl arenes in good yield and excellent functional group tolerance. Importantly, this transformation is amenable to cross-couplings of pyridyl or quinolinyll boronic acids and pyridinium salts derived

from drug-intermediates or amino acids. Mechanistic studies, including radical clock and radical trap experiments, suggest that a Ni<sup>II/III</sup> catalytic cycle is operative.

Chapter 3 describes a nickel-catalyzed Negishi alkylation of alkyl pyridinium salts with primary alkyl zinc halides. Ni(acac)<sub>2</sub>·xH<sub>2</sub>O, in conjunction with a redox non-innocent terpyrine or bis(*N*-pyrazolyl)pyridine ligand, has been identified as an optimal catalyst system that furnishes a variety of functionally diverse products with new alkyl-alkyl bonds. Both primary and secondary alkyl pyridinium salts can be efficiently cross-coupled. Additionally, a number of pyridinium salts derived from drugs or drug-intermediates are competent electrophiles in this transformation.

Chapter 4 describes my efforts toward the development of a nickel-catalyzed reductive coupling of alkyl pyridinium salts with heteroaromatic halides. A variety of reaction parameters have been screened including nickel precursors, ligands, and stoichiometric reductants. However, the identity of the reductant and the inclusion of a salt additive have proven most crucial in this transformation, with Mn<sup>0</sup> and LiCl delivering the highest yield to date (64%). Optimization of this reaction is ongoing.

Chapter 5 describes a nickel-catalyzed Suzuki-Miyaura arylation of α-pyridinium salts with aryl and heteroaryl boroxines. The pyridinium salts are synthesized in a single step from commercially available α-amino esters and serve as a readily available electrophile for the metal-catalyzed formation of α-aryl propionic acid derivatives.

## Chapter 1

### STEREOSPECIFIC MIYAJIMA BORYLATION OF ENANTIOENRICHED BENZYLIC AMMONIUM SALTS

Work described here has already been published (Basch, C. H.; Cobb, K. M.; Watson, M. P. *Org. Lett.* **2016**, *18* (1), 136-139.). It is reprinted in this chapter with permissions of *Organic Letters* (Copyright © 2016, American Chemical Society).

#### 1.1 Introduction

The synthesis and utility of enantioenriched organoboronates has been, and continues to be, a subject of intense interest in the field of methodology development.<sup>1</sup> Their unique reactivity profile has led to the establishment of a number of synthetically useful transformations which convert the boronate motif into various other functional groups, including amines, alcohols, or halides. Importantly, these transformations are often highly stereospecific. In this regard, alkyl boronate derivatives, especially boronate esters, have found widespread use as enantioenriched reagents or intermediates for asymmetric synthesis. Despite the existence of many well-developed methods that utilize these versatile precursors, the synthesis of highly enantioenriched alkyl boronates still presents challenges, many of which will be discussed below.

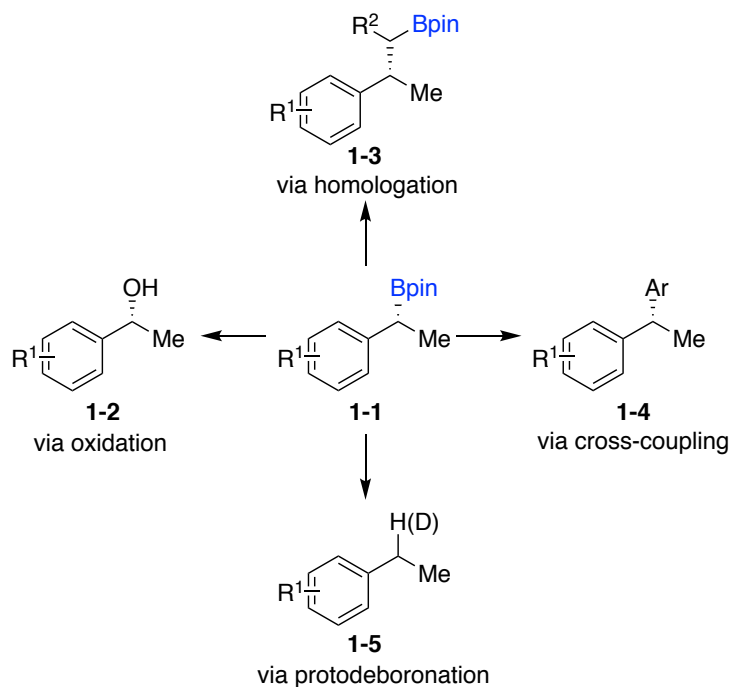
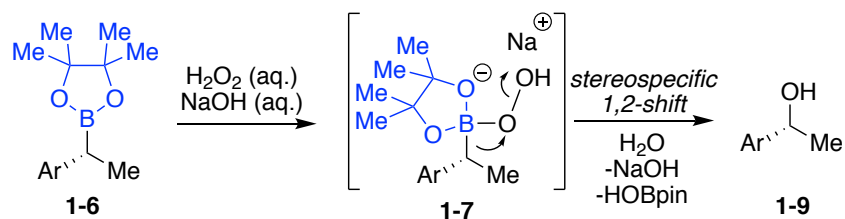


Figure 1.1 Examples of the synthetic utility of enantioenriched organoboronates

Enantioenriched organoboronates (**1-6**) are often converted to the corresponding enantioenriched alcohols (**1-9**) via Brown oxidation<sup>2</sup> with H<sub>2</sub>O<sub>2</sub> and NaOH (Figure 1.2A), or extended by one carbon via a Matteson homologation<sup>3</sup> (**1-11**) using a combination of <sup>n</sup>BuLi and CH<sub>2</sub>Cl<sub>2</sub> (Figure 1.2B). Alternatively, they can be stereoretentively cross-coupled with aryl halides under Pd-catalyzed conditions.<sup>4</sup> or converted to the reduced alkane (**1-5**) via protodeboronation. Other reactions include, for example, the conversion of enantioenriched alkyl boronates to alkyl amines, halides (e.g. bromination or fluorination), olefins, or alkynes.

A. Brown oxidation



B. Matteson homologation

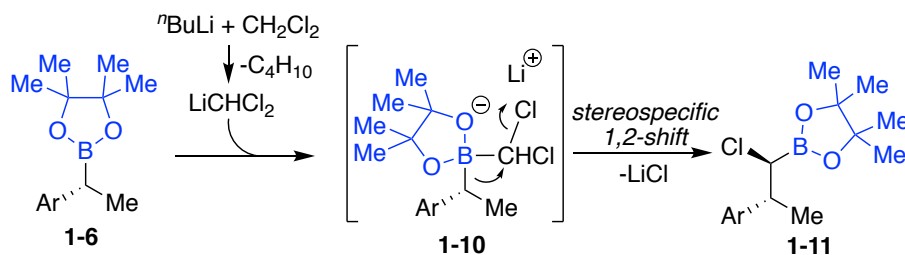


Figure 1.2 Two commonly used 1,2-shift reactions of enantioenriched organoboronates

Although they are generally employed as reagents or synthetic intermediates, alkyl boronic acids, have recently garnered interest from the medicinal community due to their bioisosteric properties. Currently, bortezomib (**1-11**, Velcade<sup>®</sup>, Millennium Pharmaceuticals Inc.) and ixazomib (**1-12**, Ninlaro<sup>®</sup>, Millennium Pharmaceuticals Inc.), both of which are protease inhibitors, are the only boron-containing drugs on the market.<sup>5</sup>

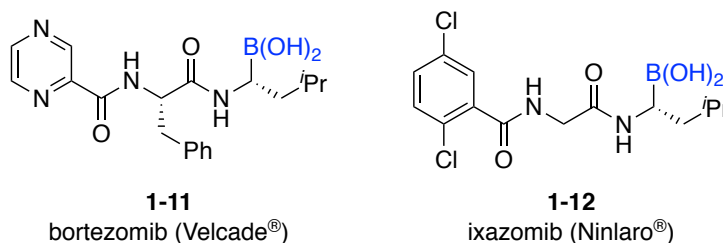


Figure 1.3 Bortezomib and ixazomib – boron-containing medications

The most common methods for synthesizing enantioenriched organoboronates are metal-catalyzed, Markovnikov hydroborations of alkenes. In 1989, Hayashi's group demonstrated the first enantioselective alkene hydroboration.<sup>6</sup> In order to override the inherent *anti*-Markovnikov selectivity of non-catalyzed hydroboration reactions, they elected to use a chiral rhodium-BINAP catalyst (Figure 1.4A). Under their optimized conditions, a number of styrenyl alkenes were hydroborated to afford a variety of branched benzylic catechol boronates (**1-15**). Because of the inherent instability of the catecholboronates, an *in situ* oxidation was performed to obtain the corresponding alcohols (**1-9**), generally in high yield and ee's. Subsequent to this ground-breaking work, the Crudden group developed a similar rhodium-catalyzed hydroboration reaction using pinacolborane (HBpin) (Figure 1.4B).<sup>7</sup> The greater stability of pinacolboronates, in comparison to catecholboronates, allowed for purification of the enantioenriched organoboronates via silica gel chromatography. More importantly, this substantially increases the synthetic utility of the products by circumventing the need for *in situ* oxidations. In a complementary approach to Rh-catalyzed hydroborations, the Yun group has shown that a copper catalyst bearing a chiral Tangphos ligand (**1-18**) can smoothly promote the hydroboration of styrenes with HBpin (Figure 1.4C).<sup>8</sup> Unlike the rhodium-catalyzed transformations which were

restricted to using terminal alkenes, the Yun group found that their Cu-based system could also promote the asymmetric hydroboration of internal alkenes (**1-19**). This was undoubtedly a significant advancement in the field of alkene hydroboration.

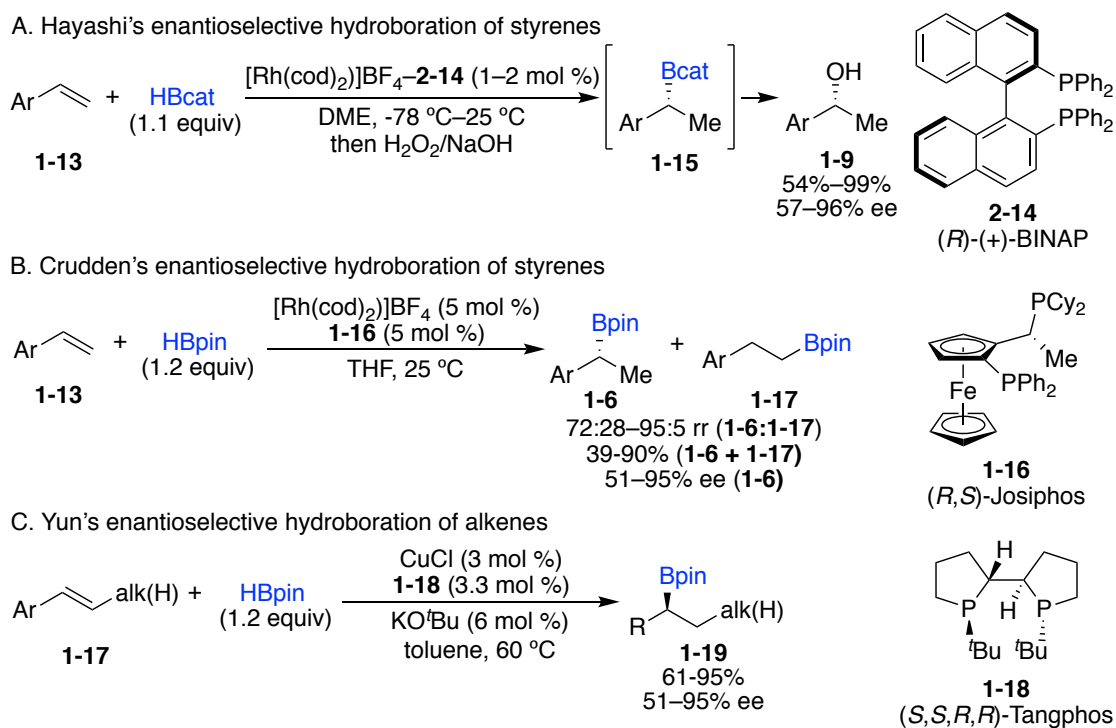
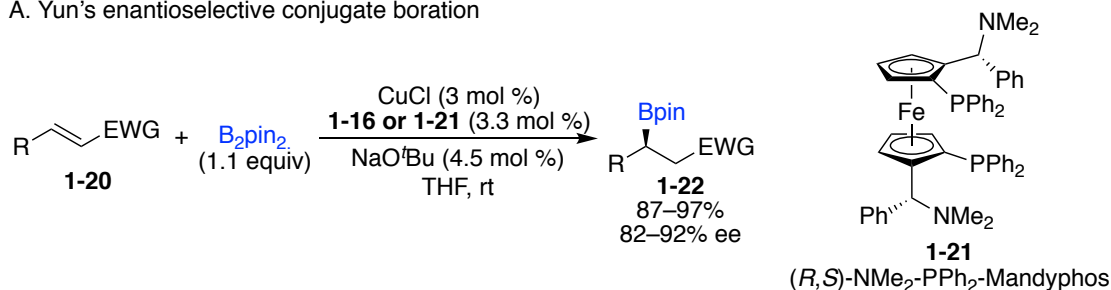


Figure 1.4 Enantioselective hydroborations of alkenes

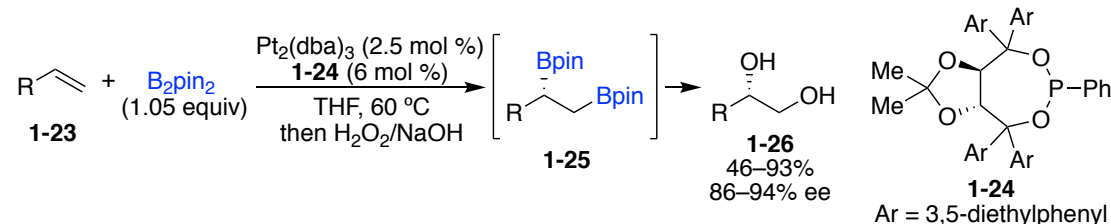
In addition to hydroborations, enantioselective metal-catalyzed additions of boron nucleophiles to alkenes have also been investigated. These methods include  $\beta$ -borations of  $\alpha,\beta$ -unsaturated carbonyls, diborations of aliphatic alkenes, and three-component couplings with aryl electrophiles. In their seminal publication on conjugate additions of boron nucleophiles, the Yun group demonstrated a highly efficient,

copper-catalyzed  $\beta$ -addition of  $B_2pin_2$  to cinnamic acid esters and nitriles (**1-20**, Figure 1.5A).<sup>9</sup> A combination of  $CuCl_2$  and chiral, ferrocenyl-based phosphine ligand (**1-16** or **1-21**) was found to be the optimal catalyst system and was able to deliver enantioenriched, benzylic  $\beta$ -boronates (**1-22**) in high yields and ee's. In the context of difunctionalization reactions, Morken and coworkers developed a platinum-catalyzed enantioselective addition of  $B_2pin_2$  to terminal aliphatic alkenes (**1-23** Figure 1.5B).<sup>10</sup> The resulting enantioenriched vicinal diboronates (**1-25**) were oxidized *in situ* to provide the corresponding diols (**1-26**) in high yields and ee's. In a different approach, the Toste group developed an arylboration of alkenes that employed a dual platinum/chiral anion-phase-transfer (CAPT) catalytic system to promote a three-component coupling between styrenes,  $B_2pin_2$ , and aryl diazonium salts (Figure 1.5C).<sup>11</sup> Despite obtaining the crude, functionally diverse benzylic boronates (**1-28**) in good to high ee's, low to moderate yields were observed. The CAPT catalyst (**1-27**) is believed to form a chiral ion pair with the insoluble aryl diazonium tetrafluoroborate salt. After oxidative addition by the Pd-catalyst and extrusion of  $N_2$  gas, the resulting electron-poor CAPT-Pd-arene complex could then coordinate to the alkene and undergo an enantioselective migratory insertion. Subsequent isomerization, transmetallation, and reductive elimination would then provide the borylated product.

A. Yun's enantioselective conjugate boration



B. Morcken's enantioselective diboration of alkenes



C. Toste's enantioselective 1,1-arylboration of alkenes

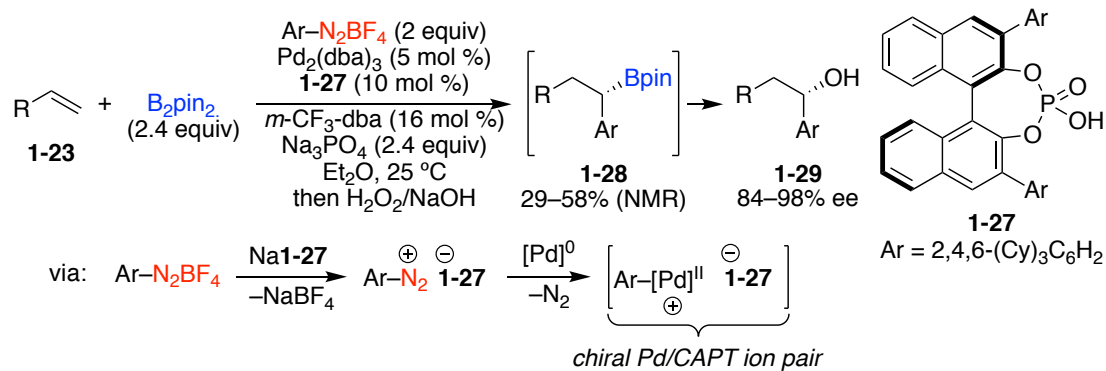


Figure 1.5 Metal-catalyzed additions of boron nucleophiles to alkenes

An alternative approach to the formation of enantioenriched organoboronates is the derivatization of boron-containing starting materials. These transformations are typically accomplished through stereospecific or stereoselective cross-couplings of *gem*-diboronates, asymmetric reductions of vinyl boronates, or homologations of achiral pinacolboronates with enantioenriched carbene equivalents. The groups of Hall and Morcken have demonstrated that *gem*-diboronate derivatives can be utilized in stereospecific and stereoselective cross-couplings, respectively, with aryl halides

(Figure 1.6). The palladium-catalyzed, stereospecific reaction developed by the Hall group takes advantage of the orthogonal reactivity between alkyl trifluoroborates and other alkyl boronate derivatives (Figure 1.6A).<sup>12</sup> In this example, a chemoselective transmetalation of the trifluoroborate unit was achieved with inversion of configuration. Notably, the  $\beta$ -ester of the diborylated starting material (**1-30**) is crucial for promoting the otherwise difficult transmetalation step. The enantioselective approach developed by the Morcken group utilizes alkyl *gem*-bis(pinacolatodiboronates) as the achiral starting material (**1-34**, Figure 1.6B).<sup>13</sup> They identified that a chiral TADDOL-based phosphine (**1-36**)/Pd catalyst leads to efficient desymmetrization of the diboronate via an enantiotopic transmetalation.

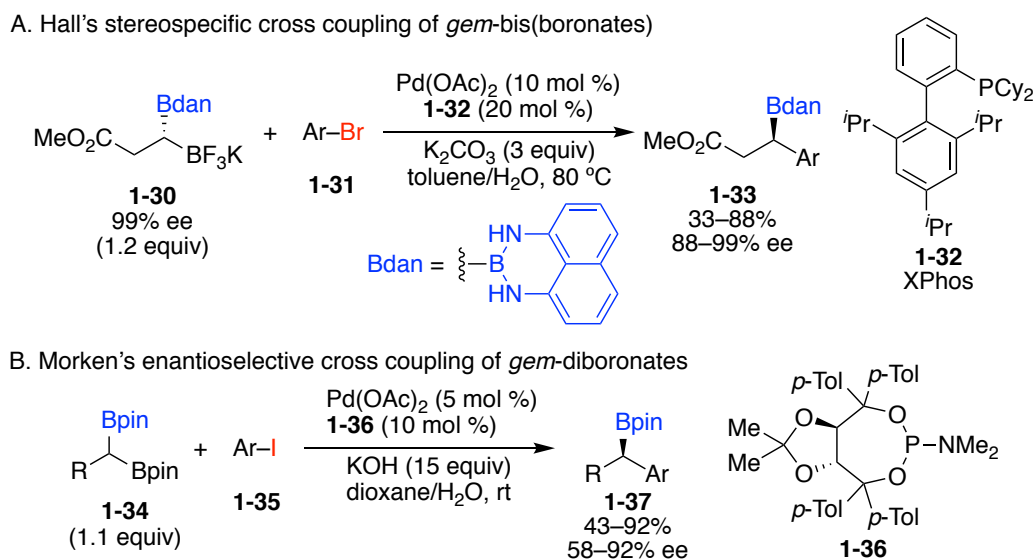


Figure 1.6 Cross couplings of *gem*-diboronate derivatives

Asymmetric conjugate additions have also been investigated as methods for obtaining enantioenriched organoboronates. The Hall group has developed an elegant

Cu-BINAP reduction of  $\beta$ -boryl- $\alpha,\beta$ -unsaturated esters (**1-38**) using polymethylhydrosiloxane (PMHS) as the hydride source (Figure 1.7A).<sup>14</sup> The method delivers both benzylic and non-benzylic  $\beta$ -boronates (**1-40**) in synthetically useful yields and modest to excellent ee's. Using a similar catalytic system, the Hall group has developed an asymmetric conjugate addition of Grignard reagents to  $\beta$ -boryl- $\alpha,\beta$ -unsaturated esters and thioesters (**1-41**, Figure 1.7B).<sup>15</sup> Like the conjugate reduction, this reaction provides a variety of highly enantioenriched alkyl  $\beta$ -boronates (**1-42**) in good to excellent yields.

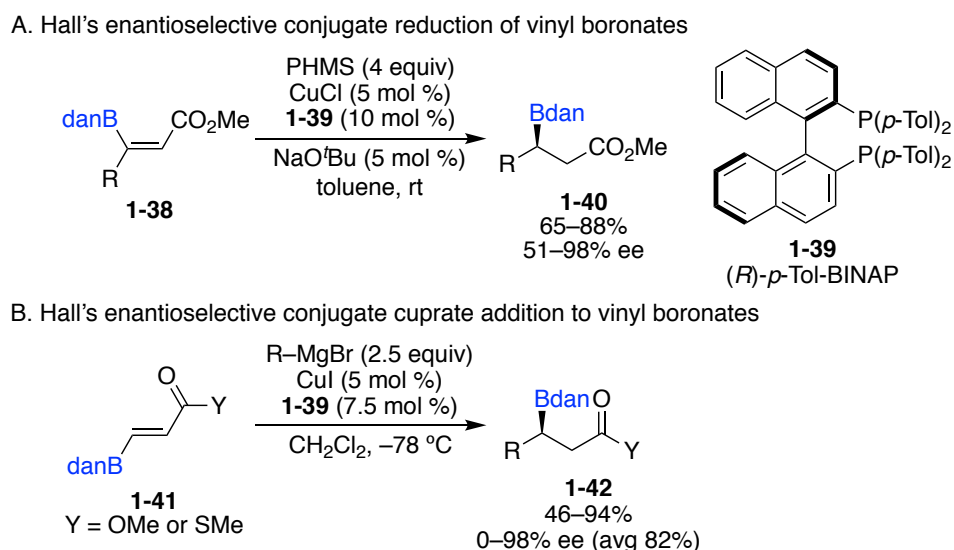


Figure 1.7 Enantioselective conjugate additions to  $\beta$ -boryl- $\alpha,\beta$ -unsaturated esters

In addition to diborations of alkenes, the Morken group has pioneered the asymmetric reduction of vinyl bis(boronates) (**1-43**) to provide enantioenriched vicinal alkyldiboronates (**1-25**).<sup>16</sup> The optimized Rh-Walphos (**1-44**)-based catalyst leads to efficient reduction of the alkene under a pressurized hydrogen atmosphere (20 bar) in

good yields and ee's. Impressively, a very sterically encumbering vinyl *tert*-butyl group has no effect on the reaction efficiency or selectivity, leading to diol **1-26** in both high yield and ee (Figure 1.8). Although the method delivers both benzylic and non-benzylic boronates, limited functional group compatibility is demonstrated.

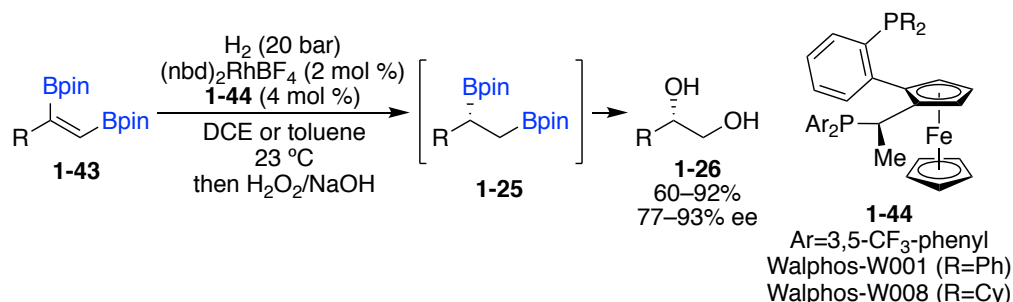


Figure 1.8 Morcken's asymmetric hydrogenation of vicinal bis(boronates)

Stereospecific homologations have become one of the most prevalent methods for the construction of enantioenriched boronates. In Matteson's seminal publication, the pinane diol backbone of the boronate ester **1-45** is used as a stoichiometric chiral auxiliary (Figure 1.9).<sup>17</sup> After treatment with LiCHCl<sub>2</sub> (derived from *n*-butyllithium and methylene chloride), the resulting boron-'ate'-complex (**1-46**) undergoes, upon warming, a stereospecific 1,2-shift to formally insert a methylene unit into the carbon–boron bond of the starting boronate. This reaction leads to an  $\alpha$ -chloroalkyl boronate (**1-47**), which can then be treated with a Grignard reagent to form a second 'ate'-complex (**1-48**). Upon warming, a second stereospecific 1,2-shift occurs. In most cases, the newly formed organoboronate (**1-49**) is obtained in high yield and  $\geq 95\%$  dr and  $\geq 95\%$  ee.



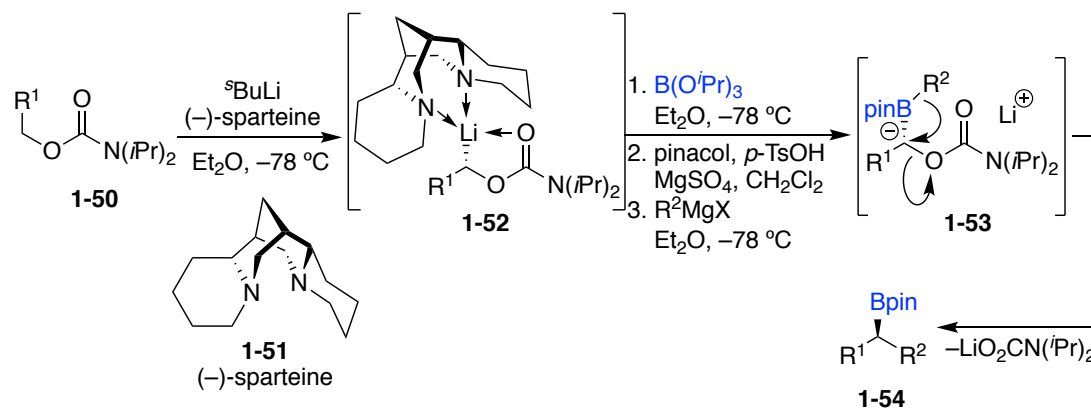
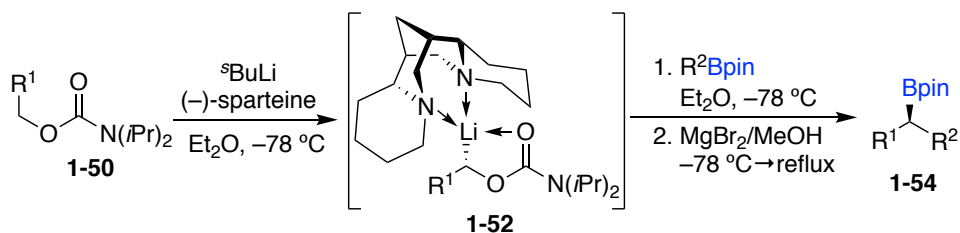


Figure 1.10 Hoppe's chiral-carbenoid-based synthesis of enantioenriched boronates

The Aggarwal group pioneered a hybrid approach to Matteson and Hoppe's work in boronate homologations. Rather than utilizing trialkylborates as the source of boron functionality, they found that using alkyl pinacolboronates can lead to the same boron-'ate' intermediate when treated with the enantioenriched, alkyllithium species (**1-52**, Figure 1.11A).<sup>19</sup> They subsequently discovered that secondary, enantioenriched carbamates (**1-55**) can also undergo an analogous stereospecific homologation in the absence of sparteine to form enantioenriched, tertiary organoboronates (**1-56**, Figure 1.11B).<sup>20</sup>

A. Lithiation-borylation strategy to form enantioenriched, secondary alkyl boronates



B. Formation of enantioenriched, tertiary alkyl boronates

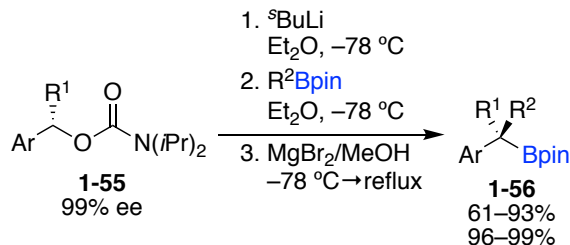
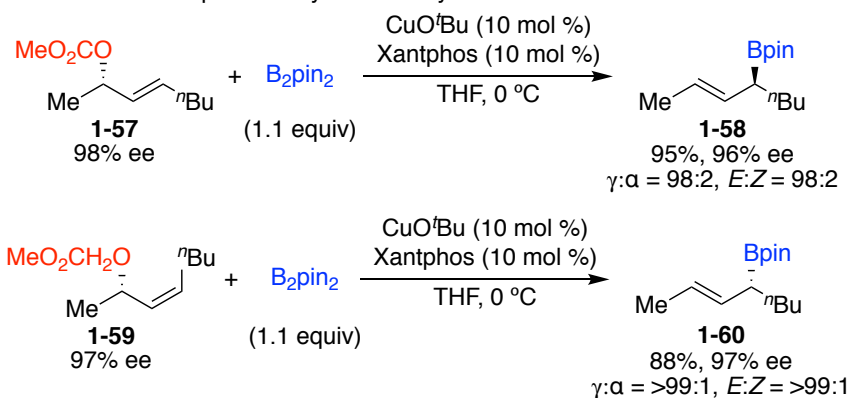


Figure 1.11 Aggarwal's lithiation-borylation strategy

Alternatively, a number of non-asymmetric Miyaura borylations of alkyl halides and pseudohalides have been developed. Despite the breadth of research targeted at constructing these valuable synthetic intermediates, only two examples of an enantioselective, or enantiospecific, Miyaura borylation have been reported. In this regard, Ito and Sawamura have shown that enantioenriched allylic carbonates are competent electrophiles in a stereospecific copper-catalyzed cross-coupling with bis(pinacolato)diboron ( $\text{B}_2\text{pin}_2$ ) (Figure 1.12A).<sup>21</sup> As the first reported example of a stereospecific Miyaura borylation, they demonstrated that a Tsuji-Trost-type C–O activation could deliver a variety of racemic, allylic boronates in both high yields and regioselectivities. Notably, they only disclosed two examples of the reaction using enantioenriched allylic carbonates. In these examples, however, they obtained the enantioenriched products with near perfect stereochemical fidelity. Similarly, the Hoveyda group has developed a stereoselective Cu-(*N*-heterocyclic carbene)

(Cu(NHC))-catalyzed boration of allylic carbonates (**1-61**) to form enantioenriched tertiary boronates (**1-62**) in high yields and ee's (Figure 1.12B).<sup>22</sup> Because of stability issues during isolation, the secondary benzylic boronates were oxidized to the alcohols (**1-63**) *in situ*. They were, however, able to successfully isolate two tertiary allylic boronates (**1-64** and **1-65**), both in very good yield and ee. This complementary approach for the synthesis of enantioenriched alkyl boronates represents the first general example of an enantioselective Miyaura borylation. However, no enantioselective or stereospecific Miyaura borylations of non-allylic electrophiles were reported before my efforts described below.

A. Ito and Sawamura's stereospecific borylation of allylic carbonates



B. Hoveyda's stereoselective borylation of allylic carbonates

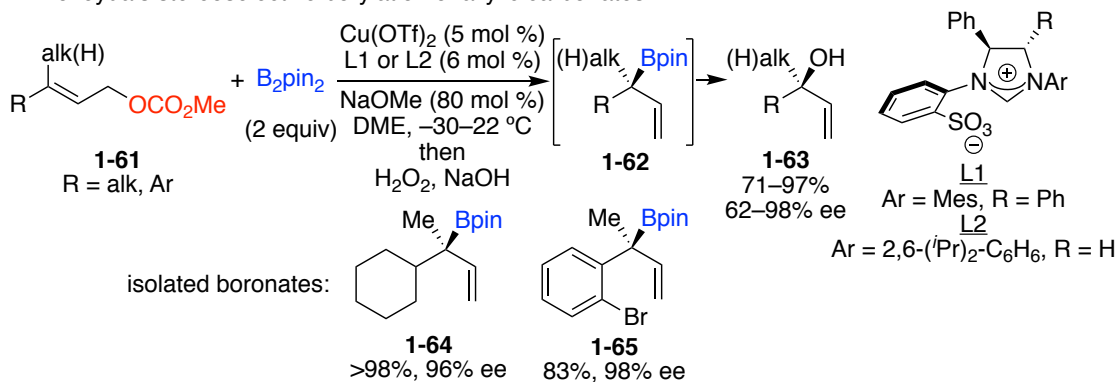


Figure 1.12 Prior art in stereospecific/stereoselective Miyaura borylations

With our group's prior success in the stereospecific Suzuki-Miyaura cross-couplings of enantioenriched benzylic ammonium salts with aryl and vinyl boronic acids (Figure 1.13A), I envisioned that an analogous Miyaura borylation might also be feasible (Figure 1.13B).<sup>23,24</sup> Furthermore, given the ease by which one can obtain enantioenriched amines (e.g., classical, kinetic, or enzymatic resolutions, chiral auxiliaries, asymmetric hydrogenations, etc.), I recognized that they would be an ideal electrophile for a stereospecific Miyaura borylation. With an opportunity to expand

the utility of enantioenriched benzylic ammonium salts, I set out to develop a nickel-catalyzed stereospecific Miyaura borylation.

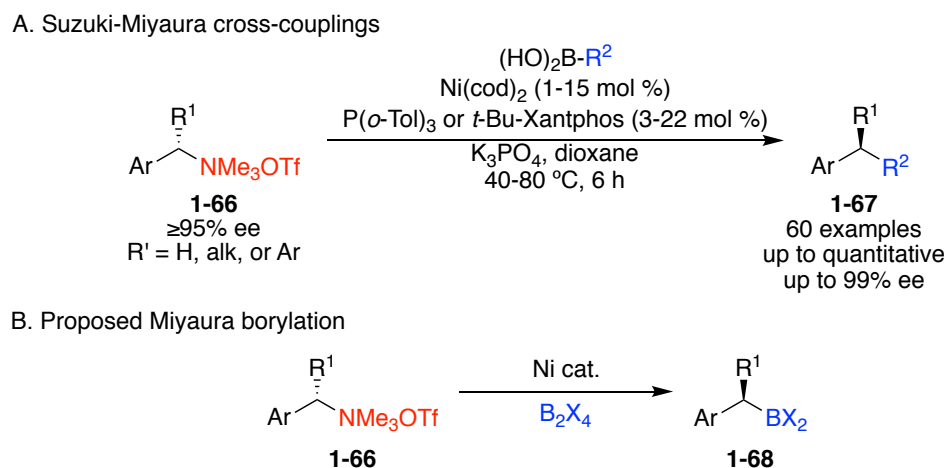


Figure 1.13 Suzuki-Miyaura cross-coupling of benzylic ammonium salts and proposed Miyaura borylation

## 1.2 Results and Discussion

The enantioenriched benzylic ammonium salts were synthesized according to Figure 1.14. Commercially available amines (**1-69**) were converted to the corresponding dimethylamines (**1-70**) via Eschenweiler-Clark conditions ( $\text{CH}_2\text{O}$ ,  $\text{HCO}_2\text{H}$ , reflux). The third methyl group was installed via treatment of **1-70** with methyl triflate ( $\text{MeOTf}$ ) in diethyl ether at  $0\text{ }^\circ\text{C}$ . In most cases, the trimethylammonium salts (**1-66**) would precipitate after 10–20 minutes of stirring. However, if precipitation failed, the salts were washed with  $\text{Et}_2\text{O}$  and hexanes and placed under hi-vacuum overnight (at which point they were obtained as foams). In order to synthesize non-commercial enantioenriched amines, I employed Ellman's

auxiliary. Enantioenriched sulfinimine **1-73** was obtained via reductive amination of (*R*)-(+)-2-methyl-2-propanesulfinamide (**1-72**, Ellman's auxiliary) with aldehyde **1-71**. A subsequent, temperature-controlled 1,2-addition of the alkyl Grignard reagent afforded sulfonamide **1-74** as a mixture of diastereomers. In all cases, the diastereomers were separable by silica gel chromatography such that only a single diastereomer was observed by <sup>1</sup>H NMR. To that end, I assumed that the dr of the purified sulfonamide **1-74** was  $\geq 95:5$  dr. With pure **1-74** in hand, I then removed the auxiliary with anhydrous HCl to reveal the hydrochloride salt of **1-69**. Subjecting the hydrochloride salt to a mild base wash provided the primary benzylic amine (**1-69**) in  $\geq 95\%$  ee. At this point, **1-69** was taken forward to the trimethylammonium salt using the previously mentioned two-step protocol.

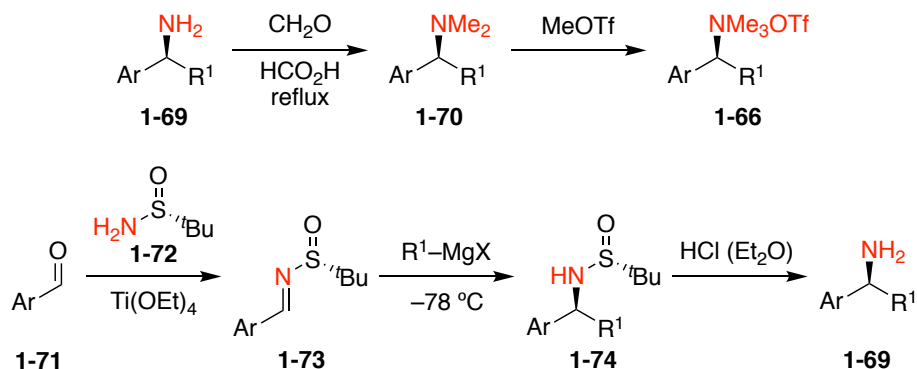
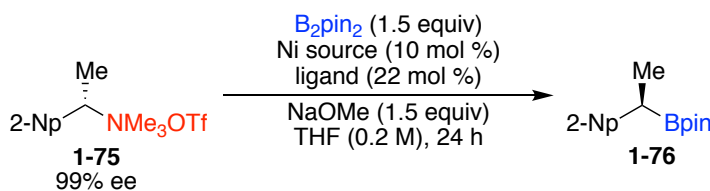


Figure 1.14 Synthesis of enantioenriched benzylic ammonium salts

My optimization began with examining the use of the optimal, first-generation Suzuki-Miyaura cross-coupling conditions. Interestingly, the desired product (**1-76**) was obtained in only 12% yield (Table 1.1, entry 1). After screening a variety of bases, I identified that alkoxides were superior in promoting the formation of the benzylic

boronate (entry 2). Lowering the temperature from 70 °C to room temperature (23 °C) greatly suppressed the formation of the protodeboronation byproduct, leading to an improvement in the yield of the desired boronate (entry 3). Air-stable and inexpensive triphenylphosphine (PPh<sub>3</sub>) was found to be an optimal ligand in this transformation and provided a slight increase in ee and yield (entry 4). Interestingly, removal of ligand gave comparable yield to the Ni/PPh<sub>3</sub> system, but in slightly lower ee (entry 5). Notably, use of air-stable Ni(OAc)<sub>2</sub>·4H<sub>2</sub>O yielded the desired benzylic boronate in both comparable yield and ee to Ni(cod)<sub>2</sub> (entry 6); however, it proved to be inferior across a broader range of substrates.

Table 1.1 Optimization of the stereospecific Miyaura borylation<sup>a</sup>

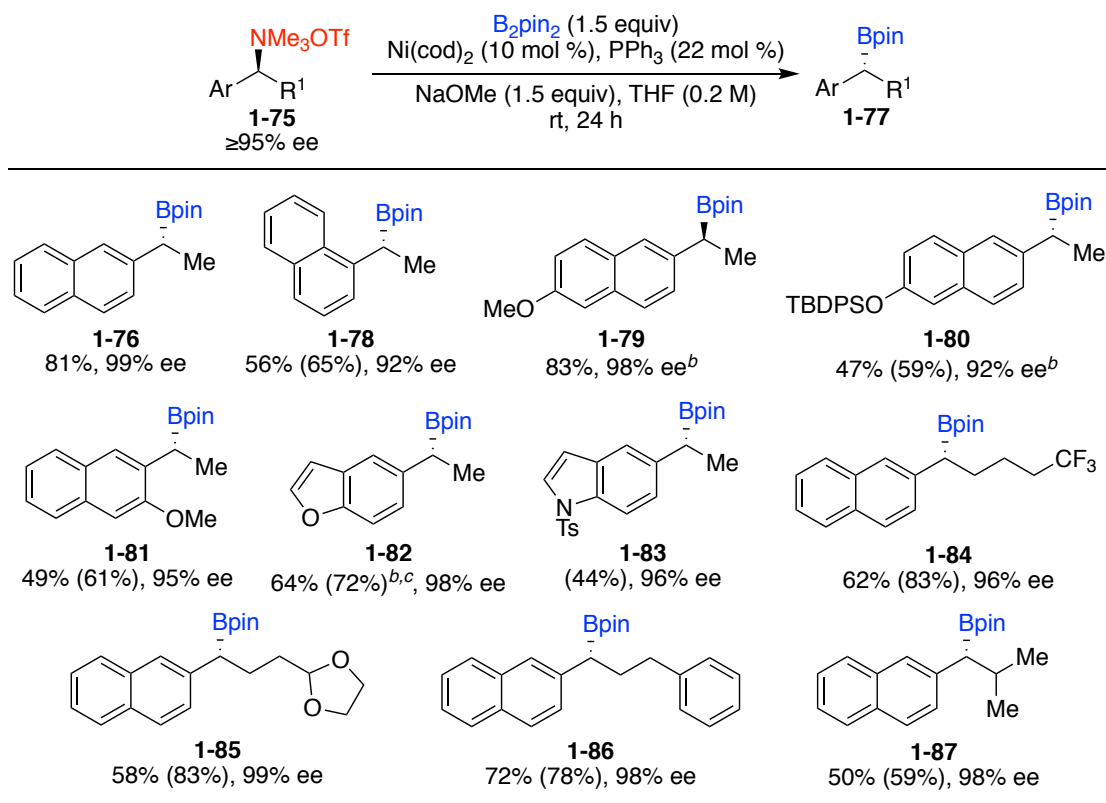


entry	Ni source	ligand	temp (°C)	yield (%)	ee (%) <sup>b</sup>
1 <sup>c</sup>	Ni(cod) <sub>2</sub>	P( <i>o</i> -Tol) <sub>3</sub>	70	12	n.d.
2	Ni(cod) <sub>2</sub>	P( <i>o</i> -Tol) <sub>3</sub>	70	78	95
3	Ni(cod) <sub>2</sub>	P( <i>o</i> -Tol) <sub>3</sub>	rt	84	98
4	Ni(cod) <sub>2</sub>	PPh <sub>3</sub>	rt	86	99
5	Ni(cod) <sub>2</sub>	none	rt	81	97
6	Ni(OAc) <sub>2</sub> ·4H <sub>2</sub> O	PPh <sub>3</sub>	rt	80	99

<sup>a</sup> Yields based on <sup>1</sup>H NMR analysis with 1,3,5-trimethoxybenzene as an internal standard. <sup>b</sup> Ee's are of the corresponding alcohol after oxidation with H<sub>2</sub>O<sub>2</sub>/NaOH. <sup>c</sup> With K<sub>3</sub>PO<sub>4</sub> instead of NaOMe.

---

With optimized conditions in hand, my colleague Kelsey Cobb and I explored the scope of the stereospecific, nickel-catalyzed Miyaura borylation (Figure 1.15). In addition to the 2-naphthyl substituent, a more sterically bulky 1-naphthyl group is well tolerated, providing product **1-78** in 56% isolated yield and 92% ee. The electron-rich 6-OMe-naphthyl substrate afforded the desired boronate **1-79** in both high yield (83%) and ee (98%). Silyl-protected ammonium salts can also be utilized in this transformation as demonstrated by boronate **1-80**, which was obtained in 47% isolated yield and 92% ee. The reaction is also amenable to the cross-coupling of ammonium salts with substituents at the 3-position of the naphthyl ring, as evidenced by 3-OMe-naphthyl benzylic boronate **1-81**. Importantly, heteroaromatic substrates bearing extended conjugation such as benzofuran and indole can also be borylated, delivering products in 64% yield and 98% ee (**1-82**), and 44% yield (NMR) and 96% ee (**1-83**), respectively. In addition to a methyl group at the benzylic position, linear alkyl substituents ( $R^1$ ) were well tolerated, such as those bearing trifluoromethyl **1-84** (62%, 96% ee), acetal **1-85** (58%, 99% ee), or phenethyl **1-86** (72%, 98% ee) groups. The acetal in particular provides a handle for further functionalization upon deprotection to the parent aldehyde. Remarkably, the substrate bearing an *i*Pr-substituent at the benzylic position also provided the corresponding boronate **1-87** in 50% isolated yield and 98% ee. Access to this type of sterically hindered alkyl boronate has not been accomplished thus far by asymmetric hydroboration methods.

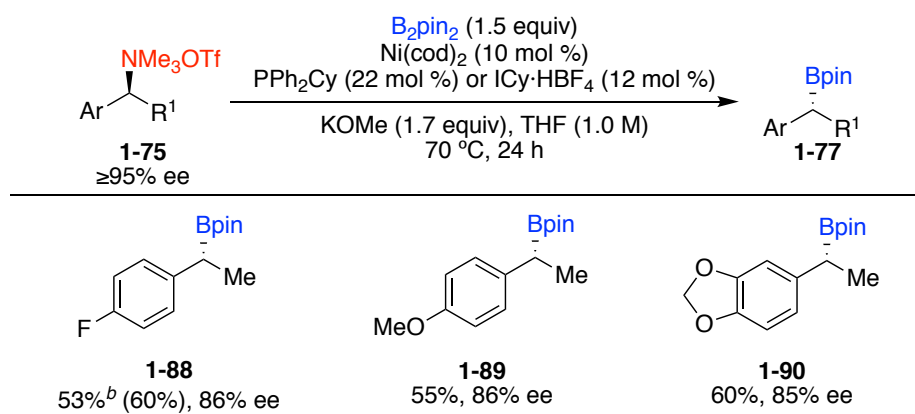


<sup>a</sup> Conditions: ammonium triflate **1-75** ( $\geq 95\%$  ee, 0.30 mmol, 1.0 equiv),  $B_2pin_2$  (1.5 equiv),  $Ni(cod)_2$  (10 mol %),  $PPh_3$  (22 mol %), NaOMe (1.5 equiv), THF (0.2 M), rt, 24 h, unless otherwise noted. Isolated yields. Yields in parentheses determined by  $^1H$  NMR analysis using 1,3,5-trimethoxybenzene as internal standard. Ee's of the subsequent alcohol, formed via oxidation with  $H_2O_2$  and NaOMe, determined by HPLC analysis using a chiral stationary phase. Enantiospecificity (es) =  $ee_{prod}/ee_{sm} \times 100$ . <sup>b</sup> Opposite enantiomer of **1-75** used. <sup>c</sup> 50 °C.

Figure 1.15 Scope in extended  $\pi$ -system<sup>a</sup>

Benzylic ammonium salts with non-extended  $\pi$ -systems provided only trace product under the optimized conditions. Recognizing that the oxidative addition step would be much less favorable in the phenyl-based system, I reinvestigated the choice of ligand. Not surprisingly, I found that more electron rich, monodentate phosphine ligands or NHC ligands proved much more effective than  $PPh_3$ . Additionally,

increasing the concentration and raising the temperature from temperature to 70 °C was necessary for obtaining synthetically useful yields of the benzylic boronates. With newly optimized conditions in hand, phenyl-substituted ammonium salts bearing *p*-fluoro (**1-88**), *p*-methoxy (**1-89**), and dioxolane (**1-90**) substituents provided useful yields of the desired products, albeit in slightly lower ee's.



<sup>a</sup> Conditions: ammonium triflate **1-75** ( $\geq 95\%$  ee, 0.3 mmol, 1.0 equiv),  $\text{B}_2\text{pin}_2$  (1.5 equiv),  $\text{Ni}(\text{cod})_2$  (10 mol %),  $\text{PPh}_2\text{Cy}$  (22 mol %), KOMe (1.7 equiv), THF (1.0 M), 70 °C, 24 h, unless otherwise noted. Average isolated yields ( $\pm 3\%$ ). Yields in parentheses determined by  $^1\text{H}$  NMR analysis using 1,3,5-trimethoxybenzene as internal standard. Average ee's ( $\pm 1\%$ ) of the subsequent alcohol, formed via oxidation with  $\text{H}_2\text{O}_2$  and NaOMe, determined by HPLC analysis using a chiral stationary phase. <sup>b</sup> 0.5 mmol scale.  $\text{ICy}\cdot\text{HBF}_4$  (12 mol %) in place of  $\text{PPh}_2\text{Cy}$ . Result of a single experiment.

Figure 1.16 Stereospecific Miyaura borylation of phenyl-substituted ammonium salts<sup>a</sup>

In order to demonstrate the practicality of this transformation, I conducted the synthesis of boronate **1-79** on a one-gram scale and outside of the glovebox (Figure 1.17). In order to circumvent air- and moisture-sensitivity, I switched the nickel source from  $\text{Ni}(\text{cod})_2$  to  $\text{Ni}(\text{OAc})_2\cdot 4\text{H}_2\text{O}$ . The benzylic boronate (**1-79**), a known precursor to

the anti-inflammatory agent (*S*)-naproxen (**1-92**), was formed in good yield (68%) and excellent ee (99%).<sup>7</sup>

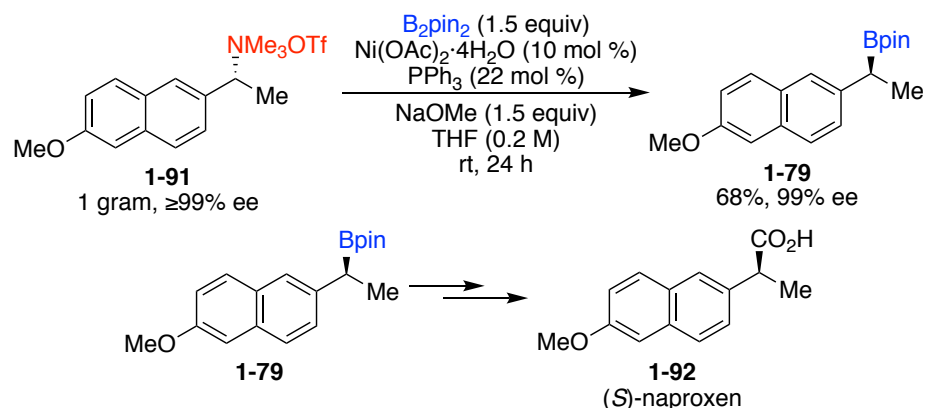


Figure 1.17 Miyaura borylation performed on a one-gram scale on the bench

The Jarvo group,<sup>25</sup> as well as our group, have proposed that an  $S_N2'$  oxidative addition is likely operative in cases where the aryl group of the electrophile has an extended  $\pi$ -system such as 2-naphthyl. In order to probe this, I synthesized both the 1- and 3-methoxynaphthyl enantioenriched benzylic ammonium salts (**1-93** and **1-96**, respectively) and subjected them to the cross-coupling conditions (Figure 1.18). The 1-methoxy (1-OMe) salt did not provide the desired product (**1-95**), likely due to hindrance of the Ni catalyst attacking C1 by the methoxy group. By blocking this position, the Ni catalyst could only attack in an  $S_N2'$ -fashion at C3. However, doing so would lead to a highly endergonic total loss of aromaticity in the naphthyl ring (**1-94**). Interestingly, the 3-methoxy (3-OMe) salt provides a synthetically useful yield of the desired enantioenriched organoboronate (**1-81**). I postulate that moving the methoxy group to C3 allows the active Ni catalyst to attack C1 via an  $S_N2'$ -addition. This  $S_N2'$ -

addition would lead to a less unfavorable, partial loss of aromaticity (**1-97**), thereby allowing for a subsequent transmetalation and reductive elimination.

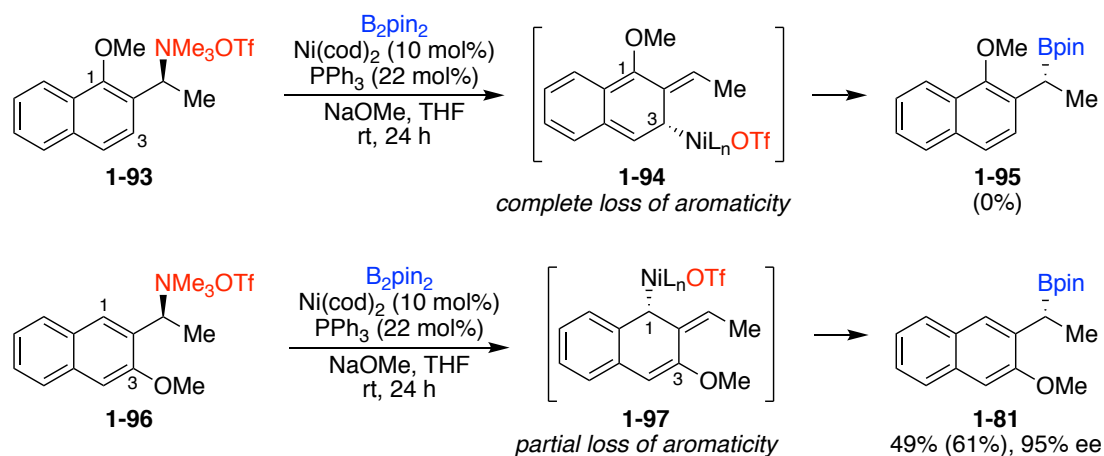


Figure 1.18 Effects of 1- and 3-OMe substituents on borylation reaction

Based on these studies, we believe that an  $\text{S}_{\text{N}}2'$ -type oxidative addition is operative (Figure 1.19). Electron-rich  $\text{Ni}^0$  species **A** can undergo a stereospecific  $\text{S}_{\text{N}}2'$  oxidative addition to the benzylic ammonium salt **1-75**. The resulting  $\text{Ni}^{\text{II}}$  species (**B**), in equilibrium benzylic  $\text{Ni}^{\text{II}}$  complex **C** via the  $\pi$ -allyl intermediate **D**, can undergo transmetalation with the boron-‘ate’ complex of  $\text{B}_2\text{pin}_2$  to form complex **E**. A subsequent reductive elimination regenerates the active  $\text{Ni}^0$  catalyst (**A**) and provides the enantioenriched boronate **1-76** with overall inversion of configuration at the benzylic carbon. The inversion of stereochemistry was determined by comparing the HPLC retention times of the alcohol derived from boronate oxidation to an enantioenriched authentic sample of known configuration.

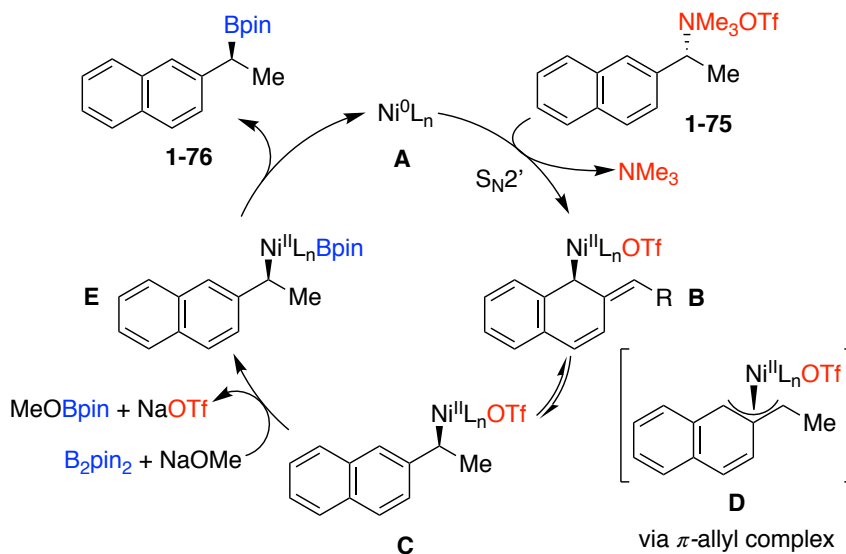


Figure 1.19 Proposed catalytic cycle

### 1.3 Conclusion

In summary, the first Miyaura borylation of a benzylic electrophile to deliver highly enantioenriched organoboronates in synthetically useful yields from readily available enantioenriched benzylic trimethylammonium salts has been described. This reaction tolerates a variety of both electronically and sterically diverse ammonium salts, including both extended and non-extended  $\pi$ -systems as well as electron-rich heterocyclic systems, and delivers versatile synthetic intermediates. This work was published in *Organic Letters* and highlighted in *Synfacts*.<sup>26,27</sup>

### 1.4 Experimental

#### 1.4.1 General Information

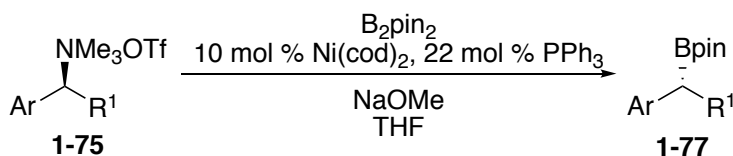
Reactions were performed in oven-dried vials with Teflon-lined caps or in oven-dried round-bottomed flasks unless otherwise noted. Flasks were fitted with

rubber septa, and reactions were conducted under a positive pressure of N<sub>2</sub>. Stainless steel syringes or cannulae were used to transfer air- and moisture-sensitive liquids. Flash chromatography was performed on silica gel 60 (40-63 μm, 60Å) unless otherwise noted. Commercial reagents were purchased from Sigma Aldrich, Acros, Fisher, Strem, TCI, Combi Blocks, Alfa Aesar, or Cambridge Isotopes Laboratories and used as received with the following exceptions: Bis(pinacolato)diboron, bis(neopentyl glycolato)diboron, and bis(hexylene glycolato)diboron were purchased from Sigma Aldrich and immediately placed in a N<sub>2</sub>-atmosphere glovebox for storage. Ni(OAc)<sub>2</sub>·4H<sub>2</sub>O was purchased from Alfa Aesar and donated by Astra Zeneca. Methyl trifluoromethanesulfonate (MeOTf) was purchased from TCI and used directly. 1,3-Bis(cyclohexyl)imidazolium tetrafluoroborate (ICy·HBF<sub>4</sub>) was purchased from Sigma Aldrich and used as received. THF was dried by passing through drying columns, then degassed by sparging with N<sub>2</sub> and stored over activated 4Å MS in a N<sub>2</sub>-atmosphere glovebox.<sup>28</sup> Commercially available enantioenriched amines were purchased from Alfa Aesar or Sigma Aldrich and used as received. Enantioenriched amines that were not commercially available were obtained through Grignard or hydride additions of Ellman's sulfinimines.<sup>29-31</sup> Dimethyl benzyl amines were prepared using Eschweiler-Clarke conditions or reductive amination of the corresponding primary benzyl amine with formaldehyde.<sup>32-33</sup> In some instances oven-dried potassium carbonate was added into CDCl<sub>3</sub> to remove trace amount of acid. Proton nuclear magnetic resonance (<sup>1</sup>H NMR) spectra, carbon nuclear magnetic resonance (<sup>13</sup>C NMR) spectra, fluorine nuclear magnetic resonance spectra (<sup>19</sup>F NMR), and silicon nuclear magnetic resonance spectra (<sup>29</sup>Si NMR) were recorded on both 400 MHz and 600 MHz spectrometers. Boron nuclear magnetic resonance spectra (<sup>11</sup>B NMR) were recorded

on a 600 MHz spectrometer. Chemical shifts for protons are reported in parts per million downfield from tetramethylsilane and are referenced to residual protium in the NMR solvent ( $\text{CHCl}_3 = \delta 7.26$ ). Chemical shifts for carbon are reported in parts per million downfield from tetramethylsilane and are referenced to the carbon resonances of the solvent ( $\text{CDCl}_3 = \delta 77.2$ ). Data are represented as follows: chemical shift, multiplicity (br = broad, s = singlet, d = doublet, t = triplet, q = quartet, m = multiplet, dd = doublet of doublets, sep = septet), coupling constants in Hertz (Hz), integration. Infrared (IR) spectra were obtained using FTIR spectrophotometers with material loaded onto a KBr plate. The mass spectral data were obtained at the University of Delaware mass spectrometry facility. Optical rotations were measured using a 2.5 mL cell with a 0.1 dm path length. Melting points were taken on a Stuart SMP10 instrument.

## 1.4.2 Stereospecific Borylation of Benzylic Ammonium Salts

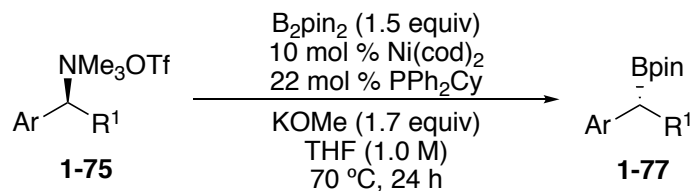
### 1.4.2.1 General Procedure A: Borylation of Naphthyl-Substituted Benzylic Ammonium Salts



In a  $\text{N}_2$ -atmosphere glovebox,  $\text{Ni(cod)}_2$  (8.3 mg, 0.030 mmol, 10 mol %),  $\text{PPh}_3$  (4.4 mg, 0.066 mmol, 22 mol %),  $\text{NaOMe}$  (24 mg, 0.45 mmol, 1.5 equiv),  $\text{B}_2\text{pin}_2$  (114 mg, 0.45 mmol, 1.5 equiv), and ammonium salt **1-75** (0.30 mmol, 1.0 equiv) were weighed into a 1-dram vial equipped with a magnetic stir bar. THF (1.5 mL, 0.2 M) was added, and the vial was capped with a Teflon-lined cap and removed from the glovebox. The mixture was stirred at room temperature for 24 h. The reaction mixture was then diluted with  $\text{Et}_2\text{O}$  (2.5 mL) and quickly filtered through a short plug of Celite<sup>®</sup>, which

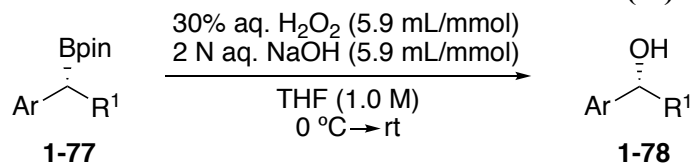
was then rinsed with Et<sub>2</sub>O (~ 10 mL). The filtrate was concentrated and purified by silica gel chromatography to give the benzylic boronate product **1-77**. The benzylic boronate was then converted to the corresponding benzylic alcohol via oxidation (see General Procedure C below) to determine the enantiomeric excess (ee).

#### 1.4.2.2 General Procedure B: Borylation of Non-Naphthyl-Substituted Benzylic Ammonium Salts

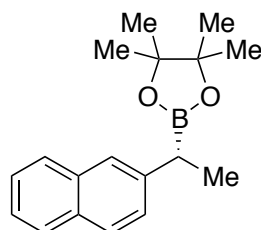


In a N<sub>2</sub>-atmosphere glovebox, Ni(cod)<sub>2</sub> (8.3 mg, 0.030 mmol, 10 mol %), PPh<sub>2</sub>Cy (18 mg, 0.066 mmol, 22 mol %), KOMe (38 mg, 0.45 mmol, 1.7 equiv), B<sub>2</sub>pin<sub>2</sub> (114 mg, 0.45 mmol, 1.5 equiv), and ammonium salt **1-75** (0.30 mmol, 1.0 equiv) were weighed into a 1-dram vial equipped with a magnetic stir bar. THF (0.3 mL, 1.0 M) was added and the vial was capped with a Teflon-lined cap and removed from the glovebox. The mixture was stirred at 70 °C for 24 h. The reaction mixture was then diluted with Et<sub>2</sub>O (2.5 mL) and quickly filtered through a plug of Celite<sup>®</sup>, which was then rinsed with Et<sub>2</sub>O (~ 10 mL). The filtrate was concentrated and then purified by silica gel chromatography to give the benzylic boronate product **1-77**. The benzylic boronate was then converted to the corresponding benzylic alcohol via oxidation (see General Procedure C below) to determine the enantiomeric excess (ee).

#### 1.4.2.3 General Procedure C: Oxidation of Benzylic Boronates to Benzylic Alcohols for Determination of Enantiomeric Excess (ee).



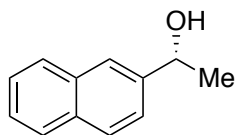
A solution of the benzylic boronate **1-77** (1.0 equiv) and Et<sub>2</sub>O (0.017 M) was cooled to 0 °C. Aqueous NaOH (2 N, 5.9 mL/mmol of **1-77**) was added, followed by aq. H<sub>2</sub>O<sub>2</sub> (30%, 5.9 mL/mmol of **1-77**). The mixture was stirred and allowed to warm slowly to room temperature overnight. The reaction mixture was diluted with H<sub>2</sub>O and Et<sub>2</sub>O, and the layers were separated. The aqueous layer was extracted with Et<sub>2</sub>O (3 x 20 mL). The combined organic layers were dried (MgSO<sub>4</sub>), filtered, and concentrated. The crude mixture was purified via silica gel chromatography to afford benzylic alcohol **3** for ee determination. For duplicate experiments, alcohol **1-78** was isolated once via column chromatography (to verify high yield in the oxidation) and once via preparatory thin-layer chromatography under the same mobile-phase conditions.



**(*R*)-4,4,5,5-Tetramethyl-2-(1-(naphthalen-2-yl)ethyl)-1,3,2-dioxaborolane (1-76).**

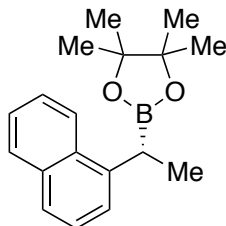
Prepared via General Procedure A using ammonium salt **1-75** (amine purchased in >99% ee). The crude mixture was purified by silica gel chromatography (5% EtOAc/hexanes) to give **1-76** (run 1: 69 mg, 82%; run 2: 79%) as a white solid: <sup>1</sup>H NMR (400 MHz, CDCl<sub>3</sub>) δ 7.83 – 7.75 (m, 3H), 7.67 (s, 1H), 7.48 – 7.37 (m, 3H), 2.64 (q, *J* = 7.4 Hz, 1H), 1.46 (d, *J* = 7.6 Hz, 3H), 1.23 (s, 6H), 1.22 (s, 6H); <sup>13</sup>C NMR (101 MHz, CDCl<sub>3</sub>) δ 142.7, 134.0, 131.8, 127.8, 127.7, 127.6, 127.4, 125.8, 125.4, 124.9, 83.5, 24.8, 24.8, 17.0.<sup>34</sup> The spectral data match that previously reported in the literature.<sup>8</sup>

Boronate **1-76** was oxidized to alcohol **1-98** via General Procedure C. The enantiomeric excess was determined to be 99% (run 1: 99% ee; run 2: 99% ee) by chiral HPLC analysis. See alcohol **1-98** below.



**(R)-1-(Naphthalen-2-yl)ethanol (1-98).** Prepared via General Procedure C using benzylic boronate **1-76**. The crude mixture was purified by silica gel chromatography (20% EtOAc/hexanes) to give **1-98** (38 mg, 95%) as a white solid. The enantiomeric excess was determined to be 99% (run 1: 99% ee; run 2: 99% ee) by chiral HPLC analysis (CHIRAPAK IA, 1.0 mL/min, 1% *i*-PrOH/hexanes,  $\lambda=254$  nm);  $t_R(\text{major}) = 43.70$  min,  $t_R(\text{minor}) = 45.74$  min);  $^1\text{H NMR}$  (400 MHz,  $\text{CDCl}_3$ )  $\delta$  7.89 – 7.79 (m, 4H), 7.56 – 7.42 (m, 3H), 5.06 (q,  $J = 6.2$  Hz, 1H), 2.07 (s, 1H), 1.58 (d,  $J = 6.4$  Hz, 3H);  $^{13}\text{C NMR}$  (101 MHz,  $\text{CDCl}_3$ )  $\delta$  143.3, 133.4, 133.0, 128.5, 128.1, 127.8, 126.3, 126.0, 123.97, 123.95, 70.7, 25.3. The spectral data match that previously reported in the literature.<sup>35</sup>

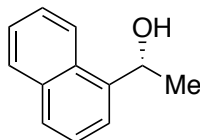
The absolute configuration of alcohol **1-98** was determined to be *R* by comparison of its HPLC trace to that of commercially available, enantioenriched **1-98**.



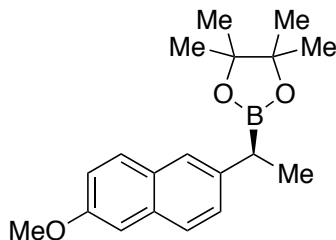
**(R)-4,4,5,5-Tetramethyl-2-(1-(naphthalen-1-yl)ethyl)-1,3,2-dioxaborolane ((R)-1-78).** Prepared via General Procedure A using ammonium salt **1-99** (amine purchased in >99% ee). The crude mixture was purified by silica gel chromatography (5% EtOAc/hexanes) to give **1-78** (run 1: 47 mg, 56%; run 2: 47 mg, 56%) as a white solid:  $^1\text{H NMR}$  (400 MHz,  $\text{CDCl}_3$ )  $\delta$  8.13 (d,  $J = 8.2$  Hz, 1H), 7.88 – 7.83 (m, 1H), 7.69 (d,  $J = 7.5$  Hz, 1H), 7.53 – 7.39 (m, 4H), 3.14 (q,  $J = 7.4$  Hz, 1H), 1.52 (d,  $J = 7.5$  Hz, 3H), 1.23 (s, 6H), 1.22 (s, 6H);  $^{13}\text{C NMR}$  (101 MHz,  $\text{CDCl}_3$ )  $\delta$  141.5, 134.0, 132.1, 128.9,

126.0, 125.5, 125.4, 124.4, 124.2, 83.6, 24.8, 24.7, 16.6.<sup>34</sup> The spectral data matches that previously reported in the literature.<sup>8</sup>

Boronate **1-78** was oxidized to alcohol **1-100** via General Procedure C. The enantiomeric excess was determined to be 92% (run 1: 92%, run 2: 91%) by chiral HPLC analysis. See alcohol **1-100** below.



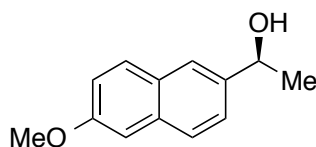
**(R)-1-(Naphthalen-1-yl)ethanol (1-100)**. Prepared via General Procedure C using benzylic boronate **1-78**. The crude mixture was purified by silica gel chromatography (20% EtOAc/hexanes) to give **1-100** (21 mg, 72%) as a colorless oil. The enantiomeric excess was determined to be 92% (run 1: 92% ee; run 2: 91% ee) by chiral HPLC analysis (CHIRAPAK IC, 1.0 mL/min, 2% *i*-PrOH/hexanes,  $\lambda=254$  nm);  $t_R(\text{major}) = 23.87$  min,  $t_R(\text{minor}) = 18.43$  min):  $^1\text{H NMR}$  (400 MHz,  $\text{CDCl}_3$ )  $\delta$  8.12 (d,  $J = 8.2$  Hz, 1H), 7.89 (d,  $J = 7.6$  Hz, 1H), 7.79 (d,  $J = 8.2$  Hz, 1H), 7.69 (d,  $J = 7.1$  Hz, 1H), 7.57 – 7.45 (m, 3H), 5.69 (q,  $J = 6.3$  Hz, 1H), 1.96 (s, 1H), 1.68 (d,  $J = 6.5$  Hz, 3H);  $^{13}\text{C NMR}$  (101 MHz,  $\text{CDCl}_3$ )  $\delta$  141.5, 133.9, 130.4, 129.1, 128.1, 126.2, 125.73, 125.70, 123.3, 122.1, 67.3, 24.5. The spectral data of this compound match that previously reported in the literature.<sup>35</sup>



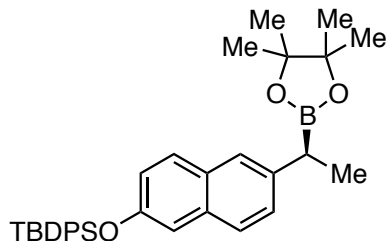
**(S)-2-(1-(6-Methoxynaphthalen-2-yl)ethyl)-4,4,5,5-tetramethyl-1,3,2-dioxaborolane (1-79)**. Prepared via General Procedure A using ammonium salt **1-91**

(amine prepared in  $\geq 95\%$  ee). The crude mixture was purified by silica gel chromatography (5% EtOAc/hexanes) to give **1-79** (run 1: 78 mg, 83%; run 2: 78 mg, 83%) as a white solid:  $^1\text{H}$  NMR (400 MHz,  $\text{CDCl}_3$ )  $\delta$  7.68 (t,  $J = 8.1$  Hz, 2H), 7.60 (s, 1H), 7.38 (dd,  $J = 8.4, 1.4$  Hz, 1H), 7.12 (d,  $J = 8.1$  Hz, 2H), 3.91 (s, 3H), 2.60 (q,  $J = 7.5$  Hz, 1H), 1.44 (d,  $J = 7.5$  Hz, 3H), 1.23 (s, 6H), 1.22 (s, 6H);  $^{13}\text{C}$  NMR (101 MHz,  $\text{CDCl}_3$ )  $\delta$  157.0, 140.3, 132.7, 129.5, 129.1, 127.8, 126.7, 125.3, 118.5, 105.7, 83.5, 55.4, 24.8, 24.7, 17.1.<sup>34</sup> The spectral data match that previously reported in the literature.<sup>7</sup>

Boronate **1-79** was oxidized to alcohol **1-101** via General Procedure C. The enantiomeric excess was determined to be 99% (run 1: 98% ee; run 2: 99% ee) by chiral HPLC analysis. See alcohol **1-101** below.

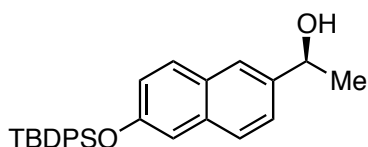


**(S)-1-(6-Methoxynaphthalen-2-yl)ethanol (1-101)**. Prepared via General Procedure C using benzylic boronate **1-79**. The crude mixture was purified by silica gel chromatography (20% EtOAc/hexanes) to give **1-101** (31 mg, 72%) as a white solid; the enantiomeric excess was determined to be 99% (run 1: 98% ee; run 2: 99% ee) by chiral HPLC analysis (CHIRAPAK IB, 1.0 mL/min, 3% *i*-PrOH/hexanes,  $\lambda = 254$  nm);  $t_{\text{R}}(\text{major}) = 19.99$  min,  $t_{\text{R}}(\text{minor}) = 25.84$  min):  $^1\text{H}$  NMR (600 MHz,  $\text{CDCl}_3$ )  $\delta$  7.75 – 7.69 (m, 3H), 7.47 (d,  $J = 8.5$  Hz, 1H), 7.18 – 7.11 (m, 2H), 5.02 (q,  $J = 6.5$  Hz, 1H), 3.92 (s, 3H), 2.03 (s, 1H), 1.57 (d,  $J = 6.5$  Hz, 3H);  $^{13}\text{C}$  NMR (151 MHz,  $\text{CDCl}_3$ )  $\delta$  157.8, 141.1, 134.2, 129.6, 128.9, 127.3, 124.5, 123.9, 119.1, 105.9, 70.6, 55.5, 25.2. The spectral data match that previously reported in the literature.<sup>36</sup>



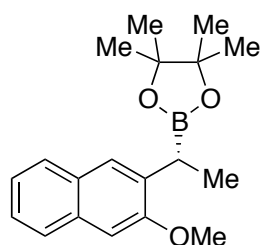
**(S)-tert-Butyldiphenyl((6-(1-(4,4,5,5-tetramethyl-1,3,2-dioxaborolan-2-yl)ethyl)naphthalen-2-yl)oxy)silane (1-80).** Prepared via General Procedure A using ammonium salt **1-102** (amine prepared in  $\geq 95\%$  ee). The crude mixture was purified by silica gel chromatography (5% EtOAc/hexanes) to give **1-80** (76 mg, 47%) as a white solid (mp 84–86 °C):  $^1\text{H}$  NMR (400 MHz,  $\text{CDCl}_3$ )  $\delta$  7.85 – 7.78 (m, 4H), 7.62 – 7.53 (m, 2H), 7.49 – 7.37 (m, 7H), 7.29 (dd,  $J = 8.5, 1.5$  Hz, 1H), 7.10 – 7.03 (m, 2H), 2.57 (q,  $J = 7.4$  Hz, 1H), 1.42 (d,  $J = 7.5$  Hz, 3H), 1.25 (s, 6H), 1.23 (s, 6H), 1.18 (s, 9H);  $^{13}\text{C}$  NMR (101 MHz,  $\text{CDCl}_3$ )  $\delta$  152.8, 140.4, 135.7, 133.2, 132.7, 130.0, 129.6, 128.8, 128.0, 127.6, 126.8, 125.2, 121.5, 114.5, 83.5, 26.8, 24.82, 24.79, 19.7, 17.2;<sup>34</sup>  $^{11}\text{B}$  NMR (193 MHz,  $\text{CDCl}_3$ )  $\delta$  33.6;  $^{29}\text{Si}$  NMR (79 MHz,  $\text{CDCl}_3$ )  $\delta$  -6.4; FTIR (neat) 2960, 2858, 1603, 1500, 1352, 1143, 975, 701  $\text{cm}^{-1}$ ; HRMS (LIFDI) calculated for  $\text{C}_{34}\text{H}_{41}\text{BO}_3\text{Si}$ : 536.2887, found: 536.2894.

Boronate **1-80** was oxidized to alcohol **1-103** via General Procedure C. The enantiomeric excess was determined to be 92% by chiral HPLC analysis. See alcohol **1-103** below.



**(S)-1-(6-((tert-Butyldiphenylsilyl)oxy)naphthalen-2-yl)ethanol (1-103).** Prepared via General Procedure C using benzylic boronate **1-80**. The crude mixture was purified by silica gel chromatography (20% EtOAc/hexanes) to give **1-103** (54 mg, 95%) as a colorless semi-solid. The enantiomeric excess was determined to be 92% by chiral HPLC analysis (CHIRALPAK IA, 1.0 mL/min, 1% *i*-PrOH/hexanes,  $\lambda = 254$

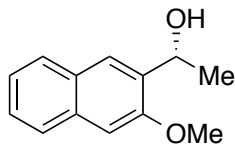
nm);  $t_R(\text{major}) = 35.70$  min,  $t_R(\text{minor}) = 33.76$  min.  $[\alpha]_D^{24} = -20.2^\circ$  (c 2.2,  $\text{CHCl}_3$ ):  $^1\text{H}$  NMR (400 MHz,  $\text{CDCl}_3$ )  $\delta$  7.83 – 7.75 (m, 4H), 7.67 (s, 1H), 7.63 – 7.59 (m, 1H), 7.50 (d,  $J = 8.5$  Hz, 1H), 7.47 – 7.34 (m, 7H), 7.12 – 7.05 (m, 2H), 4.98 (q,  $J = 6.4$  Hz, 1H), 1.99 (bs, 1H), 1.54 (d,  $J = 6.5$  Hz, 3H), 1.16 (s, 9H);  $^{13}\text{C}$  NMR (101 MHz,  $\text{CDCl}_3$ )  $\delta$  153.6, 141.1, 135.7, 134.0, 133.0, 130.1, 129.3, 128.9, 128.0, 127.3, 124.2, 123.7, 122.0, 114.7, 70.6, 26.7, 25.2, 19.7;  $^{29}\text{Si}$  NMR (119 MHz,  $\text{CDCl}_3$ )  $\delta$  -5.9; FTIR (neat) 3347 (broad), 3051, 2931, 2858, 1606, 1482, 1263, 1175, 114, 76, 701, 504  $\text{cm}^{-1}$ ; HRMS (CI+) calculated for  $\text{C}_{28}\text{H}_{30}\text{BO}_2\text{Si}$ : 427.2093, found: 427.2090.



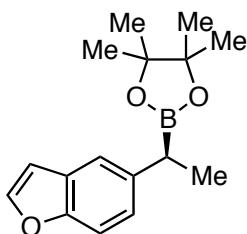
**(*R*)-2-(1-(3-Methoxynaphthalen-2-yl)ethyl)-4,4,5,5-tetramethyl-1,3,2-**

**dioxaborolane (1-81).** Prepared via General Procedure A using ammonium salt **1-96** (amine prepared in  $\geq 95\%$  ee). The crude mixture was purified by silica gel chromatography (5% EtOAc/hexanes) to give **1-81** (46 mg, 49%) as an opaque semi-solid:  $^1\text{H}$  NMR (400 MHz,  $\text{CDCl}_3$ )  $\delta$  7.77 – 7.69 (m, 2H), 7.60 (s, 1H), 7.38 (ddd,  $J = 8.1, 6.8, 1.4$  Hz, 1H), 7.31 (ddd,  $J = 8.1, 6.9, 1.3$  Hz, 1H), 7.08 (s, 1H), 3.93 (s, 3H), 2.63 (q,  $J = 7.5$  Hz, 1H), 1.43 (d,  $J = 7.5$  Hz, 3H), 1.26 (s, 12H);  $^{13}\text{C}$  NMR (101 MHz,  $\text{CDCl}_3$ )  $\delta$  156.2, 135.7, 133.1, 129.4, 127.3, 126.5, 126.3, 125.3, 123.5, 104.4, 83.2, 55.1, 24.80, 24.77, 14.8;<sup>34</sup>  $^{11}\text{B}$  NMR (193 MHz,  $\text{CDCl}_3$ )  $\delta$  33.6; FTIR (neat) 2976, 1472, 1388, 1251, 1144, 847, 746  $\text{cm}^{-1}$ ; HRMS (LIFDI) calculated for  $\text{C}_{19}\text{H}_{25}\text{BO}_3$ : 312.1897, found: 312.1884.

Boronate **1-81** was oxidized to alcohol **1-104** via General Procedure C. The enantiomeric excess was determined to be 95% by chiral HPLC analysis. See alcohol **1-104** below.



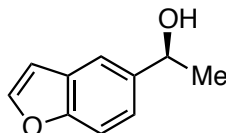
**(R)-1-(3-Methoxynaphthalen-2-yl)ethanol (1-104).** Prepared via General Procedure C using benzylic boronate **1-81**. The crude mixture was purified by silica gel chromatography (20% EtOAc/hexanes) to give **1-104** (25 mg, 83%) as a clear oil. The enantiomeric excess was determined to be 95% (CHIRALPAK IB, 1.0 mL/min, 5% *i*-PrOH/hexanes,  $\lambda=254$  nm);  $t_R(\text{major}) = 22.47$  min,  $t_R(\text{minor}) = 14.96$  min.  $[\alpha]_D^{24} = -35.7^\circ$  (c 0.11,  $\text{CHCl}_3$ ):  $^1\text{H NMR}$  (600 MHz,  $\text{CDCl}_3$ )  $\delta$  7.80 – 7.76 (m, 2H), 7.73 (d,  $J = 8.2$  Hz, 1H), 7.44 (t,  $J = 7.5$  Hz, 1H), 7.35 (t,  $J = 7.9$  Hz, 1H), 7.13 (s, 1H), 5.22 (q,  $J = 6.0$  Hz, 1H), 3.97 (s, 3H), 2.77 (s, 1H), 1.61 (d,  $J = 6.6$  Hz, 3H);  $^{13}\text{C NMR}$  (151 MHz,  $\text{CDCl}_3$ )  $\delta$  155.6, 135.0, 133.9, 128.9, 127.9, 126.5, 126.4, 125.3, 124.1, 105.6, 67.0, 55.5, 23.1. The spectral data match that previously reported in the literature for the racemic compound.<sup>37</sup>



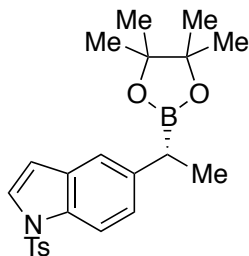
**(S)-2-(1-(Benzofuran-5-yl)ethyl)-4,4,5,5-tetramethyl-1,3,2-dioxaborolane (1-82).** Prepared via General Procedure A, except that the reaction temperature was 50 °C, using ammonium salt **1-105** (amine prepared in  $\geq 95\%$  ee). The crude mixture was purified by silica gel chromatography (5% EtOAc/hexanes) to give **1-82** (run 1: 48 mg, 59%; run 2: 55 mg, 67%) as a white solid (mp 58–59 °C):  $^1\text{H NMR}$  (400 MHz,  $\text{CDCl}_3$ )  $\delta$  7.57 (d,  $J = 2.2$  Hz, 1H), 7.45 (d,  $J = 1.8$  Hz, 1H), 7.41 (d,  $J = 8.5$  Hz, 1H), 7.17 (dd,  $J = 8.6, 1.9$  Hz, 1H), 6.71 (dd,  $J = 2.2, 1.0$  Hz, 1H), 2.54 (q,  $J = 7.5$  Hz, 1H), 1.39 (d,  $J = 7.5$  Hz, 3H), 1.23 (s, 6H), 1.21 (s, 6H);  $^{13}\text{C NMR}$  (101 MHz,  $\text{CDCl}_3$ )  $\delta$  153.4, 144.9, 139.6, 127.7, 124.7, 119.8, 111.1, 106.7, 83.4, 24.79, 24.75, 17.9;<sup>34</sup>  $^{11}\text{B}$

NMR (193 MHz, CDCl<sub>3</sub>)  $\delta$  33.6; FTIR (neat) 2976, 1467, 1319, 1144, 843, 737 cm<sup>-1</sup>; HRMS (LIFDI) calculated for C<sub>16</sub>H<sub>21</sub>BO<sub>3</sub>: 272.1584, found: 272.1611.

Boronate **1-82** was oxidized to alcohol **1-106** via General Procedure C. The enantiomeric excess was determined to be 98% (run 1: 97% ee; run 2: 98% ee) by chiral HPLC analysis. See alcohol **1-106** below.



**(S)-1-(Benzofuran-5-yl)ethanol (1-106)**. Prepared via General Procedure C using benzylic boronate **1-82**. The crude mixture was purified by silica gel chromatography (20% EtOAc/hexanes) to give **1-106** (run 1 (41 mg of **1-82**): 15 mg, 61%) as a clear oil. The enantiomeric excess was determined to be 98% (run 1: 97% ee; run 2: 98% ee) by chiral HPLC analysis (CHIRALPAK IC, 0.5 mL/min, 2% *i*-PrOH/hexanes,  $\lambda=254$  nm);  $t_R(\text{major}) = 45.76$  min,  $t_R(\text{minor}) = 43.97$  min.  $[\alpha]_D^{24} = -33.0^\circ$  (c 0.79, CHCl<sub>3</sub>): <sup>1</sup>H NMR (400 MHz, CDCl<sub>3</sub>)  $\delta$  7.67 – 7.57 (m, 2H), 7.48 (d,  $J = 8.5$  Hz, 1H), 7.32 (dd,  $J = 8.6, 1.8$  Hz, 1H), 6.76 (d,  $J = 1.1$  Hz, 1H), 5.01 (q,  $J = 6.4$  Hz, 1H), 1.92 (bs, 1H), 1.54 (d,  $J = 6.4$  Hz, 3H); <sup>13</sup>C NMR (101 MHz, CDCl<sub>3</sub>)  $\delta$  154.5, 145.6, 140.7, 127.6, 122.2, 118.1, 111.5, 106.8, 70.8, 25.7; FTIR (neat) 3344 (broad), 2921, 1444, 1261, 1129, 1072, 891, 813, 738 cm<sup>-1</sup>; HRMS (CI+) calculated for C<sub>10</sub>H<sub>11</sub>O<sub>2</sub>: 163.0759, found: 163.0756.

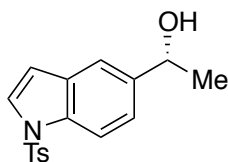


**(R)-5-(1-(4,4,5,5-Tetramethyl-1,3,2-dioxaborolan-2-yl)ethyl)-1-tosyl-1H-indole (1-83)**. Prepared via General Procedure A using ammonium salt **1-107** (prepared in  $\geq 95\%$

ee). Instead of filtering through Celite<sup>®</sup>, the diluted mixture was filtered through a small plug of silica gel and then concentrated. 1,3,5-Trimethoxybenzene was added as internal standard, and the yield was determined by <sup>1</sup>H NMR to be 44% (run 1: 46%, run 2: 41%). The reaction mixture was complicated, preventing effective purification and isolation on scale. However, an analytical sample of **1-83** (contaminated with ~15% B<sub>2</sub>pin<sub>2</sub>) was purified by silica gel chromatography (prep TLC, 30% EtOAc/hexanes) to enable characterization: <sup>1</sup>H NMR (600 MHz, CDCl<sub>3</sub>) δ 7.85 (d, *J* = 8.6 Hz, 1H), 7.75 (d, *J* = 8.3 Hz, 2H), 7.49 (d, *J* = 3.6 Hz, 1H), 7.34 (s, 1H), 7.20 (d, *J* = 8.1 Hz, 2H), 7.17 (dd, *J* = 8.6, 1.3 Hz, 1H), 6.57 (d, *J* = 3.6 Hz, 1H), 2.48 (q, *J* = 7.5 Hz, 1H), 2.33 (s, 3H), 1.32 (d, *J* = 7.5 Hz, 3H), 1.20 (s, 6H), 1.18 (s, 6H); <sup>13</sup>C NMR (101 MHz, CDCl<sub>3</sub>) δ 144.9, 140.2, 135.6, 133.1, 131.2, 130.0, 127.0, 126.3, 125.2, 120.0, 113.4, 109.3, 83.5, 24.79, 24.76, 21.7, 17.6;<sup>34</sup> <sup>11</sup>B (193 MHz, CDCl<sub>3</sub>) δ 33.8; FTIR (neat, cm<sup>-1</sup>) 2977, 2930, 1459, 1372, 1173, 676, 583; HRMS (CI) calculated for C<sub>23</sub>H<sub>28</sub>BNO<sub>4</sub>S: 425.1832, found: 425.1840.

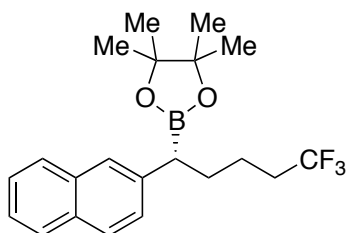
The sample was then concentrated and subjected to General Procedure C for oxidation and determination of enantiomeric excess.

Boronate **1-83** was oxidized to alcohol **1-108** via General Procedure C. The enantiomeric excess was determined to be 96% by chiral HPLC analysis. See alcohol **1-108** below.



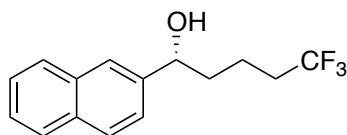
**(R)-1-(1-Tosyl-1H-indol-5-yl)ethanol (1-108)**. Prepared via General Procedure C using benzylic boronate **1-83**. The crude mixture was purified by silica gel chromatography (40% EtOAc/hexanes) to give **1-108** (34 mg, 79%) as a pale yellow semi-solid. The enantiomeric excess was determined to be 96% (run 1: 96% ee; run 2: 95% ee) by chiral HPLC analysis (CHIRALPAK IA, 1.0 mL/min, 5% *i*-

PrOH/hexanes,  $\lambda=254$  nm);  $t_R(\text{major}) = 58.15$  min,  $t_R(\text{minor}) = 53.38$  min.  $[\alpha]_D^{24} = -18.7^\circ$  (c 0.165,  $\text{CHCl}_3$ );  $^1\text{H NMR}$  (400 MHz,  $\text{CDCl}_3$ )  $\delta$  7.94 (d,  $J = 8.6$  Hz, 1H), 7.75 (d,  $J = 8.4$  Hz, 2H), 7.55 (d,  $J = 3.6$  Hz, 1H), 7.52 (s, 1H), 7.31 (dd,  $J = 8.6, 1.5$  Hz, 1H), 7.20 (d,  $J = 8.2$  Hz, 2H), 6.62 (d,  $J = 3.6$  Hz, 1H), 4.94 (q,  $J = 6.4$  Hz, 1H), 2.32 (s, 3H), 1.99 (s, 1H), 1.49 (d,  $J = 6.4$  Hz, 3H);  $^{13}\text{C NMR}$  (101 MHz,  $\text{CDCl}_3$ )  $\delta$  145.1, 141.2, 135.3, 134.3, 131.0, 130.0, 126.9, 126.9, 122.5, 118.2, 113.7, 109.2, 70.6, 25.5, 21.7; FTIR (neat) 3379 (broad), 2971, 1596, 1369, 1173, 1128, 676, 579  $\text{cm}^{-1}$ ; HRMS (CI+)  $[\text{M}+\text{H}]^+$  calculated for  $[\text{C}_{17}\text{H}_{18}\text{NO}_3\text{S}]^+$ : 316.1007, found: 316.1017.

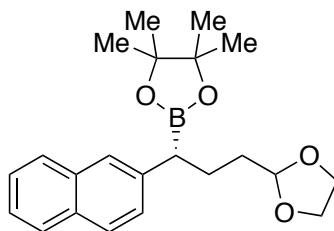


**(R)-4,4,5,5-Tetramethyl-2-(5,5,5-trifluoro-1-(naphthalen-2-yl)pentyl)-1,3,2-dioxaborolane (1-84).** Prepared via General Procedure A using ammonium salt **1-109** (amine prepared in  $\geq 95\%$  ee). The crude mixture was purified by silica gel chromatography (5% EtOAc/hexanes) to give **1-84** (run 1: 73 mg, 64%; run 2: 69 mg, 60%) as a white solid (mp 74–76  $^\circ\text{C}$ );  $^1\text{H NMR}$  (400 MHz,  $\text{CDCl}_3$ )  $\delta$  7.86 – 7.74 (m, 3H), 7.65 (s, 1H), 7.50 – 7.33 (m, 3H), 2.50 (t,  $J = 7.9$  Hz, 1H), 2.19 – 1.96 (m, 3H), 1.91 – 1.78 (m, 1H), 1.65 – 1.50 (m, 2H), 1.23 (s, 6H), 1.20 (s, 6H);  $^{13}\text{C NMR}$  (151 MHz,  $\text{CDCl}_3$ )  $\delta$  140.2, 134.0, 132.1, 128.1, 127.7, 127.6, 127.4 (q,  $J_{\text{C-F}} = 276.4$  Hz), 127.3, 126.5, 126.0, 125.2, 83.7, 33.9 (q,  $J_{\text{C-F}} = 28.4$  Hz), 31.6, 24.8, 24.7, 21.7 (q,  $J_{\text{C-F}} = 2.7$  Hz);<sup>34</sup>  $^{11}\text{B NMR}$  (193 MHz,  $\text{CDCl}_3$ )  $\delta$  33.1;  $^{19}\text{F NMR}$  (376.5 MHz,  $\text{CDCl}_3$ )  $\delta$  –66.3; FTIR (neat) 2978, 1361, 1259, 1141, 857, 749  $\text{cm}^{-1}$ ; HRMS (CI+) calculated for  $\text{C}_{21}\text{H}_{26}\text{BF}_3\text{O}_2$ : 379.2049, found: 379.2034.

Boronate **1-84** was oxidized to alcohol **1-110** via General Procedure C. The enantiomeric excess was determined to be 96% (run 1: 96% ee; run 2: 96% ee) by chiral HPLC analysis. See alcohol **1-110** below.



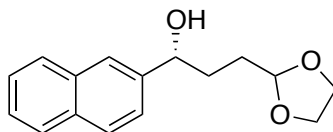
**(R)-5,5,5-Trifluoro-1-(naphthalen-2-yl)pentan-1-ol (1-110).** Prepared via General Procedure C using benzylic boronate **1-84**. The crude mixture was purified by silica gel chromatography (20% EtOAc/hexanes) to give **1-110** (40 mg, 93%) as a white solid (mp 48–50 °C). The enantiomeric excess was determined to be 96% (run 1: 96% ee; run 2: 96% ee) by chiral HPLC analysis (CHIRALPAK IB, 1.0 mL/min, 3% *i*-PrOH/hexanes,  $\lambda=254$  nm);  $t_R(\text{major}) = 28.25$  min,  $t_R(\text{minor}) = 25.09$  min.  $[\alpha]_D^{24} = +38.4^\circ$  (c 0.75, CHCl<sub>3</sub>); <sup>1</sup>H NMR (400 MHz, CDCl<sub>3</sub>)  $\delta$  7.89 – 7.80 (m, 3H), 7.76 (s, 1H), 7.55 – 7.48 (m, 2H), 7.46 (dd,  $J = 8.6, 1.8$  Hz, 1H), 4.87 – 4.79 (m, 1H), 2.20 – 2.02 (m, 3H), 1.99 – 1.67 (m, 3H), 1.68 – 1.52 (m, 1H); <sup>13</sup>C NMR (101 MHz, CDCl<sub>3</sub>)  $\delta$  141.7, 133.4, 133.2, 128.7, 128.1, 127.9, 127.2 (q,  $J_{C-F} = 277.5$  Hz), 126.5, 126.2, 124.7, 123.9, 74.4, 37.8, 33.7 (q,  $J_{C-F} = 28.6$  Hz), 18.6 (q,  $J_{C-F} = 3.0$  Hz); <sup>19</sup>F NMR (376.5 Hz, CDCl<sub>3</sub>)  $\delta$  –66.3; FTIR (neat) 3350 (broad), 2947, 1391, 1259, 1134, 1028, 821, 749, 479 cm<sup>-1</sup>; HRMS (CI+) calculated for C<sub>15</sub>H<sub>16</sub>F<sub>3</sub>O: 269.1153, found: 269.1158.



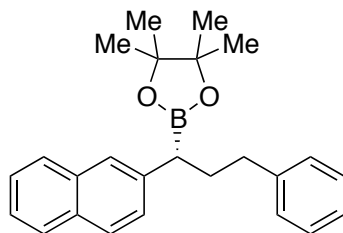
**(R)-2-(3-(1,3-Dioxolan-2-yl)-1-(naphthalen-2-yl)propyl)-4,4,5,5-tetramethyl-1,3,2-dioxaborolane (1-85).** Prepared via General Procedure A using ammonium salt **1-111** (amine prepared in  $\geq 95\%$  ee). The crude mixture was purified by silica gel chromatography (10% EtOAc/hexanes) to give **1-85** (64 mg, 58%) as a white solid (mp 82–84 °C) (note: a 10:1 mixture of product to B<sub>2</sub>pin<sub>2</sub> was observed): <sup>1</sup>H NMR

(400 MHz, CDCl<sub>3</sub>)  $\delta$  7.81 – 7.72 (m, 3H), 7.65 (s, 1H), 7.47 – 7.36 (m, 3H), 4.86 (t,  $J$  = 4.8 Hz, 1H), 3.98 – 3.77 (m, 4H), 2.51 (t,  $J$  = 8.0 Hz, 1H), 2.15 – 2.01 (m, 1H), 1.99 – 1.84 (m, 1H), 1.76 – 1.59 (m, 2H), 1.21 (s, 6H), 1.19 (s, 6H); <sup>13</sup>C NMR (101 MHz, CDCl<sub>3</sub>)  $\delta$  140.5, 133.9, 131.9, 127.9, 127.63, 127.59, 127.5, 126.5, 125.8, 125.0, 104.7, 83.5, 64.9, 33.5, 26.8, 24.8, 24.7; <sup>11</sup>B NMR (193 MHz, CDCl<sub>3</sub>)  $\delta$  33.2; FTIR (neat) 2977, 2882, 1371, 1324, 1141, 857, 750 cm<sup>-1</sup>; HRMS (LIFDI) calculated for C<sub>22</sub>H<sub>29</sub>BO<sub>4</sub>: 368.2140, found: 368.2143.

Boronate **1-85** was oxidized to alcohol **1-112** via General Procedure C. The enantiomeric excess was determined to be 98% by chiral HPLC analysis. See alcohol **1-112** below.

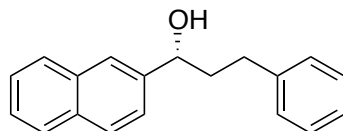


**(R)-3-(1,3-Dioxolan-2-yl)-1-(naphthalen-2-yl)propan-1-ol (1-112)**. Prepared via General Procedure C using benzylic boronate **1-85**. The crude mixture was purified by silica gel chromatography (40% EtOAc/hexanes) to give **1-112** (36 mg, 84%) as a white solid (mp 67–69 °C). The enantiomeric excess was determined to be 98% by chiral HPLC analysis (CHIRALPAK IB, 1.0 mL/min, 5% *i*-PrOH/hexanes,  $\lambda$ =254 nm);  $t_R$ (major) = 31.06 min,  $t_R$ (minor) = 27.49 min.  $[\alpha]_D^{24} = -18.4^\circ$  (c 1.78, CHCl<sub>3</sub>): <sup>1</sup>H NMR (400 MHz, CDCl<sub>3</sub>)  $\delta$  7.87 – 7.78 (m, 4H), 7.53 – 7.40 (m, 3H), 4.96 – 4.85 (m, 2H), 4.03 – 3.81 (m, 4H), 2.74 (d,  $J$  = 3.5 Hz, 1H), 2.05 – 1.92 (m, 2H), 1.91 – 1.73 (m, 2H); <sup>13</sup>C NMR (101 MHz, CDCl<sub>3</sub>)  $\delta$  142.1, 133.4, 133.0, 128.4, 128.1, 127.8, 126.2, 125.9, 124.6, 124.2, 104.4, 74.3, 65.2, 65.1, 33.1, 30.1; FTIR (neat) 3434 (broad), 2882, 1409, 1139, 1031, 822, 751, 479 cm<sup>-1</sup>; HRMS (CI+) calculated for C<sub>16</sub>H<sub>18</sub>O<sub>3</sub>: 241.1229, found: 241.1225.



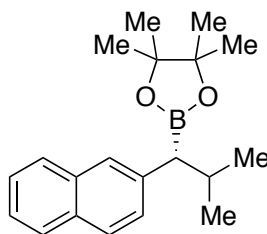
**(R)-4,4,5,5-Tetramethyl-2-(1-(naphthalen-2-yl)-3-phenylpropyl)-1,3,2-dioxaborolane (1-86).** Prepared via General Procedure A using ammonium salt **1-113** (amine prepared in  $\geq 95\%$  ee). The crude mixture was purified by silica gel chromatography (5% EtOAc/hexanes) to give **1-86** (80 mg, 72%) as a white solid (mp 77–79 °C):  $^1\text{H}$  NMR (400 MHz,  $\text{CDCl}_3$ )  $\delta$  7.87 – 7.79 (m, 3H), 7.71 (s, 1H), 7.52 – 7.41 (m, 3H), 7.34 – 7.28 (m, 2H), 7.24 – 7.18 (m, 3H), 2.65 (t,  $J = 7.9$  Hz, 2H), 2.60 (t,  $J = 7.9$  Hz, 1H), 2.37 – 2.26 (m, 1H), 2.21 – 2.10 (m, 1H), 1.25 (s, 6H), 1.23 (s, 6H);  $^{13}\text{C}$  NMR (101 MHz,  $\text{CDCl}_3$ )  $\delta$  142.6, 140.6, 133.9, 131.9, 128.7, 128.4, 128.0, 127.7, 127.6, 127.5, 126.5, 125.84, 125.81, 125.0, 83.6, 35.6, 34.3, 24.84, 24.76;<sup>34</sup>  $^{11}\text{B}$  NMR (193 MHz,  $\text{CDCl}_3$ )  $\delta$  33.7; FTIR (neat) 2977, 2930, 1323, 1141, 857, 748, 699  $\text{cm}^{-1}$ ; HRMS (LIFDI) calculated for  $\text{C}_{25}\text{H}_{29}\text{BO}_2$ : 372.2261, found: 372.2270.

Boronate **1-86** was oxidized to alcohol **1-114** via General Procedure C. The enantiomeric excess was determined to be 98% by chiral HPLC analysis. See alcohol **1-114** below.



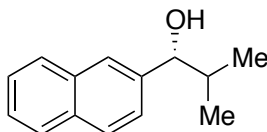
**(R)-1-(Naphthalen-2-yl)-3-phenylpropan-1-ol (1-114).** Prepared via General Procedure C using benzylic boronate **1-86**. The crude mixture was purified by silica gel chromatography (20% EtOAc/hexanes) to give **1-114** (43 mg, 94%) as a white solid (mp 85–86 °C). The enantiomeric excess was determined to be 98% by chiral HPLC analysis (CHIRALPAK IA, 1.0 mL/min, 2% *i*-PrOH/hexanes,  $\lambda = 254$  nm);  $t_{\text{R}}(\text{major}) = 35.44$  min,  $t_{\text{R}}(\text{minor}) = 38.33$  min:  $^1\text{H}$  NMR (400 MHz,  $\text{CDCl}_3$ )  $\delta$  7.89 – 7.81 (m, 3H), 7.79 (s, 1H), 7.55 – 7.44 (m, 3H), 7.34 – 7.27 (m, 2H), 7.25 – 7.16 (m,

3H), 4.87 (ddd,  $J = 8.1, 5.5, 2.9$  Hz, 1H), 2.85 – 2.65 (m, 2H), 2.30 – 2.06 (m, 2H), 2.02 (d,  $J = 3.1$  Hz, 1H);  $^{13}\text{C}$  NMR (151 MHz,  $\text{CDCl}_3$ )  $\delta$  142.1, 141.9, 133.5, 133.2, 128.56, 128.59, 128.63, 128.1, 127.9, 126.4, 126.1, 126.0, 124.9, 124.2, 74.2, 40.5, 32.2. The spectral data match that of the literature.<sup>38</sup>

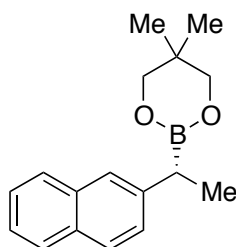


**(*R*)-4,4,5,5-Tetramethyl-2-(2-methyl-1-(naphthalen-2-yl)propyl)-1,3,2-dioxaborolane (1-87).** Prepared via General Procedure A using ammonium salt **1-115** (amine prepared in  $\geq 95\%$  ee). The crude mixture was purified by silica gel chromatography (5% EtOAc/hexanes) to give **1-87** (run 1: 46 mg, 49%; run 2: 47 mg, 50%) as a white solid (mp 85–86 °C);  $^1\text{H}$  NMR (400 MHz,  $\text{CDCl}_3$ )  $\delta$  7.83 – 7.71 (m, 3H), 7.66 (s, 1H), 7.47 – 7.36 (m, 3H), 2.33 – 2.19 (m, 1H), 2.16 (d,  $J = 10.5$  Hz, 1H), 1.21 (s, 6H), 1.18 (s, 6H), 1.10 (d,  $J = 6.4$  Hz, 3H), 0.77 (d,  $J = 6.4$  Hz, 3H);  $^{13}\text{C}$  NMR (101 MHz,  $\text{CDCl}_3$ )  $\delta$  140.2, 133.9, 132.0, 128.1, 127.7, 127.6, 127.3, 125.7, 124.9, 83.4, 31.1, 24.8, 24.7, 23.4, 22.3;<sup>34</sup>  $^{13}\text{C}$  NMR (151 MHz,  $\text{C}(\text{O})(\text{CD}_3)_2$ )  $\delta$  141.2, 134.7, 132.9, 128.7, 128.3, 128.3, 128.2, 127.9, 126.6, 125.7, 83.9, 31.7, 25.0, 24.9, 23.5, 22.4;<sup>4</sup>  $^{11}\text{B}$  NMR (193 MHz,  $\text{CDCl}_3$ )  $\delta$  33.2; FTIR (neat) 2922, 2850, 1382, 1323, 1143, 1103  $\text{cm}^{-1}$ ; HRMS (LIFDI) calculated for  $\text{C}_{20}\text{H}_{27}\text{BO}_2$ : 310.2104, found: 310.2126.

Boronate **1-87** was oxidized to alcohol **1-116** via General Procedure C. The enantiomeric excess was determined to be 98% (run 1: 97%, run 2: 98%) by chiral HPLC analysis. See alcohol **1-116** below.

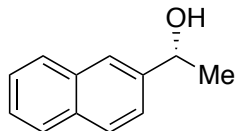


**(R)-2-Methyl-1-(naphthalen-2-yl)propan-1-ol (1-116).** Prepared via General Procedure C using benzylic boronate **1-87**. The crude mixture was purified by silica gel chromatography (20% EtOAc/hexanes) to give **1-116** (run 1 (39 mg of **1-87**): 7 mg, 28%) as a clear oil. The enantiomeric excess was determined to be 98% (run 1: 97%, run 2: 98%) by chiral HPLC analysis (CHIRALPAK IC, 1.0 mL/min, 2% *i*-PrOH/hexanes,  $\lambda=254$  nm);  $t_R(\text{major}) = 17.49$  min,  $t_R(\text{minor}) = 16.15$  min;  $^1\text{H NMR}$  (600 MHz,  $\text{CDCl}_3$ )  $\delta$  7.86 – 7.80 (m, 3H), 7.76 (s, 1H), 7.51 – 7.44 (m, 3H), 4.54 (d,  $J = 6.9$  Hz, 1H), 2.12 – 2.03 (m,  $J = 6.7$  Hz, 1H), 1.93 (s, 1H), 1.05 (d,  $J = 6.7$  Hz, 3H), 0.84 (d,  $J = 6.8$  Hz, 3H);  $^{13}\text{C NMR}$  (101 MHz,  $\text{CDCl}_3$ )  $\delta$  141.2, 133.3, 133.1, 128.2, 128.1, 127.8, 126.2, 125.9, 125.6, 124.8, 80.4, 35.4, 19.3, 18.4. The spectral data match that previously reported in the literature.<sup>39</sup>

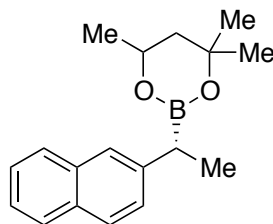


**(R)-5,5-Dimethyl-2-(1-(naphthalen-2-yl)ethyl)-1,3,2-dioxaborinane (1-117).** Prepared via General Procedure A using ammonium salt **1-75** (amine purchased in >99% ee) and bis(neopentyl glycolato)diboron ( $\text{B}_2\text{neop}_2$ ) instead of  $\text{B}_2\text{pin}_2$ . Instead of filtering through Celite<sup>®</sup>, the diluted mixture was filtered through a small plug of silica gel and then concentrated. 1,3,5-Trimethoxybenzene was added as internal standard, and the yield of the reaction was determined by  $^1\text{H NMR}$  analysis to be 61%. The sample was then concentrated and subjected to General Procedure C for oxidation and determination of enantiomeric excess.

Boronate **1-117** was oxidized to alcohol **1-98** via General Procedure C. The enantiomeric excess was determined to be 95% by chiral HPLC analysis. See alcohol **1-98** below.

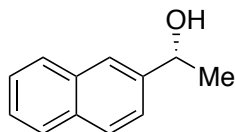


**(R)-1-(Naphthalen-2-yl)ethanol (1-98).** Prepared via General Procedure C using benzylic boronate **1-118**. The crude mixture was purified by silica gel chromatography (20% EtOAc/hexanes) to give **1-98** (29 mg, 93%) as a white solid. The enantiomeric excess was determined to be 95% by chiral HPLC analysis (CHIRALPAK IA, 1.0 mL/min, 1% *i*-PrOH/hexanes,  $\lambda=254$  nm);  $t_R(\text{major}) = 45.06$  min,  $t_R(\text{minor}) = 47.29$  min. The spectral data match that of alcohol **1-98** above.

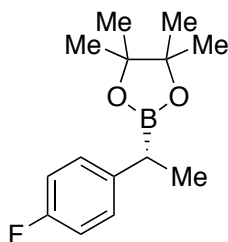


**4,4,6-Trimethyl-2-((R)-1-(naphthalen-2-yl)ethyl)-1,3,2-dioxaborinane (1-118).** Prepared via General Procedure A using ammonium salt **1-75** (amine purchased in >99% ee) and bis(hexylene glycolato)diboron ( $B_2\text{hex}_2$ ) instead of  $B_2\text{pin}_2$ . Instead of filtering through Celite<sup>®</sup>, the diluted mixture was filtered through a small plug of silica gel and then concentrated. 1,3,5-Trimethoxybenzene was added as internal standard, and the yield of the reaction was determined by  $^1\text{H}$  NMR analysis to be 74%. The sample was then concentrated and subjected to General Procedure C for oxidation and determination of enantiomeric excess.

Boronate **1-118** was oxidized to alcohol **1-98** via General Procedure C. The enantiomeric excess was determined to be 95% by chiral HPLC analysis. See alcohol **1-98** below.

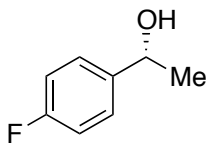


**(R)-1-(Naphthalen-2-yl)ethanol (1-98).** Prepared via General Procedure C using benzylic boronate **1-118**. The crude mixture was purified by silica gel chromatography (20% EtOAc/hexanes) to give **1-98** (35 mg, quant.) as a white solid. The enantiomeric excess was determined to be 95% by chiral HPLC analysis (CHIRALPAK IA, 1.0 mL/min, 1% *i*-PrOH/hexanes,  $\lambda=254$  nm);  $t_R(\text{major}) = 44.64$  min,  $t_R(\text{minor}) = 46.84$  min. The spectral data match that of alcohol **1-98** above.

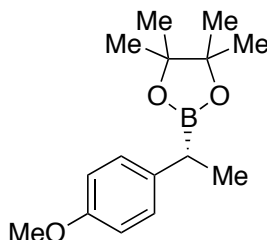


**(R)-2-(1-(4-Fluorophenyl)ethyl)-4,4,5,5-tetramethyl-1,3,2-dioxaborolane (1-88).** Prepared via General Procedure B on a 0.5-mmol scale using ammonium salt **1-119** (amine purchased in >99% ee) and ICy·HBF<sub>4</sub> (19.2 mg, 0.060 mmol, 12 mol %) instead of PPh<sub>2</sub>Cy. The crude mixture was purified by silica gel chromatography (5% EtOAc/hexanes) to give **1-88** (66 mg, 53%) as a clear oil (please note that **1-88** was not subjected to high vacuum due to its volatility): <sup>1</sup>H NMR (400 MHz, CDCl<sub>3</sub>)  $\delta$  7.20 – 7.13 (m, 2H), 6.98 – 6.91 (m, 2H), 2.42 (q,  $J = 7.5$  Hz, 1H), 1.31 (d,  $J = 7.5$  Hz, 3H), 1.21 (s, 6H), 1.20 (s, 6H); <sup>13</sup>C NMR (101 MHz, CDCl<sub>3</sub>)  $\delta$  161.0 (d,  $J_{C-F} = 243.2$  Hz), 140.7 (d,  $J_{C-F} = 3.1$  Hz), 129.1 (d,  $J_{C-F} = 7.7$  Hz), 115.1 (d,  $J_{C-F} = 21.0$  Hz), 83.5, 24.8, 17.4. The spectral data match that reported in the literature.<sup>40</sup> The sample was then concentrated and subjected to General Procedure C for oxidation and determination of enantiomeric excess.

Boronate **1-88** was oxidized to alcohol **1-120** via General Procedure C. The enantiomeric excess was determined to be 86% (run 1 from oxidation of isolated **1-88**: 87% ee; run 2 from oxidation of crude **1-88**: 85% ee) by chiral HPLC analysis. See alcohol **1-120** below.

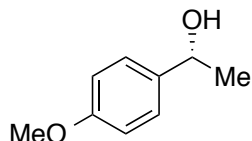


**(R)-1-(4-Fluorophenyl)ethanol (1-120).** Prepared via General Procedure C using benzylic boronate **1-88**. The crude mixture was purified by silica gel chromatography (20% EtOAc/hexanes) to give **1-120** (16 mg, 62%) as a clear oil. The enantiomeric excess was determined to be 86% (run 1 from oxidation of isolated **1-88**: 87% ee; run 2 from oxidation of crude **1-88**: 85% ee) by chiral HPLC analysis (CHIRALPAK IF, 1.0 mL/min, 2% *i*-PrOH/hexanes,  $\lambda=254$  nm);  $t_R(\text{major}) = 16.25$  min,  $t_R(\text{minor}) = 17.65$  min:  $^1\text{H}$  NMR (600 MHz,  $\text{CDCl}_3$ )  $\delta$  7.34 (dd,  $J = 8.3, 5.6$  Hz, 2H), 7.03 (t,  $J = 8.6$  Hz, 2H), 4.89 (q,  $J = 6.4$  Hz, 1H), 1.87 (s, 1H), 1.48 (d,  $J = 6.5$  Hz, 3H);  $^{13}\text{C}$  NMR (151 MHz,  $\text{CDCl}_3$ )  $\delta$  162.3 (d,  $J_{\text{C-F}} = 244.6$  Hz), 141.7, 127.2 (d,  $J_{\text{C-F}} = 7.6$  Hz), 115.4 (d,  $J_{\text{C-F}} = 22.7$  Hz), 70.0, 25.5;  $^{19}\text{F}$  NMR (565 MHz,  $\text{CDCl}_3$ )  $\delta$  -115.4. The spectral data match that of the literature.<sup>41</sup>

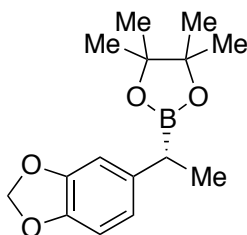


**(R)-2-(1-(4-Methoxyphenyl)ethyl)-4,4,5,5-tetramethyl-1,3,2-dioxaborolane (1-89).** Prepared via General Procedure B using ammonium salt **1-121** (amine precursor purchased in >99% ee). The crude mixture was purified by silica gel chromatography (5% EtOAc/hexanes) to give **1-89** (run 1: 45 mg, 57%; run 2: 41 mg, 52%) as a clear oil:  $^1\text{H}$  NMR (400 MHz,  $\text{CDCl}_3$ )  $\delta$  7.14 (d,  $J = 8.6$  Hz, 2H), 6.82 (d,  $J = 8.6$  Hz, 2H), 3.78 (s, 3H), 2.38 (q,  $J = 7.5$  Hz, 1H), 1.30 (d,  $J = 7.6$  Hz, 3H), 1.22 (s, 6H), 1.20 (s, 6H);  $^{13}\text{C}$  NMR (101 MHz,  $\text{CDCl}_3$ )  $\delta$  157.2, 137.0, 128.6, 113.8, 83.2, 55.2, 24.7, 24.6, 17.4.<sup>34</sup> The spectral data matches that previously reported in the literature.<sup>42</sup>

Boronate **1-89** was oxidized to alcohol **1-122** via General Procedure C. The enantiomeric excess was determined to be 86% (run 1: 85% ee; run 2: 87% ee) by chiral HPLC analysis. See alcohol **1-122** below.



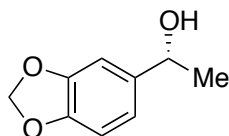
**(R)-1-(4-Methoxyphenyl)ethanol (1-122)**. Prepared via General Procedure C using benzylic boronate **1-89**. The crude mixture was purified by silica gel chromatography (20% EtOAc/hexanes) to give **1-122** (run 1 (45 mg of **1-89**): 19 mg, 72%) as a clear oil. The enantiomeric excess was determined to be 86% (run 1: 85%, run 2: 87%) by chiral HPLC analysis (CHIRALPAK IB, 1.0 mL/min, 2% *i*-PrOH/hexanes,  $\lambda=254$  nm);  $t_R(\text{major}) = 20.16$  min,  $t_R(\text{minor}) = 22.24$  min:  $^1\text{H NMR}$  (400 MHz,  $\text{CDCl}_3$ )  $\delta$  7.30 (d,  $J = 8.6$  Hz, 2H), 6.88 (d,  $J = 8.6$  Hz, 2H), 4.86 (q,  $J = 6.4$  Hz, 1H), 3.80 (s, 3H), 1.84 (bs, 1H), 1.48 (d,  $J = 6.4$  Hz, 3H);  $^{13}\text{C NMR}$  (101 MHz,  $\text{CDCl}_3$ )  $\delta$  159.1, 138.1, 126.8, 114.0, 70.2, 55.5, 25.2. The spectral data match that previously reported in the literature.<sup>43</sup>



**(R)-2-(1-(Benzo[d][1,3]dioxol-5-yl)ethyl)-4,4,5,5-tetramethyl-1,3,2-dioxaborolane (1-90)**. Prepared via General Procedure B using ammonium salt **1-123** (amine prepared in  $\geq 95\%$  ee). The crude mixture was purified by silica gel chromatography (5% EtOAc/hexanes) to give **1-90** (run 1: 48 mg, 58%; run 2: 53 mg, 63%) as a clear oil:  $^1\text{H NMR}$  (400 MHz,  $\text{CDCl}_3$ )  $\delta$  6.74 (d,  $J = 1.7$  Hz, 1H), 6.71 (d,  $J = 8.0$  Hz, 1H), 6.65 (dd,  $J = 8.0, 1.7$  Hz, 1H), 5.90 (s, 2H), 2.35 (q,  $J = 7.5$  Hz, 1H), 1.28 (d,  $J = 7.5$  Hz, 3H), 1.22 (s, 6H), 1.20 (s, 6H);  $^{13}\text{C NMR}$  (101 MHz,  $\text{CDCl}_3$ )  $\delta$  147.6, 145.2, 139.0, 120.5, 108.6, 108.3, 100.8, 83.5, 24.8, 24.8, 17.7;<sup>34</sup>  $^{11}\text{B NMR}$  (193 MHz,

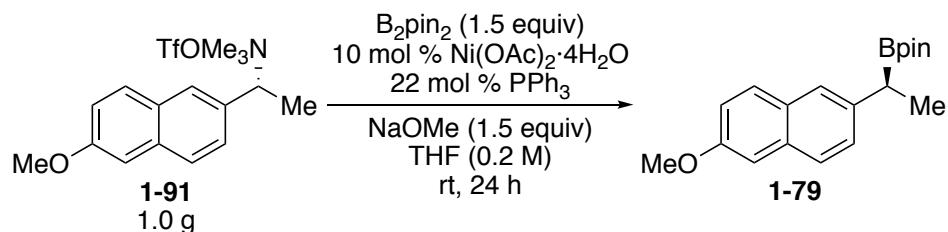
CDCl<sub>3</sub>)  $\delta$  33.3; FTIR (neat) 2977, 1487, 1321, 1237, 1144, 1041, 938, 811 cm<sup>-1</sup>; HRMS (CI) calculated for C<sub>15</sub>H<sub>21</sub>BO<sub>4</sub>: 277.1611, found: 277.1609.

Boronate **1-90** was oxidized to alcohol **1-124** via General Procedure C. The enantiomeric excess was determined to be 85% (run 1: 84% ee; run 2: 85% ee) by chiral HPLC analysis. See alcohol **1-124** below.



**(R)-1-(Benzo[d][1,3]dioxol-5-yl)ethanol (1-124)**. Prepared via General Procedure C using benzylic boronate **1-90**. The crude mixture was purified by silica gel chromatography (20% EtOAc/hexanes) to give **1-124** (run 1 (40 mg of **1-90**): 21 mg, 87%) as a clear oil. The enantiomeric excess was determined to be 85% (run 1: 85%, run 2: 84%) by chiral HPLC analysis (CHIRALPAK IA, 1.0 mL/min, 3% *i*-PrOH/hexanes,  $\lambda$ =210 nm);  $t_R$ (major) = 19.60 min,  $t_R$ (minor) = 22.01 min: <sup>1</sup>H NMR (400 MHz, CDCl<sub>3</sub>)  $\delta$  6.92 – 6.88 (m, 1H), 6.85 – 6.75 (m, 2H), 5.95 (s, 2H), 4.82 (q,  $J$  = 6.4 Hz, 1H), 1.76 (bs, 1H), 1.46 (d,  $J$  = 6.4 Hz, 3H); <sup>13</sup>C NMR (101 MHz, CDCl<sub>3</sub>)  $\delta$  147.9, 147.0, 140.1, 118.9, 108.3, 106.2, 101.2, 70.5, 25.3. The spectral data match that previously reported in the literature.<sup>43</sup>

#### 1.4.2.4 Gram-Scale Synthesis of (*S*)-2-(1-(6-Methoxynaphthalen-2-yl)ethyl)-4,4,5,5-tetramethyl-1,3,2-dioxaborolane (**1-79**)



An oven-dried, 50-mL Schlenk flask equipped with a magnetic stir bar was evacuated and backfilled with N<sub>2</sub> (x 4). Ni(OAc)<sub>2</sub>·4H<sub>2</sub>O (63 mg, 0.254 mmol, 10 mol %), PPh<sub>3</sub> (147 mg, 0.559 mmol, 22 mol %), B<sub>2</sub>pin<sub>2</sub> (0.968 g, 3.81 mmol, 1.5 equiv), and

ammonium salt **1-91** ( $\geq 95\%$  ee, 1.00 g, 2.54 mmol, 1.0 equiv) were added. NaOMe (0.206 g, 3.81 mmol, 1.5 equiv) was quickly added and the flask was sealed with a rubber septum. The flask was evacuated and then backfilled with N<sub>2</sub> (x 4). THF (13 mL, 0.2 M) was then added. The mixture was stirred vigorously at room temperature for 24 h. Over the course of the reaction, the solution turned from light yellow to dark orange. Et<sub>2</sub>O (~ 40 mL) was added, and the mixture was stirred for five minutes. The mixture was filtered through a pad of Celite<sup>®</sup>, which was then washed multiple times with Et<sub>2</sub>O (~ 120 mL total volume). The filtrate was concentrated, and the crude material was purified by silica gel chromatography (5% EtOAc/hexanes) to give **1-79** (68%, 99% ee) as a white solid. The spectra of this material match that of **1-79** prepared on 0.3 mmol scale, as described above.

Boronate **1-79** was oxidized to alcohol **1-102** via General Procedure C. The enantiomeric excess was determined to be 99% by chiral HPLC analysis. The spectral data of this alcohol match that of alcohol **1-102** as described above.

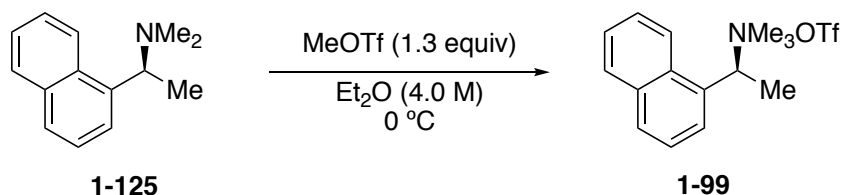
### 1.4.3 Preparation of Benzyl Ammonium Salts

Enantioenriched amines that were not commercially available were obtained through Grignard or hydride additions to Ellman's sulfinimines.<sup>29-31</sup> Via these reactions, a single diastereomer of each sulfinamine was isolated (as determined by <sup>1</sup>H NMR analysis). We thus assume  $\geq 95\%$  ee of the subsequent amine after removal of Ellman's auxiliary. Dimethyl benzyl amines were then prepared using Eschweiler-Clarke conditions or reductive amination of the corresponding primary benzyl amine with formaldehyde.<sup>32-33</sup> We assume no loss of ee in the formation of the trimethyl ammonium triflates from this intermediate. For enantioenriched amines that were commercially available, we also assume no loss of ee in the formation of the trimethyl ammonium triflates.

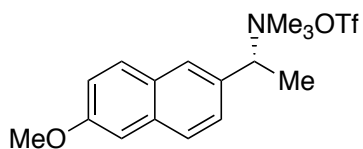
Ammonium triflates **1-75**, **1-99**, **1-115**, **1-119**, and **1-121** have been previously prepared in our laboratory.<sup>23, 44</sup>

Ammonium triflates prepared via these procedures were used as is in the stereospecific borylation reaction, without further purification. In some cases, impurities are present in the ammonium triflates.

#### 1.4.3.1 General Procedure D: Preparation of (*S*)-*N,N,N*-Trimethyl-1-(naphthalen-1-yl)ethanaminium trifluoromethanesulfonate (**1-99**)

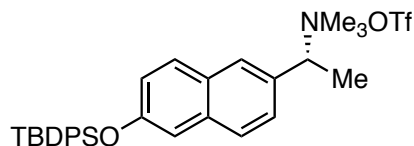


(*S*)-*N,N*-Dimethyl-1-(naphthalen-1-yl)ethanamine (0.806 g, 4.04 mmol, 1.0 equiv), which was prepared using Eschweiler-Clarke conditions<sup>32</sup> from (*S*)-(-)-1-(1-naphthyl)ethylamine (purchased in >99% ee), was dissolved in Et<sub>2</sub>O (1.01 mL, 4.0 M). MeOTf (0.58 mL, 5.25 mmol, 1.3 equiv) was added dropwise at 0 °C. After complete addition, the mixture was allowed to stir for an additional 30 minutes at 0 °C. The mixture was diluted with Et<sub>2</sub>O (~ 2 mL), taken out of the ice bath, and allowed to warm to room temperature while stirring. The white precipitate was filtered and washed with Et<sub>2</sub>O (3 x 15 mL). The solid was dried under high vacuum to afford salt **1-99** (1.377 g, 94%) as a white solid, which was used directly in the benzylic borylation. This compound was previously prepared in our laboratory via this method.<sup>15</sup>



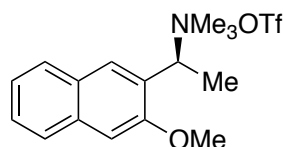
**(*R*)-1-(6-Methoxynaphthalen-2-yl)-*N,N,N*-trimethylethanaminium trifluoromethanesulfonate (**1-91**)**. Prepared according to General Procedure D on a 5.64 mmol scale from (*R*)-1-(6-methoxynaphthalen-2-yl)-*N,N*-dimethylethanamine,

which was prepared using Eschweiler-Clarke conditions<sup>32</sup> from (*R*)-1-(6-methoxynaphthalen-2-yl)ethanamine (prepared using Ellman's auxiliary<sup>29-31</sup>), to afford salt **1-91** (2.085 g, 94%) as a white solid (mp 109–111 °C): <sup>1</sup>H NMR (600 MHz, CDCl<sub>3</sub>) δ 7.94 (s, 1H), 7.84-7.74 (m, 2H), 7.49 (d, *J* = 8.3 Hz, 1H), 7.19 (dd, *J* = 9.0, 2.4 Hz, 1H), 7.13 (d, *J* = 2.1 Hz, 1H), 4.98 (q, *J* = 6.9 Hz, 1H), 3.92 (s, 3H), 3.15 (s, 9H), 1.88 (d, *J* = 6.8 Hz, 3H); <sup>13</sup>C NMR (151 MHz, CDCl<sub>3</sub>) δ 159.3, 135.6, 130.2, 128.4, 128.1, 127.2, 121.0 (q, *J*<sub>C-F</sub> = 320.1 Hz), 120.4, 105.7, 74.5, 55.6, 51.2, 15.2; <sup>19</sup>F NMR (376.5 MHz, CDCl<sub>3</sub>) δ -78.4; FTIR (neat) 3043, 1608, 1488, 1270, 1160, 846, 639 cm<sup>-1</sup>; LRMS (ESI+) [M-OTf]<sup>+</sup> calculated for [C<sub>16</sub>H<sub>22</sub>NO<sup>+</sup>]: 244.2, found: 244.2.



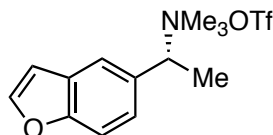
**(*R*)-1-(6-((*tert*-Butyldiphenylsilyl)oxy)naphthalen-2-yl)-*N,N,N*-trimethylethanaminium trifluoromethanesulfonate (**1-102**).** Prepared according to General Procedure D on a 1.50 mmol scale from (*R*)-1-(6-((*tert*-butyldiphenylsilyl)oxy)naphthalen-2-yl)-*N,N*-dimethylethanamine, which was prepared by reductive amination<sup>33</sup> from (*R*)-1-(6-((*tert*-butyldiphenylsilyl)oxy)naphthalen-2-yl)ethanamine (prepared using Ellman's auxiliary<sup>29-31</sup>). In this case, stirring ceased as a result of precipitate formation. The solution was diluted with Et<sub>2</sub>O to 2.0 M and the stir bar was agitated with a spatula to resume stirring. The reaction afforded salt **1-102** (0.698 g, 75%) as a white solid (mp 180–182 °C): <sup>1</sup>H NMR (600 MHz, CDCl<sub>3</sub>) δ 7.87 (s, 1H), 7.74 (d, *J* = 6.9 Hz, 4H), 7.69 (d, *J* = 8.9 Hz, 1H), 7.53 (d, *J* = 8.6 Hz, 1H), 7.45 – 7.40 (m, 2H), 7.39 – 7.33 (m, 5H), 7.13 (dd, *J* = 8.9, 2.4 Hz, 1H), 7.05 (d, *J* = 2.1 Hz, 1H), 4.92 (q, *J* = 6.9 Hz, 1H), 3.13 (s, 9H), 1.84 (d, *J* = 6.9 Hz, 3H), 1.13 (s, 9H); <sup>13</sup>C NMR (151 MHz, CDCl<sub>3</sub>) δ 155.3, 135.6, 135.4, 132.6, 130.3, 130.1, 128.5, 128.14, 128.09, 127.2, 123.3, 120.9 (q, *J*<sub>C-F</sub> = 320.1 Hz), 114.6, 74.6, 51.2, 26.7, 19.7, 15.2; <sup>19</sup>F NMR (565 MHz, CDCl<sub>3</sub>) δ

-78.4;  $^{29}\text{Si}$  NMR (119 MHz,  $\text{CDCl}_3$ )  $\delta$  -5.0; FTIR (neat) 3051, 2933, 2859, 1605, 1483, 1266, 1161, 1031, 879, 703, 639  $\text{cm}^{-1}$ ; LRMS (ESI+)  $[\text{M-OTf}]^+$  calculated for  $[\text{C}_{31}\text{H}_{38}\text{NOSi}^+]$ : 468.3, found: 468.4.



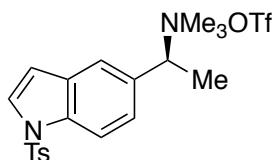
**(S)-1-(3-Methoxynaphthalen-2-yl)-N,N,N-trimethylethanaminium**

**trifluoromethanesulfonate (1-96)** Prepared according to General Procedure D on a 1.45 mmol scale from (S)-1-(3-methoxynaphthalen-2-yl)-N,N-dimethylethanamine, which was prepared using Eschweiler-Clarke conditions<sup>32</sup> from (S)-1-(3-methoxynaphthalen-2-yl)ethanamine (prepared using Ellman's auxiliary<sup>29-31</sup>). In this case, a white precipitate did not form upon addition of MeOTf. Instead, two distinct layers formed. The top layer was decanted off. The bottom layer was washed with  $\text{Et}_2\text{O}$  (5 x 2 mL) and then hexanes (5 x 2 mL, HPLC grade) and then dried under high vacuum to give salt **1-96** (0.359 g, 63%) as a clear viscous oil. By NMR, an ~8:1 mixture of rotamers was observed:  $^1\text{H}$  NMR (600 MHz,  $\text{CDCl}_3$ , major rotamer)  $\delta$  7.97 (s, 1H), 7.87 (d,  $J = 8.2$  Hz, 1H), 7.73 (d,  $J = 8.3$  Hz, 1H), 7.50 (t,  $J = 7.6$  Hz, 1H), 7.38 (t,  $J = 7.5$  Hz, 1H), 7.22 (s, 1H), 5.29 (q,  $J = 7.1$  Hz, 1H), 3.98 (s, 3H), 3.11 (s, 9H), 1.85 (d,  $J = 7.0$  Hz, 3H);  $^{13}\text{C}$  NMR (151 MHz,  $\text{CDCl}_3$ , major rotamer)  $\delta$  154.8, 135.3, 130.7, 128.7, 128.5, 128.1, 126.6, 125.1, 122.5, 120.7 (q,  $J_{\text{C-F}} = 320.0$  Hz), 106.8, 65.9, 56.0, 51.09, 51.07, 51.05, 15.4;<sup>45</sup>  $^{19}\text{F}$  NMR (376.5 MHz,  $\text{CDCl}_3$ )  $\delta$  -78.4; FTIR (neat) 3048, 1634, 1474, 1260, 1163, 1031, 756, 639  $\text{cm}^{-1}$ ; LRMS (ESI+)  $[\text{M-OTf}]^+$  calculated for  $[\text{C}_{16}\text{H}_{22}\text{NO}^+]$ : 244.2, found: 244.2.



**(R)-1-(Benzofuran-5-yl)-N,N,N-trimethylethanaminium**

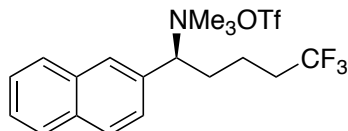
**trifluoromethanesulfonate (1-105).** Prepared according to General Procedure D on a 6.12 mmol scale from (R)-1-(benzofuran-5-yl)-N,N-dimethylethanamine, which was prepared using Eschweiler-Clarke conditions<sup>32</sup> from (R)-1-(benzofuran-5-yl)ethanamine (prepared using Ellman's auxiliary<sup>29-31</sup>). In this case, a white precipitate did not form upon addition of MeOTf. Instead, two distinct layers formed. The top layer was decanted off. The bottom layer was washed with Et<sub>2</sub>O (2 mL), which caused white precipitate to form. The precipitate was filtered and washed with Et<sub>2</sub>O (3 x 15 mL) and dried under high vacuum to afford salt **1-105** (2.076 g, 96%) as a white solid (mp 106–108 °C): <sup>1</sup>H NMR (600 MHz, CDCl<sub>3</sub>) δ 7.81 (s, 1H), 7.68 (d, *J* = 2.1 Hz, 1H), 7.55 (d, *J* = 8.5 Hz, 1H), 7.41 (d, *J* = 8.2 Hz, 1H), 6.85 – 6.81 (m, 1H), 4.98 (q, *J* = 7.0 Hz, 1H), 3.13 (s, 9H), 1.85 (d, *J* = 6.9 Hz, 3H); <sup>13</sup>C NMR (151 MHz, CDCl<sub>3</sub>) δ 155.8, 146.9, 128.5, 127.1, 120.9 (q, *J*<sub>C-F</sub> = 320.1 Hz), 112.4, 107.0, 74.4, 51.18, 51.15, 51.1, 15.5;<sup>45</sup> <sup>19</sup>F NMR (565 MHz, CDCl<sub>3</sub>) δ –78.4; FTIR (neat) 3042, 1472, 1263, 1158, 1030, 838, 750, 639, 518 cm<sup>-1</sup>; LRMS (ESI+) [M-OTf]<sup>+</sup> calculated for [C<sub>13</sub>H<sub>18</sub>NO<sup>+</sup>]: 204.1, found: 204.2.



**(S)-N,N,N-Trimethyl-1-(1-tosyl-1H-indol-5-yl)ethanaminium**

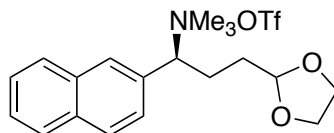
**trifluoromethanesulfonate (1-107).** Prepared according to General Procedure D on a 2.97 mmol scale from (S)-N,N-dimethyl-1-(1-tosyl-1H-indol-5-yl)ethanamine, which was prepared using Eschweiler-Clarke conditions<sup>32</sup> from (S)-1-(1-tosyl-1H-indol-5-yl)ethanamine (prepared using Ellman's auxiliary<sup>29-31</sup>) to afford salt **1-107** (1.277 g, 85%) as a white solid (mp 73-75 °C): <sup>1</sup>H NMR (600 MHz, CDCl<sub>3</sub>) δ 8.01 (d, *J* = 8.6 Hz, 1H), 7.79 – 7.73 (m, 3H), 7.62 (d, *J* = 3.7 Hz, 1H), 7.42 (d, *J* = 8.6 Hz, 1H), 7.25 (s, 1H), 6.71 (d, *J* = 3.6 Hz, 1H), 4.91 (q, *J* = 6.9 Hz, 1H), 3.09 (s, 9H), 2.34 (s, 3H),

1.80 (d,  $J = 6.9$  Hz, 3H);  $^{13}\text{C}$  NMR (151 MHz,  $\text{CDCl}_3$ )  $\delta$  145.8, 135.6, 135.0, 131.3, 130.4, 128.0, 127.4, 127.1, 120.9 (q,  $J_{\text{C-F}} = 320.12$  Hz), 114.2, 109.1, 74.3, 51.2, 21.8, 15.4;  $^{19}\text{F}$  NMR (565 MHz,  $\text{CDCl}_3$ )  $\delta$  -78.4; FTIR (neat) 3051, 1464, 1373, 1273, 1175, 1031, 639, 581  $\text{cm}^{-1}$ ; LRMS (ESI+)  $[\text{M-OTf}]^+$  calculated for  $[\text{C}_{20}\text{H}_{25}\text{N}_2\text{O}_2\text{S}^+]$ : 357.2, found: 357.3.

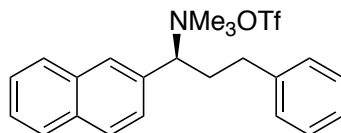


**(S)-5,5,5-Trifluoro-N,N,N-trimethyl-1-(naphthalen-2-yl)pentan-1-aminium**

**trifluoromethanesulfonate (1-109).** Prepared according to General Procedure D on a 3.47 mmol scale from (*S*)-5,5,5-trifluoro-*N,N*-dimethyl-1-(naphthalen-2-yl)pentan-1-amine, which was prepared using Eschweiler-Clarke conditions<sup>32</sup> from (*S*)-5,5,5-trifluoro-1-(naphthalen-2-yl)pentan-1-amine (prepared using Ellman's auxiliary<sup>29-31</sup>). In this case, a precipitate did not form upon addition of MeOTf. Instead, two distinct layers were observed. The top layer was decanted. The bottom layer was washed with a 1:1 (v/v) solution of  $\text{Et}_2\text{O}$ /hexanes (5 x 4 mL) and dried under high vacuum at 50 °C to afford salt **1-109** (1.492 g, 94%) as a sticky solid:  $^1\text{H}$  NMR (600 MHz,  $\text{CDCl}_3$ )  $\delta$  8.15 – 7.88 (m, 3H), 7.86 (d,  $J = 8.2$  Hz, 1H), 7.64 – 7.44 (m, 3H), 4.87 – 4.76 (m, 1H), 3.16 (s, 9H), 2.41 (s, 2H), 2.29 – 2.03 (m, 2H), 1.53 – 1.36 (m, 1H), 1.32 – 1.13 (m, 1H);  $^{13}\text{C}$  NMR (101 MHz,  $\text{CDCl}_3$ )  $\delta$  135.0, 134.1, 133.1, 130.0, 129.6, 128.7, 128.2, 127.9, 127.5, 126.9 (q,  $J_{\text{C-F}} = 277.5$  Hz), 122.9, 120.7 (q,  $J_{\text{C-F}} = 320.1$  Hz), 78.7, 51.8, 32.8 (q,  $J_{\text{C-F}} = 29.0$  Hz) 26.3, 19.2;  $^{19}\text{F}$  NMR (565 MHz,  $\text{CDCl}_3$ )  $\delta$  -78.4, -66.2; FTIR (neat) 3053, 2957, 1491, 1260, 1154, 1031, 831, 639  $\text{cm}^{-1}$ ; LRMS (ESI+)  $[\text{M-OTf}]^+$  calculated for  $[\text{C}_{18}\text{H}_{23}\text{F}_3\text{N}^+]$ : 310.2, found: 310.4. Two-dimensional NMR experiments were used to verify  $^1\text{H}$  and  $^{13}\text{C}$  assignments due to the complex nature of the spectra.

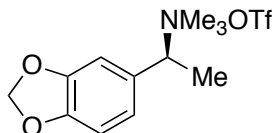


**(S)-3-(1,3-Dioxolan-2-yl)-N,N,N-trimethyl-1-(naphthalen-2-yl)propan-1-aminium trifluoromethanesulfonate (1-111).** Prepared according to General Procedure D on a 1.93 mmol scale from (S)-3-(1,3-dioxolan-2-yl)-N,N-dimethyl-1-(naphthalen-2-yl)propan-1-amine, which was prepared by reductive amination<sup>33</sup> from (S)-3-(1,3-dioxolan-2-yl)-1-(naphthalen-2-yl)propan-1-amine (prepared using Ellman's auxiliary<sup>29-31</sup>). In this case, a white precipitate did not form upon addition of MeOTf. Instead, two distinct layers formed. The top layer was decanted off. The bottom layer was washed with Et<sub>2</sub>O (5 x 2 mL) and then hexanes (5 x 2 mL, HPLC grade) and then dried under high vacuum to give salt **1-111** (0.854 g, 98%) as a sticky white solid: <sup>1</sup>H NMR (600 MHz, CDCl<sub>3</sub>) δ 8.15 – 7.89 (m, 3H), 7.86 (d, *J* = 7.9 Hz, 1H), 7.63 – 7.41 (m, 3H), 4.89 – 4.83 (m, 1H), 4.81 (t, *J* = 4.0 Hz, 1H), 3.97 – 3.86 (m, 2H), 3.82 – 3.63 (m, 2H. Please note: this peak is contaminated with an unknown impurity. At 50 °C the peak corresponding to the impurity shifts and an accurate integration of two protons is obtained), 3.17 (s, 9H), 2.50 – 2.29 (m, 2H), 1.60 – 1.24 (m, 2H); <sup>1</sup>H NMR (400 MHz, CDCl<sub>3</sub>, 50 °C) δ 8.14 – 7.99 (m, 1H), 7.99 – 7.90 (m, 2H), 7.90 – 7.82 (m, 1H), 7.62 – 7.46 (m, 3H), 4.97 – 4.74 (m, 2H), 4.00 – 3.67 (m, 4H), 3.18 (s, 9H), 2.59 – 2.26 (m, 2H), 1.61 – 1.29 (m, 2H); <sup>13</sup>C NMR (101 MHz, CDCl<sub>3</sub>) δ 135.2, 134.1, 133.1, 129.9, 129.5, 128.8, 128.1, 127.8, 127.4, 123.0, 120.8 (q, *J*<sub>C-F</sub> = 321.1 Hz), 102.8, 78.9, 65.1, 65.0, 51.8, 30.0; <sup>19</sup>F NMR (565 MHz, CDCl<sub>3</sub>) δ –78.3; FTIR (neat) 3054, 2890, 1489, 1264, 1159, 1031, 830, 639, 518 cm<sup>-1</sup>; LRMS (ESI+) [M-OTf]<sup>+</sup> calculated for [C<sub>19</sub>H<sub>26</sub>NO<sub>2</sub><sup>+</sup>]: 300.2, found: 300.3. Two-dimensional NMR experiments were used to verify <sup>1</sup>H and <sup>13</sup>C assignments due to the complex nature of the spectra.



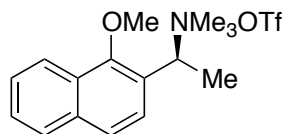
**(S)-N,N,N-Trimethyl-1-(naphthalen-2-yl)-3-phenylpropan-1-aminium**

**trifluoromethanesulfonate (1-113).** Prepared according to General Procedure D on a 1.93 mmol scale from (*S*)-*N,N*-dimethyl-1-(naphthalen-2-yl)-3-phenylpropan-1-amine, which was prepared using Eschweiler-Clarke conditions<sup>32</sup> from (*S*)-3-(1,3-dioxolan-2-yl)-1-(naphthalen-2-yl)propan-1-amine (prepared using Ellman's auxiliary<sup>29-31</sup>). In this case, a white precipitate did not form upon addition of MeOTf. Instead, two distinct layers formed. The top layer was decanted off. The bottom layer was washed with Et<sub>2</sub>O (5 x 2 mL) and then hexanes (5 x 2 mL, HPLC grade) and then dried under high vacuum to give salt **1-113** (0.854 g, 98%) as a beige solid that slowly turned yellow (mp 65–68°C): <sup>1</sup>H NMR (600 MHz, CDCl<sub>3</sub>) δ 8.07 – 7.92 (m, 3H), 7.90 (d, *J* = 7.8 Hz, 1H), 7.64 – 7.56 (m, 2H), 7.53 (s, 1H), 7.22 (t, *J* = 7.5 Hz, 2H), 7.14 (t, *J* = 7.3 Hz, 1H), 7.05 (d, *J* = 7.3 Hz, 2H), 4.78 – 4.65 (m, 1H. Please note: this peak is contaminated with an unknown impurity; however at 50 °C the peak corresponding to the impurity shifts and a more accurate integration is obtained.), 3.12 (s, 9H), 2.60 (d, *J* = 6.7 Hz, 2H), 2.49 – 2.27 (m, 2H); <sup>1</sup>H NMR (400 MHz, CDCl<sub>3</sub>, 50 °C) δ 8.05 (s, 1H), 8.02 – 7.93 (m, 2H), 7.93 – 7.87 (m, 1H), 7.64 – 7.55 (m, 2H), 7.55 – 7.50 (m, 1H), 7.25 – 7.18 (m, 2H), 7.17 – 7.11 (m, 1H), 7.08 – 7.02 (m, 2H), 4.77 – 4.60 (m, 1H), 3.13 (s, 9H), 2.66 – 2.55 (m, 2H), 2.51 – 2.33 (m, 2H); <sup>13</sup>C NMR (101 MHz, CDCl<sub>3</sub>) δ 139.6, 135.1, 134.1, 133.1, 130.0, 129.5, 128.8, 128.4, 128.2, 127.9, 127.5, 127.3, 126.7, 123.0, 120.8 (q, *J*<sub>C-F</sub> = 320.9 Hz), 78.9, 51.7, 32.3, 29.3; <sup>19</sup>F NMR (565 MHz, CDCl<sub>3</sub>) δ –78.3; FTIR (neat) 3058, 2969, 1490, 1262, 1160, 1030, 829, 638 cm<sup>-1</sup>; LRMS (ESI+) [M-OTf]<sup>+</sup> calculated for [C<sub>22</sub>H<sub>26</sub>N<sup>+</sup>]: 304.2, found: 304.3. Two-dimensional NMR experiments were used to verify <sup>1</sup>H and <sup>13</sup>C assignments due to the complex nature of the spectra.



**(S)-1-(Benzo[d][1,3]dioxol-5-yl)-N,N,N-trimethylethanaminium**

**trifluoromethanesulfonate (1-123).** Prepared according to General Procedure D on a 1.52 mmol scale from (S)-1-(benzo[d][1,3]dioxol-5-yl)-N,N-dimethylethanamine, which was prepared using Eschweiler-Clarke conditions<sup>32</sup> from (S)-1-(benzo[d][1,3]dioxol-5-yl)ethanamine (prepared using Ellman's auxiliary<sup>29-31</sup>), to afford salt **1-119** (0.471 g, 87%) as an off-white solid (mp 136–138 °C); <sup>1</sup>H NMR (600 MHz, CDCl<sub>3</sub>) δ 7.01 (d, *J* = 7.8 Hz, 1H), 6.95 (s, 1H), 6.85 (d, *J* = 8.0 Hz, 1H), 6.01 (s, 2H), 4.80 (q, *J* = 7.0 Hz, 1H), 3.11 (s, 9H), 1.76 (d, *J* = 6.9 Hz, 3H); <sup>13</sup>C NMR (151 MHz, CDCl<sub>3</sub>) δ 149.8, 148.6, 125.9, 120.9 (q, *J*<sub>C-F</sub> = 320.1 Hz), 109.0, 102.1, 74.1, 51.13, 51.11, 51.08, 15.3;<sup>45</sup> <sup>19</sup>F NMR (565 MHz, CDCl<sub>3</sub>) δ -78.5; FTIR (neat) 3045, 2909, 1493, 1256, 1159, 1031, 835, 639 cm<sup>-1</sup>; LRMS (ESI+) [M-OTf]<sup>+</sup> calculated for [C<sub>12</sub>H<sub>18</sub>NO<sub>2</sub><sup>+</sup>]: 208.1, found: 208.2.



**(S)-1-(1-Methoxynaphthalen-2-yl)-N,N,N-trimethylethanaminium**

**trifluoromethanesulfonate (1-126)** Prepared according to General Procedure D on a 5.64 mmol scale from (S)-1-(1-methoxynaphthalen-2-yl)-N,N-dimethylethanamine, which was prepared using Eschweiler-Clarke conditions<sup>32</sup> from (S)-1-(1-methoxynaphthalen-2-yl)ethanamine (prepared using Ellman's auxiliary<sup>29-31</sup>), to afford salt **1-126** (2.085 g, 94%) as a white solid (mp 123–124 °C); <sup>1</sup>H NMR (600 MHz, CDCl<sub>3</sub>) δ 8.14 – 8.09 (m, 1H), 7.91 – 7.86 (m, 1H), 7.74 (d, *J* = 8.7 Hz, 1H), 7.62 – 7.58 (m, 2H), 7.50 (d, *J* = 8.7 Hz, 1H), 5.30 (q, *J* = 7.1 Hz, 1H), 4.00 (s, 3H), 3.16 (s, 9H), 1.94 (d, *J* = 7.0 Hz, 3H); <sup>13</sup>C NMR (151 MHz, CDCl<sub>3</sub>) δ 156.4, 135.9, 128.5, 128.3, 127.5, 127.4, 125.6, 124.4, 123.3, 120.94, 120.90 (q, *J*<sub>C-F</sub> = 320.1 Hz), 67.1,

63.9, 51.38, 51.36 51.34, 15.4;<sup>45</sup>  $^{19}\text{F}$  NMR (565 MHz,  $\text{CDCl}_3$ )  $\delta$  -78.4; FTIR (neat) 3051, 1471, 1272, 1158, 1031, 827, 639  $\text{cm}^{-1}$ ; LRMS (ESI+)  $[\text{M-OTf}]^+$  calculated for  $[\text{C}_{16}\text{H}_{22}\text{NO}^+]$ : 244.2, found: 244.2.

## REFERENCES

1. Collins, B. S. L.; Wilson, C. M.; Myers, E. L.; Aggarwal, V. K. *Angew. Chem., Int. Ed.* **2017**, *56* (39), 11700-11733.
2. Brown, H. C.; Rao, B. C. S. *J. Am. Chem. Soc.* **1956**, *78* (21), 5694-5695.
3. Matteson, D. S. *Tetrahedron* **1998**, *54* (36), 10555-10607.
4. Imao, D.; Glasspoole, B. W.; Laberge, V. S.; Crudden, C. M. *J. Am. Chem. Soc.* **2009**, *131* (14), 5024-5025.
5. Smoum, R.; Rubinstein, A.; Dembitsky, V. M.; Srebnik, M. *Chem. Rev.* **2012**, *112* (7), 4156-4220.
6. Hayashi, T.; Matsumoto, Y.; Ito, Y. *J. Am. Chem. Soc.* **1989**, *111* (9), 3426-3428.
7. Crudden, C. M.; Hleba, Y. B.; Chen, A. C. *J. Am. Chem. Soc.* **2004**, *126* (30), 9200-9201.
8. Noh, D.; Chea, H.; Ju, J.; Yun, J. *Angew. Chem., Int. Ed.* **2009**, *48* (33), 6062-6064.
9. Lee, J.-E.; Yun, J. *Angew. Chem., Int. Ed.* **2008**, *47* (1), 145-147.
10. Kliman, L. T.; Mlynarski, S. N.; Morken, J. P. *J. Am. Chem. Soc.* **2009**, *131* (37), 13210-13211.
11. Nelson, H. M.; Williams, B. D.; Miró, J.; Toste, F. D. *J. Am. Chem. Soc.* **2015**, *137* (9), 3213-3216.
12. Lee, J. C. H.; McDonald, R.; Hall, D. G. *Nat. Chem.* **2011**, *3* (11), 894-899.
13. Sun, C.; Potter, B.; Morken, J. P. *J. Am. Chem. Soc.* **2014**, *136* (18), 6534-6537.
14. Ding, J.; Lee, J. C. H.; Hall, D. G. *Org. Lett.* **2012**, *14* (17), 4462-4465.
15. Lee, J. C. H.; Hall, D. G. *J. Am. Chem. Soc.* **2010**, *132* (16), 5544-5545.
16. Morgan, J. B.; Morken, J. P. *J. Am. Chem. Soc.* **2004**, *126* (47), 15338-15339.
17. Matteson, D. S.; Ray, R. *J. Am. Chem. Soc.* **1980**, *102* (25), 7590-7591.
18. Beckmann, E.; Desai, V.; Hoppe, D. *Synlett* **2004**, (EFirst), 2275-2280.
19. Stymiest, J. L.; Dutheil, G.; Mahmood, A.; Aggarwal, V. K. *Angew. Chem., Int. Ed.* **2007**, *46* (39), 7491-7494.
20. Stymiest, J. L.; Bagutski, V.; French, R. M.; Aggarwal, V. K. *Nature* **2008**, *456* (7223), 778-782.
21. Ito, H.; Kawakami, C.; Sawamura, M. *J. Am. Chem. Soc.* **2005**, *127* (46), 16034-16035.
22. Guzman-Martinez, A.; Hoveyda, A. H. *J. Am. Chem. Soc.* **2010**, *132* (31), 10634-10637.
23. Maity, P.; Shacklady-McAtee, D. M.; Yap, G. P. A.; Sirianni, E. R.; Watson, M. P. *J. Am. Chem. Soc.* **2013**, *135* (1), 280-285.

24. Shacklady-McAtee, D. M.; Roberts, K. M.; Basch, C. H.; Song, Y.-G.; Watson, M. P. *Tetrahedron* **2014**, *70* (27), 4257-4263.
25. Taylor, B. L. H.; Swift, E. C.; Waetzig, J. D.; Jarvo, E. R. *J. Am. Chem. Soc.* **2011**, *133* (3), 389-391.
26. Basch, C. H.; Cobb, K. M.; Watson, M. P. *Org. Lett.* **2016**, *18* (1), 136-139.
27. Yamamoto, H.; Shimoda, Y. *Synfacts* **2016**, *12* (04), 0375-0375.
28. Pangborn, A. B.; Giardello, M. A.; Grubbs, R. H.; Rosen, R. K.; Timmers, F. J. *Organometallics* **1996**, *15*, 1518.
29. Procopiou, G.; Lewis, W.; Harbottle, G.; Stockman, R. A. *Org. Lett.* **2013**, *15*, 2030-2033.
30. Aggarwal, V. K.; Barbero, N.; McGarrigle, E. M.; Mickle, G.; Navas, R.; Suarez, R.; Unthank, M. G.; Yar, M. *Tetrahedron Lett.* **2009**, *50*, 3482-3483.
31. Tanuwidjaja, J.; Peltier, H. M.; Ellman, J. A. *J. Org. Chem.* **2007**, *72* (2), 626-629.
32. Icke, R. N.; Wisegarver, B. B.; Alles, G. A. *Org. Synth.* **1955**, *Coll. Vol. 3*, 723.
33. Borch, R. F.; Hassid, A. I. *J. Org. Chem.* **1972**, *37* (10), 1673-1674.
34. quadrupole.
35. Ren, X.; Li, G.; Wei, S.; Du, H. *Org. Lett.* **2015**, *17* (4), 990-993.
36. Yadav, J. S.; Nanda, S.; Reddy, P. T.; Rao, A. B. *J. Org. Chem.* **2002**, *67* (11), 3900-3903.
37. Legouin, B.; Gayral, M.; Uriac, P.; Cupif, J.-F.; Levoin, N.; Toupet, L.; van de Weghe, P. *Eur. J. Org. Chem.* **2010**, *2010* (28), 5503-5508.
38. Liu, Y.; Da, C.-S.; Yu, S.-L.; Yin, X.-G.; Wang, J.-R.; Fan, X.-Y.; Li, W.-P.; Wang, R. *J. Org. Chem.* **2010**, *75* (20), 6869-6878.
39. El-Shehawy, A. A.; Sugiyama, K.; Hirao, A. *Tetrahedron Asym.* **2008**, *19* (4), 425-434.
40. Li, H.; Wang, L.; Zhang, Y.; Wang, J. *Angew. Chem., Int. Ed.* **2012**, *51* (12), 2943-2946.
41. Wei, S.; Du, H. *J. Am. Chem. Soc.* **2014**, *136* (35), 12261-12264.
42. Balieu, S.; Hallett, G. E.; Burns, M.; Bootwicha, T.; Studley, J.; Aggarwal, V. K. *J. Am. Chem. Soc.* **2015**, *137* (13), 4398-4403.
43. Zuo, Z.; Zhang, L.; Leng, X.; Huang, Z. *Chem. Commun.* **2015**, *51* (24), 5073-5076.
44. Shacklady-McAtee, D. M.; Roberts, K. M.; Basch, C. H.; Song, Y.-G.; Watson, M. P. *Tetrahedron* **2014**, *70* (27-28), 4257-4263.
45. In several of the ammonium triflates, the methyl groups of the NMe<sub>3</sub> fragment appear as three, nearly coincident peaks. We hypothesize that this may be due to hindered rotation about the benzylic C–N bond. rotation.

## Chapter 2

### SUZUKI-MIYaura CROSS-COUPLING OF ALKYL PYRIDINIUM SALTS AND ARYL BORONIC ACIDS

Work described here has already been published (Basch, C. H.; Liao, J.; Xu, J.; Piane, J. J.; Watson, M. P. *J. Am. Chem. Soc.* **2017**, *139* (15), 5313-5316.). It is reprinted in this chapter with permissions of *Organic Letter* (Copyright © 2017, American Chemical Society).

#### 2.1 Introduction

Alkyl primary amines are present in a wide array of molecules, ranging from cheap and abundant feedstock chemicals to complex synthetic or natural bioactive compounds (Figure 2.1).<sup>1</sup>

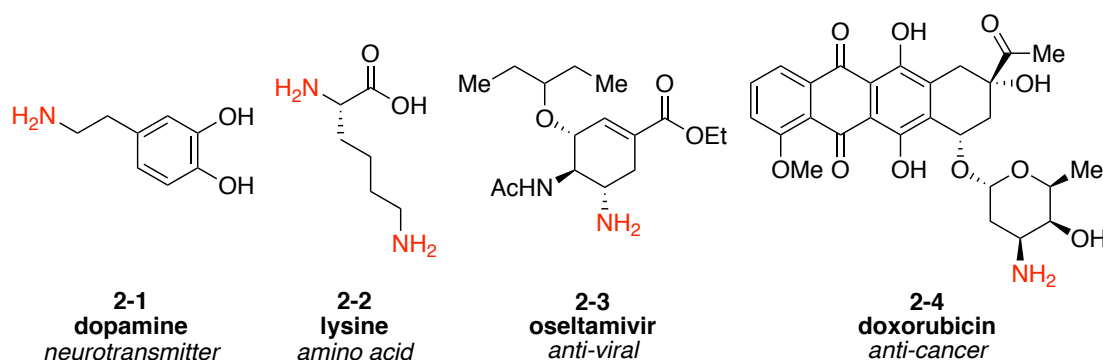


Figure 3.1: Examples of bioactive natural or synthetic alkyl primary amines

Compounds bearing the amino (NH<sub>2</sub>) group have been extensively utilized for the synthesis of simple and complex nitrogen-containing products. Despite the existence of a wide array of well-established methods for installing NH<sub>2</sub> groups and forming new carbon–nitrogen bonds, the use of alkyl amines with unactivated alkyl groups as electrophiles in a metal-catalyzed cross-coupling was not reported (Figure 2.2).

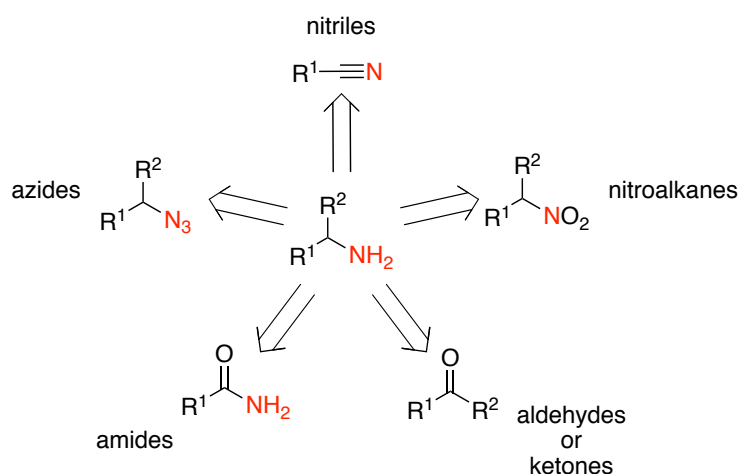


Figure 2.2 Synthetic precursors to primary alkyl amines

Such a transformation of unactivated systems would allow for the expedient formation of new carbon–carbon bonds from abundant and inexpensive primary amines, as well as from complex biological or synthetic primary amines via late-stage functionalization. Indeed, there has been intense effort in the activation of C<sub>sp<sup>2</sup></sub>–N bonds in metal-catalyzed cross-couplings, including those of enamine- (2-5),<sup>2</sup> aniline- (2-6),<sup>3,4</sup> and amide-derivatives (2-7) (Figure 2.3).<sup>5,6</sup>

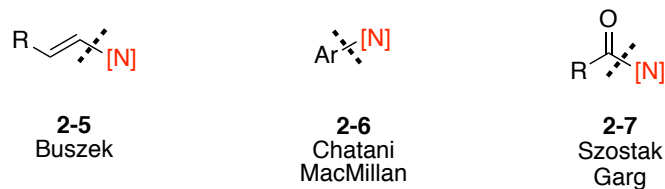


Figure 2.3  $C_{sp^2}$ -N electrophiles used in transition metal-catalyzed cross-couplings

However, until we began utilizing alkyl pyridinium salts,  $C_{sp^3}$ -N activation had only been achieved with electronically activated benzylic (**2-8**)<sup>7,8</sup> or allylic (**2-9**) amine derivatives,<sup>9</sup> or strain-activated aziridines (**2-10**) (Figure 2.4).<sup>10,11,12</sup>

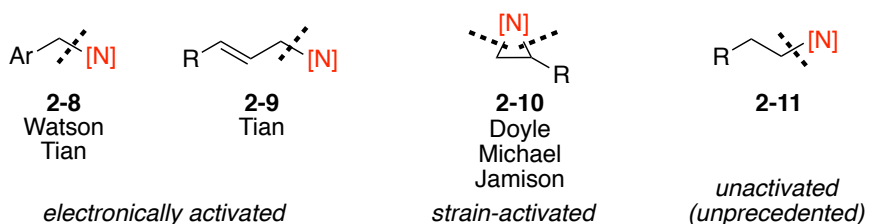


Figure 2.4  $C_{sp^3}$ -N electrophiles used in transition metal-catalyzed cross-couplings

In contrast, intense efforts have identified other reagents to install alkyl groups lacking activation. Following pioneering developments with alkyl halides, pseudohalides, redox-active esters (RAEs), and organometallic nucleophiles (i.e.,  $M=SnR_3$ ,  $MgX$ ,  $ZnX$ ), metallophotoredox chemistry has enabled use of oxalates, carboxylic acids, 1,4-dihydropyridines, organoboronates, and organosilicates (Figure 2.5).

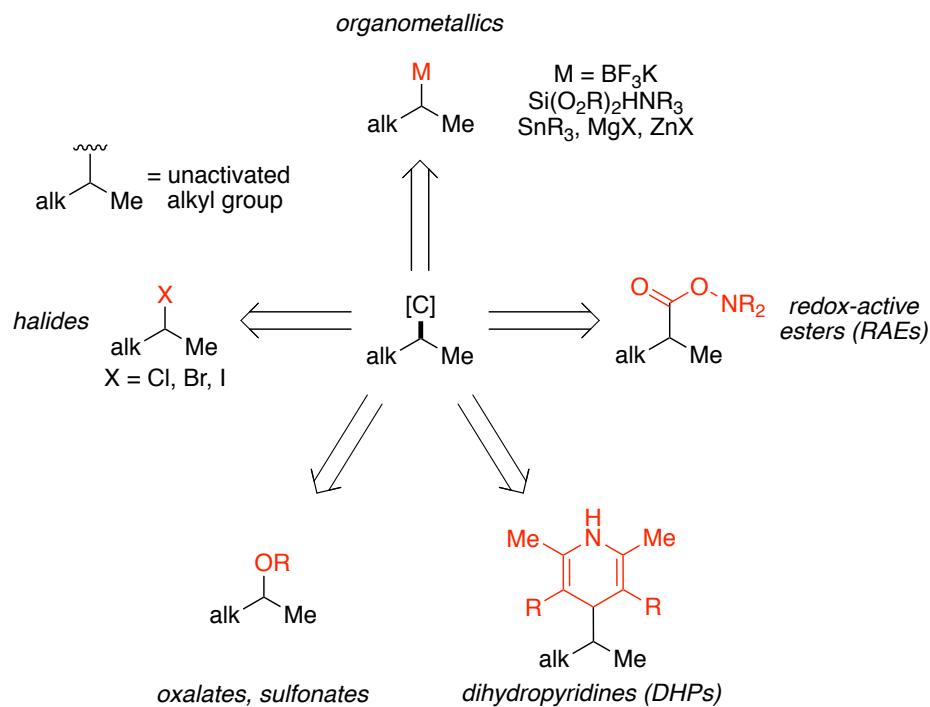


Figure 2.5 Reagents used to install unactivated alkyl groups via metal-catalyzed cross-couplings

### 2.1.1 Non-Photoredox, Metal-Catalyzed Cross-Couplings

In a seminal report by the Fu group in 2003, they demonstrated a Negishi cross-coupling of unactivated secondary alkyl bromides and iodides.<sup>13</sup> Using readily available primary alkyl zinc halides and a  $\text{Ni}(\text{cod})_2/\text{Pybox}$  ligand system, they successfully coupled a number of primary and secondary cyclic and acyclic halides in good yields under mild conditions (Figure 2.6). Following intense mechanistic studies by Vicic,<sup>14</sup> it is hypothesized that a  $\text{Ni}^{\text{I}}$  species **A** undergoes transmetalation with the alkyl zinc halide to afford a  $\text{Ni}^{\text{I}}$ -alkyl species **B**. Single-electron transfer (SET) from **B** to the alkyl halide generates a solvent-caged  $\text{Ni}^{\text{II}}$ -alkyl intermediate and an alkyl radical. Upon recombination, a  $\text{Ni}^{\text{III}}$  dialkyl species **D** is formed, which after reductive elimination, furnishes the cross-coupled product **E** and the active  $\text{Ni}^{\text{I}}$  catalyst **A**.

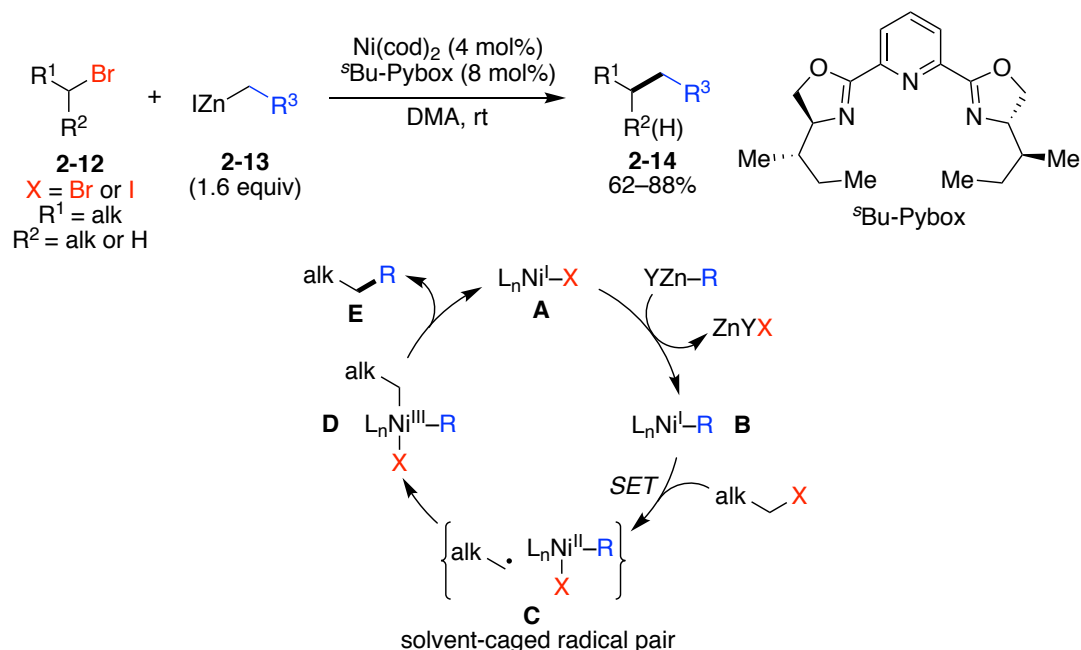


Figure 2.6 Fu's nickel-catalyzed Negishi cross-coupling of alkyl halides

Recently, the Baran and Weix groups have shown that redox-active esters (RAEs) are also potent alkylating agents in traditional nickel-catalyzed cross-couplings and reductive cross-couplings, respectively. These methods take advantage of utilizing alkyl carboxylic acids, which are not only abundant feedstock chemicals, but are also present in many complex bioactive molecules, giving rise to opportunities for late-stage functionalization. In their first publication, the Baran group demonstrated the Negishi cross-coupling of aryl zinc halides with a wide variety of electronically and sterically diverse, secondary RAEs (**2-15**) (Figure 2.7).<sup>15</sup> They have proposed a  $Ni^{I/III}$  catalytic cycle in which an active  $Ni^I$  species **A** undergoes a transmetalation with the aryl zinc halide to form aryl-nickel species **B**. This species can then undergo single-electron transfer with the phthalimide unit of the RAE to generate an intermediate  $Ni^{II}$  species **C** and phthalimide radical **D**. A subsequent self-

immolation of the **D** leads to the extrusion of CO<sub>2</sub> and an alkyl radical **E**. This newly formed alkyl radical can then recombine with Ni<sup>II</sup> species **C** to form a high-valent Ni<sup>III</sup> species (**F**). Upon reductive elimination, the cross-coupling product (**2-17**) is produced and the active, low-valent Ni<sup>I</sup> species (**A**) is regenerated.

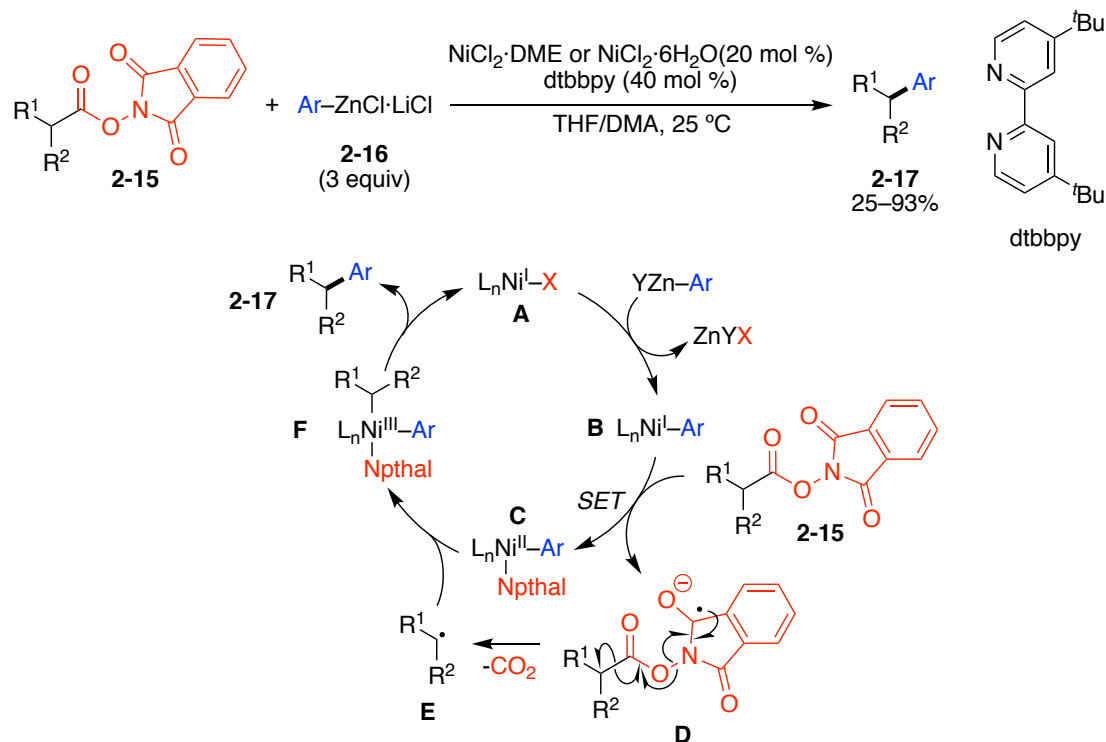


Figure 2.7 Baran's Negishi cross-coupling of redox-active esters

Since this seminal publication, a number of other cross-couplings using RAEs have also been demonstrated, including Negishi or Kumada alkylations and Suzuki-Miyaura arylations.<sup>16</sup>

Alternatively, Weix has shown that RAEs can serve as alkyl electrophiles in a nickel-catalyzed reductive coupling with aryl iodides.<sup>17</sup> The reaction enjoyed

relatively broad scope in both the alkyl and aryl electrophile, delivering the primary or secondary alkyl arenes (**2-19**) in modest to very high yields (41–97%). Importantly, this is the first example of using a Barton-type ester in a nickel-catalyzed reductive coupling. Although mechanistic studies suggest that a radical-chain bimetallic catalytic cycle may be operative, the current mechanistic understanding is very limited.

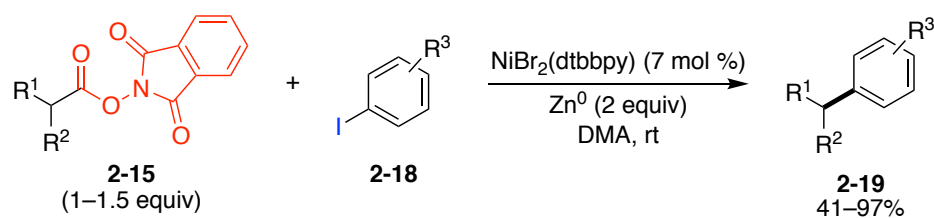
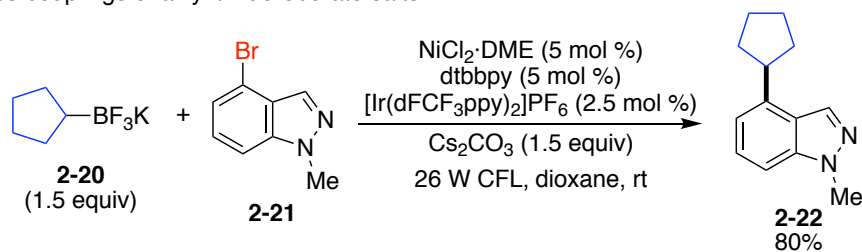


Figure 2.8 Weix's nickel-catalyzed reductive cross-coupling of RAEs and aryl iodides

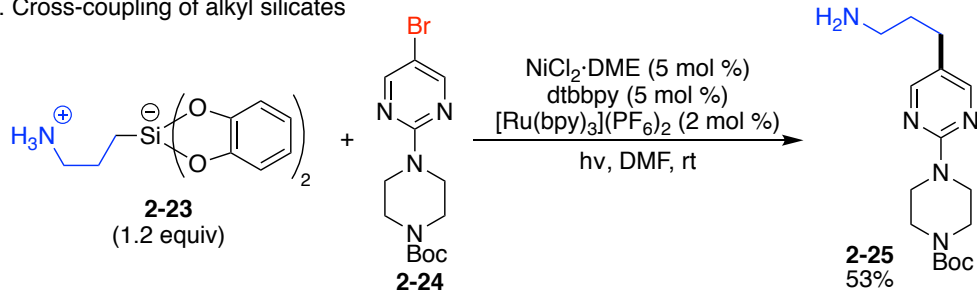
### 2.1.2 Metallophotoredox Dual-Catalyzed Cross-Couplings

Dual metallophotoredox/nickel catalysis has also been shown to efficiently promote cross-couplings that employ nucleophiles, or electrophiles, with unactivated alkyl groups. In this regard, the Molander group has communicated a number of metallophotoredox-catalyzed transformations using alkyl trifluoroborate salts (Figure 2.9A),<sup>18</sup> silicates (Figure 2.9B),<sup>19</sup> or dihydropyridines (Figure 2.9C)<sup>20</sup> as the source of unactivated alkyl groups. Notably, all these reagents can be easily prepared from readily available starting materials.

A. Cross-couplings of alkyl trifluoroborate salts



B. Cross-coupling of alkyl silicates



C. Cross-coupling of alkyl dihydropyridines

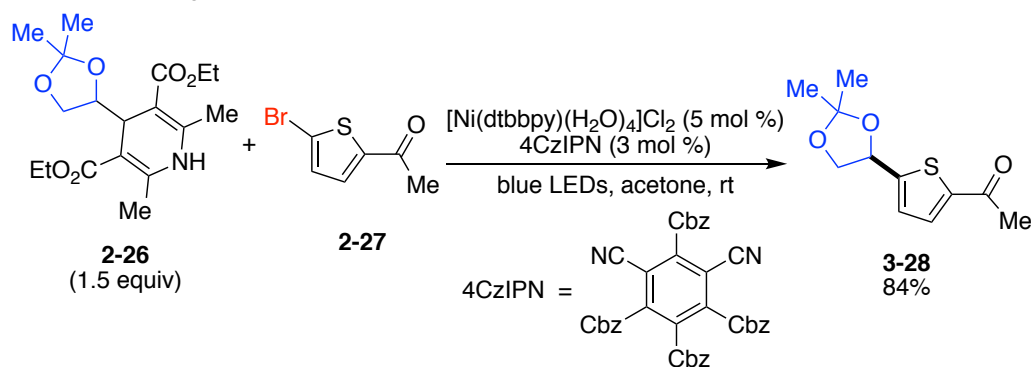


Figure 2.9 Molander's dual metallophotoredox/nickel-catalyzed cross-couplings of alkyl trifluoroborate salts, silicates, and dihydropyridines

A similar approach was employed by MacMillan and coworkers who showed that alcohols can serve as sources of “latent” alkyl nucleophiles through the formation of the corresponding oxalate (**2-29**) (Figure 2.10).<sup>21</sup> Due to the instability of the oxalate salts, they cannot be stored for extended periods of time, and are thus used

directly in the cross-coupling without prior purification via recrystallization or chromatography.

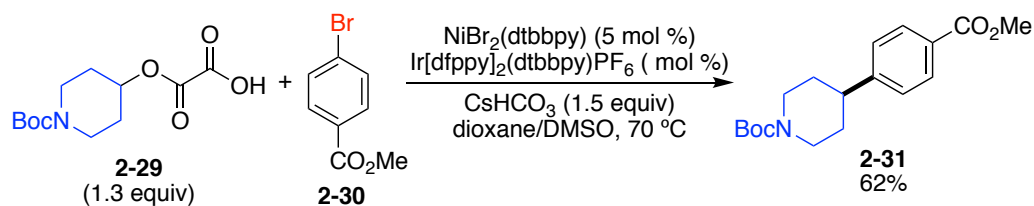
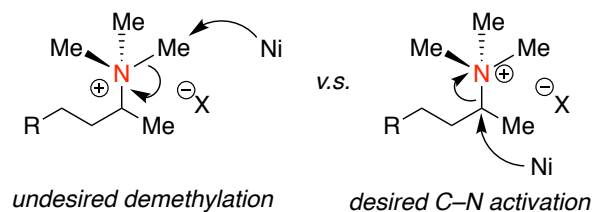


Figure 2.10 MacMillan's dual metallophotoredox/nickel-catalyzed decarboxylative cross-couplings of alkyl oxalates

Contrary to our previously developed cross-coupling of electronically activated benzylic trimethylammonium salts, we envisioned that an oxidative addition into the C–N bond of an amine electrophile without an adjacent activating group would be challenging. If we used a tetralkyl ammonium salt, the catalyst would need to differentiate between the four alkyl groups bound to the nitrogen, so that it could selectively activate the target C–N bond (Figure 2.11A). Utilizing a methylation strategy would also preclude the presence of other basic or nucleophilic nitrogen atoms within the framework of the electrophile, and would therefore limit the utility of the cross-coupling reaction (Figure 2.11B).

A. Potential chemoselectivity problems with oxidative addition



B. Chemoselective methylation is problematic

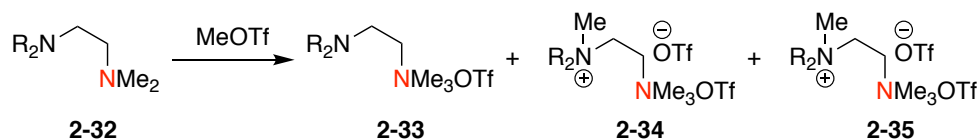


Figure 2.11 Potential issues with C–N bond activation using our previous methylation strategy

With these problems in mind, I turned to a new strategy for activating the alkyl C–N bond via the formation of a Katritzky (2,4,6-triphenyl) pyridinium salt. Notably, these salts are air- and moisture-stable solids, which are easily prepared in a single condensation step with the commercially available 2,4,6-triphenylpyrylium tetrafluoroborate. Advantageously, this condensation is chemoselective for primary amines, thereby allowing the incorporation of secondary or tertiary alkyl amines, as well as nitrogen heterocycles, within the molecular scaffold of the electrophile.

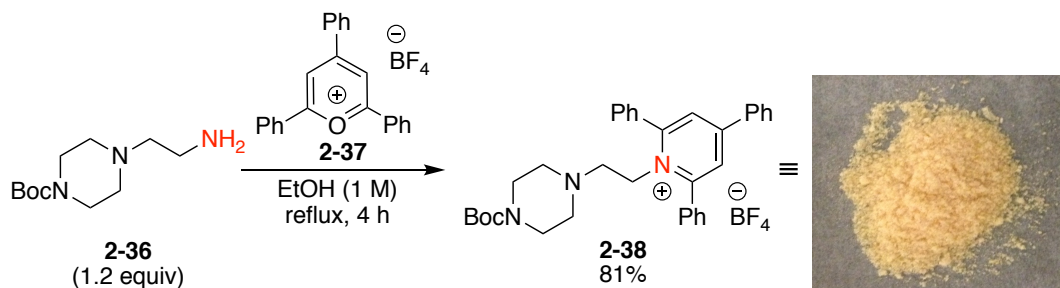


Figure 2.12 Synthesis and physical appearance of an alkyl pyridinium salt



ammonium salt was used, triethylamine was added to the reaction mixture in an equimolar amount. After stirring for 4 hours, the pyridinium salts were triturated by the addition of Et<sub>2</sub>O with rapid stirring. Typically, the salts crashed out within an hour; however, in the event that one did not, the flask containing the mixture was sealed and placed in a -27 °C freezer until a precipitate formed (typically 1–3 days). The solid was filtered through a fritted funnel and subsequently washed with Et<sub>2</sub>O. If a hydrochloride salt was used instead of its free-base, the solid was first washed with water to remove the triethylammonium chloride byproduct and then washed with Et<sub>2</sub>O. If precipitation did not occur, the salts were easily purified via silica gel chromatography using an acetone/methylene chloride solution as the mobile phase.

As shown by the representative examples in Figure 2.14, a variety of alkyl pyridinium salts were prepared via this method. Both primary (**2-42**, **2-43**, and **2-45**) and secondary (**2-44**) alkyl groups can be incorporated. Excellent functional group tolerance was observed, as shown by the inclusion of acid-sensitive acetals (**2-42**) and basic heteroatoms (**2-43** and **2-45**). Perhaps most importantly, and as described above, pyridinium salt formation was chemoselective for primary amines. Tertiary and Boc-protected amines were untouched in this reaction (**2-43**, **2-44**, and **2-45**).

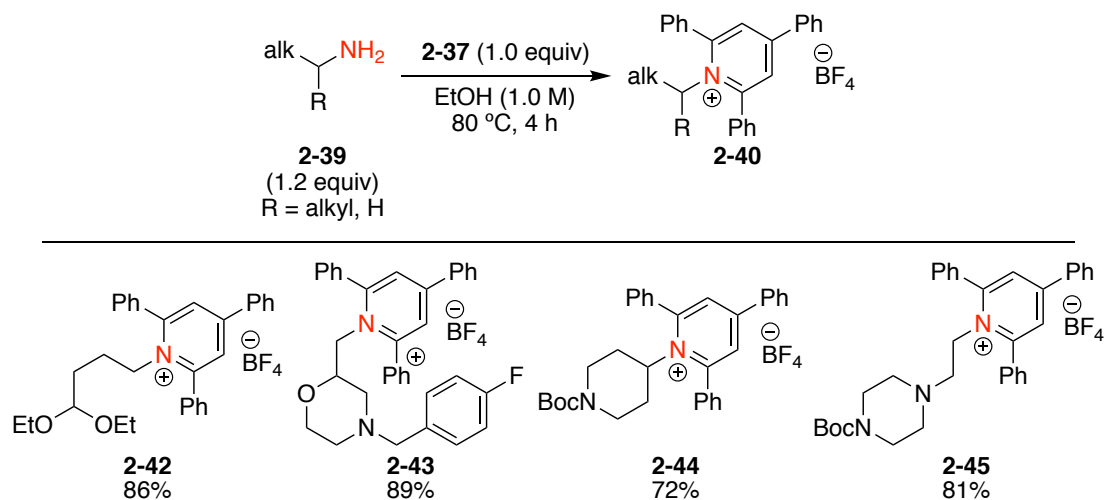


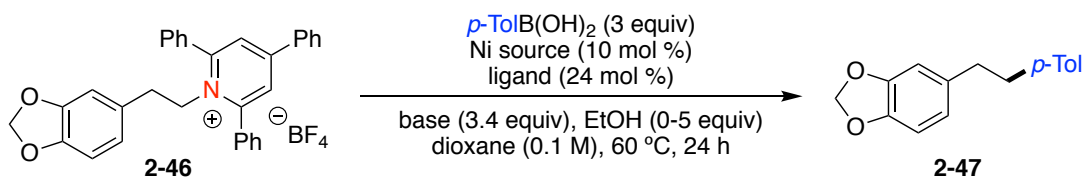
Figure 2.14 Selected examples of alkyl pyridinium salts formed

### 2.2.2 Optimization

I began the optimization with the first-generation Suzuki-Miyaura cross-coupling conditions that our group had published previously for the activation of benzylic trimethylammonium salts.<sup>8</sup> A trace amount of desired 1,2-diarylethane product **2-47** was obtained (Table 2.1, entry 1). After screening a variety of ligands, including mono- and bidentate phosphines, diamines, and bipyridines, I found that redox non-innocent phenanthroline-based ligands were the most effective ligand class (entry 2). Switching from a Ni<sup>0</sup> precatalyst, Ni(cod)<sub>2</sub>, to a Ni<sup>II</sup> precatalyst, Ni(OAc)<sub>2</sub>·4H<sub>2</sub>O, further improved the yield (entry 4). Additionally, a combination of potassium *tert*-butoxide and ethanol improved the yield of the reaction substantially, likely by increasing solubility of the base or boronic acid (entry 6). By optimizing the reaction setup, I found that pre-stirring Ni(OAc)<sub>2</sub>·4H<sub>2</sub>O and BPhen separately from the pyridinium salt, boronic acid, and base led to higher yields (entry 6). Currently, the reason for this increase in reaction yield is not well understood; however, in the interest of developing a more practical, user-friendly reaction, future efforts will be

aimed at eliminating this step in the reaction set-up. Importantly, control reactions revealed that metal, ligand, and base are all required in order to obtain the coupling product.

Table 2.1 Reaction optimization<sup>a</sup>



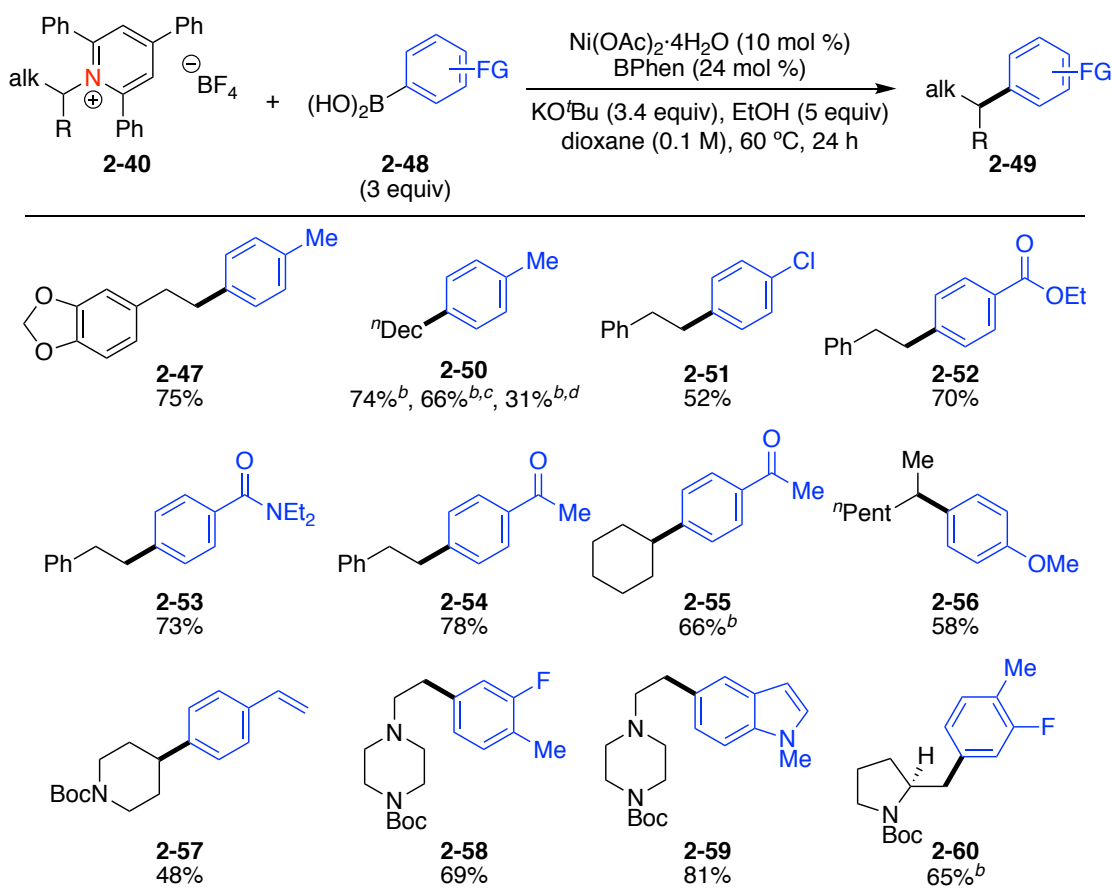
entry	Ni source	ligand	base	additive	pre-stir	yield (%)
1	Ni(cod) <sub>2</sub>	PPh <sub>2</sub> Cy	K <sub>3</sub> PO <sub>4</sub>	none	–	6
2	Ni(cod) <sub>2</sub>	BPhen	K <sub>3</sub> PO <sub>4</sub>	none	–	21
3	Ni(cod) <sub>2</sub>	BPhen	KO <sup>t</sup> Bu	none	–	24
4	Ni(OAc) <sub>2</sub> ·4H <sub>2</sub> O	BPhen	KO <sup>t</sup> Bu	none	–	39
5	Ni(OAc) <sub>2</sub> ·4H <sub>2</sub> O	BPhen	KO <sup>t</sup> Bu	none	1 h	52
6	Ni(OAc) <sub>2</sub> ·4H <sub>2</sub> O	BPhen	KO <sup>t</sup> Bu	EtOH	1 h	81
7	none	BPhen	KO <sup>t</sup> Bu	EtOH	1 h	0
8	Ni(OAc) <sub>2</sub> ·4H <sub>2</sub> O	none	KO <sup>t</sup> Bu	EtOH	1 h	0
9	Ni(OAc) <sub>2</sub> ·4H <sub>2</sub> O	BPhen	none	EtOH	1 h	0

<sup>a</sup> Yields based on <sup>1</sup>H NMR with 1,3,5-trimethoxybenzene as an internal standard. Pre-stir: Ni source + ligand (vial 1), *p*-TolB(OH) + base + **2-46** + EtOH (vial 2).

### 2.2.3 Reaction Scope

With optimized conditions in hand, I, along with my colleagues Jennie Liao, Jianyu Xu, and Jacob Piane, investigated the scope of the transformation (Figure

2.15). The model reaction provided the corresponding cross-coupled product **2-47** in a 75% isolated yield. The *p*-tolyl boronic acid was also cross-coupled effectively with the pyridinium salt derived from *n*-decylamine (**2-50**). With non-oven-dried glassware, this cross-coupling delivers similar yields. A minimal precaution set-up, in which no care was taken to exclude air or moisture, led to a significant decrease in yield. Functional groups such as chlorides (**2-51**), esters (**2-52**), amides (**2-53**), and ketones (**2-54** and **2-55**) were well tolerated in the reaction. Furthermore, styrenyl and indole boronic acids were effectively cross-coupled. In addition to primary alkyl groups in the pyridinium salts, substrates with both cyclic (**2-55**) and acyclic (**2-56**) alkyl groups provided the products in synthetically useful yields.

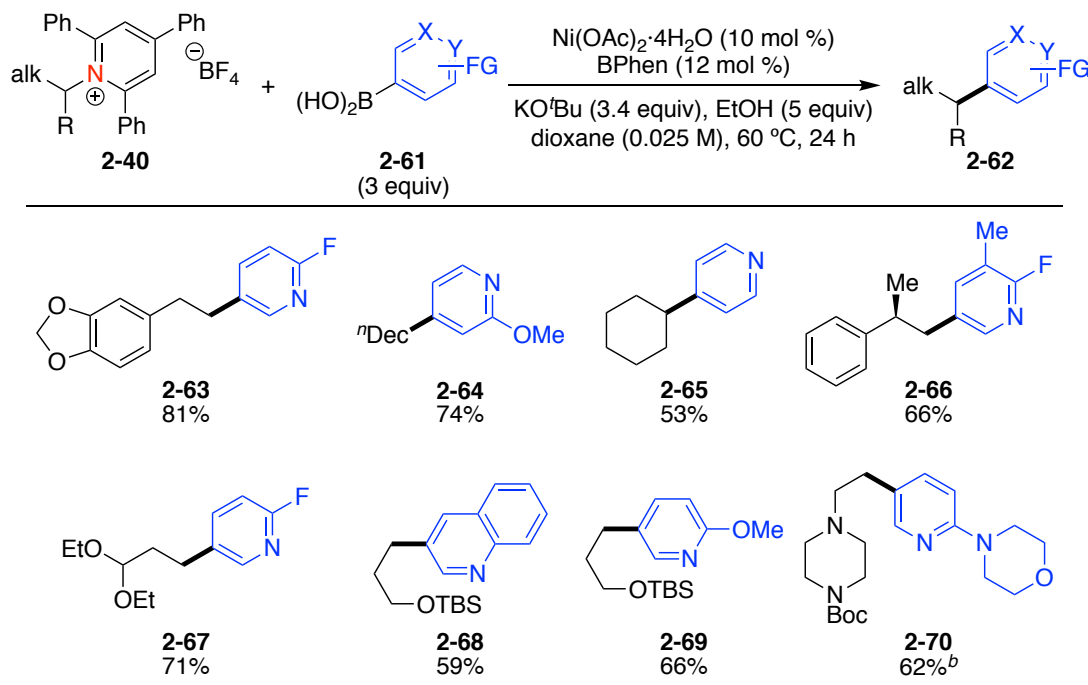


<sup>a</sup> Conditions: pyridinium salt **2-47** (1.0 mmol), Ni(OAc)<sub>2</sub>·4H<sub>2</sub>O (10 mol %), BPhen (24 mol %), ArB(OH)<sub>2</sub> **2-48** (3.0 equiv), KO<sup>t</sup>Bu (3.4 equiv), EtOH (5 equiv), dioxane (0.1 M), 60 °C, 24 h. Average isolated yields (±6%) from duplicate experiments. <sup>b</sup> Single experiment. <sup>c</sup> Glassware not oven-dried before use. <sup>d</sup> Minimal precautions to protect from air and moisture.

Figure 2.15 Scope of non-pyridyl boronic acid<sup>a</sup>

Recognizing the biological importance of pyridines, I prioritized the use of pyridyl boronic acids in the transformation. Under slightly modified conditions, a number of pyridyl boronic acids were effectively cross-coupled with both primary and secondary alkyl pyridinium salts (Figure 2.16). Both 3- and 4-pyridyl boronic acids

were effective. In addition, 2-fluoropyridyl groups can be incorporated, enabling elaboration of these products via subsequent  $S_NAr$  reactions.



<sup>a</sup> Conditions: pyridinium salt **2-40** (1.0 mmol),  $Ni(OAc)_2 \cdot 4H_2O$  (10 mol %), BPhen (12 mol %),  $ArB(OH)_2$  **2-61** (3.0 equiv), KOtBu (3.4 equiv), EtOH (5 equiv), dioxane (0.025 M), 60 °C, 24 h. Average isolated yields ( $\pm 6\%$ ) from duplicate experiments.

<sup>b</sup> Single experiment.

Figure 2.16 Scope of pyridyl boronic acid<sup>a</sup>

I was also very interested in exploring the potential of this reaction for late-stage functionalization of advanced intermediates. Gratifyingly, a number of biologically relevant primary amines were efficiently transformed into the corresponding pyridinium salt and subsequently coupled under the optimized conditions. For example, Boc-protected *L*-isoleucine (**2-71**, Boc-Ile-OH) was easily

converted to diastereomerically pure diamine (**2-73**) via an amidation-reduction sequence (Figure 2.17). The pyridinium salt (**2-74**) was formed in good yield and subsequently cross-coupled to deliver a single diastereomer of product **2-76** in 52% yield. This formation of a single diastereomer is indicative that an epimerization pathway, such as a reversible  $\beta$ -hydride elimination, is not in effect for non-acidic stereocenters under the optimized reaction conditions.

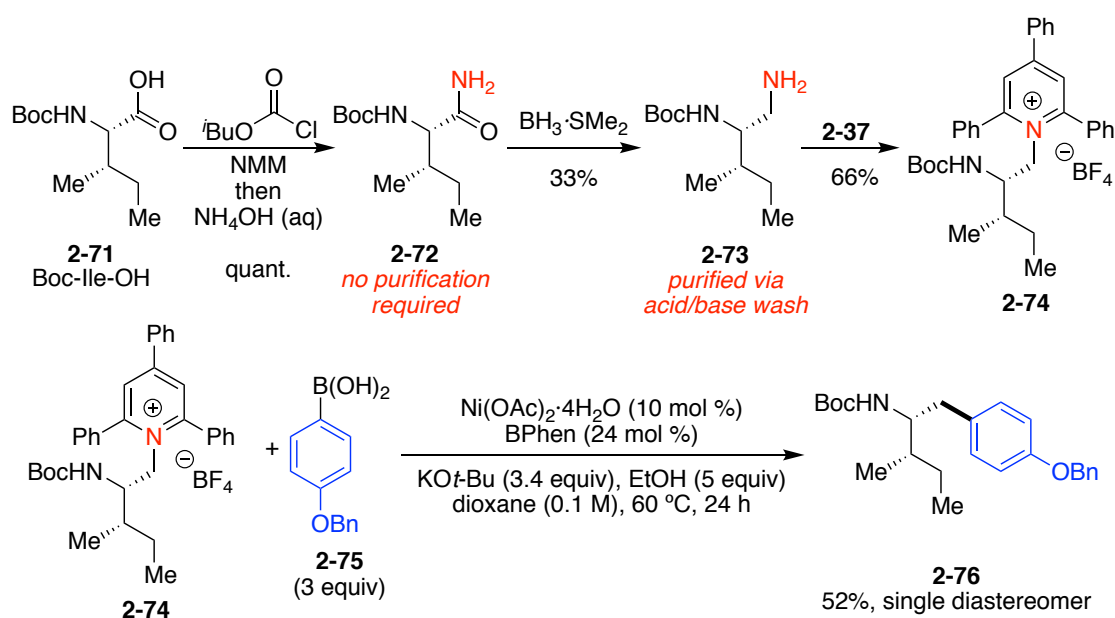
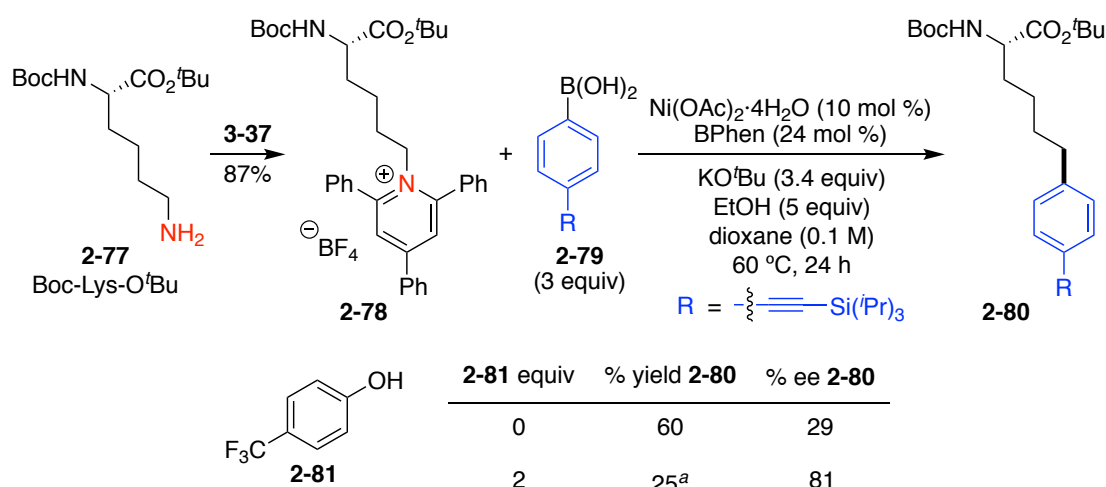


Figure 2.17 Synthesis and cross-coupling of isoleucine-derived pyridinium salt

In addition to isoleucine, I was interested in applying this chemistry to the cross-coupling of the primary amine on the side-chain of *L*-lysine. After forming the *L*-lysine pyridinium salt (**2-78**) in good yield, I subjected it to the cross-coupling conditions (Figure 2.18). Interestingly, the product (**2-80**) was formed in synthetically useful yield (60%) but low ee (29%). Suspecting that the epimerization was base-

promoted, I screened a variety of acid additives to buffer the solution. I found that the addition of 4-trifluoromethylphenol (**2-81**) dramatically improved the ee of the cross-coupled product (**2-80**).<sup>24</sup> However, a significant decrease in the yield was observed, likely due to the lower concentration of activated ‘ate’ complex of the boronic acid. Although a low yield was observed, this promising result suggests that further optimization will result in a high-yielding cross-coupling of the side-chain of lysine without loss of ee.



<sup>a</sup> Yield based on <sup>1</sup>H NMR integration with 1,3,5-trimethoxybenzene as an internal standard.

Figure 2.18 Cross coupling of lysine pyridinium salt

I then turned my attention toward exploring the functionalization of synthetic drug intermediates. Pyridinium **2-43**, derived from an intermediate (**2-83**) used in the synthesis of the gastrointestinal medication Mosapride (**2-82**), was efficiently cross-coupled with both an electron-poor *m*-cyano aryl boronic acid (**2-84**) and an electron-

rich dioxolane aryl boronic acid (**2-85**) in 62% and 71% yield, respectively (Figure 2.20).<sup>25</sup>

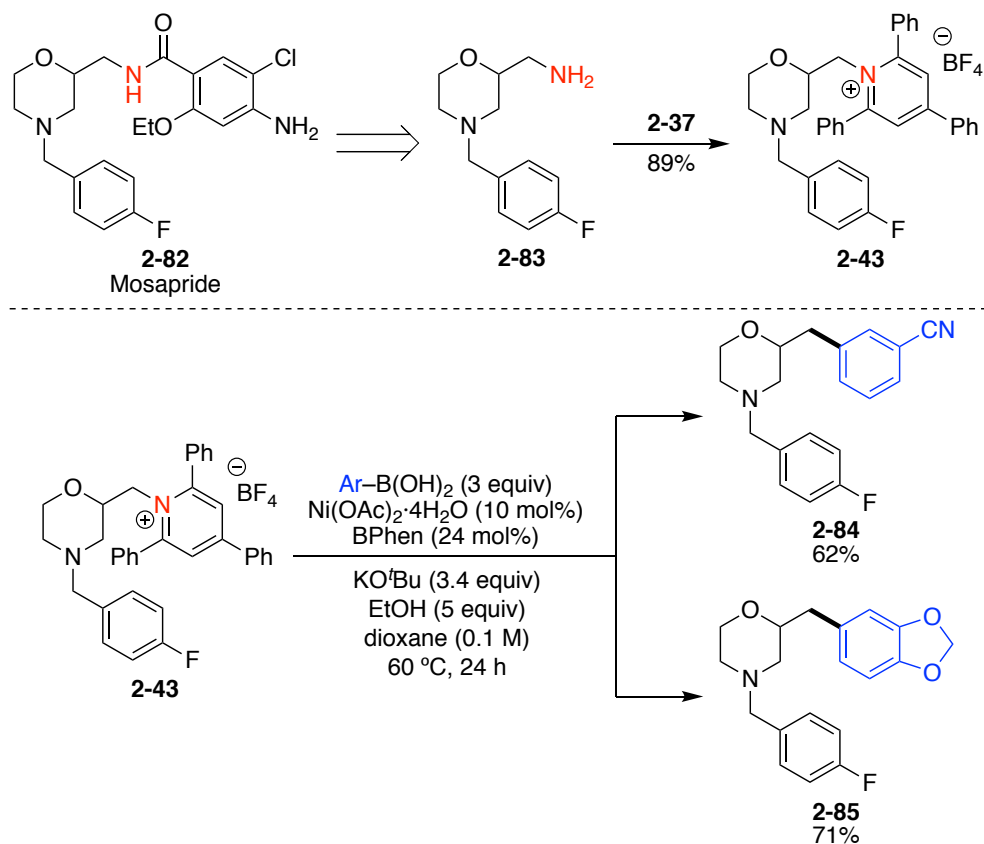


Figure 2.19 Synthesis and cross-coupling of the pyridinium salt derived from Mosapride intermediate

Moreover, the pyridinium salt **2-88**, derived from an amine (**2-87**) used in the synthesis of the anti-cholesterol drug atorvastatin (**2-86**, Lipitor<sup>®</sup>, Pfizer), was coupled with 3-fluoropyridyl boronic acid (**2-89**) to deliver **2-90** in synthetically useful yield

(Figure 2.20).<sup>26</sup> Notably, the 2-fluoro-substituent allows for rapid downstream diversification of the pyridine ring via S<sub>N</sub>Ar chemistry.

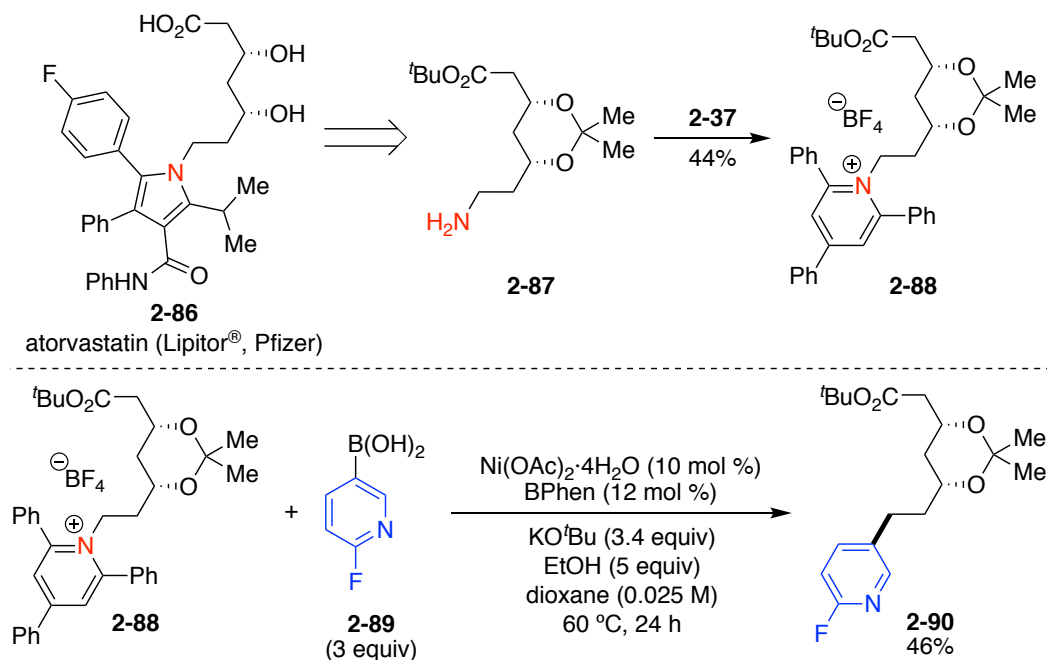


Figure 2.20 Synthesis and cross-coupling of pyridinium salt derived from atorvastatin intermediate

Interestingly, another well-known anti-cholesterol medication, rosuvastatin (**2-91**, Crestor<sup>®</sup>, AstraZeneca), contains a very similar 1,3-diol alkyl chain to atorvastatin (**2-86**) (Figure 2.21). However, unlike atorvastatin which contains an electron-rich pyrrole ring, rosuvastatin is substituted with an electron-poor pyrimidine ring. Despite this electronic difference, both compounds display similar biological effects. With this in mind, it is possible that derivatives (**2-92**) of product **2-90** (Figure 2.20), which contains an electron-poor pyridine ring, could exhibit some of the same effects.

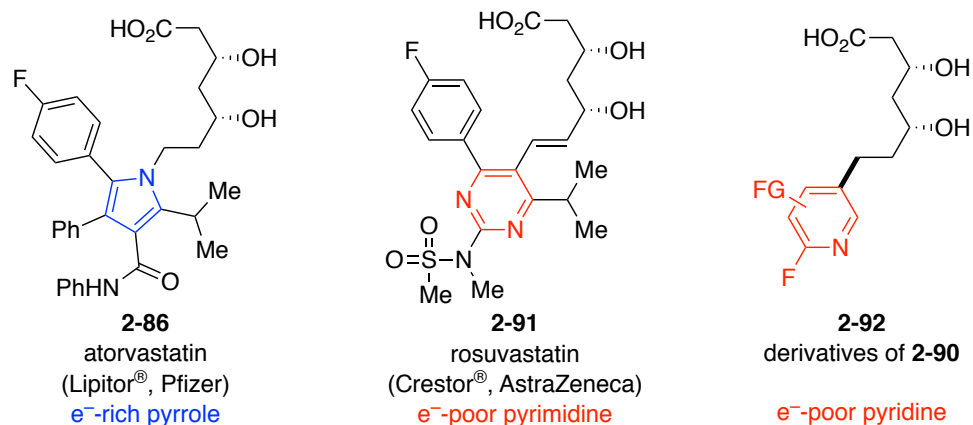


Figure 2.21 Comparison of the ring-systems in atorvastatin, rosuvastatin, and **2-92**

This example, along with the cross-couplings of the drug-intermediates described above, demonstrates the potential utility of this chemistry within discovery efforts in the pharmaceutical industry.

### 2.3 Mechanistic Studies

In addition to demonstrating the synthetic potential of this reaction, I led efforts to investigate the mechanism of this novel C–N bond activation reaction. In addition to  $S_N2$  reactions, it has been demonstrated that these Katritzky pyridinium salts can act as single-electron acceptors. As such, they have been used as alkyl electrophiles for C-alkylation of nitronate anions (Figure 2.22), and shown to be effective photosensitizers and sources of nitrogen-centered radicals.<sup>27</sup>

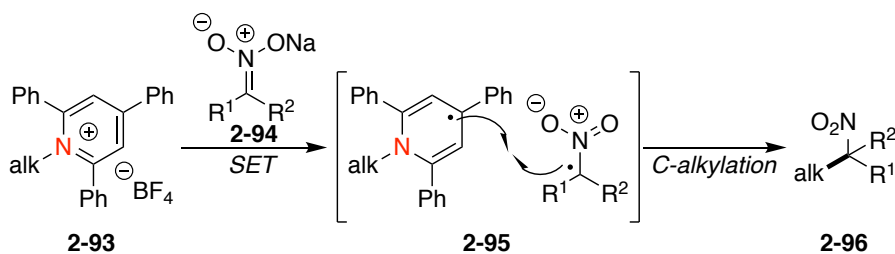


Figure 2.22 C-alkylation of nitronate anions with alkyl pyridinium salts

With this in mind, a series of mechanistic experiments were conducted to aid in understanding the mechanism of this reaction. Thus, we considered that this reaction may be proceeding through a Ni<sup>0/II</sup> catalytic cycle, involving an oxidative addition via S<sub>N</sub>2-like attack of the nickel to the alkyl pyridinium, or a Ni<sup>I/III</sup> cycle, in which single-electron transfer (SET) from the nickel to the pyridinium initiates oxidative addition. This SET mechanism would result in an alkyl radical intermediate. Due to the rapid interconversion of alkyl radicals, we postulated that a full racemization of an enantioenriched alkyl pyridinium salt should occur if the reaction proceeded via an alkyl radical. As predicted, under the optimized conditions, the cross-coupling of enantioenriched pyridinium salt **2-97** led to the desired diarylethane (**2-99**), racemically, in 54% yield (Figure 2.23A). In addition, cross-coupling of the radical-clock containing cyclopropyl methyl pyridinium salt **2-100** provided the ring-opened adduct (**2-102**) in 33% yield, indicating the intermediacy of either a cationic or radical species (Figure 2.23B). The addition of TEMPO to the reaction provided the trapped product **2-104**, thereby supporting a radical intermediate (Figure 2.23C).

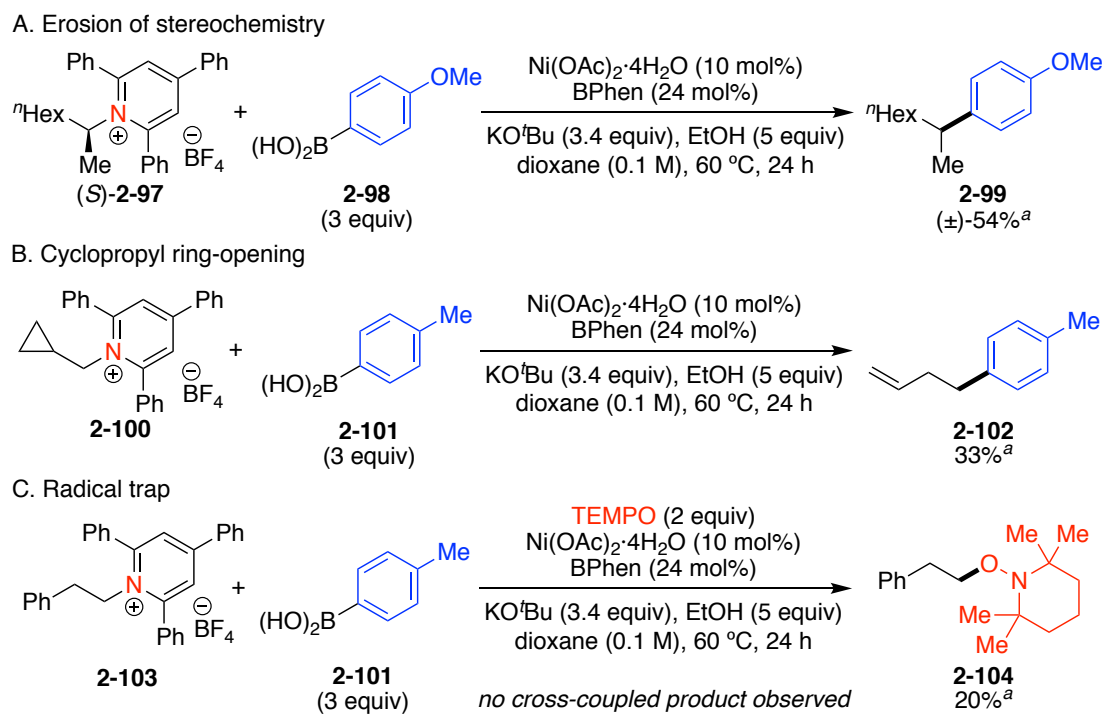


Figure 2.23 Mechanistic studies of the Suzuki-Miyaura cross-coupling.

On the basis of these mechanistic studies, and the identification of the redox-active non-innocent BPhen as the optimal ligand, we have proposed the following Ni<sup>I</sup>/Ni<sup>III</sup> catalytic cycle (Figure 2.24). Ni<sup>I</sup> species **A** undergoes transmetalation with the activated aryl boronic acid, generating Ni<sup>I</sup> species **B**. Pyridinium **A** undergoes SET with **B**, leading to fragmentation and homolytic cleavage of the C–N  $\sigma$ -bond to generate alkyl radical **E**. This transient alkyl radical can then recombine with the aryl Ni<sup>II</sup> intermediate **D** to generate an alkyl-aryl Ni<sup>III</sup> species **F**. A subsequent reductive elimination would thus provide the desired product **G** and regenerate the active Ni<sup>I</sup> catalyst **A**. This type of mechanism is analogous to that proposed by Vicic for Fu's

cross-coupling of alkyl halides and alkyl zinc halides. Notably, Baran's redox-active esters are also proposed to proceed via this type of pathway.<sup>15</sup>

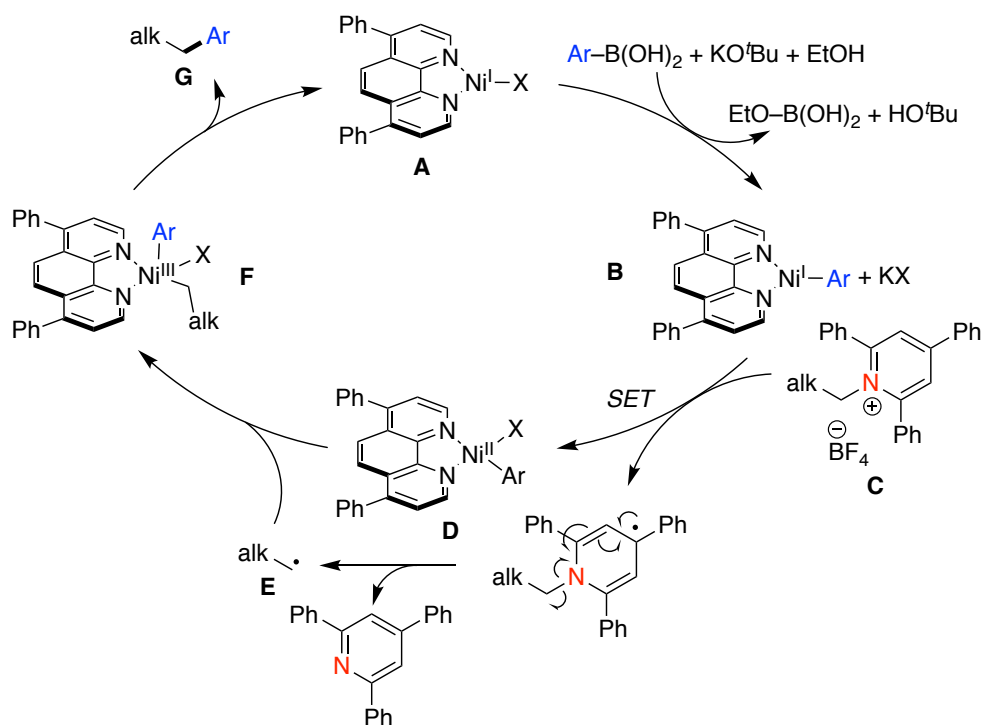


Figure 2.24 Possible “transmetalation first” catalytic cycle.

Alternatively, a radical chain bimetallic SET pathway is also possible (Figure 2.25). Pyridinium salt **B** could undergo SET with Ni<sup>I</sup> species **A**, which would lead to alkyl radical **C** and Ni<sup>II</sup> intermediate **D**. The activated aryl boronic acid could then transmetalate the aryl group to **D**, forming Ni<sup>II</sup> intermediate **E**. Subsequently, intermediate **E** can recombine with alkyl radical **C**, formed in the first step, to generate Ni<sup>III</sup> species **F** which could then reductively eliminate to form the desired product **G**

and regenerate the active  $\text{Ni}^{\text{I}}$  species **A**. This type of mechanism has been proposed for the nickel-catalyzed cross-coupling of propargylic bromides.<sup>28</sup>

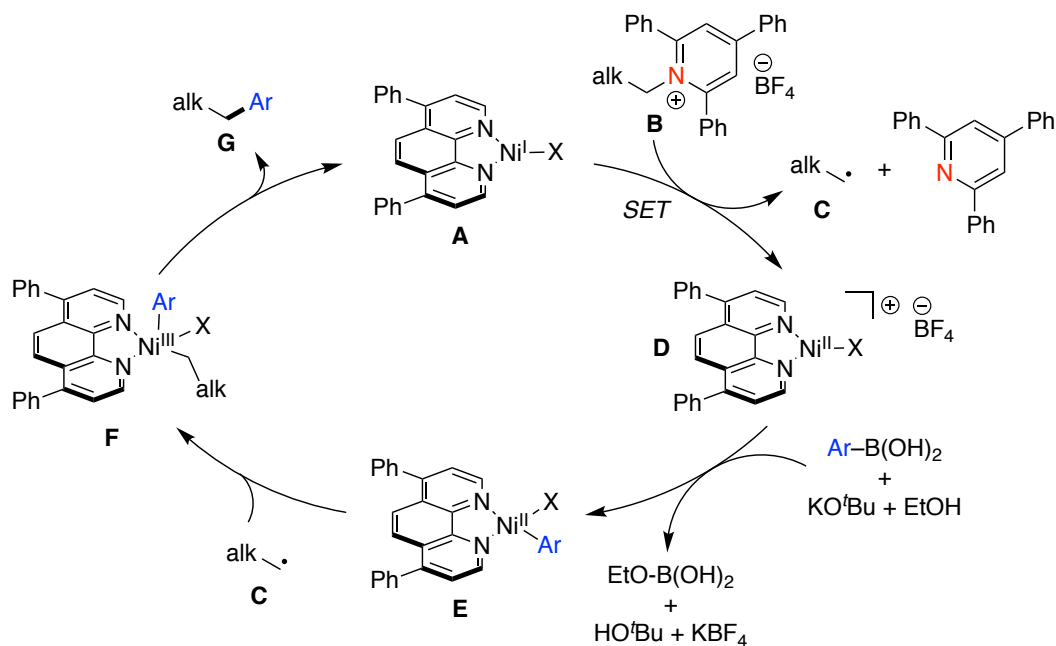


Figure 2.25 Alternative catalytic cycle.

Our current, experiments do not allow us to distinguish between the proposed “transmetalation-first” and radical-chain bimetallic pathway mechanisms. However, future work in our group will be directed toward exploring the fundamental steps of this catalytic process.

## 2.4 Conclusion

In summary, I have developed the first transition metal-catalyzed cross-coupling reaction with unactivated alkyl amine derivatives as the electrophile. A variety of primary amines with unactivated alkyl groups were efficiently converted to

the corresponding 2,4,6-triphenylpyridinium salts and subsequently cross-coupled to afford a variety of functionalized alkyl arene products. A number of amino acid derivatives and drug intermediates were also cross-coupled, demonstrating the amenability of this reaction to late-stage functionalization. This work was published in the *Journal of the American Chemical Society*.<sup>29</sup>

## 2.5 Experimental

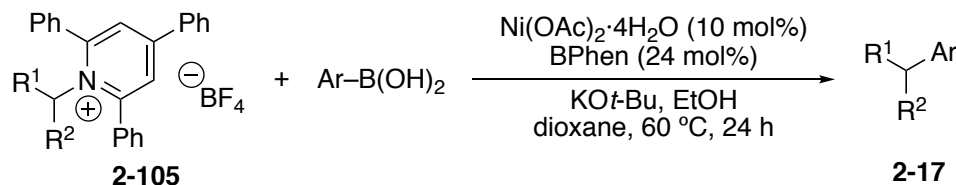
### 2.5.1 General Information

Reactions were performed in oven-dried Schlenk flasks or in oven-dried round-bottomed flasks unless otherwise noted. Round-bottomed flasks were fitted with rubber septa, and reactions were conducted under a positive pressure of N<sub>2</sub>. Stainless steel syringes or cannulae were used to transfer air- and moisture-sensitive liquids. Silica gel chromatography was performed on silica gel 60 (40-63 μm, 60Å) unless otherwise noted. Commercial reagents, including 2,4,6-triphenylpyrylium tetrafluoroborate and the primary and secondary alkyl amines (or corresponding hydrochloride salts), were purchased from Sigma Aldrich, Acros, Fisher, Strem, TCI, Combi Blocks, Alfa Aesar, AK Scientific, Oakwood, or Cambridge Isotopes Laboratories and used as received with the following exceptions: anhydrous ethanol was degassed by sparging with N<sub>2</sub> for 20-30 minutes prior to use in the cross-coupling reactions; dioxane was dried by passing through drying columns, then degassed by sparging with N<sub>2</sub>.<sup>30</sup> In some instances oven-dried potassium carbonate was added to CDCl<sub>3</sub> to remove trace acid. Proton nuclear magnetic resonance (<sup>1</sup>H NMR) spectra, carbon nuclear magnetic resonance (<sup>13</sup>C NMR) spectra, fluorine nuclear magnetic resonance spectra (<sup>19</sup>F NMR), and silicon nuclear magnetic resonance spectra (<sup>29</sup>Si NMR) were recorded on both 400 MHz and 600 MHz spectrometers. Chemical shifts for protons are reported in parts per million downfield from tetramethylsilane and are referenced to residual protium in the NMR solvent (CHCl<sub>3</sub> = δ 7.26). Chemical shifts

for carbon are reported in parts per million downfield from tetramethylsilane and are referenced to the carbon resonances of the solvent ( $\text{CDCl}_3 = \delta$  77.16). Data are represented as follows: chemical shift, multiplicity (br = broad, s = singlet, d = doublet, t = triplet, q = quartet, m = multiplet, dd = doublet of doublets, sep = septet) coupling constants in Hertz (Hz), integration. Infrared (IR) spectra were obtained using FTIR spectrophotometers with material loaded onto a KBr plate. The mass spectral data were obtained at the University of Delaware mass spectrometry facility. Optical rotations were measured using a 2.5 mL cell with a 0.1 dm path length. Melting points were taken on a Thomas-Hoover Uni-Melt Capillary Melting Point Apparatus.

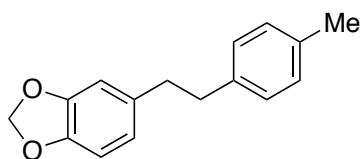
## 2.5.2 Suzuki–Miyaura Cross-Couplings of Alkyl Pyridinium Salts

### 2.5.2.1 General Procedure A: Cross-Coupling with Non-Pyridyl Aryl Boronic Acids

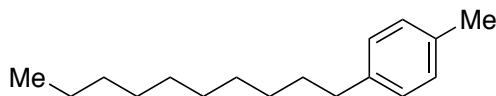


To an oven-dried, 25-mL pear-shaped flask, was added  $\text{Ni(OAc)}_2 \cdot 4\text{H}_2\text{O}$  (25 mg, 0.10 mmol, 10 mol %) and bathophenanthroline (BPhen, 80 mg, 0.24 mmol, 24 mol %). The flask was fitted with a rubber septum, sealed with Parafilm, and then evacuated and refilled with  $\text{N}_2$  (x 3). To an oven-dried, 50-mL Schlenk flask was added the alkyl pyridinium salt (1.0 mmol, 1.0 equiv), arylboronic acid (3.0 equiv, 3.0 mmol), and  $\text{KO}t\text{-Bu}$  (382 mg, 3.4 mmol, 3.4 equiv). The flask was fitted with a rubber septum, sealed with Parafilm, and then evacuated and refilled with  $\text{N}_2$  (x 3). To the pear-shaped flask containing  $\text{Ni(OAc)}_2 \cdot 4\text{H}_2\text{O}$  and BPhen was added dioxane (sparged, anhydrous; 2.5 mL). To the Schlenk flask containing the pyridinium salt, boronic acid, and  $\text{KO}t\text{-Bu}$  was added dioxane (sparged, anhydrous; 2.5 mL), followed by EtOH (sparged, anhydrous; 0.29 mL, 5.0 mmol, 5.0 equiv). After vigorously stirring of the

resulting mixtures for 1 h at room temperature, the heterogeneous mixture containing the catalyst was transferred via cannula to the mixture containing the pyridinium salt and activated boronate complex. The pear-shaped flask was rinsed multiple times with dioxane (totaling 5 mL; each rinse was transferred via cannula to the reaction mixture) to bring the total volume of dioxane in the reaction flask to 10 mL (0.1 M). The resulting reaction mixture was stirred at 60 °C for 24 h. The mixture was allowed to cool to room temperature. EtOAc (10 mL) was added. The mixture was stirred for 2–5 min, and then filtered through a small plug of silica gel. The filter cake was washed with EtOAc (4 x 20 mL), and the resulting solution was concentrated. The cross-coupled product was then purified via silica gel chromatography.

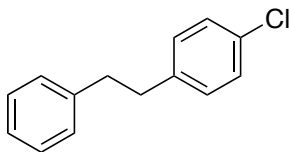


**5-(4-Methylphenethyl)benzo[*d*][1,3]dioxole (2-47).** Prepared via General Procedure A using pyridinium salt **2-46**. The crude mixture was purified by silica gel chromatography (step gradient: 1→5→10→20% toluene/hexanes) to give **2-47** (run 1: 183 mg, 76%; run 2: 177 mg, 74%) as a white solid (mp 81–82 °C): <sup>1</sup>H NMR (600 MHz, CDCl<sub>3</sub>) δ 7.12–7.03 (m, 4H), 6.72 (d, *J* = 7.9 Hz, 1H), 6.69 (d, *J* = 1.5 Hz, 1H), 6.62 (dd, *J* = 7.9, 1.5 Hz, 1H), 5.92 (s, 2H), 2.87 – 2.78 (m, 4H), 2.32 (s, 3H); <sup>13</sup>C NMR (151 MHz, CDCl<sub>3</sub>) δ 147.6, 145.8, 138.7, 135.9, 135.5, 129.2, 128.4, 121.3, 109.1, 108.2, 100.9, 37.9, 37.9, 21.2; FTIR (neat) 2940, 1490, 1246, 1038, 927, 815, 741 cm<sup>-1</sup>; HRMS (ESI+) [*M*+*H*]<sup>+</sup> calculated for C<sub>16</sub>H<sub>17</sub>O<sub>2</sub>: 241.1223, found 241.1222.

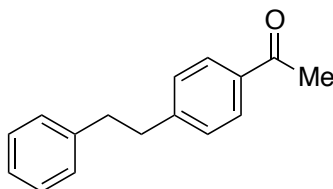


**1-Decyl-4-methylbenzene (2-50).** Prepared via General Procedure A using pyridinium salt **2-106**. The crude mixture was purified by silica gel chromatography (100% pentane) to give **2-50** (run 1: 173 mg, 74%; run 2: 161 mg, 69%) as a clear oil (Note: This product is slightly volatile. Care should be used when drying under high

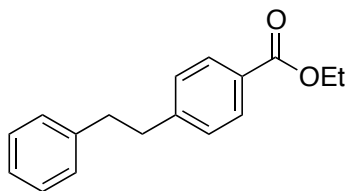
vacuum.):  $^1\text{H}$  NMR (400 MHz,  $\text{CDCl}_3$ )  $\delta$  7.14 – 7.02 (m, 4H), 2.59 – 2.52 (m, 2H), 2.32 (s, 3H), 1.63 – 1.54 (m, 2H), 1.45 – 1.07 (m, 14H), 0.92 – 0.83 (m, 3H);  $^{13}\text{C}$  NMR (101 MHz,  $\text{CDCl}_3$ )  $\delta$  140.0, 135.1, 129.0, 128.4, 35.7, 32.1, 31.8, 29.79, 29.76, 29.7, 29.5, 22.9, 21.2, 14.3. The spectral data matches that of the literature.<sup>31</sup>



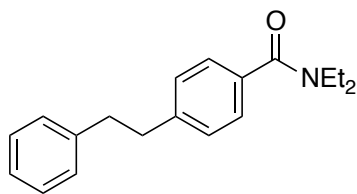
**1-Chloro-4-phenethylbenzene (2-51).** Prepared via General Procedure A using pyridinium salt **2-103**. The crude mixture was purified by silica gel chromatography (100% pentanes) to give **2-51** (run 1: 109 mg, 50%; run 2: 114 mg, 53%) as a white solid:  $^1\text{H}$  NMR (600 MHz,  $\text{CDCl}_3$ )  $\delta$  7.30 – 7.26 (m, 2H), 7.25 – 7.22 (m, 2H), 7.22 – 7.18 (m, 1H), 7.17 – 7.13 (m, 2H), 7.11 – 7.05 (m, 2H), 2.89 (s, 4H);  $^{13}\text{C}$  NMR (151 MHz,  $\text{CDCl}_3$ )  $\delta$  141.4, 140.3, 131.8, 130.0, 128.6, 128.54, 128.52, 126.2, 37.9, 37.3. The spectral data matches that of the literature.<sup>32</sup>



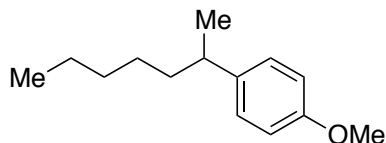
**1-(4-Phenethylphenyl)ethanone (2-54).** Prepared via General Procedure A using pyridinium salt **2-103**. The crude mixture was purified by silica gel chromatography (5% EtOAc/hexanes) to give **2-54** (run 1: 175 mg, 78%; run 2: 172 mg 77%) as a white solid:  $^1\text{H}$  NMR (600 MHz,  $\text{CDCl}_3$ )  $\delta$  7.90 – 7.85 (m, 2H), 7.30 – 7.26 (m, 2H), 7.26 – 7.23 (m, 2H), 7.22 – 7.18 (m, 1H), 7.17 – 7.13 (m, 2H), 3.01 – 2.96 (m, 2H), 2.96 – 2.91 (m, 2H), 2.59 (s, 3H);  $^{13}\text{C}$  NMR (151 MHz,  $\text{CDCl}_3$ )  $\delta$  197.9, 147.6, 141.2, 135.4, 128.9, 128.7, 128.58, 128.55, 126.3, 38.0, 37.6, 26.7. The spectral data matches that of the literature.<sup>33</sup>



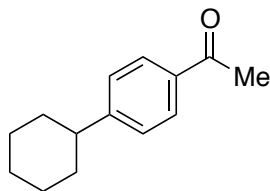
**Ethyl 4-phenethylbenzoate (2-52).** Prepared via General Procedure A using pyridinium salt **2-103**. The crude mixture was purified by silica gel chromatography (50% toluene/hexanes) to give **2-52** (run 1: 178 mg, 70%; run 2: 176 mg, 69%) as an off-white solid:  $^1\text{H}$  NMR (400 MHz,  $\text{CDCl}_3$ )  $\delta$  7.98 – 7.92 (m, 2H), 7.30 – 7.26 (m, 2H), 7.24 – 7.18 (m, 3H), 7.15 (d,  $J = 7.15$  Hz, 2H), 4.37 (q,  $J = 7.1$  Hz, 2H), 3.00 – 2.96 (m, 2H), 2.95 – 2.91 (m, 2H), 1.39 (t,  $J = 7.1$  Hz, 3H);  $^{13}\text{C}$  NMR (101 MHz,  $\text{CDCl}_3$ )  $\delta$  166.8, 147.2, 141.3, 129.8, 128.63, 128.58, 128.5, 128.4, 126.2, 61.0, 38.0, 37.6, 14.5. The spectral data matches that of the literature.<sup>34</sup>



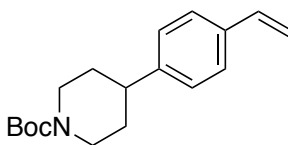
***N,N*-Diethyl-4-phenethylbenzamide (2-53).** Prepared via General Procedure A using pyridinium salt **2-103**. The crude mixture was purified by silica gel chromatography (50% EtOAc/hexanes) to give **2-53** (run 1: 211 mg, 75%; run 2: 200 mg, 71%) as a yellow oil:  $^1\text{H}$  NMR (600 MHz,  $\text{CDCl}_3$ )  $\delta$  7.32 – 7.26 (m, 4H), 7.23 – 7.14 (m, 5H), 3.62 – 3.41 (m, br, 2H), 3.37 – 3.16 (m, br, 2H), 2.97 – 2.88 (m, 4H), 1.34 – 1.18 (m, br, 3H), 1.18 – 1.02 (m, br, 3H);  $^{13}\text{C}$  NMR (101 MHz,  $\text{CDCl}_3$ )  $\delta$  171.5, 143.0, 141.6, 135.0, 128.59, 128.58, 128.5, 126.5, 126.1, 43.4, 39.4, 37.87, 37.85, 14.4, 13.0; FTIR (neat) 2972, 1630, 1426, 1287, 1095, 700  $\text{cm}^{-1}$ ; HRMS (ESI+)  $[\text{M}+\text{H}]^+$  calculated for  $\text{C}_{19}\text{H}_{24}\text{NO}$ : 282.1852, found 282.1852.



**1-(Heptan-2-yl)-4-methoxybenzene (2-56).** Prepared via General Procedure A using pyridinium salt **2-107**. The crude mixture was purified by silica gel chromatography (step gradient: 0→2→5% toluene/hexanes) to give **2-56** (run 1: 119 mg, 58%; run 2: 118 mg, 57%) as a colorless oil:  $^1\text{H}$  NMR (600 MHz,  $\text{CDCl}_3$ )  $\delta$  7.14 – 7.04 (m, 2H), 6.89 – 6.78 (m, 2H), 3.79 (s, 3H), 2.63 (sep,  $J = 7.1$  Hz, 1H), 1.56 – 1.48 (m, 2H), 1.31 – 1.12 (m, 9H), 0.90 – 0.81 (m, 3H);  $^{13}\text{C}$  NMR (151 MHz,  $\text{CDCl}_3$ )  $\delta$  157.8, 140.3, 127.9, 113.8, 55.4, 39.2, 38.7, 32.1, 27.5, 22.75, 22.67, 14.2; FTIR (neat) 2956, 2926, 1513, 1247, 828  $\text{cm}^{-1}$ ; HRMS (ESI+)  $[\text{M}+\text{H}]^+$  calculated for  $\text{C}_{14}\text{H}_{23}\text{O}$ : 207.1743, found 207.1741.

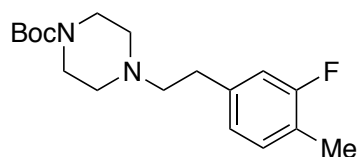


**1-(4-Cyclohexylphenyl)ethanone (2-55).** Prepared via General Procedure A using pyridinium salt **2-108**. The crude mixture was purified by silica gel chromatography (step gradient: 50→75% toluene/hexanes) to give **2-55** (run 1: 134 mg, 66%) as a pale yellow solid:  $^1\text{H}$  NMR (600 MHz,  $\text{CDCl}_3$ )  $\delta$  7.94 – 7.83 (m, 2H), 7.33 – 7.27 (m, 2H), 2.63 – 2.49 (m, 4H), 1.93 – 1.80 (m, 4H), 1.80 – 1.73 (m, 1H), 1.48 – 1.35 (m, 4H), 1.31 – 1.23 (m, 1H);  $^{13}\text{C}$  NMR (151 MHz,  $\text{CDCl}_3$ )  $\delta$  198.0, 153.9, 135.2, 128.7, 127.2, 44.8, 34.3, 26.9, 26.7, 26.2. The spectral data matches that of the literature.<sup>35</sup>



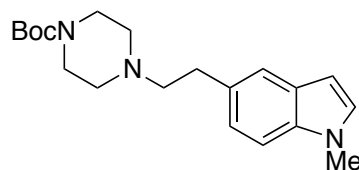
**tert-Butyl 4-(4-vinylphenyl)piperidine-1-carboxylate (2-57).** Prepared via General Procedure A using pyridinium salt **2-44**. The crude mixture was purified by silica gel chromatography (3% EtOAc/hexanes) to give **2-57** (run 1: 148 mg, 51%; run 2: 130 mg, 45%) as a clear oil:  $^1\text{H}$  NMR (600 MHz,  $\text{CDCl}_3$ )  $\delta$  7.38 – 7.33 (m, 2H), 7.19 – 7.14 (m, 2H), 6.69 (dd,  $J = 17.6, 10.9$  Hz, 1H), 5.72 (dd,  $J = 17.6, 0.9$  Hz, 1H), 5.21

(dd,  $J = 10.9, 0.8$  Hz, 1H), 4.42 – 4.08 (m, br, 2H), 2.88 – 2.70 (m, 2H), 2.63 (tt,  $J = 12.1, 3.5$  Hz, 1H), 1.85 – 1.76 (m, br, 2H), 1.67 – 1.55 (m, 2H), 1.48 (s, 9H);  $^{13}\text{C}$  NMR (151 MHz,  $\text{CDCl}_3$ )  $\delta$  155.0, 145.7, 136.6, 135.9, 127.1, 126.5, 113.5, 79.6, 44.5 (br), 42.6, 33.3, 28.6; FTIR (neat) 2933, 1693, 1424, 1170, 840  $\text{cm}^{-1}$ ; HRMS (ESI+)  $[\text{M}+\text{H}]^+$  calculated for  $\text{C}_{18}\text{H}_{26}\text{NO}_2$ : 288.1958, found 288.1956.



**tert-Butyl 4-(3-fluoro-4-methylphenethyl)piperazine-1-carboxylate (2-58).**

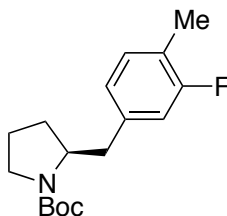
Prepared via General Procedure A using pyridinium salt **2-45**. The crude mixture was purified by silica gel chromatography (step gradient: 0→10→20→40% EtOAc/hexanes) to give **2-58** (run 1: 214 mg, 66%; run 2: 228 mg, 71%) as a yellow semi-solid;  $^1\text{H}$  NMR (600 MHz,  $\text{CDCl}_3$ )  $\delta$  7.07 (t,  $J = 8.0$  Hz, 1H), 6.89 – 6.81 (m, 2H), 3.50 – 3.41 (m, 4H), 2.79 – 2.72 (m, 2H), 2.61 – 2.55 (m, 2H), 2.50 – 2.40 (m, br, 4H), 2.23 (s, 3H), 1.46 (s, 9H);  $^{13}\text{C}$  NMR (151 MHz,  $\text{CDCl}_3$ )  $\delta$  161.4 (d,  $J_{\text{C-F}} = 244.6$  Hz), 154.9, 139.9 (d,  $J_{\text{C-F}} = 9.1$  Hz), 131.4 (d,  $J_{\text{C-F}} = 6.0$  Hz), 124.1 (d,  $J_{\text{C-F}} = 3.0$  Hz), 122.5 (d,  $J_{\text{C-F}} = 16.6$  Hz), 115.3 (d,  $J_{\text{C-F}} = 22.7$  Hz), 79.8, 60.3, 53.1, 43.3 (br), 33.0, 28.6, 14.3;  $^{19}\text{F}$  NMR (565 MHz,  $\text{CDCl}_3$ )  $\delta$  -118.0; FTIR (neat) 2930, 2809, 1698, 1422, 1249, 1173, 1123, 1004; HRMS (ESI+)  $[\text{M}+\text{H}]^+$  calculated for  $\text{C}_{18}\text{H}_{28}\text{FN}_2\text{O}_2$ : 323.2129, found 323.2128.



**tert-Butyl 4-(2-(1-methyl-1H-indol-5-yl)ethyl)piperazine-1-carboxylate (2-59).**

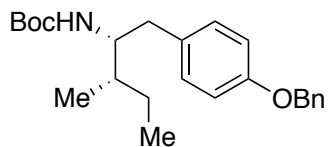
Prepared via General Procedure A using pyridinium salt **2-45**. The crude mixture was purified by silica gel chromatography (step gradient: 30→70% EtOAc/hexanes) to give **2-59** (run 1: 272 mg, 79%; run 2: 282 mg, 82%) as a light orange/yellow solid (mp 80–83 °C):  $^1\text{H}$  NMR (600 MHz,  $\text{CDCl}_3$ )  $\delta$  7.46 – 7.41 (m, 1H), 7.26 – 7.23 (m,

1H), 7.10 – 7.05 (m, 1H), 7.03 (d,  $J = 3.1$  Hz, 1H), 6.43 – 6.39 (m, 1H), 3.77 (m, br, 3H), 3.59 – 3.41 (m, br, 4H), 2.91 (m, br, 2H), 2.66 (m, br, 2H), 2.50 (s, 4H), 1.47 (s, 9H);  $^{13}\text{C}$  NMR (101 MHz,  $\text{CDCl}_3$ )  $\delta$  154.9, 135.6, 130.9, 129.2, 128.8, 122.7, 120.5, 109.2, 100.5, 79.7, 61.6, 53.2, 43.7, 33.7, 33.0, 28.6; FTIR (neat) 2929, 2808, 1694, 1422, 1247, 1171, 1002, 718  $\text{cm}^{-1}$ ; HRMS (ESI+)  $[\text{M}+\text{H}]^+$  calculated for  $\text{C}_{20}\text{H}_{30}\text{N}_3\text{O}_2$ : 344.2333, found 344.2331.

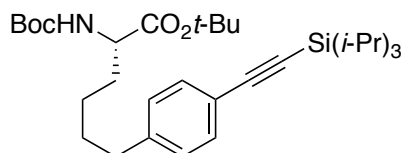


**(S)-tert-Butyl 2-(3-fluoro-4-methylbenzyl)pyrrolidine-1-carboxylate (2-60).**

Prepared via General Procedure A using pyridinium salt **2-109**. The crude mixture was purified by silica gel chromatography (5%  $\text{Et}_2\text{O}$ /toluene) to give **2-60** (189 mg, 65%) as a yellow oil (mixture of rotamers):  $^1\text{H}$  NMR (400 MHz,  $\text{CDCl}_3$ )  $\delta$  7.13 – 7.02 (m, br, 1H), 6.92 – 6.76 (m, br, 2H), 4.05 – 3.85 (m, br, 1H), 3.45 – 3.18 (m, br, 2H), 3.16 – 2.95 (m, br, 1H), 2.59 – 2.41 (m, br, 1H), 2.23 (s, br, 3H), 1.84 – 1.64 (m, br, 4H), 1.57 – 1.44 (s, br, 9H);  $^{13}\text{C}$  NMR (101 MHz,  $\text{CDCl}_3$ )  $\delta$  161.3 (d,  $J_{\text{C-F}} = 245.1$  Hz), 154.6, 138.9 (d,  $J_{\text{C-F}} = 7.4$  Hz), 131.4 (d,  $J_{\text{C-F}} = 4.9$  Hz, major), 131.2 (d,  $J_{\text{C-F}} = 4.4$  Hz, minor), 125.0 (minor), 124.8 (major), 122.6 (d,  $J_{\text{C-F}} = 17.6$  Hz, major), 122.4 (d,  $J_{\text{C-F}} = 16.4$  Hz, minor), 116.1 (d,  $J_{\text{C-F}} = 20.3$  Hz, minor), 115.8 (d,  $J_{\text{C-F}} = 22.2$  Hz, major), 79.5 (major), 79.2 (minor), 58.9 (major), 58.6 (minor), 47.0 (minor), 46.4 (major), 40.1 (major), 39.1 (minor), 29.8 (major), 29.0 (minor), 28.7, 23.6 (minor), 22.8 (major), 14.4, 14.3;  $^{19}\text{F}$  NMR (565 MHz,  $\text{CDCl}_3$ )  $\delta$  -118.0 (major), -118.4 (minor); FTIR (neat) 2973, 2875, 1694, 1394, 1172, 1114, 771  $\text{cm}^{-1}$ ; HRMS (ESI+)  $[\text{M}+\text{H}]^+$  calculated for  $\text{C}_{17}\text{H}_{25}\text{FNO}_2$ : 294.1864, found 294.1862.



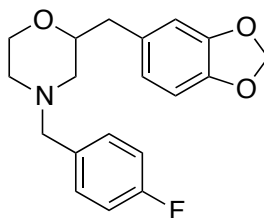
***tert*-Butyl ((2*R*,3*S*)-1-(4-(benzyloxy)phenyl)-3-methylpentan-2-yl)carbamate (2-76).** Prepared via General Procedure A using pyridinium salt **2-74**. The crude mixture was purified by silica gel chromatography (gradient: 1→2% EtOAc/toluene) to give **2-76** (201 mg, 52%) as an off-white solid (mp 121–123 °C): <sup>1</sup>H NMR (600 MHz, CDCl<sub>3</sub>) δ 7.44 – 7.40 (m, 2H), 7.40 – 7.35 (m, 2H), 7.34 – 7.29 (m, 1H), 7.12 – 7.05 (m, 2H), 6.92–6.86 (m, 2H), 5.03 (s, 2H), 4.36 – 4.24 (m, 1H), 3.80 – 3.68 (m, br, 1H), 2.79 – 2.73 (m, 1H), 2.57 – 2.53 (m, 1H), 1.55–1.47 (m, 2H), 1.35 (s, br, 9H), 1.15 – 1.05 (m, br, 1H), 0.97–0.86 (m, 6H); <sup>13</sup>C NMR (101 MHz, CDCl<sub>3</sub>) δ 157.4, 155.7, 137.3, 131.3, 130.3, 128.7, 128.0, 127.6, 114.8, 79.0, 70.1, 56.1, 37.7, 37.0, 28.5, 24.8, 15.8, 11.9; FTIR (neat) 3384, 2962, 1684, 1518, 1240, 744 cm<sup>-1</sup>; HRMS (ESI+) [M+H]<sup>+</sup> calculated for C<sub>24</sub>H<sub>34</sub>NO<sub>3</sub>: 384.2533, found 384.2526



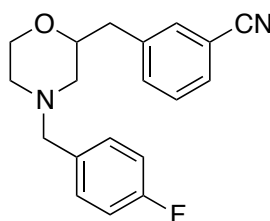
**(*S*)-*tert*-Butyl 2-((*tert*-butoxycarbonyl)amino)-6-(4-((triisopropylsilyl)ethynyl)phenyl)hexanoate (2-80).** Prepared via General Procedure A using pyridinium salt **2-78** and (4-((triisopropylsilyl)ethynyl)phenyl)boronic acid<sup>36</sup> with the following exceptions: the reaction was run on a 0.5 mmol scale and pyridinium salt **2-78** was pre-stirred with Ni(OAc)<sub>2</sub>·4H<sub>2</sub>O and BPhen instead of with the boronic acid, KO*t*-Bu, and EtOH. The crude mixture was purified by silica gel chromatography (5% EtOAc/hexanes) to give **2-80** (165 mg, 60%) as a clear oil. The enantiomeric excess was determined to be 29% by chiral HPLC analysis (CHIRALPAK IA, 1.0 mL/min, 2% *i*-PrOH/hexanes, λ=254 nm); t<sub>R</sub>(major) = 14.52 min, t<sub>R</sub>(minor) = 9.78 min. [α]<sub>D</sub><sup>26</sup> = +40.1° (c 1.6, CHCl<sub>3</sub>): <sup>1</sup>H NMR (600 MHz, CDCl<sub>3</sub>) δ 7.38 (d, *J* = 8.0 Hz, 2H), 7.09 (d, *J* = 8.1 Hz, 2H), 4.98 (d, *J* = 7.8 Hz, 1H), 4.23 – 4.07 (m, 1H), 2.59 (t, *J* = 7.6 Hz, 2H), 1.81 – 1.72 (m, 1H), 1.68 – 1.57 (m, 3H), 1.44 (s, 9H), 1.43 (s, 9H), 1.40 – 1.35 (m, 1H), 1.35 – 1.29 (m, 1H), 1.12 (s, 21H); <sup>13</sup>C NMR (151 MHz, CDCl<sub>3</sub>) δ 172.1, 155.5, 142.9, 132.2, 128.4,

121.1, 107.4, 89.8, 81.9, 79.7, 54.0, 35.7, 33.0, 30.9, 28.5, 28.1, 24.7, 18.8, 11.5;  $^{29}\text{Si}$  NMR (119 MHz,  $\text{CDCl}_3$ )  $\delta$  -2.0; FTIR (neat) 3358, 2942, 2865, 2155, 1717, 1504, 1367, 1155, 677  $\text{cm}^{-1}$ ; HRMS (ESI+)  $[\text{M}+\text{H}]^+$  calculated for  $\text{C}_{32}\text{H}_{54}\text{NO}_4\text{Si}$ : 544.3817, found 544.3811.

The arylation of pyridinium salt **2-78** was also performed in the presence of 4-(trifluoromethyl)phenol. In a  $\text{N}_2$ -atmosphere glovebox.  $\text{Ni}(\text{OAc})_2 \cdot 4\text{H}_2\text{O}$  (1.2 mg, 0.005 mmol, 10 mol %), BPhen (4.0 mg, 0.0012 mmol, 24 mol %), 4-(trifluoromethyl)phenol **2-81** (16 mg, 0.1 mmol, 2.0 equiv), and pyridinium salt **2-78** (34 mg, 0.05 mmol, 1.0 equiv) were added to an oven-dried 1-dram vial. To a separate oven-dried 1-dram vial was added  $\text{KO}t\text{-Bu}$  (19 mg, 0.17 mmol, 3.4 equiv) and 4-((triisopropylsilyl)ethynyl)phenylboronic acid (45 mg, 0.15 mmol, 3.0 equiv). Dioxane (125  $\mu\text{L}$ ) was added to each vial. Each vial was then equipped with a micro stir bar, capped with a pierceable Teflon-coated cap, and removed from the glovebox. To the vial containing the boronic acid and  $\text{KO}t\text{-Bu}$  was added EtOH (15  $\mu\text{L}$ ) via a  $\text{N}_2$ -purged syringe. Both mixtures were stirred for 1 h at rt. After pre-stirring was complete, the catalyst mixture containing the pyridinium salt and 4-(trifluoromethyl)phenol was transferred to the “activated boronate” mixture via a  $\text{N}_2$ -purged syringe. Dioxane (250  $\mu\text{L}$  total) was used to insure complete transfer of the catalyst mixture and bring the total concentration of the reaction to 0.1 M. The resulting reaction mixture was heated to 60  $^\circ\text{C}$  and stirred vigorously for 24 h. Upon completion, the mixture was diluted with EtOAc (approx. 1.5 mL) and filtered through a short plug of silica gel. The filter cake was washed with EtOAc (5 x 1.5 mL) and the resulting solution was concentrated. The yield of the crude product was determined to be 25% and was obtained by integration by  $^1\text{H}$ -NMR with 1,3,5-trimethoxybenzene as an internal standard. A small sample of the product was purified via preparatory thin-layer chromatography (5% EtOAc/hexanes) and the enantiomeric excess was determined to be 81% by chiral HPLC analysis (CHIRALPAK IA, 1.0 mL/min, 2% *i*-PrOH/hexanes,  $\lambda=254$  nm);  $t_{\text{R}}(\text{major}) = 14.57$  min,  $t_{\text{R}}(\text{minor}) = 9.84$  min.



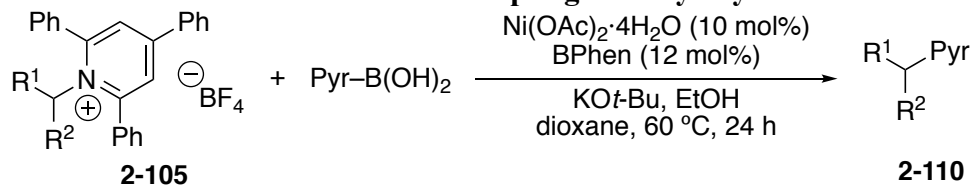
**2-(Benzo[*d*][1,3]dioxol-5-ylmethyl)-4-(4-fluorobenzyl)morpholine (2-86).** Prepared via General Procedure A using pyridinium salt **2-43**. After the silica gel filtration, the crude mixture was dissolved in Et<sub>2</sub>O (20 mL) and washed with HCl (1 N, 4 x 25 mL). The combined aqueous layers were extracted with Et<sub>2</sub>O (4 x 50 mL, these organic layers were discarded), basified to pH ≥ 12 with NaOH (4 N), and then extracted with Et<sub>2</sub>O (4 x 50 mL). The combined organic layers were dried (MgSO<sub>4</sub>), filtered, and concentrated. The residue was then purified by silica gel chromatography (step gradient: 10→20% EtOAc/hexanes) to give **2-86** (run 1: 224 mg, 68%; run 2: 240 mg, 73%) as a yellow oil: <sup>1</sup>H NMR (600 MHz, CDCl<sub>3</sub>) δ 7.28 – 7.23 (m, 2H, *overlaps with CHCl<sub>3</sub>*), 7.04 – 6.94 (m, 2H), 6.76 – 6.67 (m, 2H), 6.65 – 6.60 (m, 1H), 5.92 (s, 2H), 3.87 – 3.81 (m, 1H), 3.74 – 3.66 (m, 1H), 3.64 – 3.57 (m, 1H), 3.52 – 3.46 (m, 1H), 3.41 – 3.34 (m, 1H), 2.78 – 2.67 (m, 2H), 2.62 – 2.55 (m, 2H), 2.16 – 2.08 (m, 1H), 1.96 – 1.87 (m, 1H); <sup>13</sup>C NMR (151 MHz, CDCl<sub>3</sub>) δ 162.2 (d, *J*<sub>C-F</sub> = 245.1 Hz), 147.6, 146.1, 133.6, 131.9, 130.7 (d, *J*<sub>C-F</sub> = 7.7 Hz), 122.2, 115.2 (d, *J*<sub>C-F</sub> = 21.3 Hz), 109.8, 108.2, 100.9, 76.7, 66.9, 62.6, 58.4, 52.8, 40.0; <sup>19</sup>F NMR (565 MHz, CDCl<sub>3</sub>) δ –115.8; FTIR (neat) 2859, 2804, 1604, 1508, 1247, 1114, 1040, 810 cm<sup>-1</sup>; HRMS (ESI+) [M+H]<sup>+</sup> calculated for C<sub>19</sub>H<sub>21</sub>FNO<sub>3</sub>: 330.1500, found 330.1491.



**3-((4-(4-Fluorobenzyl)morpholin-2-yl)methyl)benzonitrile (2-85).** Prepared via General Procedure A using pyridinium salt **2-43**. After the silica gel filtration, the crude mixture was dissolved in Et<sub>2</sub>O (20 mL) and washed with HCl (1 N, 4 x 25 mL).

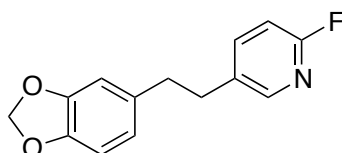
The combined aqueous layers were extracted with Et<sub>2</sub>O (4 x 50 mL, these organic layers were discarded), basified to pH  $\geq$  12 with NaOH (4 N), and then extracted with Et<sub>2</sub>O (4 x 50 mL). The combined organic layers were dried (MgSO<sub>4</sub>), filtered, and concentrated. The residue was then purified by silica gel chromatography (20% EtOAc/hexanes) to give **2-85** (run 1: 201 mg, 65%; run 2: 180 mg, 58%) as a yellow oil: <sup>1</sup>H NMR (600 MHz, CDCl<sub>3</sub>)  $\delta$  7.51 – 7.50 (m, 2H), 7.44 – 7.43 (m, 1H), 7.39 – 7.36 (m, 1H), 7.28 – 7.25 (m, 2H, *overlaps with CHCl<sub>3</sub>*), 7.02– 6.99 (m, 2H), 3.82 – 3.84 (m, 1H), 3.72 (m, 1H), 3.61 – 3.57 (m, 1H), 3.48–3.41 (m, 2H), 2.82 – 2.79 (m, 1H), 2.72 – 2.69 (m, 2H), 2.63 – 2.61 (m, 1H), 2.16 – 2.12 (m, 1H), 1.94 – 1.90 (m, 1H); <sup>13</sup>C NMR (151 MHz, CDCl<sub>3</sub>)  $\delta$  162.2 (d,  $J_{C-F}$  = 245.4 Hz), 139.9, 134.0, 133.4, 133.0, 130.7 (d,  $J_{C-F}$  = 7.6 Hz), 130.2, 129.1, 119.1, 115.3 (d,  $J_{C-F}$  = 21.1 Hz), 112.4, 75.9, 66.9, 62.5, 58.2, 52.9, 39.7; <sup>19</sup>F NMR (376 MHz, CDCl<sub>3</sub>)  $\delta$  –115.6; FTIR (neat) 2933, 2807, 2229, 1508, 1221, 1114, 693 cm<sup>-1</sup>; HRMS (ESI+) [M+H]<sup>+</sup> calculated for C<sub>19</sub>H<sub>20</sub>FN<sub>2</sub>O: 311.1554, found 311.1551.

### 2.5.2.2 General Procedure B: Cross-Coupling with Pyridyl Boronic Acids

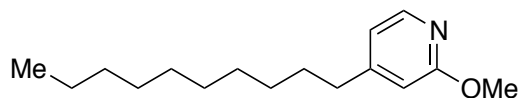


To an oven-dried, 25-mL pear-shaped flask was added Ni(OAc)<sub>2</sub>·4H<sub>2</sub>O (25 mg, 0.10 mmol, 10 mol %), bathophenanthroline (BPhen, 40 mg, 0.12 mmol, 12 mol %), and the alkyl pyridinium salt (1.0 mmol, 1.0 equiv). The flask was fitted with a rubber septum, sealed with Parafilm, and then evacuated and refilled with N<sub>2</sub> (x 3). To an oven-dried, 100-mL Schlenk flask was added the arylboronic acid (3.0 equiv, 3.0 mmol) and KO<sup>t</sup>-Bu (382 mg, 3.4 mmol, 3.4 equiv). The flask was fitted with a rubber septum, sealed with Parafilm, and then evacuated and refilled with N<sub>2</sub> (x 3). To the pear-shaped flask containing Ni(OAc)<sub>2</sub>·4H<sub>2</sub>O and BPhen was added dioxane (sparged, anhydrous; 10 mL). To the Schlenk flask containing the boronic acid and KO<sup>t</sup>-Bu was

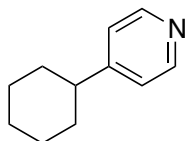
added dioxane (sparged, anhydrous; 10 mL), followed by EtOH (sparged, anhydrous; 0.29 mL, 5.0 mmol, 5.0 equiv). After vigorously stirring the resulting mixtures for 2 h at room temperature, the mixture (heterogeneous in some cases) of catalyst and pyridinium salt was transferred via large-gauge cannula to the mixture containing the activated boronate complex. The pear-shaped flask was rinsed multiple times with dioxane (totaling 20 mL; each rinse was transferred via cannula to the reaction mixture) to bring the total volume of dioxane in the reaction to 40 mL (0.025 M). The resulting reaction mixture was stirred at 60 °C for 24 h. The mixture was allowed to cool to room temperature. EtOAc (10 mL) was added. The mixture was stirred 2–5 min, and then filtered through a small plug of silica gel. The filter cake was washed with EtOAc (4 x 20 mL), and the resulting solution was concentrated. The cross-coupled product was then purified via silica gel chromatography.



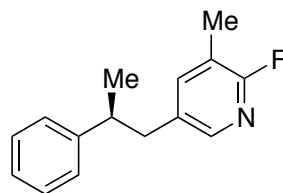
**5-(2-(Benzo[*d*][1,3]dioxol-5-yl)ethyl)-2-fluoropyridine (2-63).** Prepared via General Procedure B using pyridinium salt **2-46**. The crude mixture was purified by silica gel chromatography (4% EtOAc/hexanes) to give **2-63** (run 1: 201 mg, 82%; run 2: 193 mg, 79%) as a yellow oil:  $^1\text{H}$  NMR (600 MHz,  $\text{CDCl}_3$ )  $\delta$  7.98 – 7.92 (m, 1H), 7.50 (td,  $J = 8.1, 2.6$  Hz, 1H), 6.82 (dd,  $J = 8.3, 2.9$  Hz, 1H), 6.71 (d,  $J = 7.9$  Hz, 1H), 6.62 (d,  $J = 1.7$  Hz, 1H), 6.54 (dd,  $J = 7.8, 1.7$  Hz, 1H), 5.93 (s, 2H), 2.90 – 2.85 (m, 2H), 2.85 – 2.80 (m, 2H);  $^{13}\text{C}$  NMR (101 MHz,  $\text{CDCl}_3$ )  $\delta$  162.4 (d,  $J_{\text{C-F}} = 238.0$  Hz), 147.8, 147.3 (d,  $J_{\text{C-F}} = 14.3$  Hz), 146.0, 141.3 (d,  $J_{\text{C-F}} = 7.7$  Hz), 134.324, 134.319 (d,  $J_{\text{C-F}} = 4.4$  Hz), 121.5, 109.1 (d,  $J_{\text{C-F}} = 37.5$  Hz), 109.0, 108.3, 101.0, 37.4, 34.2;  $^{19}\text{F}$  NMR (376 MHz,  $\text{CDCl}_3$ )  $\delta$  -71.9; FTIR (neat) 2925, 1596, 1486, 1246, 1040, 932, 811  $\text{cm}^{-1}$ ; HRMS (ESI+)  $[\text{M}+\text{H}]^+$  calculated for  $\text{C}_{14}\text{H}_{13}\text{FNO}_2$ : 246.0925, found 246.0925.



**4-Decyl-2-methoxypyridine (2-64).** Prepared via General Procedure B using pyridinium salt **2-106**. The crude mixture was purified by silica gel chromatography (step gradient: 100% toluene→2% EtOAc/hexanes) to give **2-64** (run 1: 195 mg, 78%; run 2: 175 mg, 70%) as a yellow oil:  $^1\text{H}$  NMR (600 MHz,  $\text{CDCl}_3$ )  $\delta$  8.03 (d,  $J = 5.3$  Hz, 1H), 6.72 – 6.67 (m, 1H), 6.58 – 6.51 (m, 1H), 3.92 (s, 3H), 2.59 – 2.49 (m, 2H), 1.62 – 1.56 (m, 2H), 1.35 – 1.19 (m, 14H), 0.88 (t,  $J = 6.9$  Hz, 3H);  $^{13}\text{C}$  NMR (151 MHz,  $\text{CDCl}_3$ )  $\delta$  164.7, 154.8, 146.6, 117.7, 110.4, 53.4, 35.3, 32.0, 30.3, 29.74, 29.68, 29.6, 29.5, 29.3, 22.8, 14.2; FTIR (neat) 2926, 1613, 1398, 1157, 1044, 820; HRMS (ESI+)  $[\text{M}+\text{H}]^+$  calculated for  $\text{C}_{16}\text{H}_{27}\text{NO}$ : 250.2165, found 250.2157.

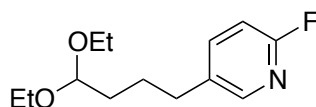


**4-Cyclohexylpyridine (2-65).** Prepared via General Procedure B using pyridinium salt **2-108**. The crude mixture was purified by silica gel chromatography (50% EtOAc/hexanes) to give **2-65** (run 1: 81 mg, 50%; run 2: 91 mg, 56%) as an orange oil:  $^1\text{H}$  NMR (400 MHz,  $\text{CDCl}_3$ )  $\delta$  8.49 – 8.47 (m, 2H), 7.13 – 7.11 (m, 2H), 2.53 – 2.45 (m, 1H), 1.91 – 1.67 (m, 5H), 1.46 – 1.19 (m, 5H);  $^{13}\text{C}$  NMR (101 MHz,  $\text{CDCl}_3$ )  $\delta$  156.7, 149.9, 122.5, 43.9, 33.6, 26.7, 26.1. The spectral data matches that of the literature.<sup>37</sup>

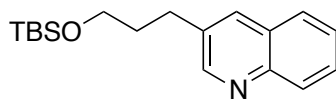


**(S)-2-Fluoro-3-methyl-5-(2-phenylpropyl)pyridine (2-66).** Prepared via General Procedure B using pyridinium salt **2-111**. The crude mixture was purified by silica gel chromatography (gradient: 10→20→30→50→70% toluene/hexanes→100% toluene) to give **2-66** (run 1: 151 mg, 66%; run 2: 152 mg, 66%) as a dark orange oil:  $^1\text{H}$  NMR (400 MHz,  $\text{CDCl}_3$ )  $\delta$  7.67 (s, br, 1H), 7.32 – 7.26 (m, 2H), 7.24 – 7.15 (m, 2H),

7.15 – 7.07 (m, 2H), 2.94 (sep,  $J = 7.0$  Hz, 1H), 2.87 – 2.72 (m, 2H), 2.22 – 2.15 (s, 3H), 1.27 (d,  $J = 6.9$  Hz, 3H);  $^{13}\text{C}$  NMR (101 MHz,  $\text{CDCl}_3$ )  $\delta$  161.1 (d,  $J_{\text{C-F}} = 237.0$  Hz), 145.8, 144.8 (d,  $J_{\text{C-F}} = 14.2$  Hz), 142.4 (d,  $J_{\text{C-F}} = 5.9$  Hz), 133.7 (d,  $J_{\text{C-F}} = 4.6$  Hz), 128.6, 127.2, 126.5, 118.8 (d,  $J_{\text{C-F}} = 32.8$  Hz), 41.8, 41.1 (d,  $J_{\text{C-F}} = 0.9$  Hz), 21.3, 14.6 (d,  $J_{\text{C-F}} = 1.5$  Hz);  $^{19}\text{F}$  NMR (376 MHz,  $\text{CDCl}_3$ )  $\delta$  -76.6; FTIR (neat) 2962, 1591, 1471, 1246, 1143, 700  $\text{cm}^{-1}$ ; HRMS (ESI+)  $[\text{M}+\text{H}]^+$  calculated for  $\text{C}_{15}\text{H}_{16}\text{FN}$ : 230.1340, found 230.1334.

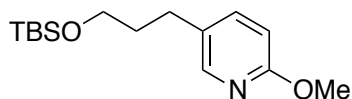


**5-(4,4-Diethoxybutyl)-2-fluoropyridine (2-67).** Prepared via General Procedure B using pyridinium salt **2-112**. The crude mixture was purified by silica gel chromatography (5% EtOAc/hexanes) to give **2-67** (run 1: 176 mg, 73%; run 2: 164 mg, 68%) as a yellow oil:  $^1\text{H}$  NMR (600 MHz,  $\text{CDCl}_3$ )  $\delta$  8.02 (s, 1H), 7.59 (td,  $J = 8.1, 2.5$  Hz, 1H), 6.84 (dd,  $J = 8.3, 2.9$  Hz, 1H), 4.49 (t,  $J = 5.3$  Hz, 1H), 3.63 (dq,  $J = 9.4, 7.1$  Hz, 2H), 3.48 (dq,  $J = 9.4, 7.1$  Hz, 2H), 2.63 (t,  $J = 7.3$  Hz, 2H), 1.72 – 1.61 (m, 4H), 1.20 (t,  $J = 7.1$  Hz, 6H);  $^{13}\text{C}$  NMR (151 MHz,  $\text{CDCl}_3$ )  $\delta$  162.5 (d,  $J_{\text{C-F}} = 236.8$  Hz), 147.2 (d,  $J_{\text{C-F}} = 14.3$  Hz), 141.1 (d,  $J_{\text{C-F}} = 7.6$  Hz), 135.2 (d,  $J_{\text{C-F}} = 4.5$  Hz), 109.1 (d,  $J_{\text{C-F}} = 37.4$  Hz), 102.8, 61.3, 33.2, 31.94, 31.93, 26.4, 15.5;  $^{19}\text{F}$  NMR (565 MHz,  $\text{CDCl}_3$ )  $\delta$  -72.3; FTIR (neat) 2975, 2872, 1593, 1485, 1249, 1126, 1065, 831  $\text{cm}^{-1}$ ; HRMS (ESI+)  $[\text{M}+\text{H}]^+$  calculated for  $\text{C}_{13}\text{H}_{21}\text{FNO}_2$ : 242.1551, found 242.1548.

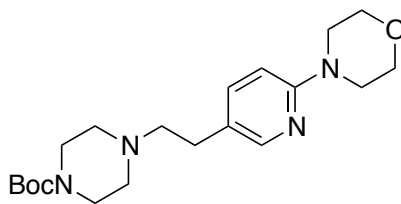


**3-(3-((tert-Butyl)dimethylsilyloxy)propyl)quinoline (2-68).** Prepared via General Procedure B using pyridinium salt **2-113**. The crude mixture was purified by silica gel chromatography (5% EtOAc/hexanes) to give **2-68** (run 1: 160 mg, 53%; run 2: 195 mg, 65%) as a yellow oil:  $^1\text{H}$  NMR (600 MHz,  $\text{CDCl}_3$ )  $\delta$  8.80 (d,  $J = 2.2$  Hz, 1H), 8.08 (d,  $J = 8.4$  Hz, 1H), 7.94 (s, 1H), 7.76 (d,  $J = 8.1$  Hz, 1H), 7.66 (t,  $J = 7.2$  Hz, 1H), 7.52 (t,  $J = 7.5$  Hz, 1H), 3.68 (t,  $J = 6.1$  Hz, 2H), 2.92 – 2.87 (m, 2H), 1.96 – 1.90 (m, 2H),

0.92 (s, 9H), 0.07 (s, 6H);  $^{13}\text{C}$  NMR (151 MHz,  $\text{CDCl}_3$ )  $\delta$  152.2, 146.9, 135.0, 134.5, 129.3, 128.7, 128.3, 127.4, 126.7, 62.0, 34.1, 29.6, 26.1, 18.5, -5.1; FTIR (neat) 2929, 2857, 1471, 1255, 1102, 836  $\text{cm}^{-1}$ ; HRMS (ESI+)  $[\text{M}+\text{H}]^+$  calculated for  $\text{C}_{18}\text{H}_{28}\text{NOSi}$ : 302.1935, found 302.1934.

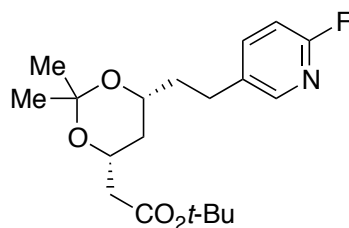


**5-(3-((*tert*-Butyldimethylsilyloxy)propyl)-2-methoxypyridine (2-69).** Prepared via General Procedure B using pyridinium salt **2-113**. The crude mixture was purified by silica gel chromatography (gradient: 50→75% toluene/hexanes→100% toluene→5% EtOAc/toluene) to give **2-69** (run 1: 196 mg, 70%; run 2: 176 mg, 62%) as a yellow oil:  $^1\text{H}$  NMR (400 MHz,  $\text{CDCl}_3$ )  $\delta$  7.97 (d,  $J = 2.1$  Hz, 1H), 7.41 (dd,  $J = 8.5, 2.5$  Hz, 1H), 6.67 (d,  $J = 8.4$  Hz, 1H), 3.91 (s, 3H), 3.62 (t,  $J = 6.2$  Hz, 2H), 2.63 – 2.55 (m, 2H), 1.83 – 1.73 (m, 2H), 0.90 (s, 9H), 0.05 (s, 6H);  $^{13}\text{C}$  NMR (101 MHz,  $\text{CDCl}_3$ )  $\delta$  162.7, 146.2, 139.2, 130.1, 110.5, 62.1, 53.4, 34.5, 28.3, 26.1, 18.5, -5.1; FTIR (neat) 2929, 2857, 1608, 1493, 1256, 1102, 835  $\text{cm}^{-1}$ ; HRMS (ESI+)  $[\text{M}+\text{H}]^+$  calculated for  $\text{C}_{15}\text{H}_{27}\text{NO}_2\text{Si}$ : 282.1884, found 282.1874.



***tert*-Butyl 4-(2-(6-morpholinopyridin-3-yl)ethyl)piperazine-1-carboxylate (2-70).** Prepared via General Procedure B using pyridinium salt **2-45**. The crude mixture was purified by silica gel chromatography (100% EtOAc) to give **2-70** (233 mg, 62%) as a yellow solid (mp 125–127 °C):  $^1\text{H}$  NMR (400 MHz,  $\text{CDCl}_3$ )  $\delta$  8.05 (d,  $J = 2.3$  Hz, 1H), 7.37 (dd,  $J = 8.6, 2.4$  Hz, 1H), 6.59 (d,  $J = 8.6$  Hz, 1H), 3.91 – 3.75 (m, 4H), 3.58 – 3.32 (m, 8H), 2.73 – 2.64 (m, 2H), 2.58 – 2.51 (m, 2H), 2.50 – 2.35 (m, 4H), 1.46 (s, 9H);  $^{13}\text{C}$  NMR (101 MHz,  $\text{CDCl}_3$ )  $\delta$  158.6, 154.9, 147.8, 138.2, 125.3, 107.0, 79.8, 66.9, 60.4, 53.1, 46.0, 43.7 (br), 29.8, 28.6; FTIR (neat) 2971, 2860, 1694, 1499, 1265,

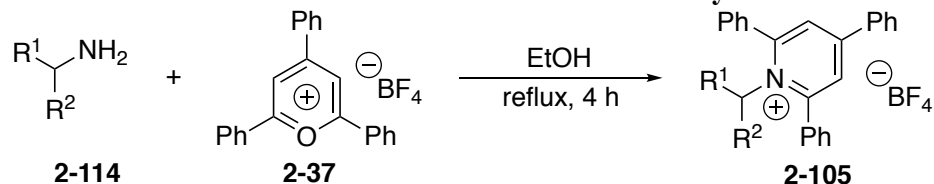
1126, 810  $\text{cm}^{-1}$ ; HRMS (ESI+)  $[\text{M}+\text{H}]^+$  calculated for  $\text{C}_{20}\text{H}_{33}\text{N}_4\text{O}_3$ : 377.2547, found 377.2544.



**tert-Butyl 2-((4R,6R)-6-(2-(6-fluoropyridin-3-yl)ethyl)-2,2-dimethyl-1,3-dioxan-4-yl)acetate (2-90).** Prepared via General Procedure B using pyridinium salt **2-88**. The crude mixture was purified by silica gel chromatography (5% EtOAc/hexanes) to give **2-90** (161 mg, 46%) as a dark pink oil:  $^1\text{H}$  NMR (400 MHz,  $\text{CDCl}_3$ )  $\delta$  8.02 – 8.01 (m, 1H), 7.59 (td,  $J = 8.1, 2.6$  Hz, 1H), 6.85 (dd,  $J = 8.4, 2.9$  Hz, 1H), 4.21 (dtd,  $J = 11.6, 6.6, 2.4$  Hz, 1H), 3.83 – 3.72 (m, 1H), 2.79 – 2.61 (m, 2H), 2.43 (dd,  $J = 15.2, 6.9$  Hz, 1H), 2.29 (dd,  $J = 15.2, 6.2$  Hz, 1H), 1.85 – 1.73 (m, 1H), 1.73 – 1.61 (m, 1H), 1.53 (dt,  $J = 12.7, 2.5$  Hz, 1H), 1.43 (s, 9H), 1.41 (s, 3H), 1.38 (s, 3H), 1.27 – 1.17 (m, 1H);  $^{13}\text{C}$  NMR (101 MHz,  $\text{CDCl}_3$ )  $\delta$  170.4, 162.4 (d,  $J_{\text{C-F}} = 237.8$  Hz), 147.2 (d,  $J_{\text{C-F}} = 14.2$  Hz), 141.3 (d,  $J_{\text{C-F}} = 7.7$  Hz), 134.9 (d,  $J_{\text{C-F}} = 4.5$  Hz), 109.2 (d,  $J_{\text{C-F}} = 37.5$  Hz), 98.9, 80.8, 67.5, 66.3, 42.8, 37.6, 36.6, 30.2, 28.2, 27.4, 19.9;  $^{19}\text{F}$  NMR (376 MHz,  $\text{CDCl}_3$ )  $\delta$  -72.2; FTIR (neat) 2981, 2940, 1730, 1484, 1249, 1159, 951, 840  $\text{cm}^{-1}$ ; HRMS (ESI+)  $[\text{M}+\text{H}]^+$  calculated for  $\text{C}_{19}\text{H}_{29}\text{FNO}_4$ : 354.2075, found 354.2072.

## 2.5.3 Preparation of Pyridinium Salts

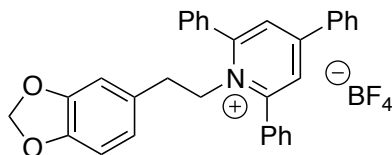
### 2.5.3.1 General Procedure C: Conversion of Amines to Pyridinium Salts



Primary amine (1.2 equiv) was added to a suspension of 2,4,6-triphenylpyrylium tetrafluoroborate (1.0 equiv) and EtOH (1.0 M) in a round-bottomed flask. The flask

was fitted with a reflux condenser. The mixture was stirred and heated at reflux in an oil bath at 80–85 °C for 4 h. The mixture was then allowed to cool to room temperature. If product precipitation occurred during reflux, the solid was filtered, washed with EtOH (3 x 25 mL) and then Et<sub>2</sub>O (3 x 25 mL), and dried under high vacuum. If product precipitation did not occur during reflux, the solution was diluted with Et<sub>2</sub>O (2–3x volume of EtOH used) and vigorously stirred for 1 h. The resulting solid pyridinium salt was filtered and washed with Et<sub>2</sub>O (3 x 25 mL). If the pyridinium salt failed to precipitate at this point, the flask containing the reaction mixture and Et<sub>2</sub>O was sealed with Parafilm and stored in a –27 °C freezer for 1–3 days (or until precipitation occurred). The cold mixture was quickly filtered and washed with Et<sub>2</sub>O (3 x 25 mL) to give the corresponding analytically pure pyridinium salt. If the salt still did not precipitate, it was subjected to silica gel chromatography with acetone/DCM.

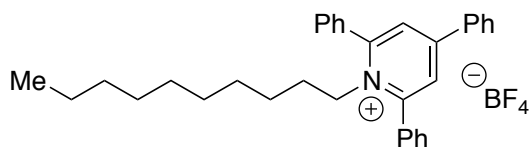
The corresponding amine hydrochloride salts can also be used (see synthesis of pyridinium salt **3l**) using the following modified procedure: Et<sub>3</sub>N (1.2 equiv) was added to a mixture of the corresponding alkyl ammonium hydrochloride salt (1.2 equiv) and EtOH (1.0 M). After stirring the mixture for 30 min at room temperature, 2,4,6-triphenylpyrylium tetrafluoroborate (1 equiv) was added. From this point forward, the same procedure was followed as for alkyl amines described above; however prior to washing the solid product with EtOH and/or Et<sub>2</sub>O, the mixture was washed with water (3 x 25 mL) to remove Et<sub>3</sub>N·HCl.



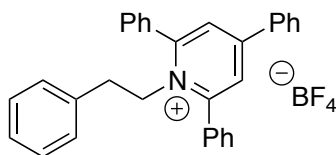
**1-(2-(Benzo[*d*][1,3]dioxol-5-yl)ethyl)-2,4,6-triphenylpyridin-1-ium**

**tetrafluoroborate (2-46).** Prepared via General Procedure C on a 7.5 mmol scale with commercially available 2-(benzo[*d*][1,3]dioxol-5-yl)ethanamine (9.0 mmol) to give **2-46** (3.64 g, 89%) as an off-white solid (mp 234–235 °C): <sup>1</sup>H NMR (600 MHz, CDCl<sub>3</sub>) δ 7.91 (s, 2H), 7.83 – 7.77 (m, 6H), 7.68 – 7.62 (m, 6H), 7.59 – 7.55 (m, 1H), 7.55 –

7.51 (m, 2H), 6.48 (d,  $J = 7.9$  Hz, 1H), 5.85 (s, 2H), 5.77 – 5.74 (m, 1H), 5.69 – 5.66 (m, 1H), 4.61 – 4.55 (m, 2H), 2.65 – 2.58 (m, 2H);  $^{13}\text{C}$  NMR (151 MHz,  $\text{CDCl}_3$ )  $\delta$  156.7, 156.3, 148.0, 146.9, 134.2, 132.9, 132.3, 131.4, 129.9, 129.6, 129.3, 128.9, 128.3, 126.9, 121.4, 108.61, 108.57, 101.2, 56.1, 35.7;  $^{19}\text{F}$  NMR (565 MHz,  $\text{CDCl}_3$ )  $\delta$  –153.27 (minor,  $^{11}\text{BF}_4$ ), –153.32 (major,  $^{10}\text{BF}_4$ ); FTIR (neat) 3060, 2903, 1624, 1489, 1053, 699  $\text{cm}^{-1}$ ; HRMS (ESI+)  $[\text{M}-\text{BF}_4]^+$  calculated for  $\text{C}_{32}\text{H}_{26}\text{NO}_4$ : 456.1958, found 456.1961.

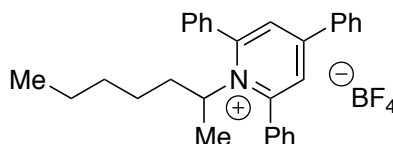


**1-Decyl-2,4,6-triphenylpyridin-1-ium tetrafluoroborate (2-106).** Prepared via General Procedure C on a 4.17 mmol scale with commercially available decan-1-amine (5.0 mmol) to give **2-106** (1.56 g, 58%) as a white solid (mp 98–100 °C):  $^1\text{H}$  NMR (600 MHz,  $\text{CDCl}_3$ )  $\delta$  7.84 (s, 2H), 7.82 – 7.76 (m, 4H), 7.76 – 7.72 (m, 2H), 7.64 – 7.56 (m, 6H), 7.56 – 7.52 (m, 1H), 7.52 – 7.47 (m, 2H), 4.45 – 4.34 (m, 2H), 1.48 – 1.38 (m, 2H), 1.25 (m,  $J = 7.1$  Hz, 2H), 1.20 – 1.08 (m, 4H), 1.05 – 0.97 (m, 2H), 0.95 – 0.81 (m, 5H), 0.79 – 0.69 (m, 4H);  $^{13}\text{C}$  NMR (151 MHz,  $\text{CDCl}_3$ )  $\delta$  156.6, 155.8, 134.2, 132.9, 132.1, 131.1, 129.8, 129.4, 129.2, 128.2, 126.8, 54.9, 31.9, 29.8, 29.3, 29.2, 29.0, 28.0, 26.1, 22.8, 14.2;  $^{19}\text{F}$  NMR (376 MHz,  $\text{CDCl}_3$ )  $\delta$  –153.4 (minor,  $^{11}\text{BF}_4$ ), –153.5 (major,  $^{10}\text{BF}_4$ ); FTIR (neat) 2926, 1625, 1566, 1056, 704  $\text{cm}^{-1}$ ; HRMS (ESI+)  $[\text{M}-\text{BF}_4]^+$  calculated for  $\text{C}_{33}\text{H}_{38}\text{N}$ : 448.2999, found 448.3004.

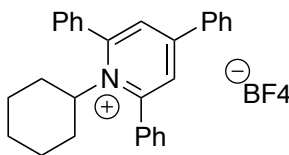


**1-Phenethyl-2,4,6-triphenylpyridin-1-ium tetrafluoroborate (2-103).** Prepared via General Procedure C on a 10 mmol scale with commercially available 2-phenylethanamine to give **2-103** (4.40 g, 88%) as a white solid (mp >260 °C):  $^1\text{H}$  NMR (400 MHz,  $\text{CDCl}_3$ )  $\delta$  7.92 (s, 2H), 7.89 – 7.73 (m, 6H), 7.73 – 7.48 (m, 9H),

7.15 – 7.09 (m, 1H), 7.09 – 7.03 (m, 2H), 6.32 – 6.26 (m, 2H), 4.69 – 4.62 (m, 2H), 2.73 – 2.66 (m, 2H);  $^{13}\text{C}$  NMR (101 MHz,  $\text{CDCl}_3$ )  $\delta$  156.8, 156.2, 135.3, 134.1, 132.8, 132.3, 131.3, 129.9, 129.5, 129.3, 128.9, 128.33, 128.30, 127.4, 126.9, 56.0, 35.8;  $^{19}\text{F}$  NMR (376 MHz,  $\text{CDCl}_3$ )  $\delta$  -153.26 (minor,  $^{11}\text{BF}_4$ ), -153.32 (major,  $^{10}\text{BF}_4$ ); FTIR (neat) 3068, 1624, 1494, 1055, 699  $\text{cm}^{-1}$ ; HRMS (ESI+)  $[\text{M}-\text{BF}_4]^+$  calculated for  $\text{C}_{31}\text{H}_{26}\text{N}$ : 412.2060, found 412.2048.

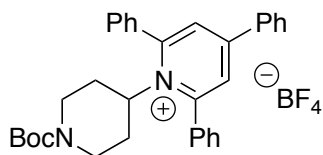


**1-(Heptan-2-yl)-2,4,6-triphenylpyridin-1-ium tetrafluoroborate (2-107).** Prepared via General Procedure C on a 5.0 mmol scale with commercially available heptan-2-amine to give **2-107** (1.21 g, 49%) as a pale yellow solid (mp 157–158 °C):  $^1\text{H}$  NMR (400 MHz,  $\text{CDCl}_3$ )  $\delta$  7.99 – 7.44 (m, 17H), 4.96 – 4.84 (m, 1H), 1.84 – 1.70 (m, 1H), 1.49 – 1.36 (m, 4H), 1.20 – 1.08 (m, 2H), 1.07 – 0.93 (m, 3H), 0.89 – 0.73 (m, 4H);  $^{13}\text{C}$  NMR (151 MHz, acetone- $d_6$ )  $\delta$  158.7, 155.3, 135.1, 134.4, 133.3, 131.9, 130.6, 130.4, 129.7, 129.4, 128.6, 68.4, 37.2, 31.7, 26.7, 22.8, 22.5, 14.1;  $^{19}\text{F}$  NMR (376 MHz,  $\text{CDCl}_3$ )  $\delta$  -153.3 (minor,  $^{11}\text{BF}_4$ ), -153.4 (major,  $^{10}\text{BF}_4$ ); FTIR (neat) 2956, 1621, 1412, 1056, 765  $\text{cm}^{-1}$ ; HRMS (ESI+)  $[\text{M}-\text{BF}_4]^+$  calculated for  $\text{C}_{30}\text{H}_{32}\text{N}$ : 406.2529, found 406.2516.



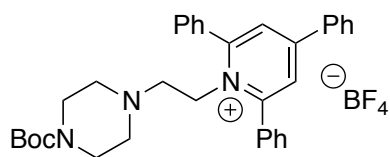
**1-Cyclohexyl-2,4,6-triphenylpyridin-1-ium tetrafluoroborate (2-108).** Prepared via General Procedure C on a 10 mmol scale with commercially available cyclohexanamine (12 mmol) to give **2-108** (2.99 g, 63%) as pale yellow solid (mp 181–182 °C):  $^1\text{H}$  NMR (400 MHz,  $\text{CDCl}_3$ )  $\delta$  7.83 – 7.76 (m, 2H), 7.76 – 7.69 (m, 6H), 7.64 – 7.54 (m, 6H), 7.54 – 7.48 (m, 1H), 7.48 – 7.42 (m, 2H), 4.61 (tt,  $J = 12.2, 2.9$  Hz, 1H), 2.12 (m, 2H), 1.64 – 1.40 (m, 4H), 1.34 (d,  $J = 13.3$  Hz, 1H), 0.74 (m, 2H),

0.61 (tt,  $J = 13.1, 3.5$  Hz, 1H);  $^{13}\text{C}$  NMR (101 MHz,  $\text{CDCl}_3$ )  $\delta$  157.1, 155.1, 134.2, 134.1, 131.9, 130.9, 129.7, 129.4, 128.9, 128.4, 128.2, 72.0, 33.7, 26.6, 24.7;  $^{19}\text{F}$  NMR (376 MHz,  $\text{CDCl}_3$ )  $\delta$  -153.36 (minor,  $^{11}\text{BF}_4$ ), -153.41 (major,  $^{10}\text{BF}_4$ ); FTIR (neat) 3061, 2934, 1621, 1055, 705  $\text{cm}^{-1}$ ; HRMS (ESI+)  $[\text{M}-\text{BF}_4]^+$  calculated for  $\text{C}_{29}\text{H}_{28}\text{N}$ : 390.2216, found 390.2199.



**1-(1-(*tert*-Butoxycarbonyl)piperidin-4-yl)-2,4,6-triphenylpyridin-1-ium**

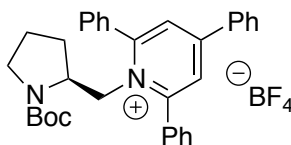
**tetrafluoroborate (2-44).** Prepared via General Procedure C on a 5.0 mmol scale with commercially available *tert*-butyl 4-aminopiperidine-1-carboxylate to give **2-44** (2.08 g, 72%) as an off-white solid (mp 165–166 °C):  $^1\text{H}$  NMR (600 MHz,  $\text{CDCl}_3$ )  $\delta$  7.86 – 7.69 (m, 6H), 7.67 (d,  $J = 7.2$  Hz, 2H), 7.64 – 7.52 (m, 6H), 7.52 – 7.46 (m, 1H), 7.46 – 7.36 (m, 2H), 4.82 – 4.69 (m, 1H), 4.04 – 3.75 (m, 2H), 2.27 – 1.95 (m, 4H), 1.74 – 1.51 (m, 2H), 1.30 (s, 9H);  $^{13}\text{C}$  NMR (101 MHz,  $\text{CDCl}_3$ )  $\delta$  157.2, 155.5, 154.3, 134.0, 133.8, 132.1, 131.2, 129.7, 129.4, 129.1, 128.4, 128.3, 80.2, 70.0, 44.3 (br), 32.8 (br), 28.3;  $^{19}\text{F}$  NMR (565 MHz,  $\text{CDCl}_3$ )  $\delta$  -153.07 (minor,  $^{11}\text{BF}_4$ ), -153.13 (major,  $^{10}\text{BF}_4$ ); FTIR (neat) 2977, 1692, 1621, 1057, 706  $\text{cm}^{-1}$ ; HRMS (ESI+)  $[\text{M}-\text{BF}_4]^+$  calculated for  $\text{C}_{33}\text{H}_{35}\text{N}_2\text{O}_2$ : 491.2693, found 491.2686.



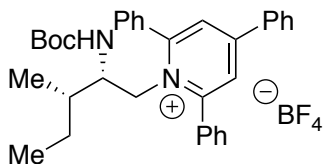
**1-(2-(4-(*tert*-Butoxycarbonyl)piperazin-1-yl)ethyl)-2,4,6-triphenylpyridin-1-ium**

**tetrafluoroborate (2-45).** Prepared via General Procedure C on a 1.67 mmol scale with commercially available *tert*-butyl 4-(2-aminoethyl)piperazine-1-carboxylate to give **2-45** (0.82 g, 81%) as an off-white solid (mp 133–135 °C):  $^1\text{H}$  NMR (600 MHz,  $\text{CDCl}_3$ )  $\delta$  7.88 – 7.75 (m, 6H), 7.74 – 7.69 (m, 2H), 7.65 – 7.56 (m, 6H), 7.55 – 7.50 (m, 1H), 7.50 – 7.44 (m, 2H), 4.66 – 4.57 (m, 2H), 3.13 – 3.00 (m, 4H), 2.41 – 2.31

(m, 2H), 1.82 – 1.73 (m, br, 4H), 1.39 (s, 9H);  $^{13}\text{C}$  NMR (151 MHz,  $\text{CDCl}_3$ )  $\delta$  157.0, 156.1, 154.6, 134.1, 133.0, 132.3, 131.3, 129.8, 129.51, 129.46, 128.3, 126.8, 79.9, 56.4, 52.4, 51.8, 43.2 (br), 28.5;  $^{19}\text{F}$  NMR (565 MHz,  $\text{CDCl}_3$ )  $\delta$  -152.96 (minor,  $^{11}\text{BF}_4$ ), -153.01 (major,  $^{10}\text{BF}_4$ ); FTIR (neat) 2976, 1690, 1623, 1169, 1056, 703  $\text{cm}^{-1}$ ; HRMS (ESI+)  $[\text{M}-\text{BF}_4]^+$  calculated for  $\text{C}_{34}\text{H}_{38}\text{N}_3\text{O}_2$ : 520.2959, found 520.2950.

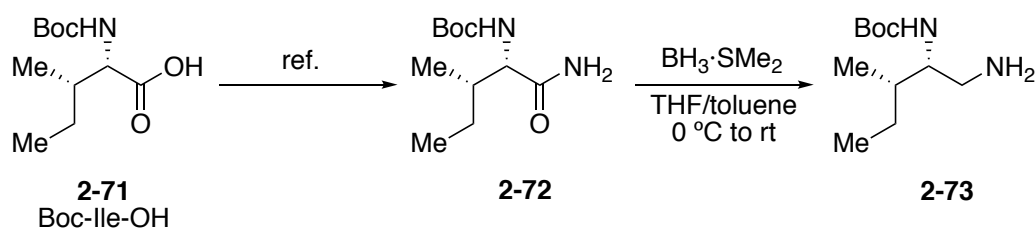


**(*S*)-1-((1-(*tert*-Butoxycarbonyl)pyrrolidin-2-yl)methyl)-2,4,6-triphenylpyridin-1-ium tetrafluoroborate (2-109).** Prepared via General Procedure C on a 4.17 mmol scale with commercially available (*S*)-*tert*-butyl 2-(aminomethyl)pyrrolidine-1-carboxylate to give **2-109** (2.08 g, 84%) as a white solid (mp 180–181 °C):  $^1\text{H}$  NMR (600 MHz,  $\text{CDCl}_3$ )  $\delta$  8.31 – 7.84 (m, br, 3H), 7.80 (s, 2H), 7.72 (d,  $J = 7.4$  Hz, 2H), 7.70 – 7.38 (m, 10H), 4.89 – 4.74 (m, 1H), 4.71 – 4.55 (m, 1H), 3.98 – 3.83 (m, 1H), 2.91 (td,  $J = 10.7, 6.5$  Hz, 1H), 2.66 (t,  $J = 9.3$  Hz, 1H), 1.58 – 1.43 (m, 2H), 1.32 (s, 9H), 1.28 – 1.22 (m, 1H), 0.88 – 0.74 (m, 1H);  $^{13}\text{C}$  NMR (151 MHz,  $\text{CDCl}_3$ )  $\delta$  158.0 (br), 155.6, 155.4, 134.3, 133.5, 132.1, 131.0, 130.4, 129.8, 129.4, 128.0, 126.3, 80.1, 57.5, 55.1, 47.3, 28.5, 28.4, 23.4;  $^{19}\text{F}$  NMR (565 MHz,  $\text{CDCl}_3$ )  $\delta$  -153.08 (minor,  $^{11}\text{BF}_4$ ), -153.13 (major,  $^{10}\text{BF}_4$ ); FTIR (neat) 2975, 1687, 1622, 1383, 1058, 704  $\text{cm}^{-1}$ ; HRMS (ESI+)  $[\text{M}-\text{BF}_4]^+$  calculated for  $\text{C}_{33}\text{H}_{35}\text{N}_2\text{O}_2$ : 491.2693, found 491.2672.



**1-((2*S*,3*S*)-2-((*tert*-Butoxycarbonyl)amino)-3-methylpentyl)-2,4,6-triphenylpyridin-1-ium tetrafluoroborate (2-74).** Prepared via General Procedure C; however a 1:1 ratio of 2,4,6-triphenylpyrylium tetrafluoroborate (1.9 mmol) to *tert*-butyl ((2*S*,3*S*)-1-amino-3-methylpentan-2-yl)carbamate (see synthesis below) was used. After stirring for the 4 h period, the reaction mixture was concentrated. The

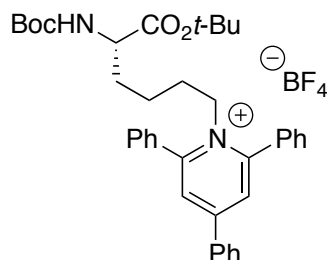
crude residue was purified via column chromatography (5% acetone/CH<sub>2</sub>Cl<sub>2</sub>) to give pyridinium salt (**2-74**) (0.74 g, 66%) as a pale yellow solid (mp 107–109 °C): <sup>1</sup>H NMR (600 MHz, CDCl<sub>3</sub>) δ 8.42 – 8.12 (m, 2H), 7.96 – 7.50 (m, 15H), 4.98 (dd, *J* = 14.6, 3.4 Hz, 1H), 4.59 (dd, *J* = 14.6, 11.7 Hz, 1H), 3.91 (d, *J* = 10.1 Hz, 1H), 3.61 – 3.54 (m, 1H), 1.31 (s, 9H), 1.09 – 1.01 (m, 1H), 0.85 – 0.72 (m, 2H), 0.49 (t, *J* = 7.4 Hz, 3H), 0.31 (d, *J* = 6.8 Hz, 3H); <sup>13</sup>C NMR (151 MHz, CDCl<sub>3</sub>) δ 158.3, 155.9, 155.1, 134.2, 133.5, 132.3, 131.2, 130.4, 129.9, 129.4, 128.0, 126.5, 80.3, 56.4, 53.6, 37.1, 28.5, 25.2, 14.2, 10.6; <sup>19</sup>F NMR (565 MHz, CDCl<sub>3</sub>) δ –153.0 (minor, <sup>11</sup>BF<sub>4</sub>), –153.1 (major, <sup>10</sup>BF<sub>4</sub>); FTIR (neat) 3442, 3357, 2968, 1707, 1621, 1057, 703 cm<sup>-1</sup>; HRMS (ESI+) [M–BF<sub>4</sub>]<sup>+</sup> calculated for C<sub>34</sub>H<sub>39</sub>N<sub>2</sub>O<sub>2</sub>: 507.3006, found 507.2995.



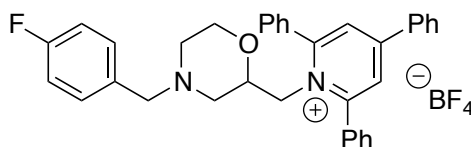
**tert-Butyl ((2*S*,3*S*)-1-amino-3-methyl-1-oxopentan-2-yl)carbamate (**2-72**).** Prepared according to the literature procedure.<sup>38</sup>

**tert-Butyl ((2*S*,3*S*)-1-amino-3-methylpentan-2-yl)carbamate (**2-73**).** Prepared according to a procedure adapted from the literature<sup>39</sup> (note: these reduction conditions are *unoptimized* for Boc-Ile-NH<sub>2</sub> **2-72**): In a round-bottomed flask, a solution of amide **2-72** (1.5 g, 6.5 mmol, 1.0 equiv) and THF (21.7 mL, 0.30 M) was cooled to 0 °C. BH<sub>3</sub>·SMe<sub>2</sub> (2.0 M in toluene, 32.6 mL, 65.1 mmol, 10.0 equiv) was added portionwise (approx. 6–7 mL/min). After the addition was complete, the solution was stirred for 5 min at 0 °C, allowed to warm room temperature, and stirred for 24 h. The solution was then concentrated, and MeOH (36 mL, 5.6 mL/mmol) was slowly added (CAUTION: add slowly to prevent violent evolution of gas!). The solution was stirred briefly and then concentrated. This dilution/concentration protocol was repeated two more times. The resulting residue was then dissolved in Et<sub>2</sub>O (50 mL) and extracted with HCl (1 N, 4 x 50 mL). The combined aqueous layers were washed with Et<sub>2</sub>O (4 x 50 mL) and

then basified with KOH (4 N) to  $\text{pH} \geq 12$ . The basic aqueous layer was then extracted with  $\text{Et}_2\text{O}$  (4 x 100 mL). The combined organic layers were washed with sat. NaCl (100 mL), dried ( $\text{MgSO}_4$ ), filtered through a cotton plug, and concentrated to afford amine **S2** (0.464 g, 33%) as a white solid, which was used without further purification.

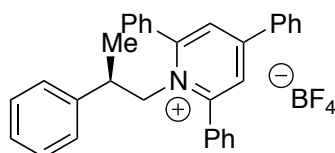


**(S)-1-(6-(tert-Butoxy)-5-((tert-butoxycarbonyl)amino)-6-oxohexyl)-2,4,6-triphenylpyridin-1-ium tetrafluoroborate (2-78)**. Prepared via General Procedure C on a 4.91 mmol scale with Boc-Lys-O<sup>t</sup>Bu.<sup>40</sup> Attempts to triturate the product failed; the crude residue was purified via column chromatography (5→20% acetone/ $\text{CH}_2\text{Cl}_2$ ) to give pyridinium salt **2-78** (2.91 g, 87%) as a tan solid (mp 96–100 °C):  $^1\text{H}$  NMR (600 MHz,  $\text{CDCl}_3$ )  $\delta$  7.91 (s, 2H), 7.85 – 7.77 (m, 6H), 7.67 – 7.61 (m, 6H), 7.61 – 7.57 (m, 1H), 7.57 – 7.53 (m, 2H), 4.84 (d, br,  $J = 7.7$  Hz, 1H), 4.49 – 4.38 (m, 2H), 3.90 – 3.78 (m, 1H), 1.55 – 1.46 (m, 2H), 1.42 (s, 9H), 1.40 (s, 9H), 1.33 – 1.26 (m, 1H), 1.11 – 1.03 (m, 1H), 0.94 – 0.76 (m, 1H);  $^{13}\text{C}$  NMR (151 MHz,  $\text{CDCl}_3$ )  $\delta$  171.3, 156.6, 156.0, 155.4, 134.2, 132.8, 132.2, 131.2, 129.8, 129.5, 129.2, 128.3, 126.9, 82.2, 79.9, 54.5, 53.5, 31.8, 29.5, 28.4, 28.1, 22.1;  $^{19}\text{F}$  NMR (376 MHz,  $\text{CDCl}_3$ )  $\delta$  –153.3 (minor,  $^{11}\text{BF}_4$ ), –153.4 (major,  $^{10}\text{BF}_4$ ); FTIR (neat) 3374, 2978, 1711, 1624, 1155, 1057, 704  $\text{cm}^{-1}$ ; HRMS (ESI+)  $[\text{M}-\text{BF}_4]^+$  calculated for  $\text{C}_{38}\text{H}_{45}\text{N}_2\text{O}_4$ : 593.3374, found 593.3366.



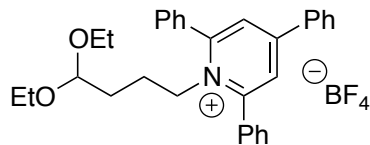
**1-((4-(4-Fluorobenzyl)morpholin-2-yl)methyl)-2,4,6-triphenylpyridin-1-ium tetrafluoroborate (2-43)**. Prepared via General Procedure C (refluxed for 22 h) on a 5

mmol scale with commercially available (4-(4-fluorobenzyl)morpholin-2-yl)methanamine (6.0 mmol) to give **2-43** (2.67 g, 89%) as a tan solid (mp 170–172 °C):  $^1\text{H}$  NMR (400 MHz,  $\text{CDCl}_3$ )  $\delta$  7.89 (s, 2H), 7.87 – 7.67 (m, 6H), 7.64 – 7.51 (m, 9H), 7.09 – 7.03 (m, 2H), 6.98 – 6.91 (m, 2H), 4.73 (dd,  $J = 14.9, 4.1$  Hz, 1H), 4.55 (dd,  $J = 14.9, 9.7$  Hz, 1H), 3.67 – 3.58 (m, 1H), 3.33 – 3.16 (m, 4H), 2.47 – 2.39 (m, 1H), 2.13 – 2.04 (m, 1H), 1.89 (td,  $J = 11.4, 3.3$  Hz, 1H), 1.33 – 1.24 (m, 1H);  $^{13}\text{C}$  NMR (151 MHz,  $\text{CDCl}_3$ )  $\delta$  162.2 (d,  $J_{\text{C-F}} = 245.7$  Hz), 157.8, 155.7, 134.0, 133.2, 132.6, 132.4, 131.1, 130.7 (d,  $J_{\text{C-F}} = 7.9$  Hz), 129.9, 129.6, 129.3, 128.2, 126.3, 115.2 (d,  $J_{\text{C-F}} = 21.4$  Hz), 72.5, 66.6, 61.9, 56.3, 55.6, 52.2;  $^{19}\text{F}$  NMR (376 MHz,  $\text{CDCl}_3$ )  $\delta$  –115.3, –153.2 (minor,  $^{11}\text{BF}_4$ ), –153.3 (major,  $^{10}\text{BF}_4$ ); FTIR (neat) 3065, 2815, 1622, 1058, 703  $\text{cm}^{-1}$ ; HRMS (ESI+)  $[\text{M}-\text{BF}_4]^+$  calculated for  $\text{C}_{35}\text{H}_{32}\text{FN}_2\text{O}$ : 515.2493, found 515.2486.



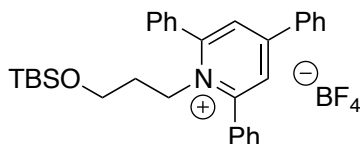
**(*R*)-2,4,6-Triphenyl-1-(2-phenylpropyl)pyridin-1-ium tetrafluoroborate (2-111).**

Prepared via General Procedure C on a 5.0 mmol scale with commercially available (*R*)-2-phenylpropan-1-aminium chloride to give **2-111** (2.27 g, 88%) as a white solid (mp 206–207 °C):  $^1\text{H}$  NMR (400 MHz,  $\text{CDCl}_3$ )  $\delta$  8.44 – 7.30 (m, 17H), 7.23 – 7.16 (m, 1H), 7.08 (t,  $J = 7.5$  Hz, 2H), 6.49 – 6.37 (m, 2H), 5.03 (dd,  $J = 14.3, 5.5$  Hz, 1H), 4.81 (dd,  $J = 14.3, 9.4$  Hz, 1H), 2.80 – 2.63 (m, 1H), 0.82 (d,  $J = 7.0$  Hz, 3H);  $^{13}\text{C}$  NMR (101 MHz,  $\text{CDCl}_3$ )  $\delta$  157.6, 155.8, 140.4, 133.8, 133.2, 132.5, 131.2, 129.9, 129.65, 129.59, 129.1, 128.2, 127.7, 126.9, 126.6, 61.3, 39.8, 17.9;  $^{19}\text{F}$  NMR (565 MHz,  $\text{CDCl}_3$ )  $\delta$  –153.1 (minor,  $^{11}\text{BF}_4$ ), –153.2 (major,  $^{10}\text{BF}_4$ ); FTIR (neat) 3062, 1620, 1562, 1057, 702  $\text{cm}^{-1}$ ; HRMS (ESI+)  $[\text{M}-\text{BF}_4]^+$  calculated for  $\text{C}_{32}\text{H}_{28}\text{N}$ : 426.2216, found 426.2220.



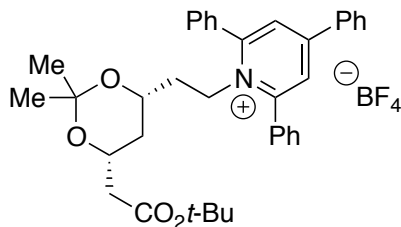
**1-(4,4-Diethoxybutyl)-2,4,6-triphenylpyridin-1-ium tetrafluoroborate (2-112).**

Prepared via General Procedure C on a 4.0 mmol scale with commercially available 4,4-diethoxybutan-1-amine (4.8 mmol) to give **2-112** (1.86 g, 86%) as a fluffy white solid (mp 139–140 °C):  $^1\text{H}$  NMR (600 MHz,  $\text{CDCl}_3$ )  $\delta$  7.87 (s, 2H), 7.83 – 7.78 (m, 4H), 7.78 – 7.74 (m, 2H), 7.63 – 7.58 (m, 6H), 7.58 – 7.54 (m, 1H), 7.54 – 7.48 (m, 2H), 4.49 – 4.42 (m, 2H), 4.01 (t,  $J = 5.2$  Hz, 1H), 3.36 (dq,  $J = 9.0, 7.0$  Hz, 2H), 3.18 (dq,  $J = 9.1, 7.0$  Hz, 2H), 1.60 – 1.52 (m, 2H), 1.10 – 0.98 (m, 8H);  $^{13}\text{C}$  NMR (101 MHz,  $\text{CDCl}_3$ )  $\delta$  156.5, 155.8, 134.0, 132.8, 132.1, 131.0, 129.7, 129.3, 129.0, 128.1, 126.8, 101.5, 61.6, 54.7, 30.5, 25.1, 15.2;  $^{19}\text{F}$  NMR (376 MHz,  $\text{CDCl}_3$ )  $\delta$  –153.4 (minor,  $^{11}\text{BF}_4$ ), –153.5 (major,  $^{10}\text{BF}_4$ ); FTIR (neat) 2975, 2880, 1624, 1566, 1056, 703  $\text{cm}^{-1}$ ; HRMS (ESI+)  $[\text{M}-\text{BF}_4]^+$  calculated for  $\text{C}_{31}\text{H}_{34}\text{NO}_2$ : 452.2584, found 452.2589.

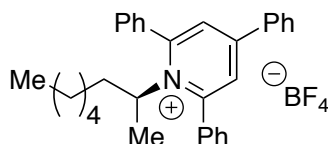


**1-(3-((*tert*-Butyldimethylsilyloxy)propyl)-2,4,6-triphenylpyridin-1-ium**

**tetrafluoroborate (2-113).** Prepared via General Procedure C on a 1.67 mmol scale with 3-((*tert*-butyldimethylsilyloxy)propan-1-amine<sup>41</sup> (2.0 mmol) to give **2-113** (0.73 g, 77%) as a white solid (mp 170–171 °C):  $^1\text{H}$  NMR (600 MHz,  $\text{CDCl}_3$ )  $\delta$  7.89 (s, 2H), 7.84 – 7.75 (m, 6H), 7.65 – 7.58 (m, 6H), 7.58 – 7.49 (m, 3H), 4.58 – 4.52 (m, 2H), 3.13 (t,  $J = 5.6$  Hz, 2H), 1.74 – 1.65 (m, 2H), 0.67 (s, 9H), –0.21 (s, 6H);  $^{13}\text{C}$  NMR (101 MHz,  $\text{CDCl}_3$ )  $\delta$  156.7, 156.0, 134.3, 133.0, 132.1, 131.2, 129.8, 129.5, 129.1, 128.3, 127.1, 60.1, 53.4, 32.8, 25.9, 18.2, –5.5;  $^{19}\text{F}$  NMR (376 MHz,  $\text{CDCl}_3$ )  $\delta$  –153.4 (minor,  $^{11}\text{BF}_4$ ), –153.5 (major,  $^{10}\text{BF}_4$ ); FTIR (neat) 2954, 2855, 1622, 1054, 837, 771, 703  $\text{cm}^{-1}$ ; HRMS (ESI+)  $[\text{M}-\text{BF}_4]^+$  calculated for  $\text{C}_{32}\text{H}_{38}\text{NO}_4$ : 480.2717, found 480.2716.

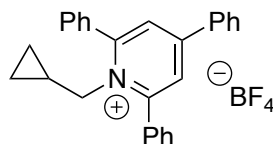


**1-(2-((4R,6R)-6-(2-(*tert*-Butoxy)-2-oxoethyl)-2,2-dimethyl-1,3-dioxan-4-yl)ethyl)-2,4,6-triphenylpyridin-1-ium tetrafluoroborate (2-88).** Prepared via General Procedure C on a 5.0 mmol scale with commercially available *tert*-butyl 2-((4R,6R)-6-(2-aminoethyl)-2,2-dimethyl-1,3-dioxan-4-yl)acetate (6.0 mmol) to give **2-88** (1.44 g, 44%) as a white solid (mp 128–130 °C):  $^1\text{H}$  NMR (600 MHz,  $\text{CDCl}_3$ )  $\delta$  7.90 (s, 2H), 7.87 – 7.72 (m, 6H), 7.70 – 7.60 (m, 6H), 7.60 – 7.56 (m, 1H), 7.56 – 7.50 (m, 2H), 4.71 – 4.63 (m, 1H), 4.55 – 4.47 (m, 1H), 4.02 – 3.96 (m, 1H), 3.33 – 3.27 (m, 1H), 2.26 (dd,  $J = 15.3, 7.2$  Hz, 1H), 2.14 (dd,  $J = 15.3, 5.9$  Hz, 1H), 1.65 – 1.54 (m, 2H), 1.42 (s, 9H), 1.16 (s, 3H), 1.13 (dt,  $J = 12.6, 2.2$  Hz, 1H), 1.03 (s, 3H), 0.72 (q,  $J = 11.7$  Hz, 1H);  $^{13}\text{C}$  NMR (101 MHz,  $\text{CDCl}_3$ )  $\delta$  170.1, 156.9, 156.0, 134.2, 132.9, 132.2, 131.2, 129.8, 129.5, 129.2, 128.2, 126.9, 98.6, 80.9, 66.1, 65.7, 51.9, 42.4, 35.9, 35.4, 29.9, 28.2, 19.6;  $^{19}\text{F}$  NMR (376 MHz,  $\text{CDCl}_3$ )  $\delta$  –153.3 (minor,  $^{11}\text{BF}_4$ ), –153.4 (major,  $^{10}\text{BF}_4$ ); FTIR (neat) 2990, 1726, 1624, 1160, 1057, 703  $\text{cm}^{-1}$ ; HRMS (ESI+)  $[\text{M}-\text{BF}_4]^+$  calculated for  $\text{C}_{37}\text{H}_{42}\text{NO}_4$ : 564.3108, found 564.3099.



**(S)-1-(Octan-2-yl)-2,4,6-triphenylpyridin-1-ium tetrafluoroborate (2-97).** Prepared via General Procedure C; however, a 1:1 ratio of 2,4,6-triphenylpyridinium tetrafluoroborate (5.0 mmol) to commercially available (*S*)-octan-2-amine was used. After refluxing overnight with stirring, the reaction mixture was concentrated. The crude residue was purified via silica gel chromatography (10% acetone/ $\text{CH}_2\text{Cl}_2$ ) to give **2-97** (1.55 g, 61%) as an orange solid (mp 67–69 °C):  $^1\text{H}$  NMR (400 MHz,  $\text{CDCl}_3$ )  $\delta$  7.93 – 7.38 (m, 17H), 4.94 – 4.82 (m, 1H), 1.82 – 1.71 (m, 1H), 1.48 – 1.32

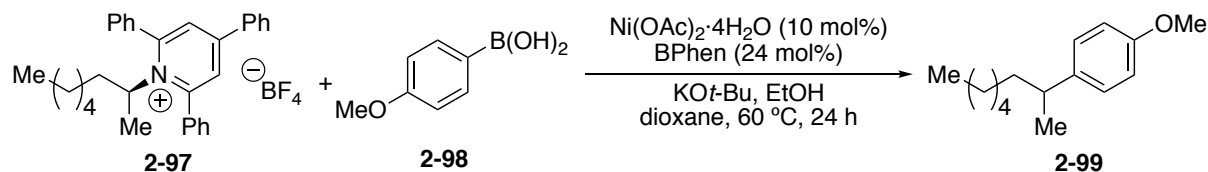
(m, 4H), 1.21 – 1.11 (m, 2H), 1.11 – 0.91 (m, 5H), 0.88 – 0.72 (m, 4H);  $^{13}\text{C}$  NMR (101 MHz,  $\text{CDCl}_3$ )  $\delta$  157.2 (br), 155.1, 134.0, 133.9, 132.0, 131.0, 129.7, 129.3 (br), 128.9 (br), 128.8 (br), 128.4, 67.1, 36.9, 31.5, 28.5, 26.6, 22.5, 21.7, 14.1;  $^{19}\text{F}$  NMR (376 MHz,  $\text{CDCl}_3$ )  $\delta$  -153.25 (minor,  $^{11}\text{BF}_4$ ), -153.31 (major,  $^{10}\text{BF}_4$ ); FTIR (neat) 2927, 2857, 1621, 1564, 1055, 765, 703  $\text{cm}^{-1}$ ; HRMS (ESI+)  $[\text{M}-\text{BF}_4]^+$  calculated for  $\text{C}_{31}\text{H}_{34}\text{N}$ : 420.2686, found 420.2685.



### 1-(Cyclopropylmethyl)-2,4,6-triphenylpyridin-1-ium tetrafluoroborate (2-100).

Prepared via General Procedure C on a 5.0 mmol scale with commercially available cyclopropylmethanamine (6.0 mmol) to give **2-100** (1.64 g, 71%) as a white solid (mp 178–180  $^{\circ}\text{C}$ ):  $^1\text{H}$  NMR (400 MHz,  $\text{CDCl}_3$ )  $\delta$  7.86 (s, 2H), 7.84 – 7.78 (m, 4H), 7.78 – 7.71 (m, 2H), 7.66 – 7.56 (m, 6H), 7.56 – 7.45 (m, 3H), 4.51 (d,  $J = 6.8$  Hz, 2H), 0.72 – 0.61 (m, 1H), 0.34 – 0.20 (m, 2H), -0.38 (q,  $J = 5.1$  Hz, 2H);  $^{13}\text{C}$  NMR (101 MHz,  $\text{CDCl}_3$ )  $\delta$  157.0, 155.7, 133.9, 133.3, 132.3, 131.2, 129.9, 129.54, 129.46, 128.2, 126.8, 59.2, 10.8, 5.1;  $^{19}\text{F}$  NMR (376 MHz,  $\text{CDCl}_3$ )  $\delta$  -153.2 (minor,  $^{11}\text{BF}_4$ ), -153.3 (major,  $^{10}\text{BF}_4$ ); FTIR (neat) 3064, 1621, 1566, 1057, 703  $\text{cm}^{-1}$ ; HRMS (ESI+)  $[\text{M}-\text{BF}_4]^+$  calculated for  $\text{C}_{27}\text{H}_{24}\text{N}$ : 362.1903, found 362.1898.

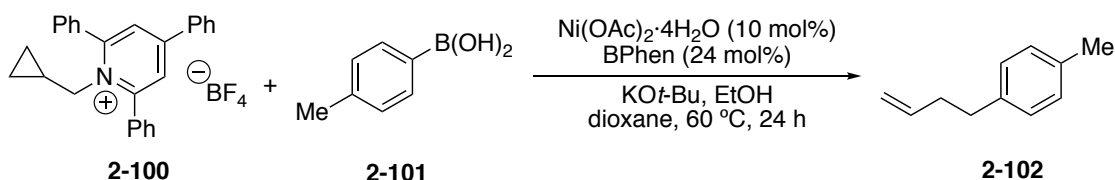
### 2.5.4 Test for Stereospecificity



In a  $\text{N}_2$ -filled glovebox: To an oven-dried 1-dram vial was added  $\text{Ni}(\text{OAc})_2 \cdot 4\text{H}_2\text{O}$  (2.5 mg, 0.01 mmol, 10 mol %) and BPhen (8.0 mg, 0.024 mmol, 24 mol %). To a separate oven-dried 1-dram vial was added  $\text{KO}t\text{-Bu}$  (38 mg, 0.17 mmol, 3.4 equiv), 4-

methoxyphenylboronic acid (46 mg, 0.30 mmol, 3.0 equiv), and pyridinium salt **2-97** (51 mg, 0.10 mmol, 1.0 equiv). Dioxane (250  $\mu$ L) was added to each vial. Each vial was then equipped with a micro stir bar, capped with a pierceable Teflon-coated cap, and removed from the glovebox. To the vial containing the boronic acid, KO*t*-Bu, and pyridinium salt **2-97**, was added EtOH (29  $\mu$ L) via a N<sub>2</sub>-purged syringe. Both mixtures were stirred for 1 h at rt. The catalyst mixture was then transferred to the “activated boronate” and pyridinium salt mixture via a N<sub>2</sub>-purged syringe. Dioxane (500  $\mu$ L total) was used to ensure complete transfer of the catalyst mixture and bring the total concentration of the reaction to 0.1 M. The resulting reaction mixture was stirred vigorously at 60 °C for 24 h. The mixture was diluted with Et<sub>2</sub>O (approx. 1.5 mL) and filtered through a short plug of silica gel. The filter cake was washed with Et<sub>2</sub>O (5 x 1.5 mL), and the resulting solution was concentrated. The yield of the crude product **2-99** was determined to be 54% by <sup>1</sup>H-NMR analysis with 1,3,5-trimethoxybenzene as an internal standard. A small sample of the product was purified via preparatory thin-layer chromatography (10% toluene/hexanes), and the enantiomeric excess was determined to be 0% by chiral HPLC analysis (CHIRALPAK IF, 0.2 mL/min, 100% hexanes,  $\lambda$ =254 nm); t<sub>R</sub> (enantiomer A) = 31.32 min, t<sub>R</sub> (enantiomer B) = 32.85 min.

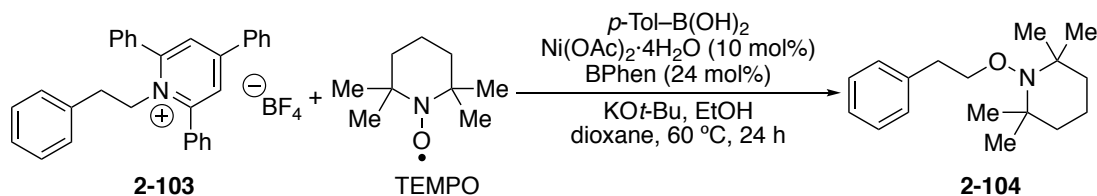
### 2.5.5 Radical Clock Experiment



In a N<sub>2</sub>-filled glovebox: To an oven-dried 1-dram vial was added Ni(OAc)<sub>2</sub>·4H<sub>2</sub>O (2.5 mg, 0.01 mmol, 10 mol %) and BPhen (8.0 mg, 0.024 mmol, 24 mol %). To a separate oven-dried 1-dram vial was added KO*t*-Bu (38 mg, 0.17 mmol, 3.4 equiv), 4-methylphenylboronic acid (41 mg, 0.30 mmol, 3.0 equiv), and pyridinium salt **2-100** (45 mg, 0.10 mmol, 1.0 equiv). Dioxane (250  $\mu$ L) was added to each vial. Each vial

was then equipped with a micro stir bar, capped with a pierceable Teflon-coated cap, and removed from the glovebox. To the vial containing the boronic acid, KO*t*-Bu, and pyridinium salt **2-100**, was added EtOH (29  $\mu$ L) via a N<sub>2</sub>-purged syringe. Both mixtures were stirred for 1 h at rt. The catalyst mixture was then transferred to the “activated boronate” and pyridinium salt mixture via a N<sub>2</sub>-purged syringe. Dioxane (500  $\mu$ L total) was used to ensure complete transfer of the catalyst mixture and bring the total concentration of the reaction to 0.1 M. The resulting reaction mixture was stirred vigorously at 60 °C for 24 h. The mixture was then diluted with Et<sub>2</sub>O (approx. 1.5 mL) and filtered through a short plug of silica gel. The filter cake was washed with Et<sub>2</sub>O (5 x 1.5 mL), and the resulting solution was concentrated. The yield of the crude ring-opened product **2-102** was determined to be 33% by <sup>1</sup>H-NMR analysis with 1,3,5-trimethoxybenzene as an internal standard.

### 2.5.6 Radical Trap Experiment



In a N<sub>2</sub>-filled glovebox: To an oven-dried 1-dram vial was added Ni(OAc)<sub>2</sub>·4H<sub>2</sub>O (2.5 mg, 0.01 mmol, 10 mol %) and BPhen (8.0 mg, 0.024 mmol, 24 mol %). To a separate oven-dried 1-dram vial was added KO*t*-Bu (38 mg, 0.17 mmol, 3.4 equiv), 4-methylphenylboronic acid (41 mg, 0.30 mmol, 3.0 equiv), 2,2,6,6-tetramethylpiperidine-*N*-oxyl (TEMPO; 31 mg, 0.20 mmol, 2.0 equiv), and pyridinium salt **2-103** (50 mg, 0.10 mmol, 1.0 equiv). Dioxane (250  $\mu$ L) was added to each vial. Each vial was then equipped with a micro stir bar, capped with a pierceable Teflon-coated cap, and removed from the glovebox. To the vial containing the boronic acid, KO*t*-Bu, TEMPO, and pyridinium salt **2-103**, was added EtOH (30  $\mu$ L) via a N<sub>2</sub>-purged syringe. Both mixtures were stirred for 1 h at rt. After pre-stirring was

complete, the catalyst mixture was transferred to the “activated boronate” and TEMPO/pyridinium salt mixture via a N<sub>2</sub>-purged syringe. Dioxane (500 μL total) was used to ensure complete transfer of the catalyst mixture and bring the total concentration of the reaction to 0.1 M. The resulting reaction mixture was heated to 60 °C and stirred vigorously for 24 h. The mixture was diluted with Et<sub>2</sub>O (approx. 1.5 mL) and filtered through a short plug of silica gel. The filter cake was washed with Et<sub>2</sub>O (5 x 1.5 mL), and the resulting solution was concentrated. 1,3,5-trimethoxybenzene (7.2 mg, 0.043 mmol, 0.43 equiv) was added as an internal standard. The yield of known TEMPO adduct **2-104**<sup>42</sup> was determined to be 20% by analysis of the <sup>1</sup>H NMR spectrum of the crude reaction mixture. No cross-coupled product was observed.

## REFERENCES

1. Ruiz-Castillo, P.; Buchwald, S. L. *Chem. Rev.* **2016**, *116* (19), 12564-12649.
2. Buszek, K. R.; Brown, N. *Org. Lett.* **2007**, *9* (4), 707-710.
3. Blakey, S.; MacMillan, D. *J. Am. Chem. Soc.* **2003**, *125* (20), 6046-6047.
4. Tobisu, M.; Nakamura, K.; Chatani, N. *J. Am. Chem. Soc.* **2014**, *136* (15), 5587-5590.
5. Shi, S.; Meng, G.; Szostak, M. *Angew. Chem., Int. Ed.* **2016**, *55* (24), 6959-6963.
6. Weires, N. A.; Baker, E. L.; Garg, N. K. *Nat. Chem.* **2016**, *8* (1), 75-79.
7. Li, M.-B.; Tang, X.-L.; Tian, S.-K. *Adv. Synth. Catal.* **2011**, *353* (11-12), 1980-1984.
8. Maity, P.; Shacklady-McAtee, D. M.; Yap, G. P. A.; Sirianni, E. R.; Watson, M. P. *J. Am. Chem. Soc.* **2013**, *135* (1), 280-285.
9. Li, M.-B.; Wang, Y.; Tian, S.-K. *Angew. Chem., Int. Ed.* **2012**, *51*, 2968-2971.
10. Huang, C.-Y.; Doyle, A. G. *J. Am. Chem. Soc.* **2012**, *134*, 9541-9544.
11. Duda, M. L.; Michael, F. E. *J. Am. Chem. Soc.* **2013**, *135* (49), 18347-18349.
12. Jensen, K. L.; Standley, E. A.; Jamison, T. F. *J. Am. Chem. Soc.* **2014**, *136* (31), 11145-11152.
13. Zhou, J. S.; Fu, G. C. *J. Am. Chem. Soc.* **2003**, *125*, 14726-14727.
14. Jones, G. D.; Martin, J. L.; McFarland, C.; Allen, O. R.; Hall, R. E.; Haley, A. D.; Brandon, R. J.; Konovalova, T.; Desrochers, P. J.; Pulay, P.; Vivic, D. A. *J. Am. Chem. Soc.* **2006**, *128* (40), 13175-13183.
15. Cornella, J.; Edwards, J. T.; Qin, T.; Kawamura, S.; Wang, J.; Pan, C. M.; Gianatassio, R.; Schmidt, M.; Eastgate, M. D.; Baran, P. S. *J. Am. Chem. Soc.* **2016**, *138* (7), 2174-7.
16. Sandfort, F.; O'Neill, M. J.; Cornella, J.; Wimmer, L.; Baran, P. S. *Angew. Chem., Int. Ed.* **2017**, *56* (12), 3319-3323.
17. Huihui, K. M.; Caputo, J. A.; Melchor, Z.; Olivares, A. M.; Spiewak, A. M.; Johnson, K. A.; DiBenedetto, T. A.; Kim, S.; Ackerman, L. K.; Weix, D. J. *J. Am. Chem. Soc.* **2016**, *138* (15), 5016-9.
18. Tellis, J. C.; Primer, D. N.; Molander, G. A. *Science* **2014**, *345* (6195), 433-436.
19. Jouffroy, M.; Primer, D. N.; Molander, G. A. *J. Am. Chem. Soc.* **2016**, *138* (2), 475-478.
20. Gutiérrez-Bonet, Á.; Tellis, J. C.; Matsui, J. K.; Vara, B. A.; Molander, G. A. *ACS Catalysis* **2016**, *6* (12), 8004-8008.
21. Zhang, X.; MacMillan, D. W. *J. Am. Chem. Soc.* **2016**, *138*, 13862.
22. Said, S. A.; Fiksdahl, A. *Tetrahedron Asym.* **2001**, *12* (13), 1947-1951.
23. Katrizky, A. R.; Marson, C. M. *Angew. Chem., Int. Ed.* **1984**, *23*, 420-429.

24. Ohshima, T.; Hayashi, Y.; Agura, K.; Fujii, Y.; Yoshiyama, A.; Mashima, K. *Chem. Commun.* **2012**, 48 (44), 5434-6.
25. Kato, S.; Morie, T.; Yoshida, N. *Chem. Pharm. Bull.* **1995**, 43 (4), 699-702.
26. Roth, B. D. Trans-6-[2-(3- or 4-carboxamido-substituted pyrrol-1-yl)alkyl]-4-hydroxypyran-2-one Inhibitors of Cholesterol Synthesis. US 4,681,893, 1987.
27. Katritzky, A. R.; De Ville, G.; Patel, R. C. *Tetrahedron* **1981**, 37, 25-30.
28. Schley, N. D.; Fu, G. C. *J. Am. Chem. Soc.* **2014**, 136 (47), 16588-16593.
29. Basch, C. H.; Liao, J.; Xu, J.; Piane, J. J.; Watson, M. P. *J. Am. Chem. Soc.* **2017**, 139 (15), 5313-5316.
30. Pangborn, A. B.; Giardello, M. A.; Grubbs, R. H.; Rosen, R. K.; Timmers, F. J. *Organometallics* **1996**, 15 (5), 1518-1520.
31. Ghorai, S. K.; Jin, M.; Hatakeyama, T.; Nakamura, M. *Org. Lett.* **2012**, 14 (4), 1066-1069.
32. Jin, L.; Zhao, Y.; Zhu, L.; Zhang, H.; Lei, A. *Adv. Synth. Catal.* **2009**, 351 (4), 630-634.
33. St. Denis, J. D.; Scully, C. C. G.; Lee, C. F.; Yudin, A. K. *Org. Lett.* **2014**, 16 (5), 1338-1341.
34. Krasovskiy, A.; Duplais, C.; Lipshutz, B. H. *J. Am. Chem. Soc.* **2009**, 131 (43), 15592-15593.
35. Patel, N. R.; Molander, G. A. *J. Org. Chem.* **2016**, 81 (16), 7271-7275.
36. Godt, A.; Ünsal, Ö.; Roos, M. *J. Org. Chem.* **2000**, 65 (9), 2837-2842.
37. Molander, G. A.; Argintaru, O. A.; Aron, I.; Dreher, S. D. *Org. Lett.* **2010**, 12 (24), 5783-5785.
38. Toumi, M.; Couty, F.; Evano, G. *J. Org. Chem.* **2008**, 73 (4), 1270-1281.
39. Bagley, M. C.; Dwyer, J. E.; Molina, M. D. B.; Rand, A. W.; Rand, H. L.; Tomkinson, N. C. O. *Org. Biomol. Chem.* **2015**, 13 (24), 6814-6824.
40. Fekner, T.; Li, X.; Lee, M. M.; Chan, M. K. *Angew. Chem. Int. Ed.* **2009**, 48 (9), 1633-1635.
41. Padwa, A.; Rashatasakhon, P.; Ozdemir, A. D.; Willis, J. *J. Org. Chem.* **2005**, 70 (2), 519-528.
42. Thuy-Boun, P. S.; Villa, G.; Dang, D.; Richardson, P.; Su, S.; Yu, J.-Q. *J. Am. Chem. Soc.* **2013**, 135 (46), 17508-17513.

## Chapter 3

### NICKEL-CATALYZED NEGISHI CROSS-COUPPLINGS OF ALKYL PYRIDINIUM SALTS AND ALKYL ZINC HALIDES

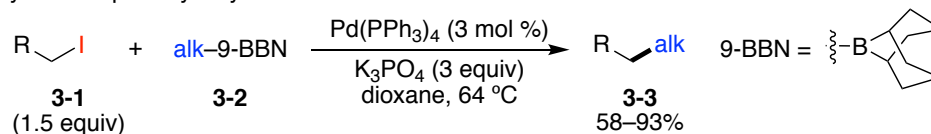
#### 3.1 Introduction

The prevalence of  $C_{sp^3}$ - $C_{sp^3}$  bonds in bioactive molecules has led to intense research efforts aimed at developing novel methods to form them. With the advent of transition metal-catalyzed cross-coupling reactions, the construction of these bonds has become significantly more facile. In contrast to the cross-coupling of  $C_{sp^3}$ -electrophiles with  $C_{sp^2}$ -hybridized carbon nucleophiles, alkyl-alkyl bond formation suffers from increased rates of  $\beta$ -hydride elimination. Thus, until the pioneering work by Fu in the early 2000's,  $C_{sp^3}$ - $C_{sp^3}$  bond formation had been restricted to couplings with primary alkyl electrophiles. Early studies by Kharasch,<sup>1</sup> Noller, Tamura, and Kochi on the cobalt-,<sup>1</sup> silver-,<sup>2</sup> and copper-catalyzed<sup>3,4</sup> cross-couplings of Grignard reagents and alkyl halides laid the groundwork for the contemporary palladium- and nickel-catalyzed methods developed by Suzuki, Knochel, Kambe, and Fu. The palladium- and nickel-catalyzed methods are detailed below.

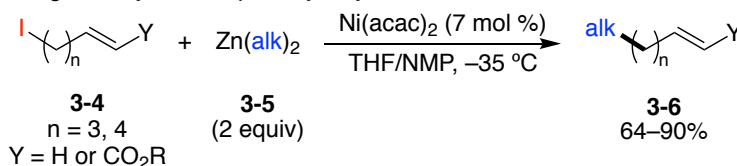
As an extension of their pioneering work in the field of  $C_{sp^2}$ - $C_{sp^2}$  cross-couplings, Suzuki and coworkers demonstrated the first, general transition metal-catalyzed alkyl-alkyl cross-coupling reaction.<sup>5</sup> They found that alkyl 9-borabicyclo(3.3.1)nonane (9-BBN) reagents were effective transmetalating agents in a  $Pd(OAc)_2/PCy_3$ -catalyzed cross-coupling with primary alkyl iodides (Figure 3.1A). Building on this groundbreaking work, Knochel reported that alkyl iodides bearing a

distal alkene could also be cross-coupled in very good yields (Figure 3.1B).<sup>6</sup> His group employed dialkyl zinc reagents as the nucleophilic coupling partner and Ni(acac)<sub>2</sub> as the catalyst. Interestingly, a tethered alkene was necessary for promoting the desired coupling through an intramolecular coordination, which they proposed would lead to a more electron-deficient Ni-center and therefore faster reductive elimination. Without this internal coordination of the alkene to the metal center, side-reactions such as zinc-bromide exchange became problematic. Another important advancement in the field of alkyl-alkyl cross-coupling was made by Kambe. In his seminal publication, he described the nickel-catalyzed Kumada-Corriu cross-coupling of primary alkyl bromides and tosylates with alkyl Grignard reagents.<sup>7</sup> With low NiCl<sub>2</sub> loadings (1–3 mol %), a number of linear alkyl electrophiles were smoothly cross-coupled with both primary and secondary Grignard reagents (Figure 3.1C). The crucial 1,3-butadiene additive was proposed to react with a reduced Ni<sup>0</sup> species to form a bis- $\pi$ -allyl Ni(II) complex. This complex would then react with an equivalent of alkyl Grignard reagent to generate a nickelate intermediate (**3-9**) that would be primed for facile oxidative addition with the alkyl electrophile, followed by subsequent reductive elimination.

A. Suzuki's alkylation of primary alkyl iodides



B. Knochel's Negishi alkylation of primary alkyl iodides



C. Kambe's Kumada alkylation of primary alkyl bromides and tosylates

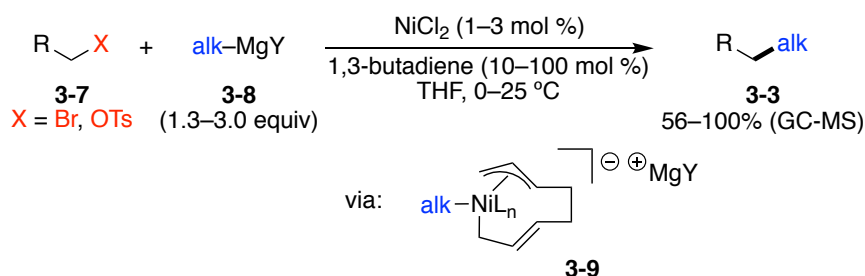


Figure 3.1 First, general metal-catalyzed cross-couplings to form alkyl-alkyl bonds

Prior to 2003, alkyl-alkyl cross-couplings of  $sp^3$ -hybridized carbon nucleophiles had been limited to the use of primary alkyl electrophiles. It was not until nearly a decade after Knochel's findings that Fu and coworkers disclosed their Negishi cross-coupling of secondary alkyl bromides with alkyl zinc halides (Figure 3.2).<sup>8</sup> This pivotal finding was the first to demonstrate that higher order alkyl electrophiles could be cross-coupled. The major advancement that contributed to their success in developing this previously elusive reaction was the use of the tridentate, redox-non-innocent <sup>s</sup>Bu-Pybox ligand. The multidentate binding ability of the ligand led to the suppression of notoriously problematic  $\beta$ -hydride elimination pathways. Additionally, the redox-active nature of the ligand contributed to significant stabilization of the odd-electron oxidation states of the metal center via metal-to-ligand charge transfer

(MLCT). Consequentially, the oxidative addition was proposed to proceed through a single-electron transfer (SET) process rather than the slower, two-electron alternative.

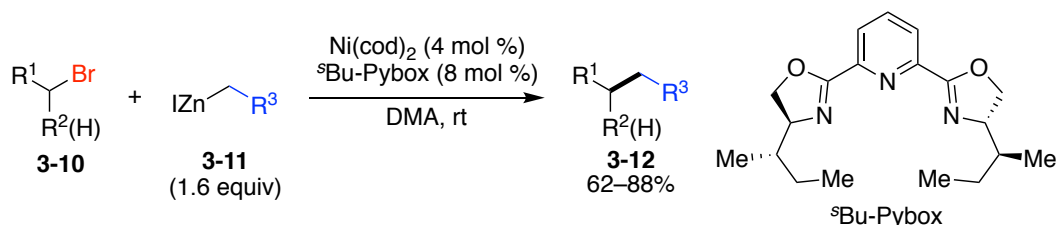


Figure 3.2 Fu's seminal publication on the cross-coupling of 2° alkyl bromides

Subsequent to this pivotal communication, Fu and others have greatly expanded the scope of alkyl-alkyl cross-couplings in both nucleophile and electrophile. Arguably, two of the most important advances in this field have been the development of enantioselective reaction variants and the inclusion of tertiary alkyl electrophiles as competent coupling partners.

The Negishi cross-coupling in particular, which utilizes alkylzinc halides or dialkylzincs as the nucleophilic coupling partner, is a highly reliable method for the construction of C<sub>sp3</sub>-C<sub>sp3</sub> bonds. Although organozinc compounds suffer from air and moisture sensitivity, they are easily prepared using standard inert-atmosphere techniques.<sup>9,10</sup> Additionally, their high degree of nucleophilicity makes them excellent transmetalating agents. Relative to alkyl lithium and alkyl magnesium reagents, organozinc halides display much broader functional group tolerance, even at non-cryogenic temperatures. Notably, alkyl boronate derivatives are superior to organozinc reagents in regard to this functional group compatibility; however, the vast majority of traditional alkyl-alkyl cross-couplings require the use of air- and moisture-sensitive 9-



electronically activated benzylic systems or ring-strained aziridinyl systems). Doyle has reported an efficient nickel-catalyzed cross-coupling of styrenyl aziridines (**3-15**) with alkyl zinc bromides (Figure 3.4A).<sup>12</sup> Notably, the ring-opening occurs via C–N bond activation at the benzylic carbon to deliver protected primary amines (**3-17**). Similarly, Jamison has developed a nickel-catalyzed cross-coupling of alkyl aziridines (**3-18**) with alkyl zinc bromides (Figure 3.4B).<sup>13</sup> In contrast to Doyle’s work, this catalytic system delivers products (**3-20**) of ring-opening at the terminal carbon.

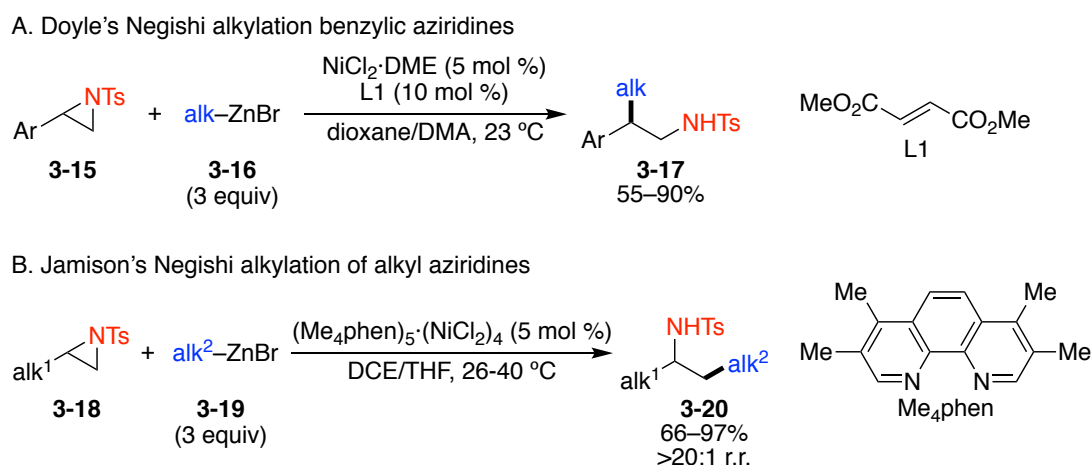


Figure 3.4 Nickel-catalyzed C–N activation of aziridinyl electrophiles

A much less developed method for the construction of alkyl-alkyl bonds is cross-electrophile coupling, or reductive coupling. To avoid chemoselectivity issues, the majority of cross-electrophile couplings involve the coupling of an C<sub>sp2</sub> electrophile with a C<sub>sp3</sub> electrophile. To that end, the Gong group developed the first, general alkyl-alkyl reductive coupling. He showed that a variety of primary and secondary alkyl halides (e.g., bromides or iodides) can be cross-coupled with other

primary and secondary alkyl electrophiles (e.g. bromides, iodides, or tosylates) using bis(pinacolato)diboron ( $B_2pin_2$ ) as the reductant (Figure 3.5).<sup>14</sup> In general, moderate to good yields of cross-coupled product (**3-23**) were obtained (36–86%); however low yields were observed for cross-couplings involving two secondary alkyl electrophiles. A similar approach to alkyl-alkyl cross-couplings was taken by the Lei group in 2014. They disclosed an elegant copper-catalyzed, cross-electrophile coupling of alkyl tosylates or mesylates with alkyl bromides.<sup>15</sup> This work will be discussed in more detail in Chapter 4 (see Figure 4.6B).

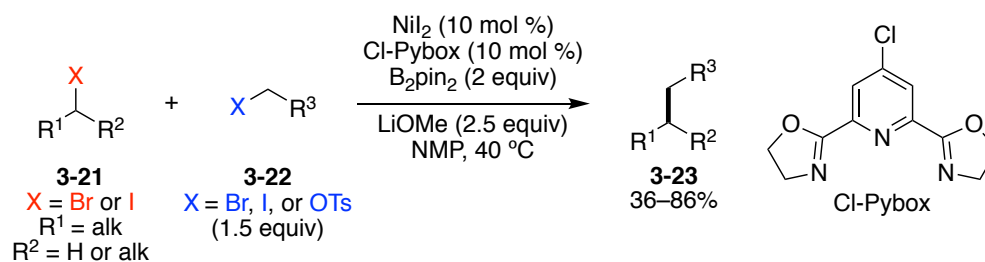


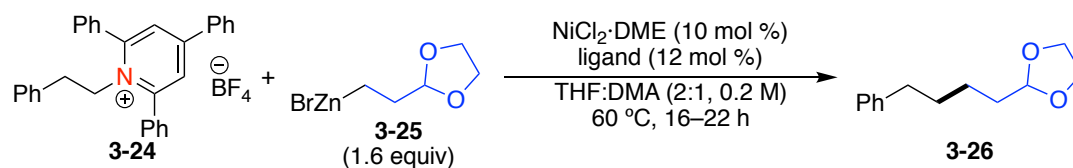
Figure 3.5 Gong's cross-electrophile coupling to form alkyl–alkyl bonds

Although the field of alkyl-alkyl cross-couplings has advanced considerably over the past several decades, all of the methods thus far have utilized alkyl halides, pseudohalides, azirdines, or redox-active esters as the electrophilic coupling partners. Aside from the cross-couplings of azirdines discussed above, the C–N activation of amine derivatives with unactivated alkyl groups has yet to be disclosed. With an opportunity to address this synthetic limitation and expand the utility of our alkyl pyridinium salts, I initiated the development of a Negishi cross-coupling to convert primary amines into alkyl groups.

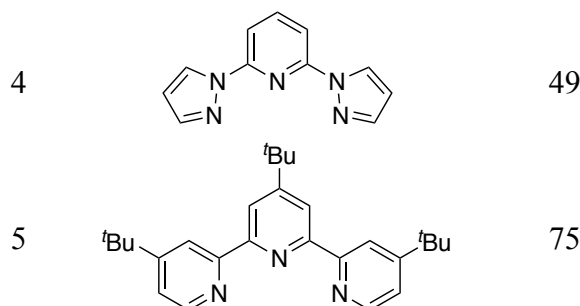
### 3.2 Results and Discussion

Alkyl zinc halides, as opposed to dialkyl zinc reagents, were chosen as the nucleophilic coupling partner due to their higher functional group tolerance and ease of handling. I began the optimization by screening a variety of redox-active, non-innocent bipyridine and phenanthroline ligands. All the bidentate ligands tried resulted in low, but promising yields of the cross-coupled product (Table 3.1, entries 1–3). Switching to tridentate ligands, however, led to a significant yield improvement, with 2,6-bis(*N*-pyrazolyl)pyridine (bpp) and 4,4',4''-tri-*tert*-butyl terpyridine (ttbtpy) leading to a 49% and 75% yield, respectively (entries 4 and 5). This observation is in accordance with recent mechanistic findings by the Vicic group on the nickel-catalyzed cross-couplings of alkyl halides with alkyl zinc reagents.<sup>16</sup>

Table 3.1 Ligand optimization



entry	ligand	yield (%) <sup>a</sup>
1		14
2		17
3		15

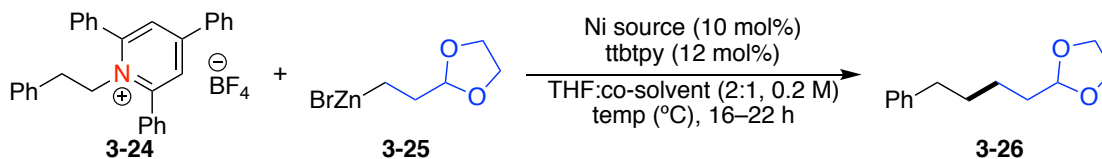


<sup>a</sup> **3-24** (1 equiv), **3-25** (1.6 equiv), NiCl<sub>2</sub>·DME (10 mol %), ligand (12 mol %), THF:DMA (2:1, 0.2 M), 60 °C, 24 h. Yields based on <sup>1</sup>H NMR analysis with 1,3,5-trimethoxybenzene as an internal standard.

The addition of a polar cosolvent led to the discovery that good yields could be obtained with dimethylacetamide (DMA) at room temperature (Table 3.2, entries 1–3). A slightly higher yield was observed at 60 °C (entry 4). Increasing the equivalents of organozinc halide from 1.4 to 1.6 further improved the yield (entry 5); however, using more than 1.6 equivalents led to a decrease in the amount of product formed (not shown).

With the help of my colleague Shane Plunkett, the final optimized conditions for the cross-coupling of primary alkyl pyridinium salts were identified. In an effort to maximize the practicality of the transformation, less expensive Ni<sup>II</sup> sources and lower catalyst loadings were screened. Although NiCl<sub>2</sub>·6H<sub>2</sub>O was ineffective (entry 6), inexpensive Ni(acac)<sub>2</sub>·xH<sub>2</sub>O was identified as a competent precatalyst, leading to slightly higher yields of the desired product compared to NiCl<sub>2</sub>·DME (entry 7). Lowering the Ni(acac)<sub>2</sub>·xH<sub>2</sub>O and bpp loading to 5 and 6 mol %, respectively, furnished a similar yield (entry 8). Control experiments confirmed that this reaction is catalytic in both nickel and ligand.

Table 3.2 Optimization of the Negishi coupling of 1° alkyl pyridinium salts



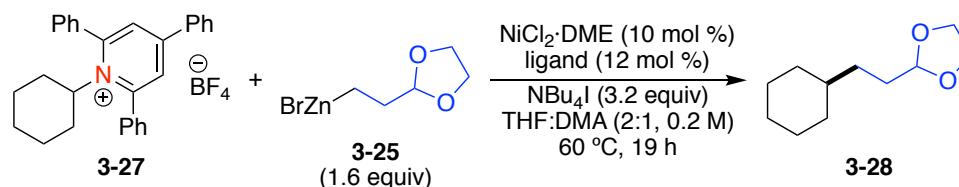
entry	Ni source	temp (°C)	cosolvent	RZnX equiv	yield (%) <sup>a</sup>
1 <sup>b</sup>	NiCl <sub>2</sub> ·DME	23	NMP	1.2	46
2 <sup>b</sup>	NiCl <sub>2</sub> ·DME	23	DMA	1.2	57
3 <sup>b</sup>	NiCl <sub>2</sub> ·DME	23	DMA	1.4	64
4	NiCl <sub>2</sub> ·DME	60	DMA	1.4	68
5	NiCl <sub>2</sub> ·DME	60	DMA	1.6	75
6	NiCl <sub>2</sub> ·6H <sub>2</sub> O	60	DMA	1.6	20
7	Ni(acac) <sub>2</sub> ·xH <sub>2</sub> O	60	DMA	1.6	81
8 <sup>c</sup>	Ni(acac) <sub>2</sub> ·xH <sub>2</sub> O	60	DMA	1.6	80
9	none	60	DMA	1.6	3
10 <sup>d</sup>	Ni(acac) <sub>2</sub> ·xH <sub>2</sub> O	60	DMA	1.6	9

<sup>a</sup> **3-24** (1 equiv), **3-25** (1.6 equiv), Ni source (10 mol %), ttbtpy (12 mol %), THF:DMA (2:1, 0.2 M), 16–22 h. Yields based on <sup>1</sup>H NMR analysis with 1,3,5-trimethoxybenzene as an internal standard. Ni source, ttbtpy, and **3-24** were pre-stirred for 20 min prior to addition of the alkyl zinc halide. <sup>b</sup> 4:1 THF:cosolvent used. <sup>c</sup> 5 mol% Ni(acac)<sub>2</sub>·xH<sub>2</sub>O and 6 mol % ttbtpy used. <sup>d</sup> Without ligand.

With optimized conditions in hand for the cross-coupling of primary alkyl pyridinium salts, we then turned our attention to the coupling of secondary systems. Unfortunately, low yield of the desired product (**3-28**) was observed (Table 3.3, entry 1). However, upon screening a number of other bidentate and tridentate ligands, we

found that the readily accessible bpp ligand promoted the coupling of secondary alkyl pyridinium salts and primary organozinc halides in very good yield (entries 2–5).<sup>17</sup>

Table 3.3 Ligand optimization for secondary alkyl pyridinium salt cross-coupling



entry	ligand	yield (%) <sup>a</sup>
1		18
2		68
3		83
4		34
5		33

<sup>a</sup> **3-27** (1 equiv), **3-25** (1.6 equiv),  $\text{NiCl}_2 \cdot \text{DME}$  (10 mol %), ligand (12 mol %),  $\text{NBu}_4\text{I}$  (3.2 equiv), THF:DMA (2:1, 0.2 M), 60 °C, 19 h. Yields based on <sup>1</sup>H NMR analysis with 1,3,5-trimethoxybenzene as an internal standard.

In contrast to primary organozinc reagents, secondary and tertiary alkylzinc halides proved vastly inferior in yielding cross-coupled product under both sets of optimized reaction conditions. We have identified that the formation of 4-addition product **3-32**, presumably arising from conjugate-addition to the pyridinium ring, is outcompeting the desired coupling (Figure 3.6). Despite preliminary attempts to suppress this undesired pathway, we currently have not identified conditions that are amenable to the coupling of these more electron-rich and sterically encumbered organozinc reagents.

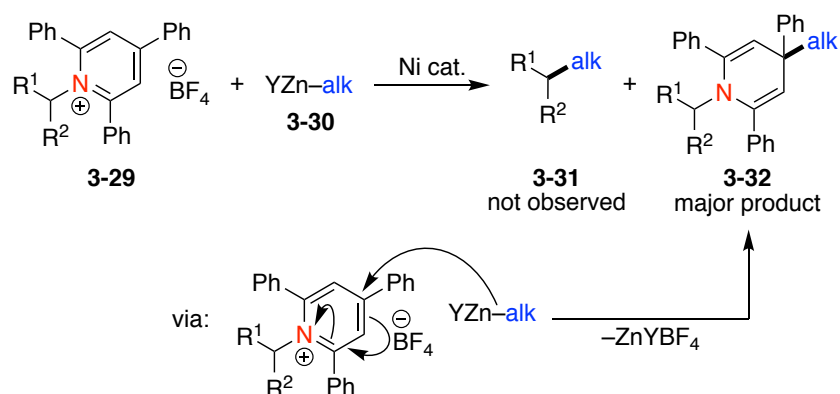
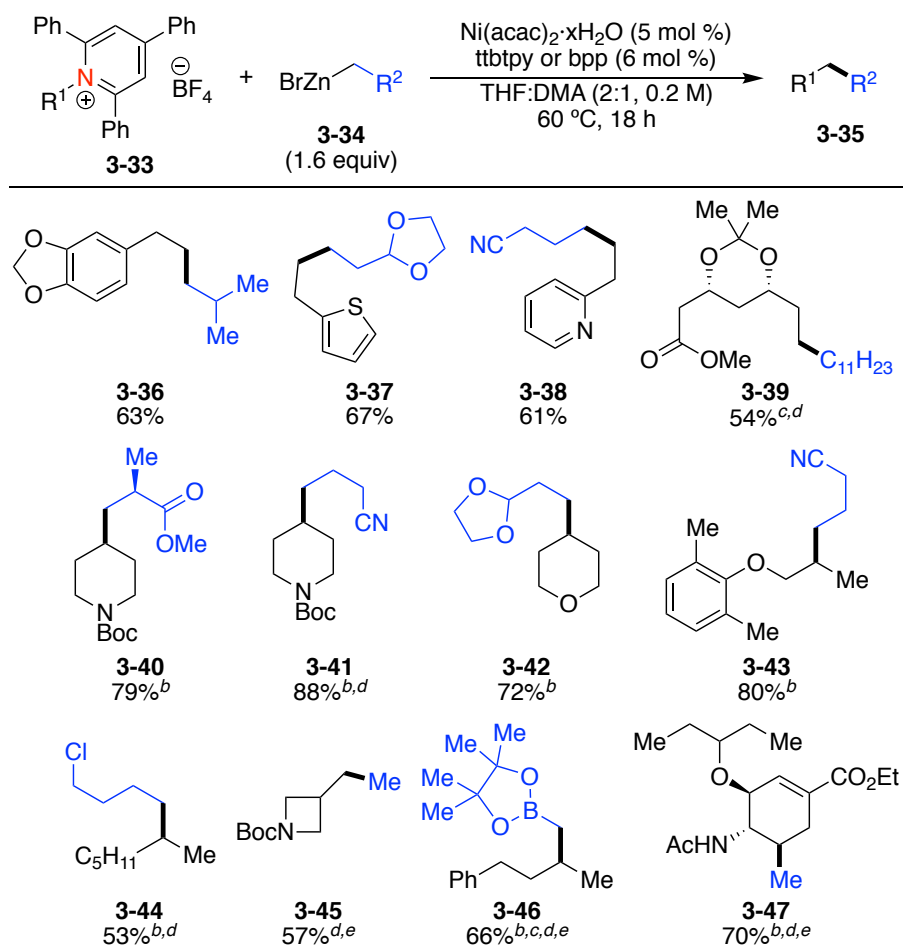


Figure 3.6 Competitive side-reaction in the coupling of secondary and tertiary alkyl zinc halides

Under the two sets of conditions identified, a preliminary scope has been examined (Figure 3.7). Primary alkyl pyridinium salts bearing dioxolane (**3-36**), thiophene (**3-37**), or pyridine (**3-38**) functionality are well tolerated. The amine intermediate used in the synthesis of the cholesterol-lowering drug atorvastatin (Lipitor<sup>®</sup>, Pfizer) was cross-coupled in synthetically useful yield with the linear undecylzinc bromide (**3-39**). Secondary alkyl pyridinium salts such as the medicinally

relevant 4-Boc-piperidine (**3-40** and **3-41**) and 4-pyranyl (**3-42**) also couple smoothly. Moreover, the anti-arrhythmic drug Mexiletine also couples efficiently, as demonstrated by **3-43**. Coupling of the 2-heptyl pyridinium salt with 4-chlorobutyl zinc bromide delivers the alkyl chloride product (**3-44**) in synthetically useful yield. Interestingly, the azetidiny pyridinium salt couples well with methylzinc iodide in the presence of tetrabutylammonium iodide (NBu<sub>4</sub>I) (**3-45**). Synthetically useful  $\alpha$ -methylpinacolboronate ( $-\text{CH}_2\text{Bpin}$ ) groups can also be installed (**3-46**) using the corresponding  $\alpha$ -methylpinacolboronate zinc bromide. Excitingly, the pyridinium salt of oseltamivir (Tamiflu<sup>®</sup>, Roche) couples well in 70% yield with methylzinc iodide in the presence of NBu<sub>4</sub>I (**3-47**).



<sup>a</sup> **3-33** (1.0 mmol), **3-34** (1.6 equiv), Ni(acac)<sub>2</sub>·xH<sub>2</sub>O (5 mol %), ttbtpy (6 mol %), THF/DMA (0.2 M), 60 °C, 18 h. Average isolated yields (±5%) from duplicate experiments. <sup>b</sup> Bpp (6 mol%) used instead of ttbtpy. <sup>c</sup> Organozinc bromide was prepared in DMA therefore THF was not used in the reaction. <sup>d</sup> Single experiment. <sup>e</sup> NBU<sub>4</sub>I (3.2 equiv) added.

Figure 3.7 Preliminary scope of the Negishi alkylation of alkyl pyridinium salts

Although mechanistic studies on this particular reaction have not been conducted thus far, the redox-active nature of the ttbtpy and bpp ligands suggests that a Ni<sup>I/III</sup> catalytic cycle is operative. We propose that a low-valent Ni<sup>I</sup> species (**A**) undergoes transmetalation with alkyl zinc halide **3-30** to produce alkyl Ni<sup>I</sup>

intermediate **B** (Figure 3.8). Single-electron transfer from electron-rich nickel species **B** to alkyl pyridinium salt **3-48** would induce formation of Ni<sup>II</sup> intermediate **C** and alkyl radical **E** via decomposition of the neutral pyridyl radical **D**. Rapid recombination of **C** and **E** would provide dialkyl Ni<sup>III</sup> species **F**. This electron-deficient Ni-intermediate would then undergo a facile reductive elimination to generate product **3-31** and complete the catalytic cycle. Like the Suzuki arylation of alkyl pyridinium salts, we cannot, at this time, rule out the possibility that a radical-chain bimetallic catalytic cycle is operating under our optimized conditions. Future mechanistic studies will investigate these possibilities. We will also continue to study the formation of the major byproduct observed with secondary and tertiary alkyl zinc halides, 4-addition adduct **3-32**. Interestingly, this reaction occurs readily in the absence of catalyst.

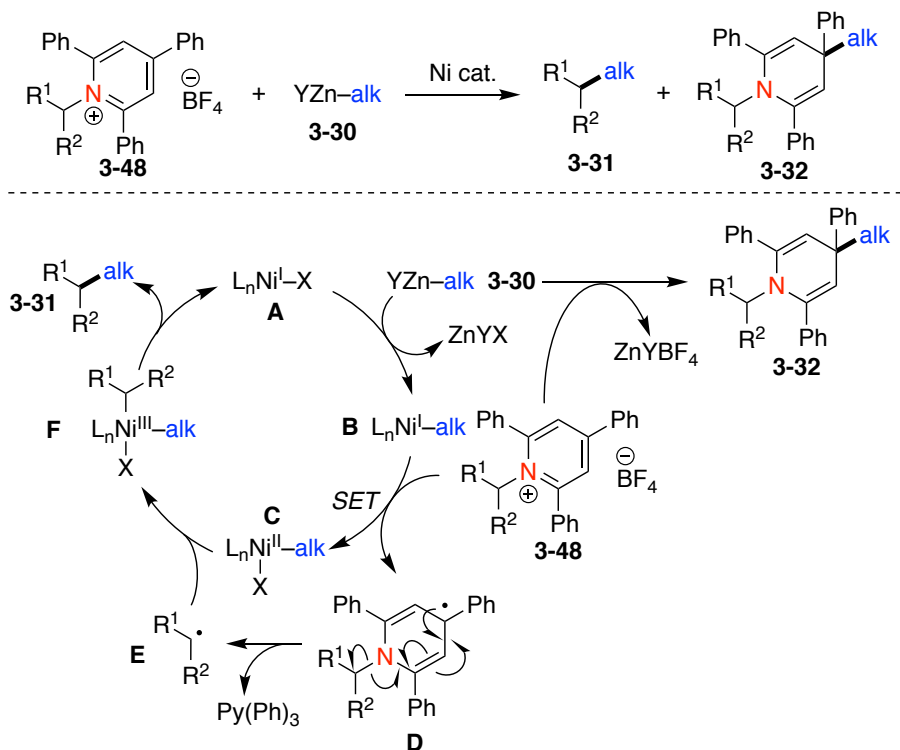


Figure 3.8 Plausible catalytic cycle of the Negishi cross-coupling

### 3.3 Conclusion

In summary, I have described our efforts toward a C<sub>sp3</sub>-C<sub>sp3</sub> cross-coupling of alkyl pyridinium salts and alkyl zinc halides. The reaction displays broad functional group tolerance in both coupling partners and is amenable to late-stage functionalization of medically relevant compounds and intermediates. Moreover, with a simple ligand switch, both primary and secondary alkyl pyridinium salts are smoothly converted to the hydrocarbon products. Based on the identities of the optimal ligands and the mechanistic experiments described in the Suzuki-Miyaura arylation of these salts (see Ch. 2), we hypothesize that the reaction proceeds through a Ni<sup>I/III</sup> catalytic cycle. However, future mechanistic studies are necessary to support this hypothesis.

## 3.4 Experimental

### 3.4.1 Optimization

In a N<sub>2</sub>-filled glovebox: To a 1-dram vial was added Ni<sup>II</sup> salt, ligand, and pyridinium salt followed by solvent. A micro stir bar was added to the vial and the mixture was stirred vigorously for 5–10 min, until a homogeneous solution was obtained. To this solution was added alkyl zinc halide (commercial bottles: 0.5 M in THF, if home-made: ~ 0.5–0.7 M in DMA). in one portion. The vial was sealed with a Teflon-coated screw cap and removed from the glovebox. The reaction mixture was stirred at the designated temperature in a heating block for 16 – 24 h. The reaction was removed from the heating block and allowed to cool to room temperature. The mixture was diluted with Et<sub>2</sub>O (~ 1.5 mL) and filtered through a short plug of silica gel. The filter cake was washed with Et<sub>2</sub>O (5 x 1.5 mL), and the resulting solution was concentrated. 1,3,5-trimethoxybenzene (5 – 15 mg) was added as an internal standard. The yield of the product was determined by analysis of the <sup>1</sup>H NMR spectrum of the crude reaction mixture.

### 3.4.2 Negishi Cross-Coupling of Alkyl Pyridinium Salts

To an oven-dried, 25-mL Schlenk flask equipped with a stir bar, was added Ni(acac)<sub>2</sub>·xH<sub>2</sub>O (13 mg, 0.05 mmol, 5 mol %), 4,4'-4''-tri-*tert*-butyl-2,2':6',2''-terpyridine (ttbtpy, 24 mg, 0.06 mmol, 6 mol %), alkyl pyridinium salt (1.0 mmol, 1.0 equiv), and if required (as noted), NBu<sub>4</sub>I (1.18 g, 3.2 mmol, 3.2 equiv). The flask was fitted with a rubber septum and then evacuated and purged with N<sub>2</sub> (x 3). DMA (Ar purged, anhydrous, 1.8 mL) was added to the flask, and the resulting mixture was stirred for ~15 min at 60 °C (Note: If using a home-made solution of alkyl zinc halide, prepared via Huo's method,<sup>10</sup> the volume of DMA is adjusted, based on the

concentration of alkyl zinc halide, such that the total concentration of alkyl pyridinium salt is 0.2 M after addition of the alkyl zinc halide). Alkyl zinc halide (0.5 M in THF, 3.2 mL, 1.6 mmol, 1.6 equiv) was added, bringing the total concentration of alkyl pyridinium salt to 0.2 M. The reaction was stirred at 60 °C for 18 h. The mixture was allowed to cool to room temperature. EtOAc (10 mL) was added. The mixture was stirred for 2–5 min, and then filtered through a small plug of silica gel. The filter cake was washed with EtOAc (3 x 20 mL), and the resulting solution was washed with brine (4 x 50 mL). The combined aqueous layers were then extracted with EtOAc (3 x 50 mL). The combined organic layers were dried with MgSO<sub>4</sub>, filtered, and concentrated. The cross-coupled product was then purified via silica gel chromatography.

## REFERENCES

1. Kharasch, M. S.; Hambling, J. K.; Rudy, T. P. *J. Org. Chem.* **1959**, *24* (3), 303-305.
2. Kochi, J. K.; Tamura, M. *J. Am. Chem. Soc.* **1971**, *93* (6), 1483-1485.
3. Kochi, J. K.; Tamura, M. *J. Am. Chem. Soc.* **1971**, *93* (6), 1485-1487.
4. Parker, V. D.; Noller, C. R. *J. Am. Chem. Soc.* **1964**, *86* (6), 1112-1116.
5. Tatsuo, I.; Shigeru, A.; Norio, M.; Akira, S. *Chem. Lett.* **1992**, *21* (4), 691-694.
6. Devasagayaraj, A.; Stüdemann, T.; Knochel, P. *Angew. Chem., Int. Ed.* **1996**, *34* (23-24), 2723-2725.
7. Terao, J.; Watanabe, H.; Ikumi, A.; Kuniyasu, H.; Kambe, N. *J. Am. Chem. Soc.* **2002**, *124* (16), 4222-4223.
8. Zhou, J. S.; Fu, G. C. *J. Am. Chem. Soc.* **2003**, *125*, 14726-14727.
9. Zhu, L.; Wehmeyer, R. M.; Rieke, R. D. *J. Org. Chem.* **1991**, *56* (4), 1445-1453.
10. Huo, S. *Org. Lett.* **2003**, *5* (4), 423-425.
11. Cornella, J.; Edwards, J. T.; Qin, T.; Kawamura, S.; Wang, J.; Pan, C. M.; Gianatassio, R.; Schmidt, M.; Eastgate, M. D.; Baran, P. S. *J. Am. Chem. Soc.* **2016**, *138* (7), 2174-7.
12. Huang, C.-Y.; Doyle, A. G. *J. Am. Chem. Soc.* **2012**, *134*, 9541-9544.
13. Jensen, K. L.; Standley, E. A.; Jamison, T. F. *J. Am. Chem. Soc.* **2014**, *136* (31), 11145-11152.
14. Wang, S.; Qian, Q.; Gong, H. *Org. Lett.* **2012**, *14* (13), 3352-3355.
15. Liu, J.-H.; Yang, C.-T.; Lu, X.-Y.; Zhang, Z.-Q.; Xu, L.; Cui, M.; Lu, X.; Xiao, B.; Fu, Y.; Liu, L. *Chem. Eur. J.* **2014**, *20* (47), 15334-15338.
16. Jones, G. D.; Martin, J. L.; McFarland, C.; Allen, O. R.; Hall, R. E.; Haley, A. D.; Brandon, R. J.; Konovalova, T.; Desrochers, P. J.; Pulay, P.; Vivic, D. A. *J. Am. Chem. Soc.* **2006**, *128* (40), 13175-13183.
17. Arendt, K. M.; Doyle, A. G. *Angew. Chem., Int. Ed.* **2015**, *54* (34), 9876-9880.

## Chapter 4

### NICKEL-CATALYZED CROSS-ELECTROPHILE COUPLINGS OF ALKYL PYRIDINIUM SALTS AND ARYL HALIDES

#### 4.1 Introduction

Within the past decade, metal-catalyzed cross-electrophile couplings have emerged as promising and robust methods for the construction of carbon-carbon bonds.<sup>1</sup> Also known as reductive couplings, they offer several advantages over traditional cross-couplings (Figure 4.1). Although extremely well established, methods that employ nucleophilic coupling partners, such as the Negishi coupling with organozinc halides or Kumada-Corriu coupling with Grignard reagents, place limitations on functional group compatibility due to their high nucleophilicity and/or basicity. In contrast, cross-electrophile couplings generally operate under neutral conditions and therefore allow the presence of base- and acid-sensitive groups within the organic framework of either coupling partner. Furthermore, not only are aryl halides more air- and moisture-stable and abundant than aryl metal species, they often serve as precursors to many aryl nucleophiles. Thus, using an aryl halide circumvents the need to pre-form the aryl nucleophile. However, despite these advantages, the reactivity patterns of reductive couplings are somewhat more difficult to control. In a traditional cross-coupling, the stark difference in reactivity between the nucleophile and electrophile dictates the overall chemoselectivity in the reaction. Because reductive cross-couplings must merge two electrophiles, the selectivity is almost entirely reliant on the redox cycle of the catalyst. To mitigate this issue, electrophiles

are often chosen such that they can be electronically or sterically differentiated by the catalyst (e.g., alkyl halide vs aryl halide) throughout the course of the catalytic cycle. Moreover, because a nucleophile is not involved, a stoichiometric reductant is required to mediate the electronic states of the catalyst. Commonly, a metal such as  $\text{Zn}^0$  or  $\text{Mn}^0$  is used to fulfill this role; however organic reductants have also been utilized, although to a lesser extent.

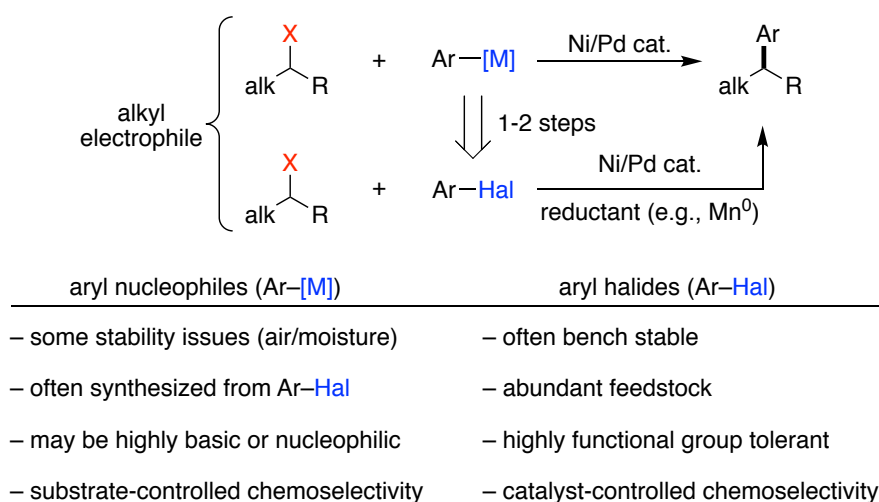


Figure 4.1 Comparison of aryl nucleophiles and aryl halides as coupling partners

It has been proposed<sup>2</sup> that reductive couplings proceed through a radical-chain bimetallic pathway in which an electron-rich, low-valent  $\text{Ni}^0$  species (**A**) can undergo a two-electron oxidative addition into the aryl electrophile (**B**) (Figure 4.2). Owing to the faster rate of two-electron oxidative addition into a  $\text{C}_{\text{sp}2}\text{-X}$  bond relative to a  $\text{C}_{\text{sp}3}\text{-X}$  bond, this is the first selective step in the cycle. The resultant  $\text{Ni}^{\text{II}}$  species **C** can then combine with an alkyl radical, **I**, to generate  $\text{Ni}^{\text{III}}$  species **D**. Subsequent reductive elimination affords the cross-coupled product, **E**, as well as a  $\text{Ni}^{\text{I}}$  intermediate (**F**).

Single-electron transfer (SET) can then occur between **F** and the alkyl electrophile (**G**) to generate another equivalent of alkyl radical and a Ni<sup>II</sup> species (**H**). Notably, this accounts for the second selective step in the cycle, such that the generation of an alkyl radical (from C<sub>sp3</sub>-X) is much more facile than the generation of an aryl radical (C<sub>sp2</sub>-X). A reduction of this Ni<sup>II</sup> intermediate by the stoichiometric metal additive (i.e., Zn<sup>0</sup> or Mn<sup>0</sup>) regenerates the active Ni<sup>0</sup> catalyst (**A**).

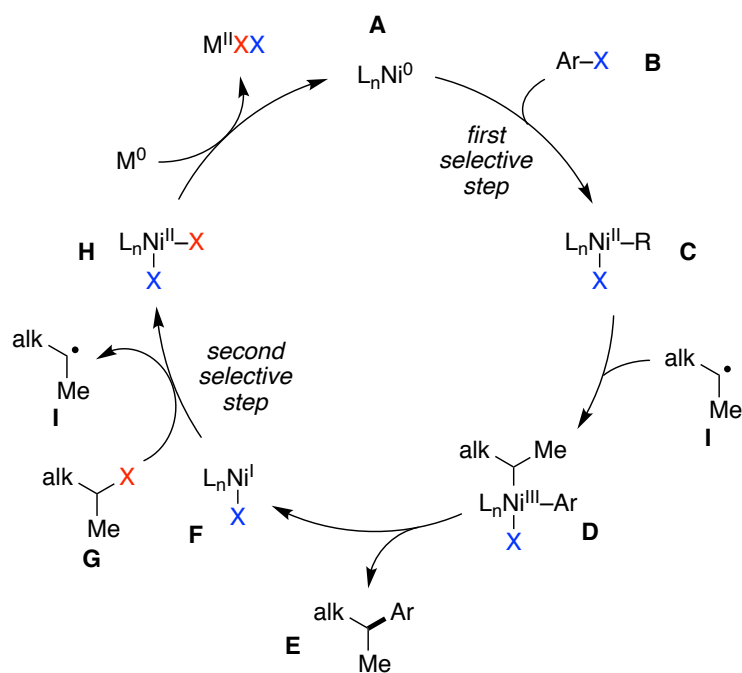


Figure 4.2 Radical-chain bimetallic catalytic cycle with stoichiometric metal reductants

In 2012, Weix disclosed the first general, transition metal-catalyzed cross-electrophile coupling between an alkyl electrophile and an aryl electrophile (Figure 4.3).<sup>3</sup> The optimal conditions utilized air- and bench-stable NiI<sub>2</sub>·xH<sub>2</sub>O in conjunction

with 4,4'-dimethoxy-2,2'-bipyridine (dOMebpy) or 1,10-phenanthroline (phen) as the redox-active supporting ligand. Screening of additives revealed that the addition of catalytic pyridine and sodium iodide led to lower levels of aryl halide homocoupling and higher conversion rates, respectively. A broad scope in both alkyl electrophile and aryl electrophile was observed, with over 40 examples, ranging from 41–96% yield. The vast majority of examples were focused on the coupling of primary alkyl bromides (**3-1**); however, in three entries, secondary cyclic and acyclic bromides led to moderate yields (61–63%) of the product (e.g., **4-8** and **4-9**).

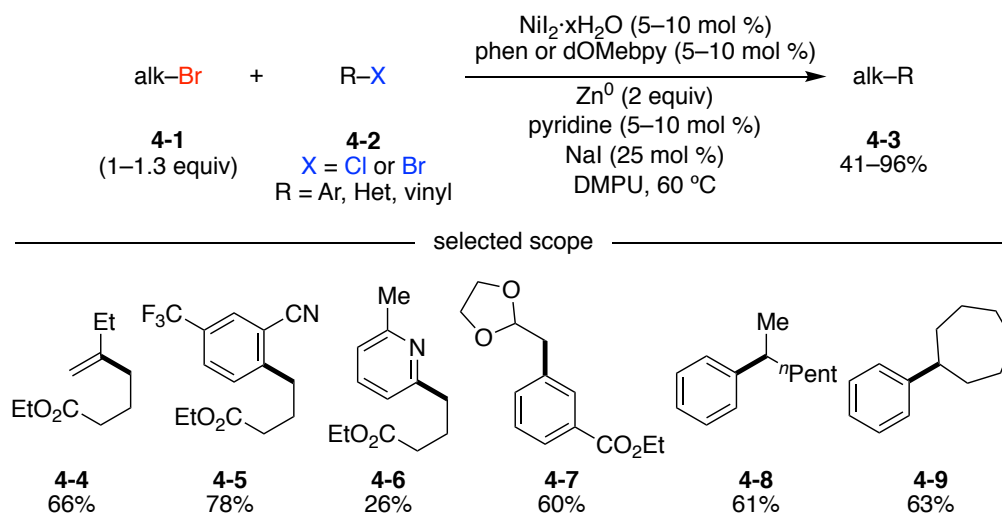
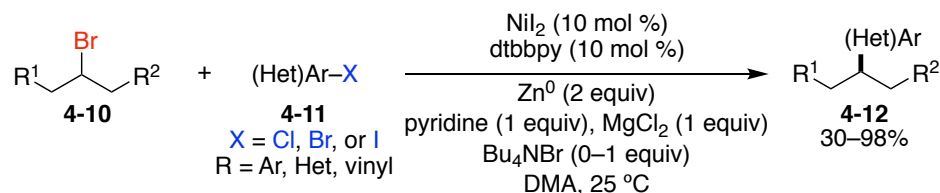


Figure 4.3 Weix's seminal publication on  $C_{sp^3}$ – $C_{sp^2}$  cross-electrophile coupling

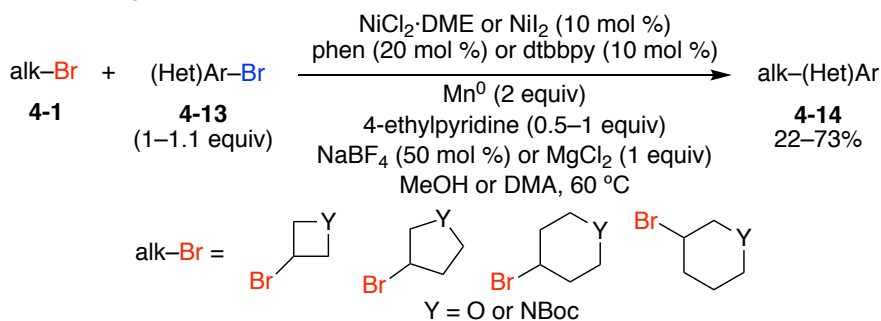
Shortly thereafter, Gong improved upon Weix's initial findings for the cross-coupling of secondary alkyl electrophiles and identified conditions that allowed the products to be obtained in good to high yields (30–98%) (Figure 4.4A).<sup>4</sup> Despite having made significant improvements, the scope of Gong's transformation lacked

breadth in regard to the couplings of heterocyclic alkyl electrophiles (**4-11**). With this in mind, Molander developed an improved, nickel-catalyzed method for the cross-couplings of 4-, 5-, and 6-membered *O*- and *N*-heterocyclic alkyl bromides (**4-1**) with aryl or heteroaryl bromides (**4-13**) (Figure 4.4B).<sup>5</sup> The biologically relevant products (**4-14**) were obtained in synthetically useful yields (22–73%). Similar products were obtained from a reaction that was developed by Buchwald in which a Pd-precatalyst, in conjunction with Zn<sup>0</sup> and a surfactant, promotes a Lipshutz-Negishi coupling under aqueous conditions (Figure 4.4C).<sup>6</sup>

A. Gong's coupling of secondary alkyl bromides and aryl/heteroaryl halides



B. Molander's coupling of heterocyclic alkyl bromides with aryl/heteroaryl bromides



C. Buchwald's coupling of heterocyclic alkyl bromides with aryl/heteroaryl halides and triflates

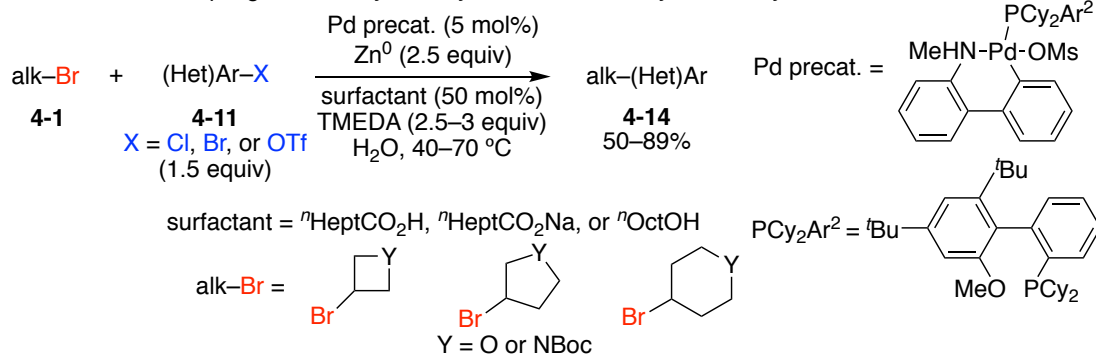


Figure 4.4 Recent advances in reductive couplings

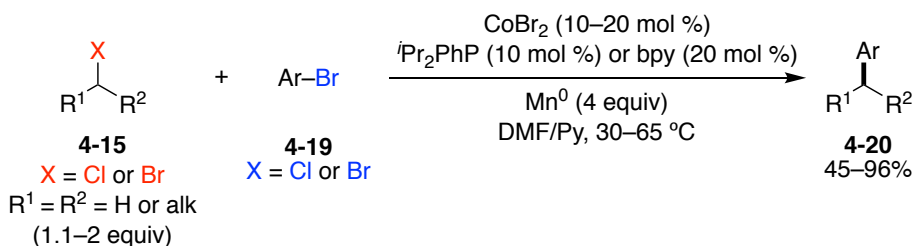
More recently, dual nickel/photoredox-catalyzed reductive couplings have been investigated. Unlike traditional cross-electrophile couplings which use a strongly reducing metal reductant (or strong organic reductant), metallophotoredox catalysis allows for milder conditions. To this end, MacMillan has shown that under blue-light irradiation, a Ni/Ir dual-photoredox-catalyzed, silyl-mediated coupling between secondary or primary alkyl halides and pseudohalides (**4-15**) with aryl bromides (**4-13**)

leads to alkyl arene products (**4-17**) in moderate to very high yields (Figure 4.5A).<sup>7</sup> It is proposed that the silane is ultimately necessary for abstracting the halide from the alkyl electrophile to generate the key alkyl radical intermediate. The alkyl radical can then intercept the nickel catalyst to continue the catalytic cycle (not shown). Alternatively, Lei has shown that secondary alkyl bromides (**4-18**) can be coupled effectively with (hetero)aryl bromides (**4-13**).<sup>8</sup> Under Ni/Ir dual-photoredox-catalyzed conditions with blue-light irradiation, they found that triethylamine can serve as the terminal reductant necessary for catalyst turnover (Figure 4.5B). In this regard, they found that with a relatively large excess (5 equivalents) of alkyl bromide, good to high yields of the alkyl arenes could be obtained. However, only a single example of a heteroaryl bromide (3-pyridyl) was shown, which resulted in a 36% yield of the desired product.



mesylates/tosylates were coupled with primary or secondary alkyl bromides, including one tertiary example in which *tert*-butyl bromide was coupled.

A. Gosmini's cobalt-catalyzed coupling of alkyl halides with aryl halides



B. Lei's copper-catalyzed coupling of alkyl mesylates or tosylates with aryl or alkyl bromides

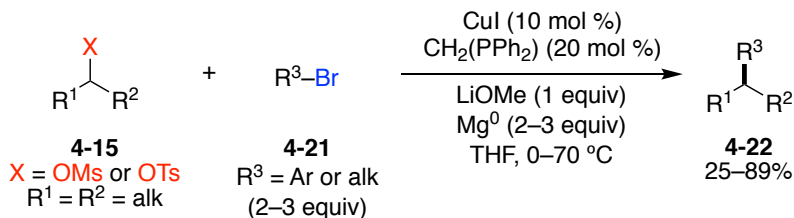


Figure 4.6 Cobalt- or copper-catalyzed cross-electrophile couplings

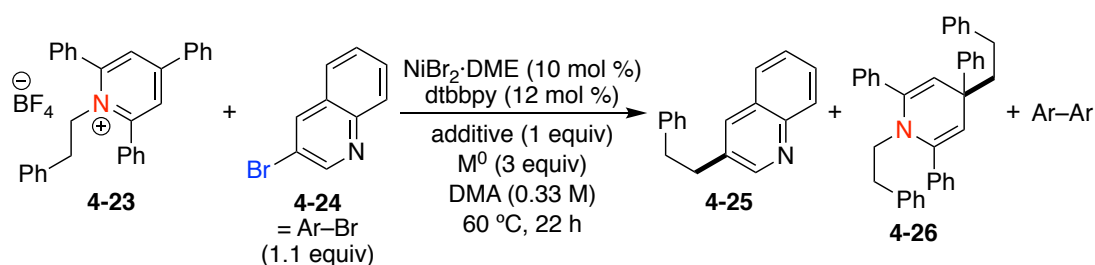
Aware of the advantages that reductive couplings can provide over traditional cross-couplings, I initiated the development of a nickel-catalyzed, cross-electrophile coupling between aryl halides and alkyl pyridinium salts.

## 4.2 Results and Discussion

I began the optimization using  $\text{NiBr}_2 \cdot \text{DME}$  and 4,4'-di-*tert*-butyl-2,2'-bipyridine (dtbbpy) in conjunction with a reducing metal and electrolytic salt additive. In regard to the stoichiometric reducing metal, I initially tested  $\text{Mn}^0$  and  $\text{Zn}^0$  and found that, despite both providing promising yields of the desired coupling product (**4-25**),

the latter provided higher yields of the major byproduct **4-26** (Table 4.1). Presumably, **4-26** arises from trapping of the alkyl radical intermediate with an equivalent of unreacted pyridinium salt. LiCl was found to be a significantly more effective additive in comparison to the other commonly employed salts, NBu<sub>4</sub>I and NaI (entries 1–3, 5–7). Without an additive, a lower yield is observed (entries 4 and 8). At this point, Mn<sup>0</sup> was taken forward as the optimal reductant.

Table 4.1 Optimization of the alkyl pyridinium salt reductive coupling



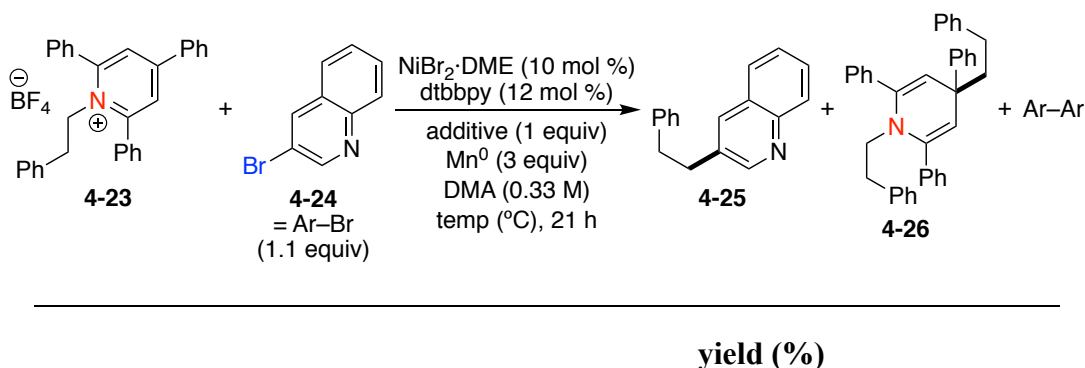
entry	M <sup>0</sup>	additive	yield (%)				
			4-25	4-26	4-25:4-26	Ar–Ar	Ph <sub>3</sub> Py
1	Mn <sup>0</sup>	NBu <sub>4</sub> I	33	20	1.6	5	68
2	Mn <sup>0</sup>	NaI	21	15	1.4	3	61
3	Mn <sup>0</sup>	LiCl	54	14	4.0	4	82
4	Mn <sup>0</sup>	none	26	25	1.0	4	63
5	Zn <sup>0</sup>	NBu <sub>4</sub> I	20	23	0.8	4	62
6 <sup>b</sup>	Zn <sup>0</sup>	NaI	17	22	0.8	3	65
7 <sup>b</sup>	Zn <sup>0</sup>	LiCl	35	19	1.9	3	80
8 <sup>c</sup>	Zn <sup>0</sup>	none	9	24	0.4	5	65

<sup>a</sup> Conditions: **4-23** (1 equiv), **4-24** (1.1 equiv), NiBr<sub>2</sub>·DME (10 mol %), dtbbpy (12 mol %), additive (1 equiv), M<sup>0</sup> (3 equiv), DMA (0.33

M), 60 °C, 22 h. PPh<sub>3</sub>Py = 2,4,6-triphenylpyridine. Yields based on <sup>1</sup>H NMR analysis with 1,3,5-trimethoxybenzene as an internal standard.

Recognizing the effectiveness of LiCl in facilitating the desired transformation, I screened a number of other salt additives. LiBr and LiI, as well as LiF (at 80 °C; Table 4.2, entry 10) led to much lower yields of **4-25**, suggesting that the identity of the anionic counter ion is critical (entries 1–3). Additionally, switching from LiCl to NaCl is also suggestive that the Li ion is crucial to the effectiveness of the salt (entry 4). KBr also proved inferior to LiCl. Increasing the equivalencies of LiCl from 1 to 2 led to nearly the same yield of desired product but improved the ratio of **4-25** to **4-26** from 1.3 to 1.9 (entries 2, 6). Interestingly, lowering the temperature from 60 to 23 °C led to only trace product, but comparable yields of 4-addition byproduct (entry 7). Lowering the equivalents of Mn<sup>0</sup> from 3 to 2 led to similar yields of **4-25** but a lower amount of byproduct. Moreover, the addition of trifluoroacetic acid (TFA), which has been used to activate the surface of reducing metals,<sup>11</sup> led to low yields of desired product. Finally, increasing the temperature of the reaction to 80 °C did not lead to improved yields of the desired product (entries 11, 12).

Table 4.2 Optimization of salt additives<sup>a</sup>

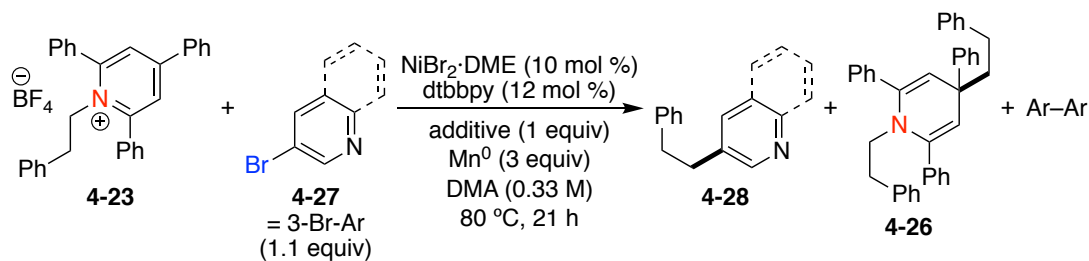


entry	additive	temp (°C)	4-25	4-26	4-25:4-26	Ar-Ar	Ph <sub>3</sub> Py
1	LiBr	60	18	28	0.6	3	64
2	LiCl	60	33	26	1.3	4	77
3	LiI	60	11	25	0.4	2	47
4	NaCl	60	7	35	0.2	3	83
5	KBr	60	12	31	0.4	3	59
6 <sup>b</sup>	LiCl	60	32	17	1.9	3	72
7	LiCl	23	1	29	0.0	3	46
8 <sup>c</sup>	LiCl	60	31	24	1.3	3	72
9 <sup>d</sup>	LiCl	60	12	32	0.4	4	62
10 <sup>e</sup>	LiF	80	26	25	1.1	6	64
11 <sup>e,f</sup>	LiCl	80	21	11	1.9	3	78
12 <sup>e</sup>	LiCl	80	26	14	1.8	5	79

<sup>a</sup> Conditions: **4-23** (1 equiv), **4-24** (1.1 equiv), NiBr<sub>2</sub>·DME (10 mol %), dtbbpy (12 mol %), additive (1 equiv), Mn<sup>0</sup> (3 equiv), DMA (0.33 M), 21 h. PPh<sub>3</sub>Py = 2,4,6-triphenylpyridine. Yields and ratios based on <sup>1</sup>H NMR analysis with 1,3,5-trimethoxybenzene as an internal standard. <sup>b</sup> 2 equivalents of LiCl used. <sup>c</sup> 2 equivalents of Mn<sup>0</sup> used. <sup>d</sup> TFA (10 mol %) added. <sup>e</sup> 3 equivalents of additive used. <sup>f</sup> 1:1 dioxane:DMA used.

In addition to 3-bromoquinoline, 3-bromopyridine also proved to be a competent aryl electrophile (Table 4.3, entries 1 and 2). Doubling the concentration from 0.33 to 0.67 M led to a drop in yield; however, decreasing the concentration to 0.17 M led to a significant improvement (entries 3 and 4). Interestingly, higher equivalents of 3-bromoquinoline or lower equivalents of LiCl did not provide better yields or ratios of desired product (**4-28**) to byproduct (**4-26**) (entries 5 and 6).

Table 4.3 Miscellaneous screens<sup>a</sup>

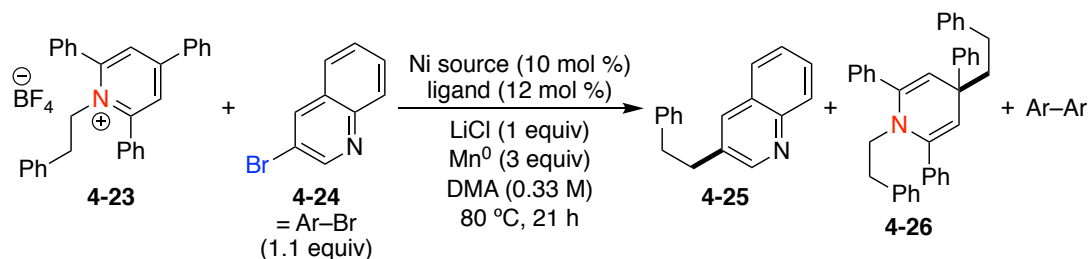


entry	Ar =	conc. (M)	yield (%)				
			4-28	4-26	4-28:4-26	Ar-Ar	Ph <sub>3</sub> Py
1	quin	0.33	43	15	2.8	4	71
2	Py	0.33	41	23	1.8	3	44
3	quin	0.67	28	19	1.4	4	63
4	quin	0.17	64	12	5.2	14	89
5 <sup>b</sup>	quin	0.33	35	15	2.3	4	69
6 <sup>c</sup>	quin	0.33	30	18	1.6	4	75

<sup>a</sup> Conditions: **4-23** (1 equiv), **4-27** (1.1 equiv),  $\text{NiBr}_2 \cdot \text{DME}$  (10 mol %), dtbbpy (12 mol %), additive (1 equiv),  $\text{Mn}^0$  (3 equiv), DMA (0.33 M), 80 °C, 21 h. PPh<sub>3</sub>Py = 2,4,6-triphenylpyridine. Yields and ratios based on <sup>1</sup>H NMR analysis with 1,3,5-trimethoxybenzene as an internal standard. Quin = quinoline. Py = pyridine <sup>b</sup> 1.5 equivalents of 3-Ar-Br used. <sup>c</sup> With 64 mol% LiCl.

In a brief ligand screen of other non-innocent ligands, including BPhen, 4,4'-dimethoxy-2,2'-bipyridine (dOMebpy), and terpyridine (tpy), I found that dtbbpy was still superior (Table 4.4, entries 1–3). Furthermore, a brief screen of nickel salts revealed that inexpensive  $\text{Ni}(\text{OAc})_2 \cdot 4\text{H}_2\text{O}$  is a much more effective Ni(II) precursor than  $\text{NiBr}_2 \cdot \text{DME}$ ,  $\text{NiCl}_2 \cdot 6\text{H}_2\text{O}$ , or  $\text{Ni}(\text{OTf})_2$  (entries 4–6).

Table 4.4 Catalyst optimization



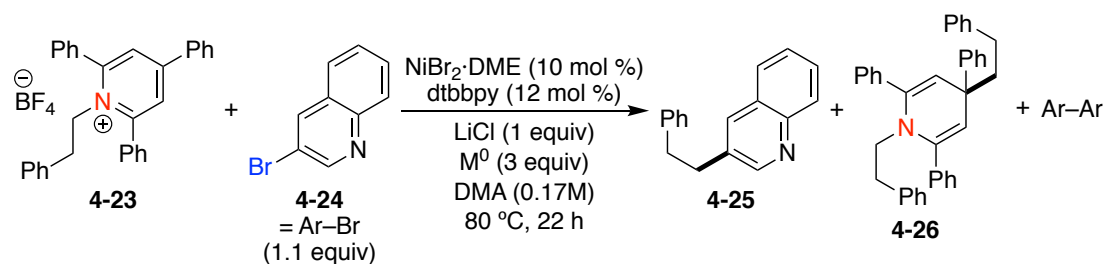
entry	Ni source	ligand	yield (%)				
			4-25	4-26	4-25:4-26	Ar-Ar	Ph <sub>3</sub> Py
1	NiBr <sub>2</sub> ·DME	Bphen	7	13	0.5	9	76
2	NiBr <sub>2</sub> ·DME	dOMebpy	32	19	1.6	3	61
3	NiBr <sub>2</sub> ·DME	tpy	27	12	2.2	8	81
4 <sup>b</sup>	NiCl <sub>2</sub> ·6H <sub>2</sub> O	dtbbpy	33	14	2.5	14	55
5	Ni(OAc) <sub>2</sub> ·4H <sub>2</sub> O	dtbbpy	64	18	5.7	18	87
6 <sup>c</sup>	Ni(OTf) <sub>2</sub>	dtbbpy	30	10	0.4	10	60

<sup>a</sup> **4-23** (1 equiv), **4-24** (1.1 equiv), Ni source (10 mol %), ligand (12 mol %), LiCl (1 equiv), Mn<sup>0</sup> (3 equiv), DMA (0.33 M), 80 °C, 21 h. PPh<sub>3</sub>Py = 2,4,6-triphenylpyridine. Yields and ratios based on <sup>1</sup>H NMR analysis with 1,3,5-trimethoxybenzene as an internal standard. Bphen = bathophenanthroline. DOMEbpy = 4,4'-dimethoxy-2,2'-bipyridine. Tpy = 2,2':6',2''-terpyridine.

Reducing metals other than Mn<sup>0</sup> were also tested under the partially optimized reaction conditions. Notably, Fe<sup>0</sup> and Cu<sup>0</sup> are completely ineffective this reaction; however, not surprisingly, Mg<sup>0</sup> shows some reactivity, albeit in lower yield than Zn<sup>0</sup> and Mn<sup>0</sup> (Table 4.5, entries 1–4). Lowering the Mn<sup>0</sup> loading from 3 equivalents to 1 led to a small drop in yield, but improved the ratio of **4-25** to **4-26** considerably (entry 5). Lastly, through a brief screen of other solvents, I identified that DMSO provides lower yields of the coupling product while, dioxane leads to complete suppression of

reactivity. Interestingly, NMP provides similar yields of **4-25** to DMA, but with a slightly higher ratio of **4-25** to **4-26** (entries 6–8).

Table 4.5 Further optimization



entry	solvent	M <sup>0</sup>	yield (%)				Ph <sub>3</sub> Py
			4-25	4-26	4-25:4-26	Ar-Ar	
1	DMA	Fe <sup>0</sup>	0	0	n/a	0	76
2	DMA	Cu <sup>0</sup>	0	0	n/a	0	61
3	DMA	Mg <sup>0</sup>	20	4	4.9	4	81
4	DMA	Zn <sup>0</sup>	41	18	2.2	15	55
5 <sup>b</sup>	DMA	Mn <sup>0</sup>	51	5	10.5	6	87
6	DMSO	Mn <sup>0</sup>	42	18	2.4	5	74
7	dioxane	Mn <sup>0</sup>	0	0	n/a	0	0
8	NMP	Mn <sup>0</sup>	62	8	7.3	21	91

<sup>a</sup> **4-23** (1 equiv), **4-24** (1.1 equiv), Ni source (10 mol %), ligand (12 mol %), LiCl (1 equiv), M<sup>0</sup> (3 equiv), solvent (0.33 M), 80 °C, 21 h. PPh<sub>3</sub>Py = 2,4,6-triphenylpyridine. Yields and ratios based on <sup>1</sup>H NMR analysis with 1,3,5-trimethoxybenzene as an internal standard. NMP = *N*-methyl-2-pyrrolidone. <sup>b</sup> 1 equivalent of Mn<sup>0</sup> used.

### 4.3 Conclusion

In summary, I have described my efforts toward the development of a reductive cross-coupling of alkyl pyridinium salts and aryl bromides. After preliminary screenings of the reaction parameters, including reductants, Ni(II) salts, and ligands, the highest yield of the model reaction currently stands at 64%. Key parameters to the success of this reaction include identification of LiCl as additive, Ni(OAc)<sub>2</sub>·4H<sub>2</sub>O/dtbbpy as catalyst, a polar solvent, and lower concentration. Further optimization to improve the yield and reduce formation of byproduct **4-26** is required. A subsequent investigation of the scope and mechanism of this transformation will also be performed. The successful development of this reductive cross-coupling has the potential to greatly impact drug discovery efforts by allowing two widely available starting materials, alkyl amines and aryl halides, to be coupled efficiently.

### 4.4 Experimental

#### 4.4.1 General Procedure A: Reaction Optimization

In a N<sub>2</sub>-filled glovebox: To a 1-dram vial was added Ni<sup>II</sup> salt and ligand, followed by pyridinium salt (0.1 mmol, 1 equiv). After the addition of solvent and a micro stir bar, the vial was sealed with a Teflon-coated screw cap and the mixture was stirred at room temperature for ~ 10 min. To the resultant green solution was added the salt additive, metal reductant, and aryl halide. The Vial was resealed with the Teflon-coated screw cap, removed from the glovebox, and stirred at the designated temperature in a heating block for 18–24 h. After allowing the mixture to cool to room temperature, it was diluted with Et<sub>2</sub>O (~ 1.5 mL) and filtered through a short plug of silica gel. The filter cake was washed with Et<sub>2</sub>O (5 x 1.5 mL), and the resulting solution was concentrated. 1,3,5-trimethoxybenzene (5 – 15 mg) was added as an

internal standard. The yield of the product was determined by analysis of the  $^1\text{H}$  NMR spectrum of the crude reaction mixture.

## REFERENCES

1. Everson, D. A.; Weix, D. J. *J. Org. Chem.* **2014**, *79* (11), 4793-4798.
2. Biswas, S.; Weix, D. J. *J. Am. Chem. Soc.* **2013**, *135* (43), 16192-16197.
3. Everson, D. A.; Jones, B. A.; Weix, D. J. *J. Am. Chem. Soc.* **2012**, *134* (14), 6146-6159.
4. Wang, S.; Qian, Q.; Gong, H. *Org. Lett.* **2012**, *14* (13), 3352-3355.
5. Molander, G. A.; Traister, K. M.; O'Neill, B. T. *J. Org. Chem.* **2014**, *79* (12), 5771-5780.
6. Bhonde, V. R.; O'Neill, B. T.; Buchwald, S. L. *Angew. Chem., Int. Ed.* **2016**, *55* (5), 1849-1853.
7. Zhang, P.; Le, C. C.; MacMillan, D. W. *J. Am. Chem. Soc.* **2016**, *138* (26), 8084-8087.
8. Duan, Z.; Li, W.; Lei, A. *Org. Lett.* **2016**, *18* (16), 4012-4015.
9. Amatore, M.; Gosmini, C. *Chem. Eur. J.* **2010**, *16* (20), 5848-5852.
10. Liu, J.-H.; Yang, C.-T.; Lu, X.-Y.; Zhang, Z.-Q.; Xu, L.; Cui, M.; Lu, X.; Xiao, B.; Fu, Y.; Liu, L. *Chem. Eur. J.* **2014**, *20* (47), 15334-15338.
11. Cherney, A. H.; Reisman, S. E. *J. Am. Chem. Soc.* **2014**, *136* (41), 14365-14368.

## Chapter 5

### SUZUKI-MIYaura CROSS-COUPPLINGS OF $\alpha$ -AMINO ACID-DERIVED PYRIDINIUM SALTS

#### 5.1 Introduction

$\alpha$ -Amino acids comprise a privileged, functionally diverse chemical feedstock with applications spanning the majority of chemistry and chemical biology.<sup>1</sup> Apart from the essentiality of amino acids in biochemical processes, they are often utilized as readily available sources of chirality in the field of synthetic organic chemistry. The majority of applications that employ amino acids lead to products in which the nitrogen functionality is ultimately maintained (Figure 5.1, top left). Such applications include, for example, the use of amino acids as chiral auxiliaries (**5-2**), chiral-pool starting materials in total syntheses (**5-3**)<sup>2</sup>, or as chiral ligand frameworks for asymmetric catalysis (**5-4**) (Figure 5.1, bottom). The use of amino acid derivatives as  $\alpha$ -carbon electrophiles via C–N bond activation has garnered much less attention from the synthetic community. Given the abundance, structural diversity, and ready availability of amino acids, they, in theory, could serve as ideal electrophiles for the synthesis of  $\alpha$ -substituted carbonyl derivatives (**5-5**) (Figure 5.1, top right).

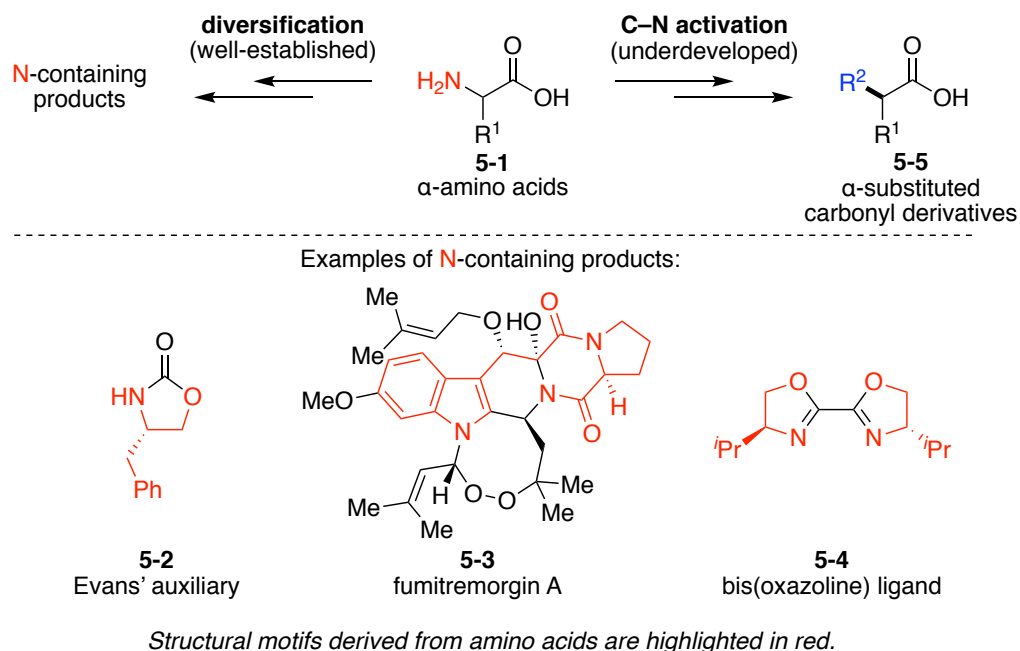


Figure 5.1 Expanding the utility of the amino acid feedstock

The common method for the activation of C–N bonds in  $\alpha$ -amino acid derivatives is the formation of  $\alpha$ -diazocompounds. Although the chemistry of these highly activated species is largely understood, their high propensity to form  $\alpha$ -carbenes through the release of  $N_2$  gas largely limits their use to carbenoid-insertion chemistry. As with most diazocompounds, stability issues often preclude their use on scale and warrant an extra level of caution when handling. Additionally,  $C_{\alpha}$ –N bond activation through the formation of diazo species, although straightforward, requires strongly acidic conditions, which inherently limit functional group tolerance. Despite these caveats, many elegant methods have been developed that harness this unique reactivity of  $\alpha$ -diazocompounds to access valuable  $\alpha$ -substituted carbonyl derivatives.<sup>3</sup>

Wang has disclosed a number of synthetically useful methods that utilize  $\alpha$ -diazocompounds. In particular, his laboratory has applied this mode of reactivity to a

transition metal-free deaminative arylation of  $\alpha$ -amino esters (**5-6** and **5-9**) with boronic acids (**5-7** and **5-10**) (Figure 5.2A, B).<sup>4</sup> Broad scope in both aryl boronic acid and amino ester was demonstrated; however, few examples of heteroaromatic boronic acids were reported. Advantageously, this method avoids independent synthesis of the diazonium salts, and instead generates them *in situ* with sodium nitrite (**5-10**). Owing to the significant carbene character at the  $\alpha$ -carbon, it is proposed that treatment of the diazo compound with an aryl boronic acid first generates an ‘ate’ complex (**5-11**), which can then undergo a 1,2-shift to tertiary boronate **5-12** and subsequently protodeboronate to give the  $\alpha$ -aryl ester (**5-13**) (Figure 5.2 C).

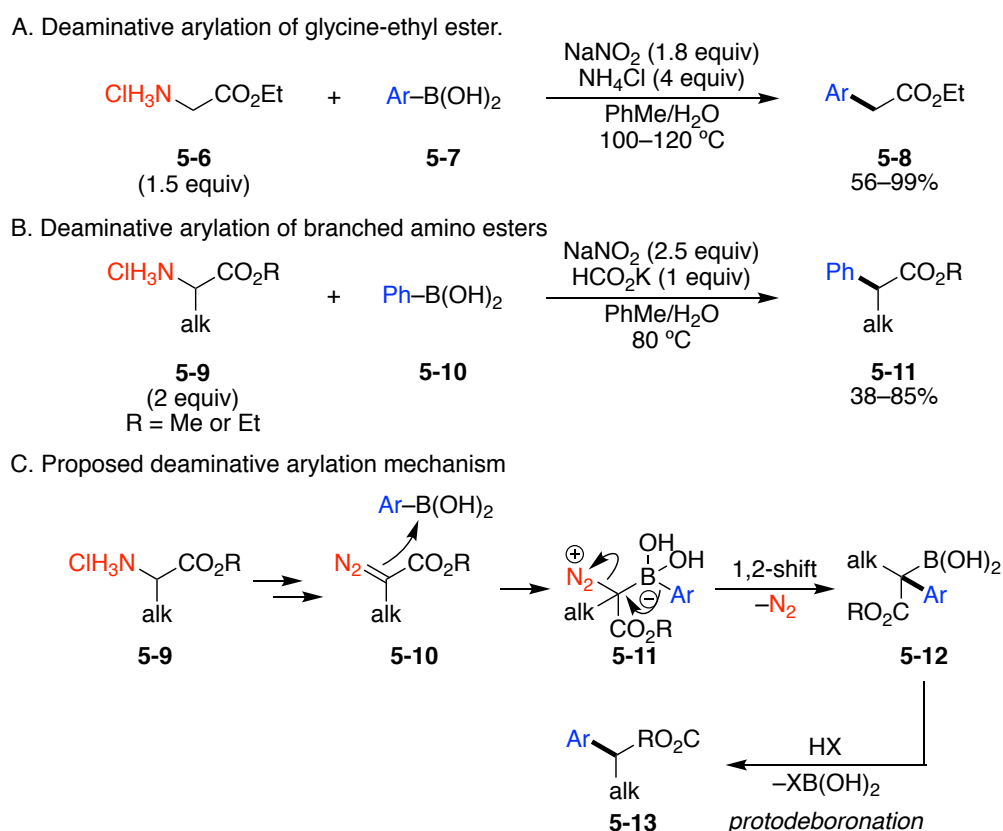


Figure 5.2 Wang’s transition metal-free coupling of  $\alpha$ -diazo esters and boronic acids

With our prior success in nickel-catalyzed cross-couplings via cleavage of C–N bonds in unactivated alkyl systems by the formation of Katritzky pyridinium salts,<sup>5</sup> I envisioned that a similar approach toward activating the C<sub>α</sub>–N bond of amino acid derivatives (**5-14**) would be possible. The pyridinium salts (**5-16**) do not suffer from the stability issues observed with diazo compounds, thus allowing them to be synthesized on scale and stored for an extended period of time without loss of efficacy using commercially. With our previous success in Suzuki-Miyaura arylations, I envisioned aryl boronic reagents would be a logical choice as coupling partners (Figure 5.3).

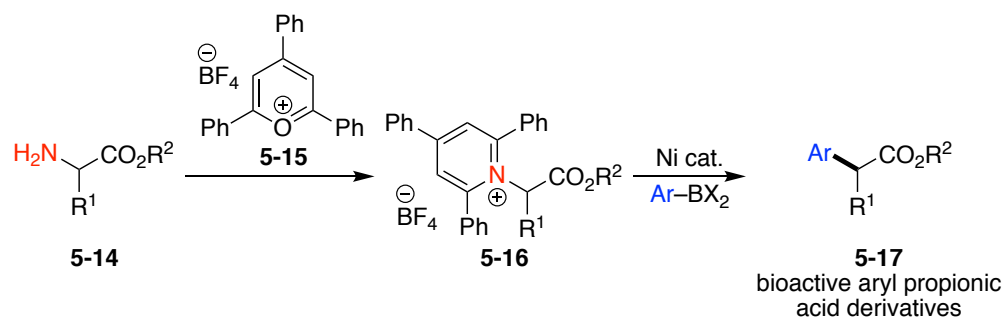


Figure 5.3 Proposed method of C<sub>α</sub>–N activation of amino acid derivatives

Due to their medicinal relevance, α-aryl carbonyl derivatives (**5-17**) have received considerable attention in recent years as synthetic targets for methods development. In this regard, non-steroidal anti-inflammatory drugs (NSAIDs) such as ibuprofen (**5-18**), ketoprofen (**5-19**), and flurbiprofen (**5-20**), are perhaps the most widely-known α-aryl carbonyl species (Figure 5.4). An NSAID is biologically active as its (*S*)-enantiomer; however, under metabolic conditions, the inactive (*R*)-

enantiomer can undergo stereochemical inversion. Thus, NSAIDs are often synthesized as racemic mixtures.<sup>6</sup>

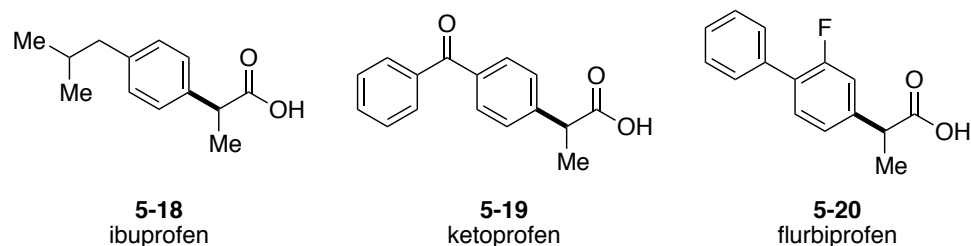
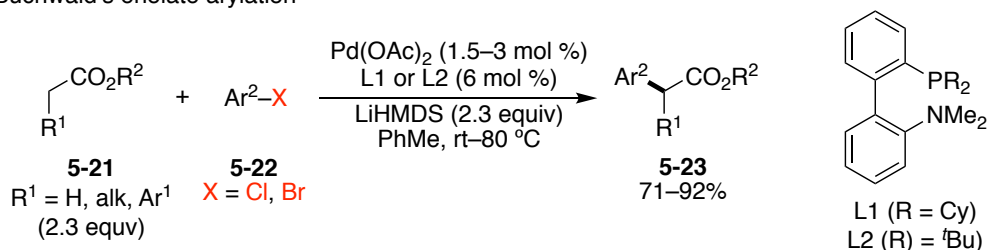


Figure 5.4 Bioactive  $\alpha$ -aryl propionic acid derivatives

Buchwald and Hartwig independently reported the formation of  $\alpha$ -aryl esters via palladium-catalyzed enolate couplings (Figure 5.5).<sup>7,8</sup> Under the two sets of conditions identified, broad scope was observed in both ester (**5-21**) and aryl halide (**5-22** or **5-24**). The only obvious drawback to these methods is the necessity of a relatively strong base to generate the enolate. In this regard, the functional group tolerance is inherently limited to systems without acidic protons.

A. Buchwald's enolate arylation



B. Hartwig's enolate arylation

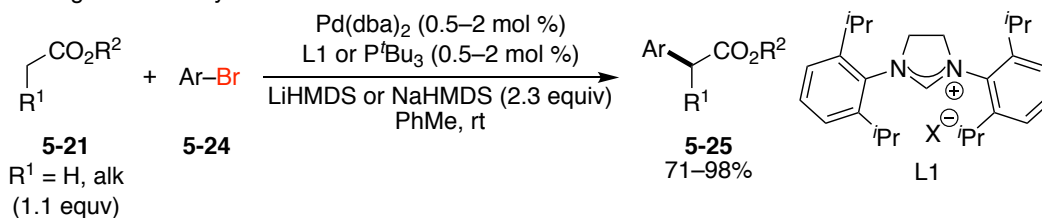


Figure 5.5 Palladium-catalyzed  $\alpha$ -arylations of enolates

Alternatively, the Fu group has demonstrated that racemic  $\alpha$ -bromo esters (**5-26**) are viable substrates in an asymmetric, nickel-catalyzed Hiyama cross-coupling with aryl silanes (**5-27**) (Figure 5.6).<sup>9</sup> A variety of alkyl substituents were well-tolerated at the  $\alpha$ -carbon; however, a limited aryl silane scope was reported. Notably, this was the first general cross-coupling of an aryl nucleophile with an  $\alpha$ -halocarbonyl electrophile.

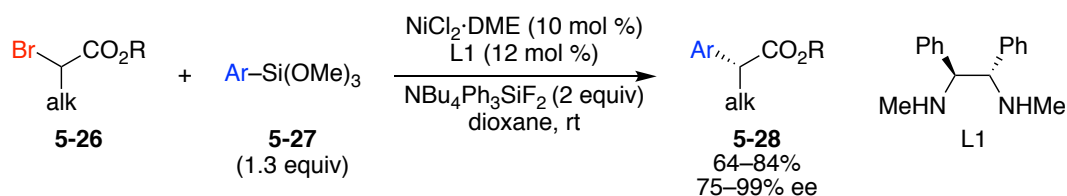


Figure 5.6 Fu's asymmetric Hiyama arylation of  $\alpha$ -bromo esters.

Recently, Glorius reported a photoredox-catalyzed Minisci-type cross-coupling of amino acid-derived  $\alpha$ -pyridinium salts with heteroarenes.<sup>10</sup> On the basis of our findings in the Suzuki-Miyaura arylation of alkyl pyridinium salts (see Ch 2), they found that single-electron transfer from an excited Ir-based photocatalyst can also lead to efficient fragmentation via C–N cleavage. Trapping of the resulting transient radical with heteroarenes such as 3-substituted indoles led to the corresponding  $\alpha$ -heteroaryl products in good yields (Figure 5.7). It is worth noting that this chemistry is predominately limited to functionalization of the heteroarene at the 2-position due to the mechanism of this reaction.

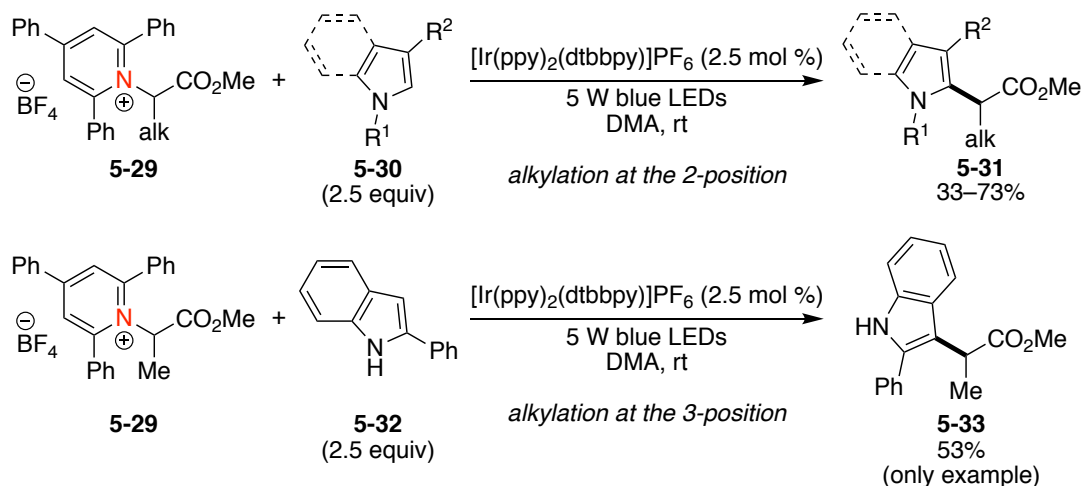


Figure 5.7 Glorius' photoredox-catalyzed, Minisci-type coupling of heteroarenes and  $\alpha$ -pyridinium salts

Building on our efforts in the cross-couplings of alkyl pyridinium salts and recognizing the potential of amino acids to serve as alkyl electrophiles, I set out to

develop a Suzuki-Miyaura arylation of  $\alpha$ -amino acid-derived pyridinium salts with aryl boronic acids. This work was ongoing at the time of Glorius' publication.

## 5.2 Results and Discussion

The  $\alpha$ -pyridinium salts were prepared in a single step from the commercially available amino acid methyl esters (**5-34**) and 2,4,6-triphenylpyrylium tetrafluoroborate (**5-15**). Generally, higher yields were obtained when using amino esters with less sterically-encumbering sidechains (R), such as glycine or alanine. This trend is likely a result of a slow rate of cyclization to form the pyridinium ring with large side-chains, as evidenced by the formation of hydrolysis byproduct **5-36** (Figure 5.8)

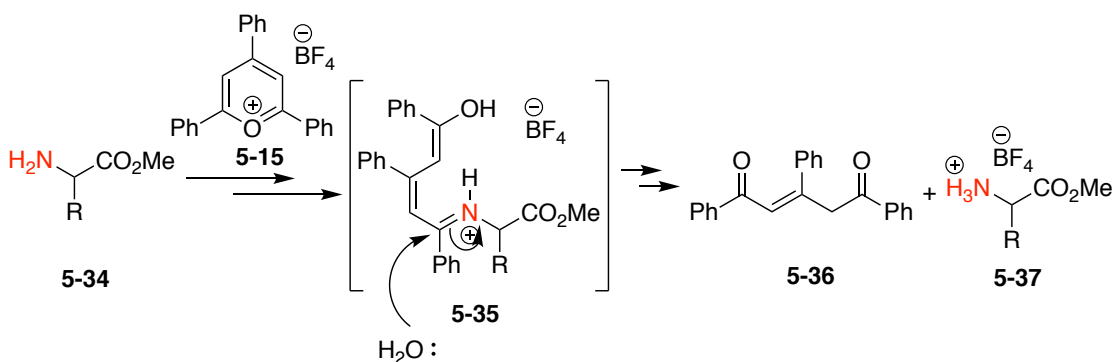
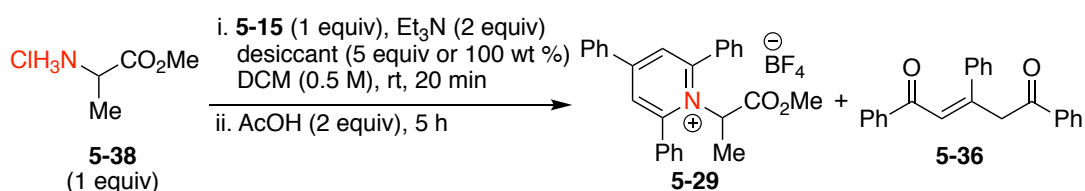


Figure 5.8 Hydrolysis of intermediate and formation of diketone byproduct

In an effort to suppress the formation of diketone byproduct **5-36**, I screened a variety of common desiccants (Table 5.1). Despite observing a minimal effect on reaction efficiency with the addition of  $\text{MgSO}_4$  or  $\text{Na}_2\text{SO}_4$ , I found that silica gel had a significant, detrimental effect on the reaction. However, switching to Drierite<sup>®</sup> led to a

promising increase in the ratio of pyridinium to diketone (96:4). Encouraged by this result, I then tested the impact of 4Å molecular sieves (4Å MS) and observed a 99:1 ratio of pyridinium to diketone. In addition to drastically improving the yield, the molecular sieves suppressed the formation of the diketone byproduct sufficiently to the point that a basic workup led to pure pyridinium salt, without the need for purification via silica gel chromatography (as was previously required).

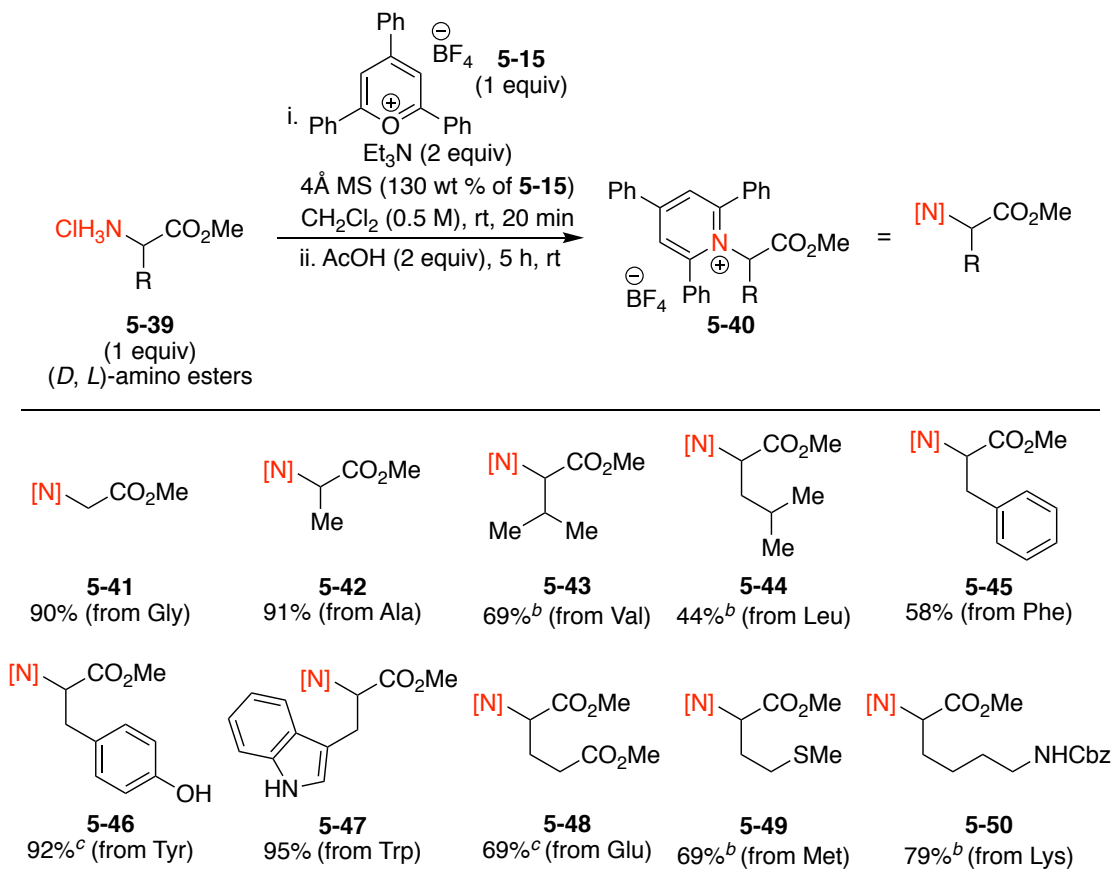
Table 5.1 Investigation into the effect of desiccants on pyridinium formation<sup>a</sup>



entry	desiccant	ratio (5-29:5-36)
1	none	86:14
2	MgSO <sub>4</sub>	84:16
3	Na <sub>2</sub> SO <sub>4</sub>	86:14
4	SiO <sub>2</sub> gel	69:31
5 <sup>b</sup>	Drierite <sup>®</sup>	96:4
6 <sup>b</sup>	4Å MS	99:1

<sup>a</sup> **5-38** (1 equiv), **5-15** (1 equiv), Et<sub>3</sub>N (2 equiv), desiccant (5 equiv), AcOH (2 equiv), CH<sub>2</sub>Cl<sub>2</sub> (0.5 M), 5 h, 23 °C. Ratios based on <sup>1</sup>H NMR analysis with 1,3,5-trimethoxybenzene as an internal standard. <sup>b</sup> 100 wt% desiccant used.

With improved conditions in hand, my colleagues Megan Hoerrner and Kristen Baker, and I, converted a series of  $\alpha$ -amino esters were to pyridinium salts (**5-40**) (Figure 5.9). The majority of the pyridinium salts were obtained in good to high yields, without need for chromatographic purifications. Not surprisingly, the bulkier <sup>i</sup>Pr and <sup>i</sup>Bu side-chains of valine (Val) and leucine (Leu) led to significant amounts of diketone formation. However, simple silica gel chromatography led to the isolation of these pyridinium salts in moderate to good yields. For reasons unclear at this time, the pyridinium salts of methionine (Met, **5-49**) and lysine (Lys, **5-50**) also required further purification via chromatography. Despite this, they were obtained in very good yields.



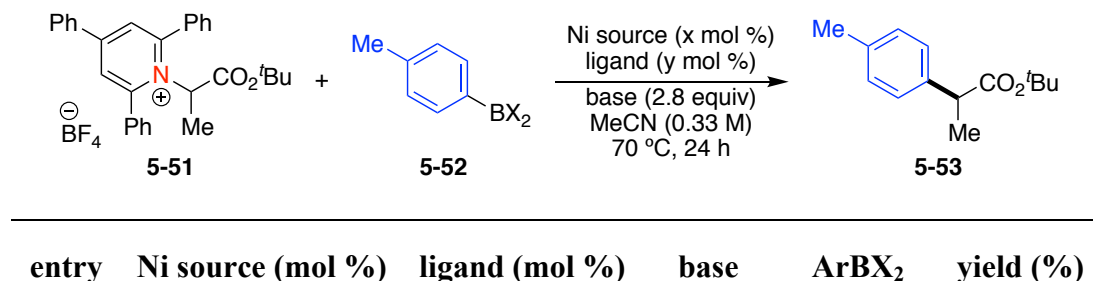
<sup>a</sup> **5-39** (1 equiv), **5-15** (1 equiv), Et<sub>3</sub>N (2 equiv), 4Å MS (130 wt %), CH<sub>2</sub>Cl<sub>2</sub> (0.5 M), AcOH (2 equiv), 5 h, 23 °C. <sup>b</sup> Purified via silica gel chromatography. <sup>c</sup> Contains <10% diketone byproduct.

Figure 5.9 Synthesis of  $\alpha$ -pyridinium salts derived from  $\alpha$ -amino acids<sup>a</sup>

I began the optimization of the Suzuki-Miyaura cross-coupling of the  $\alpha$ -pyridinium salts with a Ni(cod)<sub>2</sub> precatalyst and phenanthroline (phen) as the ancillary ligand (Table 5.2). Using an aryl boronic acid in conjunction with NaOMe as the base led to only 10% of the desired  $\alpha$ -aryl ester (**5-53**) (entry 1). Despite a similar result with the weaker base K<sub>3</sub>PO<sub>4</sub> (6%), K<sub>2</sub>CO<sub>3</sub> provided a 69% yield (entries 2 and 3). In the interest of translating the reaction out of the glove-box and onto the bench, Ni(II)

salts were also screened. In this regard, NiCl<sub>2</sub>·DME proved slightly more effective than Ni(cod)<sub>2</sub> (entry 4). In combination with the addition of 4Å molecular sieves, lowering the nickel and ligand loading to 5 and 6 mol %, respectively, led to a roughly 10% increase in yield to 88% (entry 5). A brief exploration of other ligands identified 4,4'-dimethyl-2,2'-bipyridine (dmbpy) as a superior ligand to phenanthroline. Under these conditions, the cross-coupling product was obtained in quantitative yield (entry 6). At this point, I investigated the amenability of these optimized conditions to other boronic acids. Unfortunately, I obtained inconsistent yields, which indicated that these conditions were not general. Aware of the favorable yield increase attributed by the molecular sieves, I hypothesized that water may be detrimental to the reaction. With this in mind, I elected to use a boroxine, rather than boronic acid, as the arylating reagent. Gratifyingly, a quantitative yield was observed (entry 7). Notably, the generality of the cross-coupling with boroxines proved vastly superior to the coupling with boronic acids. At this point, with the help of my colleague Megan Hoerrner, lower loadings of NiCl<sub>2</sub>·DME and dmbpy were tested; however, a lower yield of the product was observed (entry 8). Moreover, control reactions indicate that both elevated temperature, and nickel are necessary to obtain the desired product.

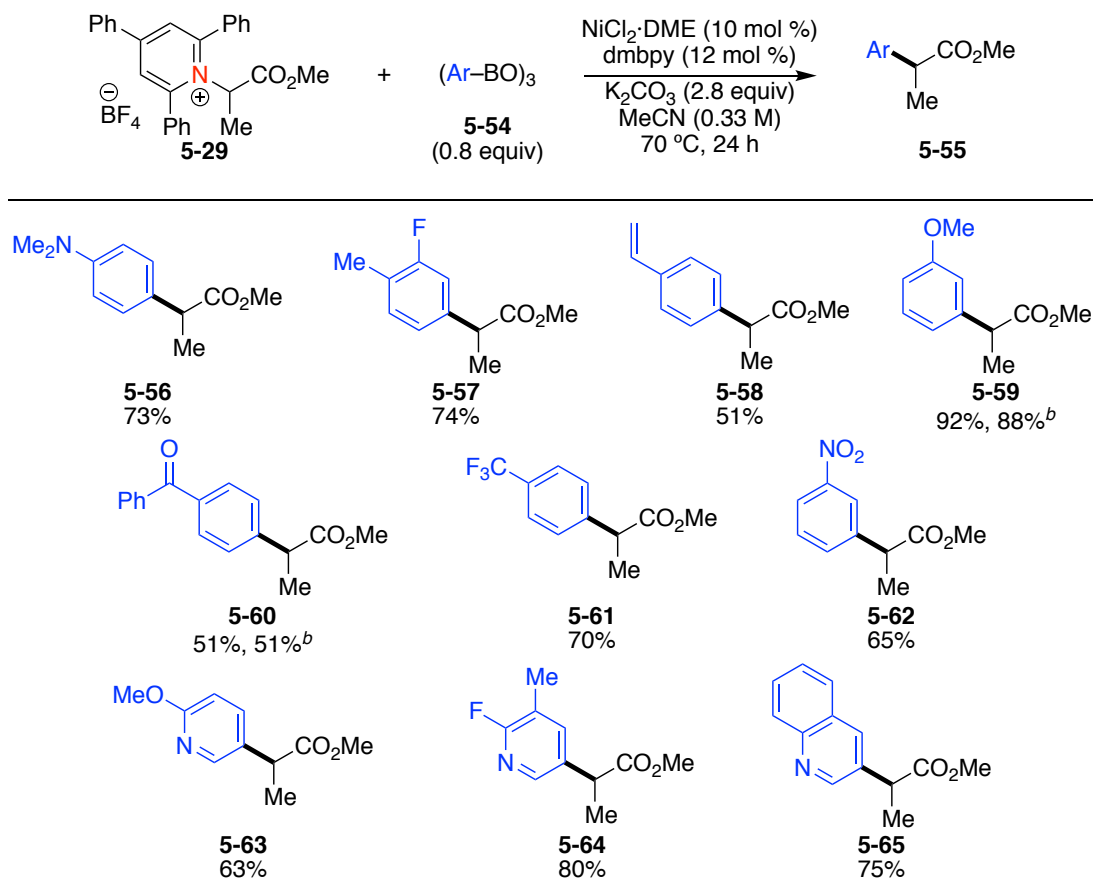
Table 5.2 Optimization of the Suzuki-Miyaura coupling of  $\alpha$ -pyridinium salts<sup>a</sup>



2	Ni(cod) <sub>2</sub> (10)	phen (12)	K <sub>3</sub> PO <sub>4</sub>	ArB(OH) <sub>2</sub>	6
3	Ni(cod) <sub>2</sub> (10)	phen (12)	K <sub>2</sub> CO <sub>3</sub>	ArB(OH) <sub>2</sub>	69
4	NiCl <sub>2</sub> ·DME (10)	phen (12)	K <sub>2</sub> CO <sub>3</sub>	ArB(OH) <sub>2</sub>	75
5 <sup>b</sup>	NiCl <sub>2</sub> ·DME (5)	phen (6)	K <sub>2</sub> CO <sub>3</sub>	ArB(OH) <sub>2</sub>	88
6 <sup>b</sup>	NiCl <sub>2</sub> ·DME (5)	dmbpy (6)	K <sub>2</sub> CO <sub>3</sub>	ArB(OH) <sub>2</sub>	>99
7	NiCl <sub>2</sub> ·DME (5)	dmbpy (6)	K <sub>2</sub> CO <sub>3</sub>	(ArBO) <sub>3</sub>	>99
8	NiCl <sub>2</sub> ·DME (2)	dmbpy (3)	K <sub>2</sub> CO <sub>3</sub>	(ArBO) <sub>3</sub>	71
9 <sup>c</sup>	NiCl <sub>2</sub> ·DME (10)	dmbpy (12)	K <sub>2</sub> CO <sub>3</sub>	(ArBO) <sub>3</sub>	0
10	none	dmbpy (6)	K <sub>2</sub> CO <sub>3</sub>	(ArBO) <sub>3</sub>	0

<sup>a</sup> **5-51** (1 equiv), ArBX<sub>2</sub> (**5-52**) equivalencies: ArB(OH)<sub>2</sub> (2.5 equiv), (ArBO)<sub>3</sub> (0.8 equiv), MeCN (0.33 M), 70 °C, 24 h. Yields based on <sup>1</sup>H NMR analysis with 1,3,5-trimethoxybenzene as an internal standard. Phen = 1,10-phenanthroline. Dmbpy = 4,4'-dimethyl-2,2'-bipyridine. <sup>b</sup> 4Å molecular sieves (MS) added (100 wt % **5-52**). <sup>c</sup> Reaction run at 23 °C.

With optimized conditions in hand, my colleagues Megan Hoerrner and Kristen Baker have explored the scope of this transformation. With regard to the scope in aryl boroxine (**5-54**), broad functional group tolerance was observed (Figure 5.10). Both electron-rich and electron-poor arenes couple smoothly, including those with *p*-NMe<sub>2</sub> (**5-56**, 73%), *p*-Bz (**5-60**, 51%), *p*-CF<sub>3</sub> (**5-61**, 70%), or *m*-NO<sub>2</sub> (**5-62**, 65%) substituents. Functionalized 3-pyridyl boroxines also cross-couple effectively, providing products **5-63** and **5-64** in 63% yield and 80% yield, respectively. Additionally, 3-quinolyl boroxine couples well to deliver **5-65** in 75%.

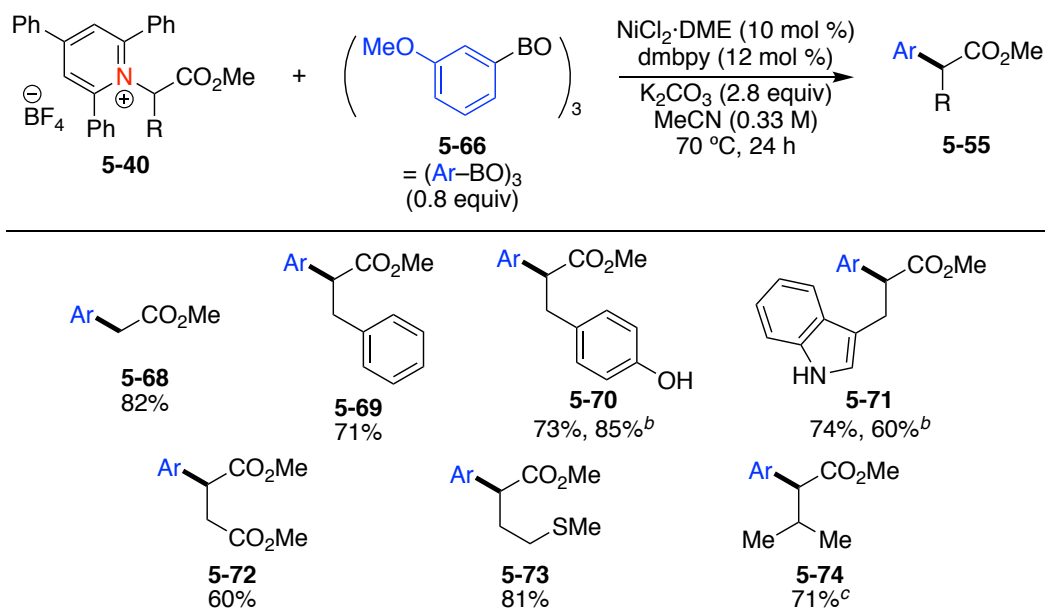


<sup>a</sup> **5-29** (1.0 mmol, 1 equiv), **5-54** (0.8 equiv), NiCl<sub>2</sub>·DME (10 mol %), dmbpy (12 mol %), K<sub>2</sub>CO<sub>3</sub> (2.8 equiv), MeCN (0.33 M), 70 °C, 24 h. Yields based on <sup>1</sup>H NMR with 1,3,5-trimethoxybenzene as an internal standard. <sup>b</sup> NiCl<sub>2</sub>·DME (5 mol %), dmbpy (6 mol %). Isolated yields (purified via silica gel chromatography).

Figure 5.10 Preliminary scope in boroxine<sup>a</sup>

Preliminary investigations into the scope of pyridinium salt (**5-40**) are also very promising (Figure 5.11). Not surprisingly, glycine-derived pyridinium salt couples well in 82% yield (**5-68**). In addition to the methyl side-chain of alanine-derived product (**5-59**), other side-chains are also well tolerated. Both benzyl- and 4-hydroxybenzyl-substituted salts couple in good yields, as does the salt derived from tryptophan (**5-69**, **5-70**, and **5-71**). Importantly, neither the free phenol of the 4-

hydroxybenzyl group (derived from tyrosine) nor the indole *N*-H appear to affect the reaction. Products bearing a  $\beta$ -ester (**5-72**) or thioether (**5-73**), also obtained in synthetically useful yields. After slightly modifying the conditions, my colleague, Kristen Baker, cross-coupled the <sup>i</sup>Pr-substituted pyridinium salt (derived from valine) in 71% (**5-74**). Key to this success was increasing the temperature from 70 to 80 °C as well as switching the solvent from MeCN to <sup>n</sup>PrCN.

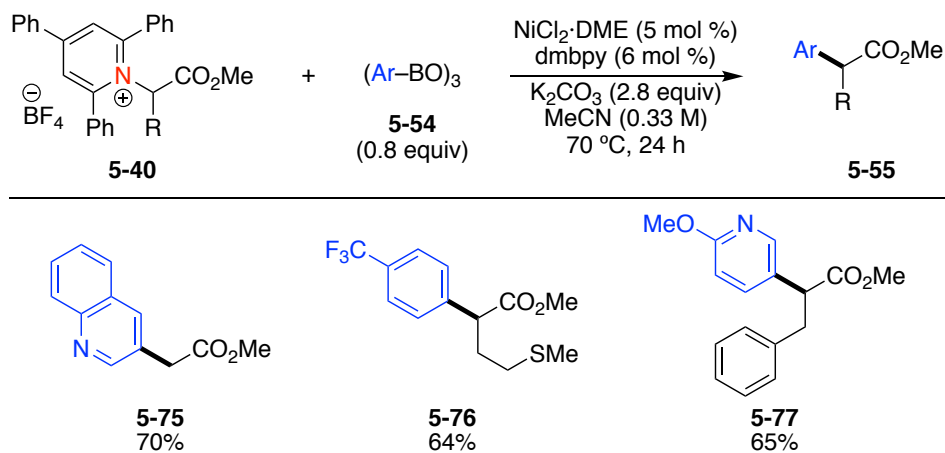


<sup>a</sup> **5-40** (1.0 mmol, 1 equiv), **5-66** (0.8 equiv),  $\text{NiCl}_2 \cdot \text{DME}$  (10 mol %), *dmbpy* (12 mol %),  $\text{K}_2\text{CO}_3$  (2.8 equiv), MeCN (0.33 M), 70 °C, 24 h. Yield based on <sup>1</sup>H NMR with 1,3,5-trimethoxybenzene as an internal standard. <sup>b</sup> Isolated yield (purified via silica gel chromatography). <sup>c</sup> Reaction run in <sup>n</sup>PrCN at 80 °C.

Figure 5.11 Preliminary scope in  $\alpha$ -pyridinium salt<sup>a</sup>

In addition to the previously mentioned scope, coupling of the Gly-pyridinium salt with 3-quinolyl boroxine delivered product **5-75** in 70% yield (Figure 5.12).

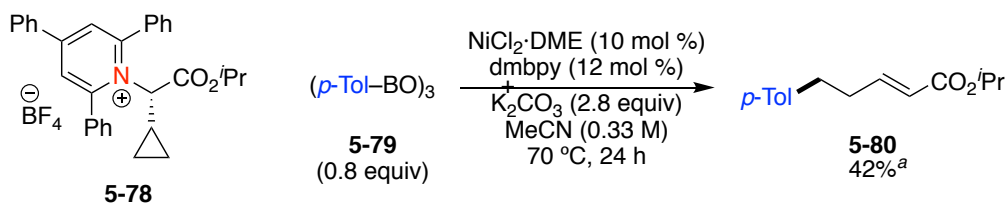
Cross-coupling of Met-pyridinium salt with 4-trifluoromethylphenyl boroxine gave 64% of the corresponding  $\alpha$ -aryl ester **5-76**, while the coupling of benzyl-substituted, Phe-pyridinium salt with the methoxy-bearing pyridyl boroxine provided the desired product (**5-77**) in 65% yield.



<sup>a</sup> **5-40** (1.0 mmol, 1 equiv), **5-54** (0.8 equiv),  $\text{NiCl}_2 \cdot \text{DME}$  (5 mol %),  $\text{dmbpy}$  (6 mol %),  $\text{K}_2\text{CO}_3$  (2.8 equiv), MeCN (0.33 M), 70 °C, 24 h. Isolated yields (purified via silica gel chromatography).

Figure 5.12 Preliminary scope<sup>a</sup>

Similar to the Suzuki-Miyaura and Negishi cross-couplings of the unactivated alkyl systems (Ch 2 and 3), we hypothesize that the identity of the optimal ligand (redox non-innocent bipyridine) suggests that the oxidative addition proceeds through a single-electron transfer (SET) pathway. In further support of this mechanism, the cross-coupling of cyclopropyl substituted pyridinium salt **5-78** results in formation of ring opened product **5-80** (Figure 5.13). These results are consistent with an alkyl radical intermediate.



<sup>a</sup> Yield based on <sup>1</sup>H NMR with 1,3,5-trimethoxybenzene as an internal standard.

Figure 5.13 Radical-clock experiment

We hypothesize that the following catalytic cycle may be operative: Ni<sup>I</sup> species **A** could undergo transmetalation with an activated aryl boron species to generate aryl Ni<sup>I</sup> species **B** (Figure 5.14). **B** can then undergo SET with the  $\alpha$ -pyridinium salt (**5-40**) to generate a Ni<sup>II</sup> species **C** and stabilized  $\alpha$ -radical **D**. A subsequent recombination between the  $\alpha$ -radical and nickel-intermediate **C** would lead to a Ni<sup>III</sup>-enolate intermediate, **E**. Reductive elimination would furnish the cross-coupled product (**5-55**) and close the catalytic cycle.

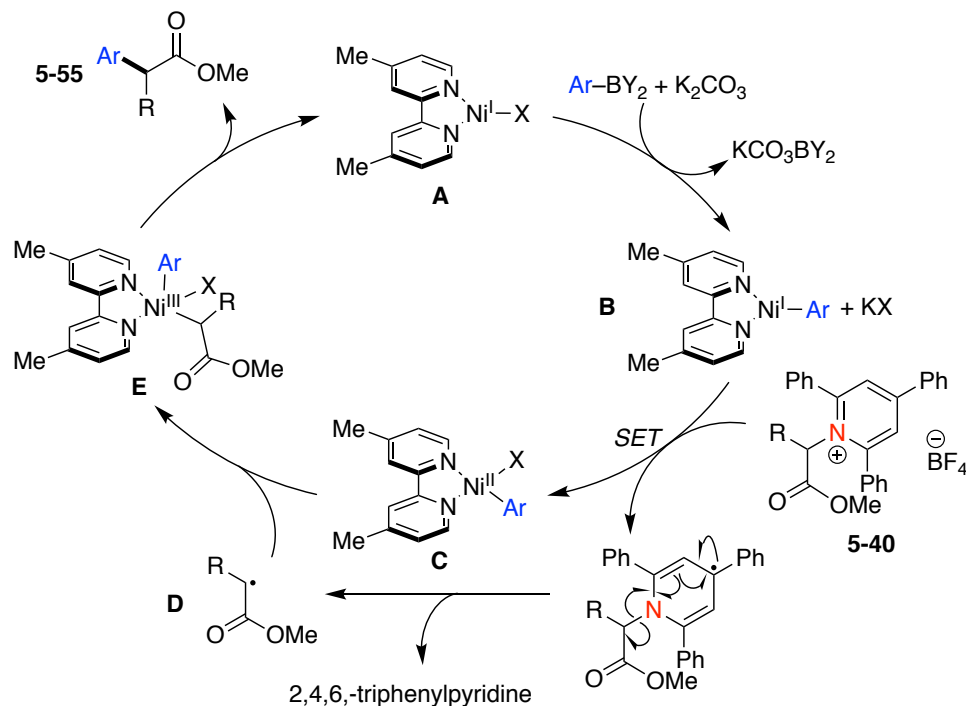


Figure 5.14 Possible catalytic cycle for the cross-coupling with  $\alpha$ -pyridinium salts

### 5.3 Conclusion

In summary, I have described our efforts toward a nickel-catalyzed Suzuki-Miyaura cross-coupling of  $\alpha$ -pyridinium salts and aryl boroxines. The  $\alpha$ -pyridinium salts were synthesized in a single, straightforward, and efficient step from  $\alpha$ -amino esters and commercially available 2,4,6-triphenylpyrylium tetrafluoroborate. In addition to high tolerance of functionally diverse aryl boroxines (e.g., nitro, ketone, pyridine, quinoline, etc.), the optimized conditions are amenable to the cross-coupling of  $\alpha$ -pyridinium salts with not only simple alkyl side-chains, but also those with sterically encumbering (e.g., from Val) or particularly reactive (e.g., from Tyr, Trp, Glu) side-chains. Future efforts will focus on expanding the scope of these cross-couplings to more complex systems, such as peptides.

## 5.4 Experimental

### 5.4.1 General Procedure A: Reaction Optimization

In a N<sub>2</sub>-filled glovebox: To a 1-dram vial was added Ni<sup>II</sup> salt and ligand, followed by base, boronic acid derivative, and pyridinium salt (0.1 mmol, 1 equiv). After the addition of solvent and a micro stir bar, the vial was sealed with a Teflon-coated screw cap and removed from the glovebox. The reaction mixture was stirred at the designated temperature in a heating block for 20–24 h then removed and allowed to cool to room temperature. The mixture was diluted with Et<sub>2</sub>O (~ 1.5 mL) and filtered through a short plug of silica gel. The filter cake was washed with Et<sub>2</sub>O (5 x 1.5 mL), and the resulting solution was concentrated. 1,3,5-trimethoxybenzene (5 – 15 mg) was added as an internal standard. The yield of the product was determined by analysis of the <sup>1</sup>H NMR spectrum of the crude reaction mixture.

### 5.4.2 General Procedure B: Suzuki-Miyaura Cross-Coupling of $\alpha$ -Pyridinium Salts

To an oven-dried 25 mL round-bottomed flask equipped with an oven-dried stir bar was added NiCl<sub>2</sub>·DME (11 mg, 0.05 equiv, 5 mol %), 4,4'-dimethyl-2,2'-bipyridine (dmbpy, 11 mg, 0.06 equiv, 6 mol %), boroxine (0.8 equiv, 0.8 mmol), K<sub>2</sub>CO<sub>3</sub> (2.8 equiv, 2.8 mmol), and pyridinium salt (1 equiv, 1.0 mmol). The flask was capped with a rubber septum, sealed with parafilm, fitted with an N<sub>2</sub> inlet needle and a vent needle, and subsequently purged for 20 min via constant flow of positive N<sub>2</sub> pressure. The vent needle was removed and MeCN (3 mL, 0.33 M, sparged, anhydrous) was added to the flask. The mixture was stirred in an oil-bath at 70 °C for 24 h and then allowed to cool to room temperature. The reaction was diluted with Et<sub>2</sub>O (10 mL) and filtered through a short plug of silica gel. The filter cake was

washed with Et<sub>2</sub>O (3 x 20 mL) and the resulting solution was concentrated. The crude product was purified via silica gel chromatography.

#### **5.4.3 General Procedure C: Synthesis of $\alpha$ -Pyridinium Salts**

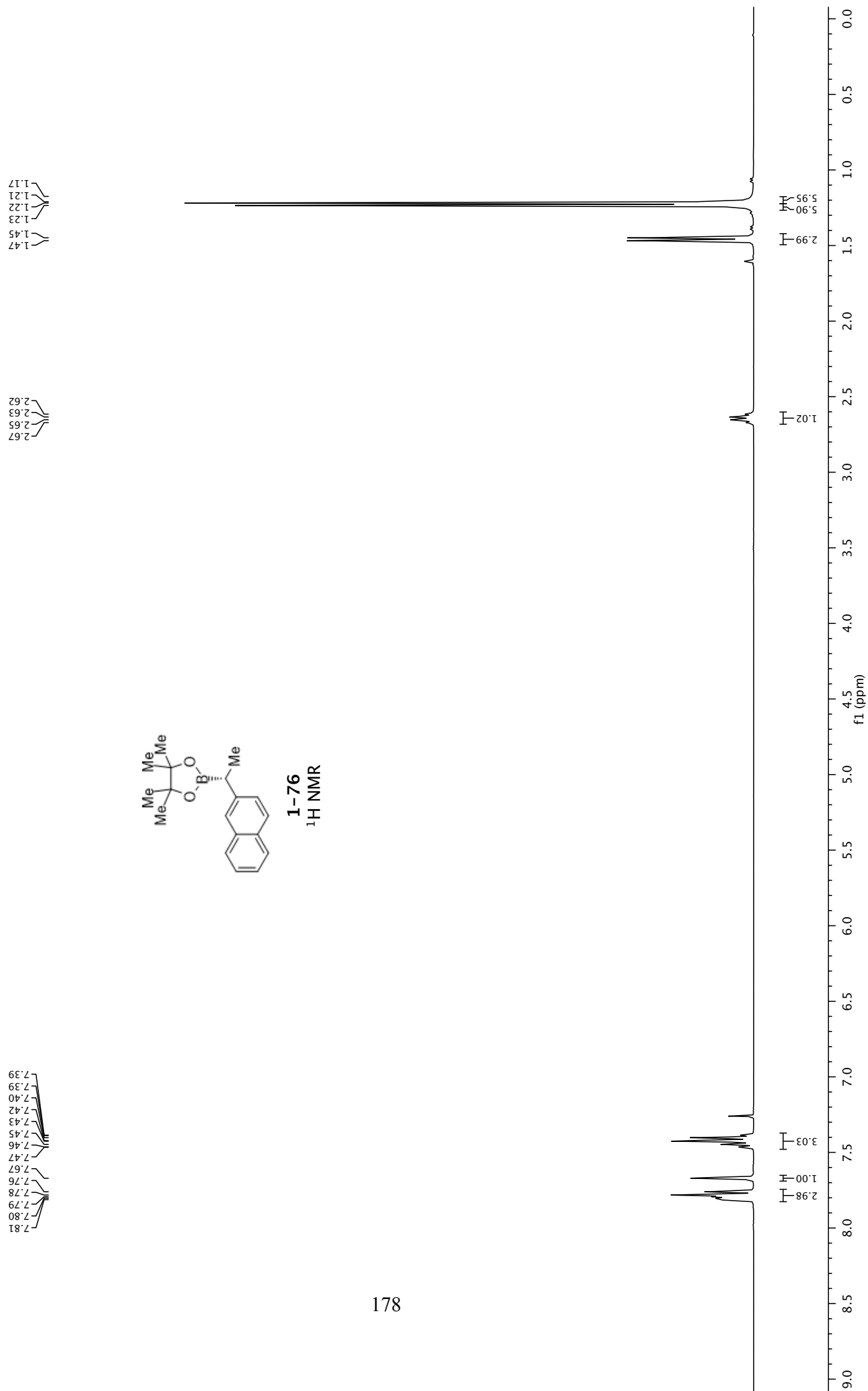
To a 25 mL round-bottomed flask equipped with a stir bar was added 2,4,6-triphenylpyrylium tetrafluoroborate (1 equiv),  $\alpha$ -amino ester hydrochloride (1 equiv), and powdered 4Å MS (500 mg/mmol, activated under hi-vacuum at 350 °C for 24 h). The flask was fitted with a rubber septum and a N<sub>2</sub> inlet. Anhydrous CH<sub>2</sub>Cl<sub>2</sub> (0.5 M) and Et<sub>3</sub>N (2 equiv) were added and the mixture was stirred for 20 min at room temperature. Glacial AcOH (2 equiv) was added and the resultant dark red suspension was stirred at room temperature for 5 h and then filtered through a short pad of celite. The filter cake was washed with CH<sub>2</sub>Cl<sub>2</sub> (3 x 20 mL). The organic layer was washed with 1 N HCl (aq., 4 x 30 mL), K<sub>2</sub>CO<sub>3</sub> (sat., aq., 4 x 30 mL), and then brine (1 x 30 mL). The organic layer was dried with MgSO<sub>4</sub>, filtered, and concentrated to give a crude residue. The product then purified via silica gel chromatography.

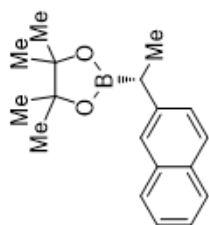
## REFERENCES

1. Scott, E.; Peter, F.; Sanders, J. *Appl. Microbiol. Biotechnol.* **2007**, *75* (4), 751-762.
2. Feng, Y.; Holte, D.; Zoller, J.; Umemiya, S.; Simke, L. R.; Baran, P. S. *J. Am. Chem. Soc.* **2015**, *137* (32), 10160-10163.
3. Ford, A.; Miel, H.; Ring, A.; Slattery, C. N.; Maguire, A. R.; McKervey, M. A. *Chem. Rev.* **2015**, *115* (18), 9981-10080.
4. Wu, G.; Deng, Y.; Wu, C.; Zhang, Y.; Wang, J. *Angew. Chem., Int. Ed.* **2014**, *53* (39), 10510-4.
5. Basch, C. H.; Liao, J.; Xu, J.; Piane, J. J.; Watson, M. P. *J. Am. Chem. Soc.* **2017**, *139* (15), 5313-5316.
6. Landoni, M. F.; Soraci, A. *Curr. Drug Metab.* **2001**, *2* (1), 37-51.
7. Moradi, W. A.; Buchwald, S. L. *J. Am. Chem. Soc.* **2001**, *123* (33), 7996-8002.
8. Lee, S.; Beare, N. A.; Hartwig, J. F. *J. Am. Chem. Soc.* **2001**, *123* (34), 8410-8411.
9. Dai, X.; Strotman, N. A.; Fu, G. C. *J. Am. Chem. Soc.* **2008**, *130* (11), 3302-3303.
10. Klauck, F. J. R.; James, M. J.; Glorius, F. *Angew. Chem., Int. Ed.* **2017**, *56* (40), 12336-12339.

**Appendix A**

**SPECTRAL AND CHROMATOGRAPHY DATA FOR CHAPTER 1**





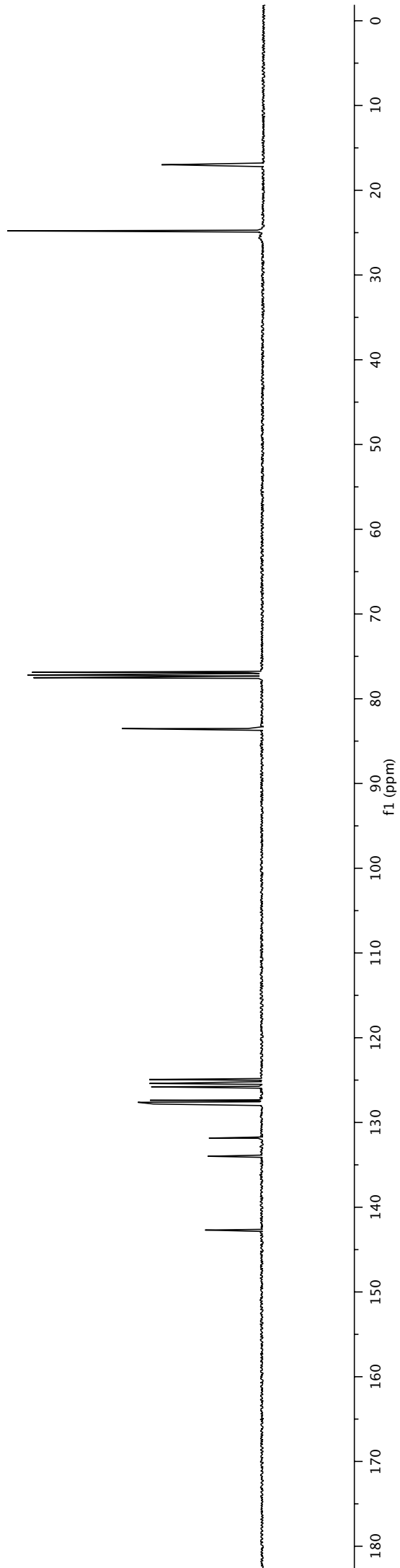
**1-76**  
<sup>13</sup>C NMR

16.99  
24.76

83.53

124.92  
125.40  
125.80  
127.38  
127.62  
127.67  
127.82  
131.84  
133.99

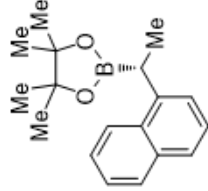
142.69



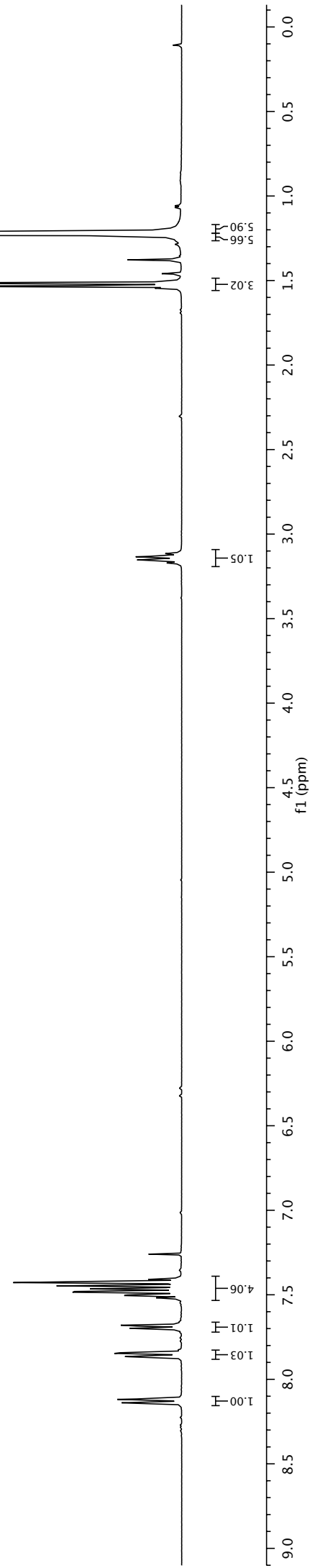
1.14  
1.15  
1.16  
1.17  
1.21  
1.22  
1.23  
1.51  
1.53

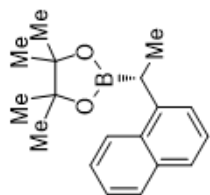
3.12  
3.13  
3.15  
3.17

7.40  
7.41  
7.42  
7.43  
7.45  
7.46  
7.48  
7.49  
7.50  
7.50  
7.52  
7.52  
7.68  
7.70  
7.84  
7.85  
7.87  
8.12  
8.14



**1-78**  
<sup>1</sup>H NMR





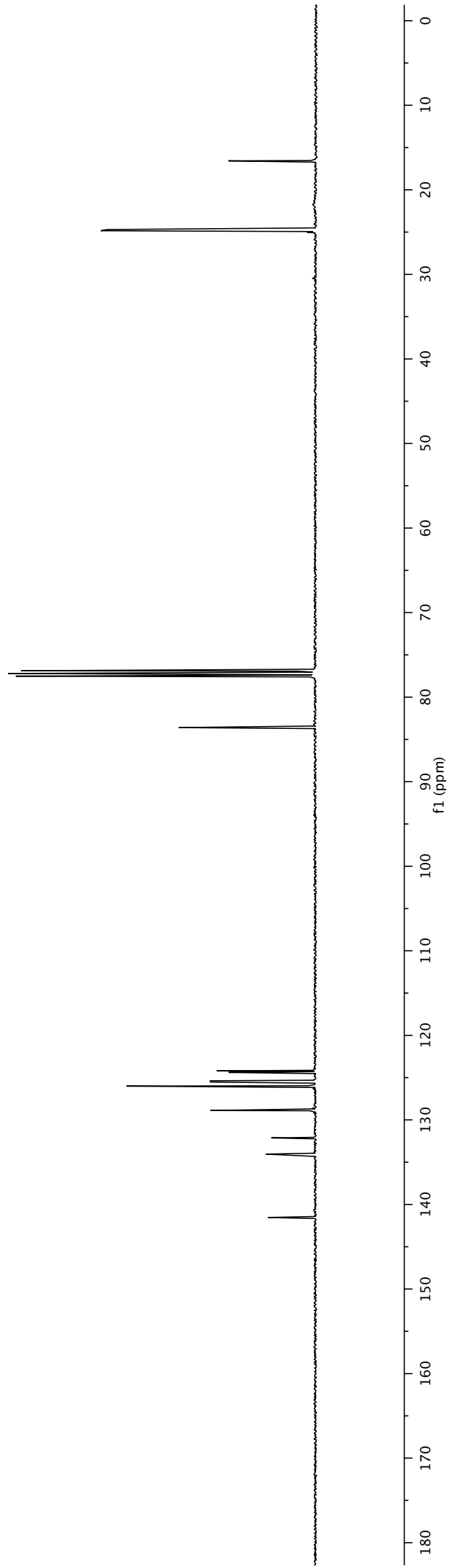
**1-78**  
<sup>13</sup>C NMR

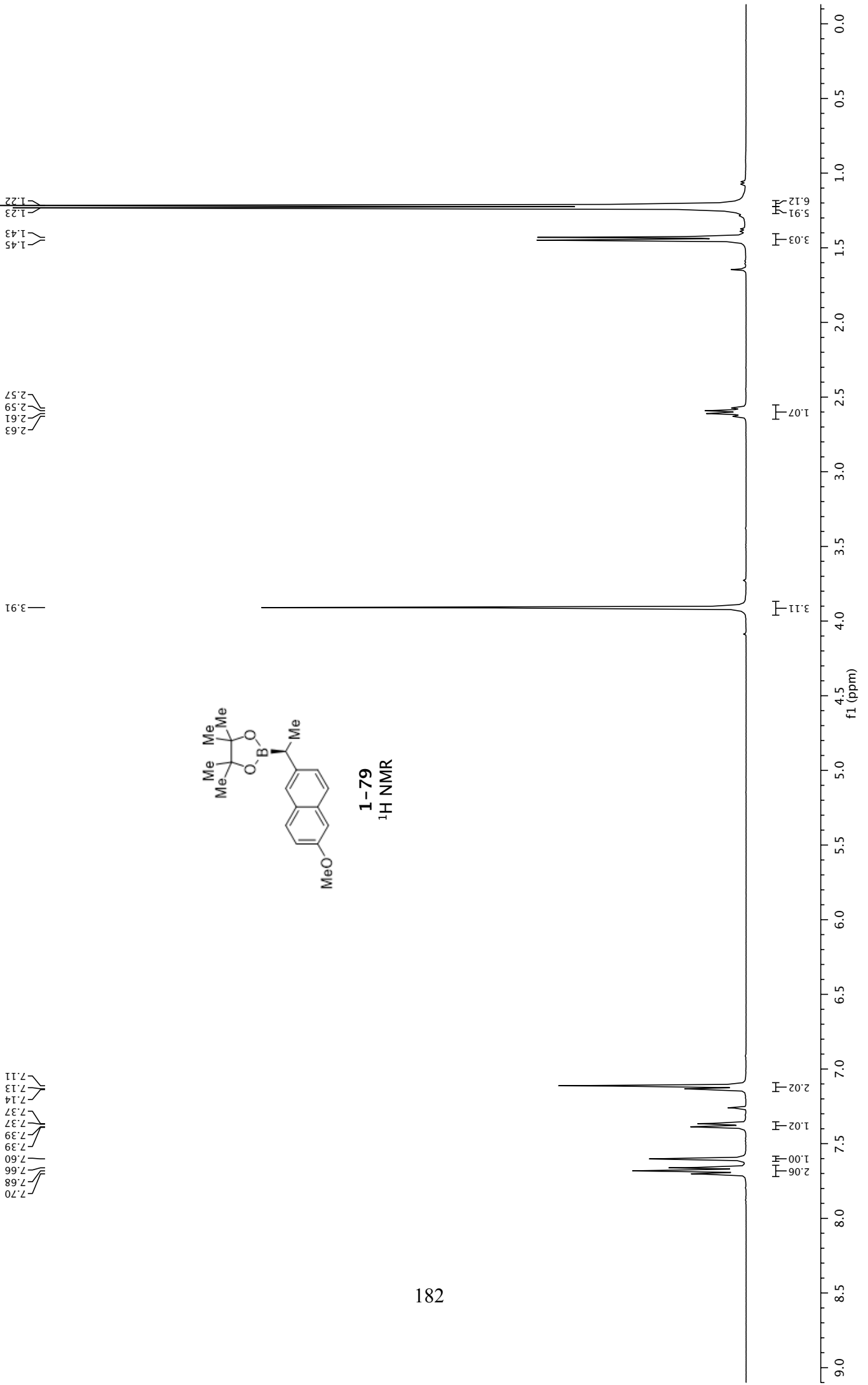
16.57  
24.70  
24.84

83.60

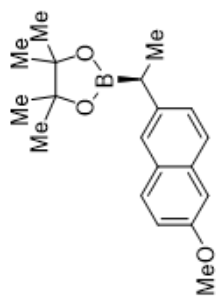
124.20  
124.39  
125.37  
125.52  
126.00  
128.89  
132.13  
134.05

141.54

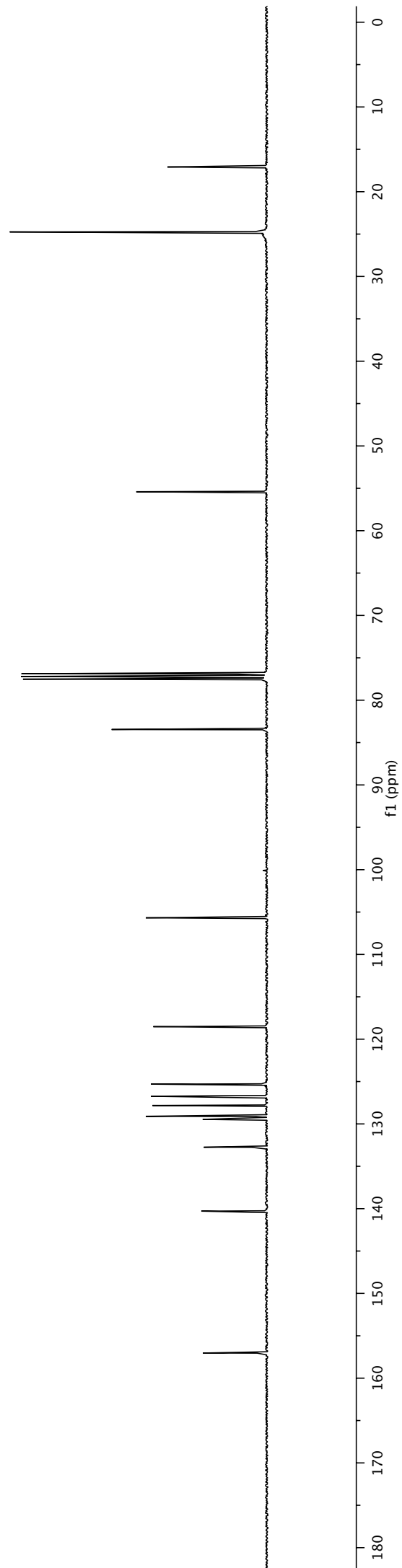




157.03  
140.29  
132.75  
129.46  
129.10  
127.82  
126.74  
125.31  
118.52  
105.68  
83.46  
55.40  
24.78  
17.08



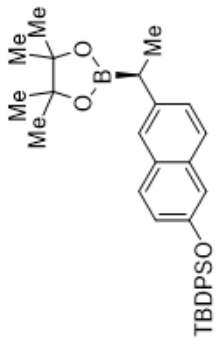
**1-79**  
<sup>13</sup>C NMR



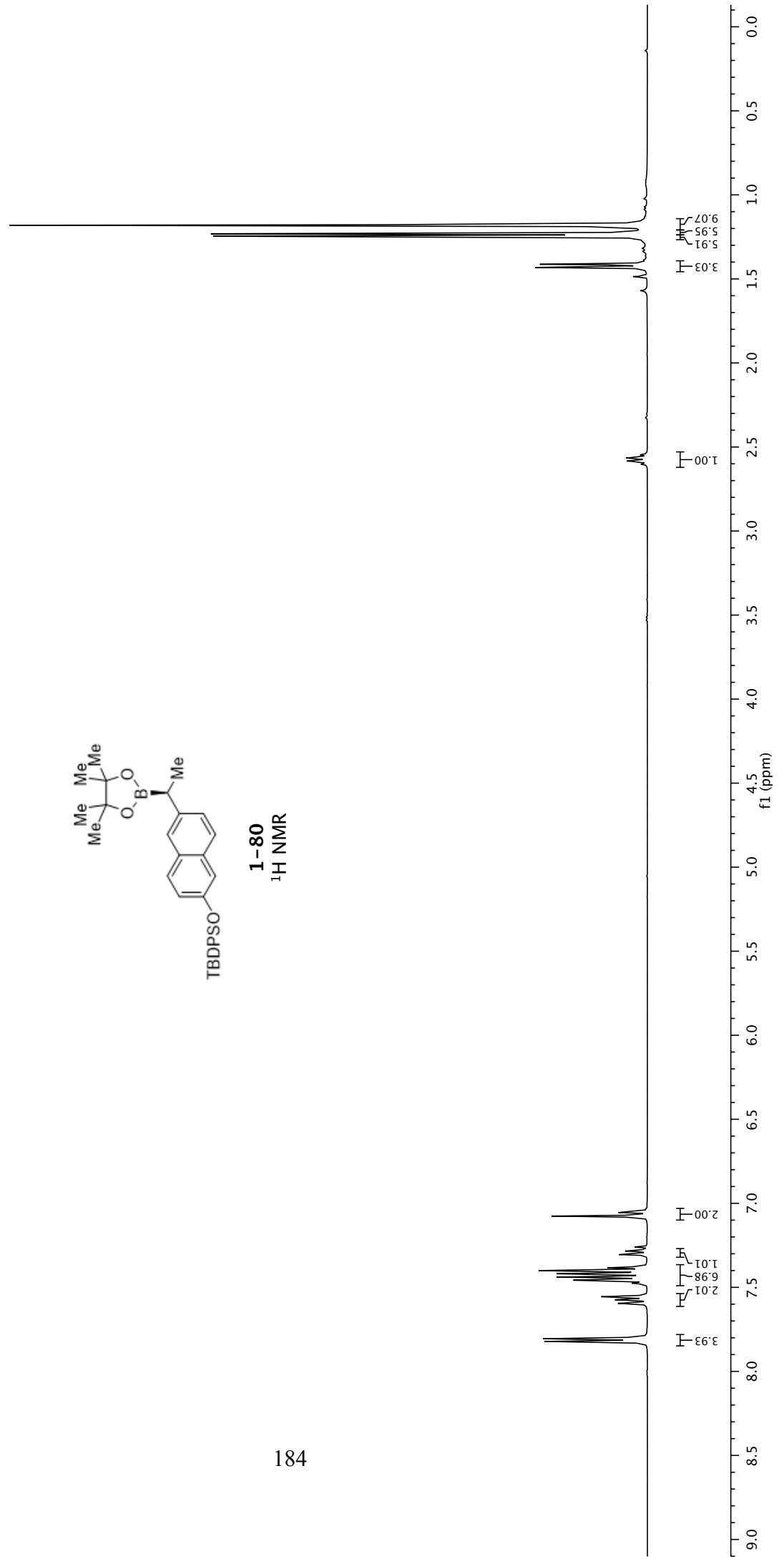
1.43  
1.41  
1.25  
1.23  
1.18

2.55  
2.56  
2.58  
2.60

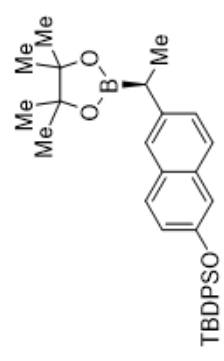
7.82  
7.81  
7.80  
7.60  
7.57  
7.56  
7.48  
7.46  
7.45  
7.44  
7.42  
7.40  
7.38  
7.38  
7.31  
7.30  
7.28  
7.28  
7.08  
7.05  
7.05



**1-80**  
<sup>1</sup>H NMR



— 17.21  
— 19.70  
— 24.79  
— 24.82  
— 26.76



**1-80**  
<sup>13</sup>C NMR

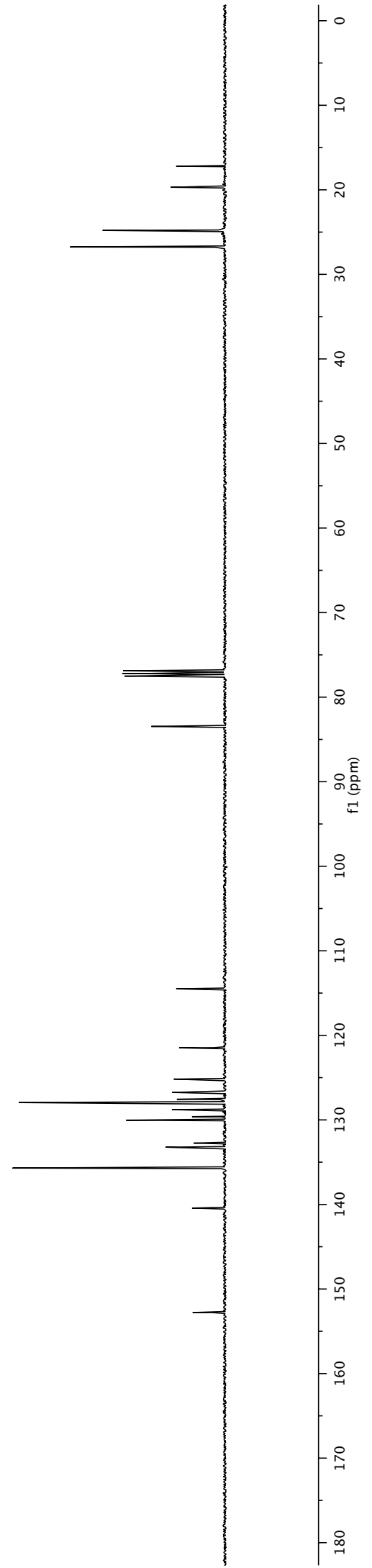
— 83.46

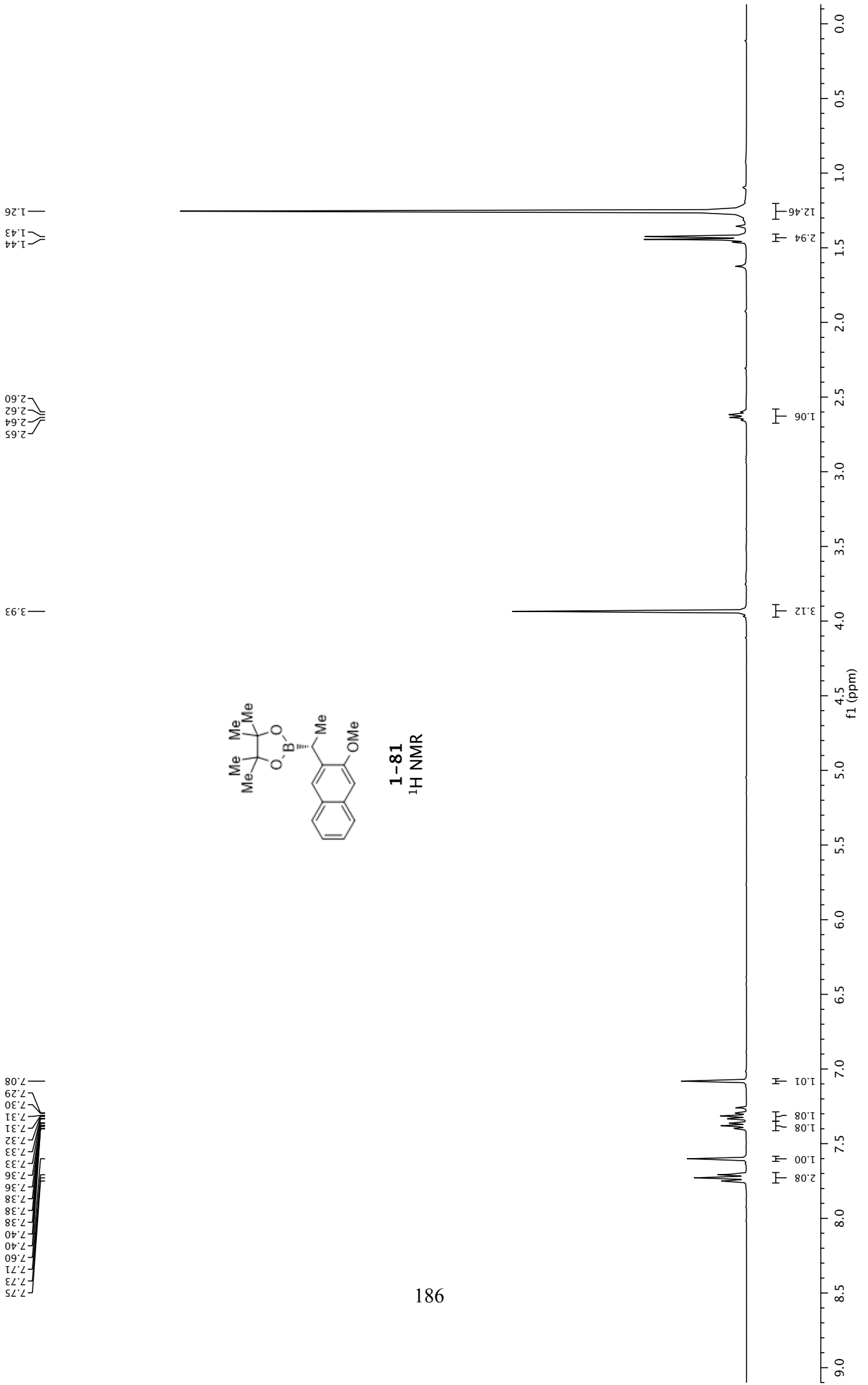
— 114.50

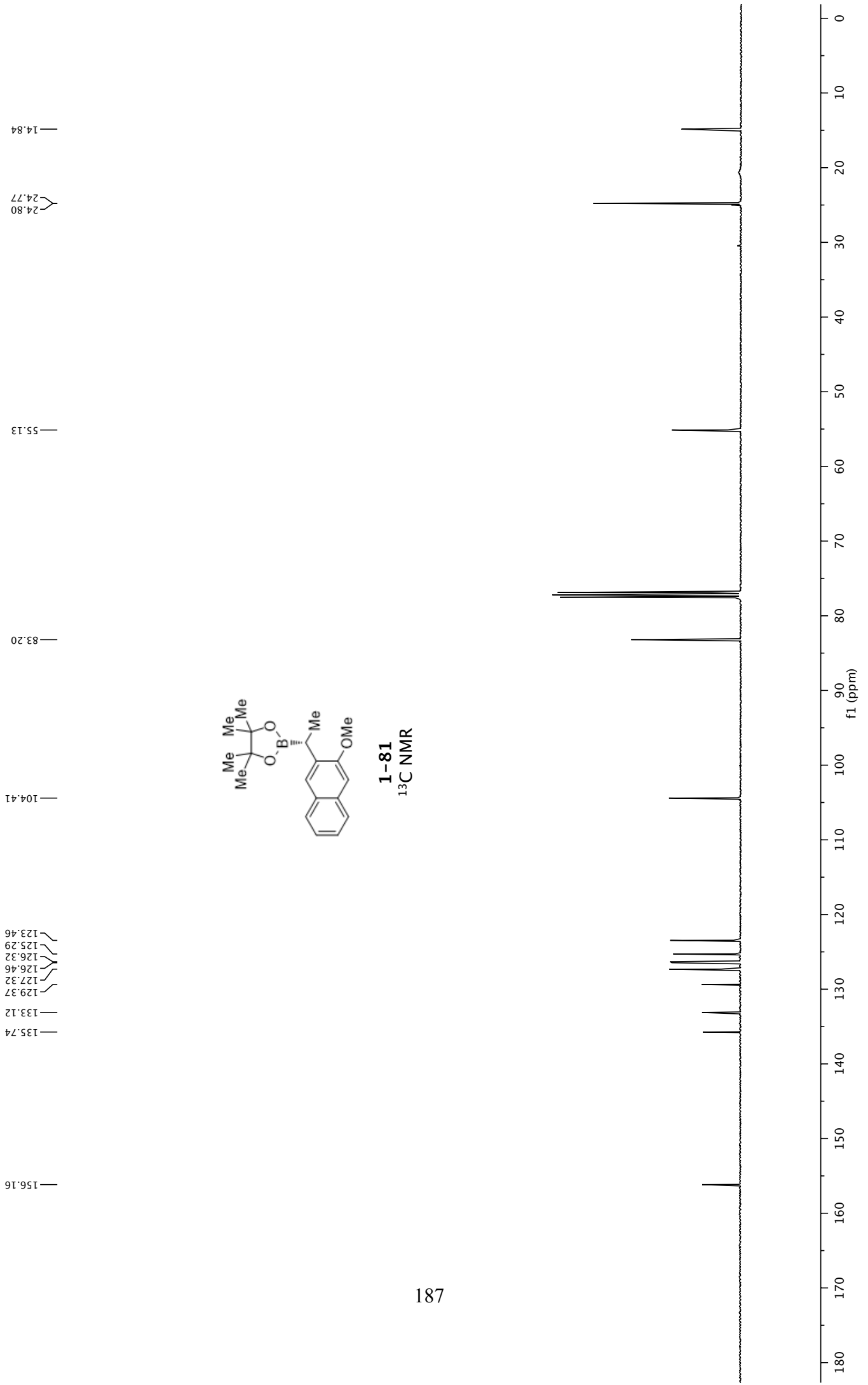
— 121.47  
— 125.18  
— 126.75  
— 127.56  
— 127.95  
— 128.78  
— 129.62  
— 130.03  
— 132.74  
— 133.23  
— 135.70

— 140.43

— 152.78





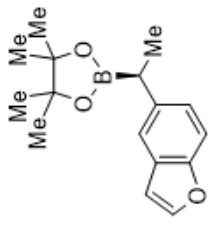


1.40  
1.38  
1.23  
1.21

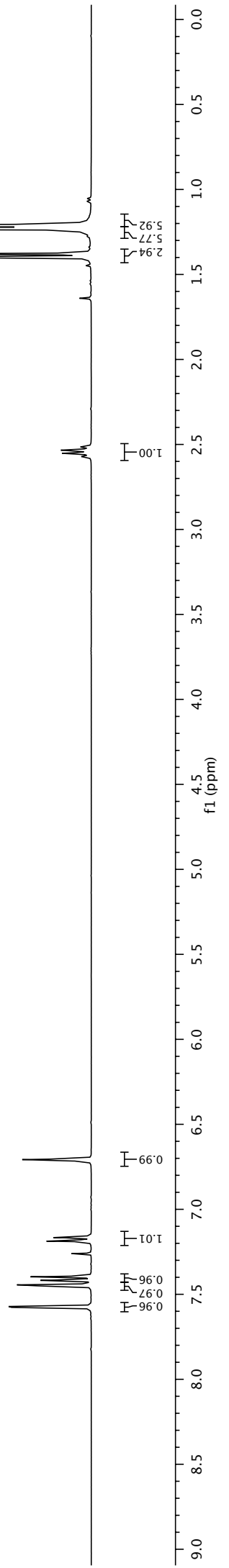
2.57  
2.55  
2.53  
2.51

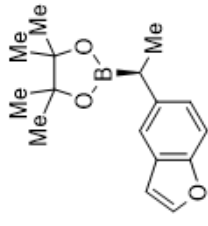
6.71  
6.71  
6.71  
6.71

7.58  
7.57  
7.45  
7.44  
7.42  
7.40  
7.19  
7.18  
7.17  
7.16



1-82  
<sup>1</sup>H NMR





1-82  
<sup>13</sup>C NMR

17.92  
24.75

83.43

106.67

111.12

119.77

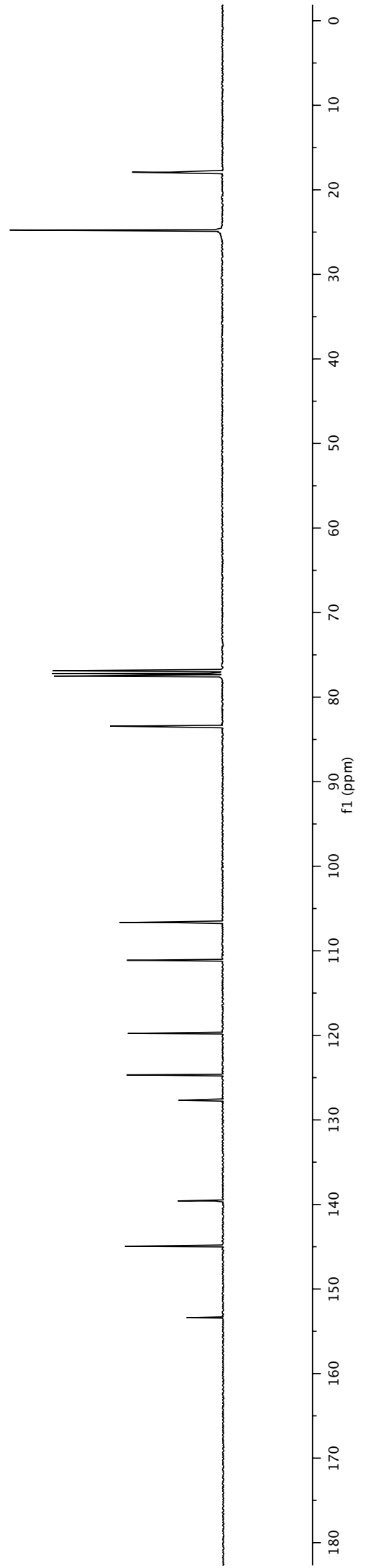
124.67

127.68

139.58

144.95

153.39

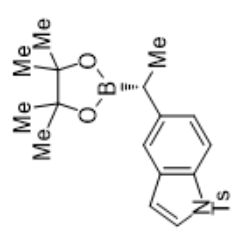


1.33  
1.32  
1.20  
1.18

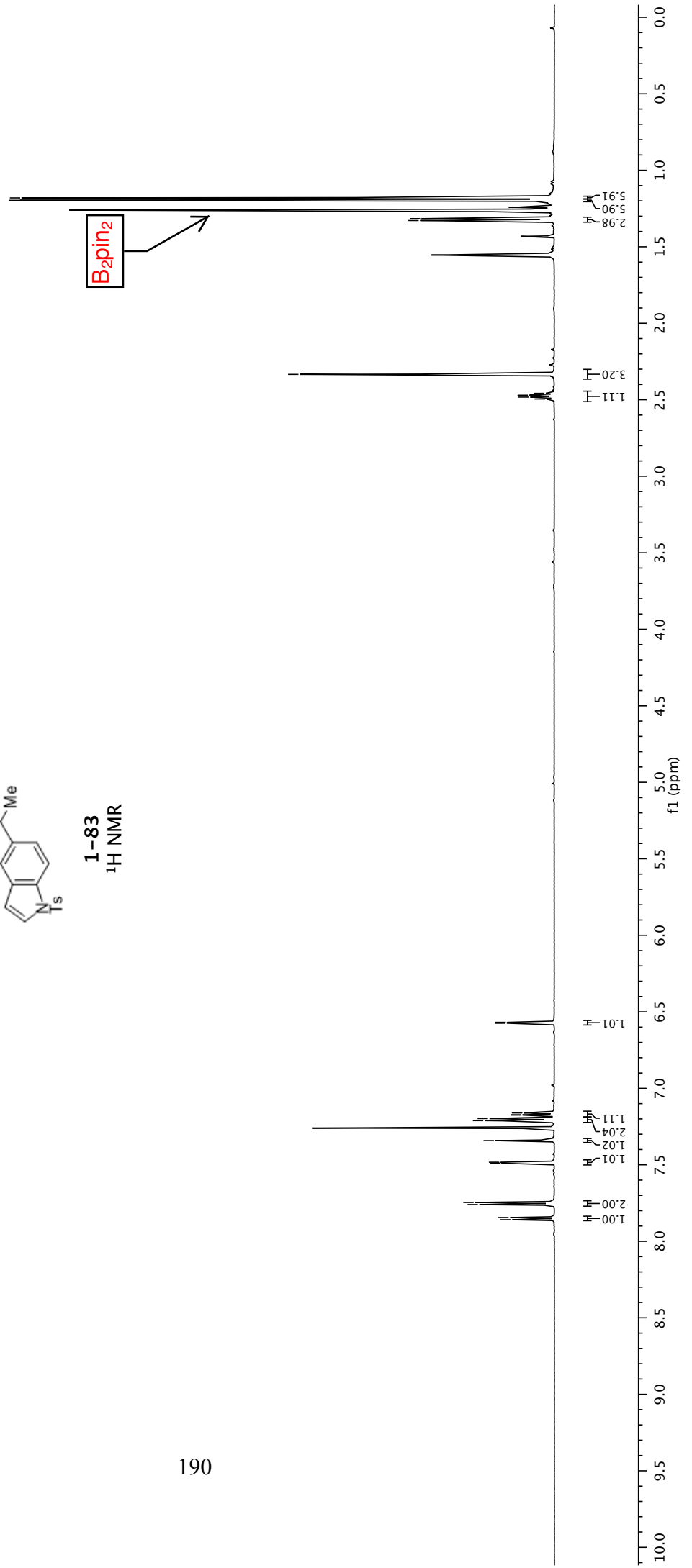
2.50  
2.48  
2.47  
2.46  
2.33

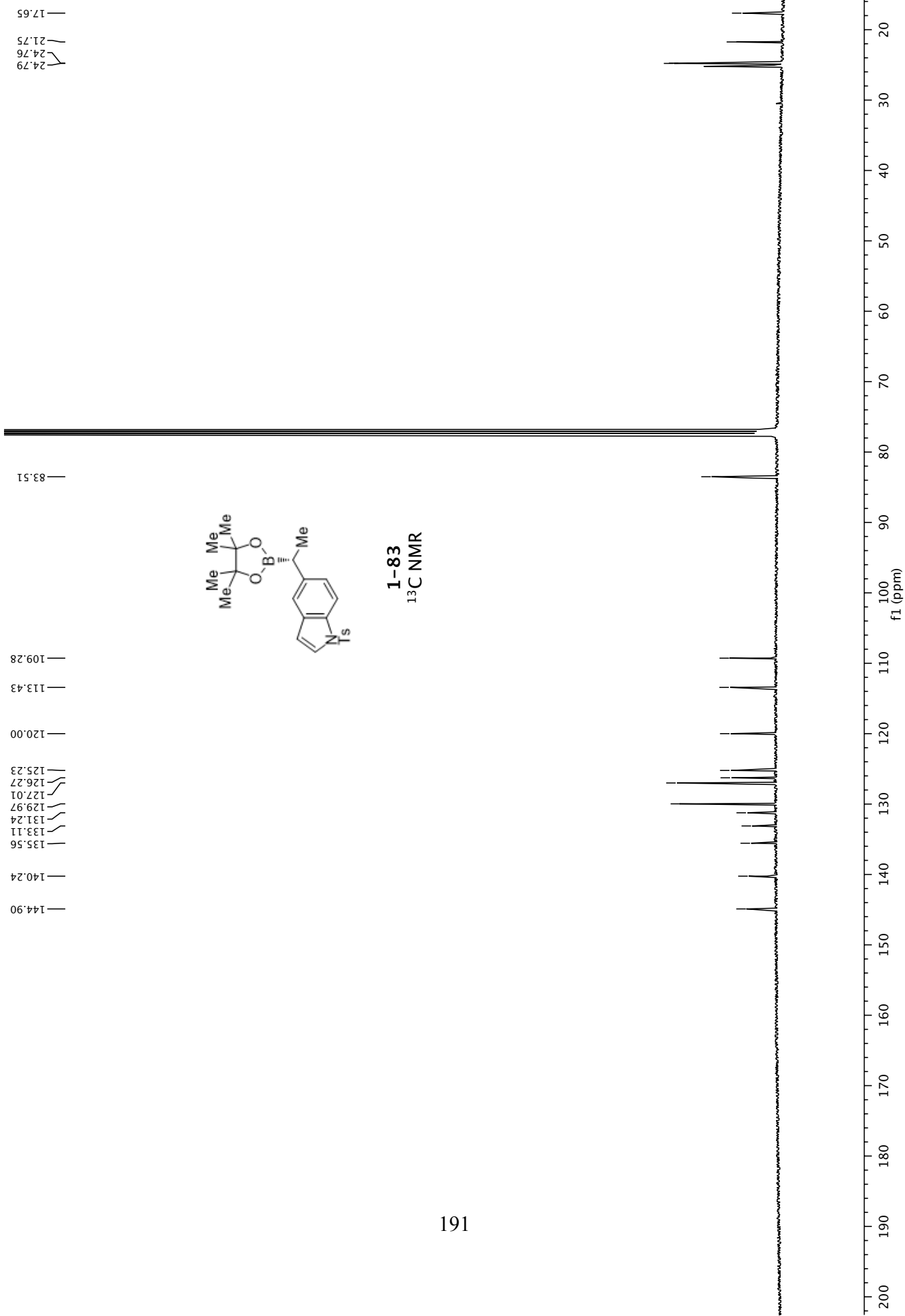
6.57

7.86  
7.84  
7.76  
7.75  
7.49  
7.48  
7.34  
7.21  
7.20  
7.18  
7.17  
7.16



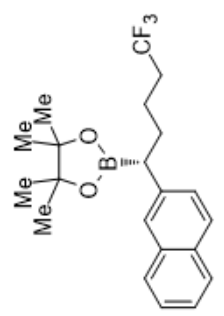
1-83  
<sup>1</sup>H NMR



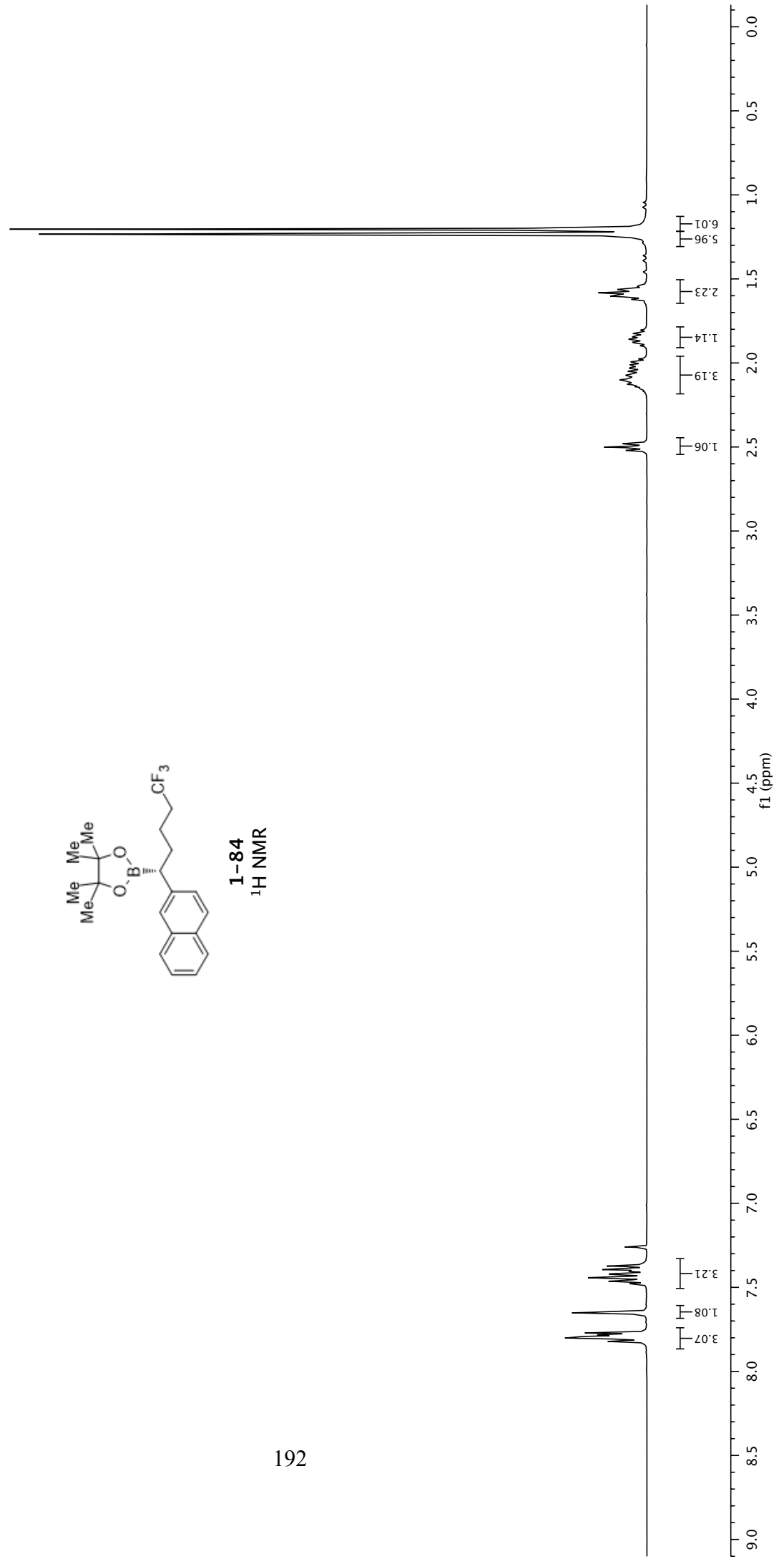


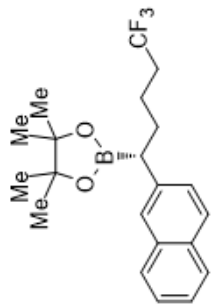
2.52  
2.50  
2.48  
2.18  
2.17  
2.15  
2.14  
2.13  
2.12  
2.11  
2.11  
2.10  
2.09  
2.08  
2.07  
2.06  
2.05  
2.03  
2.03  
2.02  
2.01  
1.99  
1.98  
1.90  
1.88  
1.86  
1.84  
1.84  
1.82  
1.80  
1.64  
1.62  
1.60  
1.60  
1.58  
1.56  
1.55  
1.54  
1.52  
1.23  
1.20

7.82  
7.80  
7.79  
7.78  
7.77  
7.65  
7.48  
7.46  
7.46  
7.44  
7.42  
7.42  
7.41  
7.40  
7.39  
7.39  
7.37



**1-84**  
<sup>1</sup>H NMR



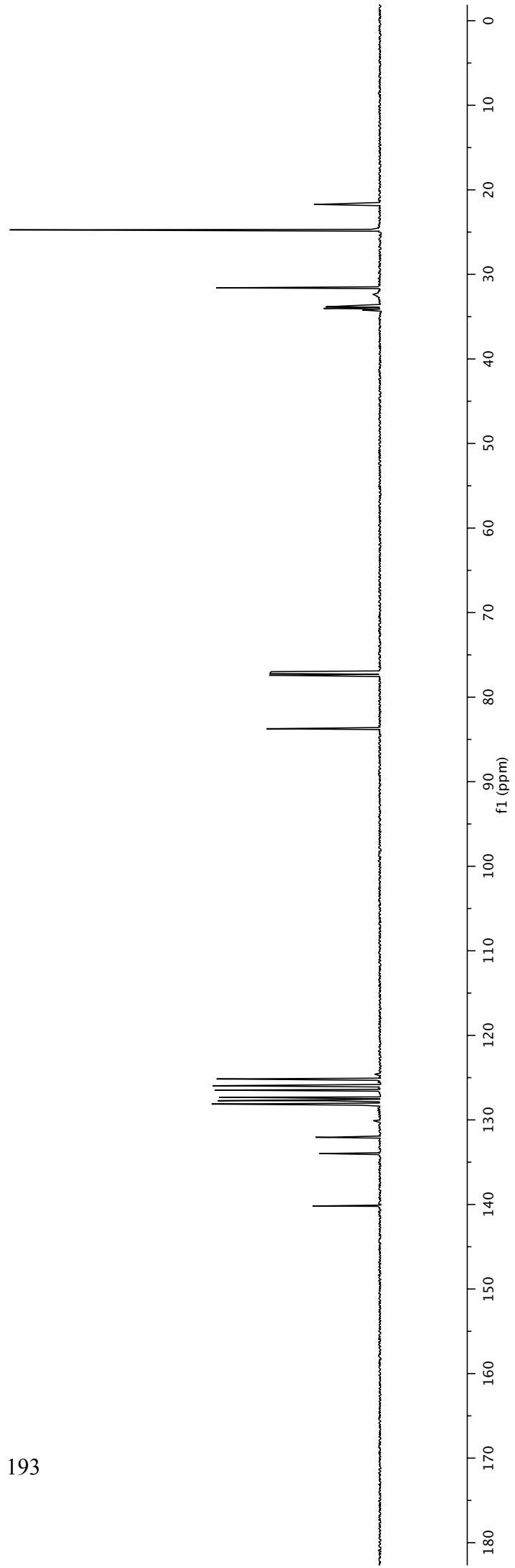


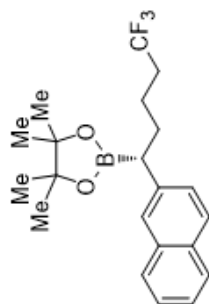
**1-84**  
<sup>13</sup>C NMR

34.22  
34.03  
33.84  
33.65  
31.59  
24.81  
24.73  
21.76  
21.74  
21.72  
21.70

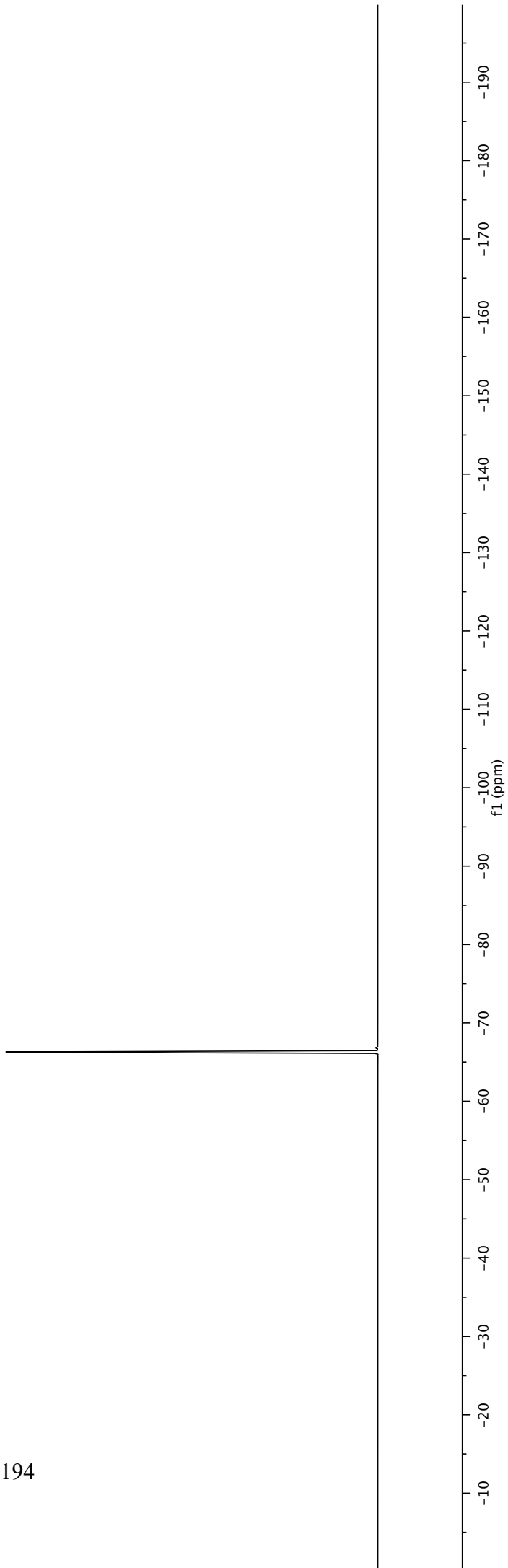
83.74

140.19  
133.98  
132.05  
130.09  
128.26  
128.13  
127.73  
127.64  
127.32  
126.48  
126.43  
125.96  
125.16  
124.60





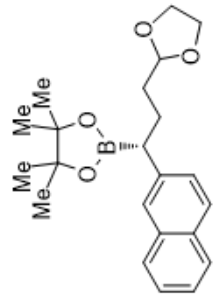
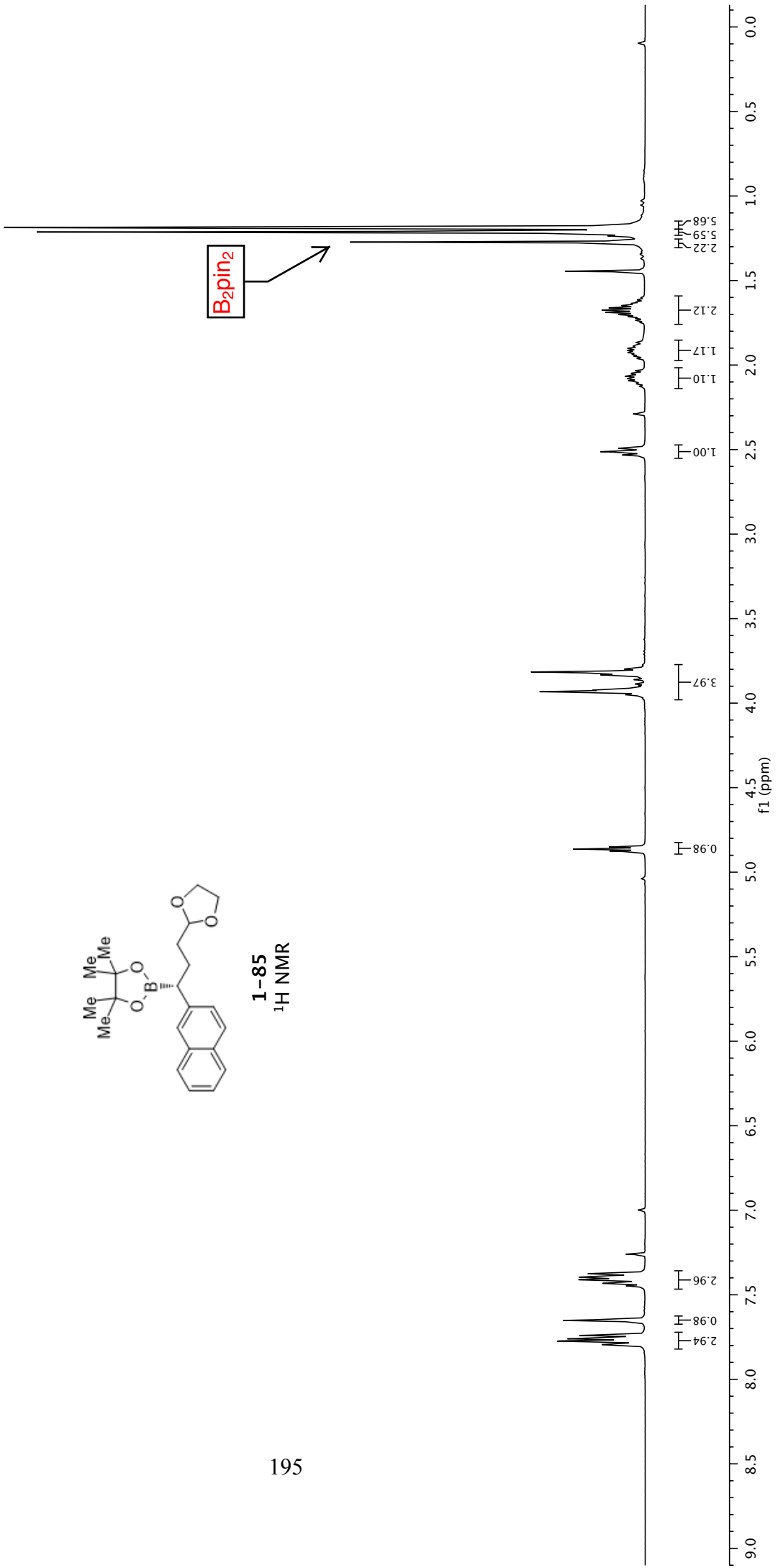
**1-84**  
<sup>19</sup>F NMR



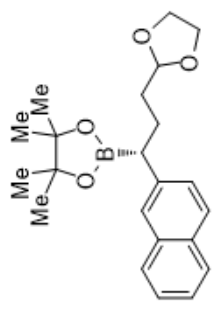
1.10  
1.21  
1.63  
1.64  
1.65  
1.66  
1.68  
1.69  
1.70  
1.71  
1.72  
1.74  
1.74  
1.89  
1.89  
1.90  
1.91  
1.91  
1.92  
1.93  
1.94  
1.94  
1.95  
2.03  
2.05  
2.05  
2.06  
2.07  
2.07  
2.08  
2.09  
2.09  
2.10  
2.49  
2.51  
2.53

3.78  
3.79  
3.80  
3.82  
3.82  
3.83  
3.83  
3.84  
3.85  
3.86  
3.89  
3.90  
3.91  
3.92  
3.92  
3.92  
3.93  
3.95  
3.95  
3.96  
3.96  
3.97  
4.85  
4.86  
4.88

7.37  
7.38  
7.40  
7.40  
7.41  
7.43  
7.43  
7.45  
7.65  
7.74  
7.75  
7.76  
7.77  
7.79



**1-85**  
<sup>1</sup>H NMR



1-85  
13C NMR

26.78  
24.79  
24.74

33.53

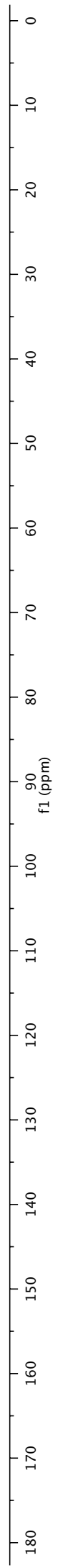
64.91

83.55

104.68

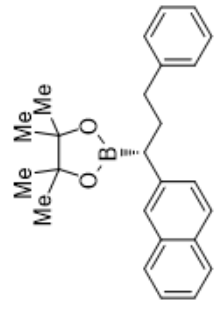
124.96  
125.77  
126.53  
127.47  
127.59  
127.63  
127.93  
131.92  
133.90

140.52

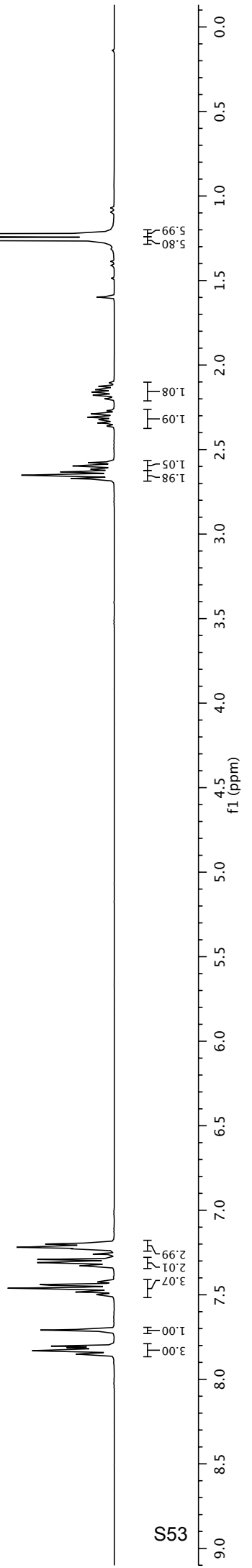


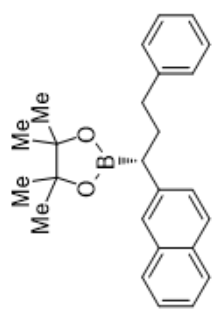
2.67  
2.65  
2.63  
2.62  
2.60  
2.58  
2.36  
2.34  
2.33  
2.32  
2.31  
2.29  
2.27  
2.20  
2.18  
2.17  
2.16  
2.15  
2.14  
2.13  
2.11  
1.25  
1.23

7.85  
7.83  
7.83  
7.81  
7.81  
7.80  
7.71  
7.50  
7.48  
7.48  
7.46  
7.46  
7.44  
7.44  
7.42  
7.42  
7.33  
7.31  
7.29  
7.23  
7.22  
7.21  
7.20



1-86  
<sup>1</sup>H NMR



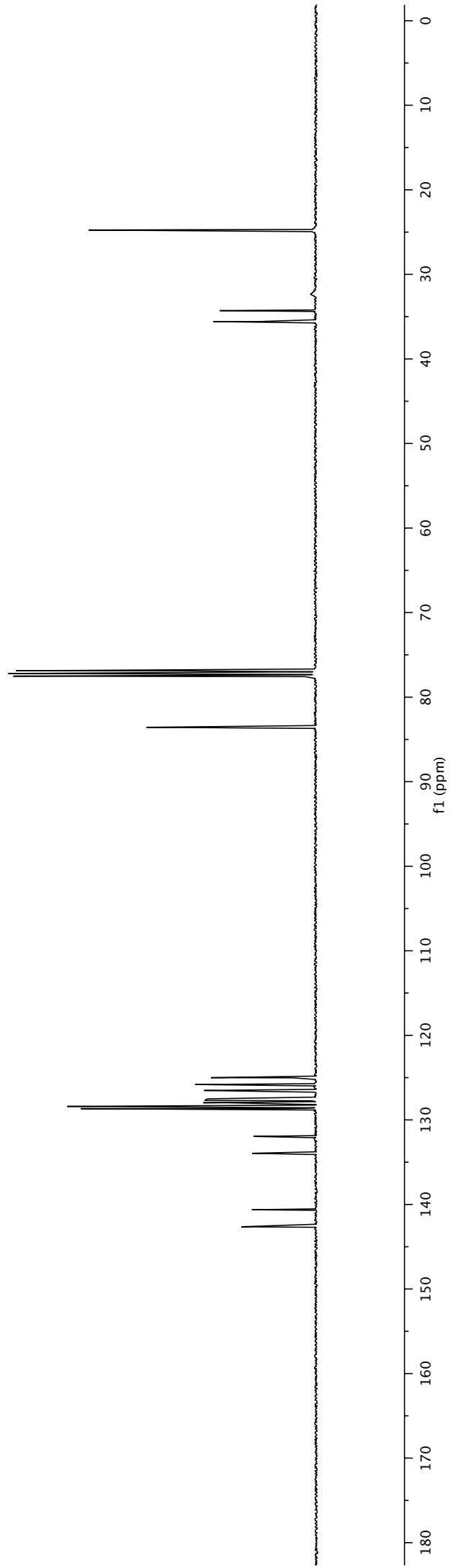


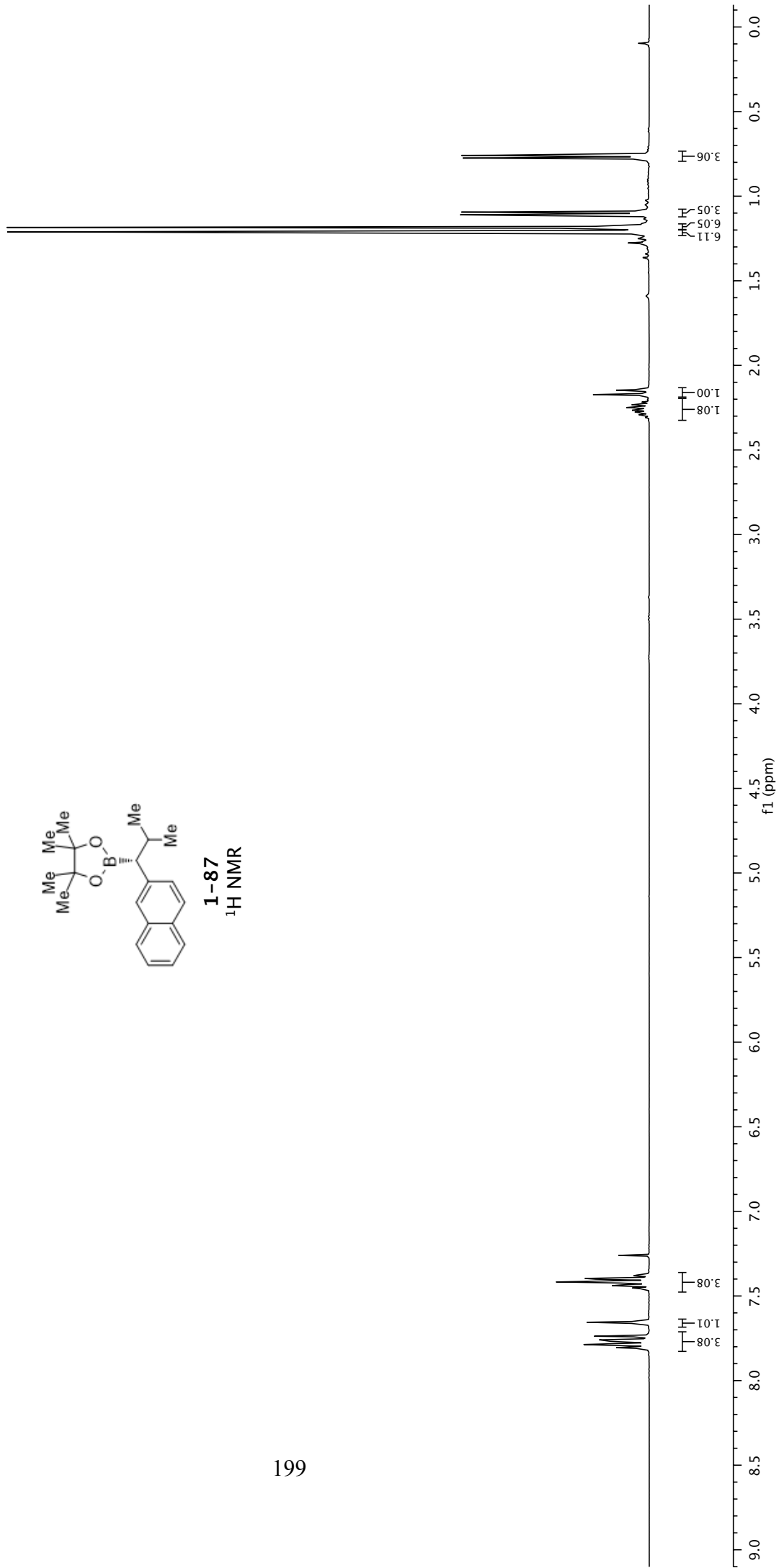
**1-86**  
<sup>13</sup>C NMR

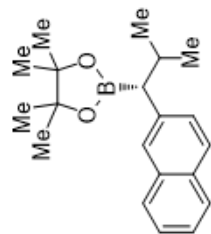
24.76  
24.84  
34.28  
35.58

83.57

125.01  
125.81  
125.84  
126.52  
127.51  
127.62  
127.70  
127.97  
128.40  
128.67  
131.95  
133.95  
140.62  
142.64





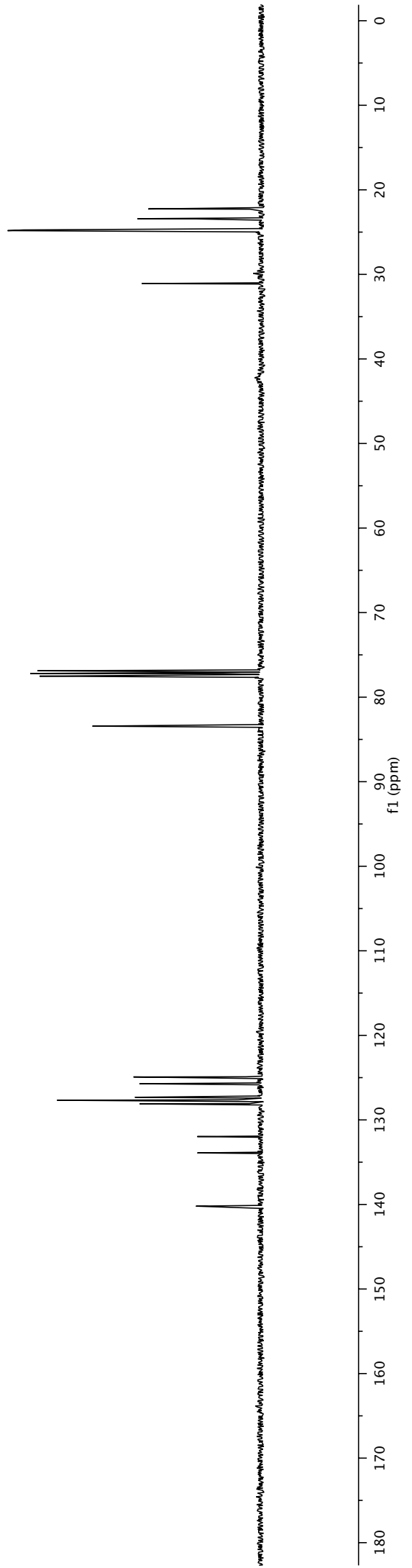


**1-87**  
<sup>13</sup>C NMR

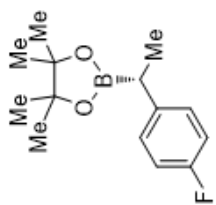
— 31.09  
 — 24.83  
 — 24.74  
 — 23.42  
 — 22.26

— 83.43

— 140.20  
 — 133.90  
 — 131.97  
 — 128.10  
 — 127.68  
 — 127.64  
 — 127.33  
 — 125.72  
 — 124.92



7.19  
7.18  
7.17  
7.16  
7.16  
7.15  
6.98  
6.97  
6.96  
6.95  
6.95  
6.94  
6.93  
6.92  
6.92



**1-88**  
H NMR

1.32  
1.30  
1.21  
1.20

2.44  
2.42  
2.41  
2.39

3.00  
5.70  
5.85

1.00

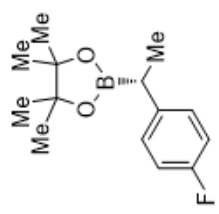
2.11

1.95

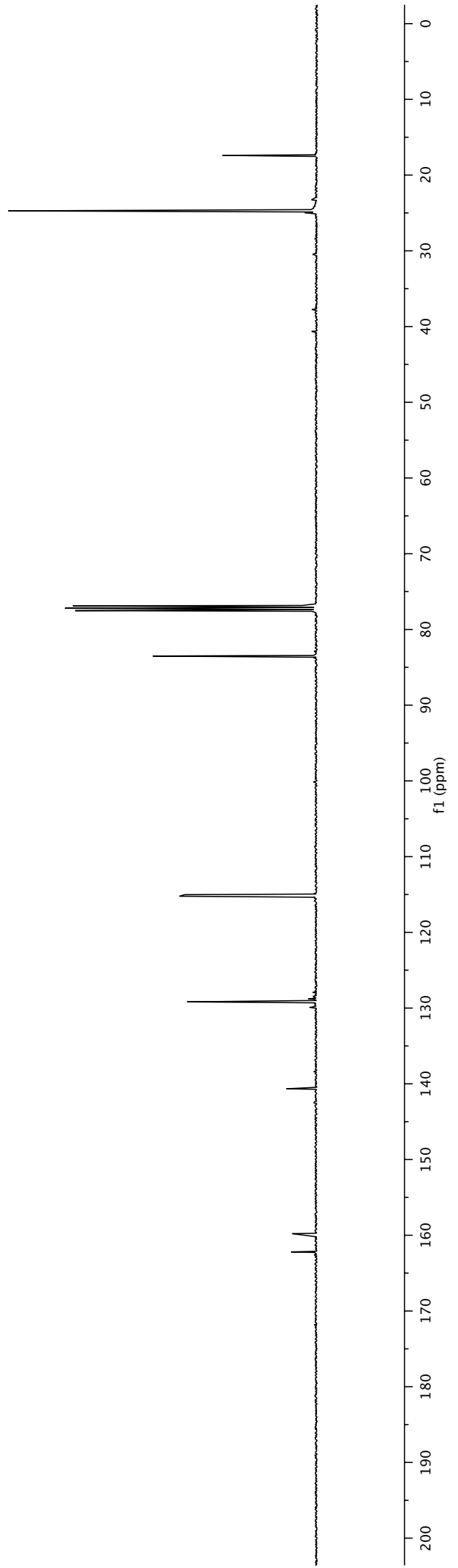
0.0  
0.5  
1.0  
1.5  
2.0  
2.5  
3.0  
3.5  
4.0  
4.5  
5.0  
5.5  
6.0  
6.5  
7.0  
7.5  
8.0  
8.5  
9.0  
9.5  
10.0

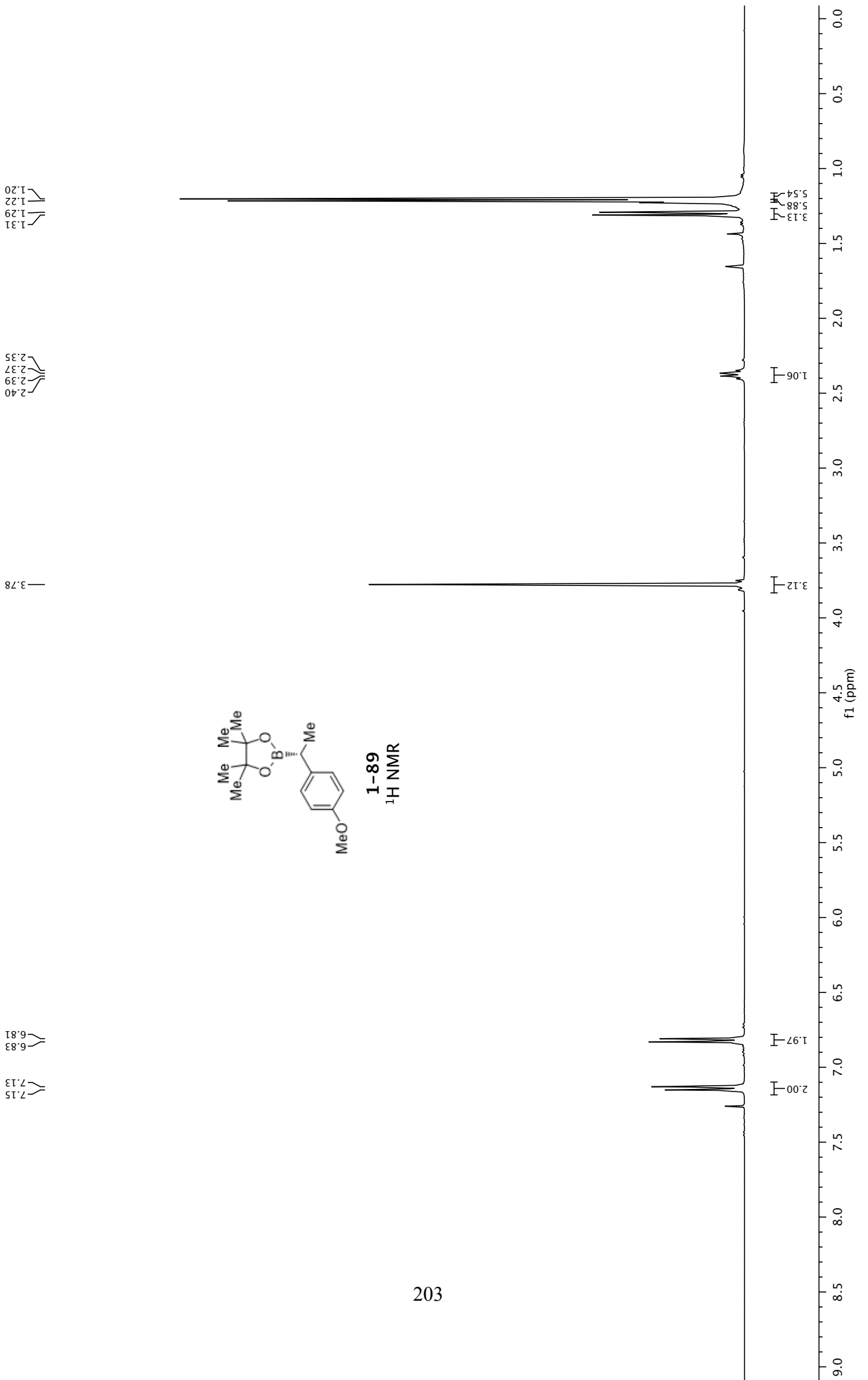
f1 (ppm)

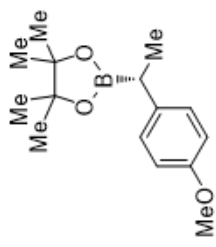
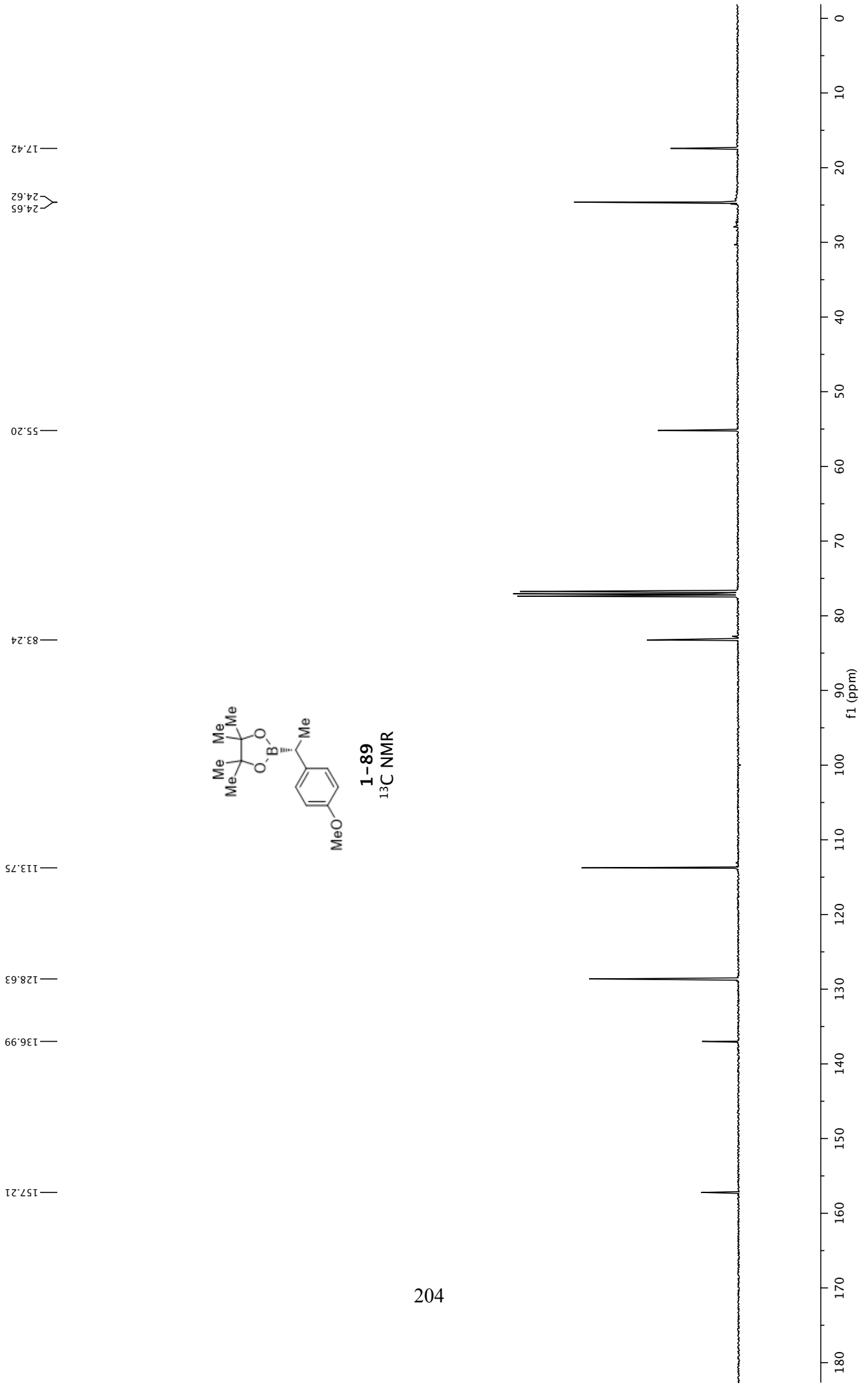
17.40  
24.77  
83.51  
115.23  
115.02  
129.18  
129.10  
140.63  
140.66  
159.79  
162.20



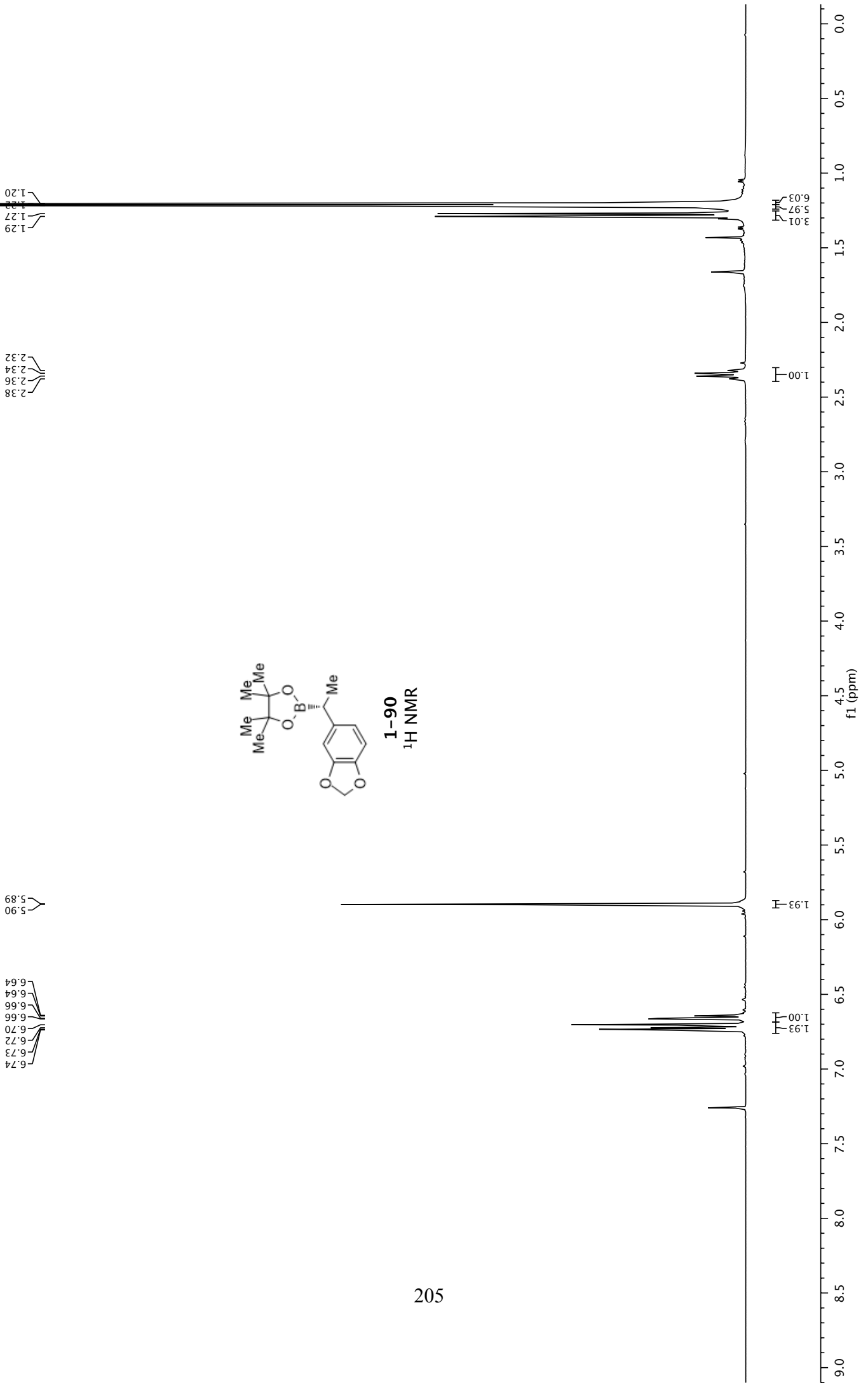
**1-88**  
<sup>13</sup>C NMR







**1-89**  
<sup>13</sup>C NMR



17.68  
24.75

83.45

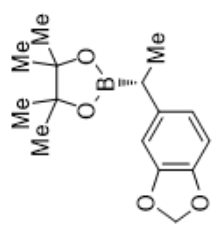
100.77

108.56  
108.31

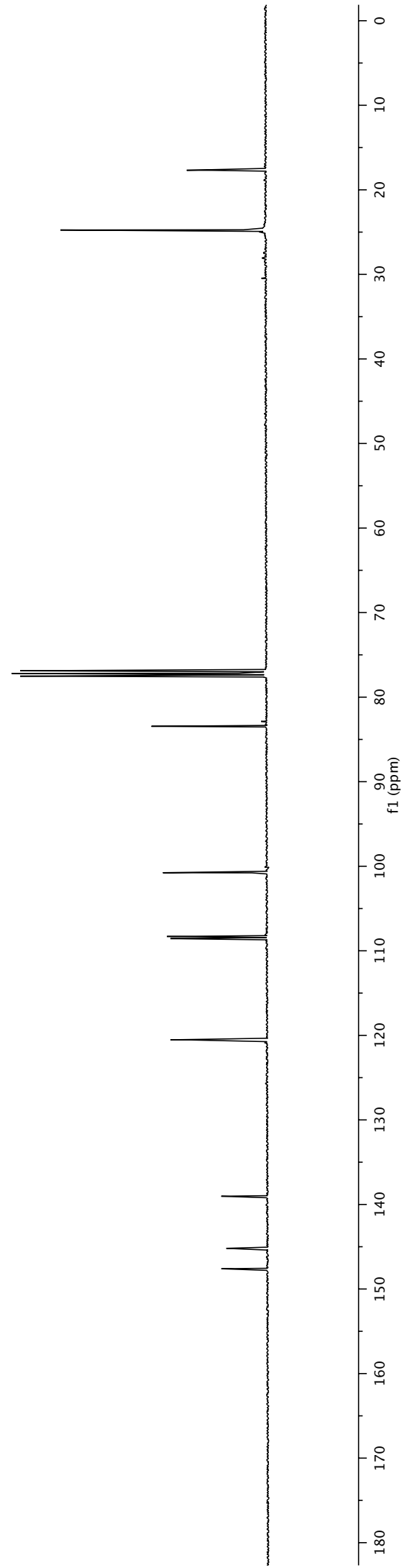
120.53

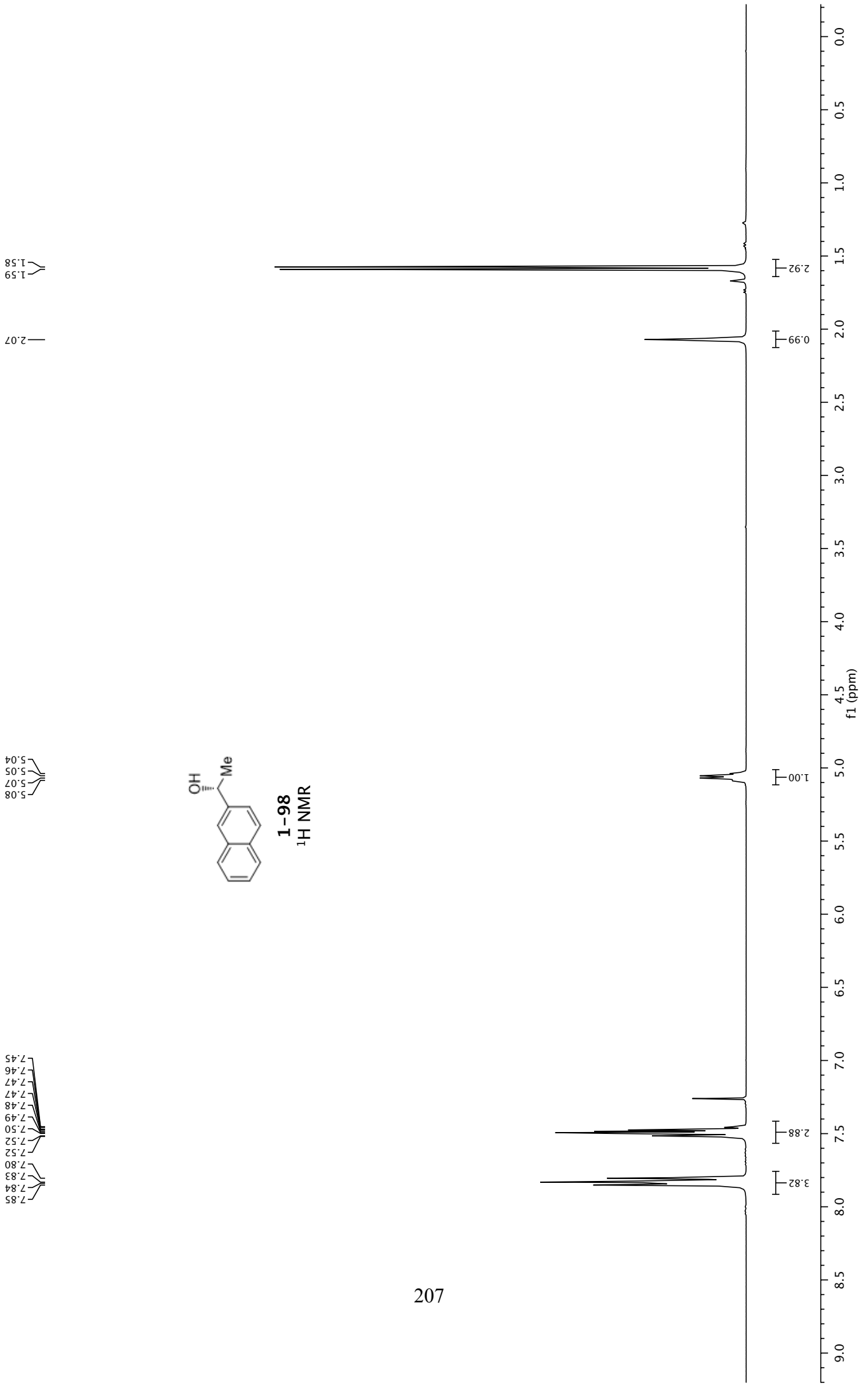
139.03

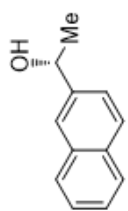
145.19  
147.60



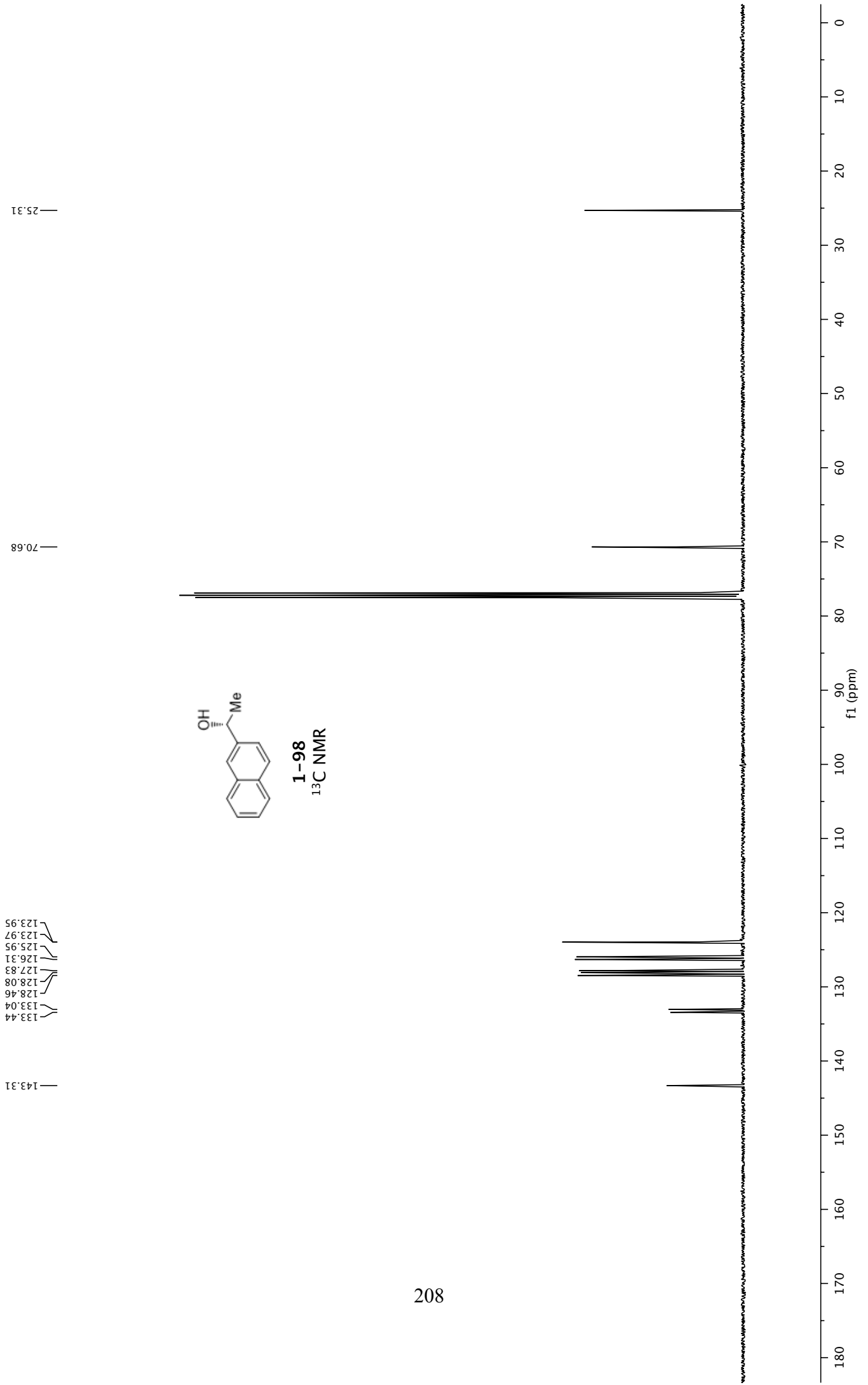
**1-90**  
<sup>13</sup>C NMR

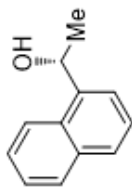






**1-98**  
<sup>13</sup>C NMR





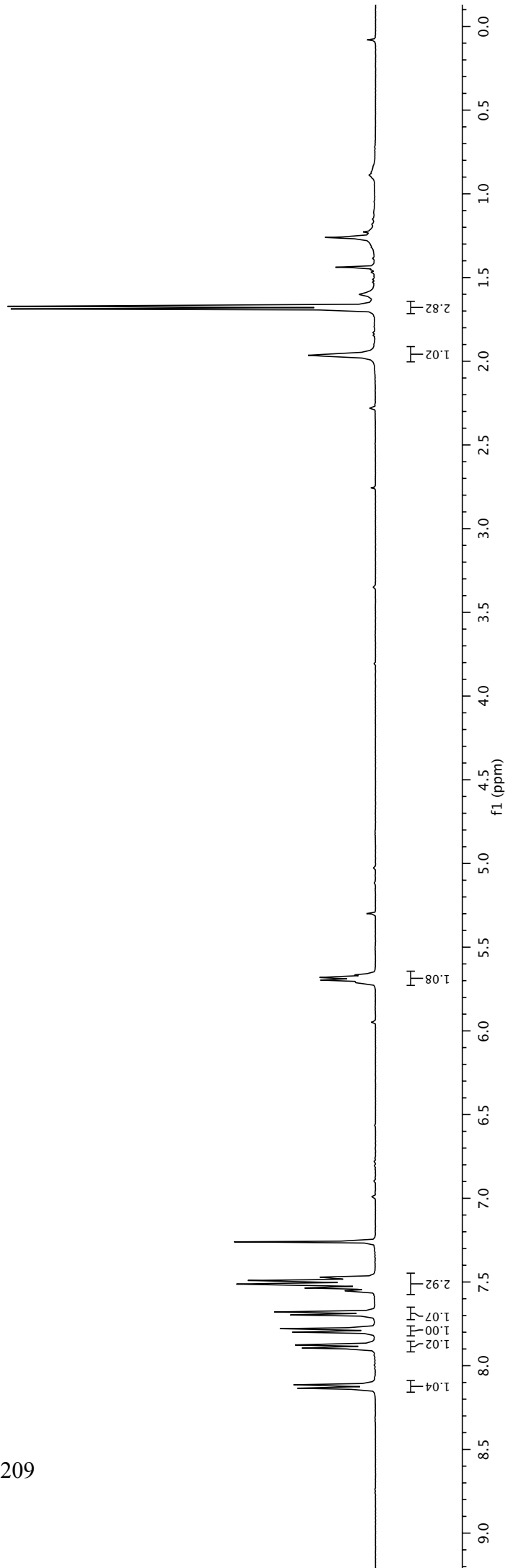
1-100  
<sup>1</sup>H NMR

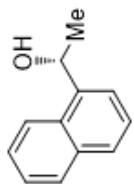
1.69  
1.67

1.96

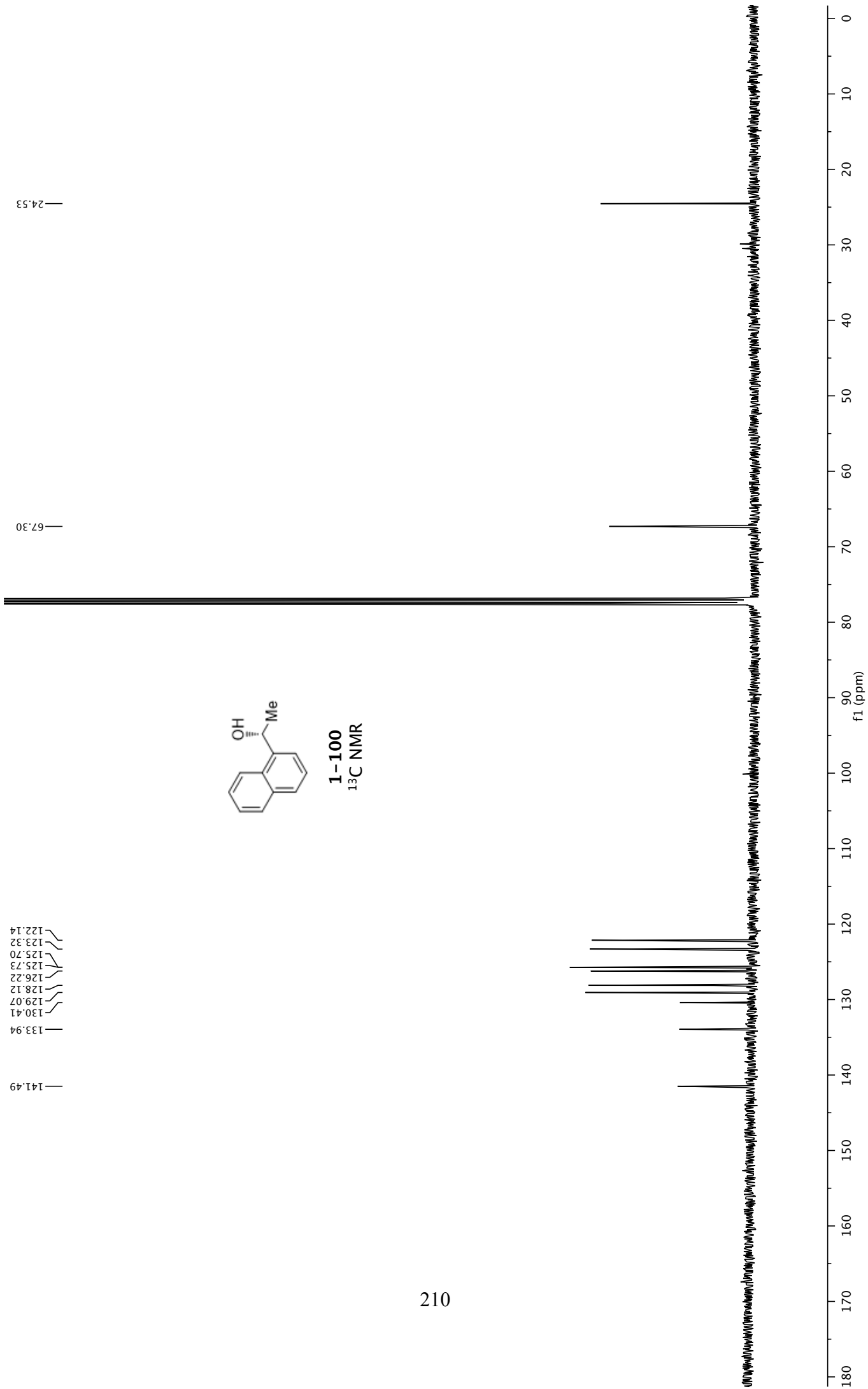
5.71  
5.70  
5.68  
5.67

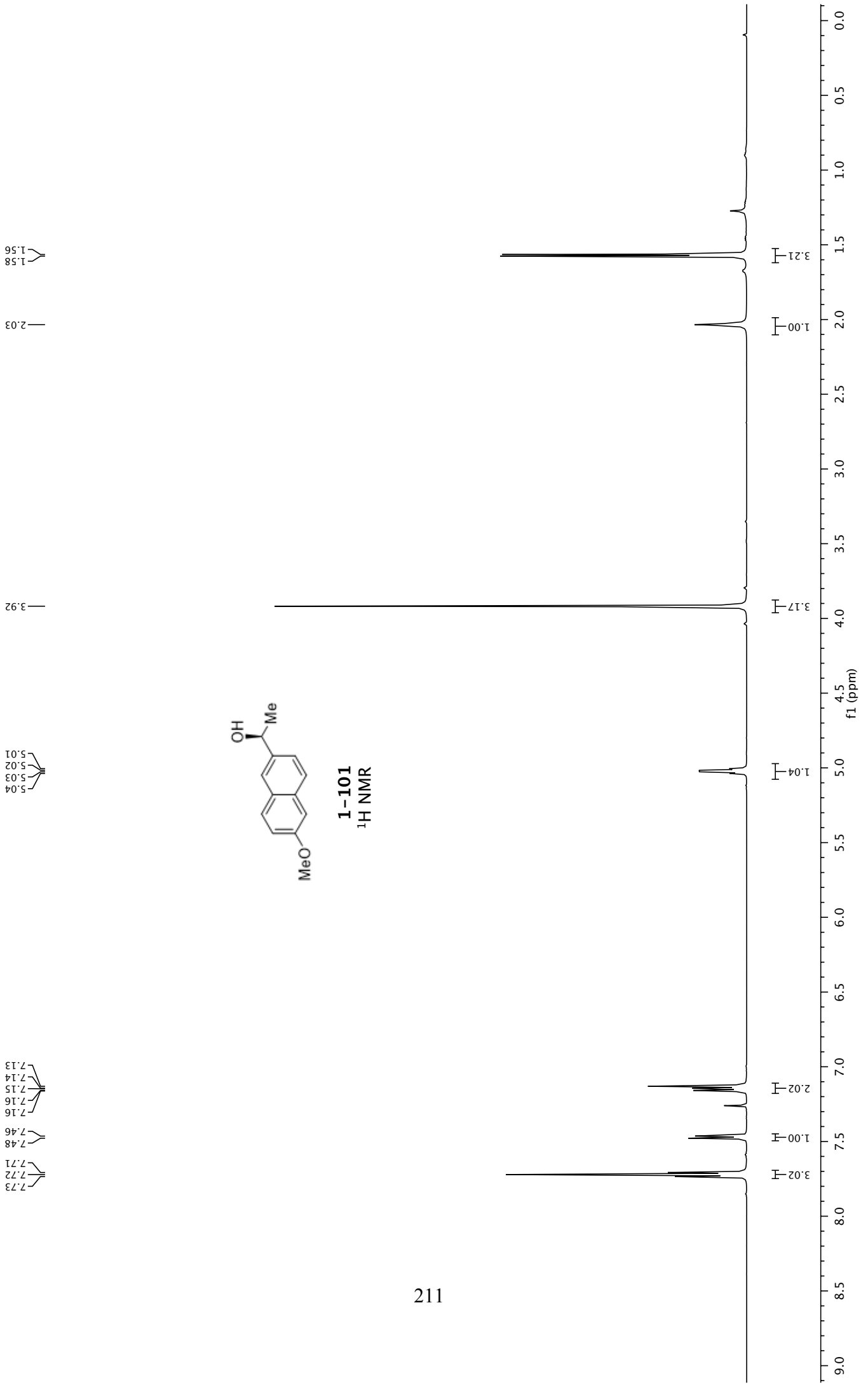
8.13  
8.11  
7.89  
7.88  
7.80  
7.78  
7.70  
7.68  
7.55  
7.54  
7.52  
7.51  
7.49  
7.48  
7.47

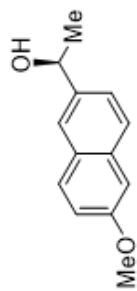




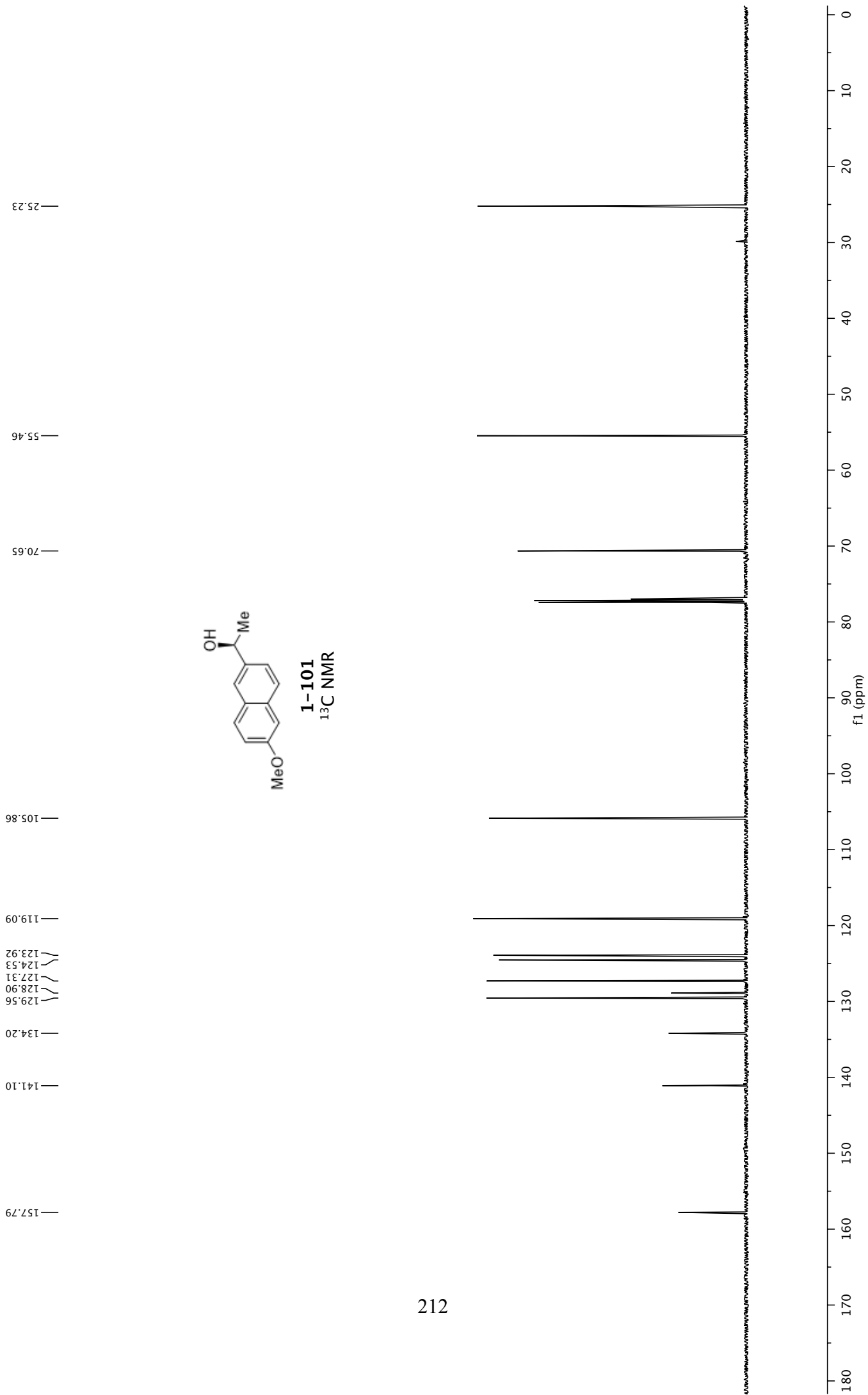
**1-100**  
<sup>13</sup>C NMR

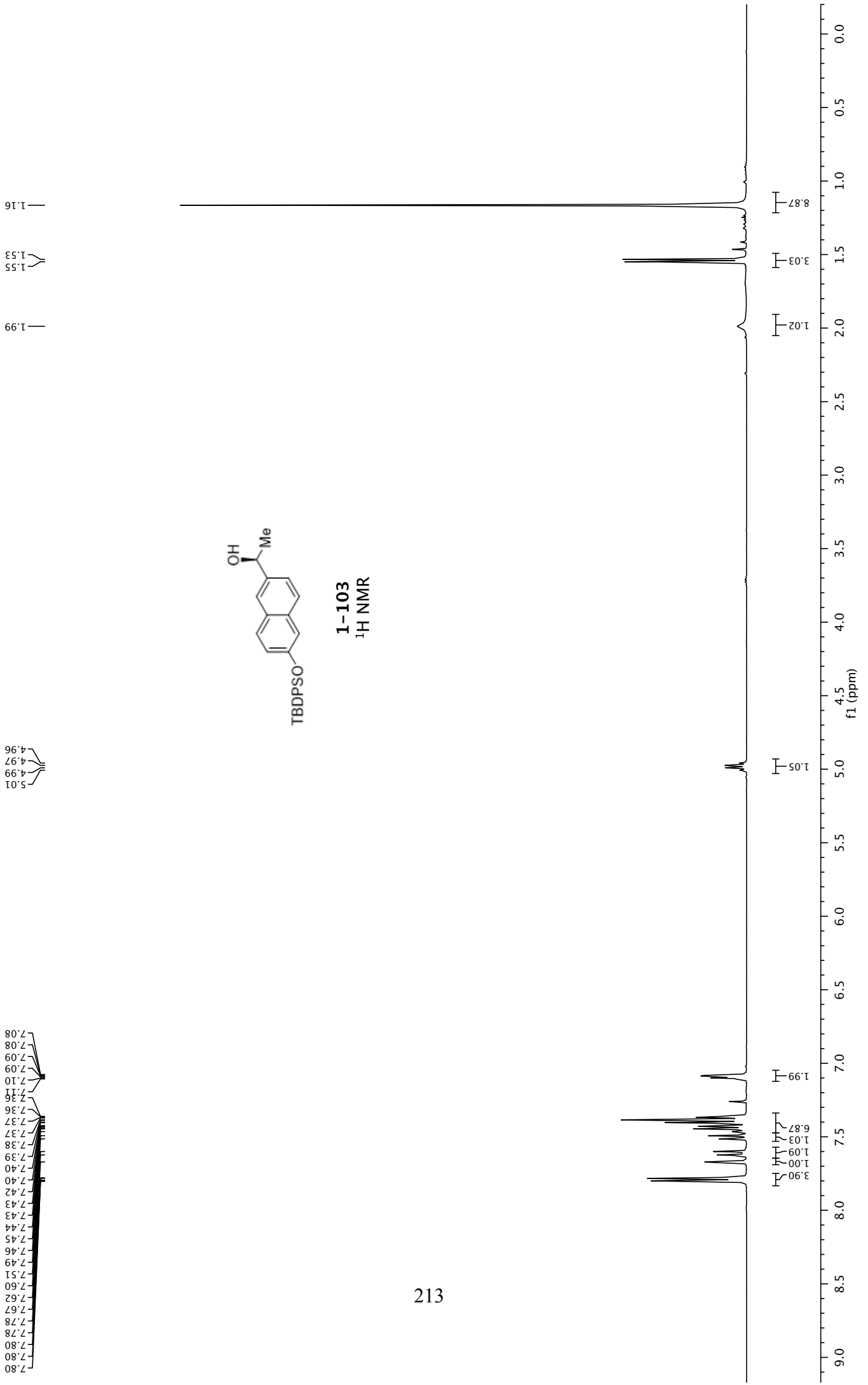


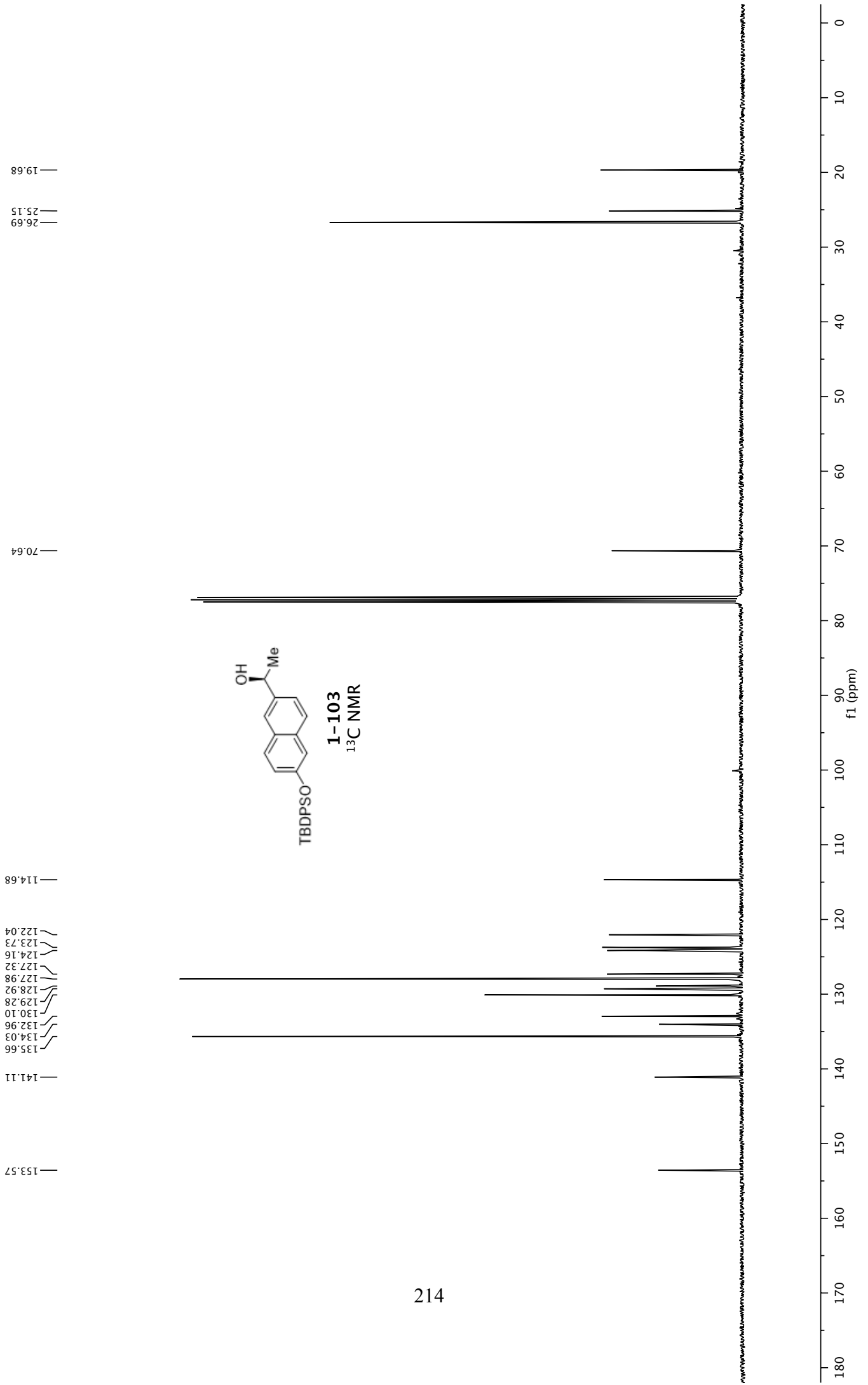


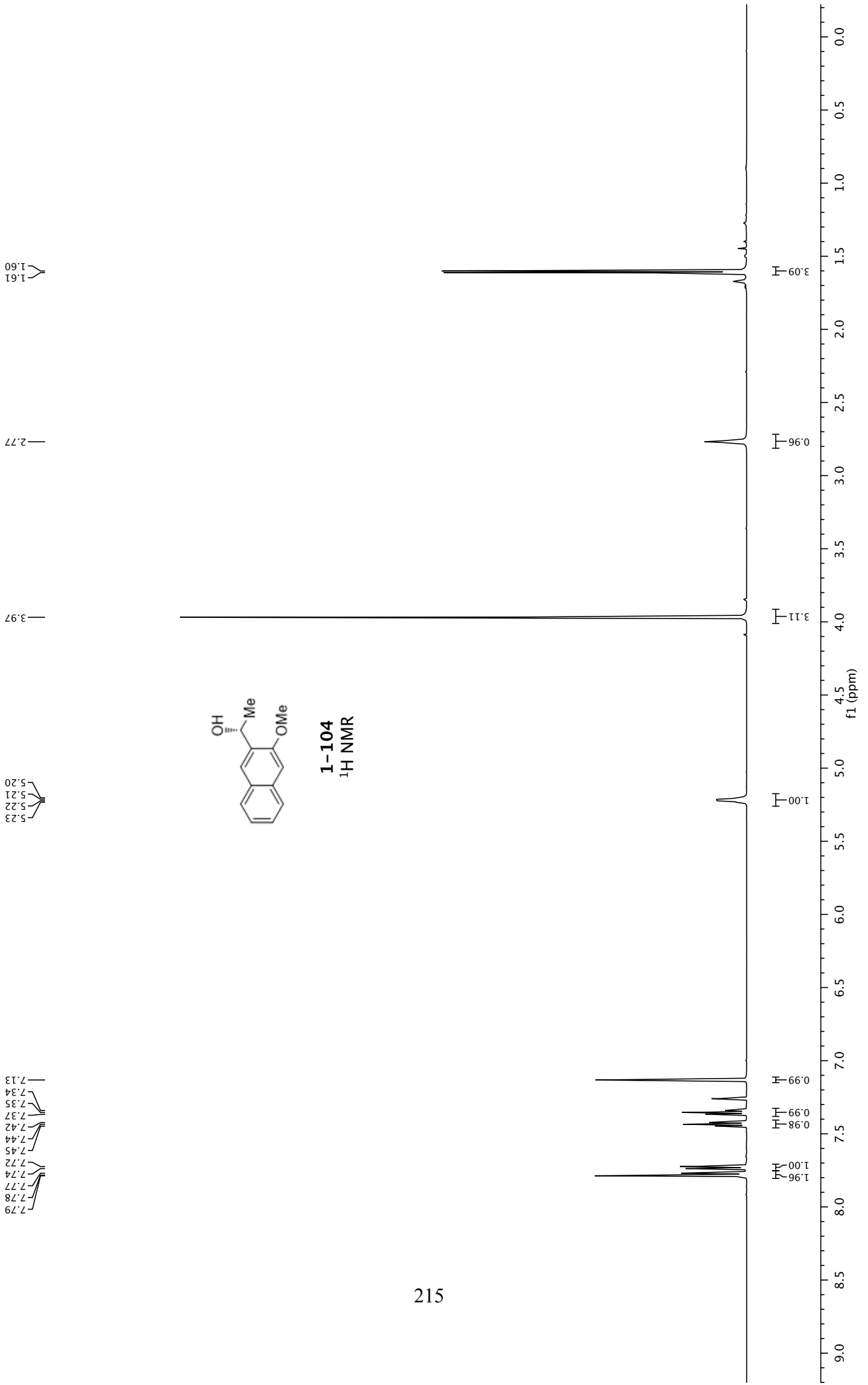


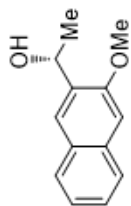
1-101  
<sup>13</sup>C NMR



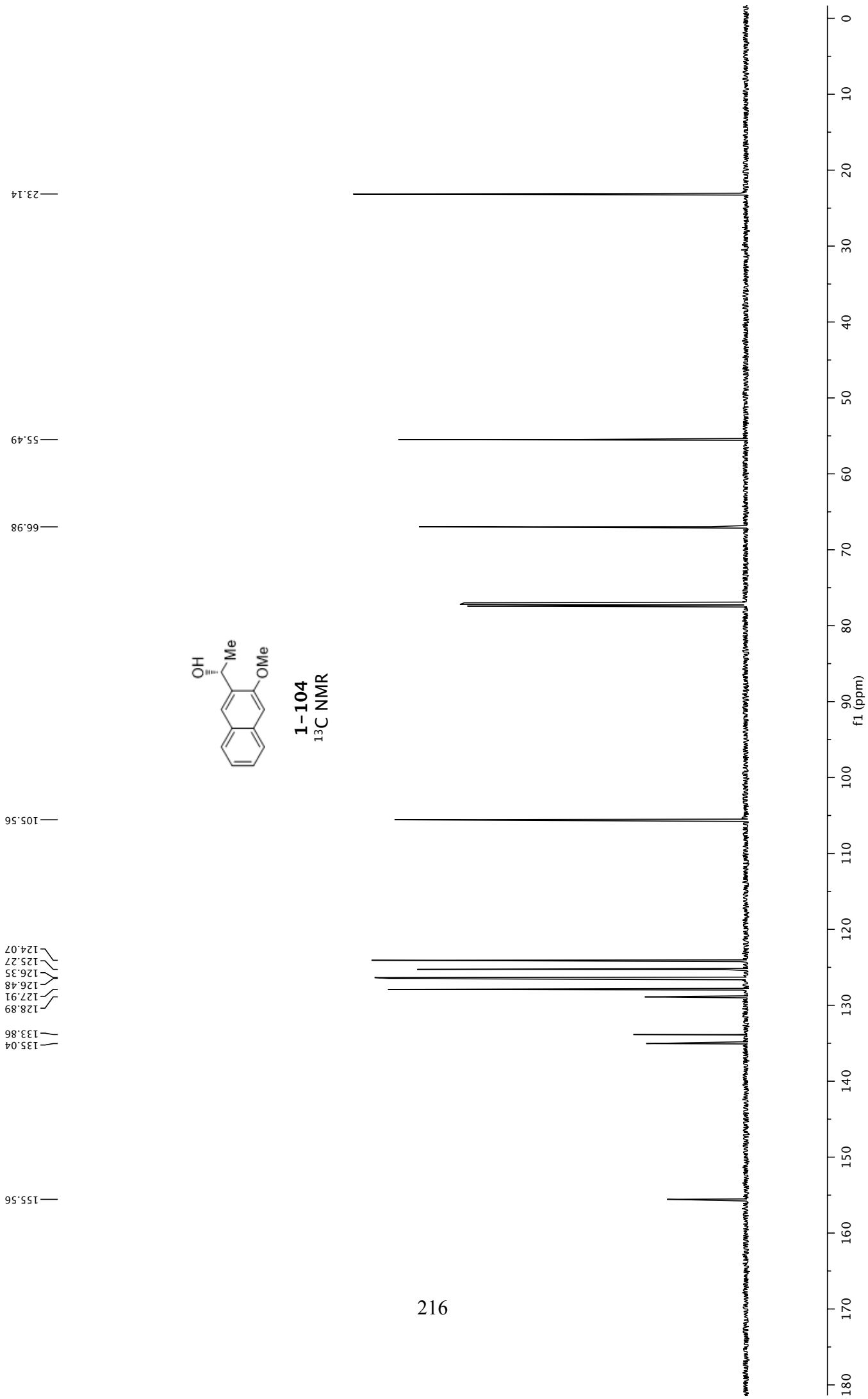


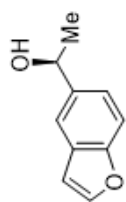






**1-104**  
<sup>13</sup>C NMR





1-106  
<sup>1</sup>H NMR

1.53  
1.55

1.92  
1.93

4.98  
5.00  
5.02  
5.03

6.75  
6.76  
6.76  
6.76

7.30  
7.31  
7.33  
7.33  
7.47  
7.49  
7.61  
7.61  
7.62  
7.63  
7.63

2.96

1.08

1.04

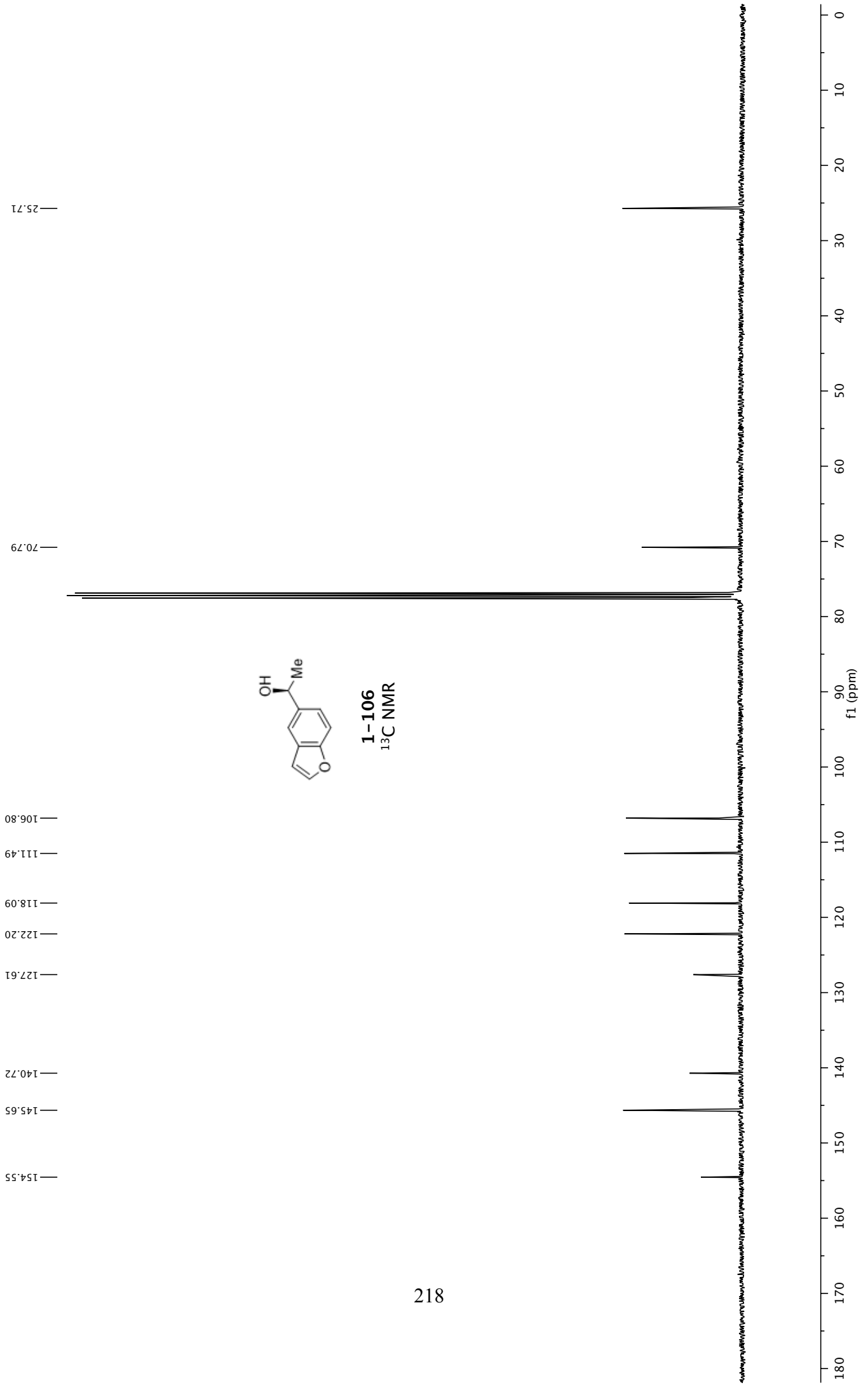
1.01

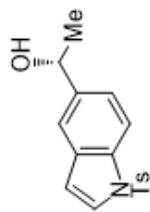
1.00

1.01

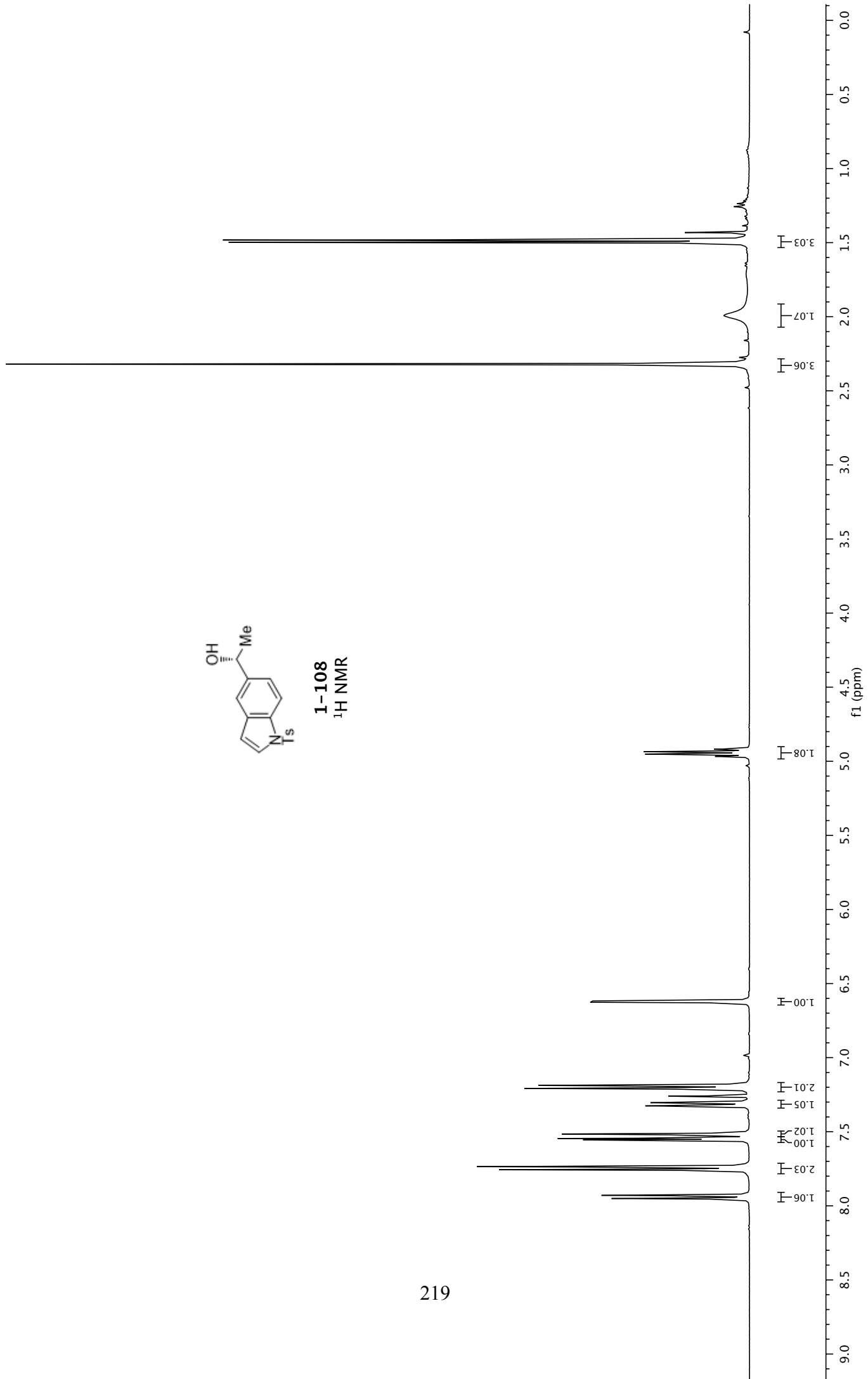
1.94

0.0  
0.5  
1.0  
1.5  
2.0  
2.5  
3.0  
3.5  
4.0  
4.5  
5.0  
5.5  
6.0  
6.5  
7.0  
7.5  
8.0  
8.5  
9.0

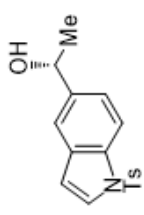




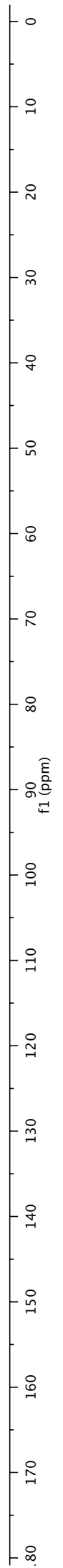
**1-108**  
<sup>1</sup>H NMR



145.11  
141.17  
135.30  
134.30  
130.96  
130.02  
126.93  
126.90  
122.54  
118.24  
113.66  
109.24  
70.56  
25.55  
21.72



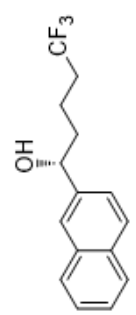
**1-108**  
<sup>13</sup>C NMR



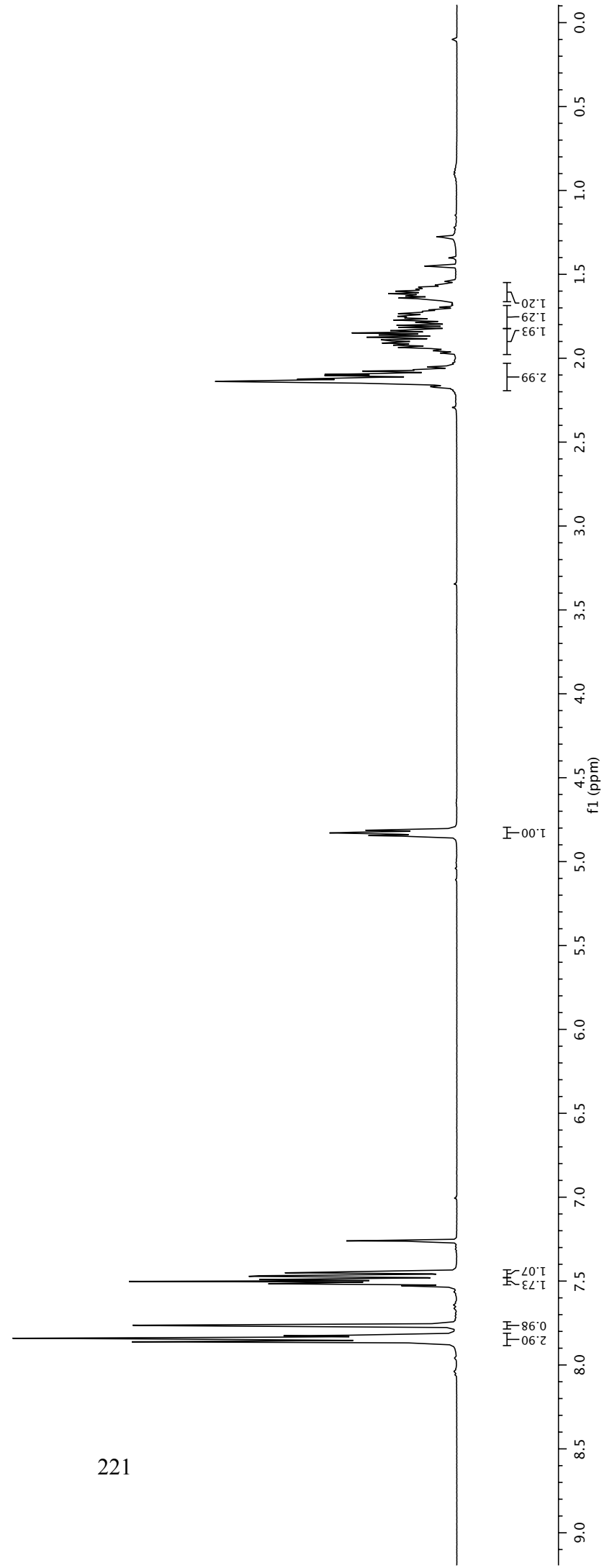
2.14  
2.12  
2.12  
2.10  
2.10  
2.08  
2.07  
1.97  
1.96  
1.94  
1.92  
1.92  
1.91  
1.90  
1.90  
1.89  
1.87  
1.86  
1.85  
1.84  
1.83  
1.82  
1.80  
1.79  
1.77  
1.76  
1.75  
1.74  
1.73  
1.72  
1.71  
1.70  
1.65  
1.64  
1.63  
1.62  
1.62  
1.60  
1.59  
1.58  
1.58  
1.56

4.85  
4.83  
4.81

7.86  
7.84  
7.83  
7.76  
7.52  
7.51  
7.50  
7.49  
7.49  
7.47  
7.47  
7.45  
7.45



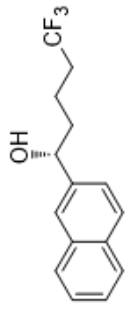
**1-110**  
<sup>1</sup>H NMR



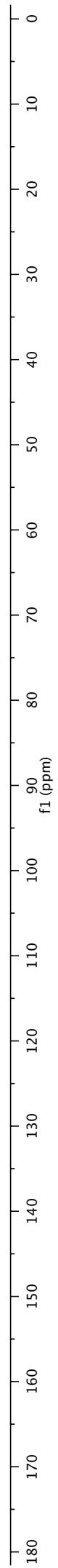
37.81  
34.16  
33.88  
33.59  
33.31  
18.69  
18.66  
18.63  
18.60

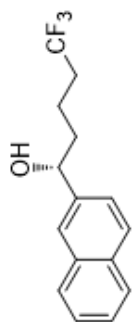
74.40

141.67  
133.37  
133.20  
131.36  
128.68  
128.61  
128.08  
127.88  
126.48  
126.18  
125.87  
124.73  
123.93  
123.12



**1-110**  
<sup>13</sup>C NMR

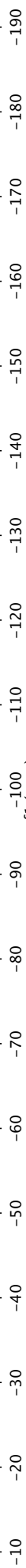


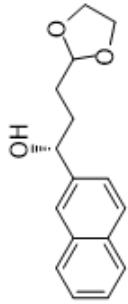
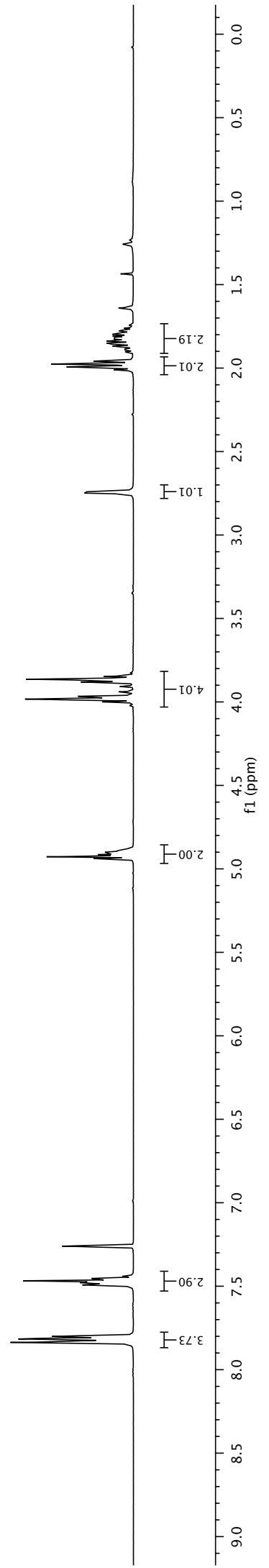


**1-110**  
<sup>19</sup>F NMR

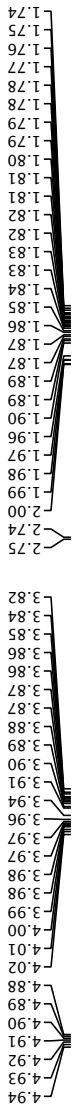


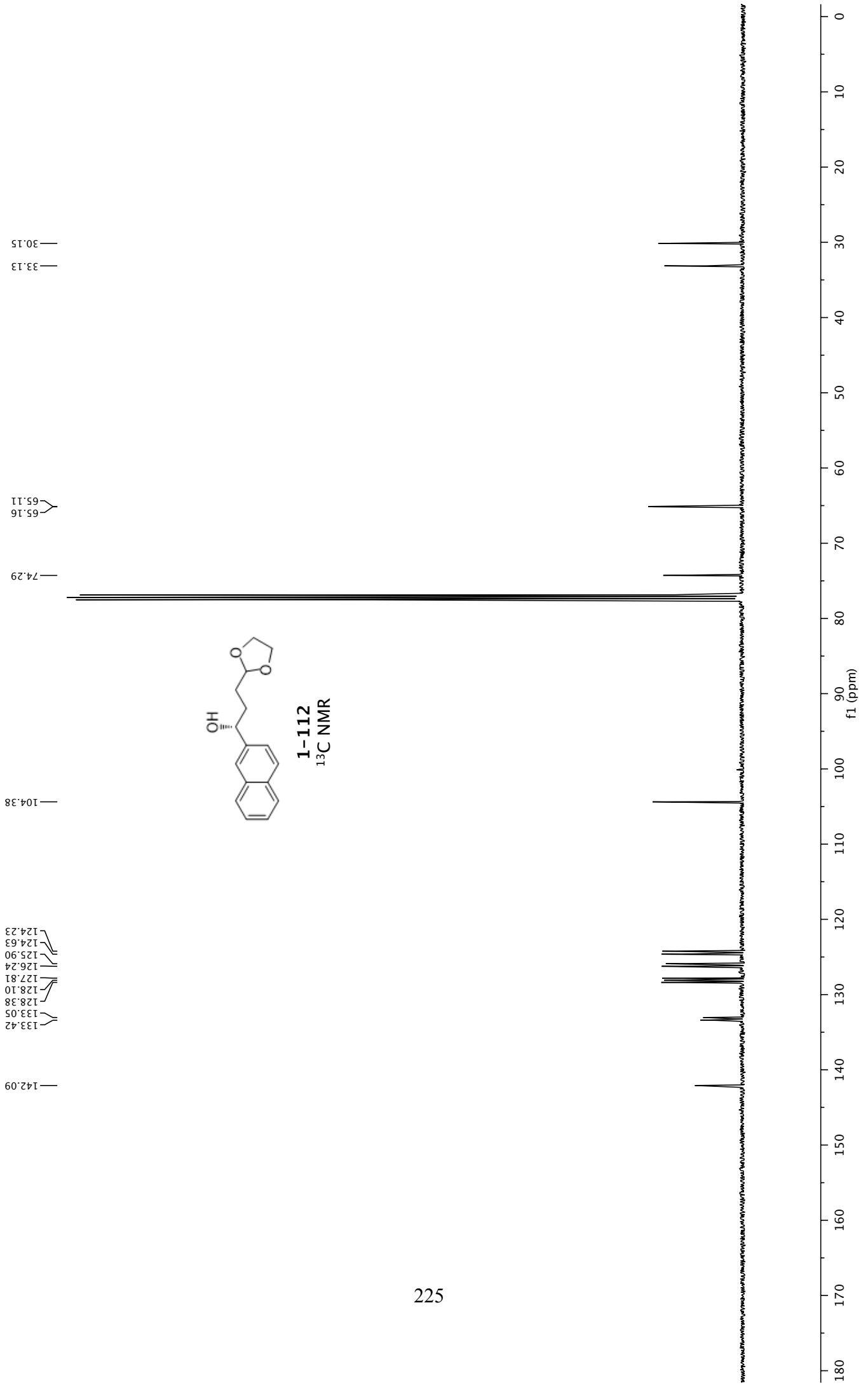
f1 (ppm)

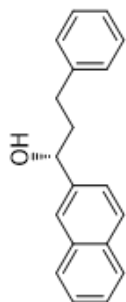




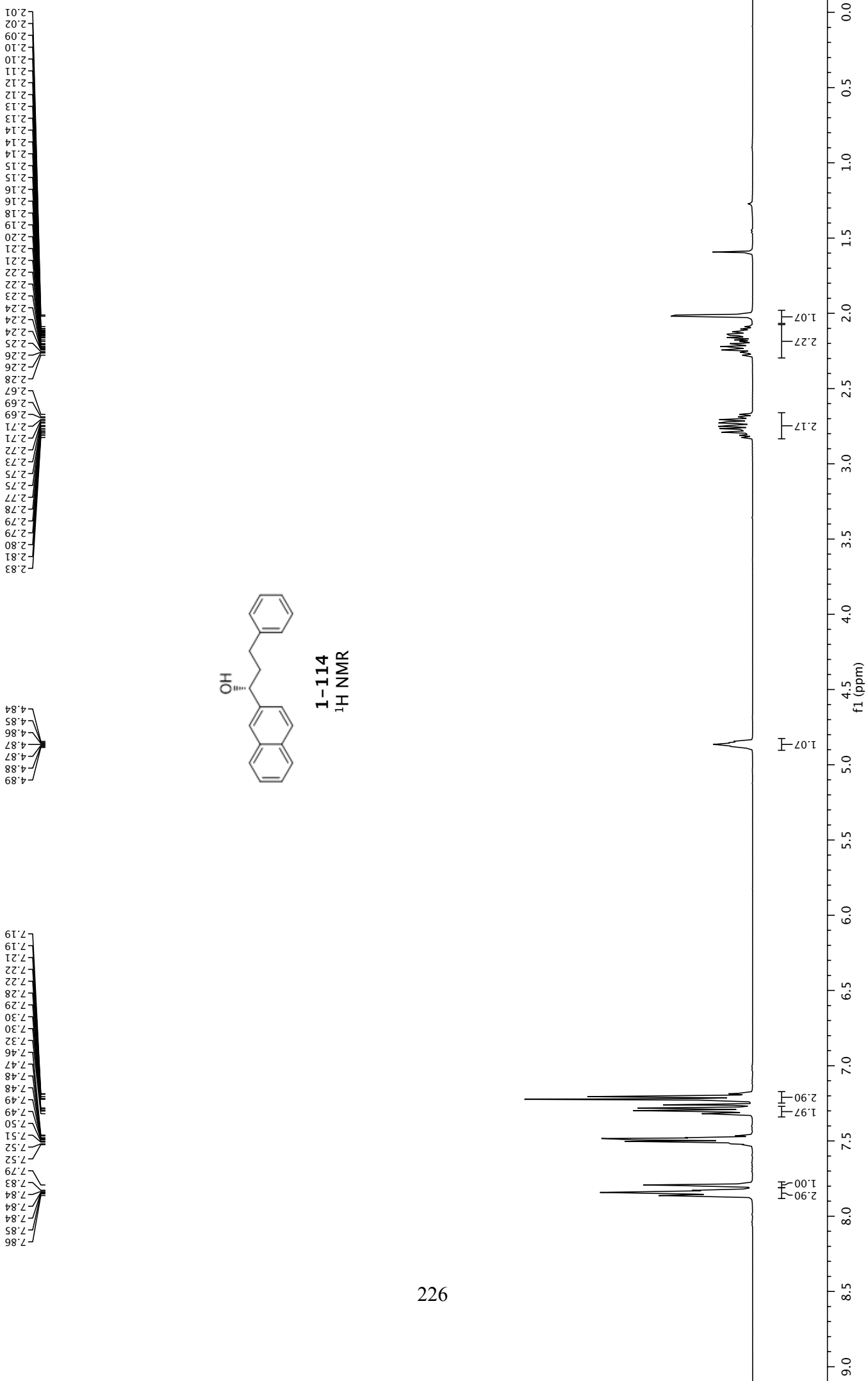
**1-112**  
<sup>1</sup>H NMR

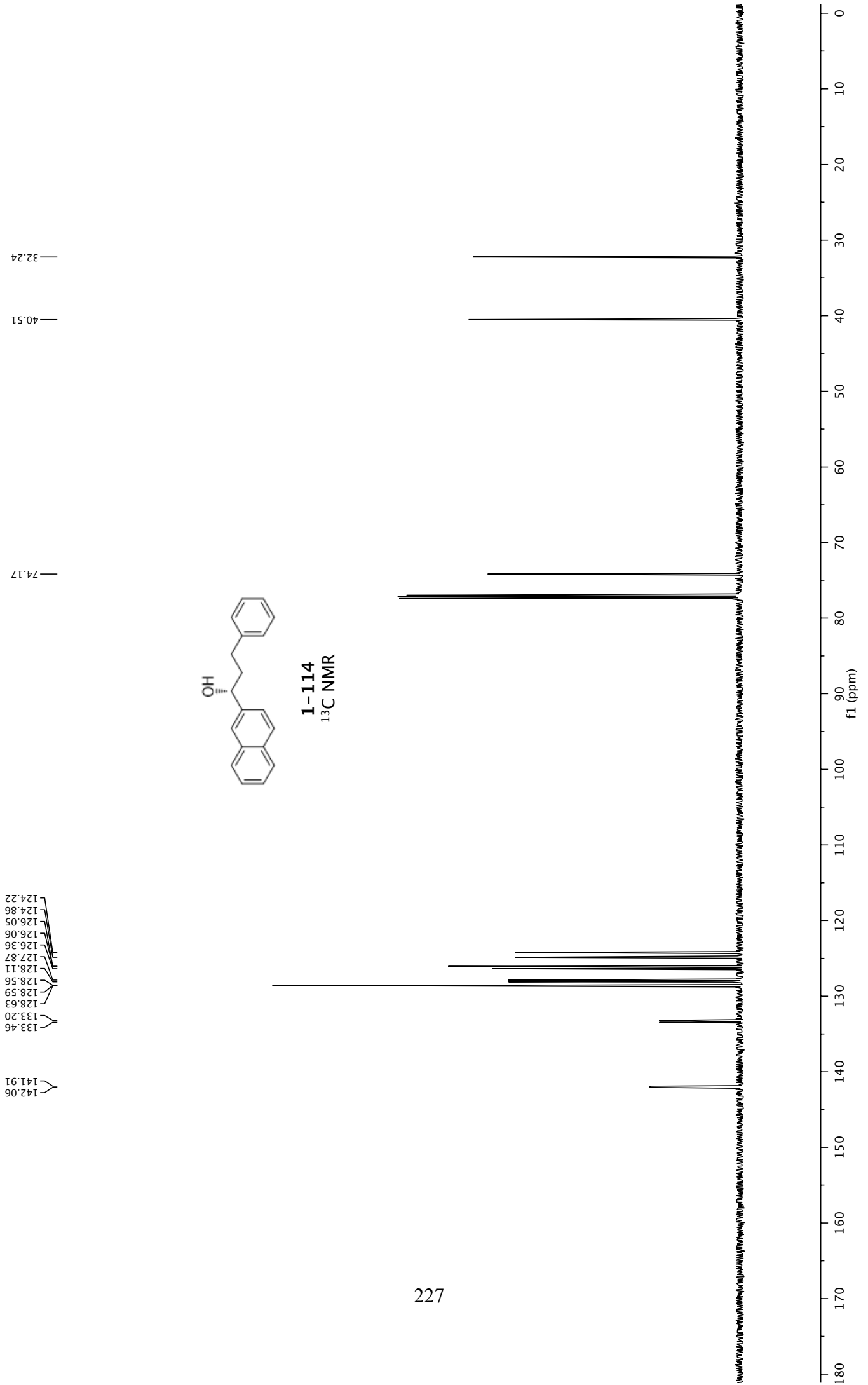






**1-114**  
<sup>1</sup>H NMR



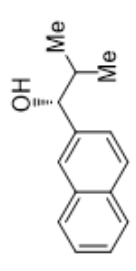


1.05  
1.04  
0.85  
0.84

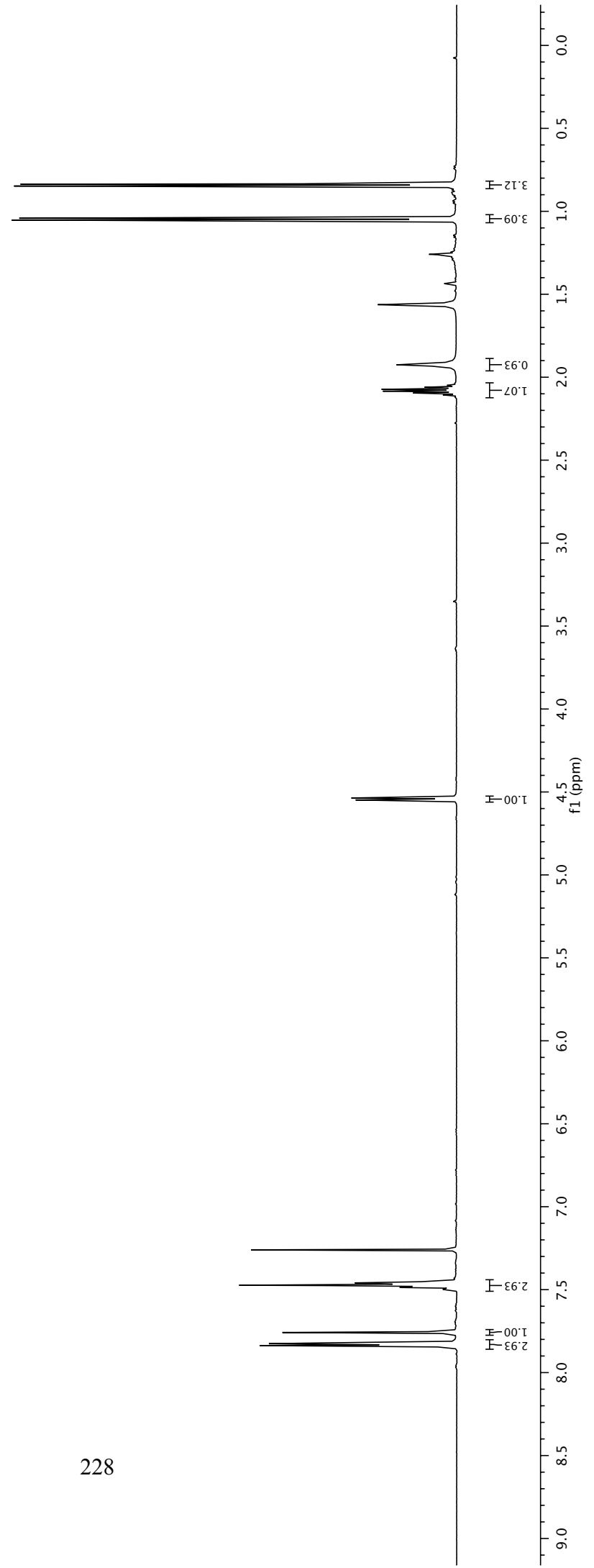
2.12  
2.11  
2.10  
2.08  
2.07  
2.06  
2.05  
2.04  
1.93

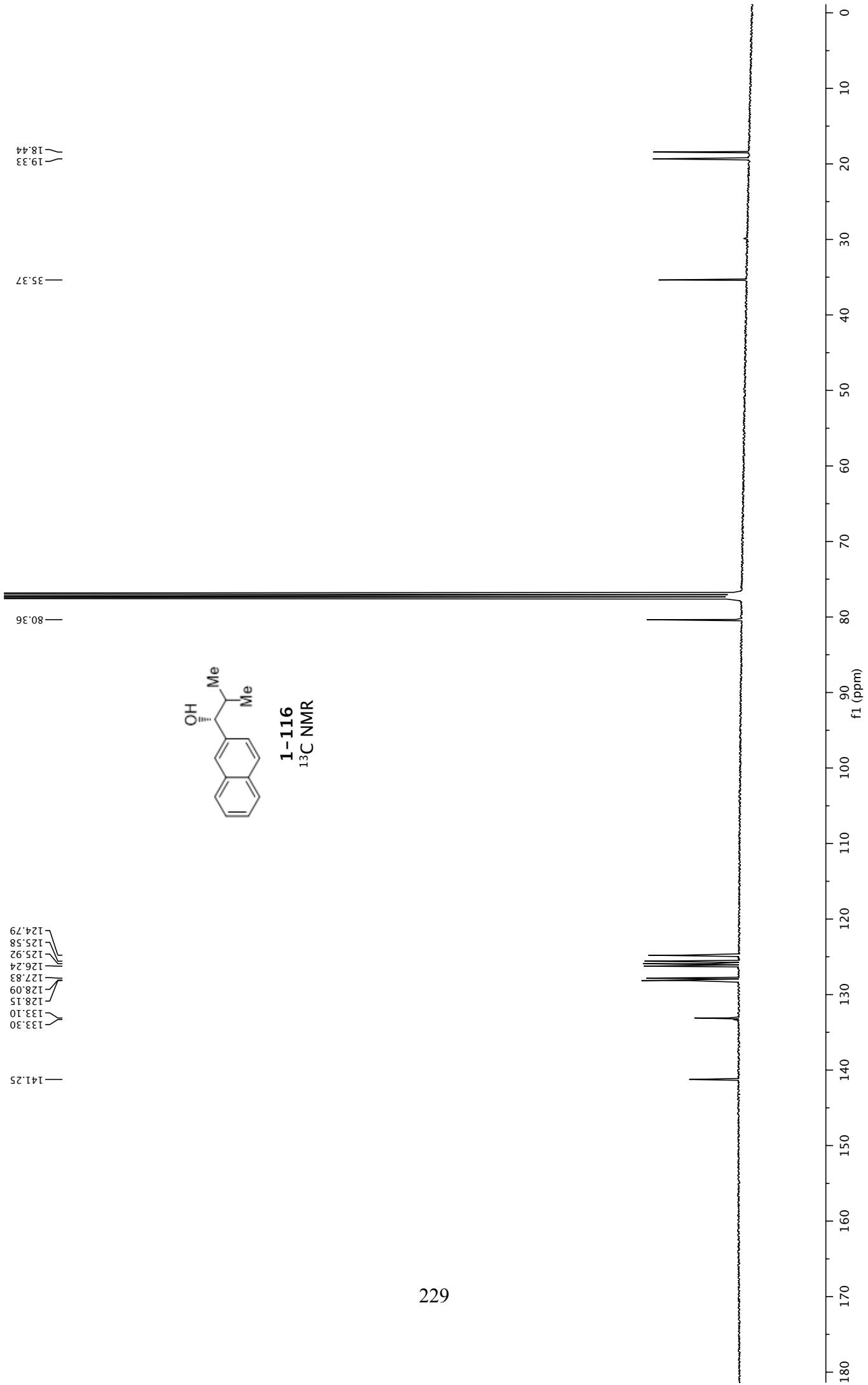
4.55  
4.54

7.84  
7.84  
7.83  
7.82  
7.76  
7.50  
7.49  
7.48  
7.47  
7.47  
7.46  
7.46  
7.46  
7.46



**1-116**  
<sup>1</sup>H NMR

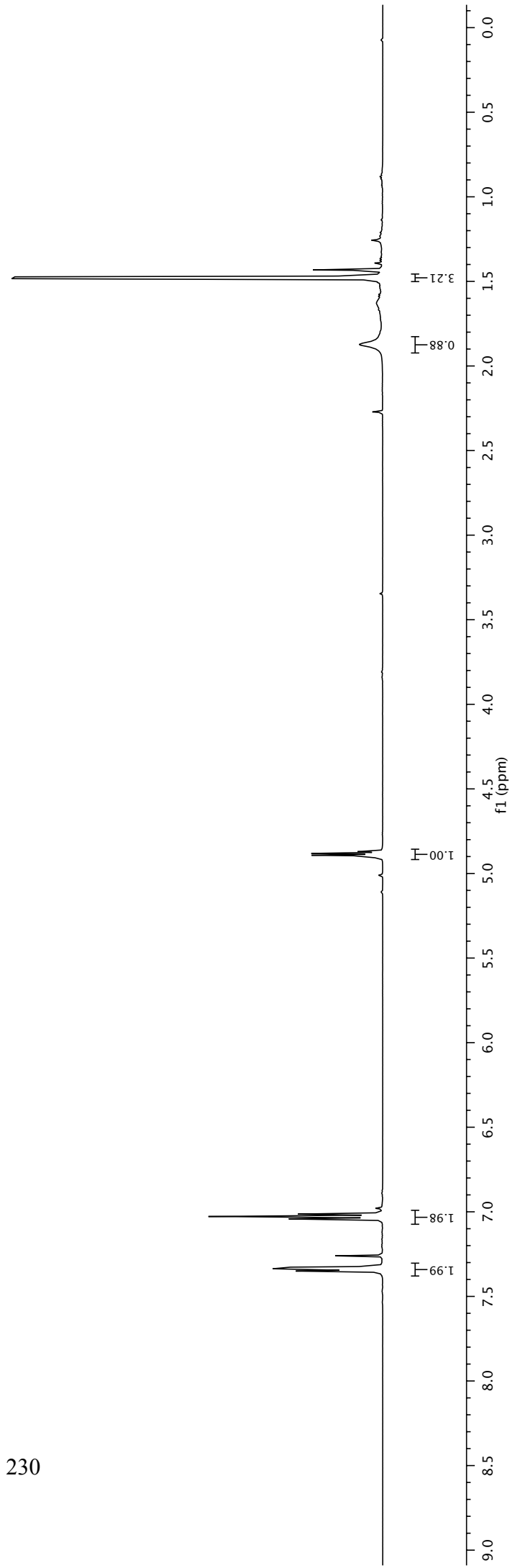
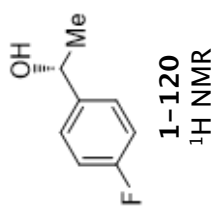


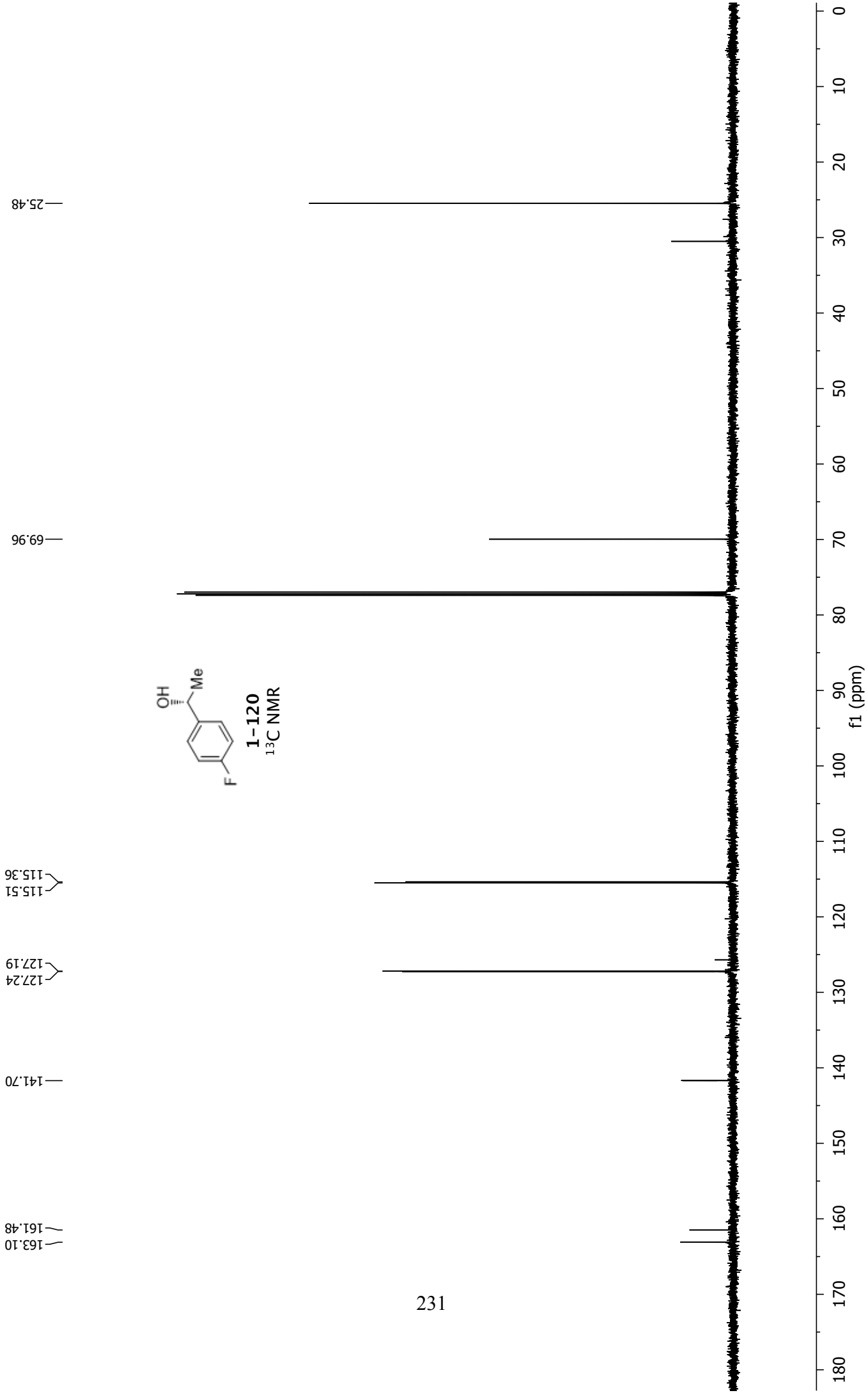


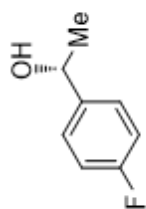
1.47  
1.48  
1.87

4.87  
4.88  
4.89  
4.90

7.01  
7.03  
7.04  
7.33  
7.34  
7.34  
7.35





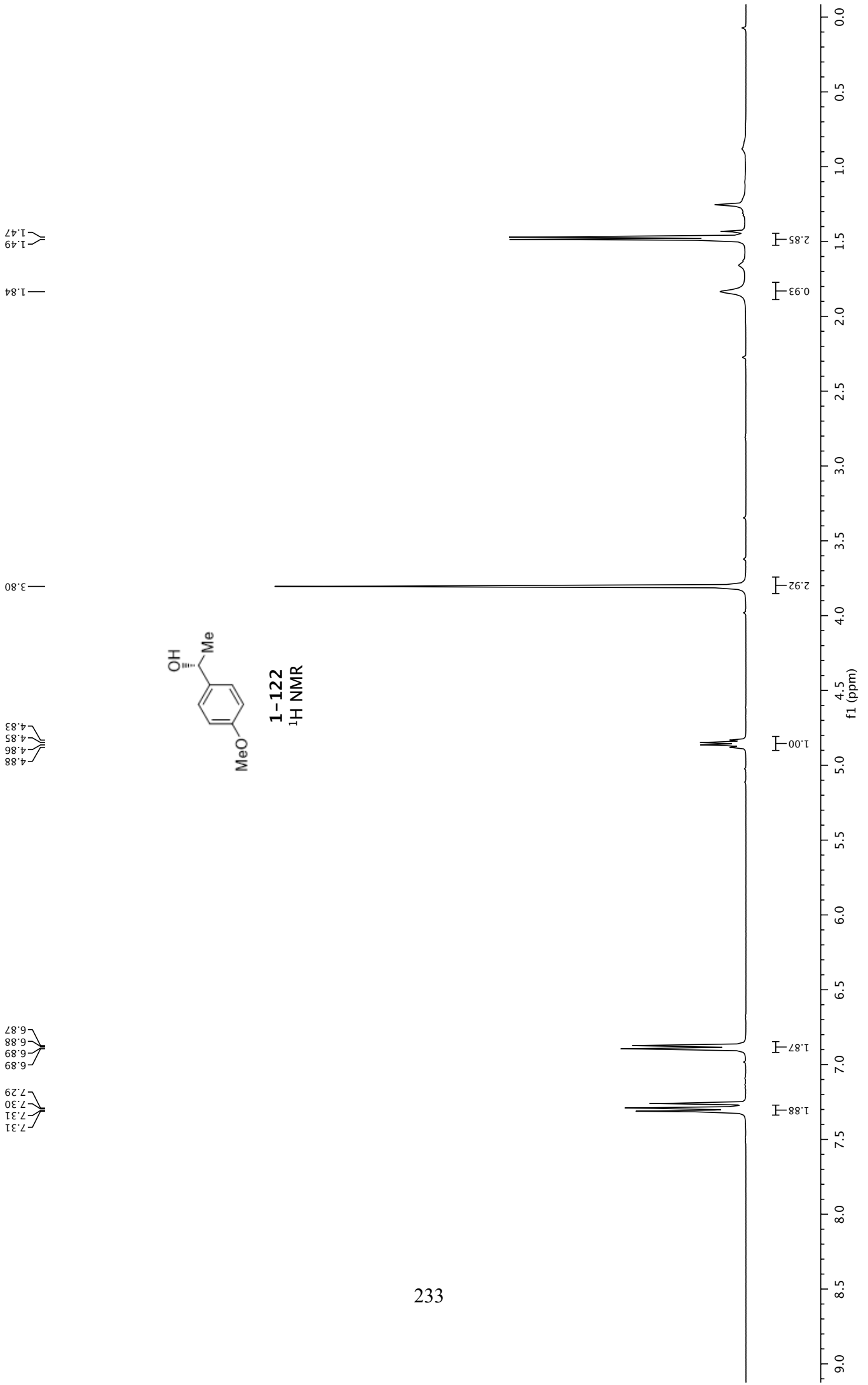


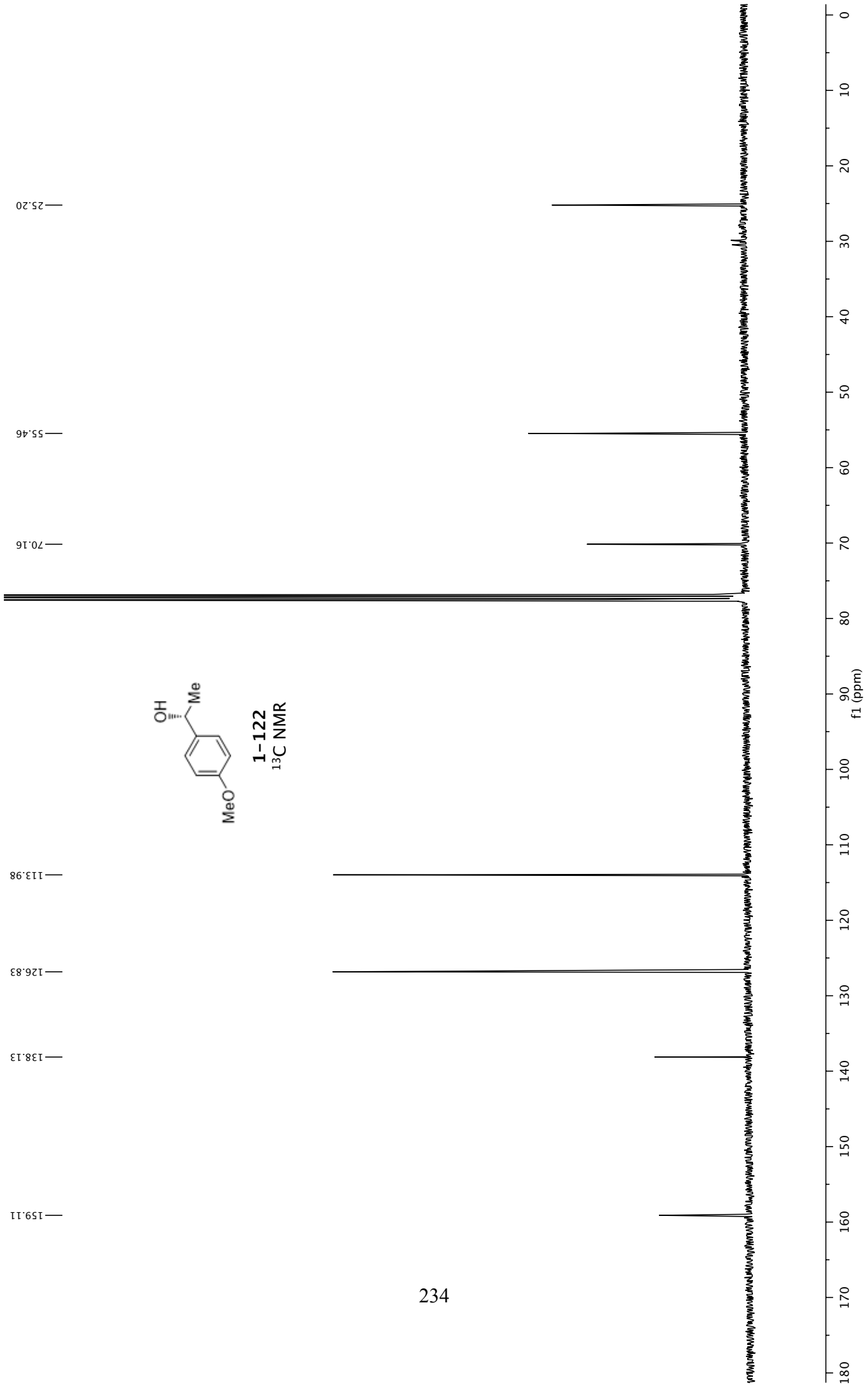
**1-120**  
<sup>19</sup>F NMR

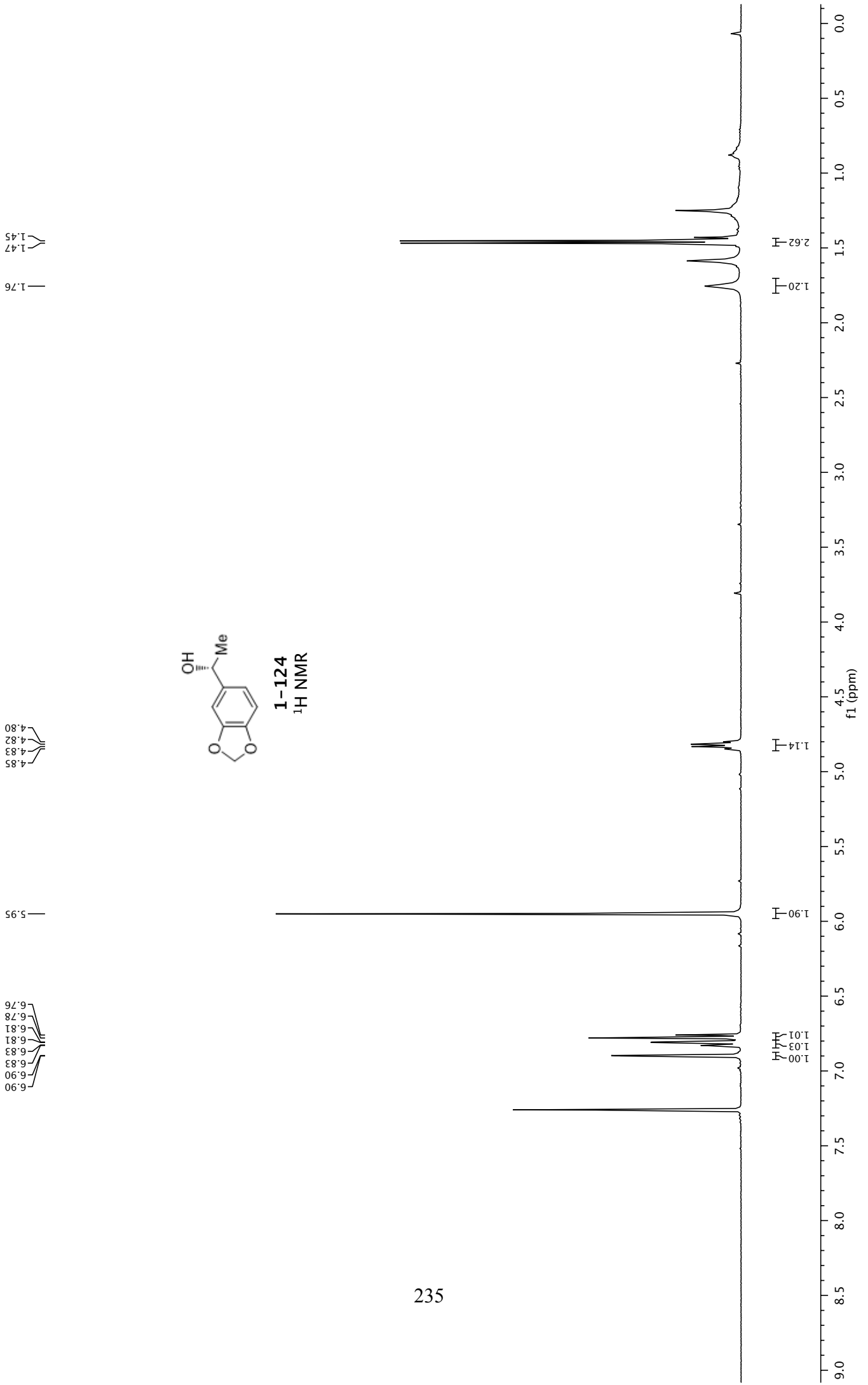
-115.36

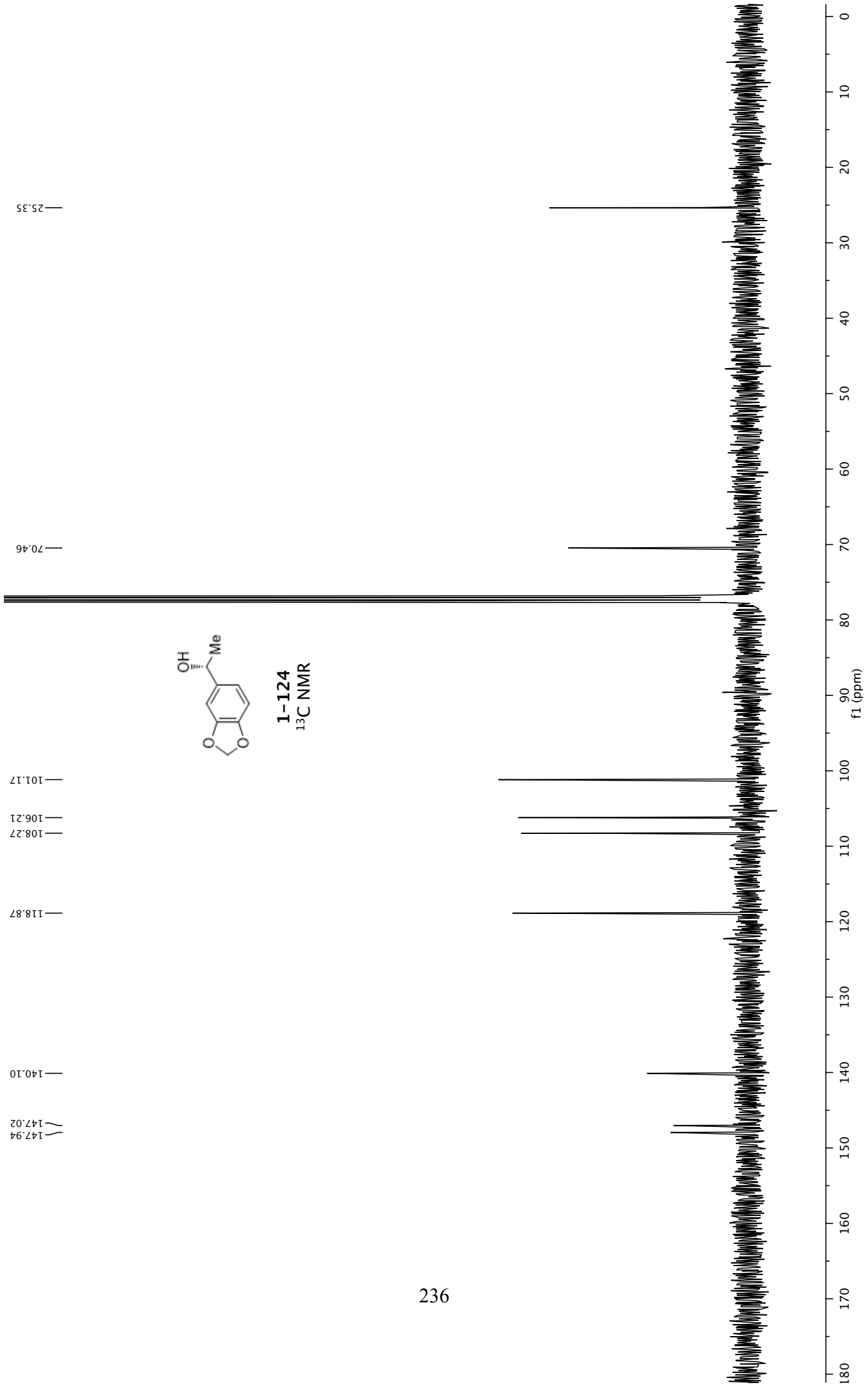
10 0 -10 -20 -30 -40 -50 -60 -70 -80 -90 -100 -110 -120 -130 -140 -150 -160 -170 -180 -190 -200 -210

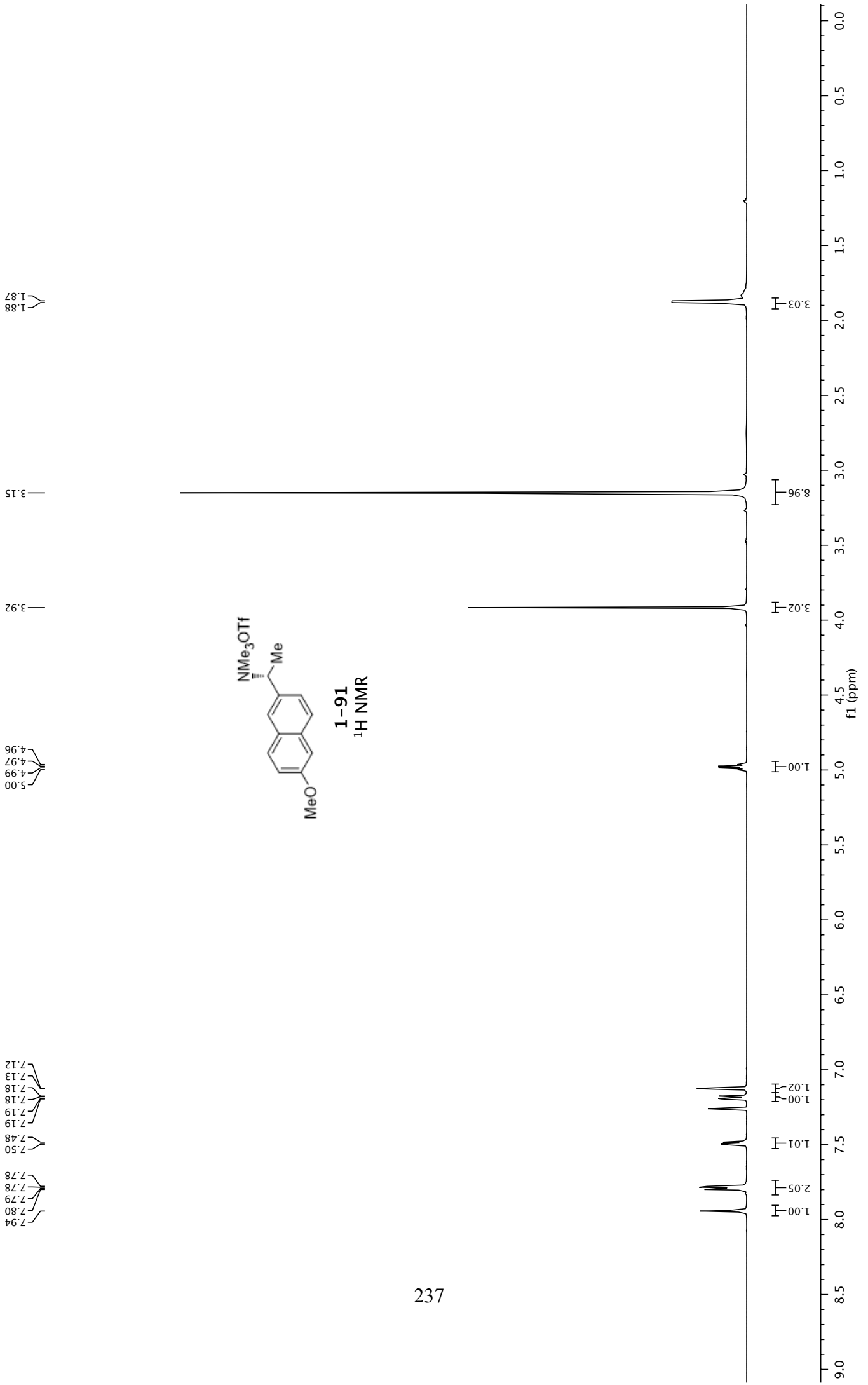
fi (ppm)

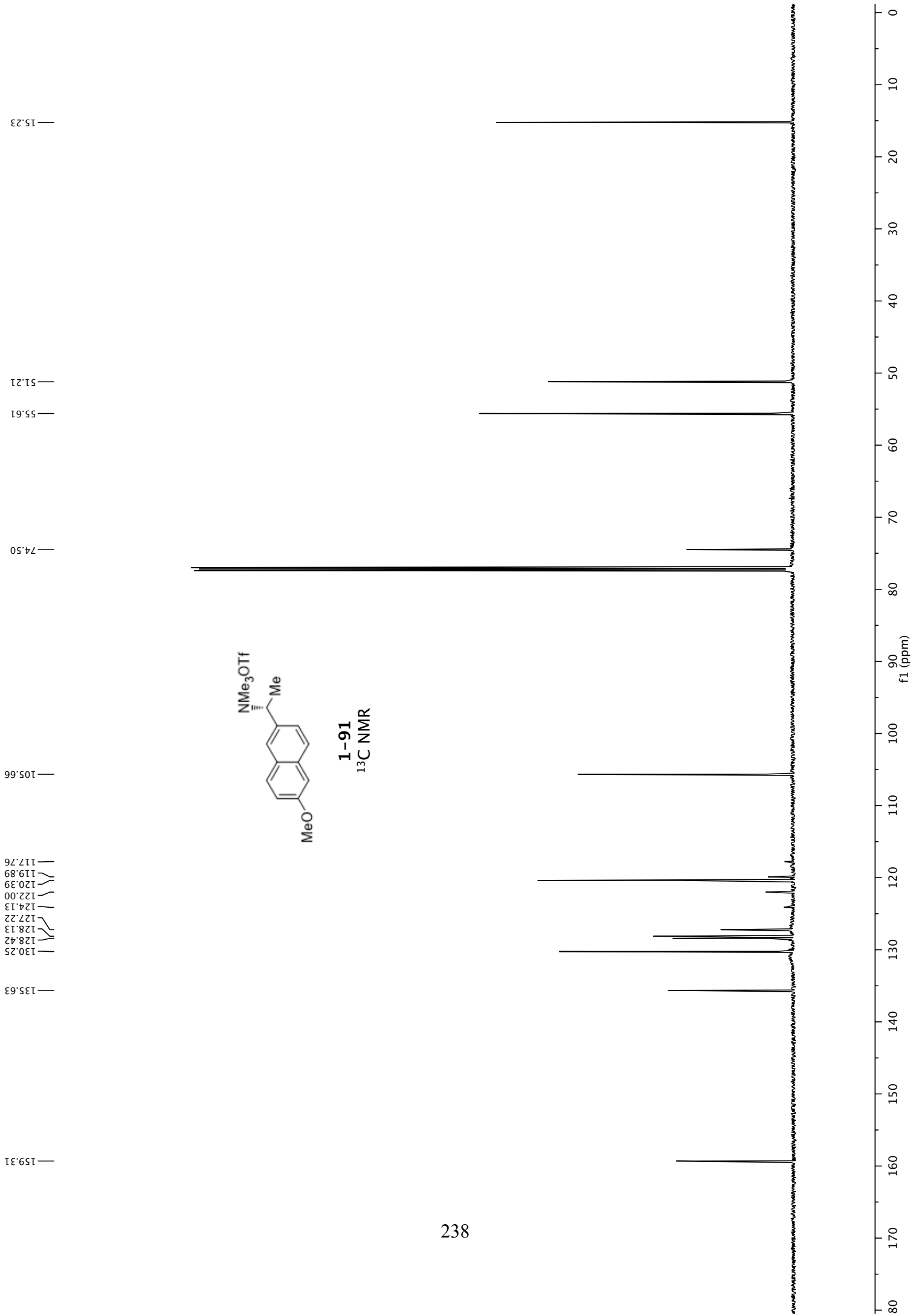




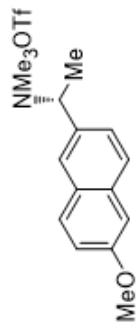








-78.39

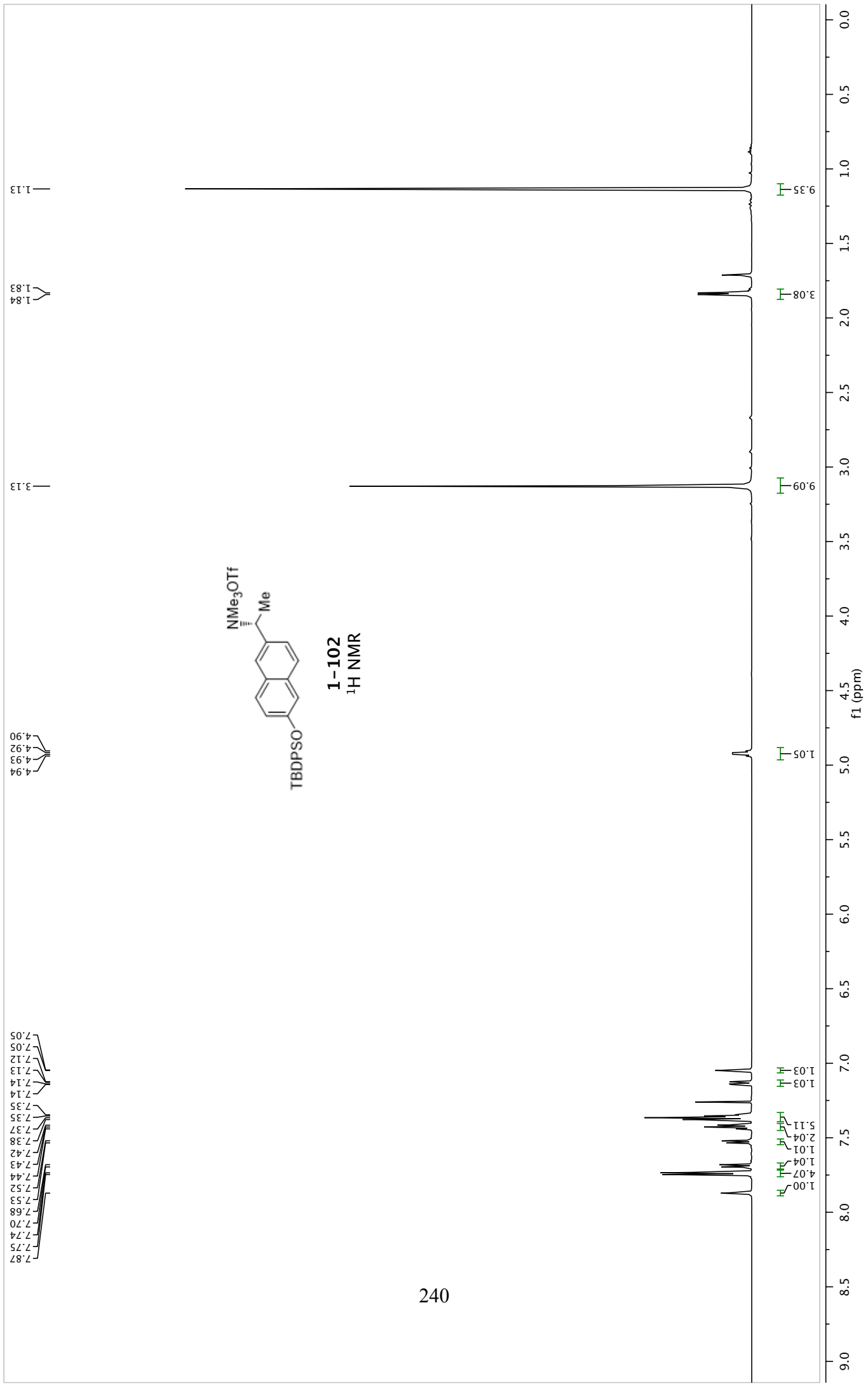


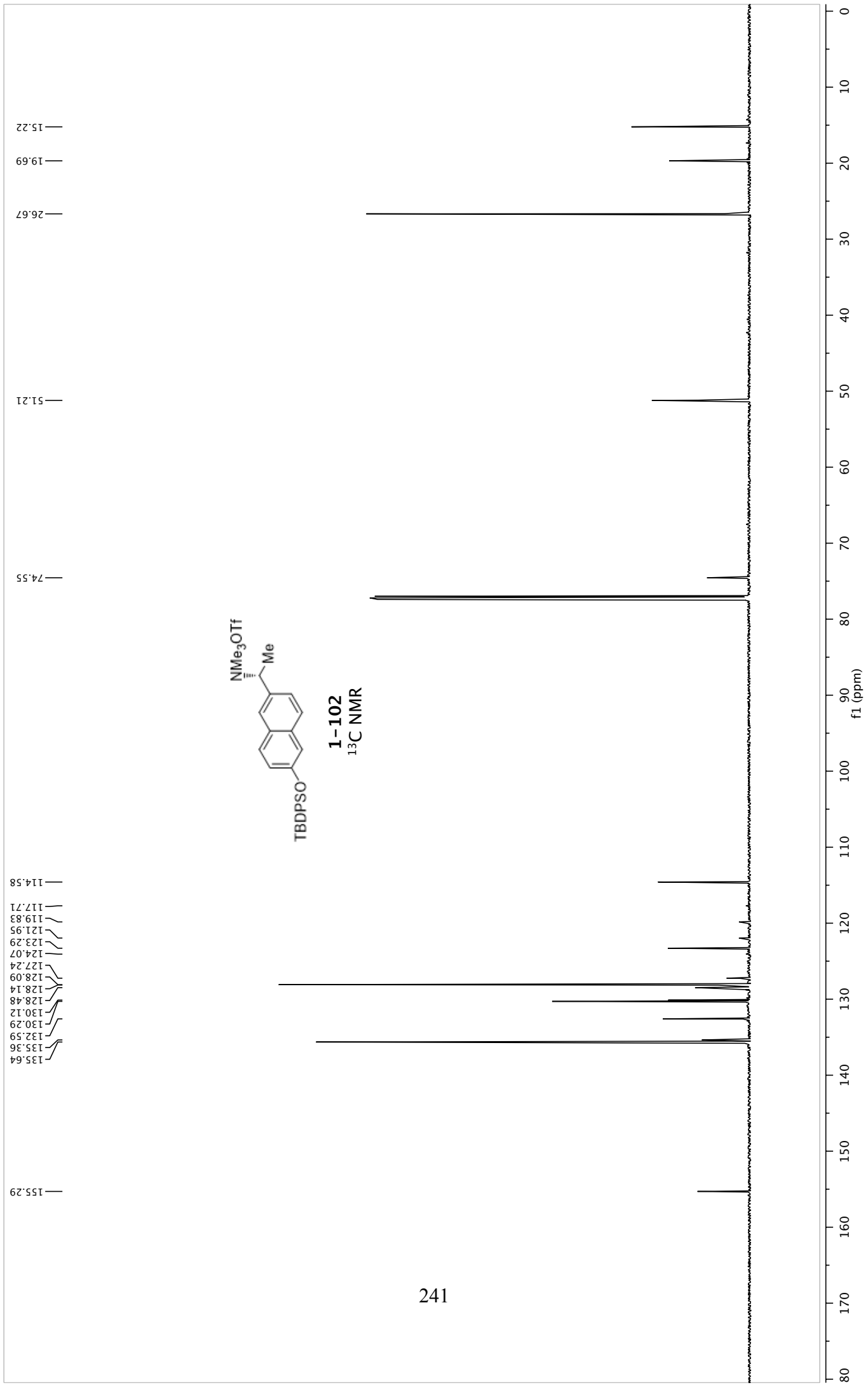
**1-91**  
<sup>19</sup>F NMR



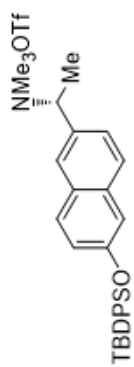
f1 (ppm)

-10 -20 -30 -40 -50 -60 -70 -80 -90 -100 -110 -120 -130 -140 -150 -160 -170 -180 -190

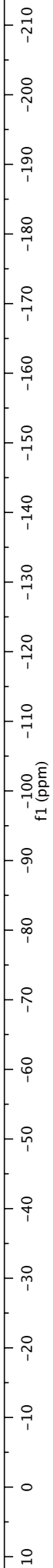


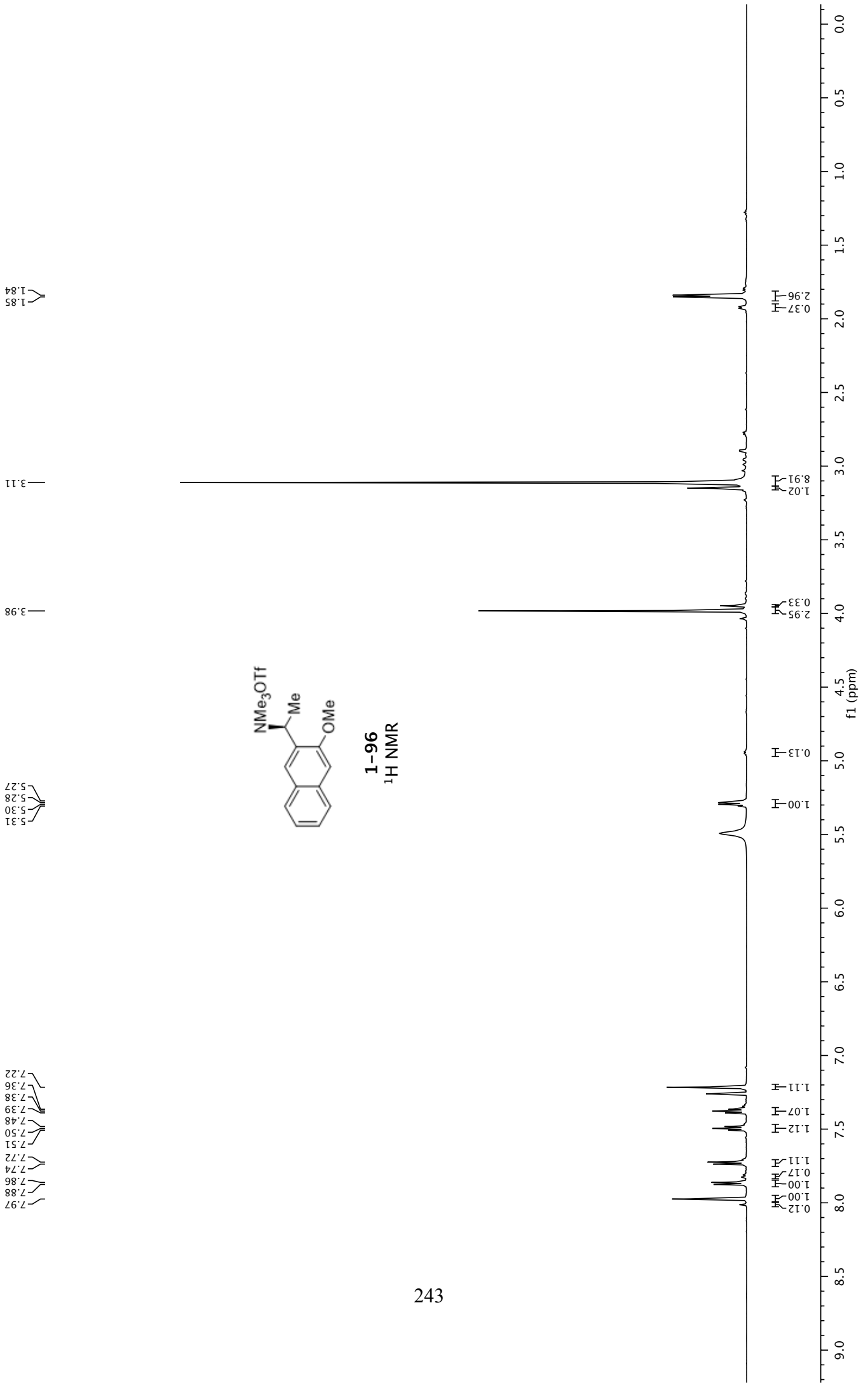


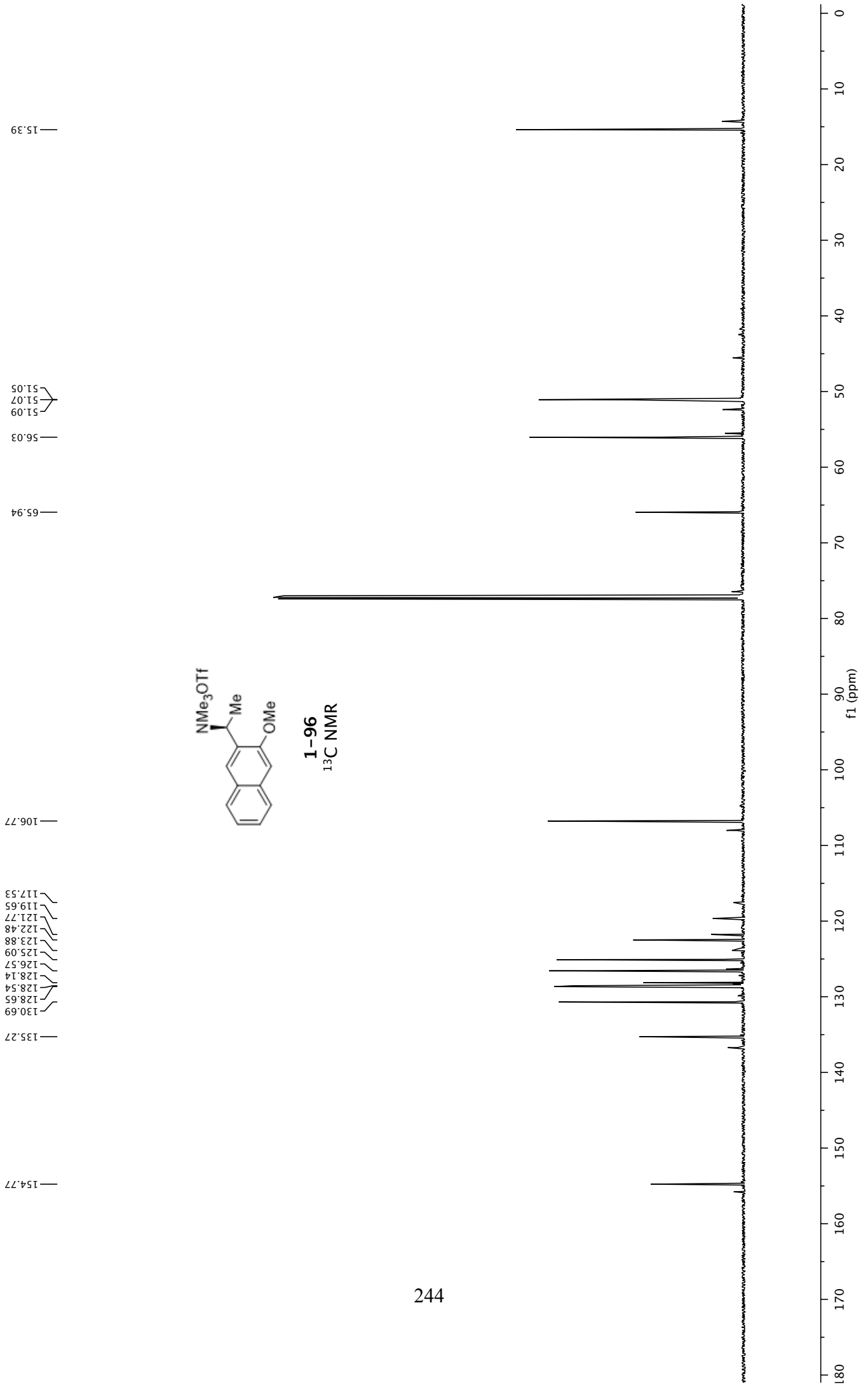
-78.38



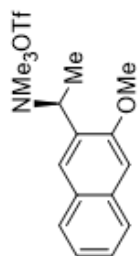
**1-102**  
<sup>19</sup>F NMR





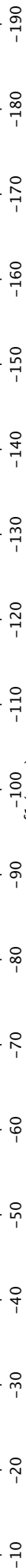


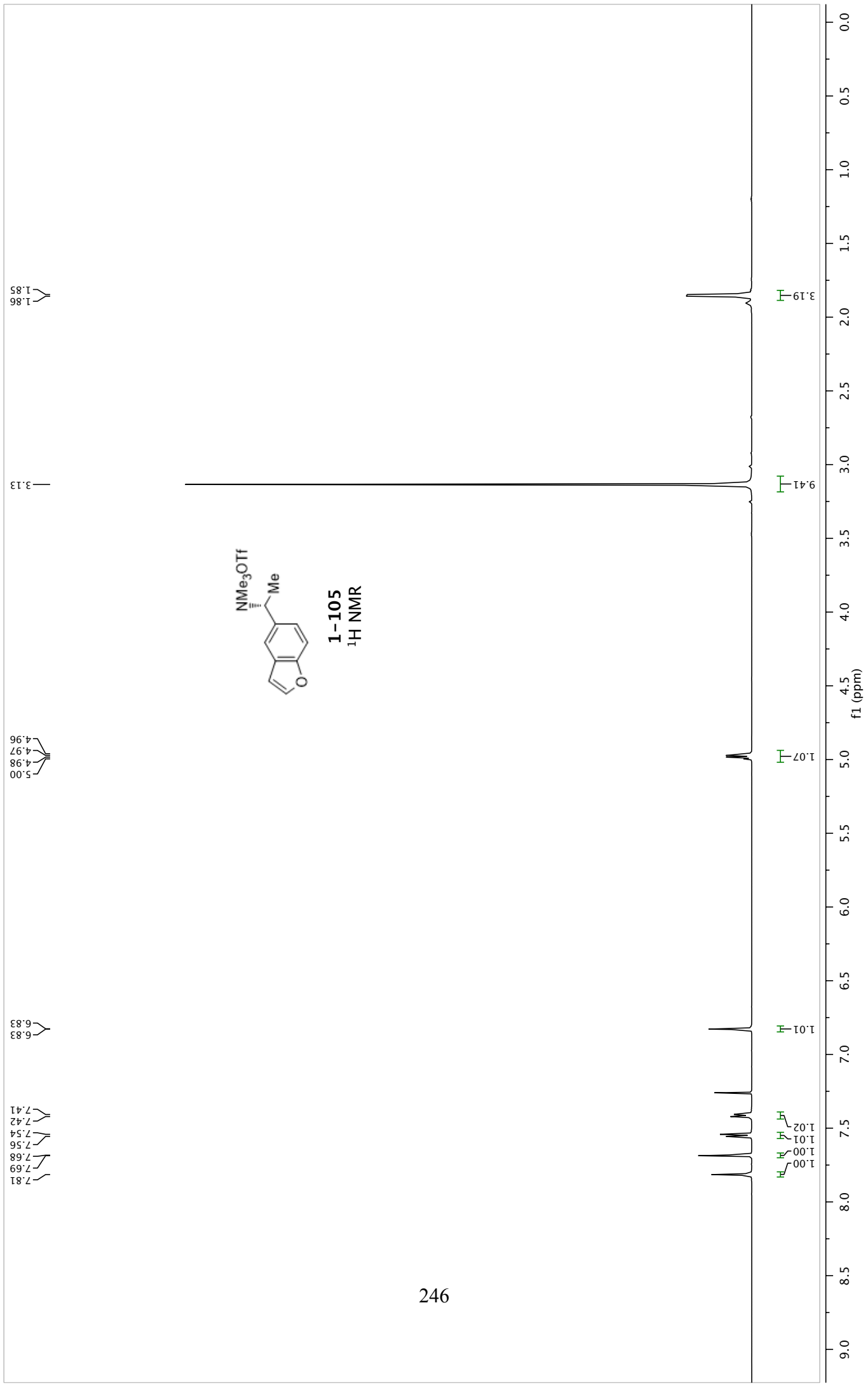
-78.42

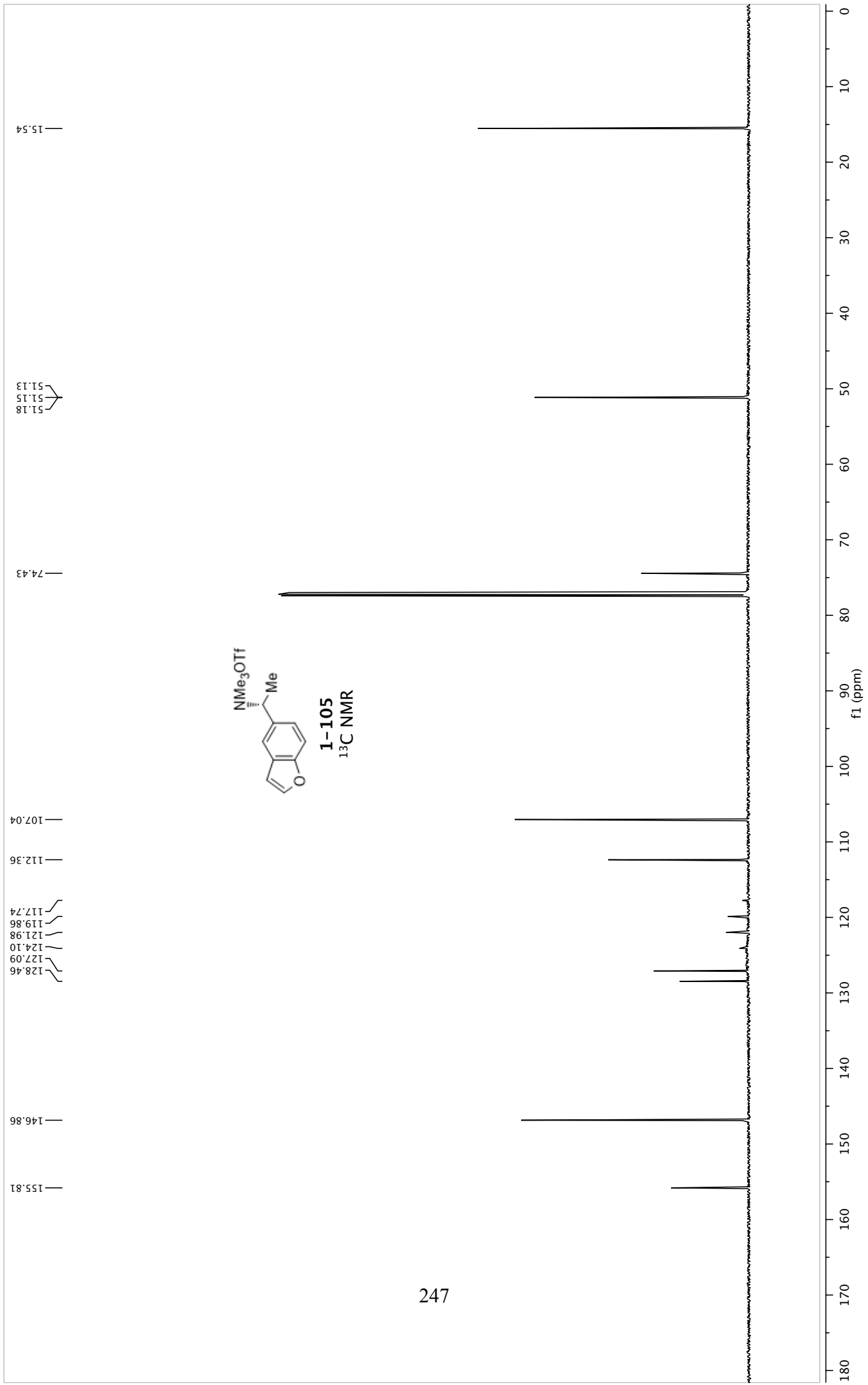


**1-96**  
<sup>19</sup>F NMR

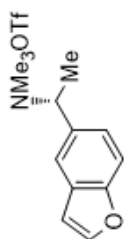
f1 (ppm)



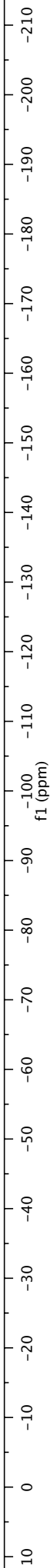


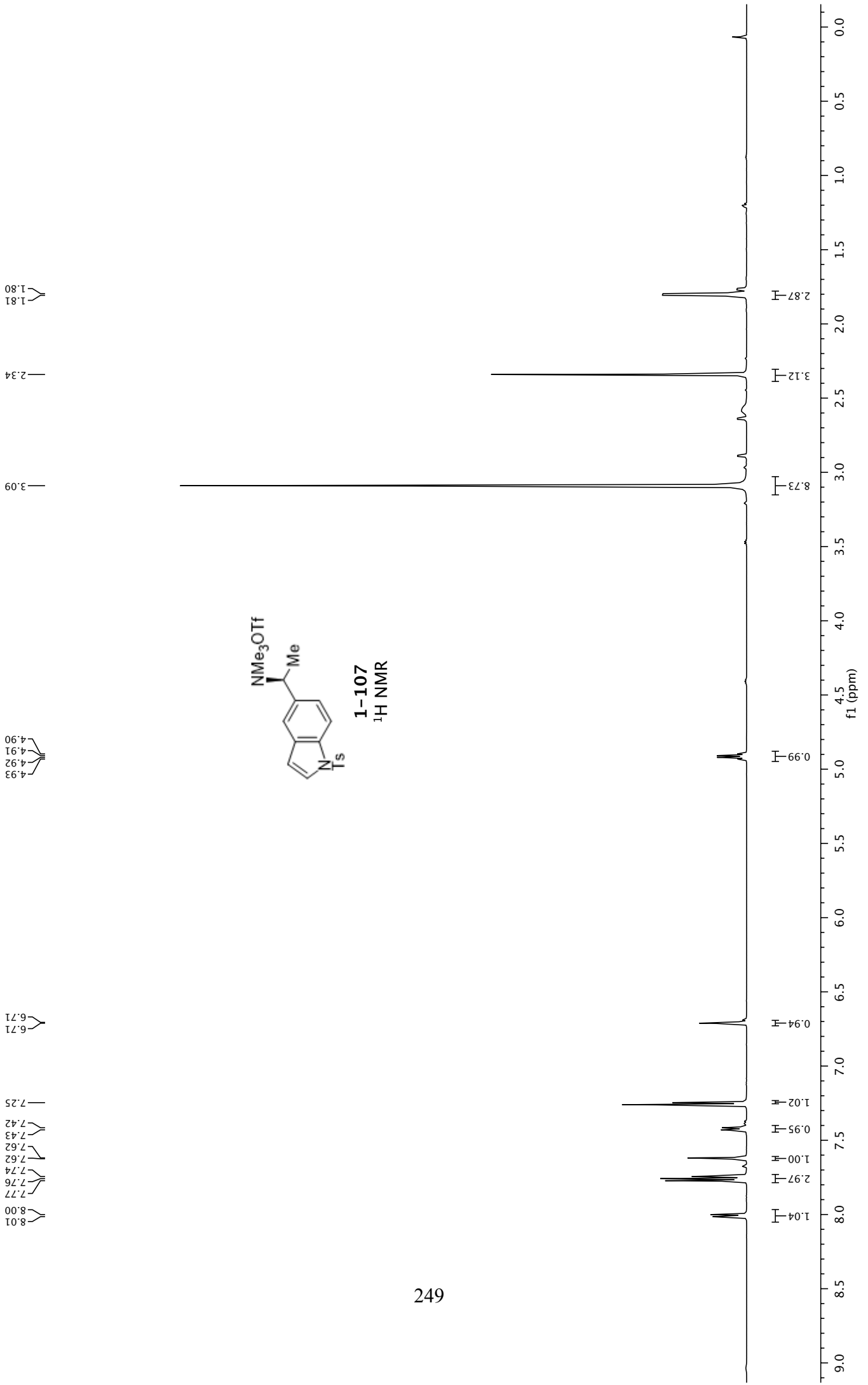


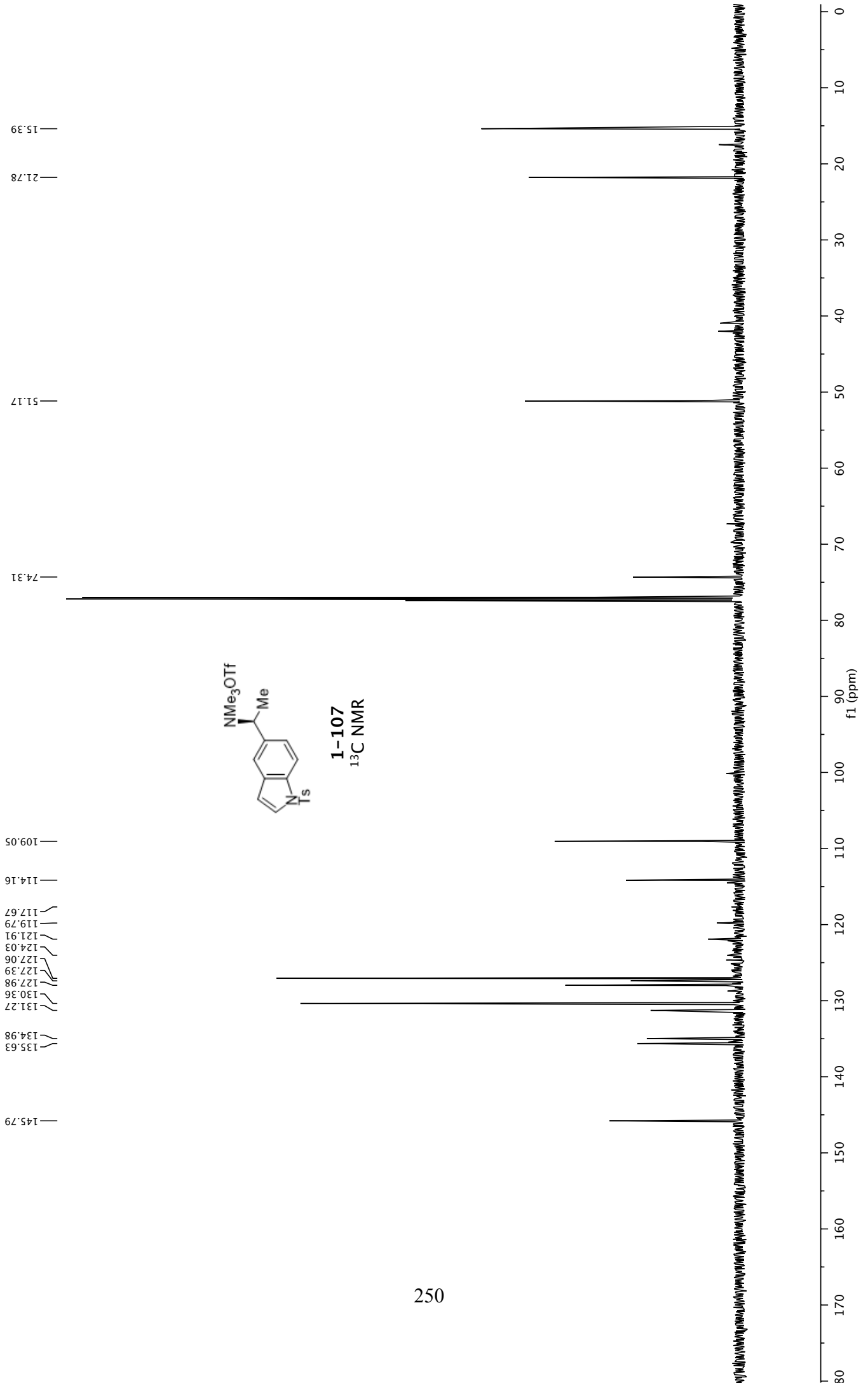
-78.39



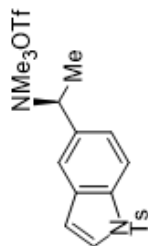
**1-105**  
<sup>19</sup>F NMR



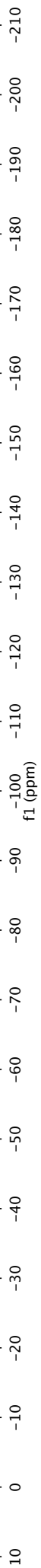




-78.36



**1-107**  
<sup>19</sup>F NMR

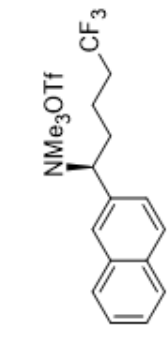


1.20  
1.27  
1.44  
2.12  
2.14  
2.16  
2.17  
2.18  
2.18  
2.19  
2.20  
2.21  
2.22  
2.23  
2.41

3.16

4.82

7.49  
7.54  
7.55  
7.56  
7.57  
7.58  
7.85  
7.86  
7.91  
7.94  
7.96  
7.97  
7.99  
8.11



1-109  
<sup>1</sup>H NMR

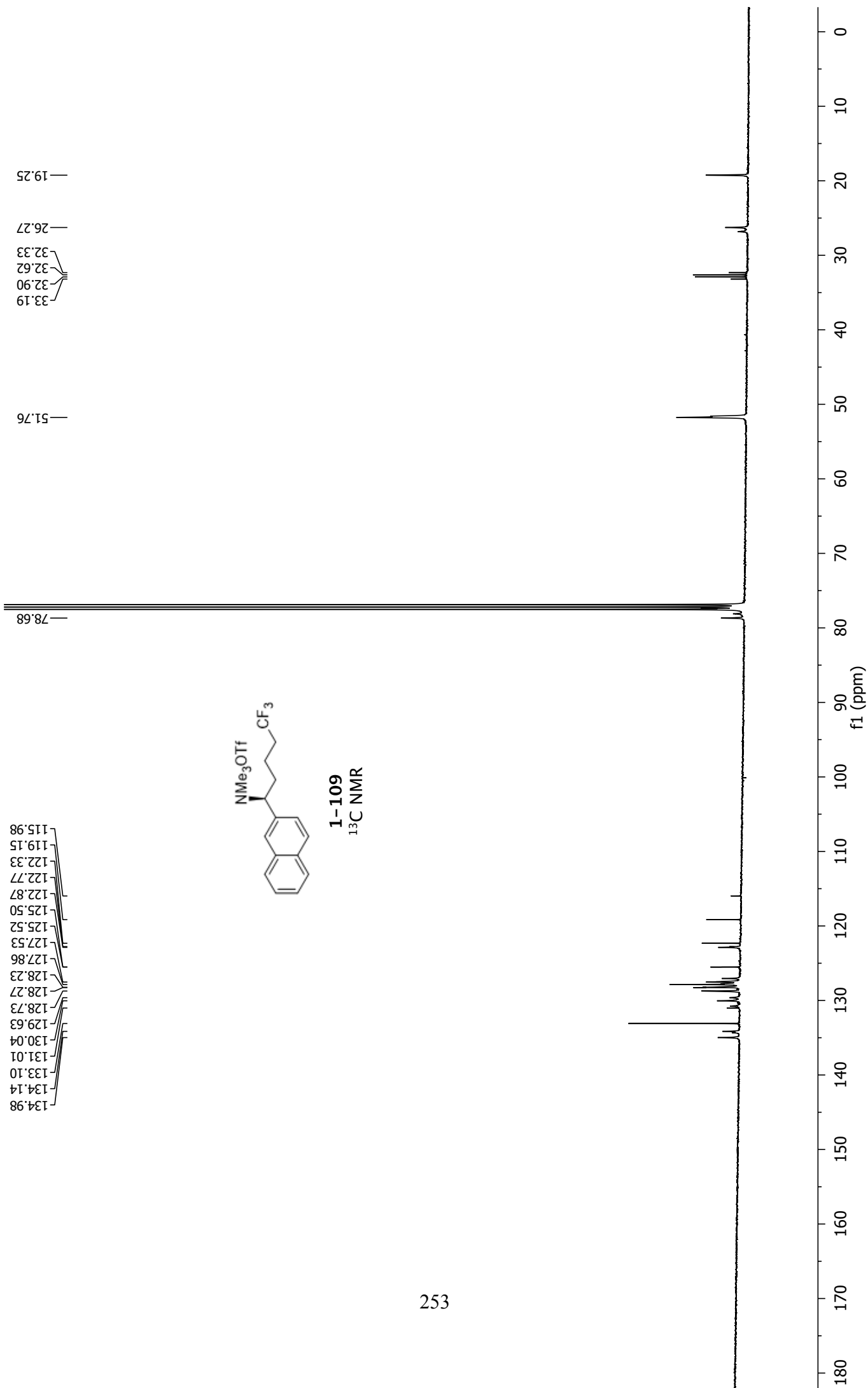
1.16  
1.05  
2.10  
2.07  
8.84

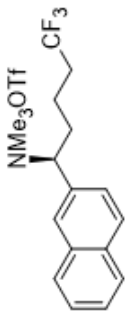
1.00

3.03

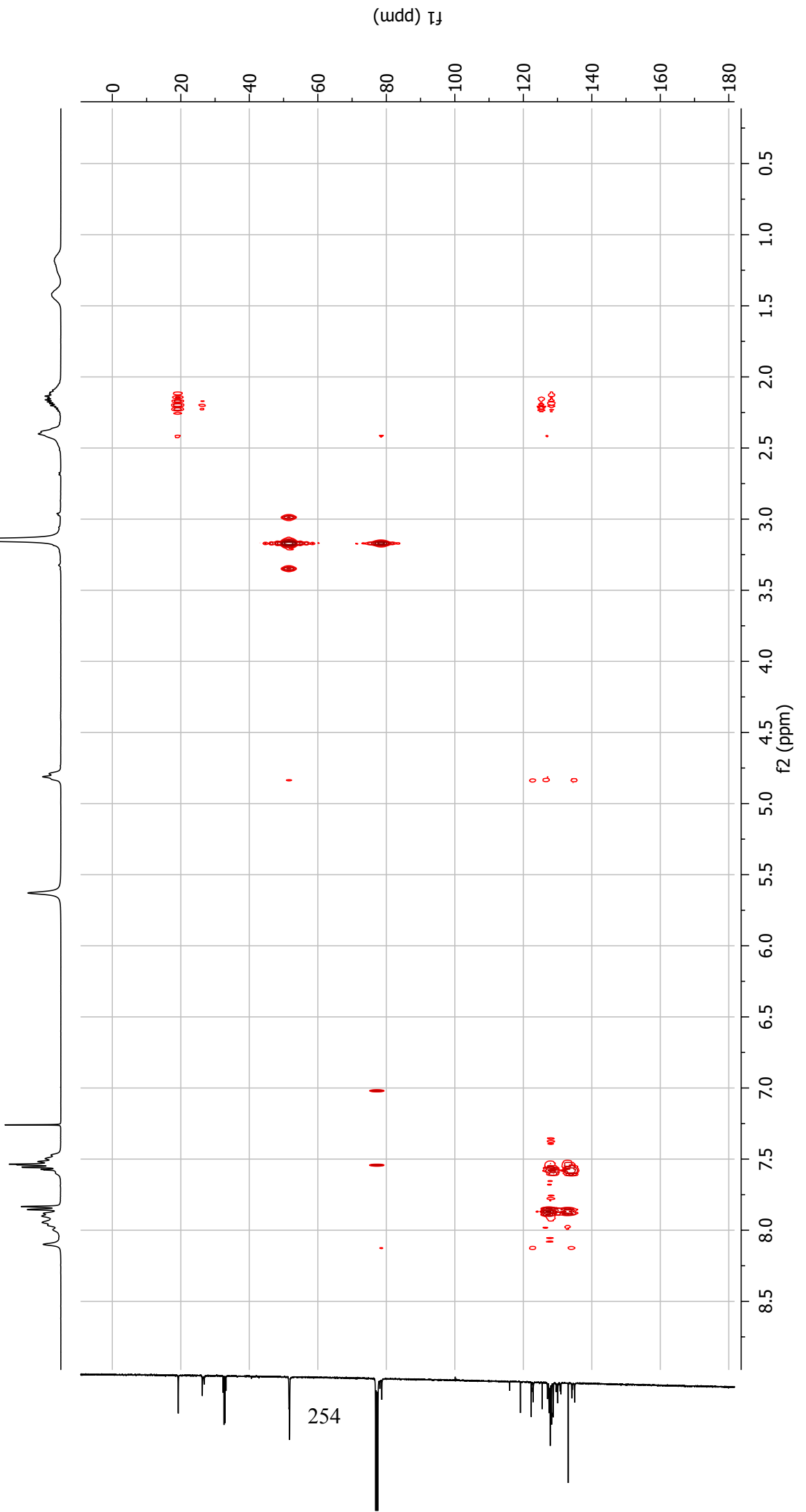
1.03  
3.05

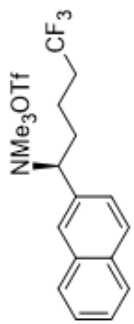




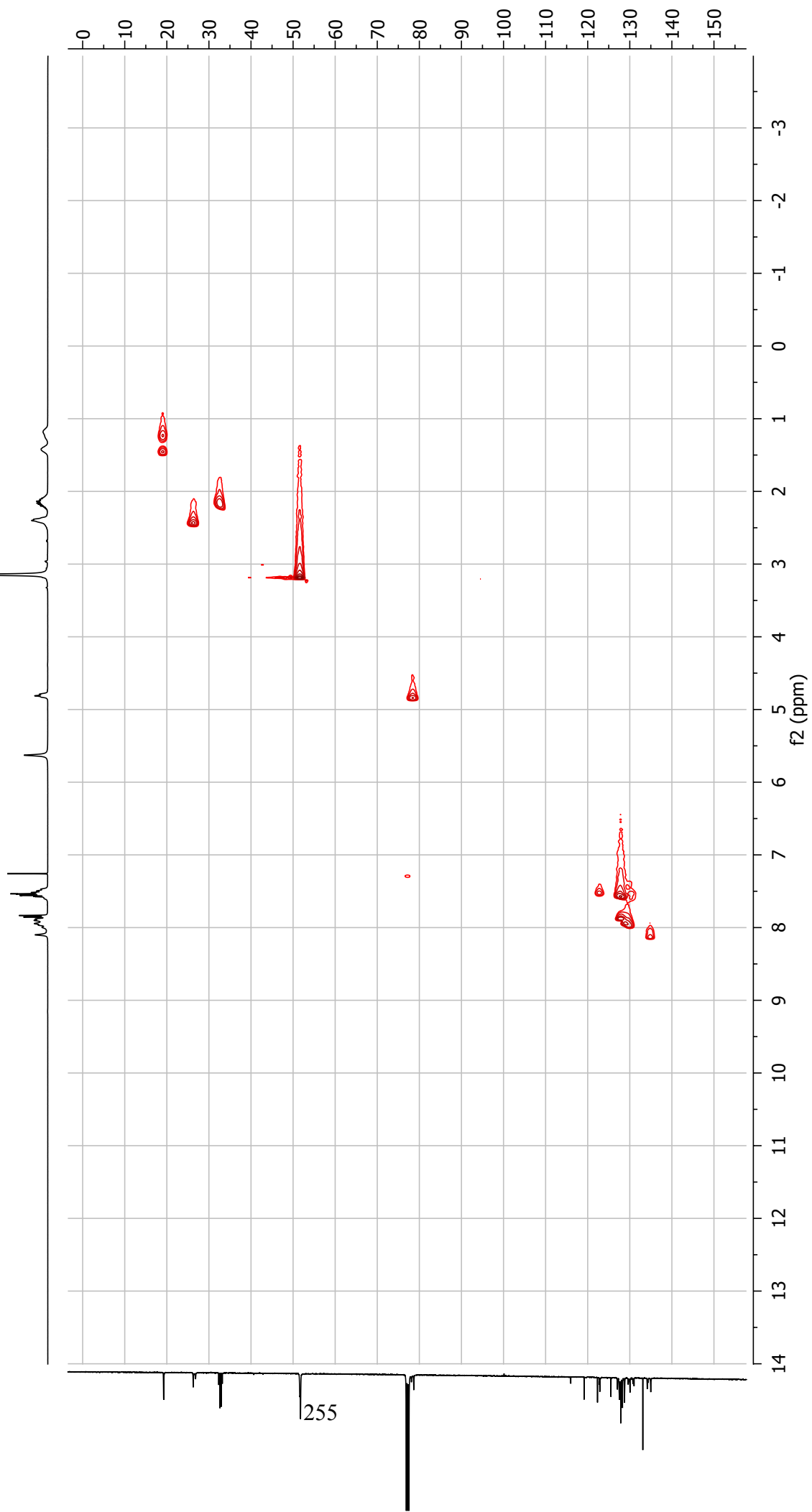


1-109  
HMBC





1-109  
HSQC

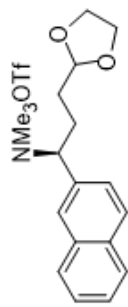


1.54  
1.43  
1.32

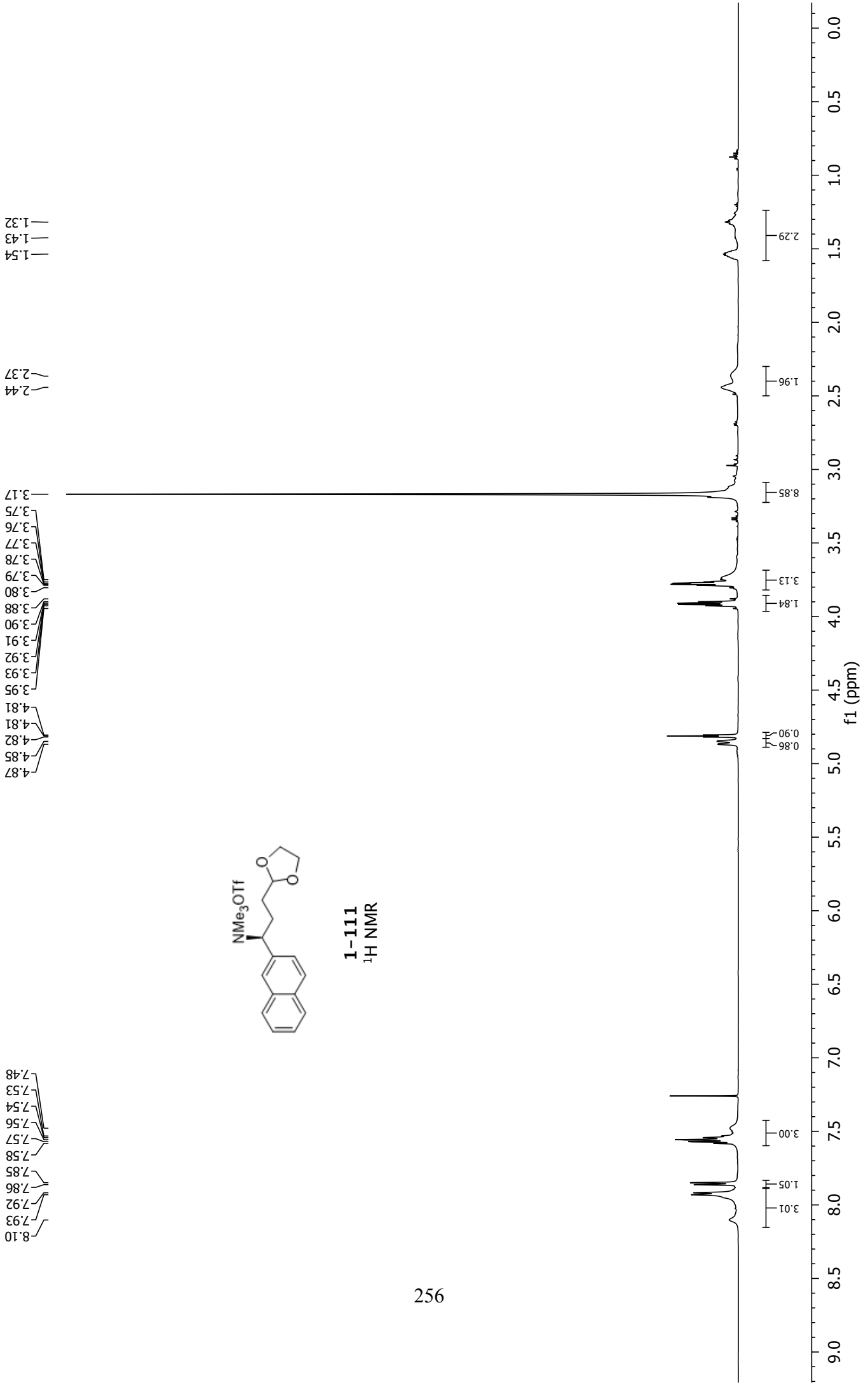
2.44  
2.37

3.17  
3.75  
3.76  
3.77  
3.78  
3.79  
3.80  
3.88  
3.90  
3.91  
3.92  
3.93  
3.95  
4.81  
4.81  
4.82  
4.85  
4.87

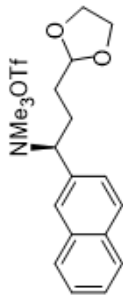
7.48  
7.53  
7.54  
7.56  
7.57  
7.58  
7.85  
7.86  
7.92  
7.93  
8.10



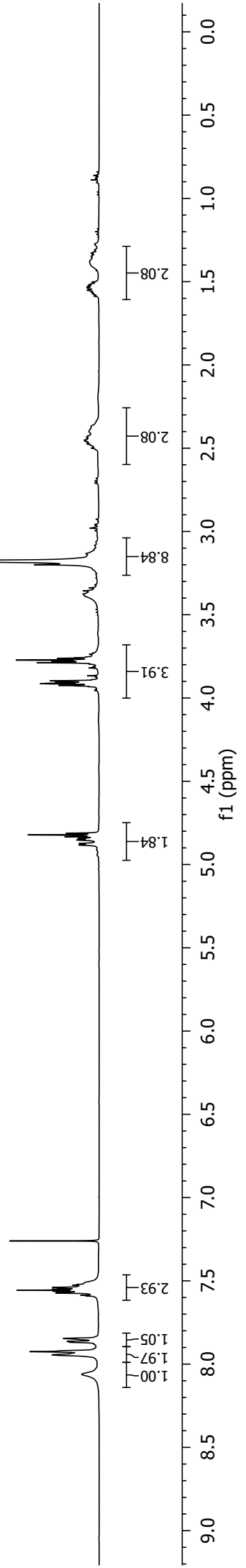
**1-111**  
<sup>1</sup>H NMR

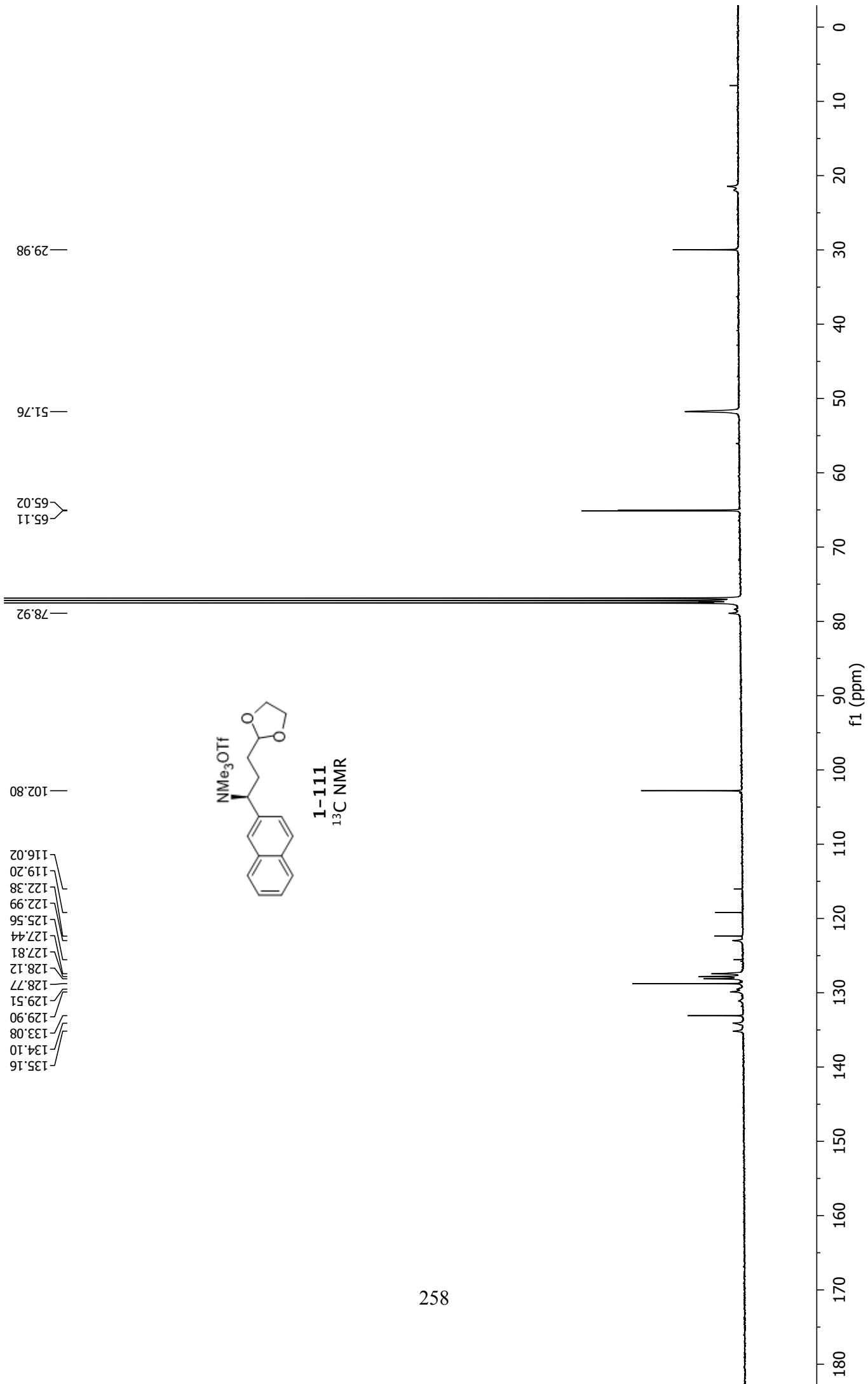


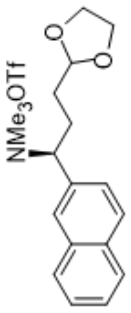
8.06  
7.94  
7.93  
7.87  
7.86  
7.85  
7.59  
7.59  
7.57  
7.57  
7.56  
7.56  
7.56  
7.55  
7.54  
7.54  
7.54  
7.53  
7.52  
4.94  
4.92  
4.88  
4.87  
4.85  
4.84  
4.83  
4.82  
4.81  
3.92  
3.91  
3.91  
3.91  
3.90  
3.79  
3.78  
3.78  
3.77  
3.76  
3.18  
2.48  
2.47  
2.46  
2.45  
2.44  
2.44  
2.43  
2.40  
2.38  
2.37  
1.59  
1.58  
1.57  
1.56  
1.55  
1.54  
1.53  
1.52  
1.51  
1.50  
1.43  
1.38  
1.35  
1.33  
1.31



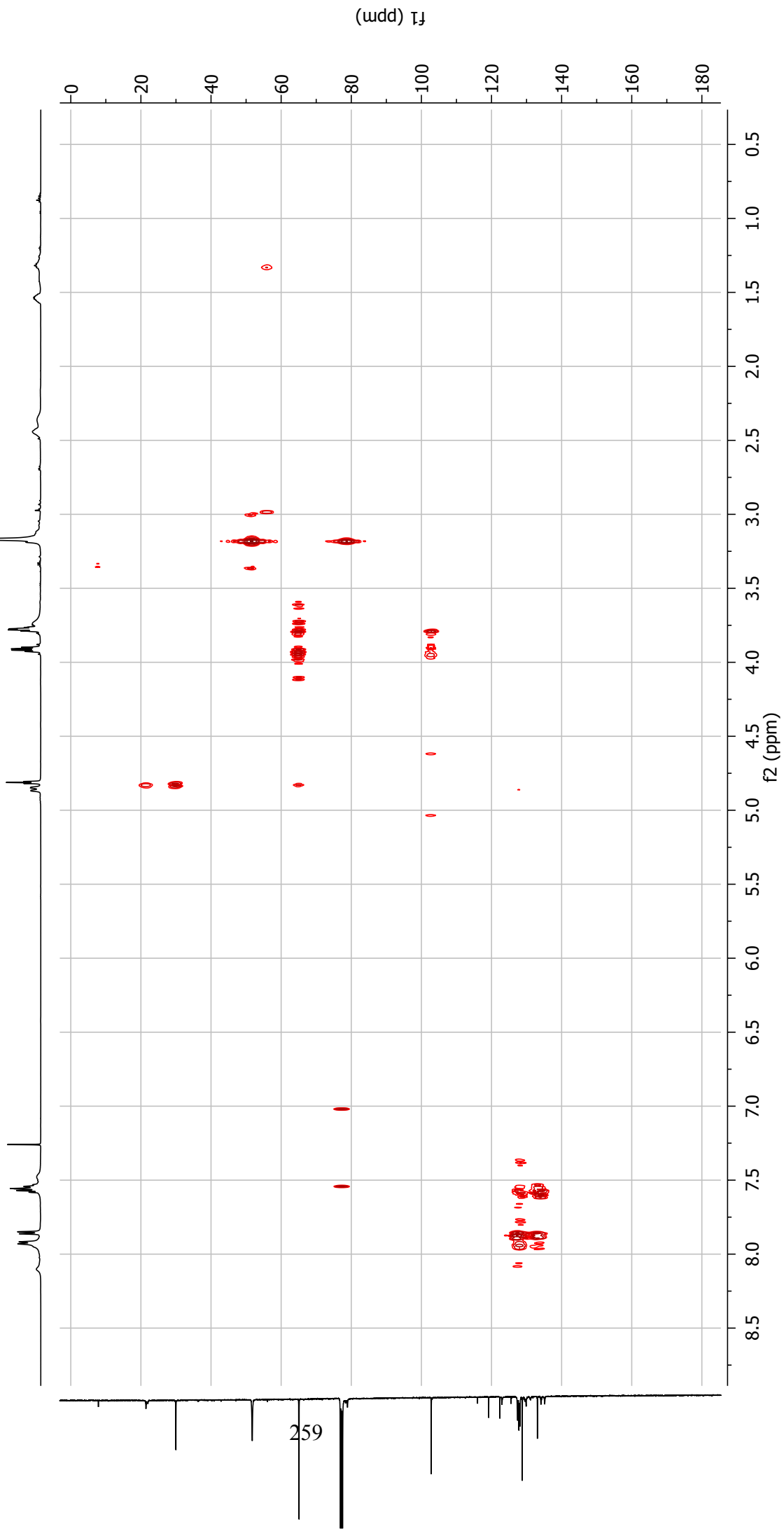
**1-111**  
<sup>1</sup>H NMR 50 °C

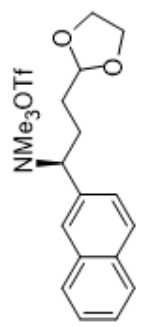




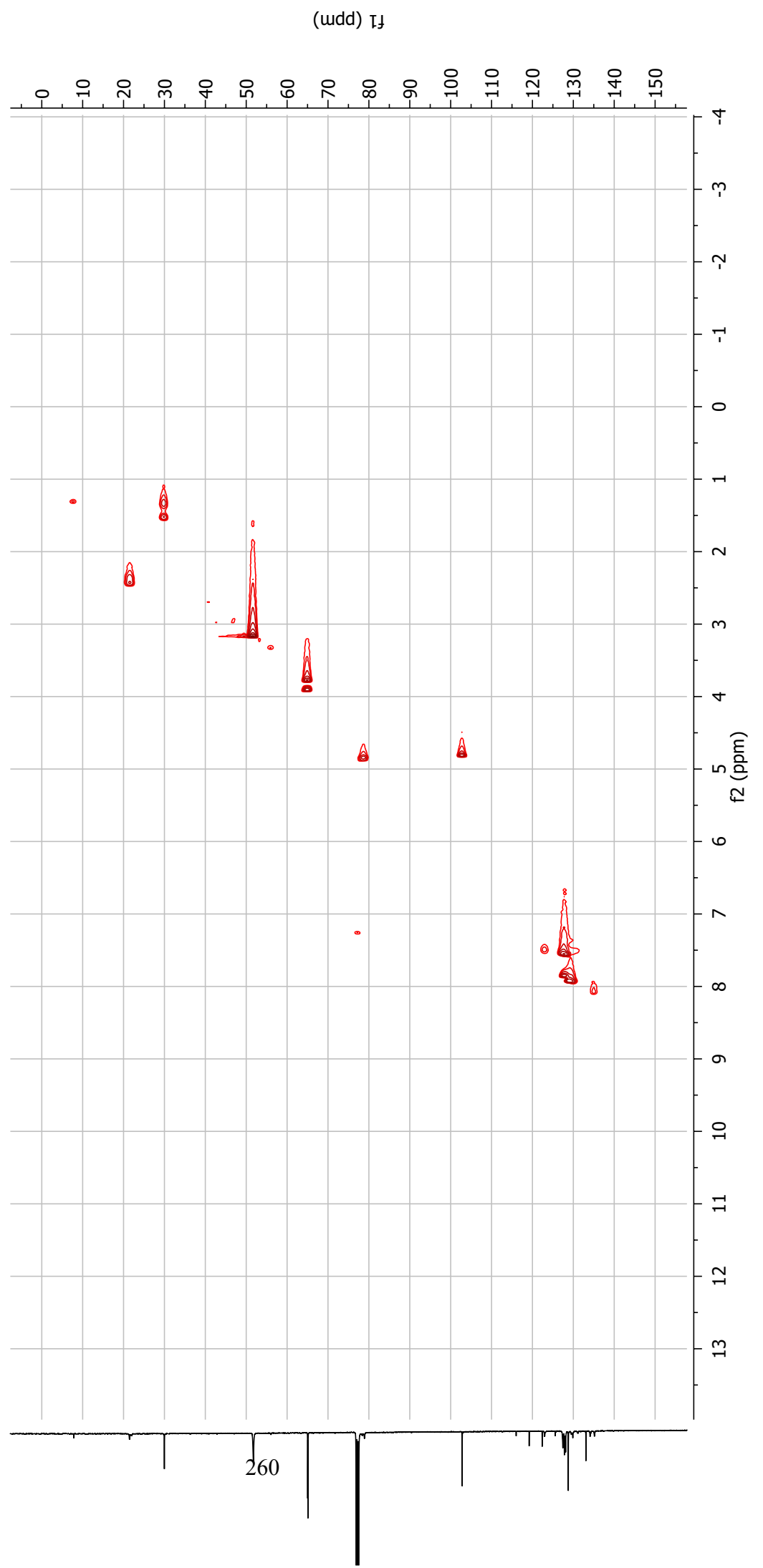


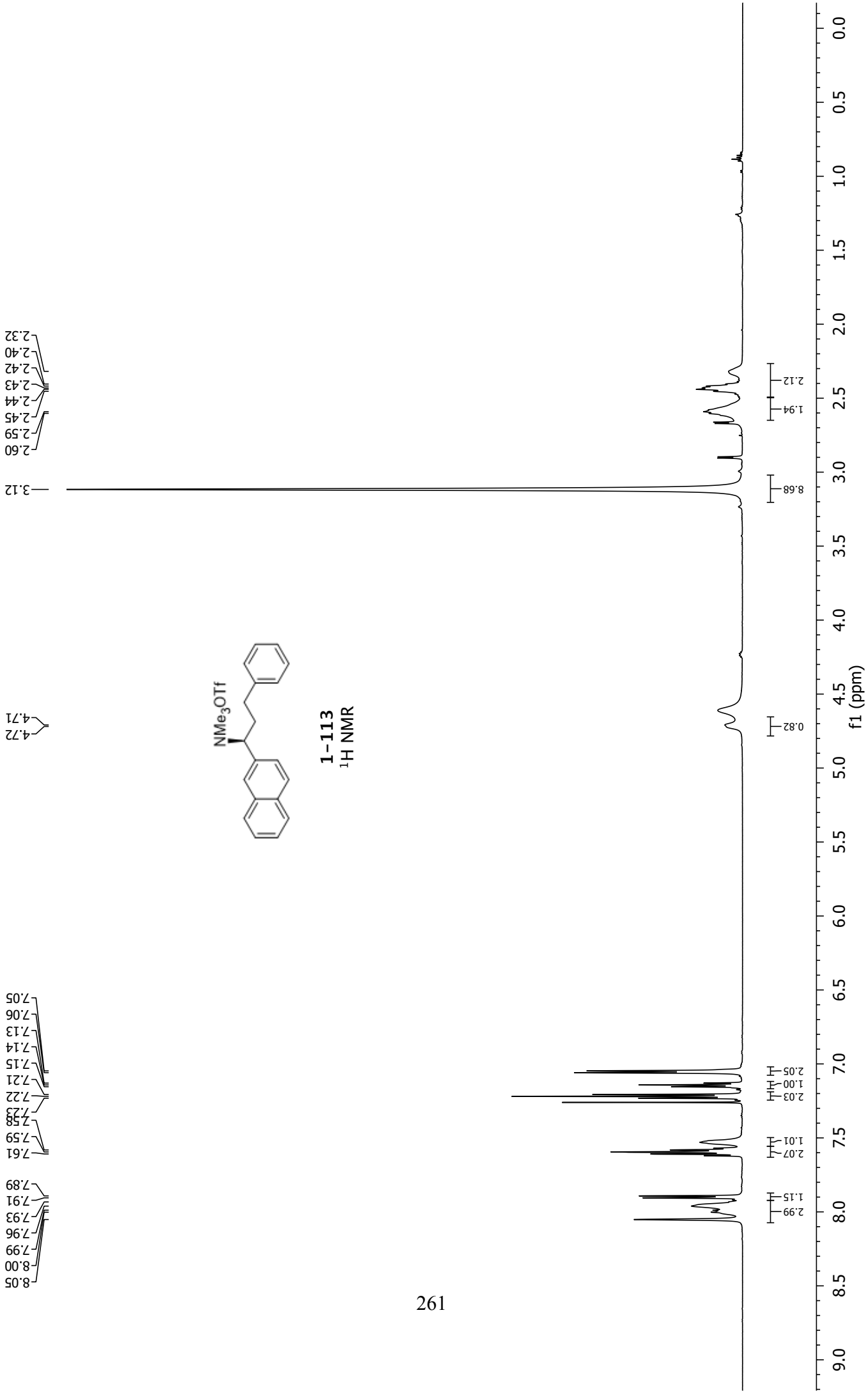
1-111  
HMBC

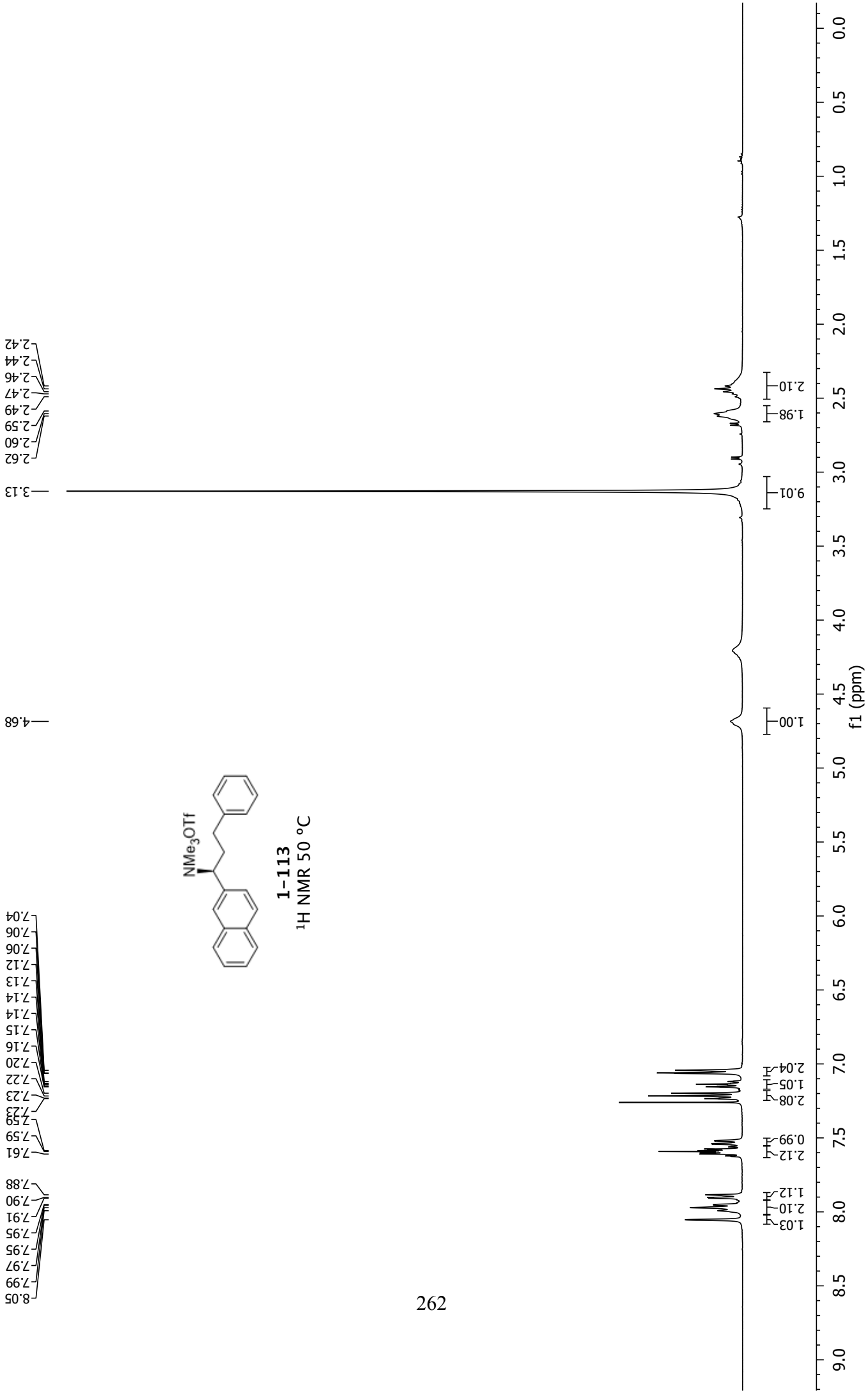


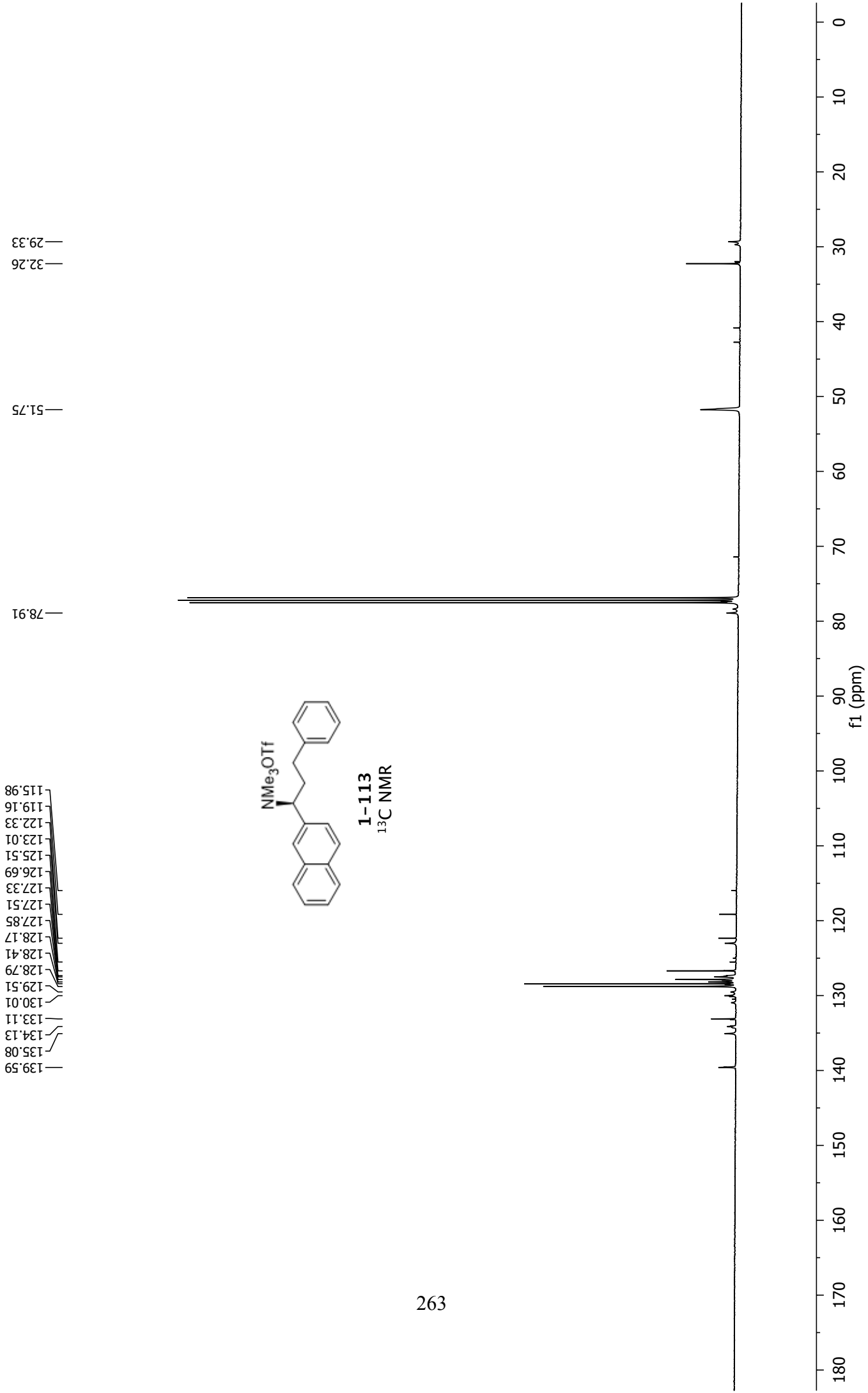


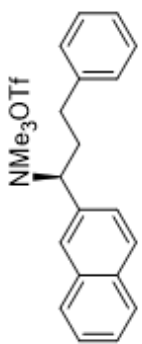
1-111  
HSQC



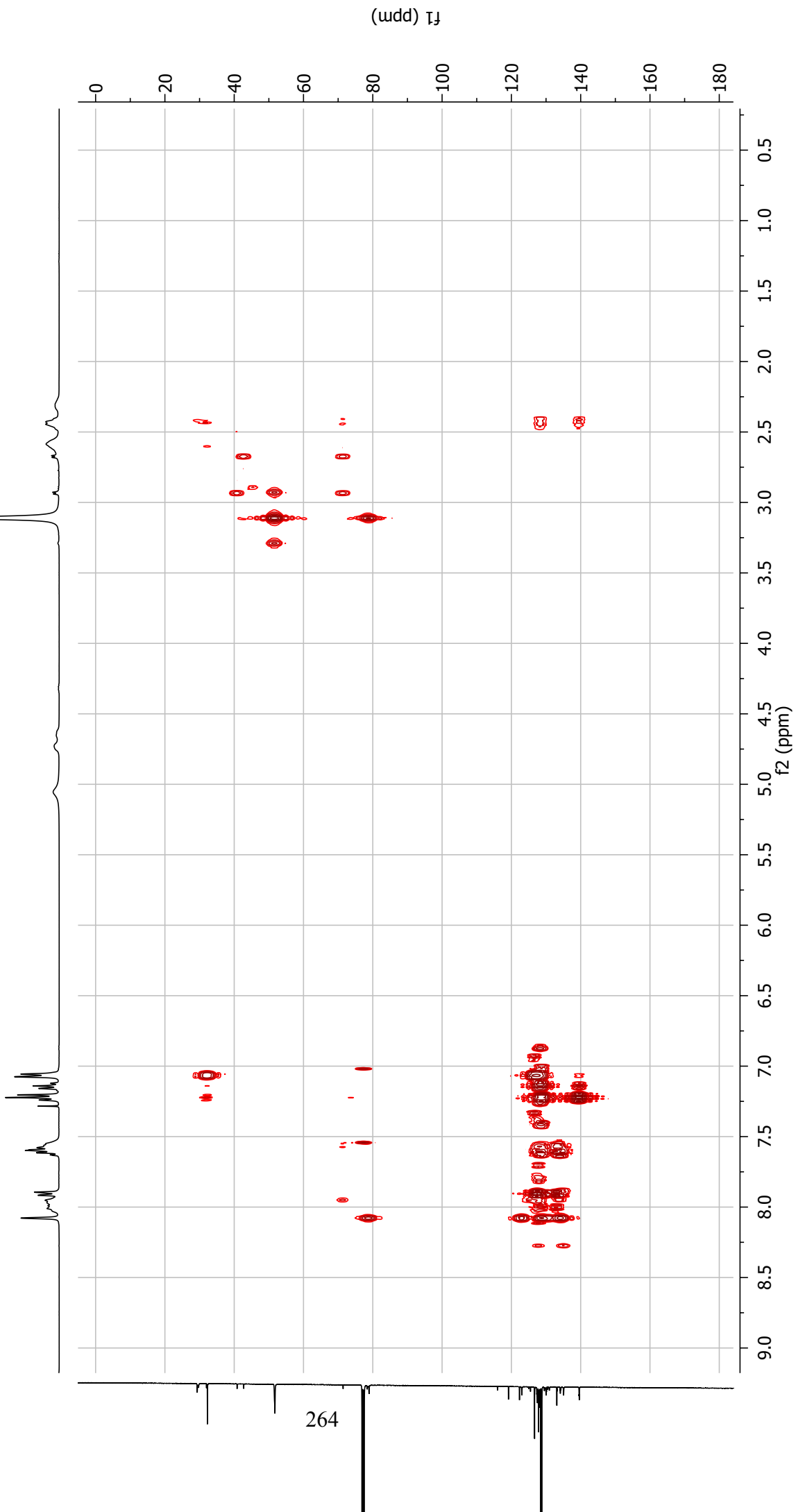




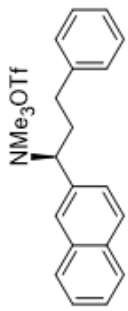




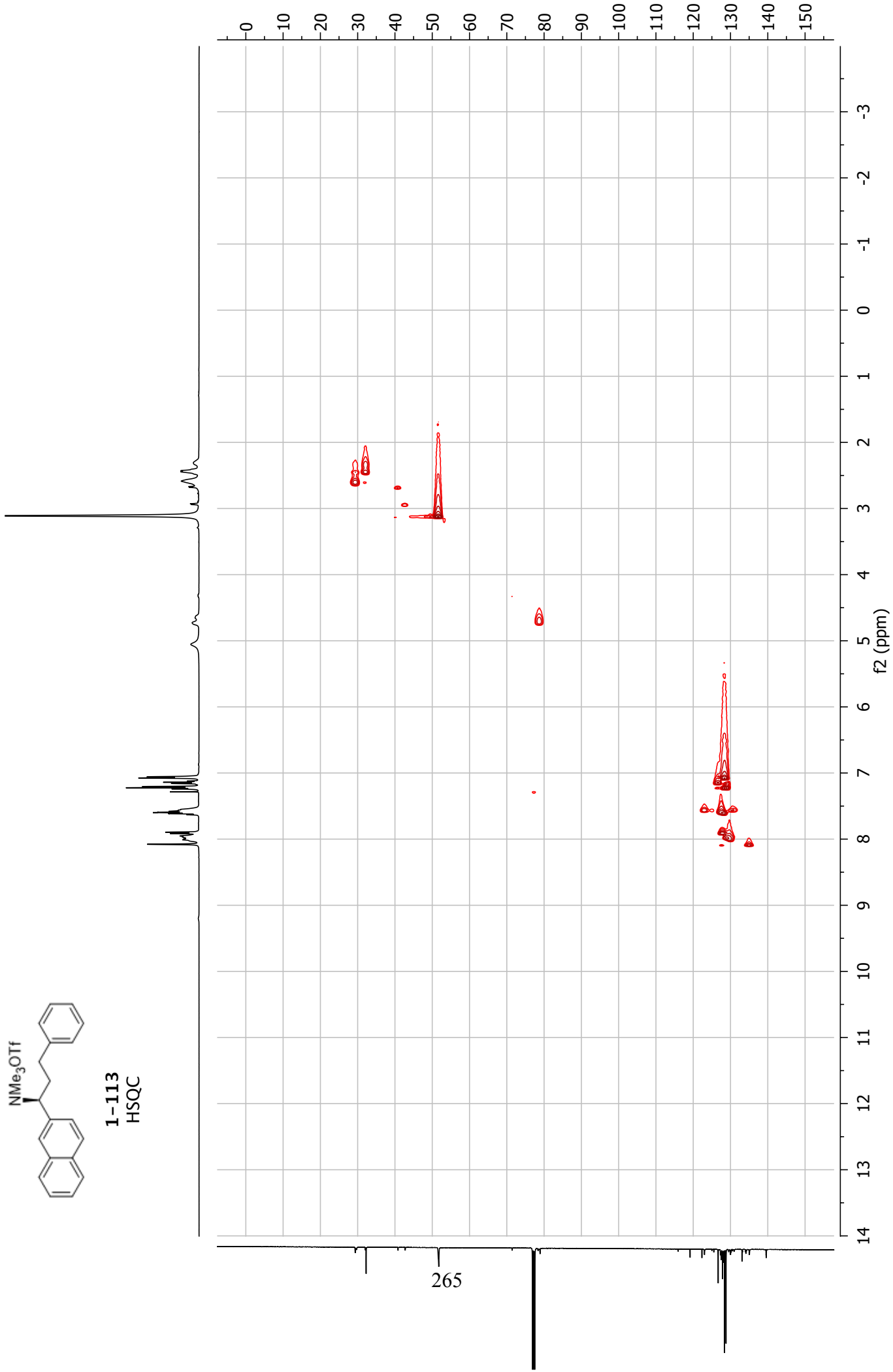
1-113  
HMBC

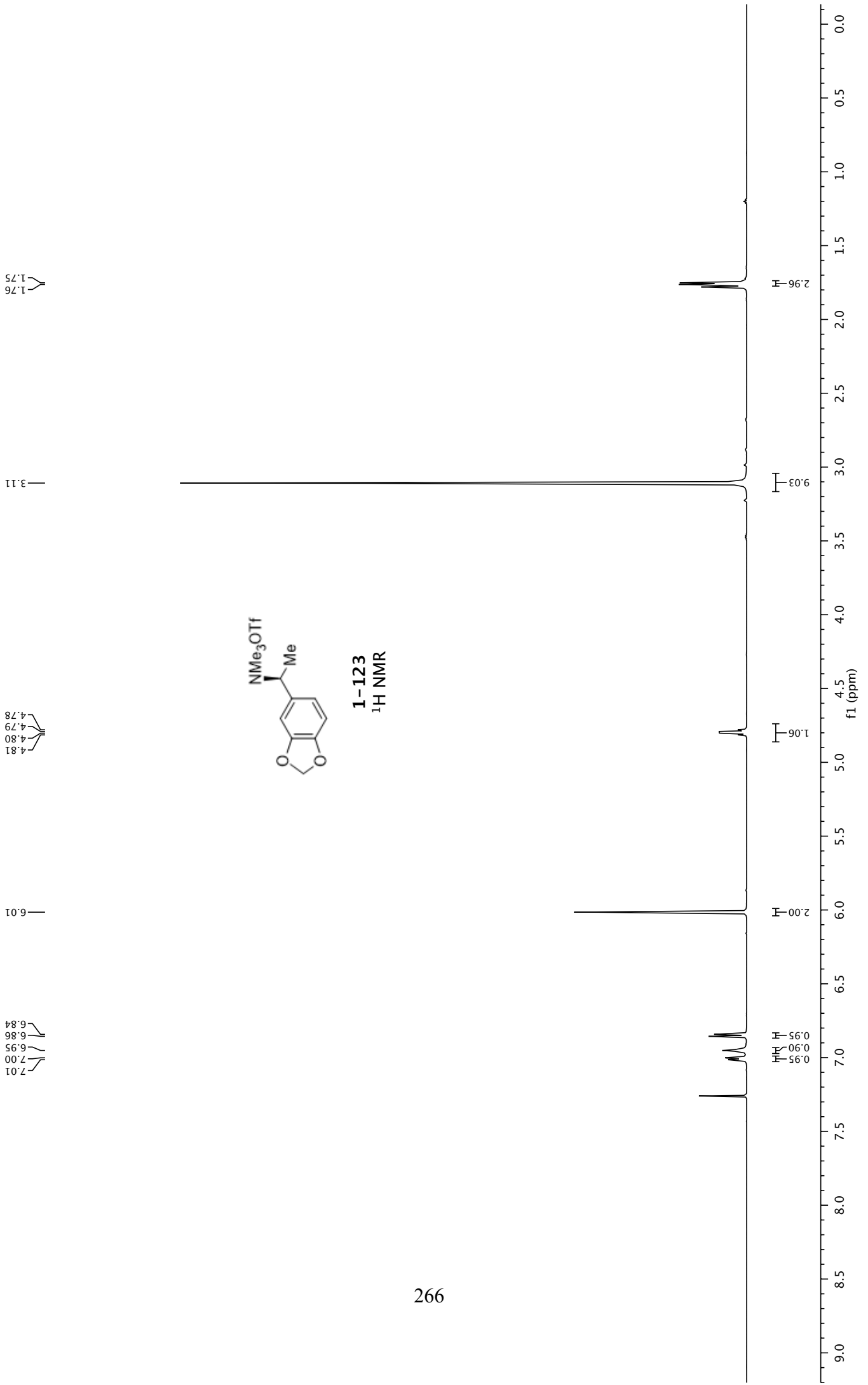


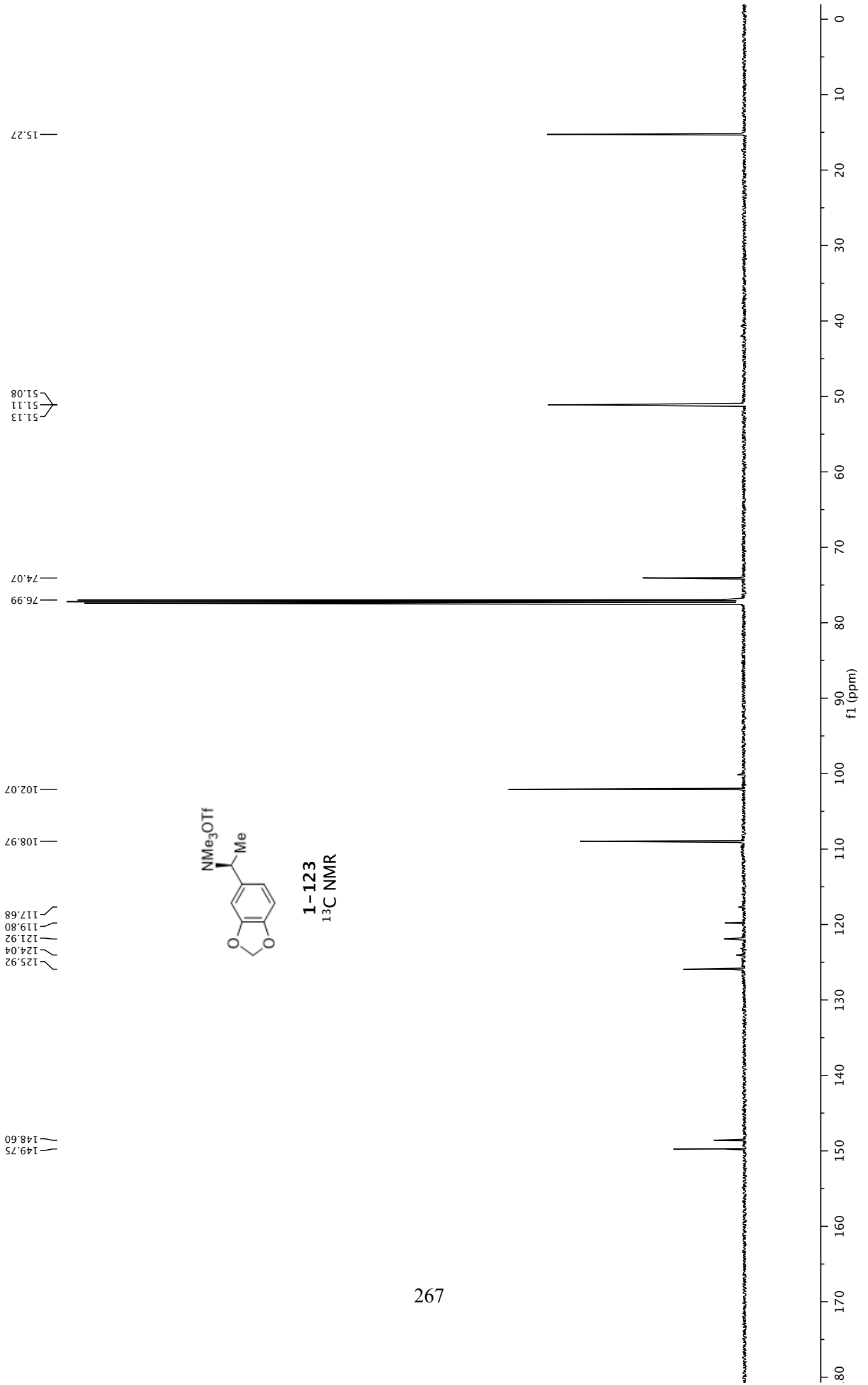
264



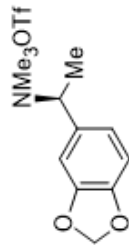
1-113  
HSQC



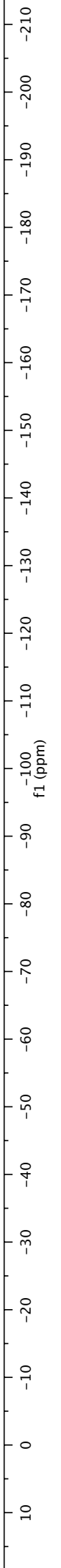


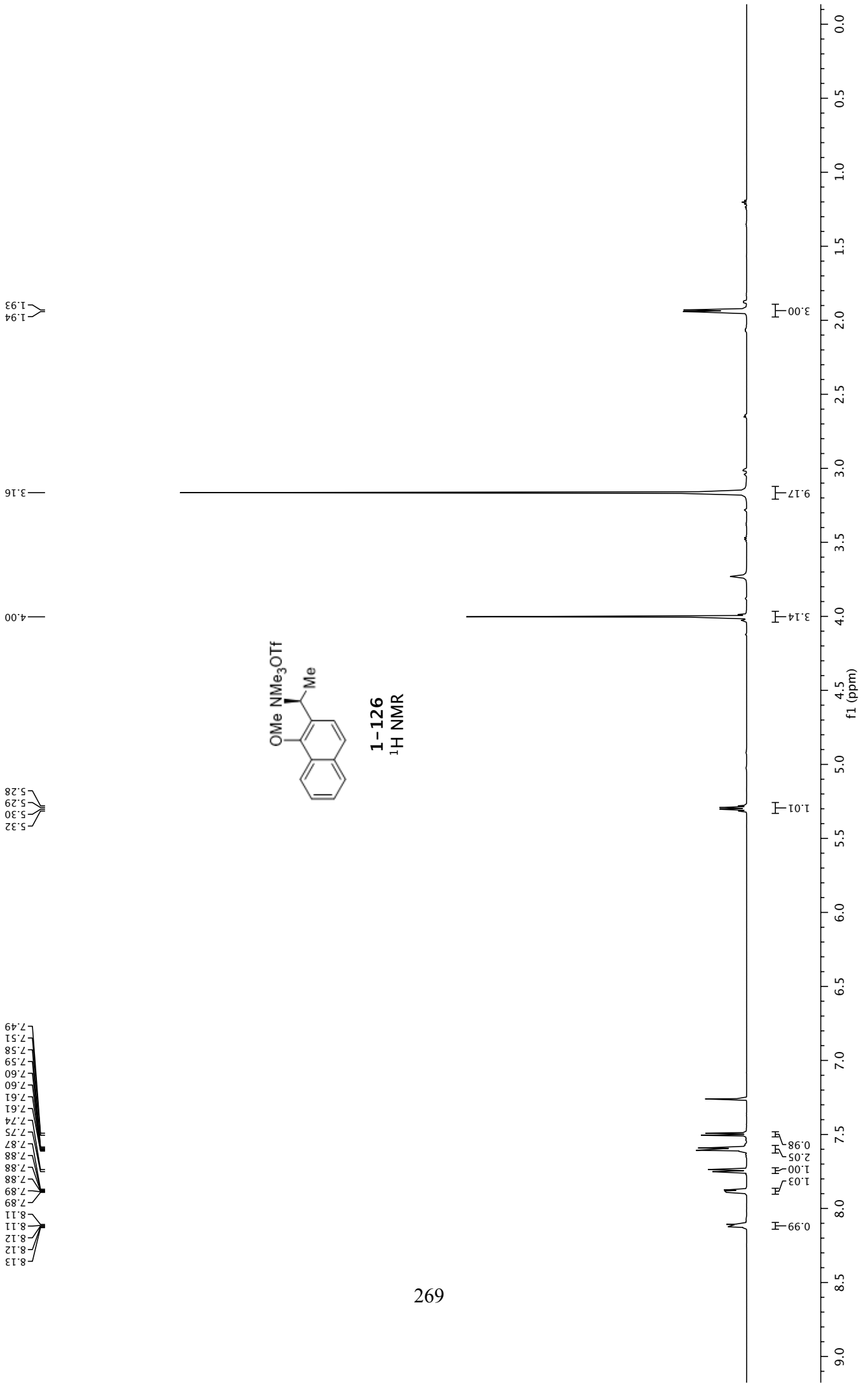


-78.45

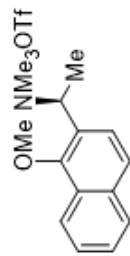


**1-123**  
<sup>19</sup>F NMR

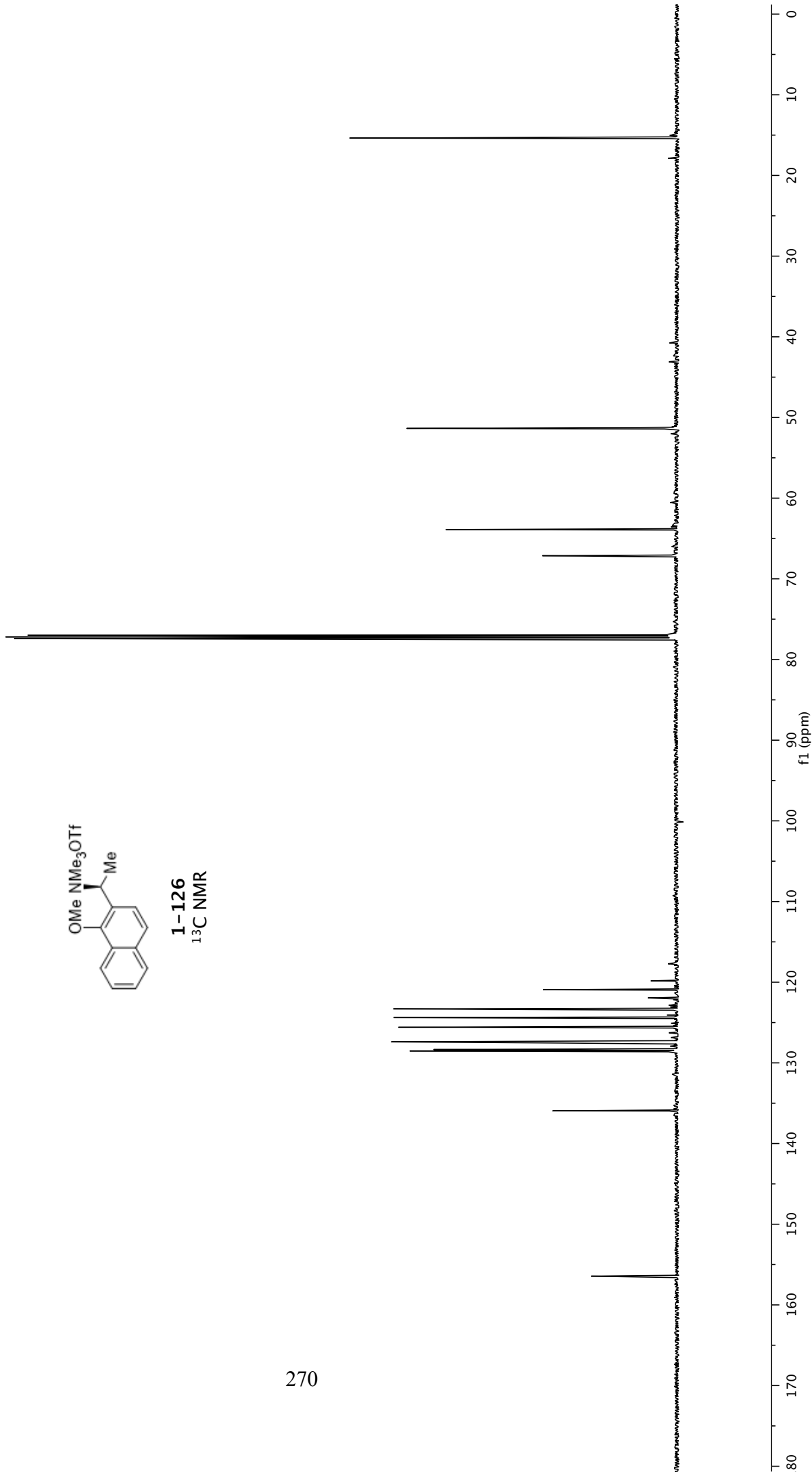




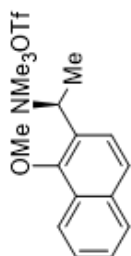
156.44  
135.95  
128.52  
128.35  
127.54  
127.40  
125.58  
124.39  
124.07  
123.30  
121.95  
120.94  
119.83  
117.71  
67.14  
63.90  
51.38  
51.36  
51.34  
15.38



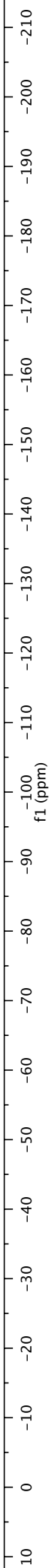
**1-126**  
<sup>13</sup>C NMR



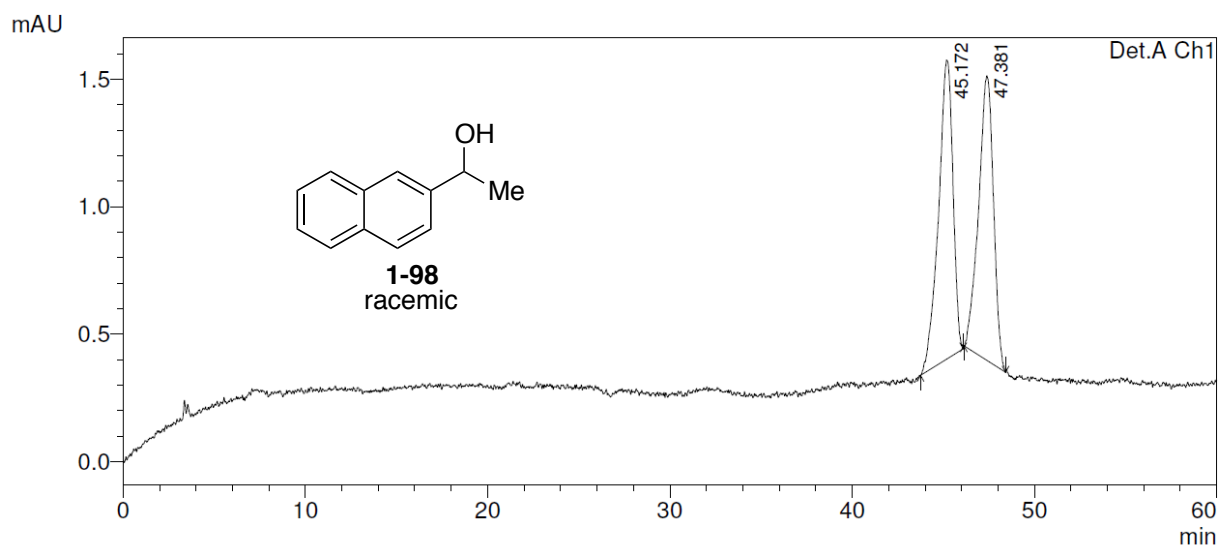
-78.36



**1-126**  
<sup>19</sup>F NMR

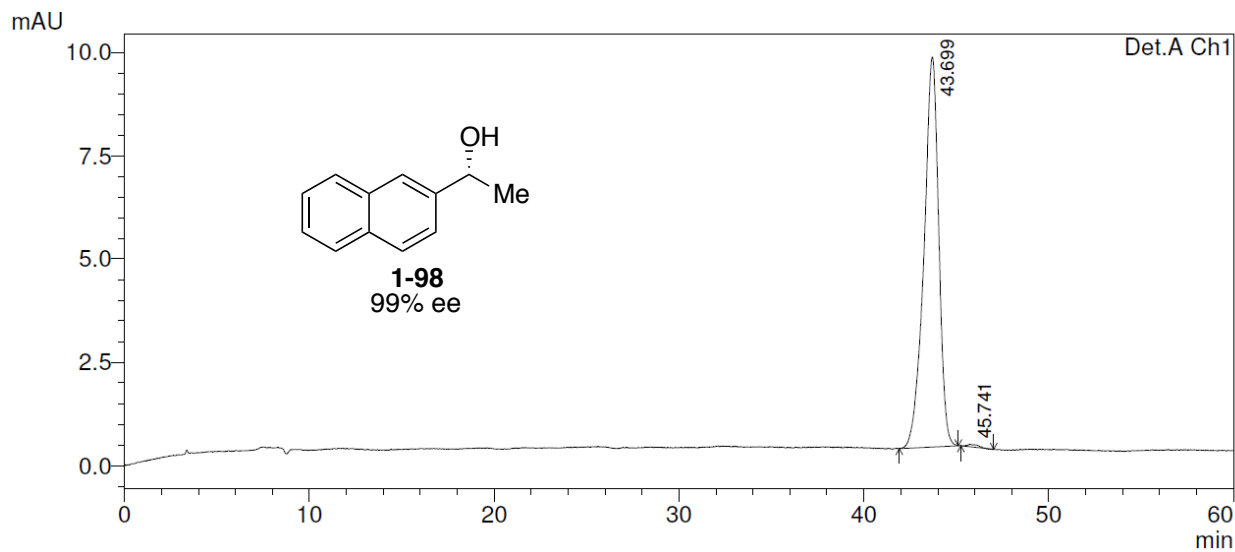


Compound **1-98**, racemic (254 nm)



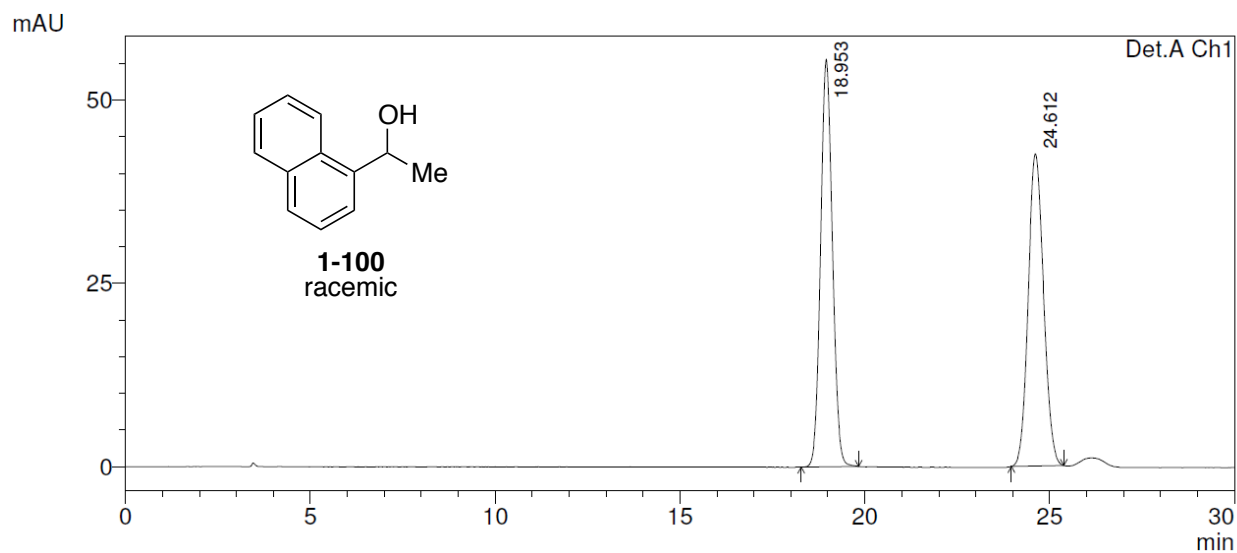
Peak#	Ret. Time	Area	Height	Area %	Height %
1	45.172	64627	1174	50.417	51.245
2	47.381	63558	1117	49.583	48.755
Total		128185	2292	100.000	100.000

Compound **1-98**, 99% ee (254 nm)



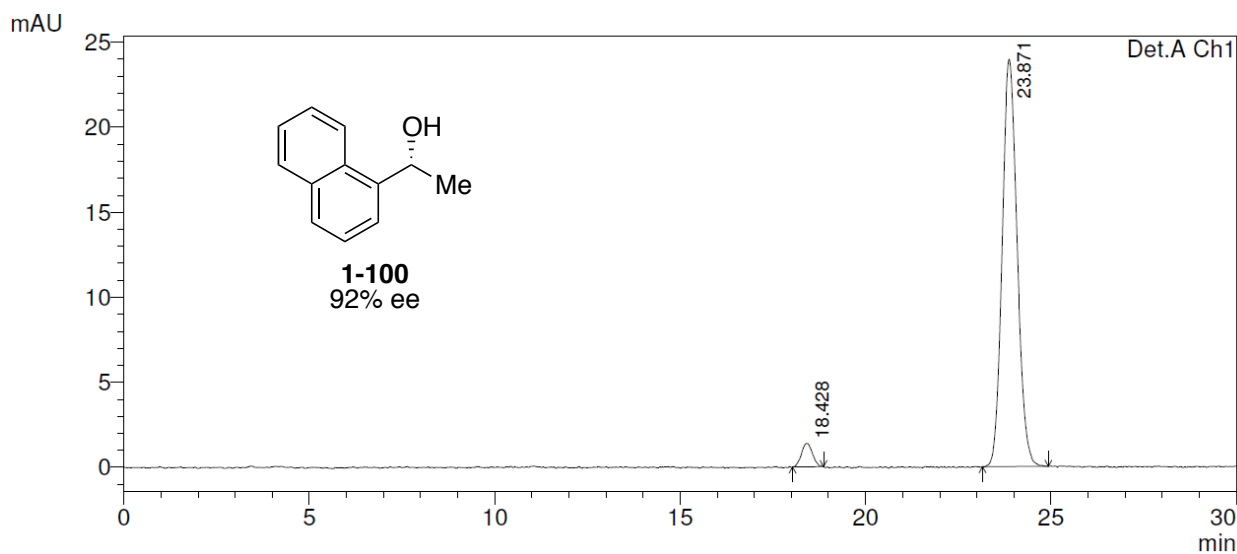
Peak#	Ret. Time	Area	Height	Area %	Height %
1	43.699	524955	9434	99.543	99.356
2	45.741	2408	61	0.457	0.644
Total		527362	9495	100.000	100.000

Compound **1-100**, racemic (254 nm)



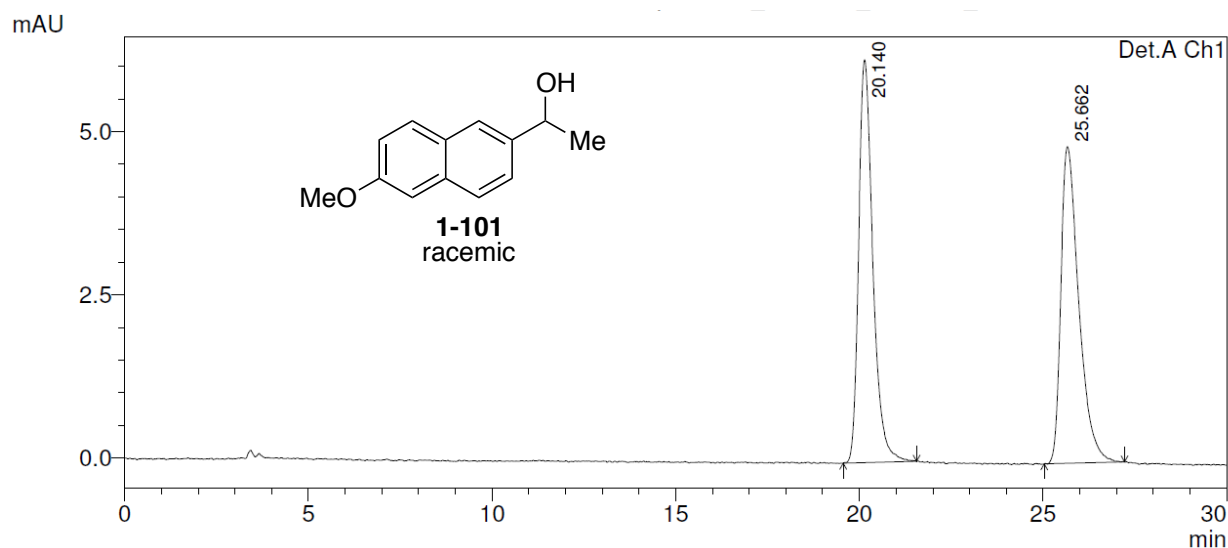
Peak#	Ret. Time	Area	Height	Area %	Height %
1	18.953	1239231	55611	50.146	56.632
2	24.612	1232017	42586	49.854	43.368
Total		2471248	98197	100.000	100.000

Compound **1-100**, 92% ee (254 nm)



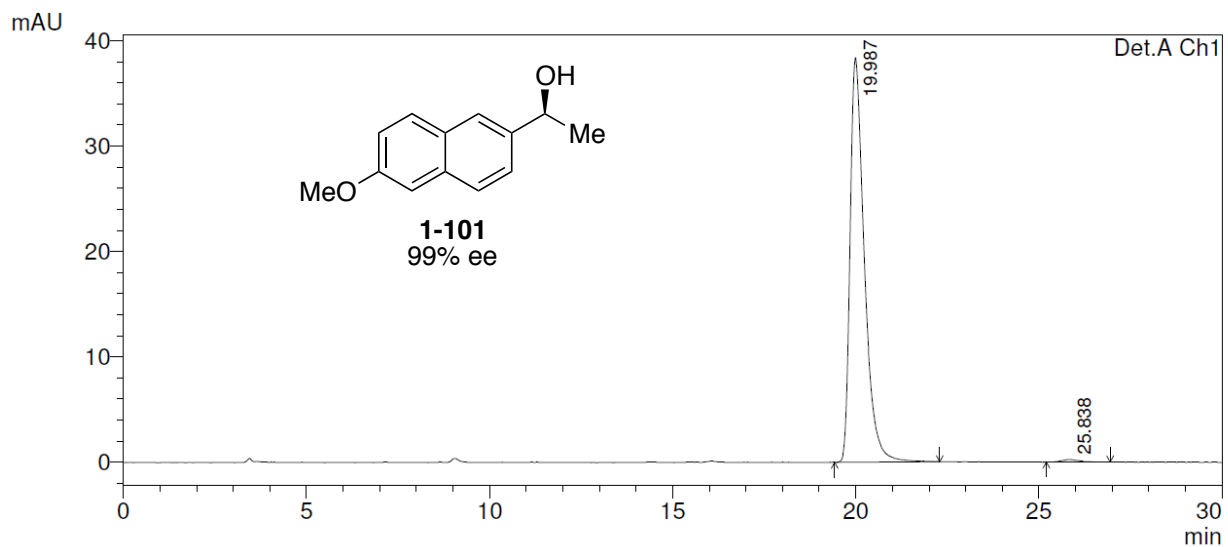
Peak#	Ret. Time	Area	Height	Area %	Height %
1	18.428	28226	1362	4.034	5.381
2	23.871	671567	23948	95.966	94.619
Total		699793	25310	100.000	100.000

Compound **1-101**, racemic (254 nm)



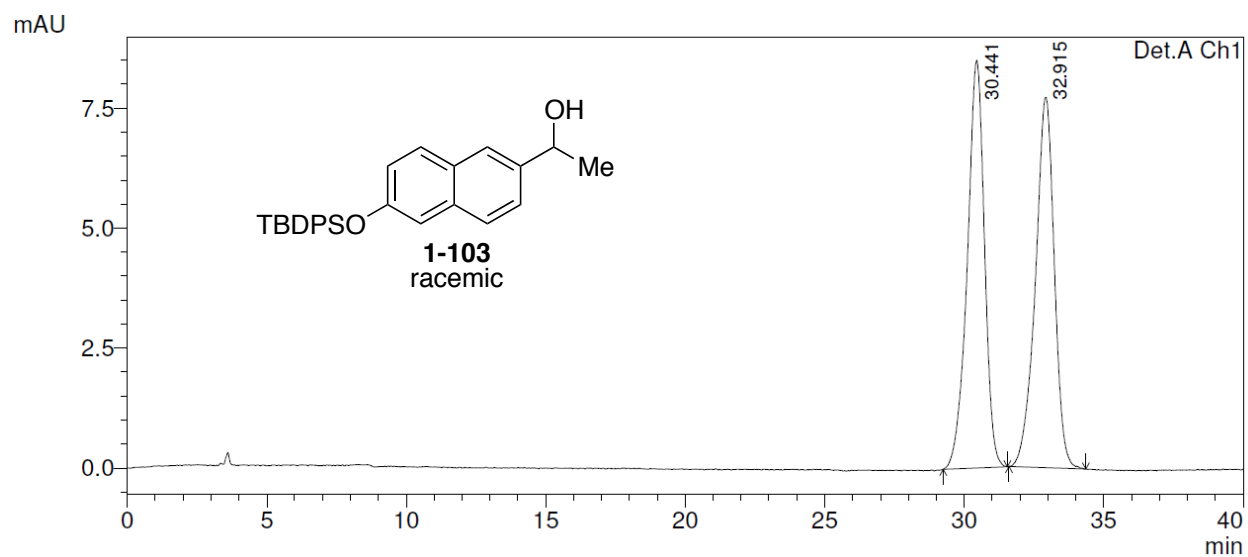
Peak#	Ret. Time	Area	Height	Area %	Height %
1	20.140	165137	6165	50.153	55.982
2	25.662	164128	4848	49.847	44.018
Total		329266	11013	100.000	100.000

Compound **1-101**, 99% ee (254 nm)



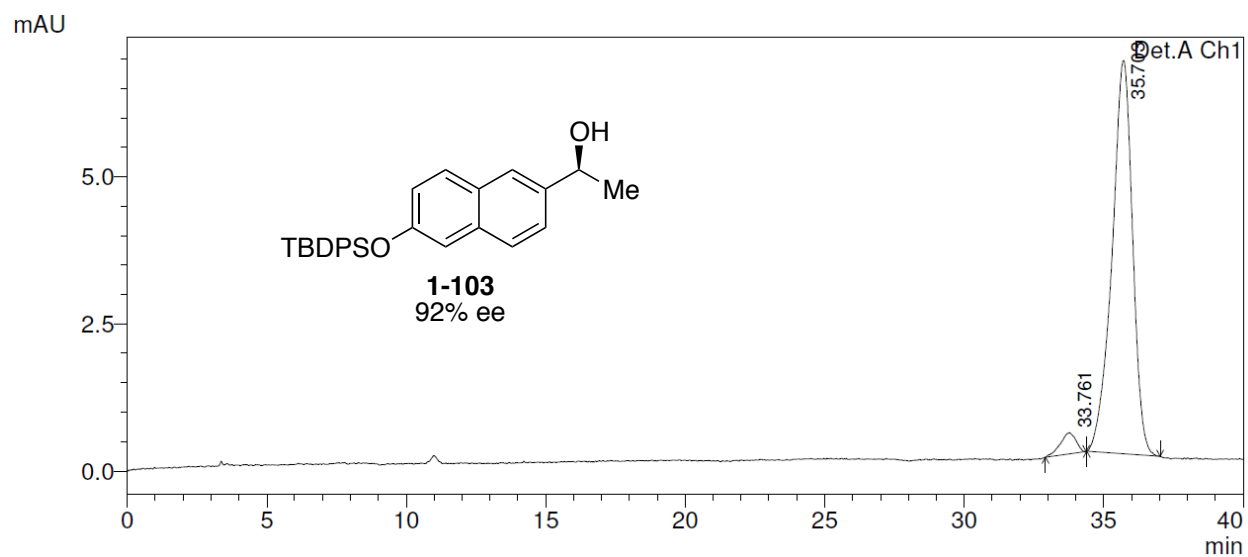
Peak#	Ret. Time	Area	Height	Area %	Height %
1	19.987	1037849	38360	99.309	99.372
2	25.838	7220	242	0.691	0.628
Total		1045069	38602	100.000	100.000

Compound **1-103**, racemic (254 nm)



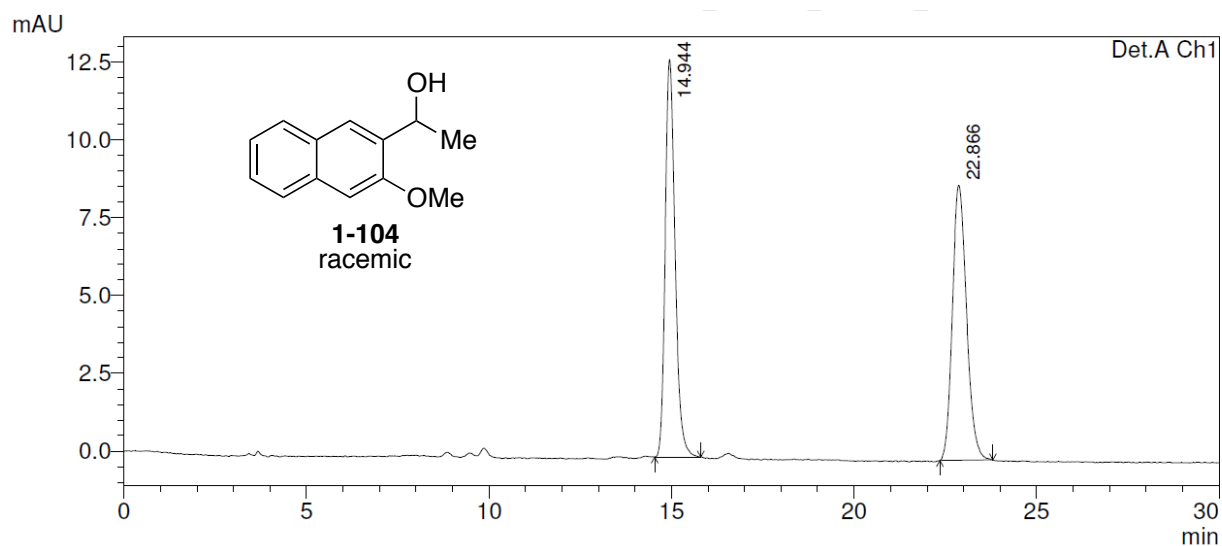
Peak#	Ret. Time	Area	Height	Area %	Height %
1	30.441	364152	8496	49.958	52.369
2	32.915	364762	7727	50.042	47.631
Total		728913	16223	100.000	100.000

Compound **1-103**, 92% ee (254 nm)



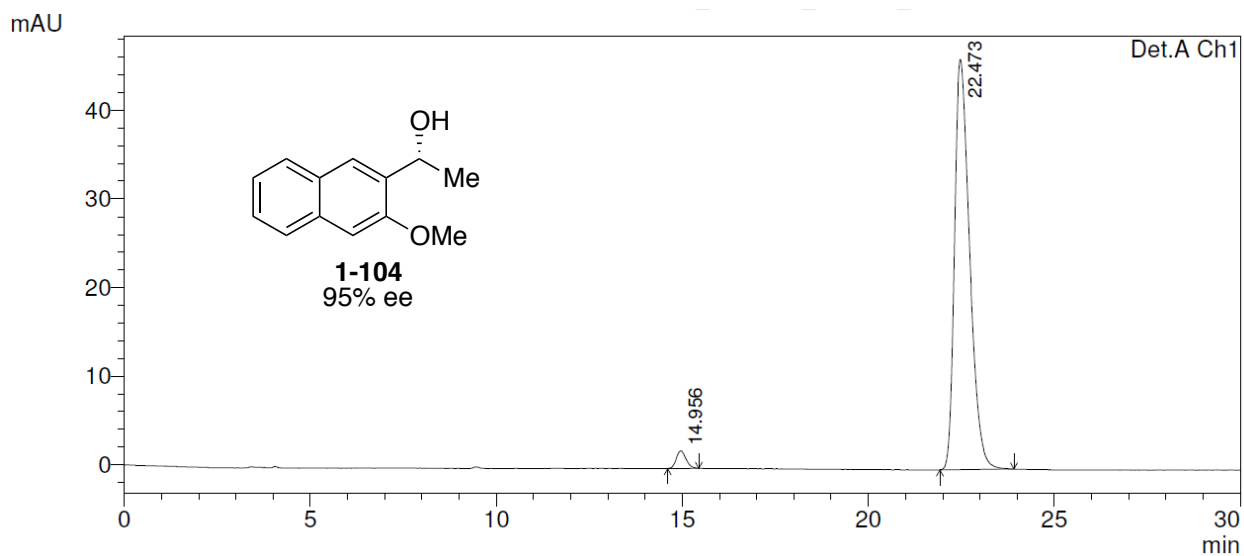
Peak#	Ret. Time	Area	Height	Area %	Height %
1	33.761	14125	358	3.958	5.084
2	35.703	342763	6682	96.042	94.916
Total		356888	7040	100.000	100.000

Compound **1-104**, racemic (254 nm)



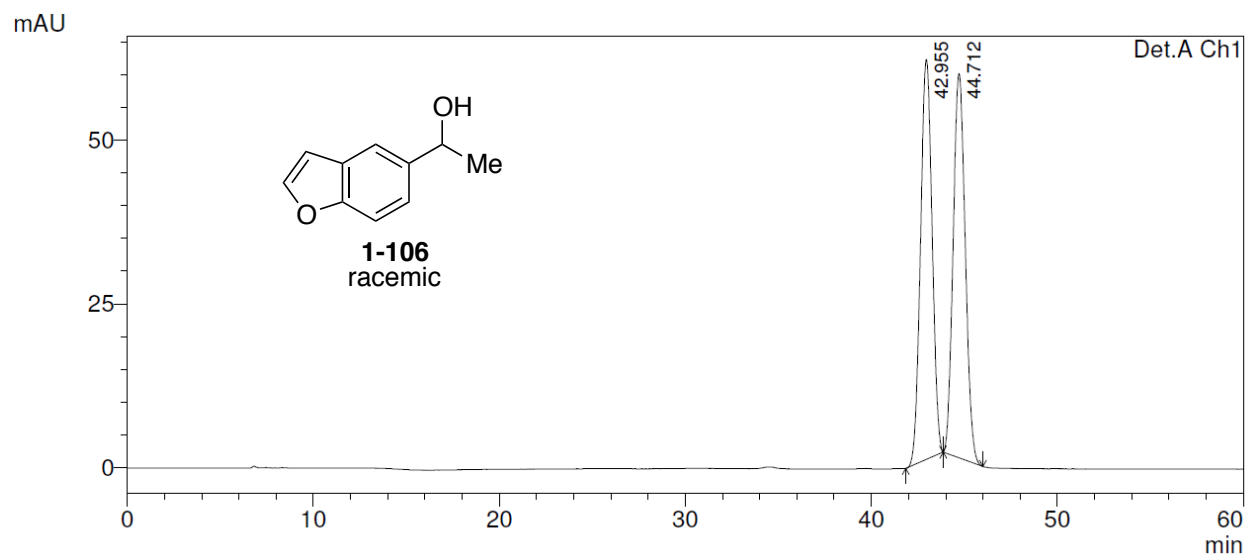
Peak#	Ret. Time	Area	Height	Area %	Height %
1	14.944	239370	12773	50.150	59.107
2	22.866	237935	8837	49.850	40.893
Total		477305	21610	100.000	100.000

Compound **1-104**, 95% ee (254 nm)



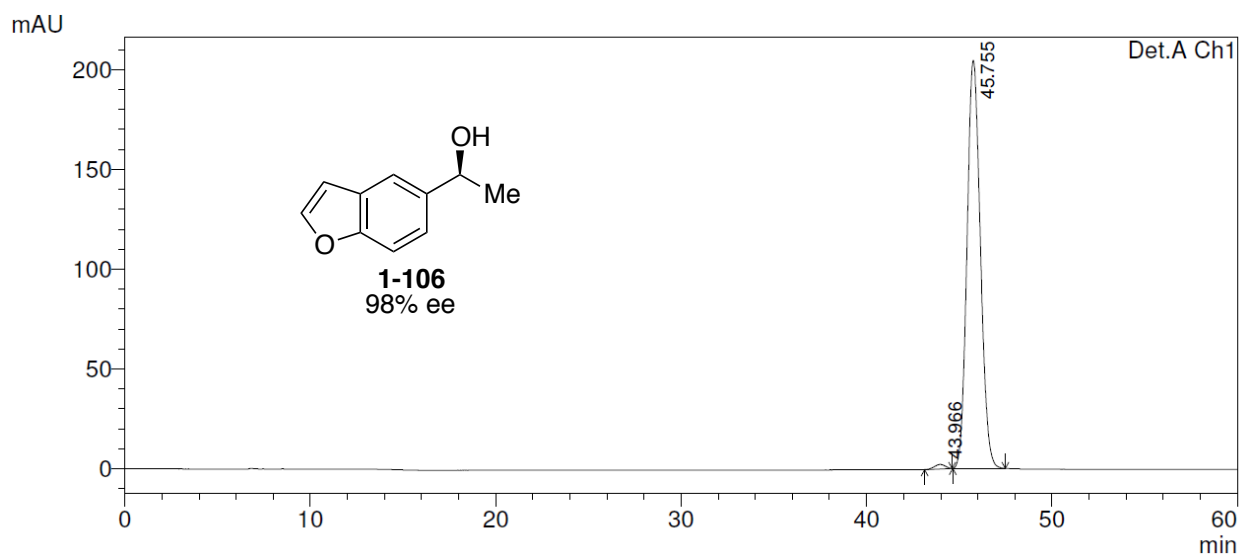
Peak#	Ret. Time	Area	Height	Area %	Height %
1	14.956	35963	1982	2.675	4.104
2	22.473	1308675	46315	97.325	95.896
Total		1344638	48297	100.000	100.000

Compound **1-106**, racemic (254 nm)



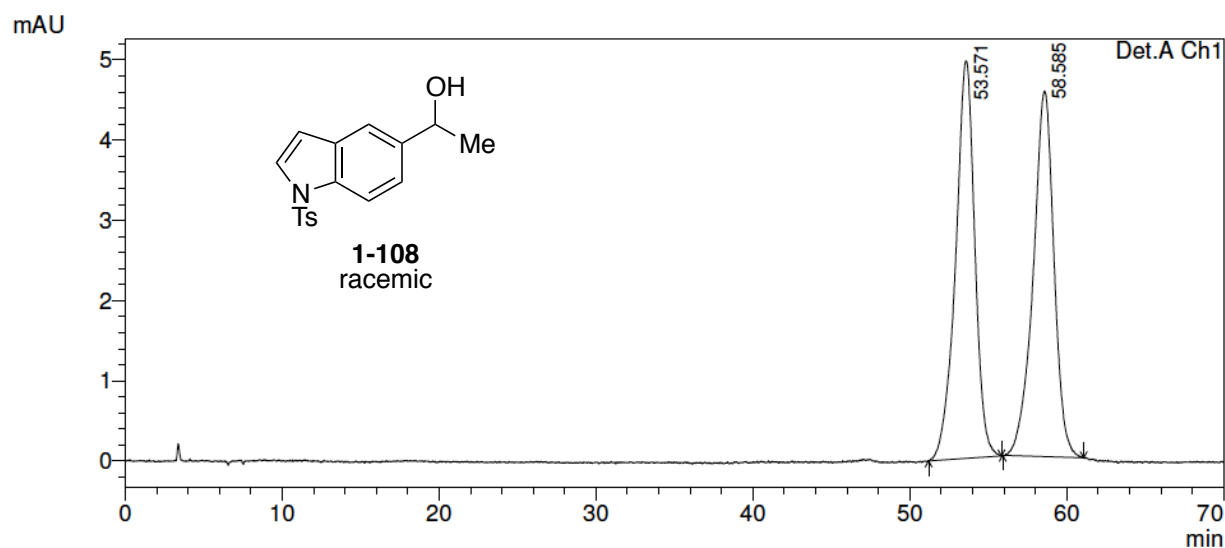
Peak#	Ret. Time	Area	Height	Area %	Height %
1	42.955	2640838	61031	49.950	51.012
2	44.712	2646127	58610	50.050	48.988
Total		5286965	119641	100.000	100.000

Compound **1-106**, 98% ee (254 nm)



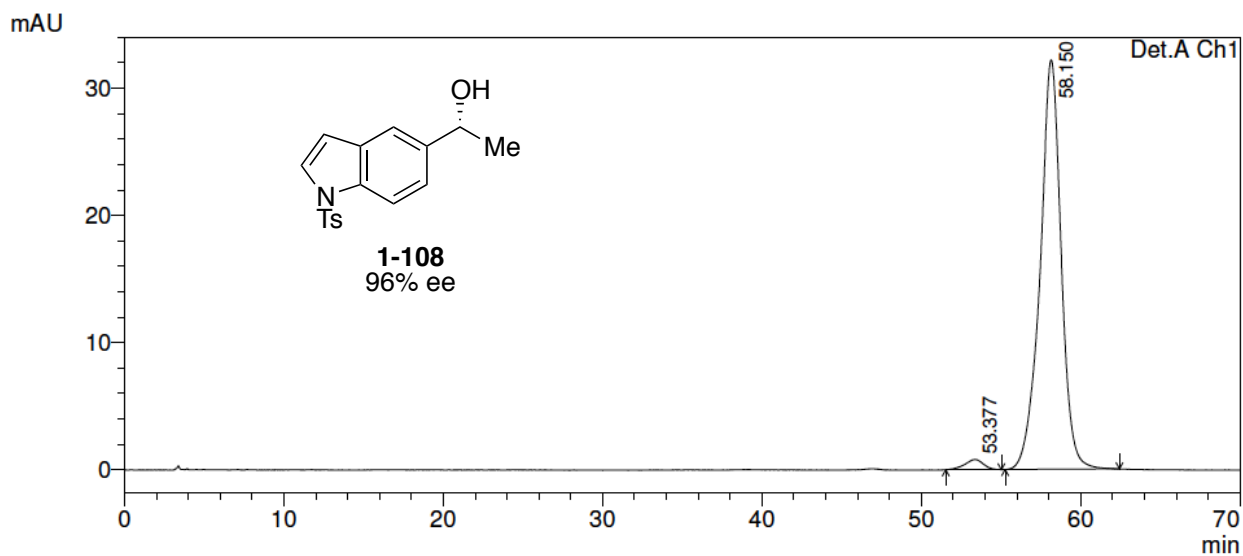
Peak#	Ret. Time	Area	Height	Area %	Height %
1	43.966	90232	2245	0.873	1.086
2	45.755	10242584	204407	99.127	98.914
Total		10332816	206652	100.000	100.000

Compound **1-108**, racemic (254 nm)



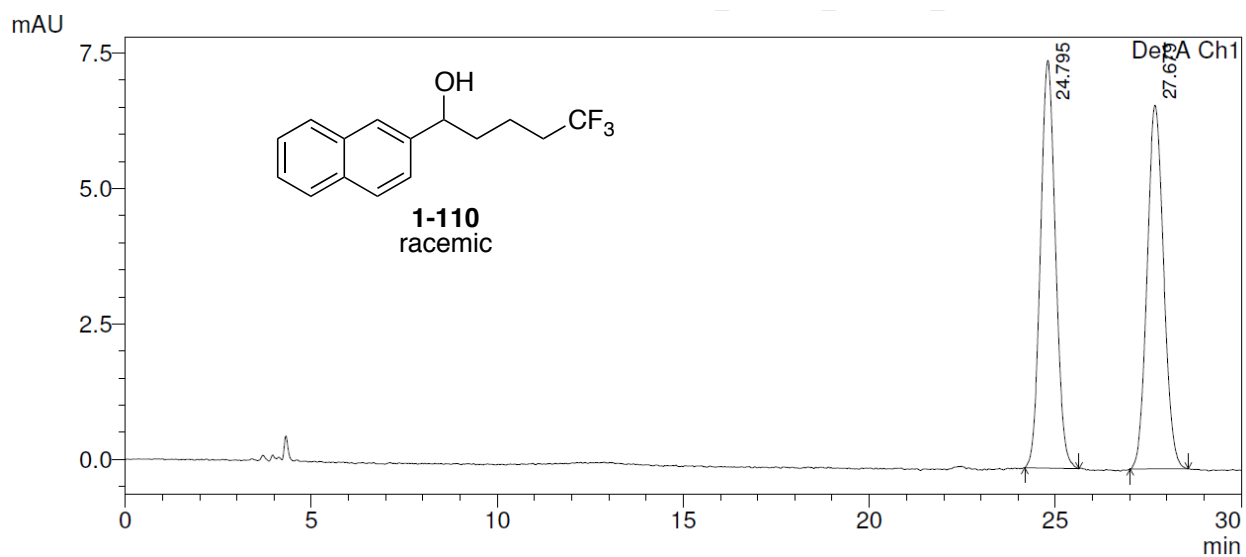
Peak#	Ret. Time	Area	Height	Area %	Height %
1	53.571	422898	4957	50.129	52.089
2	58.585	420722	4559	49.871	47.911
Total		843620	9516	100.000	100.000

Compound **1-108**, 96% ee (254 nm)



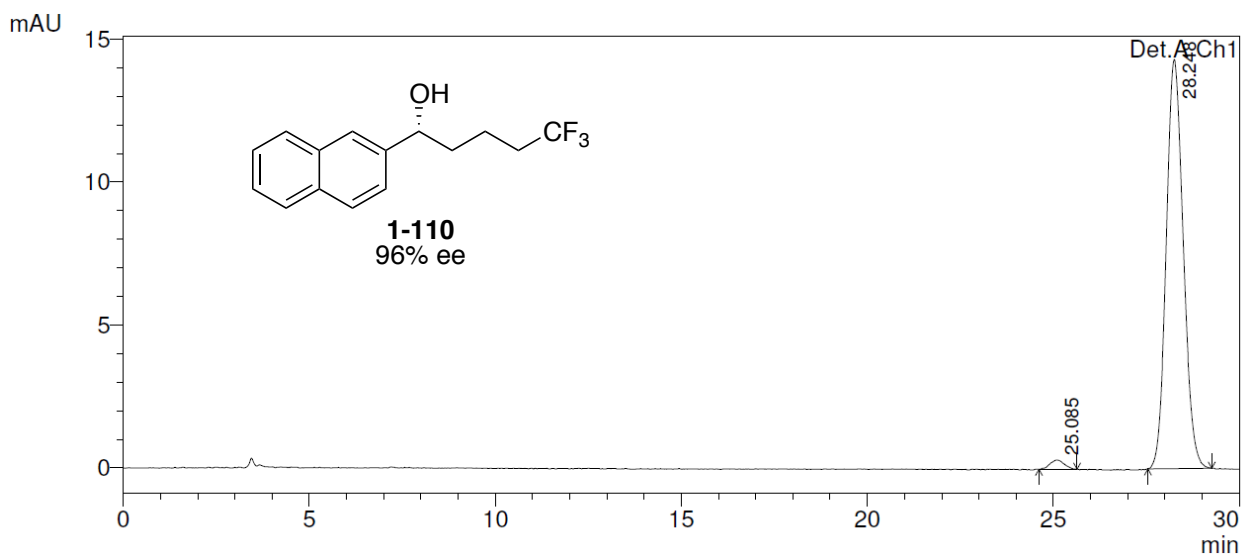
Peak#	Ret. Time	Area	Height	Area %	Height %
1	53.377	64936	808	2.149	2.450
2	58.150	2956179	32179	97.851	97.550
Total		3021114	32987	100.000	100.000

Compound **1-110**, racemic (254 nm)



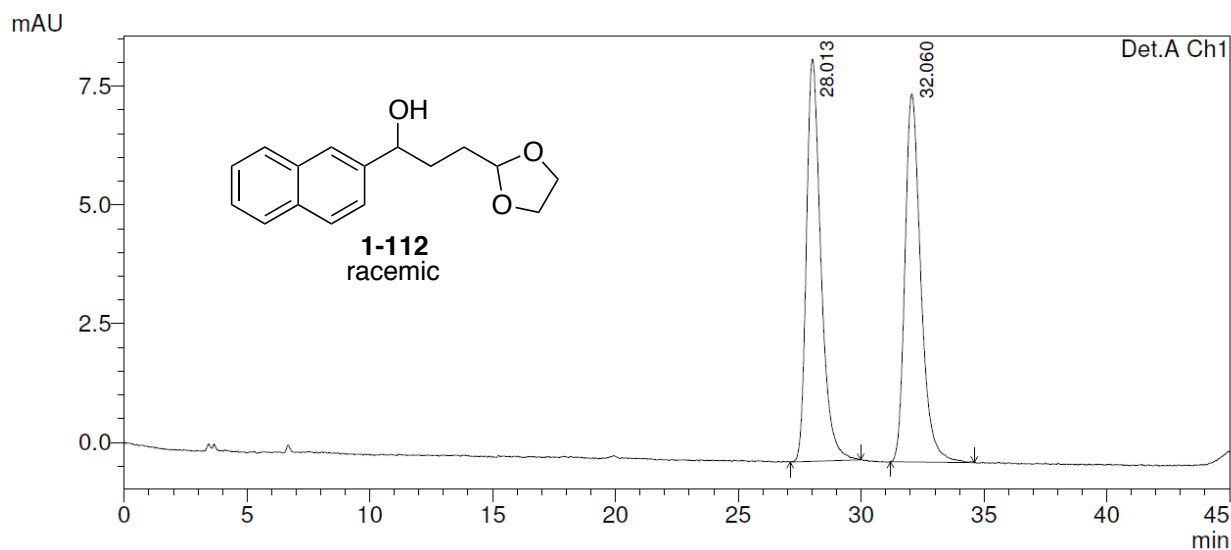
Peak#	Ret. Time	Area	Height	Area %	Height %
1	24.795	210483	7521	50.324	52.855
2	27.679	207772	6708	49.676	47.145
Total		418255	14229	100.000	100.000

Compound **1-110**, 96% ee (254 nm)



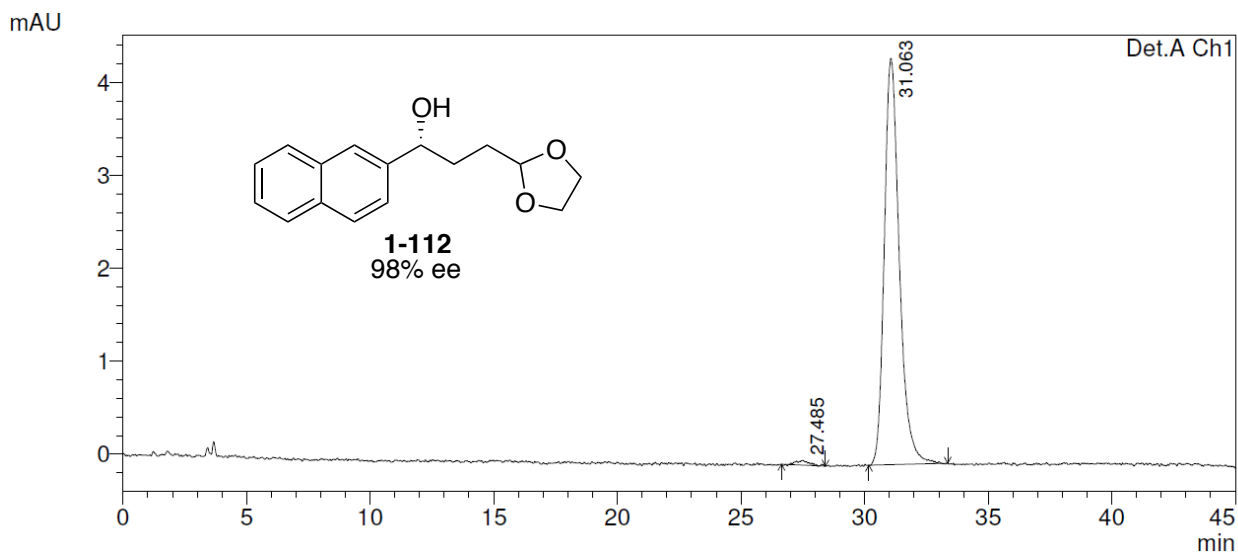
Peak#	Ret. Time	Area	Height	Area %	Height %
1	25.085	8553	324	1.840	2.212
2	28.248	456259	14308	98.160	97.788
Total		464812	14632	100.000	100.000

Compound **1-112**, racemic (254 nm)



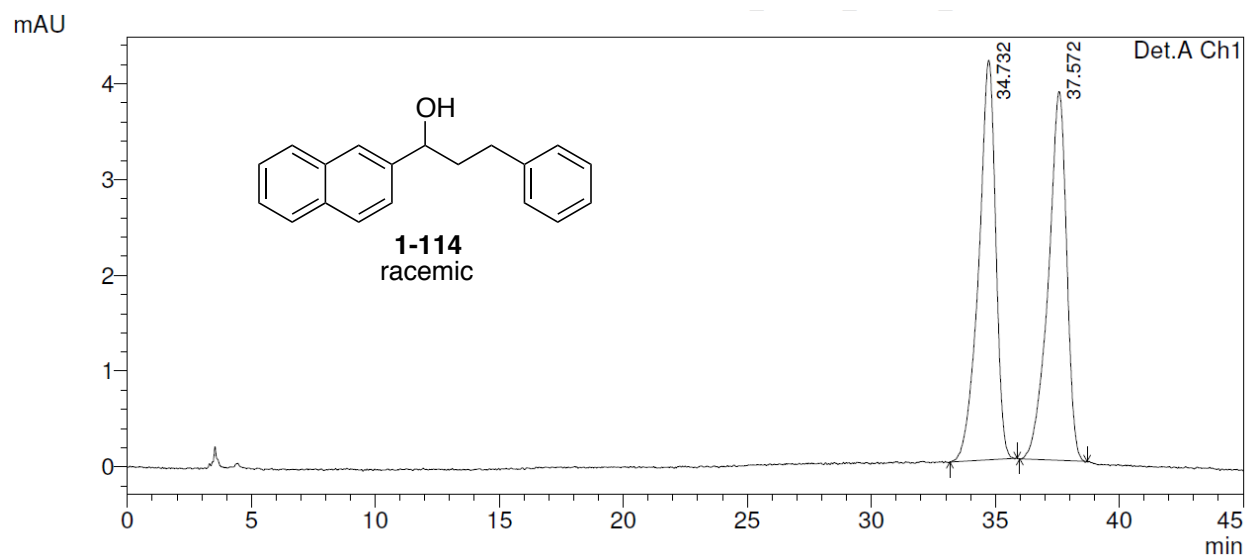
Peak#	Ret. Time	Area	Height	Area %	Height %
1	28.013	346583	8466	49.977	52.224
2	32.060	346898	7745	50.023	47.776
Total		693481	16211	100.000	100.000

Compound **1-112**, 98% ee (254 nm)



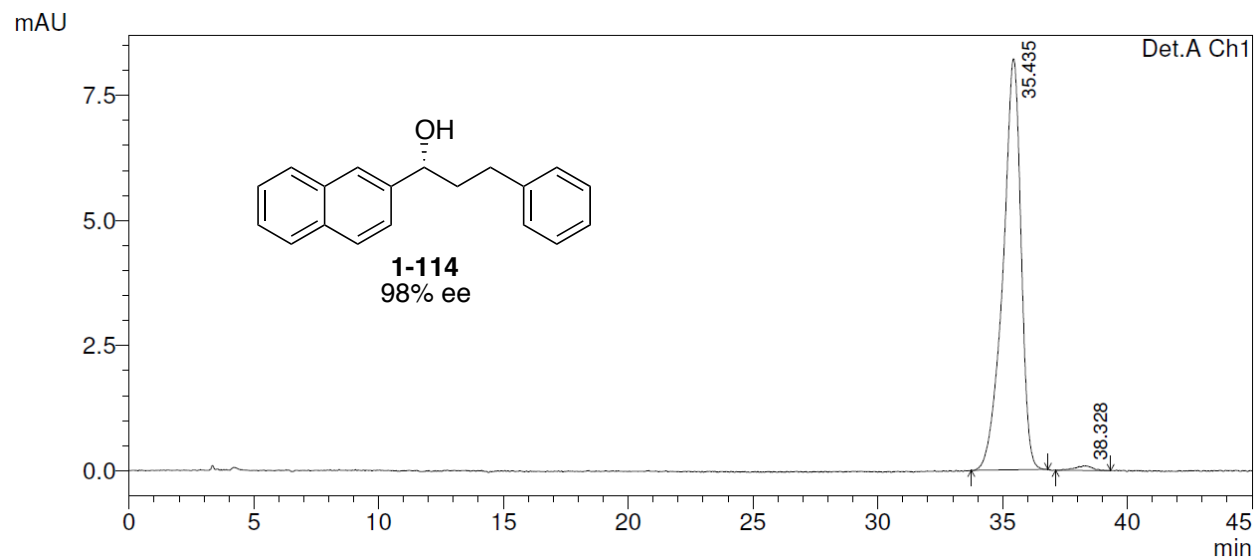
Peak#	Ret. Time	Area	Height	Area %	Height %
1	27.485	1806	53	0.968	1.191
2	31.063	184751	4374	99.032	98.809
Total		186557	4426	100.000	100.000

Compound **1-114**, racemic (254 nm)



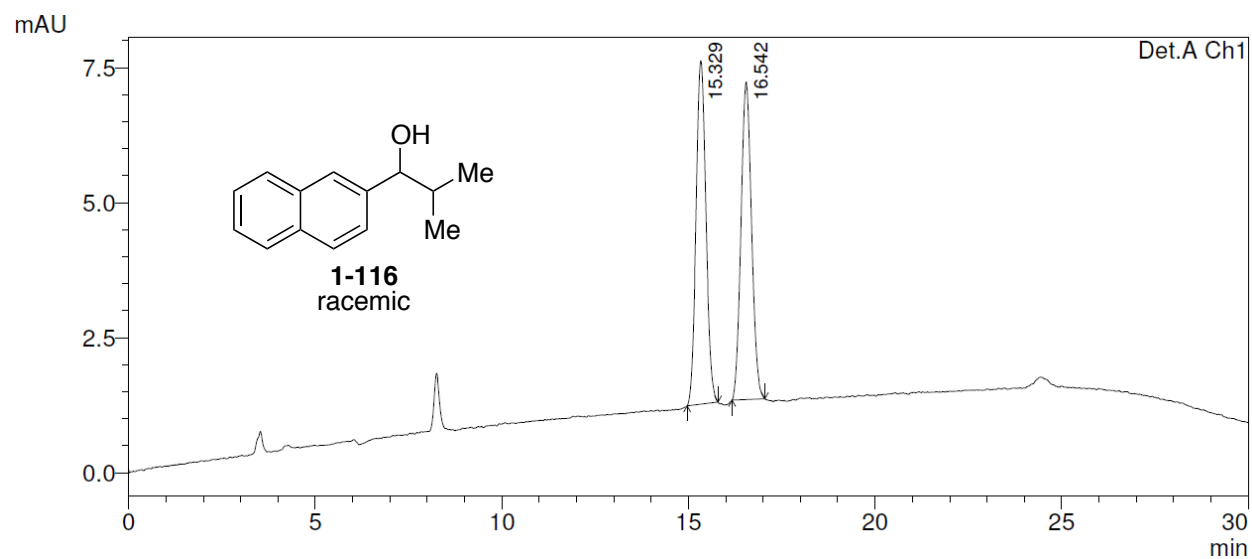
Peak#	Ret. Time	Area	Height	Area %	Height %
1	34.732	198596	4170	50.141	51.978
2	37.572	197482	3853	49.859	48.022
Total		396078	8023	100.000	100.000

Compound **1-114**, 98% ee (254 nm)



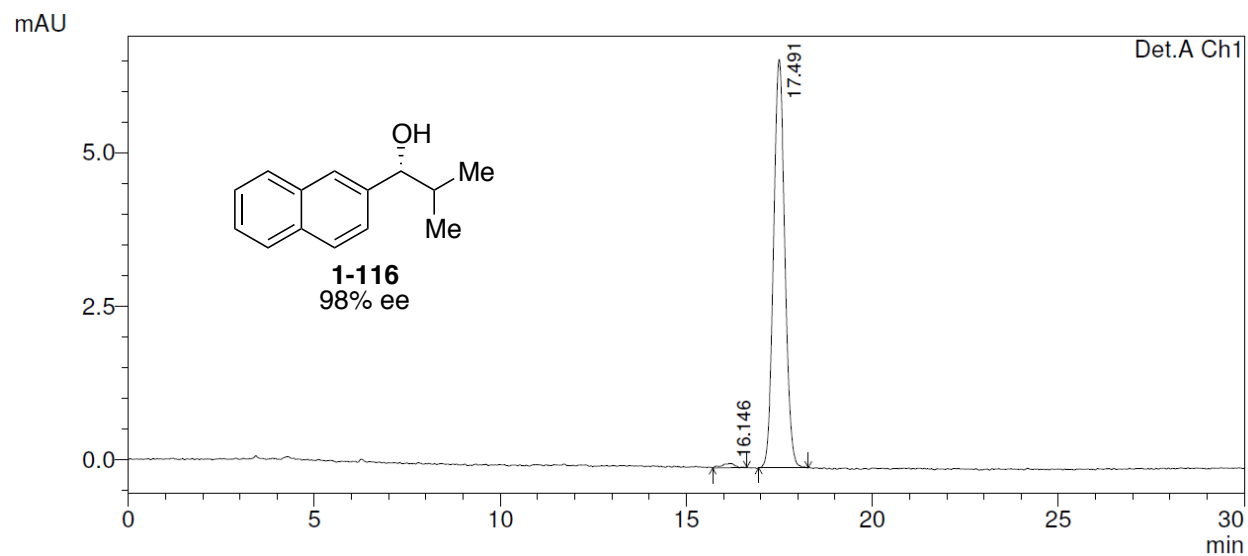
Peak#	Ret. Time	Area	Height	Area %	Height %
1	35.435	412336	8222	98.853	98.861
2	38.328	4783	95	1.147	1.139
Total		417119	8317	100.000	100.000

Compound **1-116**, racemic (254 nm)



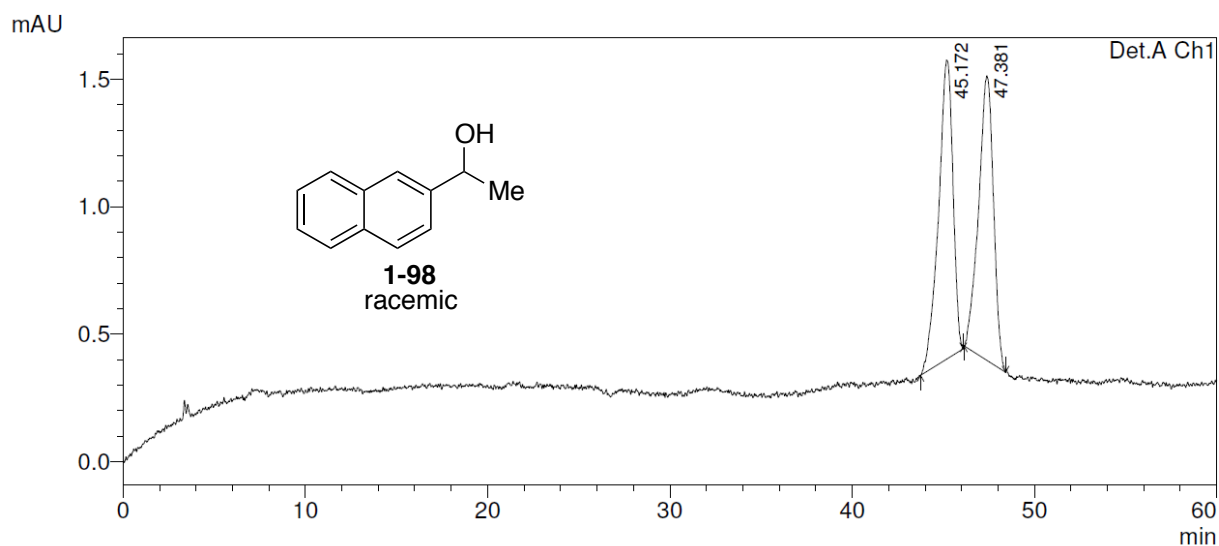
Peak#	Ret. Time	Area	Height	Area %	Height %
1	15.329	116684	6363	50.105	51.956
2	16.542	116193	5884	49.895	48.044
Total		232877	12246	100.000	100.000

Compound **1-116**, 98% ee (254 nm)



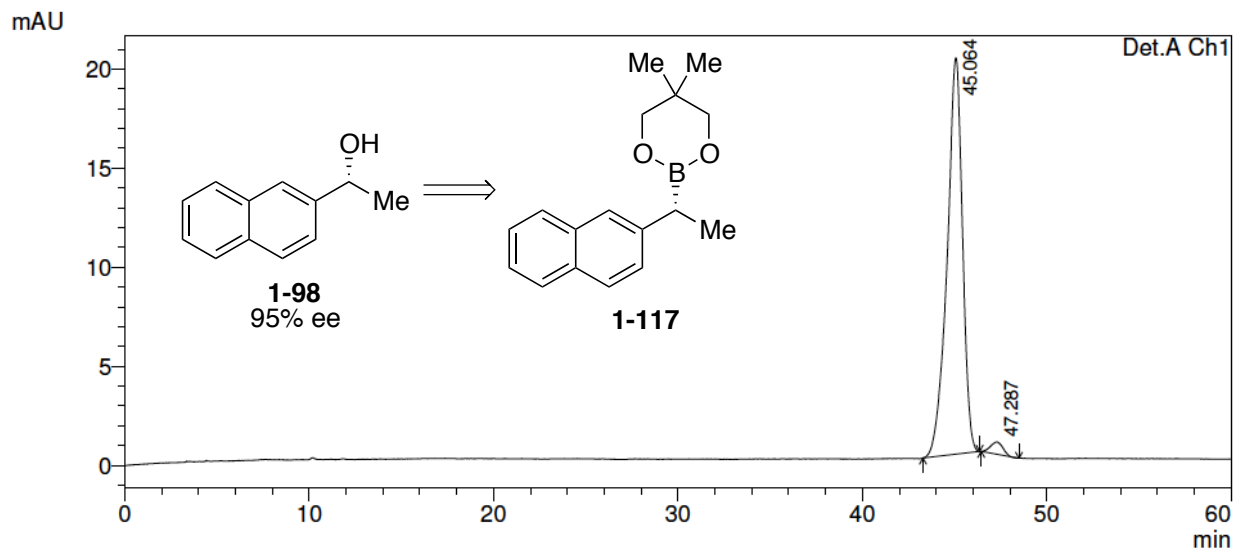
Peak#	Ret. Time	Area	Height	Area %	Height %
1	16.146	1594	70	1.126	1.034
2	17.491	140016	6657	98.874	98.966
Total		141610	6726	100.000	100.000

Compound **1-98**, racemic (254 nm)



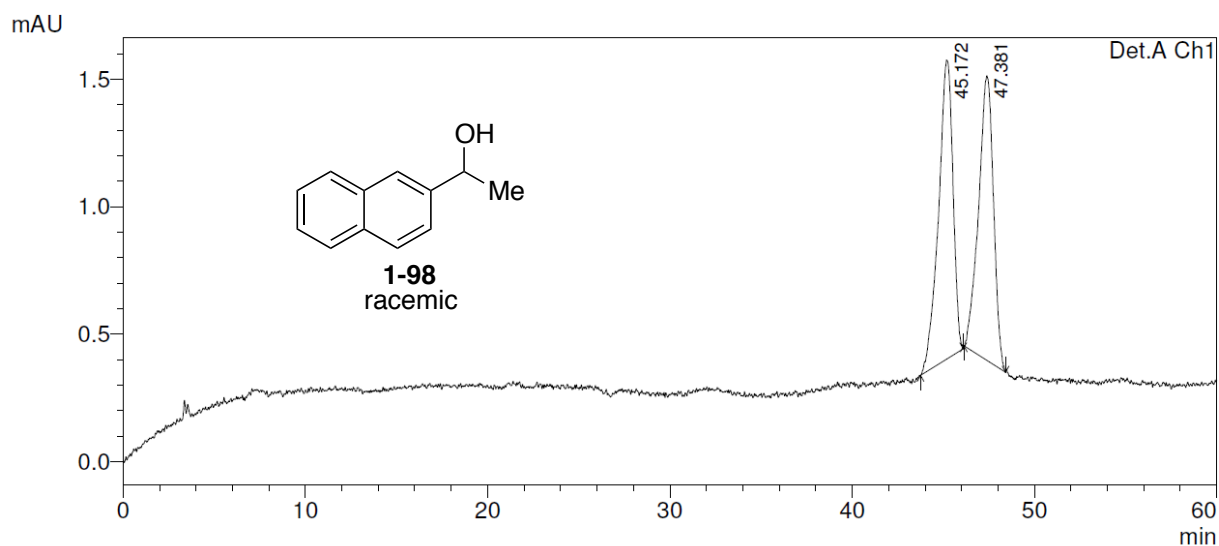
Peak#	Ret. Time	Area	Height	Area %	Height %
1	45.172	64627	1174	50.417	51.245
2	47.381	63558	1117	49.583	48.755
Total		128185	2292	100.000	100.000

Compound **1-19**, 95% ee (254 nm)



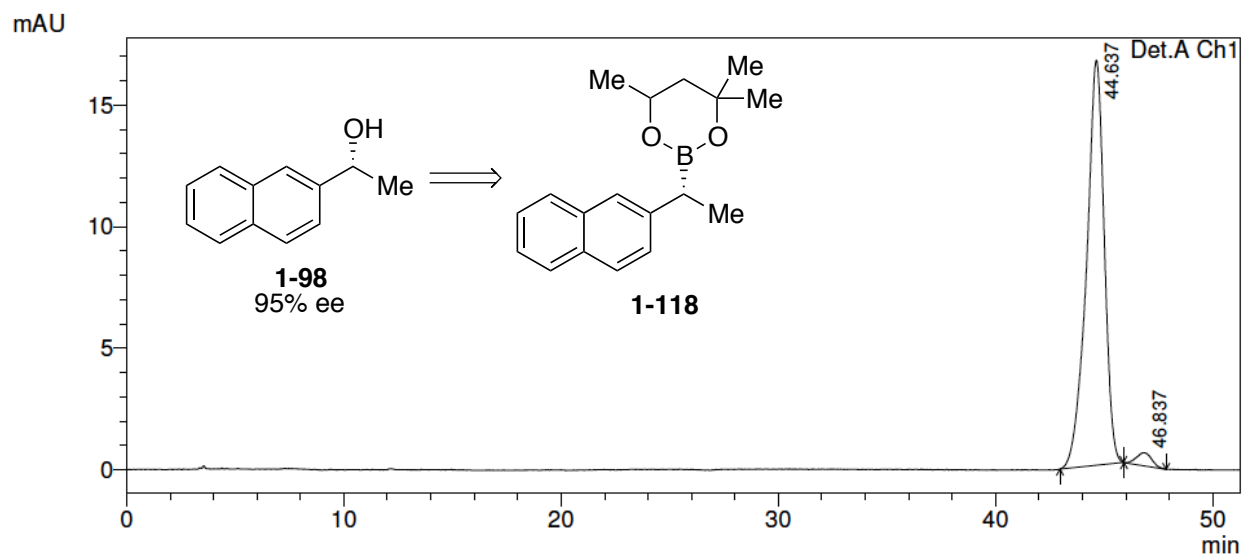
Peak#	Ret. Time	Area	Height	Area %	Height %
1	45.064	1159668	20005	97.571	97.019
2	47.287	28864	615	2.429	2.981
Total		1188532	20620	100.000	100.000

Compound **1-98**, racemic (254 nm)



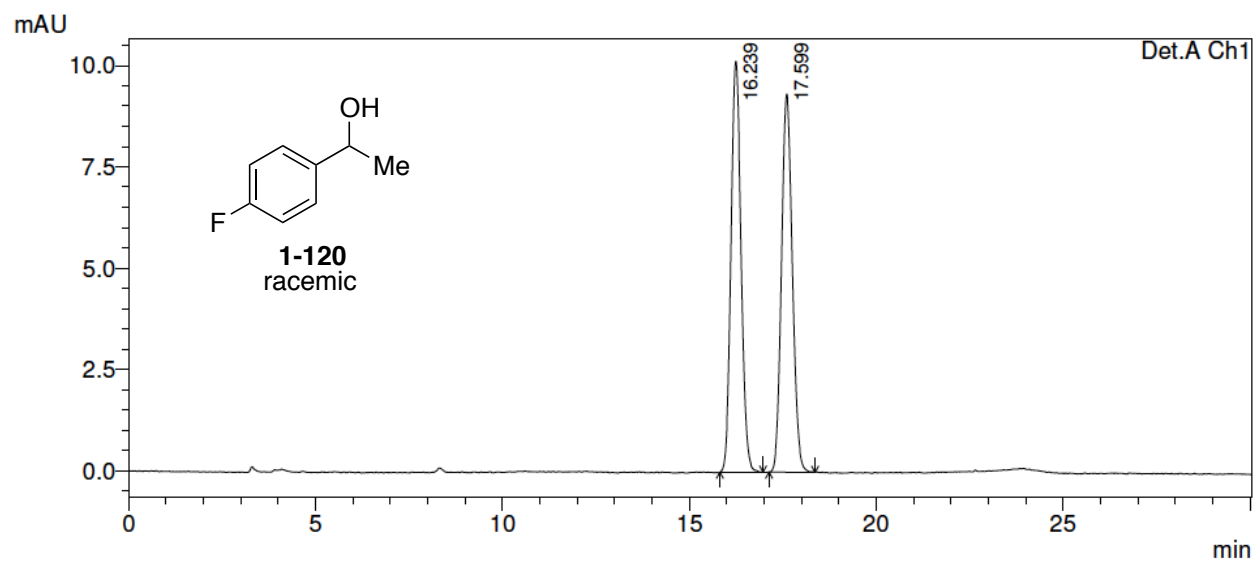
Peak#	Ret. Time	Area	Height	Area %	Height %
1	45.172	64627	1174	50.417	51.245
2	47.381	63558	1117	49.583	48.755
Total		128185	2292	100.000	100.000

Compound **1-98**, 95% ee (254 nm)



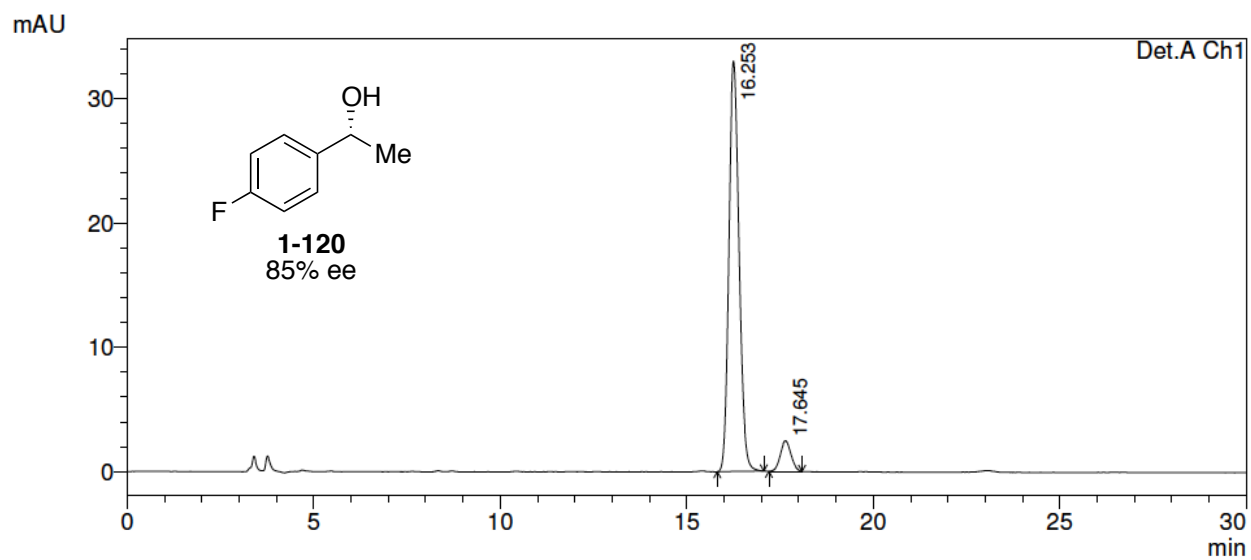
Peak#	Ret. Time	Area	Height	Area %	Height %
1	44.637	946536	16673	97.303	96.868
2	46.837	26234	539	2.697	3.132
Total		972770	17212	100.000	100.000

Compound **1-120**, racemic (254 nm)



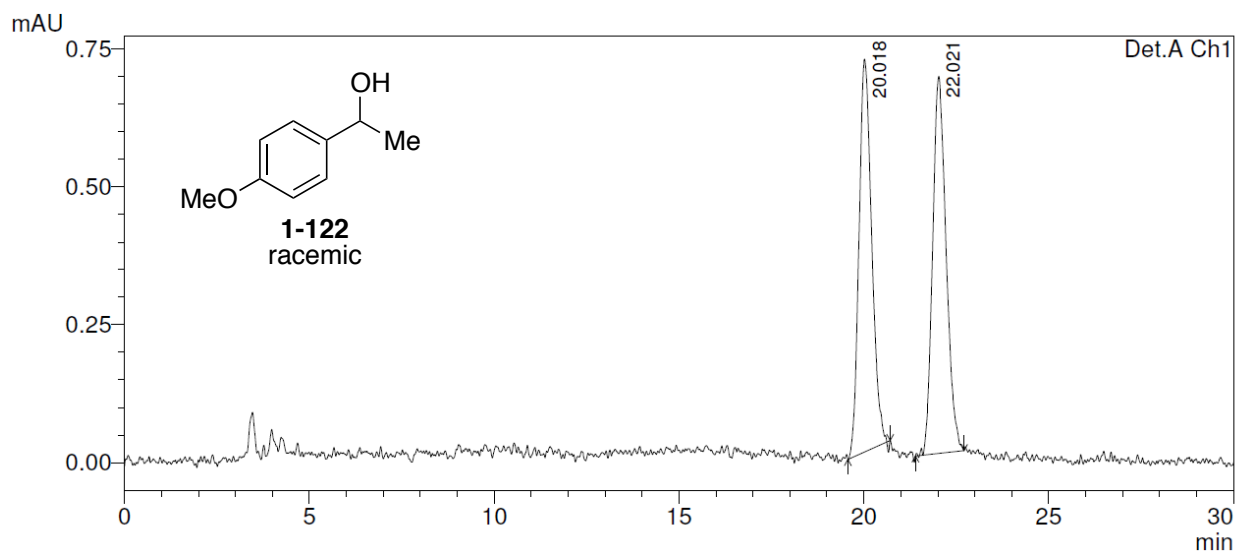
Peak#	Ret. Time	Area	Height	Area %	Height %
1	16.239	189291	10142	50.049	52.077
2	17.599	188917	9333	49.951	47.923
Total		378208	19476	100.000	100.000

Compound **1-120**, 85% ee (254 nm)



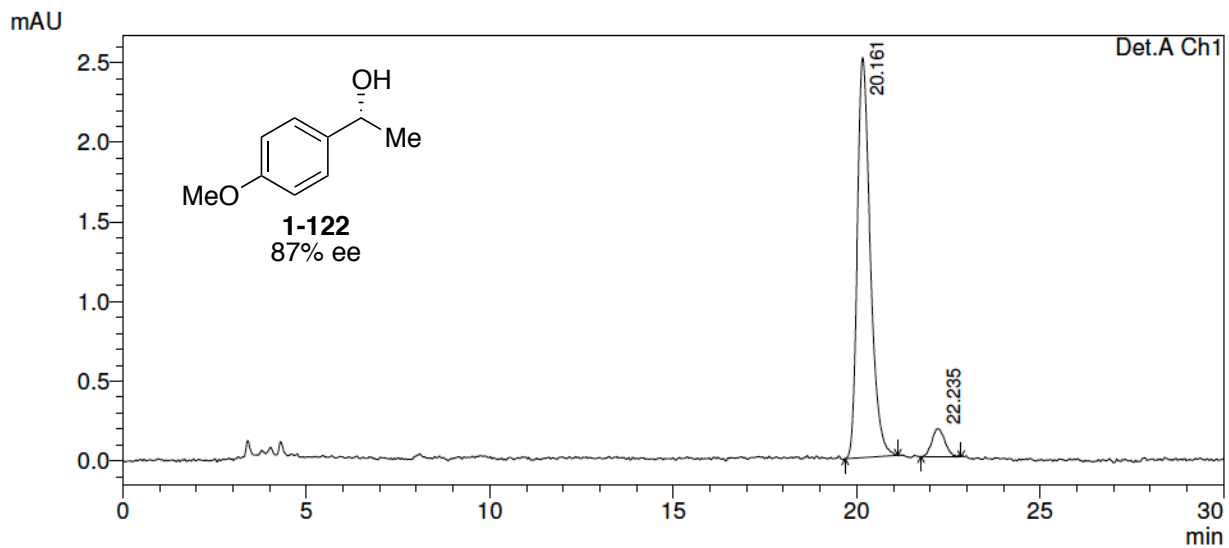
Peak#	Ret. Time	Area	Height	Area %	Height %
1	16.253	625785	33025	92.796	93.094
2	17.645	48585	2450	7.204	6.906
Total		674370	35475	100.000	100.000

Compound **1-122**, racemic (254 nm)



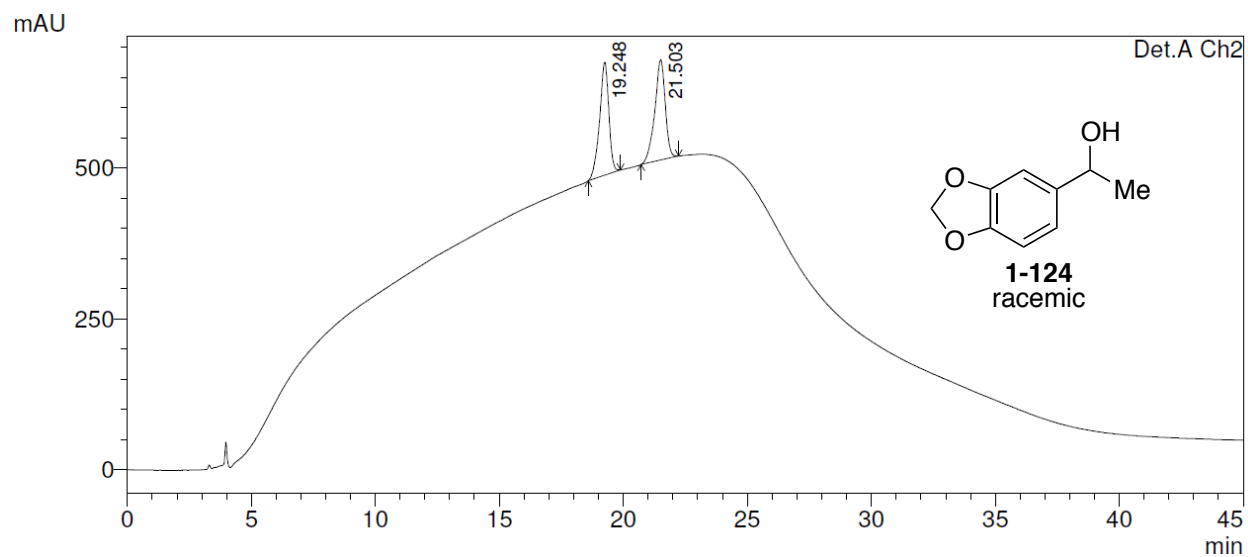
Peak#	Ret. Time	Area	Height	Area %	Height %
1	20.018	16955	713	49.424	51.024
2	22.021	17351	684	50.576	48.976
Total		34306	1397	100.000	100.000

Compound **1-122**, 87% ee (254 nm)



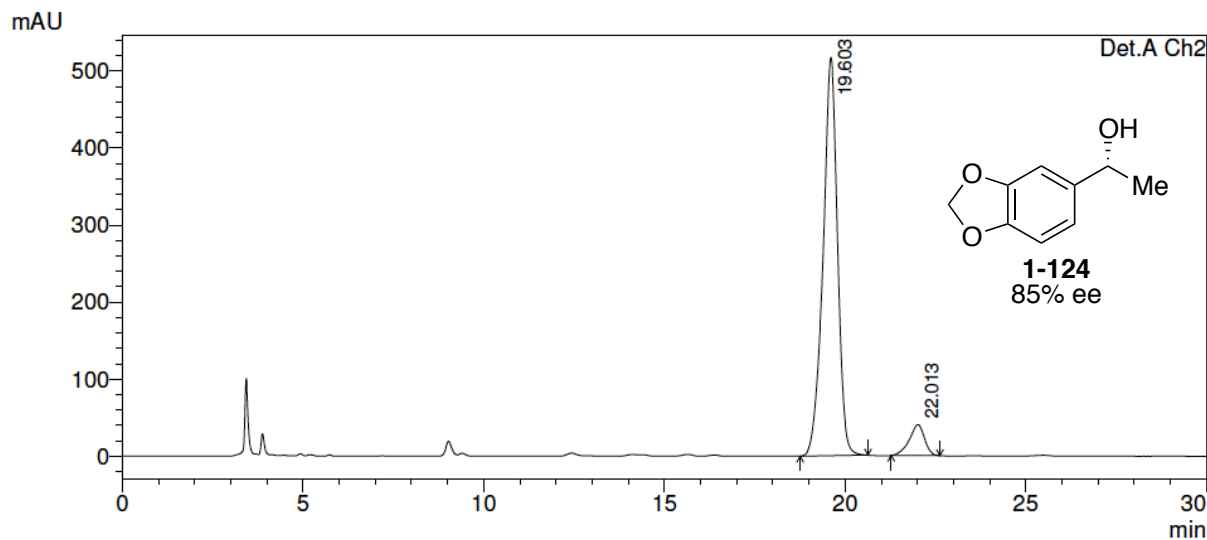
Peak#	Ret. Time	Area	Height	Area %	Height %
1	20.161	61611	2512	93.425	93.488
2	22.235	4336	175	6.575	6.512
Total		65947	2687	100.000	100.000

Compound **1-124**, racemic (210 nm)



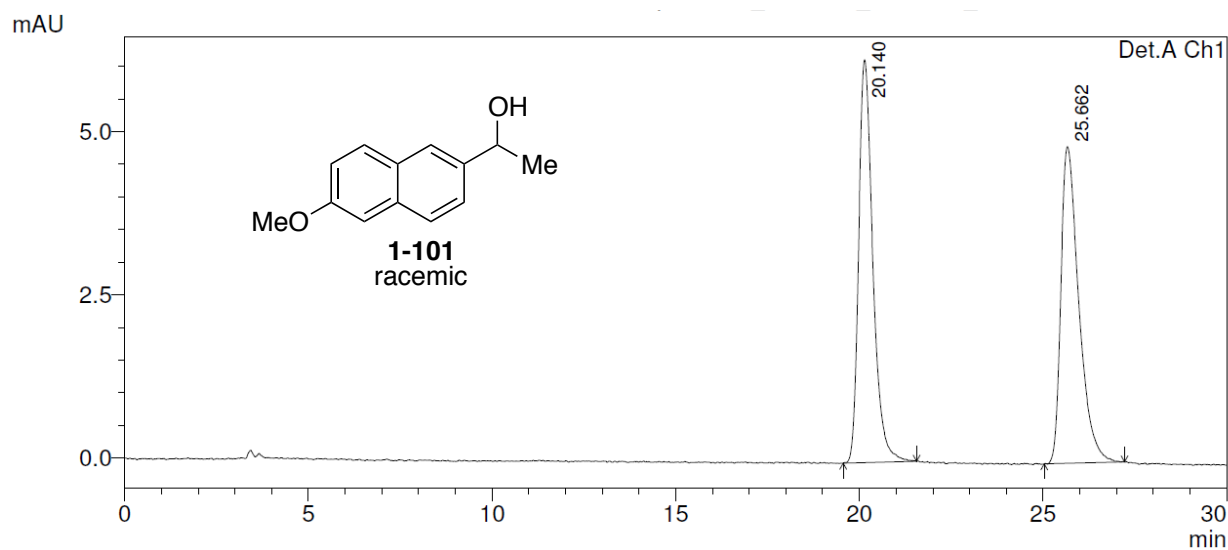
Peak#	Ret. Time	Area	Height	Area %	Height %
1	19.248	4853386	187177	49.816	52.913
2	21.503	4889175	166570	50.184	47.087
Total		9742560	353746	100.000	100.000

Compound **1-124**, 85% ee (210 nm)



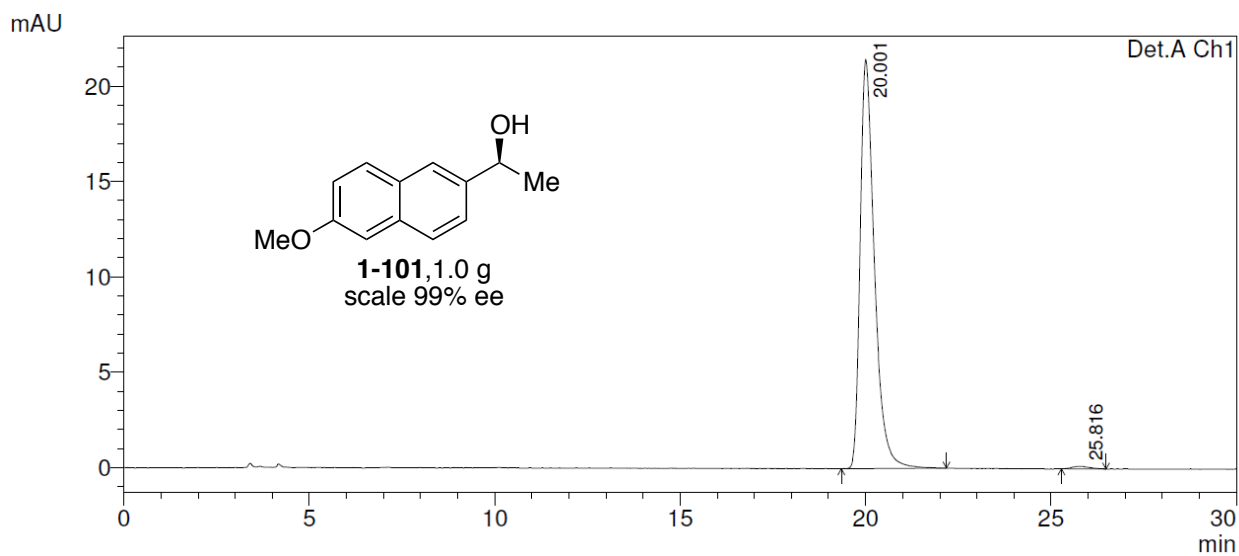
Peak#	Ret. Time	Area	Height	Area %	Height %
1	19.603	14324275	516565	92.465	92.804
2	22.013	1167262	40056	7.535	7.196
Total		15491537	556621	100.000	100.000

Compound **1-101**, racemic (254 nm)



Peak#	Ret. Time	Area	Height	Area %	Height %
1	20.140	165137	6165	50.153	55.982
2	25.662	164128	4848	49.847	44.018
Total		329266	11013	100.000	100.000

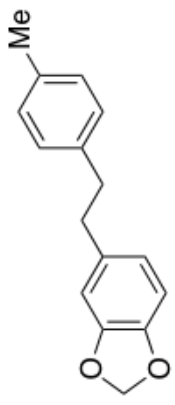
Compound **1-101**, 99% ee (254 nm)



Peak#	Ret. Time	Area	Height	Area %	Height %
1	20.001	574869	21457	99.271	99.399
2	25.816	4222	130	0.729	0.601
Total		579091	21587	100.000	100.000

**Appendix B**

**SPECTRAL AND CHROMATOGRAPHY DATA FOR CHAPTER 2**

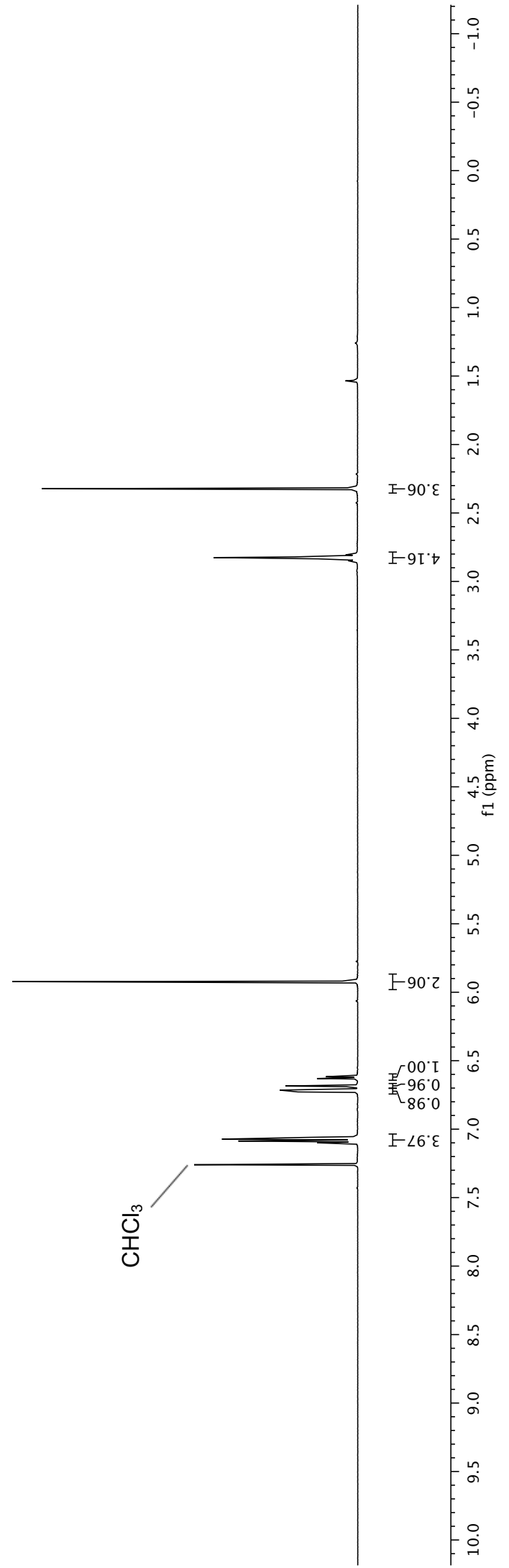


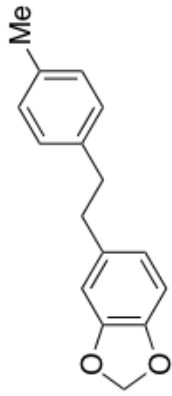
**2-47**

<sup>1</sup>H NMR (600 MHz, CDCl<sub>3</sub>)

2.857  
2.848  
2.840  
2.833  
2.828  
2.826  
2.821  
2.814  
2.806  
2.797  
2.323

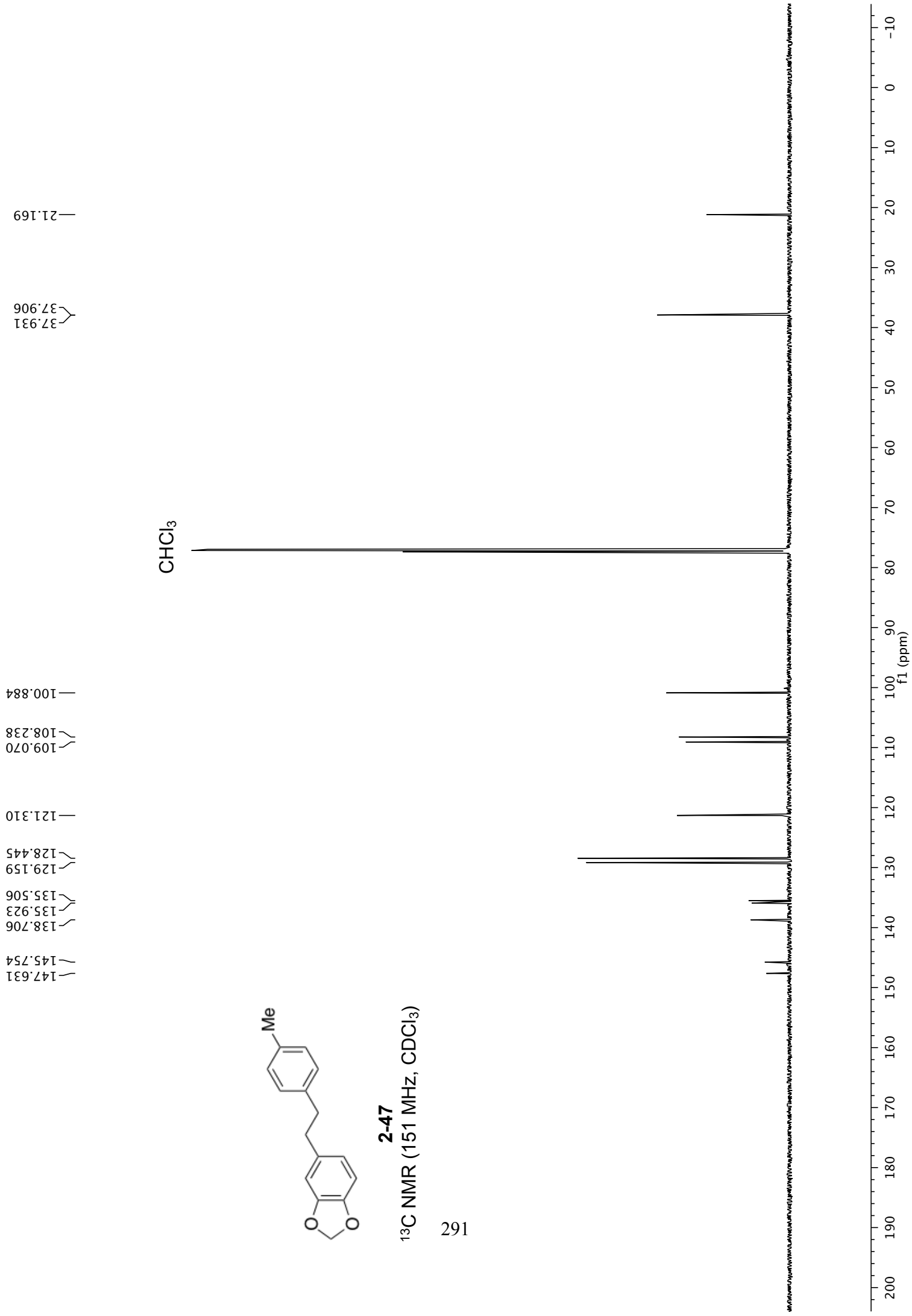
7.100  
7.086  
7.073  
7.059  
6.728  
6.715  
6.687  
6.685  
6.630  
6.627  
6.617  
6.614  
5.923

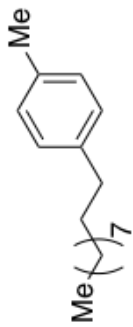




**2-47**  
 $^{13}\text{C}$  NMR (151 MHz,  $\text{CDCl}_3$ )

161



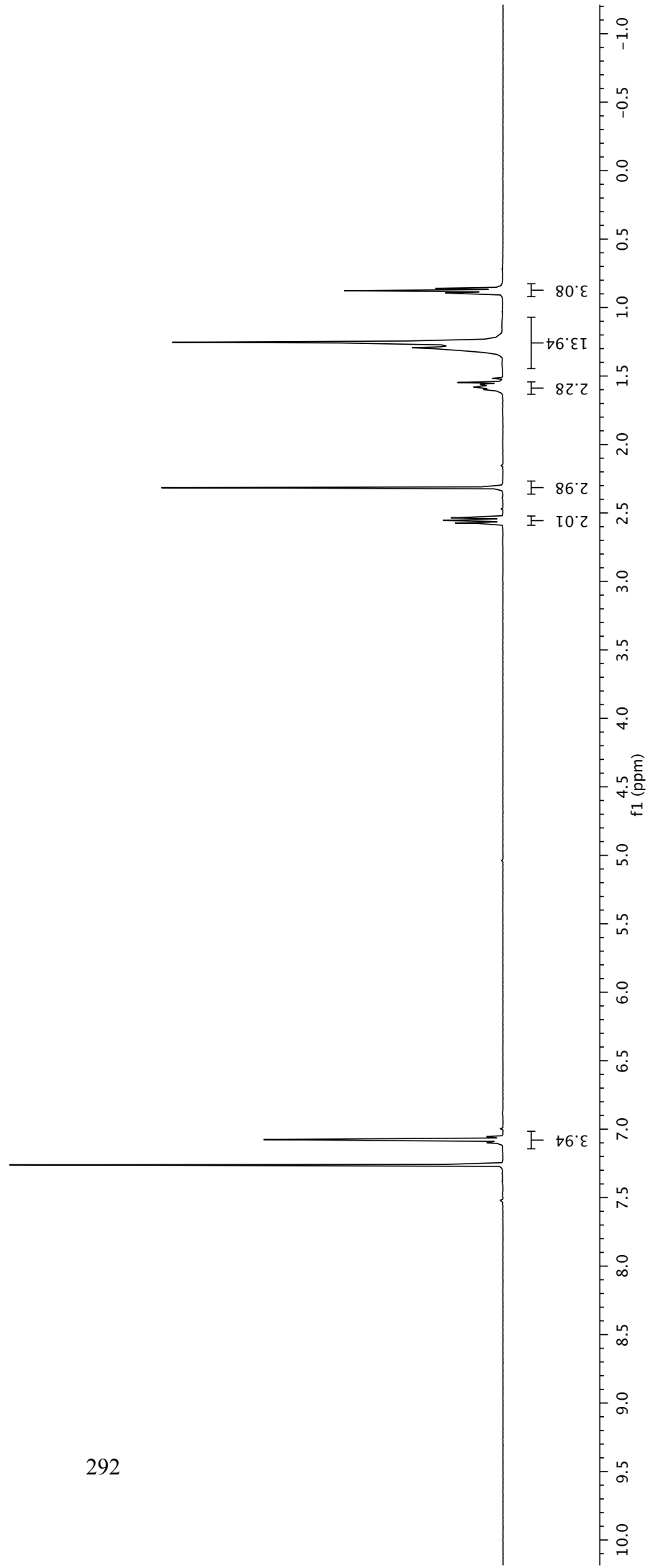


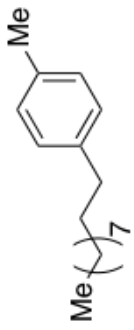
**2-50**  
<sup>1</sup>H NMR (400 MHz, CDCl<sub>3</sub>)

2.574  
 2.555  
 2.535  
 2.315  
 1.618  
 1.599  
 1.581  
 1.561  
 1.294  
 1.275  
 1.253  
 1.212  
 0.894  
 0.877  
 0.860  
 0.853

7.100  
 7.094  
 7.087  
 7.079  
 7.076  
 7.068  
 7.061  
 7.054

CHCl<sub>3</sub>





**2-50**

<sup>13</sup>C NMR (101 MHz, CDCl<sub>3</sub>)

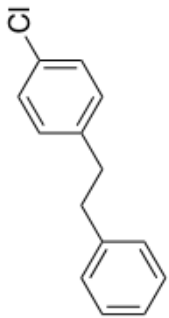
263

CHCl<sub>3</sub>

35.682  
32.063  
31.845  
29.790  
29.763  
29.693  
29.505  
22.851  
21.152  
14.295

140.023  
135.057  
129.033  
128.406





**2-51**

<sup>1</sup>H NMR (600 MHz, CDCl<sub>3</sub>)

294

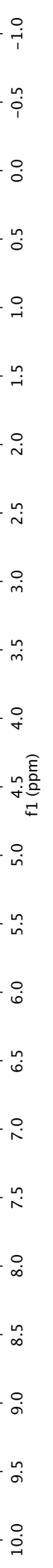
7.291  
7.279  
7.266  
7.245  
7.241  
7.238  
7.230  
7.227  
7.223  
7.211  
7.199  
7.187  
7.156  
7.144  
7.091  
7.077

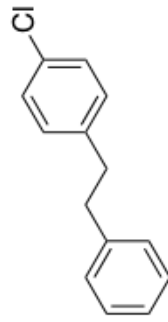
2.895

CHCl<sub>3</sub>

2.05  
1.94  
1.95  
2.00

4.07





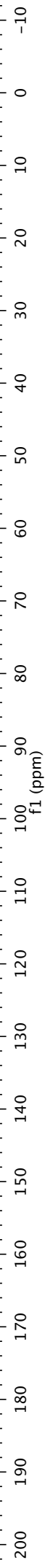
**2-51**

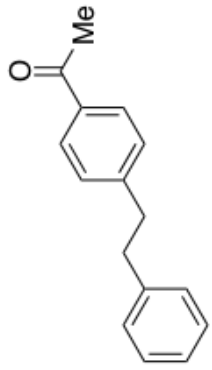
<sup>13</sup>C NMR (151 MHz, CDCl<sub>3</sub>)

CHCl<sub>3</sub>

37.899  
37.344

141.419  
140.254  
131.773  
129.983  
128.608  
128.538  
128.519  
126.184





CHCl<sub>3</sub>

**2-54**  
<sup>1</sup>H NMR (600 MHz, CDCl<sub>3</sub>)

296

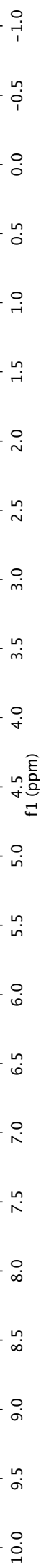
3.003  
2.999  
2.989  
2.984  
2.974  
2.943  
2.939  
2.928  
2.924  
2.586

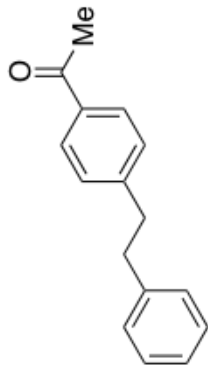
7.881  
7.878  
7.870  
7.867  
7.291  
7.289  
7.279  
7.266  
7.257  
7.243  
7.216  
7.214  
7.212  
7.205  
7.202  
7.199  
7.192  
7.190  
7.188  
7.165  
7.163  
7.151

3.03 H  
2.07 H  
1.99 H

1.93 H  
2.09 H  
1.00 H  
1.98 H

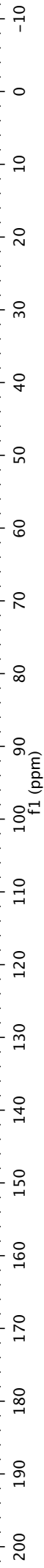
1.99 H



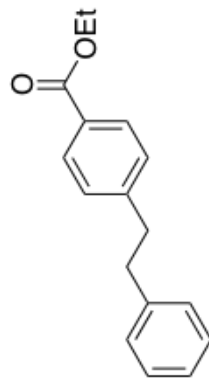


**2-54**

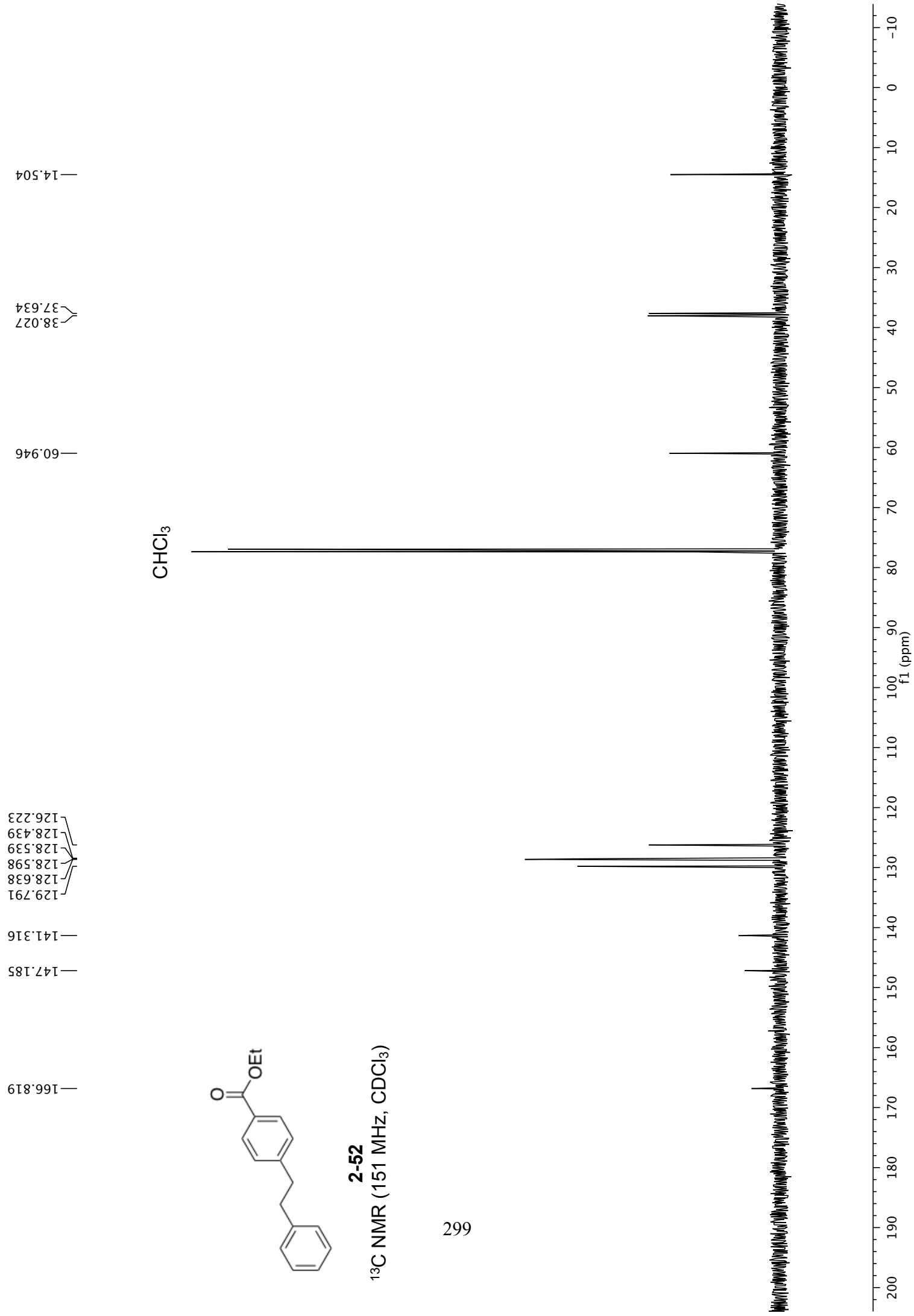
<sup>13</sup>C NMR (101 MHz, CDCl<sub>3</sub>)

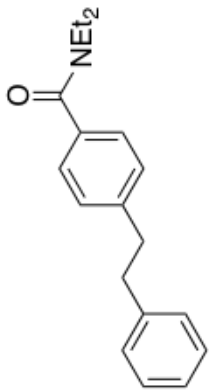






**2-52**  
<sup>13</sup>C NMR (151 MHz, CDCl<sub>3</sub>)





**2-53**

<sup>1</sup>H NMR (600 MHz, CDCl<sub>3</sub>)

300

1.112  
1.238

2.263  
2.294  
2.291  
2.288  
2.284  
2.281  
2.276  
2.263  
2.208  
2.206  
2.196  
2.191  
2.178  
2.175  
2.172  
2.161

3.541

CHCl<sub>3</sub>

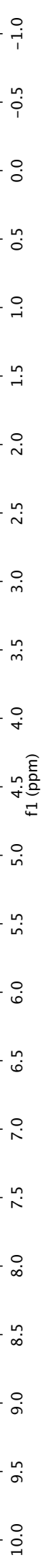
3.13  
3.14

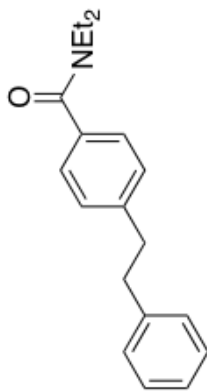
3.97

1.98

2.00

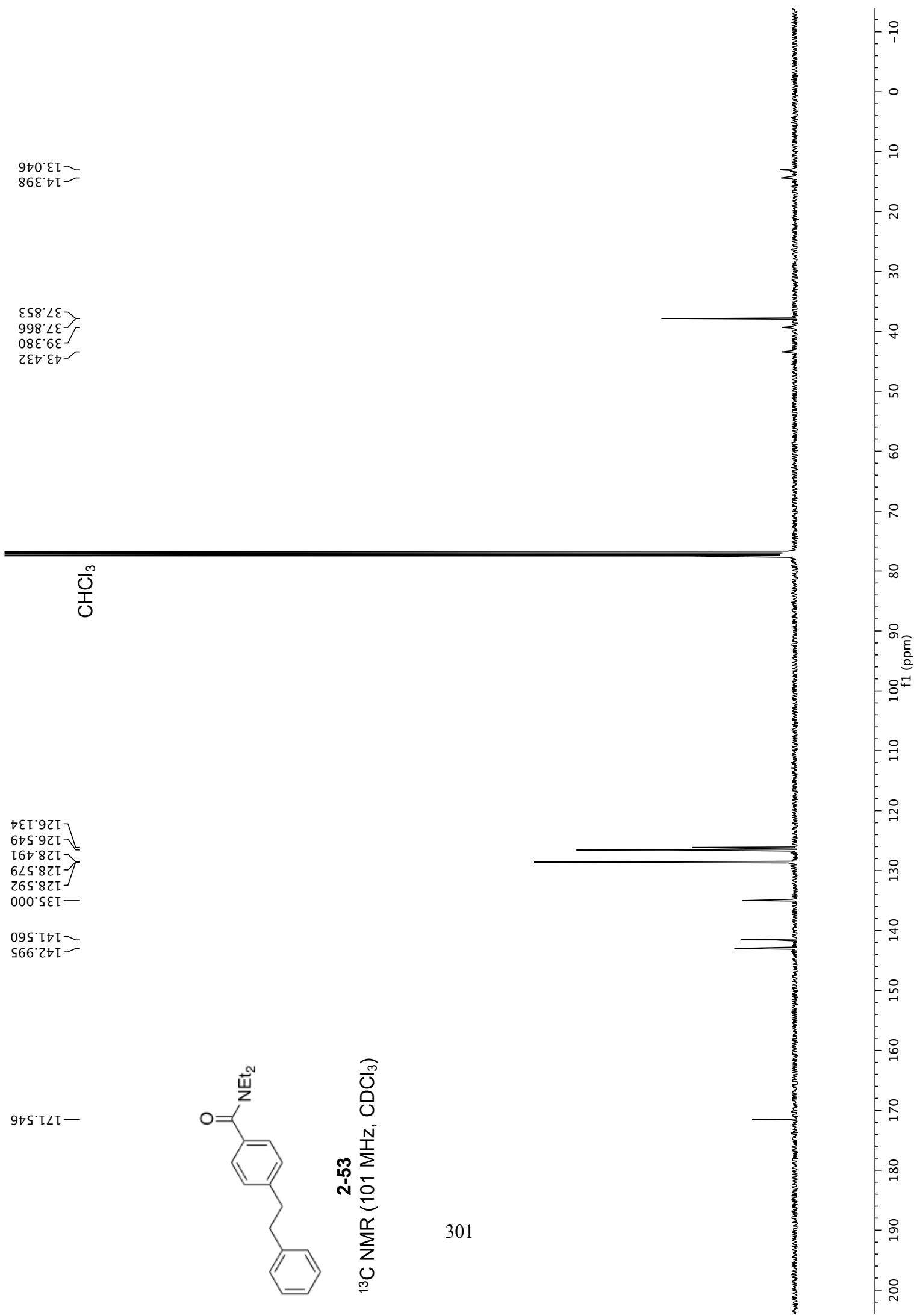
3.93  
4.93

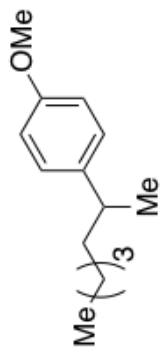




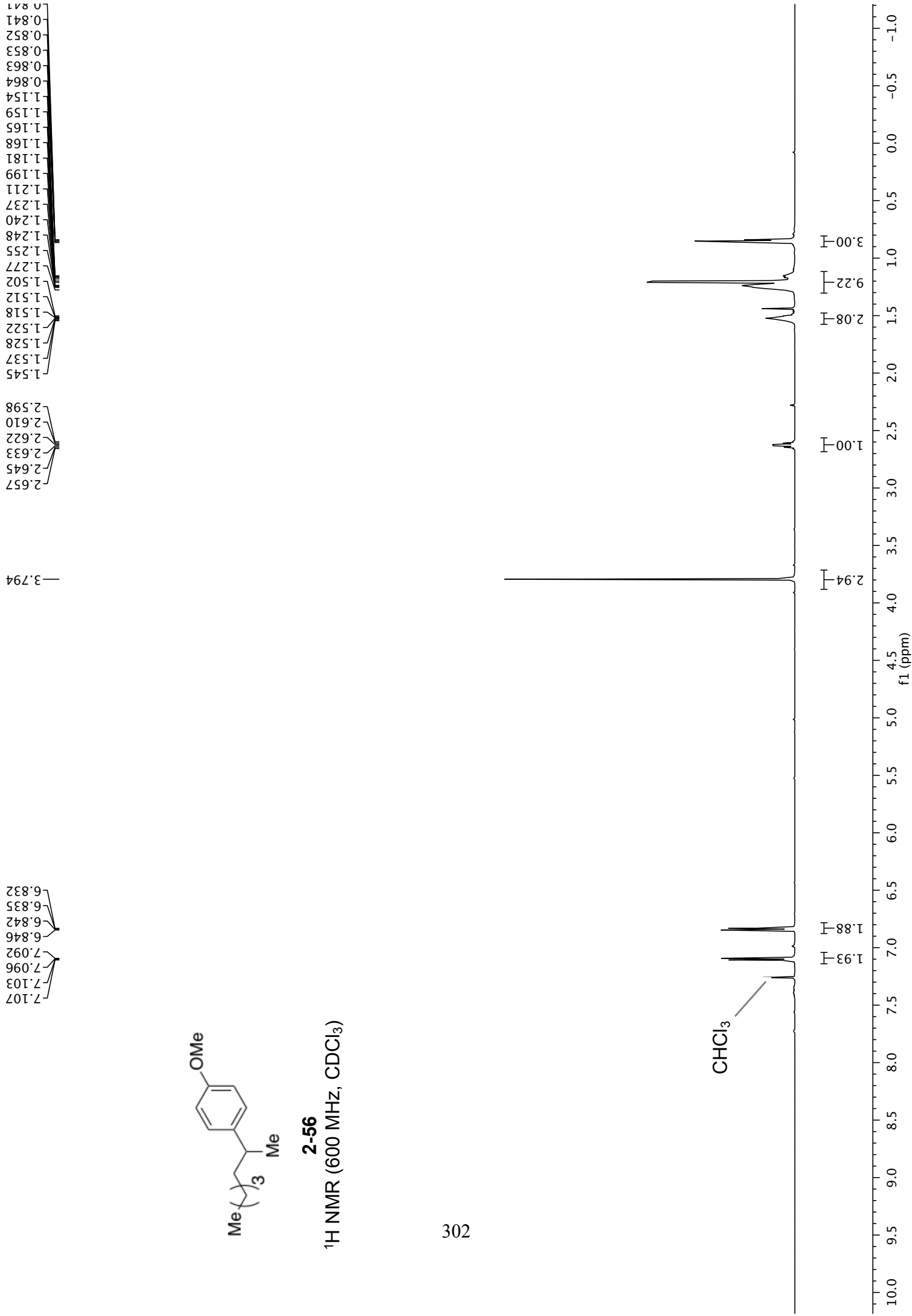
**2-53**

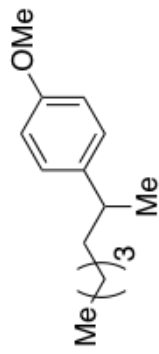
<sup>13</sup>C NMR (101 MHz, CDCl<sub>3</sub>)





**2-56**  
<sup>1</sup>H NMR (600 MHz, CDCl<sub>3</sub>)

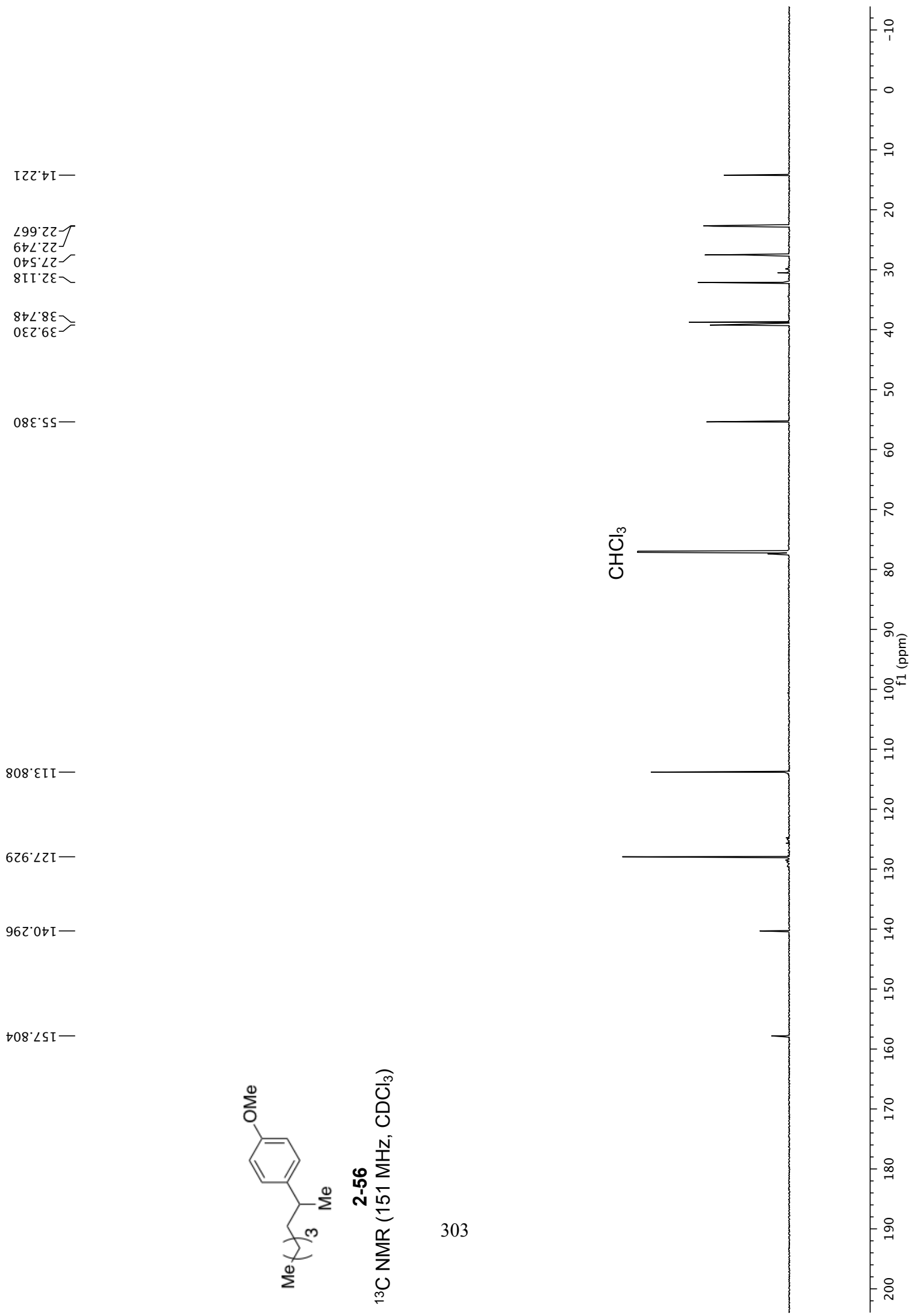


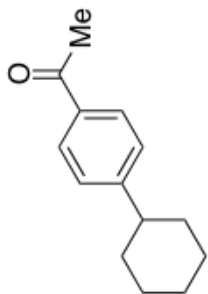


**2-56**

<sup>13</sup>C NMR (151 MHz, CDCl<sub>3</sub>)

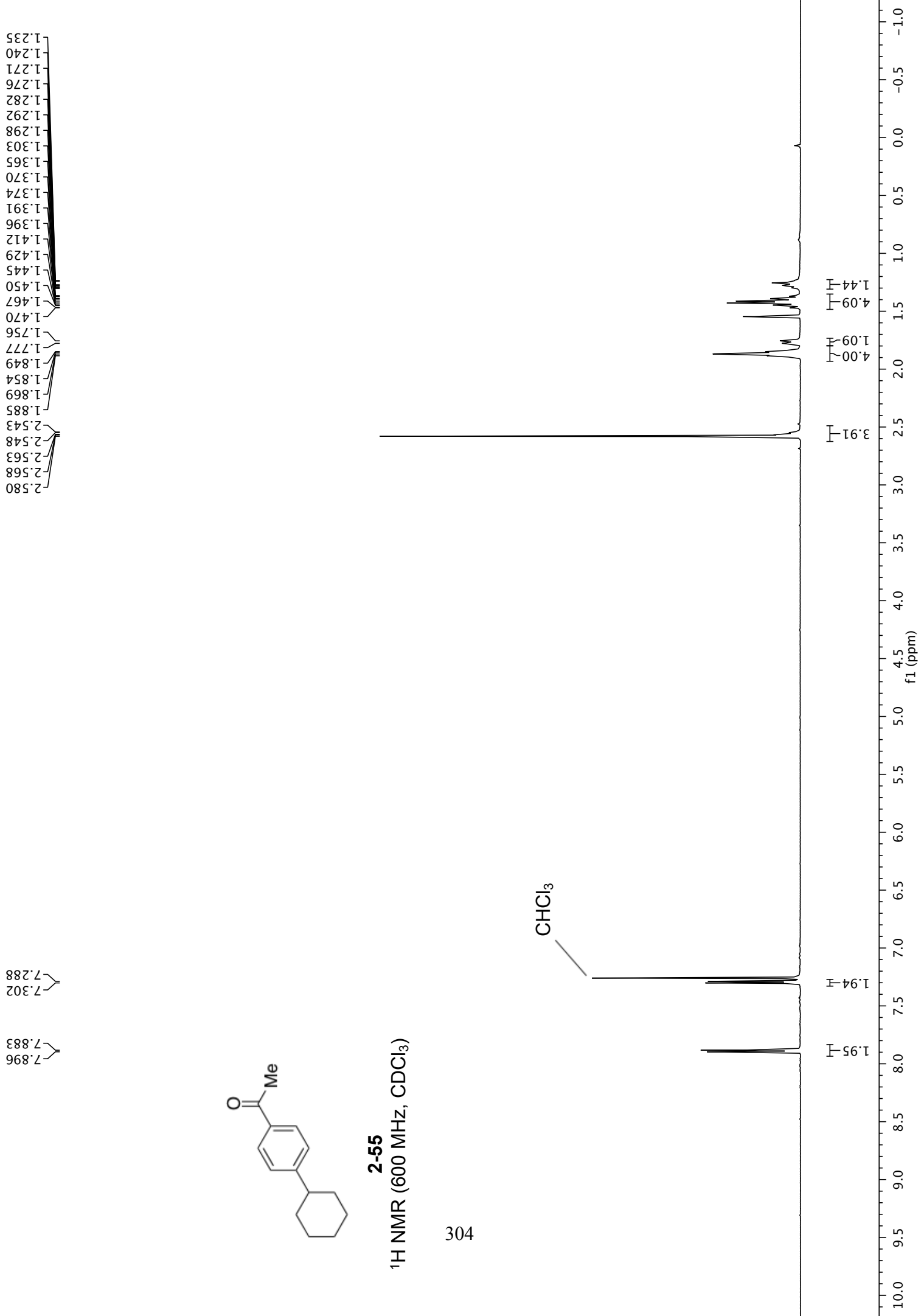
303

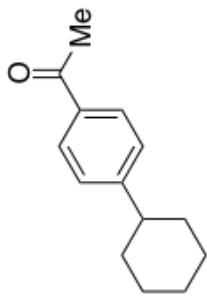




**2-55**  
<sup>1</sup>H NMR (600 MHz, CDCl<sub>3</sub>)

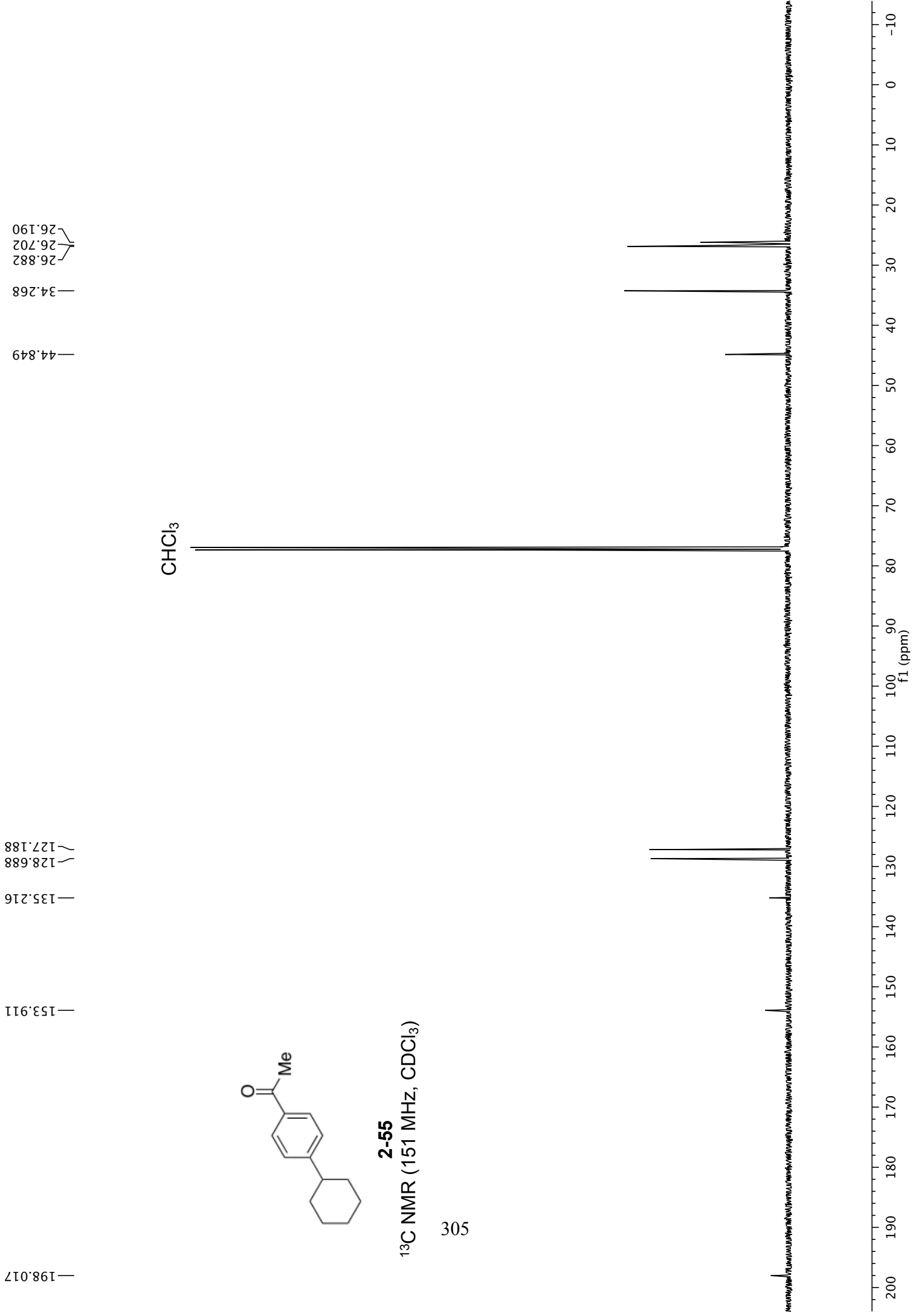
304

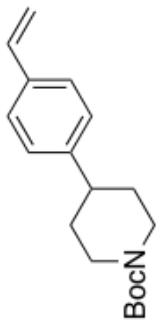




**2-55**  
 $^{13}\text{C}$  NMR (151 MHz,  $\text{CDCl}_3$ )

305



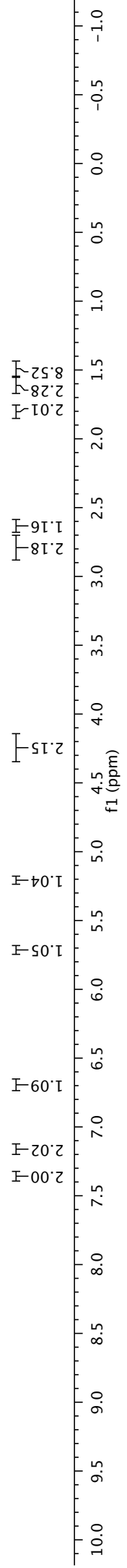


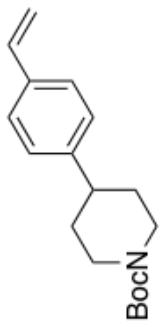
**2-57**

<sup>1</sup>H NMR (400 MHz, CDCl<sub>3</sub>)

7.370, 7.349, 7.175, 7.155, 6.730, 6.702, 6.686, 6.658, 5.738, 5.736, 5.694, 5.692, 5.223, 5.221, 5.196, 5.194, 4.243, 2.825, 2.796, 2.771, 2.673, 2.664, 2.655, 2.643, 2.634, 2.625, 2.612, 2.604, 2.595, 1.826, 1.794, 1.664, 1.654, 1.639, 1.635, 1.622, 1.601, 1.591, 1.569, 1.559, 1.484

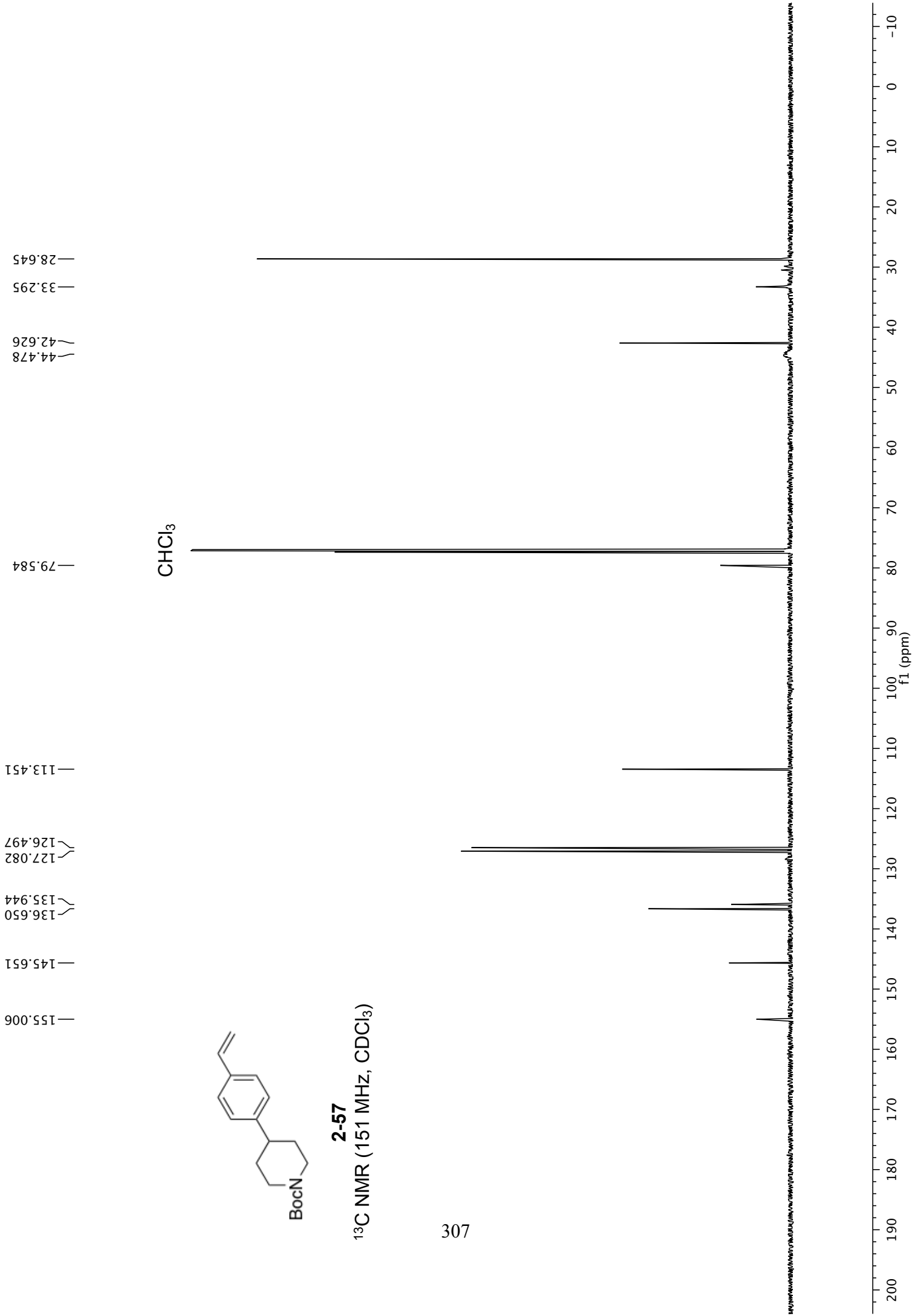
CHCl<sub>3</sub>

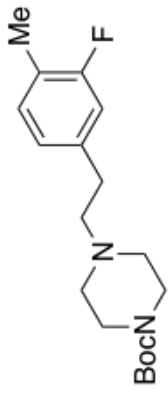




**2-57**

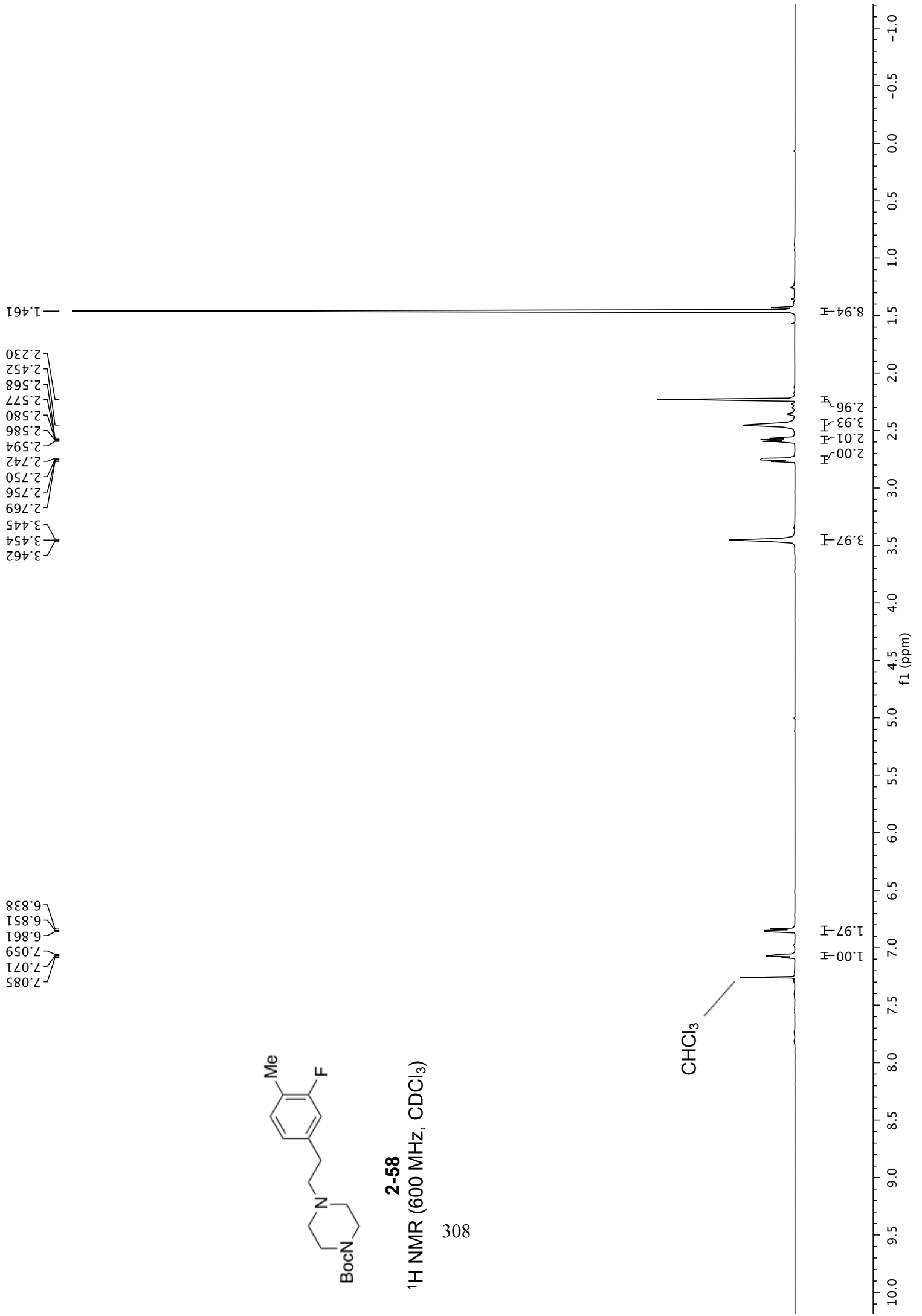
<sup>13</sup>C NMR (151 MHz, CDCl<sub>3</sub>)

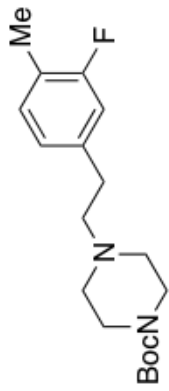




**2-58**  
<sup>1</sup>H NMR (600 MHz, CDCl<sub>3</sub>)

308





**2-58**

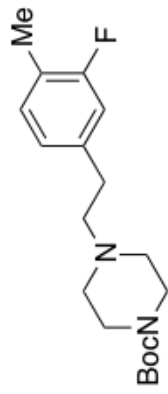
<sup>19</sup>F NMR (565 MHz, CDCl<sub>3</sub>)

309

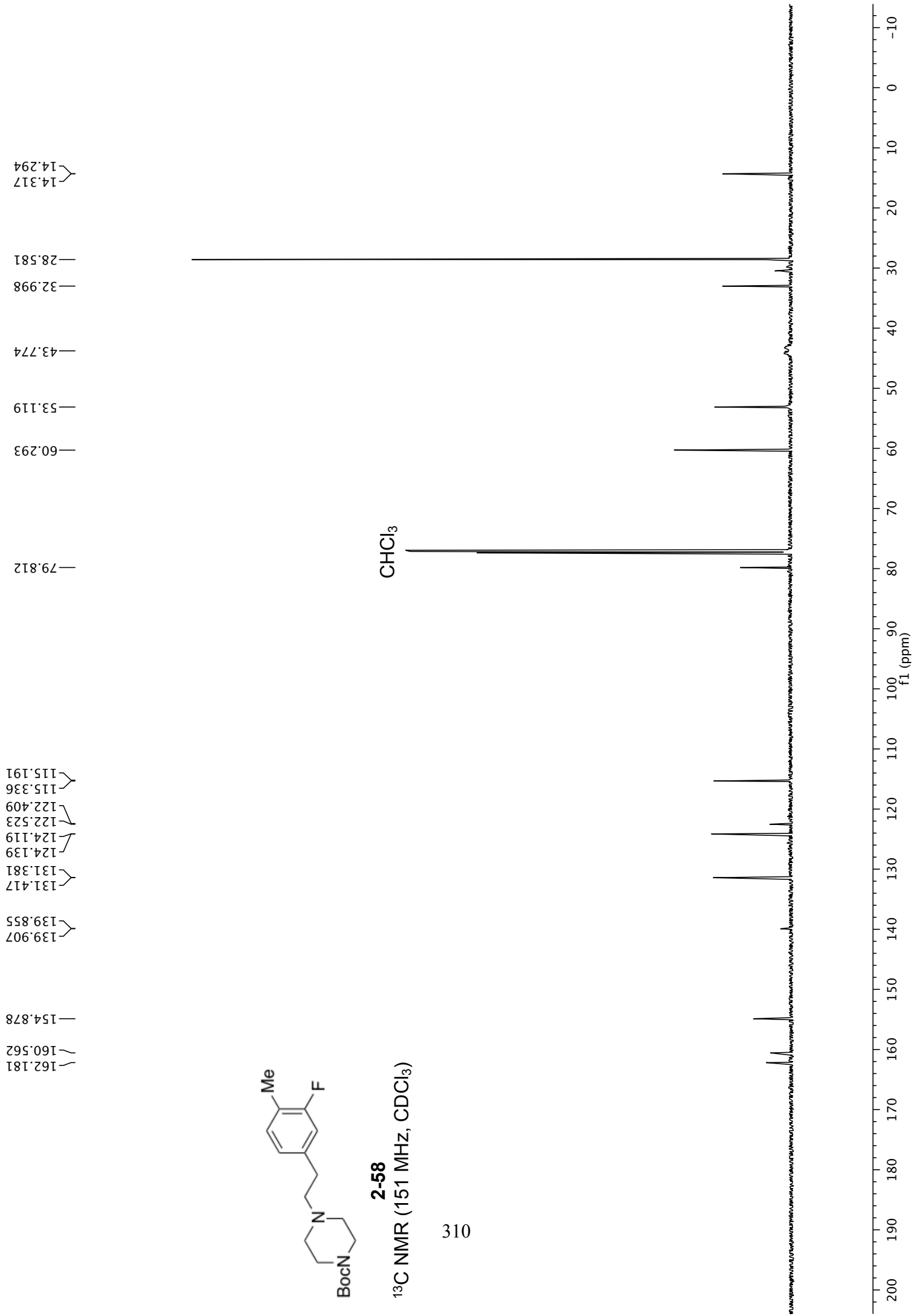
—117.975



-40 -45 -50 -55 -60 -65 -70 -75 -80 -85 -90 -95 -100 -105 -110 -115 -120 -125 -130 -135 -140 -145 -150 -155 -160 -165 -170 -175 -180



**2-58**  
<sup>13</sup>C NMR (151 MHz, CDCl<sub>3</sub>)

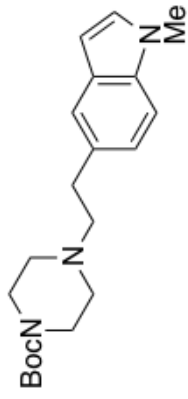


7.439  
7.258  
7.239  
7.078  
7.075  
7.064  
7.061  
7.029  
7.024  
6.418  
6.416  
6.412  
6.411

3.773  
3.485

2.911  
2.657  
2.497

1.466

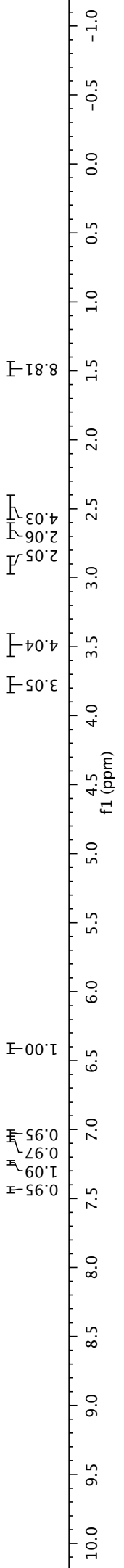


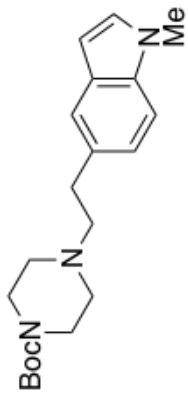
**2-59**

<sup>1</sup>H NMR (600 MHz, CDCl<sub>3</sub>)

311

CHCl<sub>3</sub>

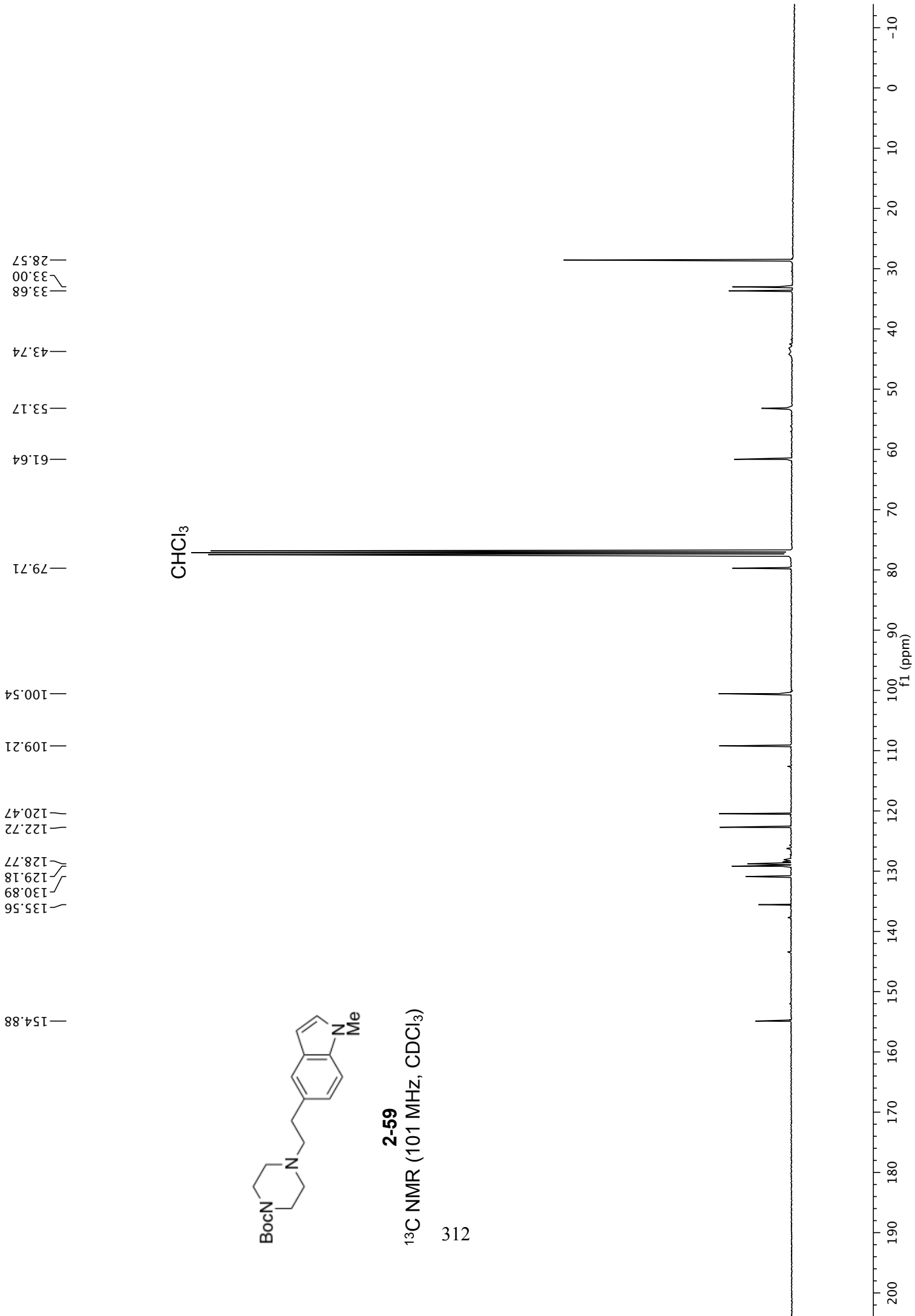


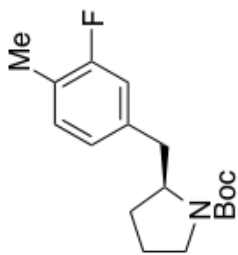


**2-59**

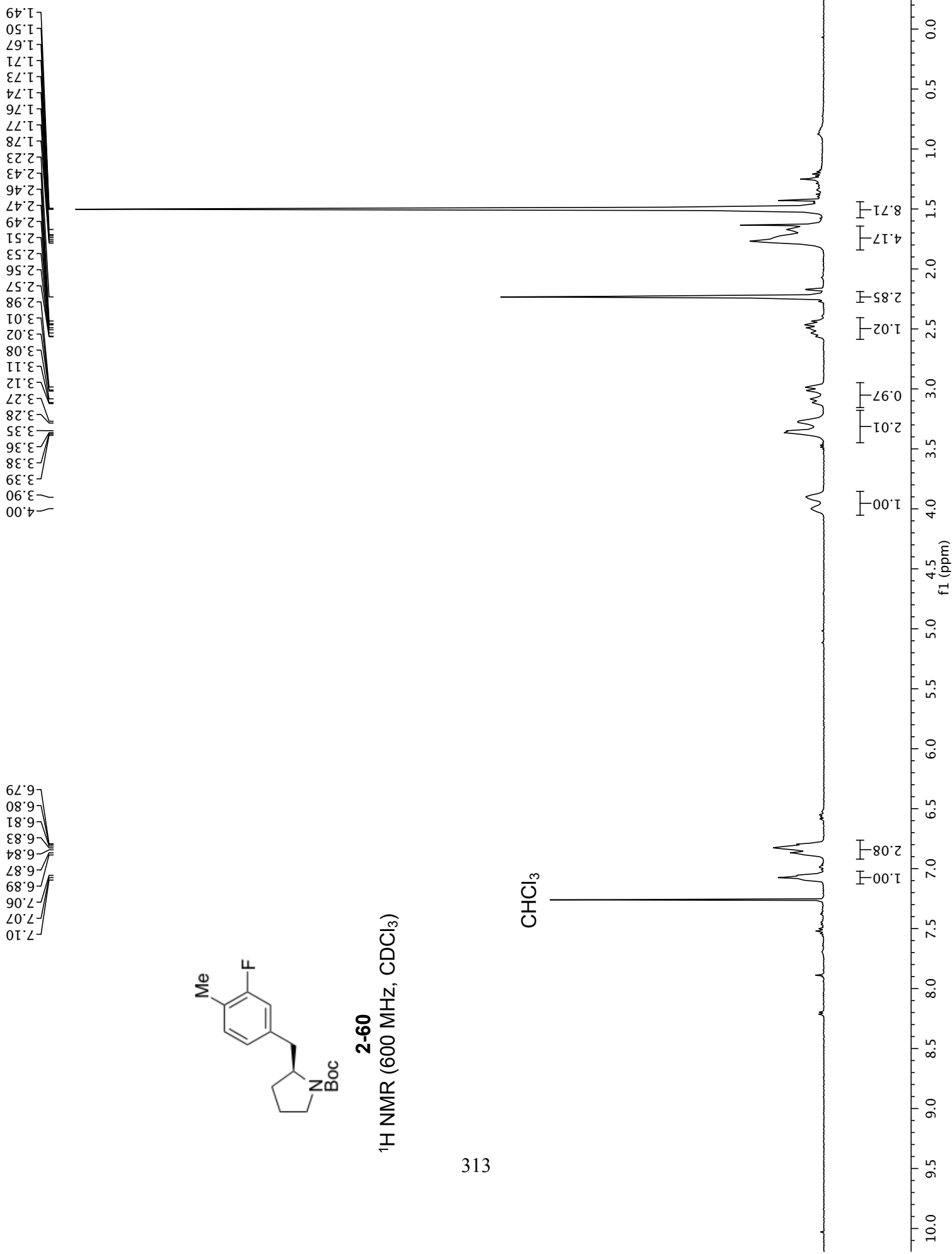
<sup>13</sup>C NMR (101 MHz, CDCl<sub>3</sub>)

312

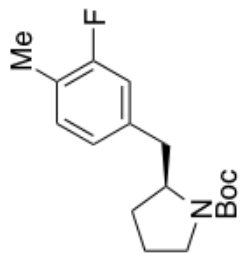




**2-60**  
<sup>1</sup>H NMR (600 MHz, CDCl<sub>3</sub>)







**2-60**

<sup>19</sup>F NMR (565 MHz, CDCl<sub>3</sub>)

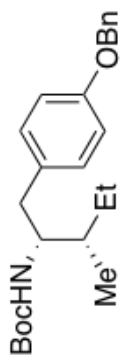
315

-117.98  
-118.39

0.04  
1.00  
0.73

f1 (ppm)

-40 -45 -50 -55 -60 -65 -70 -75 -80 -85 -90 -95 -100 -105 -110 -115 -120 -125 -130 -135 -140 -145 -150 -155 -160 -165 -170 -175 -180

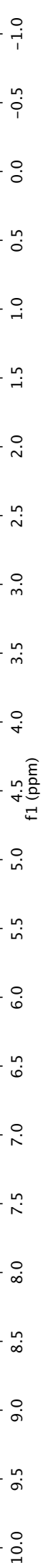


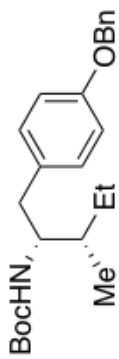
CHCl<sub>3</sub>

<sup>1</sup>H NMR (600 MHz, CDCl<sub>3</sub>)

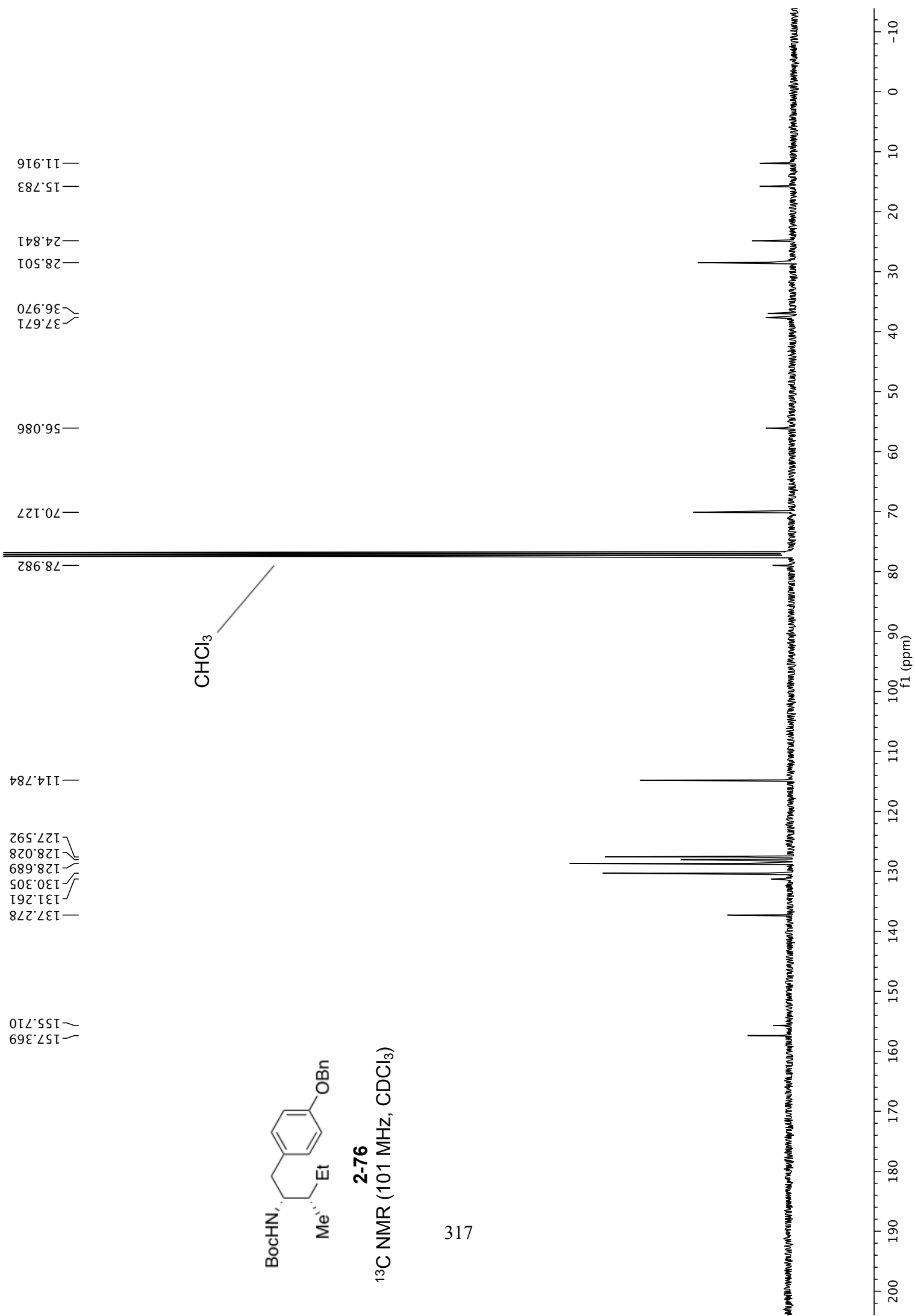
7.431, 7.418, 7.390, 7.377, 7.365, 7.328, 7.316, 7.304, 7.100, 7.087, 6.905, 6.900, 6.886, 6.881, 5.034, 4.318, 4.304, 3.745, 2.779, 2.771, 2.756, 2.747, 2.568, 2.553, 2.547, 2.531, 1.554, 1.547, 1.541, 1.534, 1.525, 1.513, 1.505, 1.501, 1.352, 1.352, 1.312, 1.105, 0.939, 0.927, 0.913, 0.901

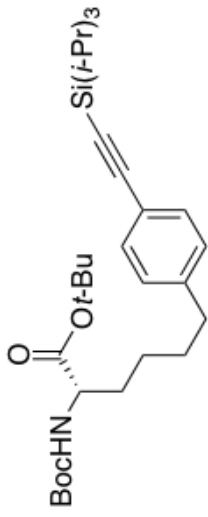
1.92, 1.98, 1.04, 2.06, 2.03, 1.99, 1.03, 1.06, 1.09, 1.00, 2.15, 9.25, 1.18, 6.08



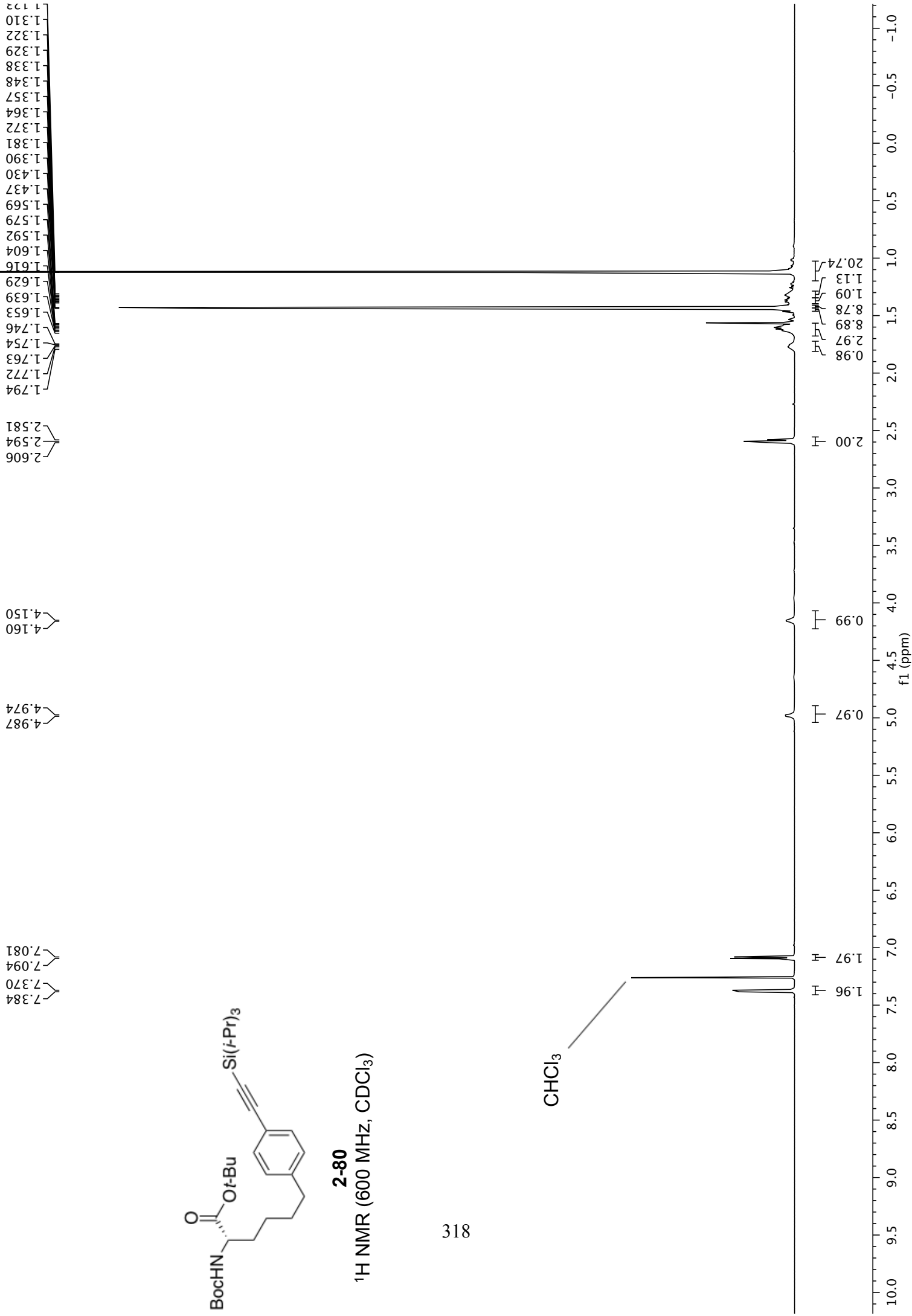


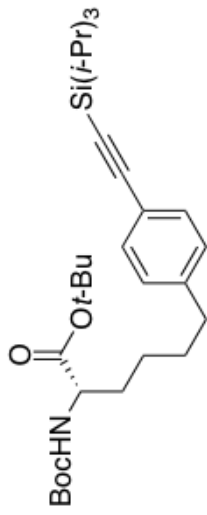
<sup>13</sup>C NMR (101 MHz, CDCl<sub>3</sub>)





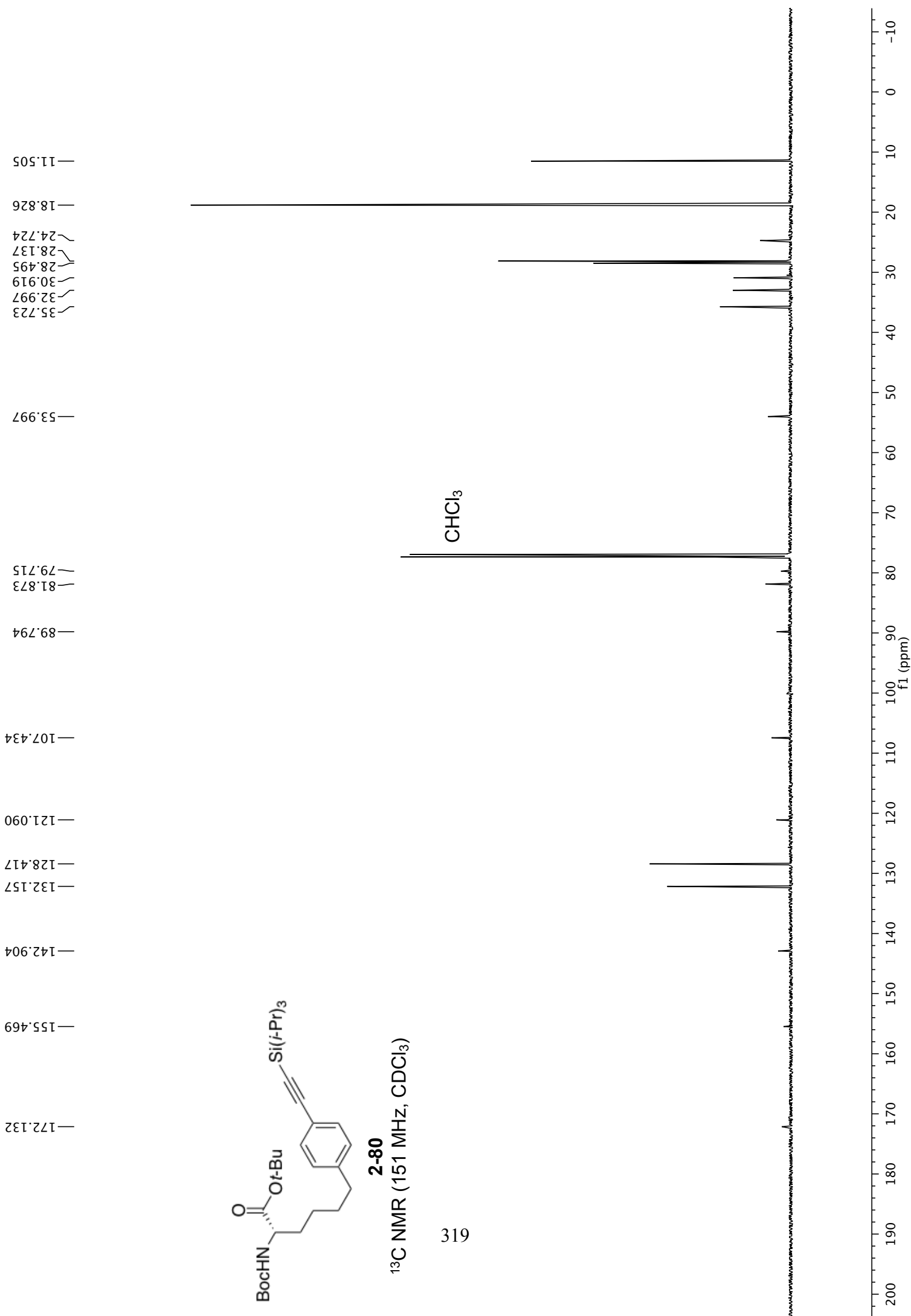
**2-80**  
 $^1\text{H NMR}$  (600 MHz,  $\text{CDCl}_3$ )

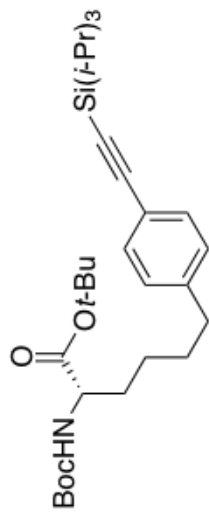




**2-80**

<sup>13</sup>C NMR (151 MHz, CDCl<sub>3</sub>)

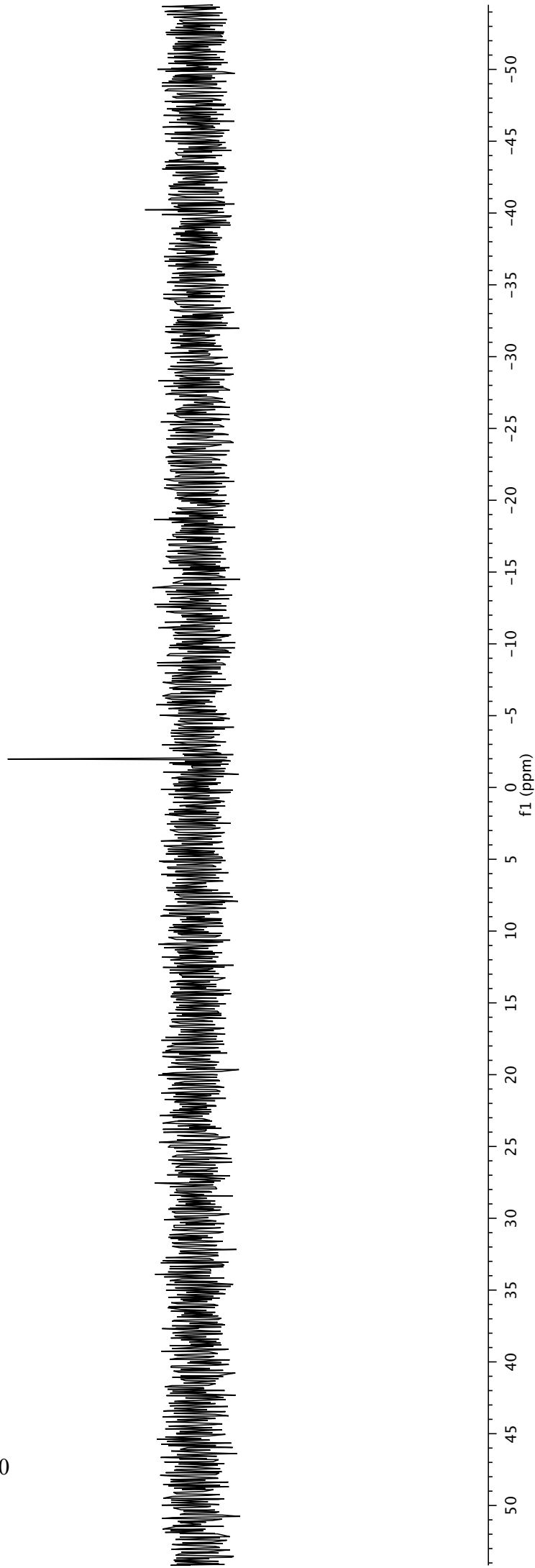


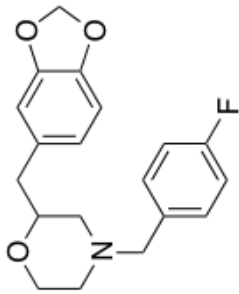


**2-80**

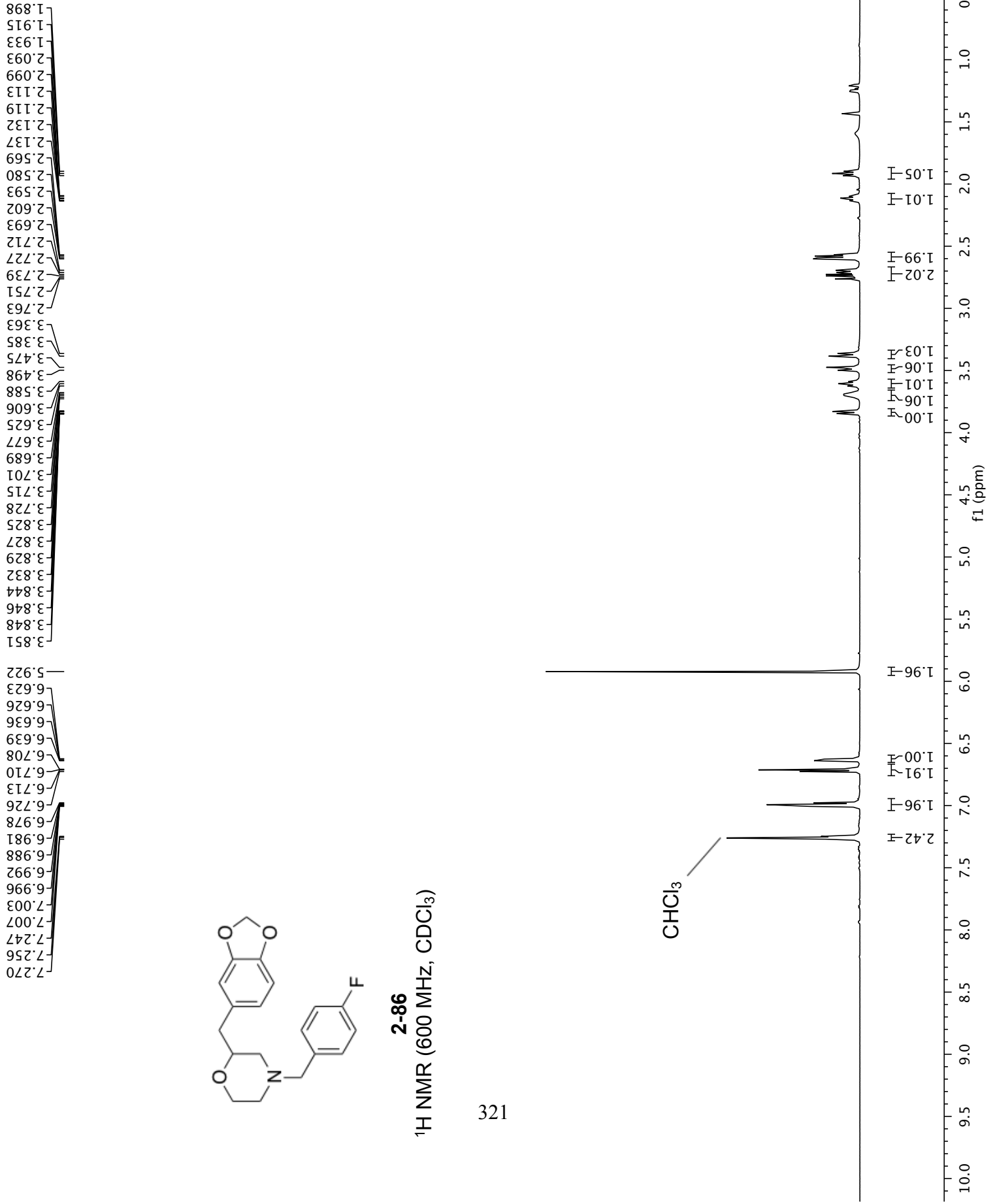
<sup>29</sup>S NMR (119 MHz, CDCl<sub>3</sub>)

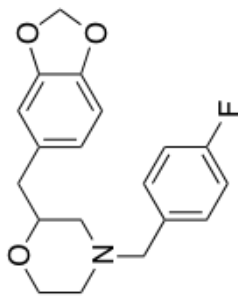
320



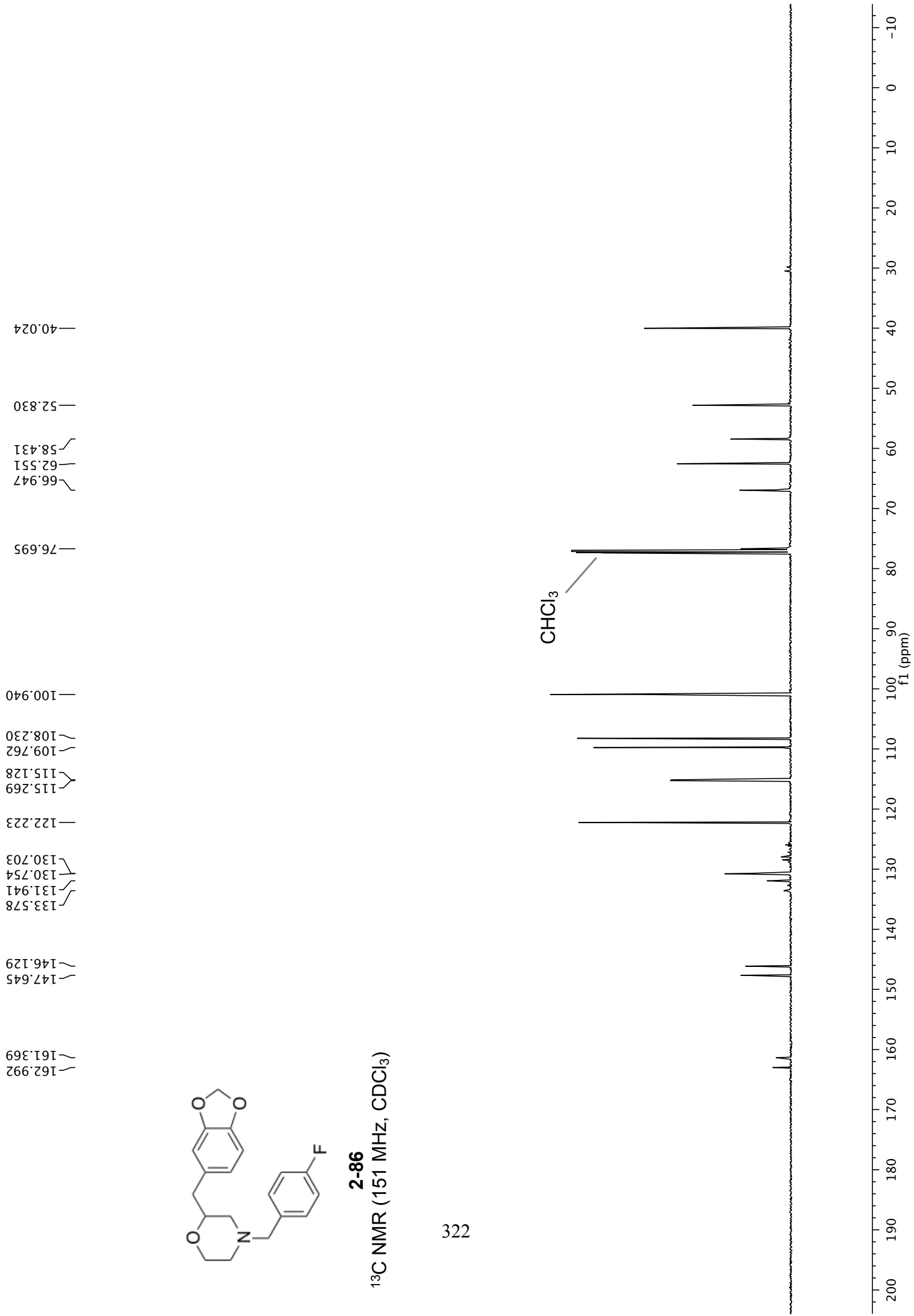


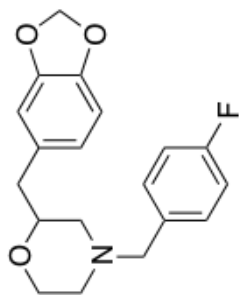
**2-86**  
<sup>1</sup>H NMR (600 MHz, CDCl<sub>3</sub>)





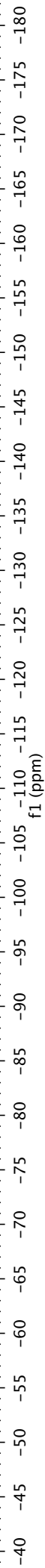
**2-86**  
 $^{13}\text{C}$  NMR (151 MHz,  $\text{CDCl}_3$ )

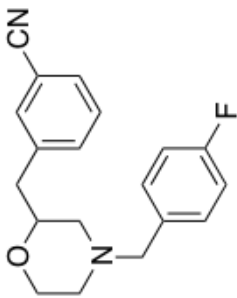




**2-86**  
<sup>19</sup>F NMR (565 MHz, CDCl<sub>3</sub>)

—115.769

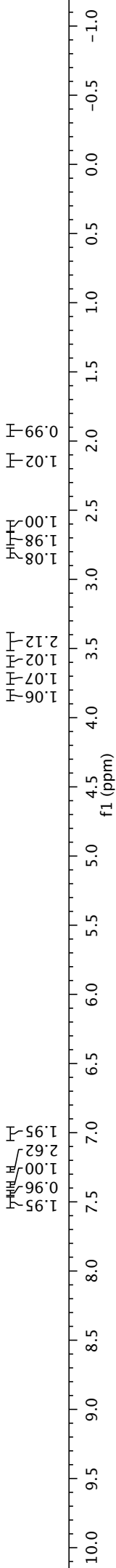


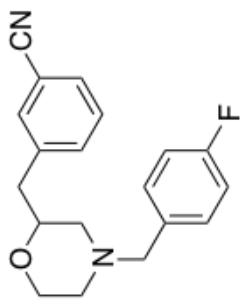


**2-85**  
<sup>1</sup>H NMR (600 MHz, CDCl<sub>3</sub>)

7.513  
7.511  
7.501  
7.499  
7.497  
7.444  
7.441  
7.439  
7.431  
7.428  
7.426  
7.388  
7.386  
7.375  
7.373  
7.364  
7.362  
7.278  
7.267  
7.260  
7.254  
7.017  
7.013  
7.002  
6.991  
6.988  
3.842  
3.840  
3.823  
3.821  
3.718  
3.605  
3.587  
3.568  
3.476  
3.453  
3.434  
3.412  
2.822  
2.809  
2.799  
2.785  
2.717  
2.709  
2.703  
2.693  
2.685  
2.626  
2.608  
2.157  
2.138  
2.120  
1.938  
1.920  
1.903

CHCl<sub>3</sub>





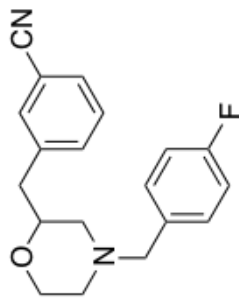
**2-85**

<sup>13</sup>C NMR (151 MHz, CDCl<sub>3</sub>)

163.027  
161.402  
139.904  
133.953  
133.438  
132.973  
130.735  
130.685  
130.219  
129.138  
119.111  
115.326  
115.186  
112.449  
75.901  
66.936  
62.484  
58.223  
52.856  
39.690

CHCl<sub>3</sub>

200 190 180 170 160 150 140 130 120 110 100 90 80 70 60 50 40 30 20 10 0 -10

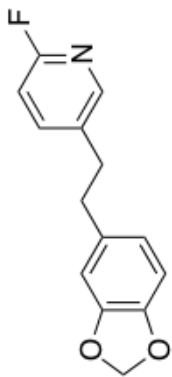


**2-85**

<sup>19</sup>F NMR (565 MHz, CDCl<sub>3</sub>)

—115.578





**2-63**

<sup>1</sup>H NMR (600 MHz, CDCl<sub>3</sub>)

2.887  
2.884  
2.873  
2.860  
2.833  
2.823  
2.820  
2.809  
2.806

7.955  
7.952  
7.515  
7.511  
7.501  
7.497  
7.488  
7.484  
6.832  
6.828  
6.819  
6.814  
6.713  
6.700  
6.621  
6.618  
6.545  
6.543  
6.532  
6.530  
5.929

327

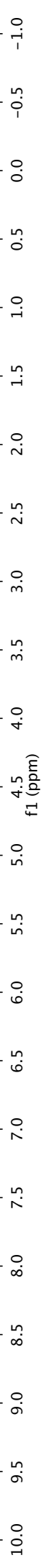
CHCl<sub>3</sub>

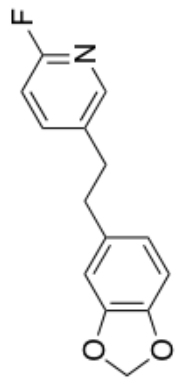
2.07  
2.08

1.00  
0.99  
0.95  
1.03

1.02

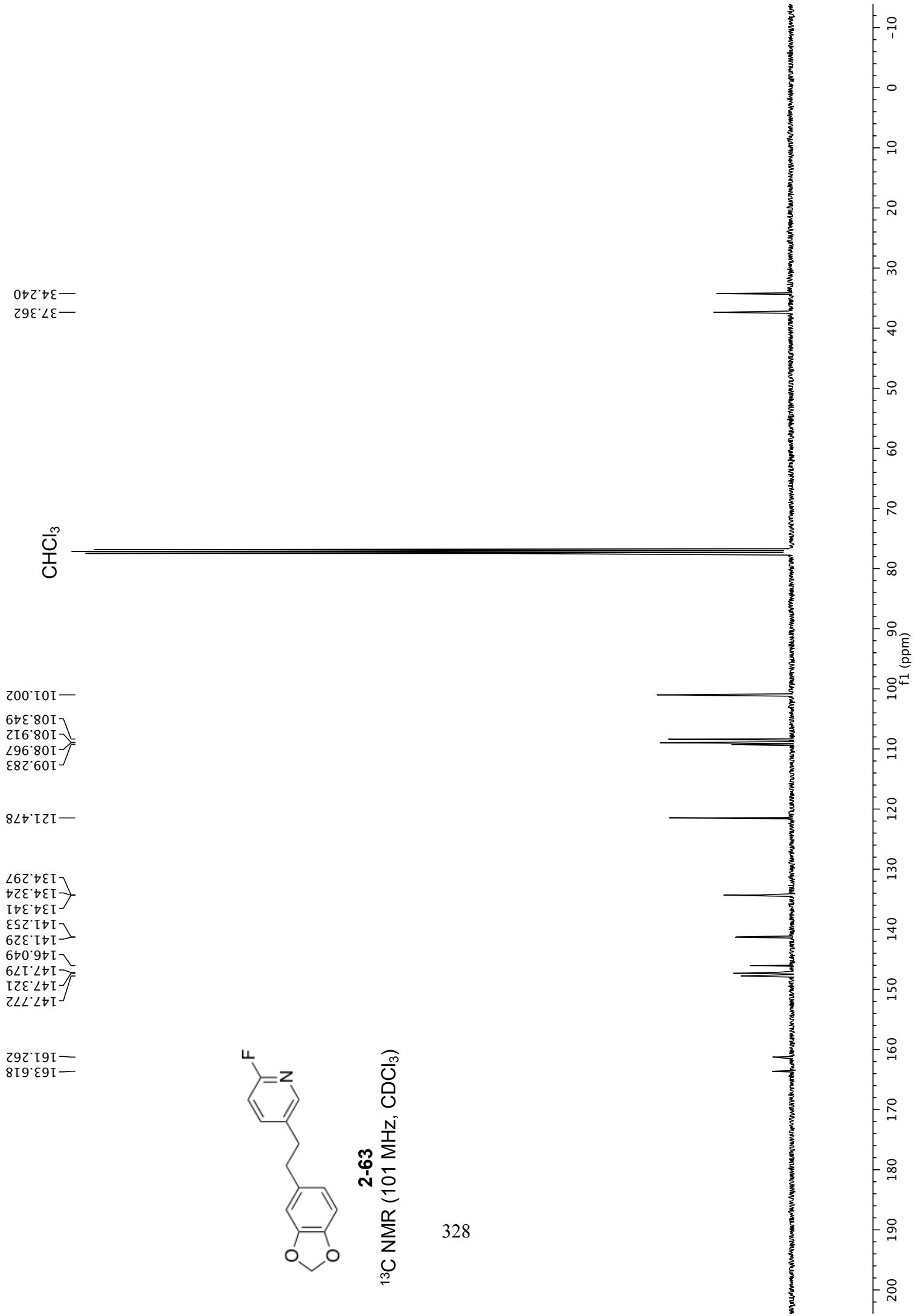
1.00

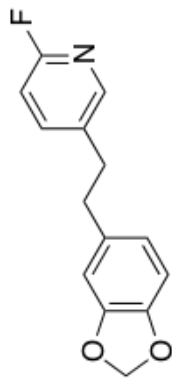




**2-63**

<sup>13</sup>C NMR (101 MHz, CDCl<sub>3</sub>)





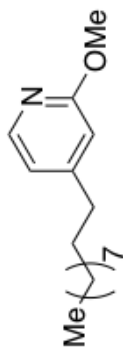
**2-63**

<sup>19</sup>F NMR (376 MHz, CDCl<sub>3</sub>)

329

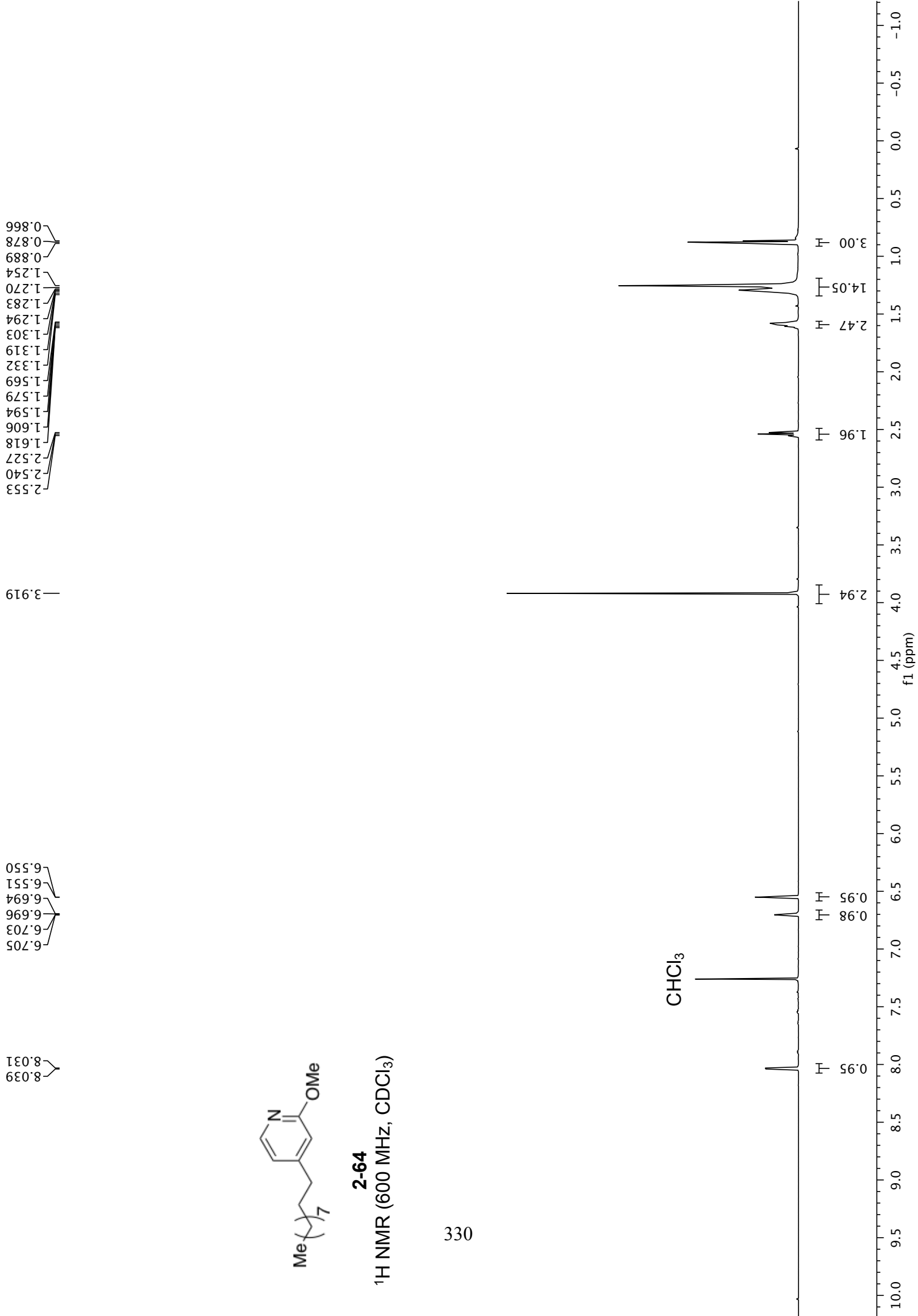
— -71.922

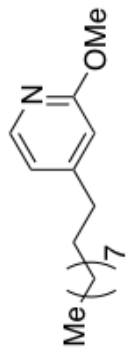




**2-64**  
<sup>1</sup>H NMR (600 MHz, CDCl<sub>3</sub>)

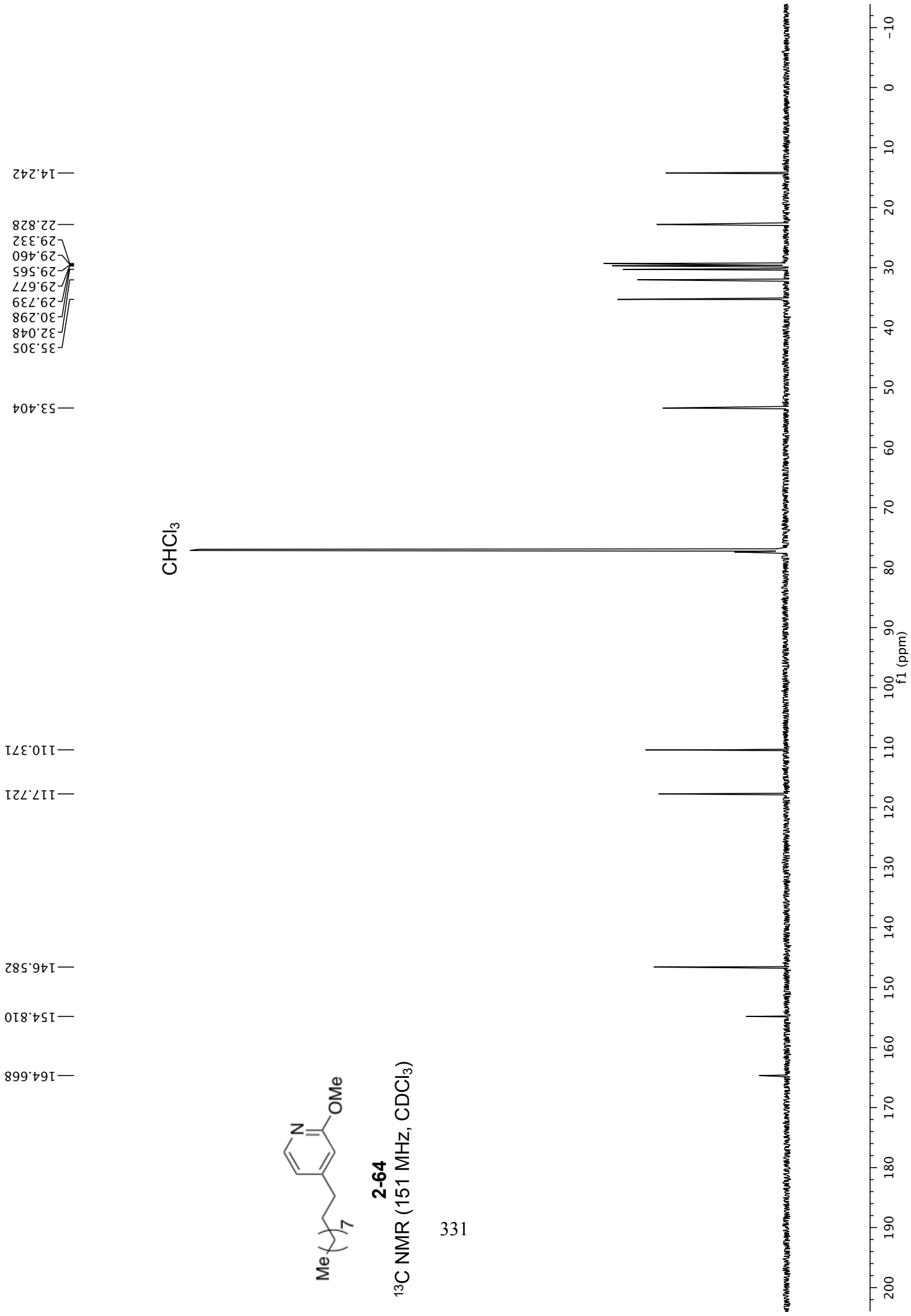
330



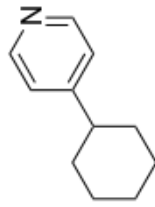


**2-64**

<sup>13</sup>C NMR (151 MHz, CDCl<sub>3</sub>)



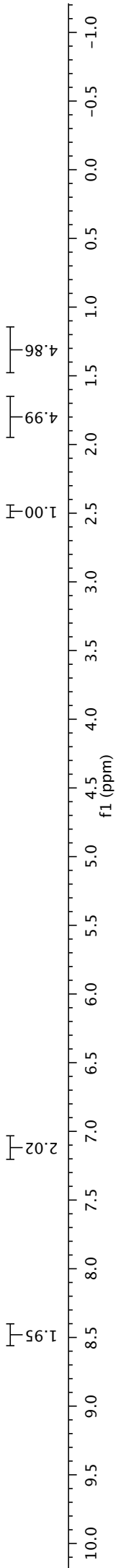
8.489  
8.485  
8.478  
8.474  
7.125  
7.121  
7.114  
7.109  
2.525  
2.517  
2.510  
2.503  
2.496  
2.488  
2.480  
2.474  
2.467  
2.458  
2.451  
1.912  
1.908  
1.877  
1.870  
1.861  
1.854  
1.848  
1.841  
1.830  
1.784  
1.781  
1.777  
1.773  
1.766  
1.757  
1.749  
1.746  
1.742  
1.735  
1.672  
1.622  
1.455  
1.449  
1.425  
1.418  
1.411  
1.402  
1.394  
1.378  
1.371  
1.363  
1.348  
1.340  
1.333  
1.304  
1.298  
1.290  
1.283  
1.274  
1.266  
1.258  
1.248  
1.241  
1.234  
1.225  
1.211  
1.207  
1.202  
1.195  
1.189

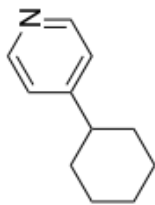


**2-65**  
<sup>1</sup>H NMR (400 MHz, CDCl<sub>3</sub>)

332

CHCl<sub>3</sub>

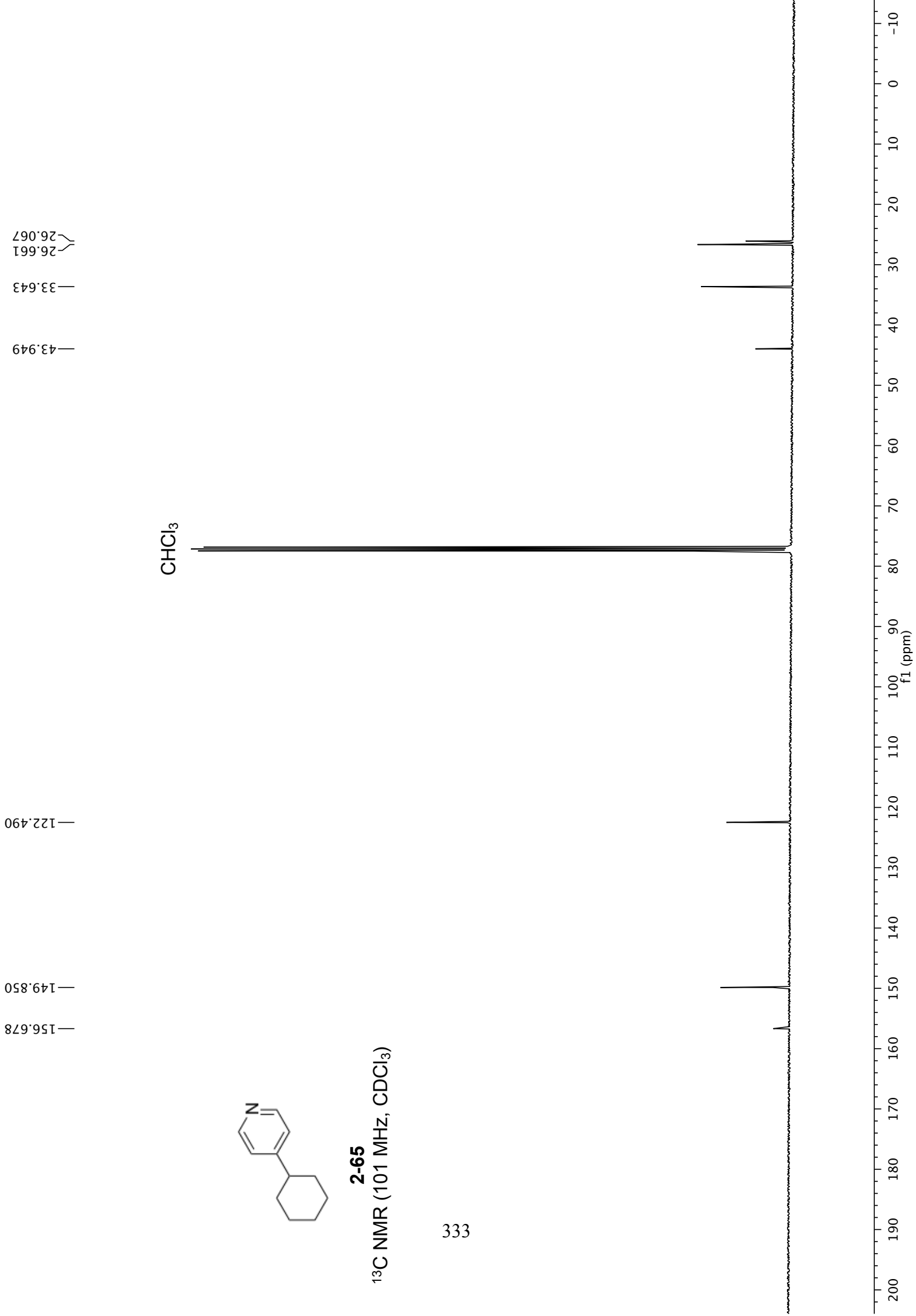


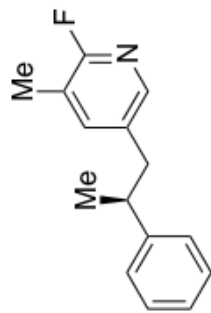


**2-65**

<sup>13</sup>C NMR (101 MHz, CDCl<sub>3</sub>)

333





**2-66**

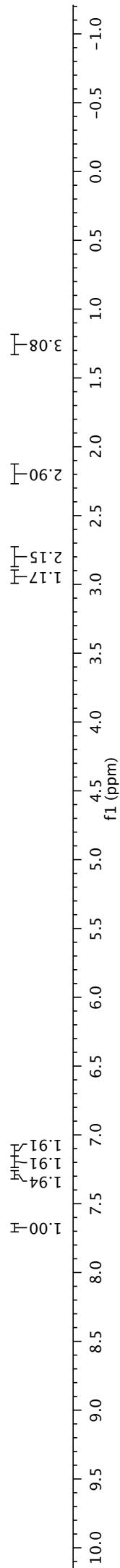
<sup>1</sup>H NMR (400 MHz, CDCl<sub>3</sub>)

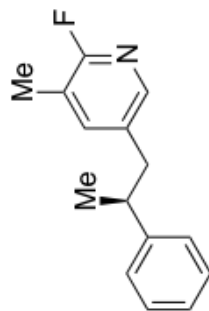
334

2.988  
2.971  
2.953  
2.935  
2.918  
2.900  
2.861  
2.844  
2.827  
2.810  
2.787  
2.768  
2.753  
2.734  
2.190  
1.278  
1.261

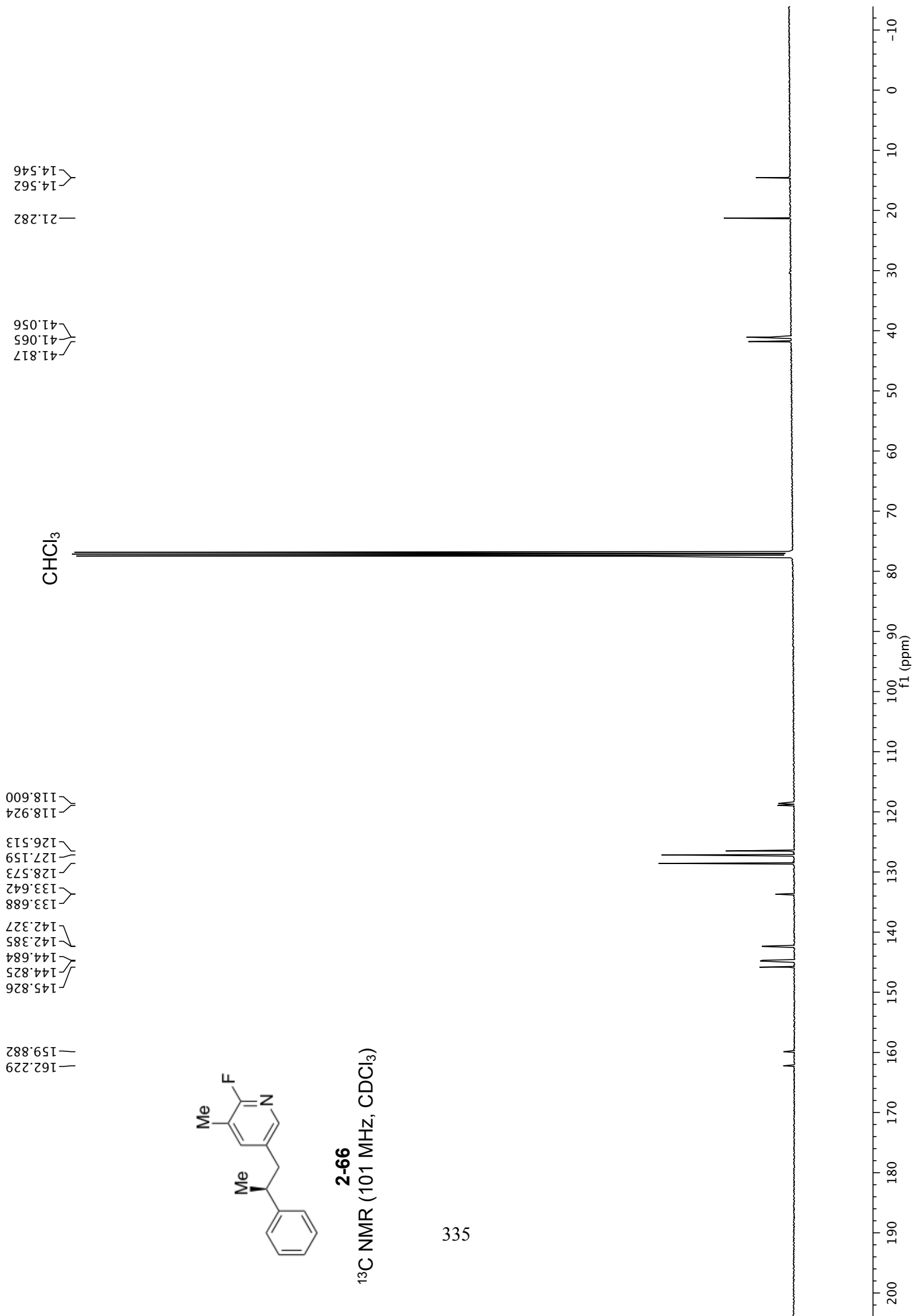
7.674  
7.297  
7.293  
7.279  
7.260  
7.213  
7.210  
7.206  
7.196  
7.191  
7.173  
7.171  
7.167  
7.138  
7.134  
7.130  
7.117  
7.110

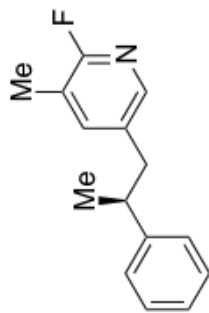
CHCl<sub>3</sub>





**2-66**  
<sup>13</sup>C NMR (101 MHz, CDCl<sub>3</sub>)

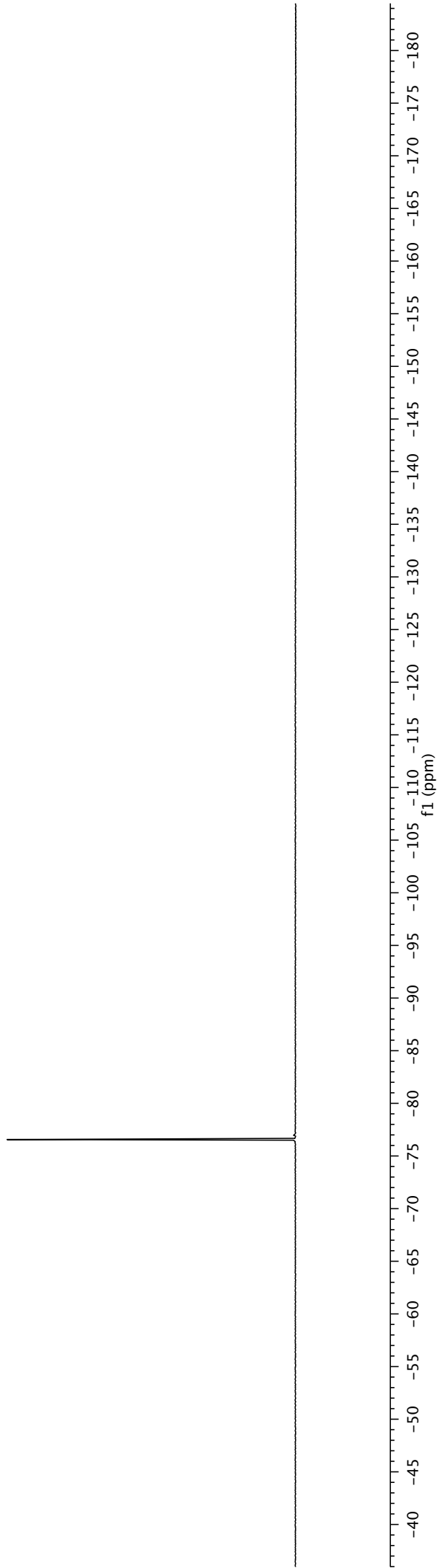


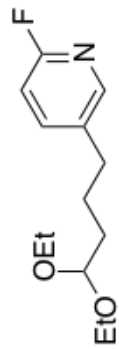


**2-66**  
<sup>19</sup>F NMR (376 MHz, CDCl<sub>3</sub>)

— -76.561

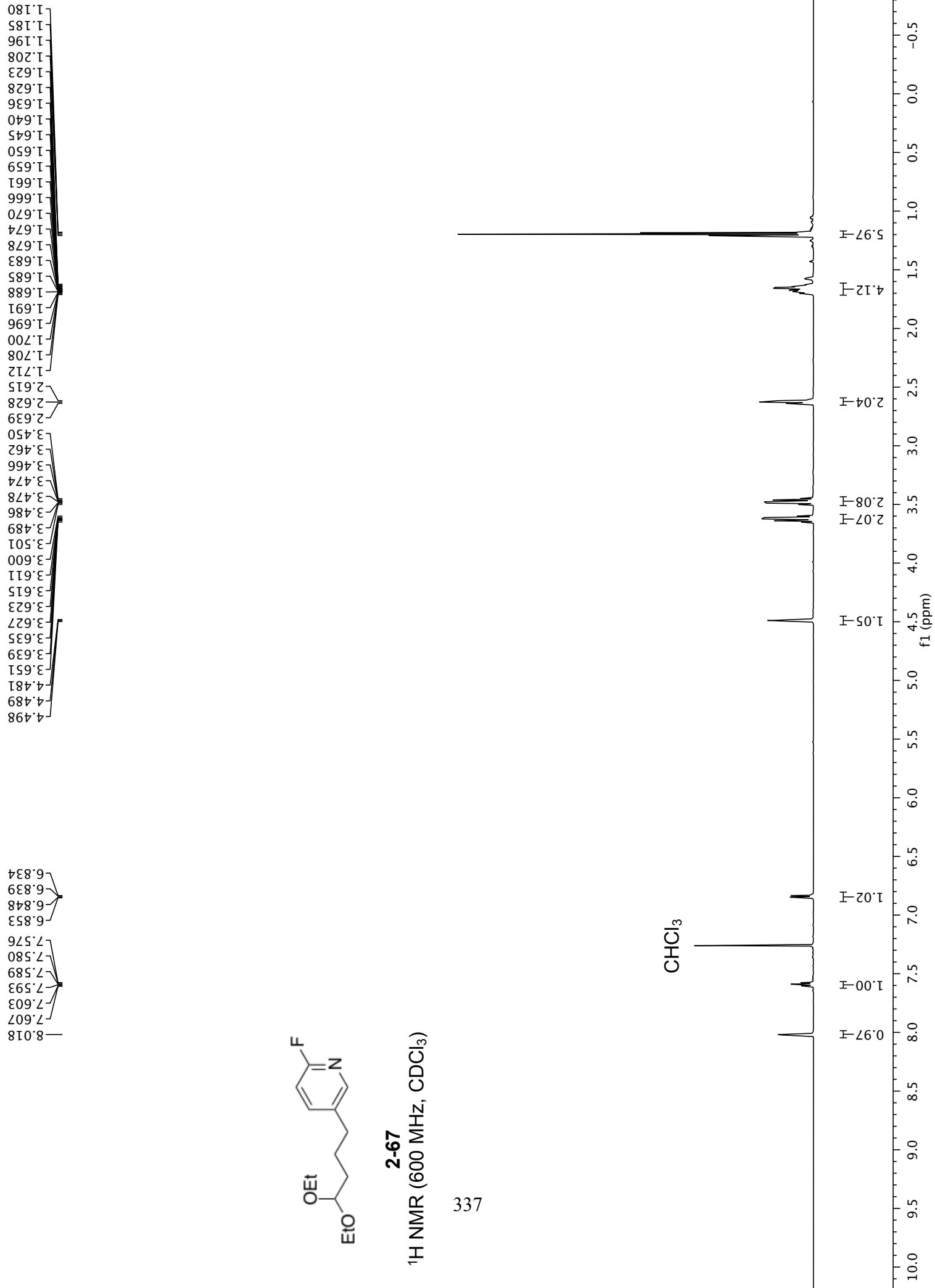
336

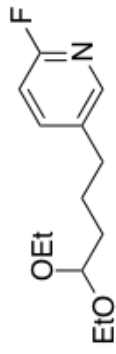




**2-67**  
<sup>1</sup>H NMR (600 MHz, CDCl<sub>3</sub>)

337

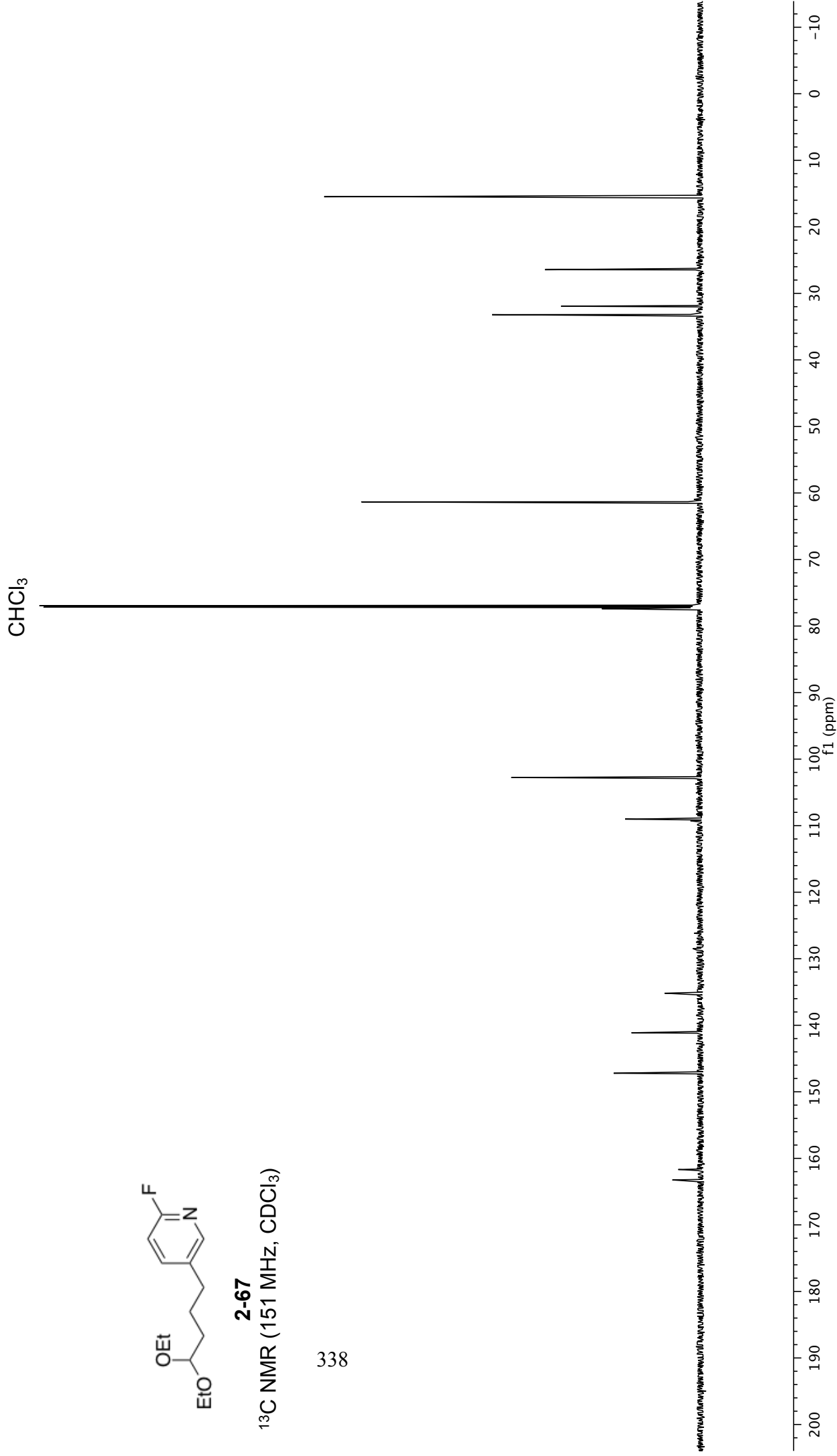




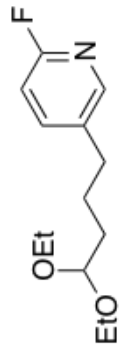
**2-67**

<sup>13</sup>C NMR (151 MHz, CDCl<sub>3</sub>)

338



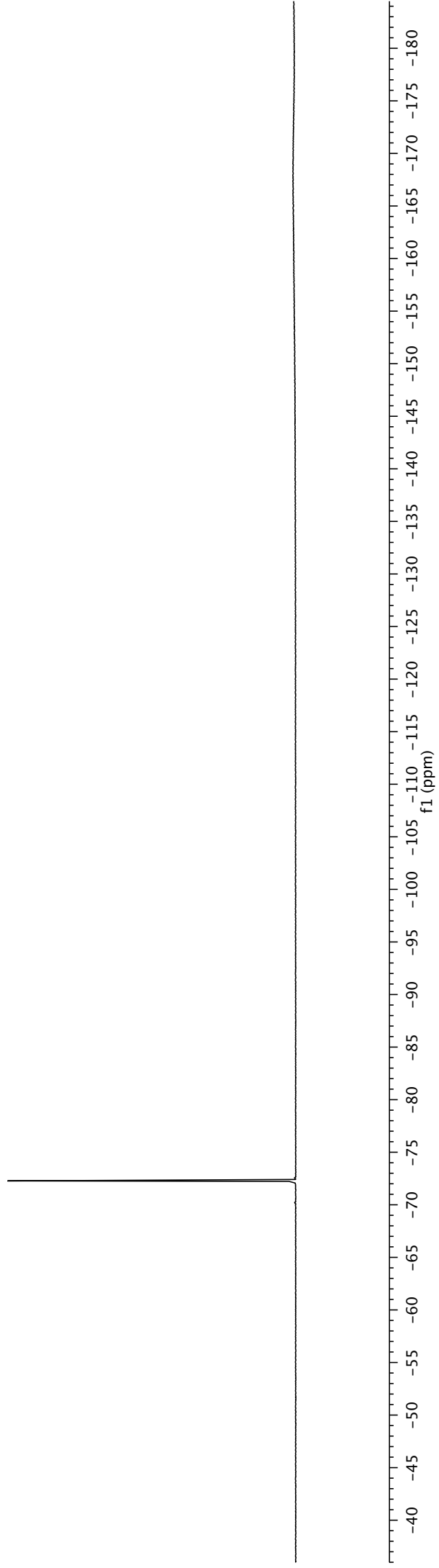
—72.271



**2-67**

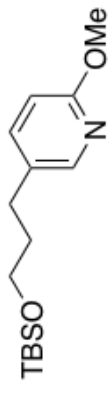
<sup>19</sup>F NMR (565 MHz, CDCl<sub>3</sub>)

339



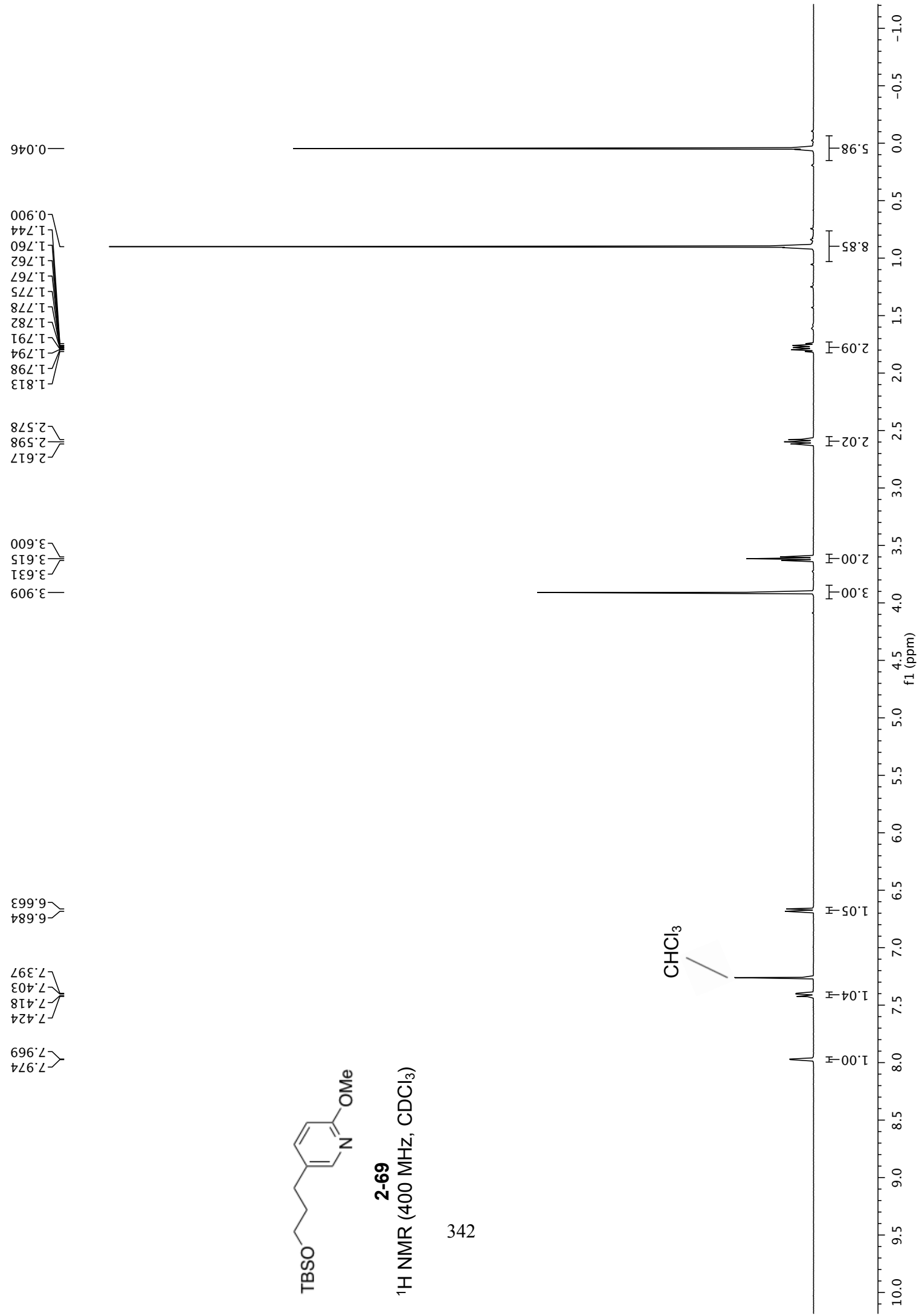


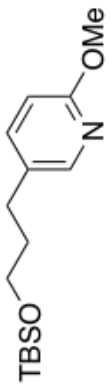




**2-69**  
<sup>1</sup>H NMR (400 MHz, CDCl<sub>3</sub>)

342

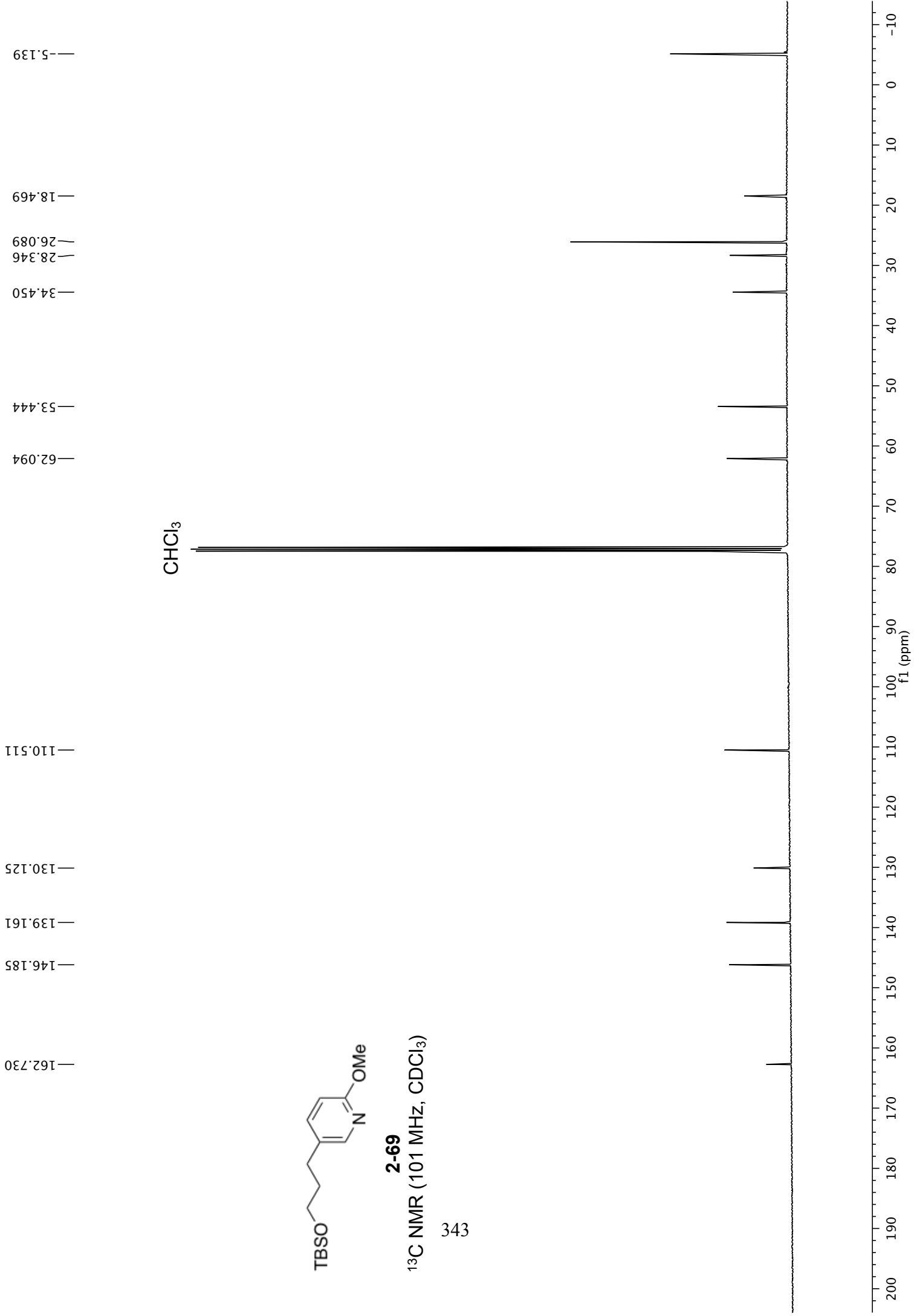


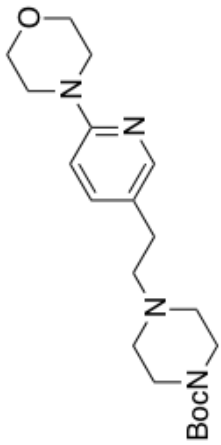


**2-69**

<sup>13</sup>C NMR (101 MHz, CDCl<sub>3</sub>)

343

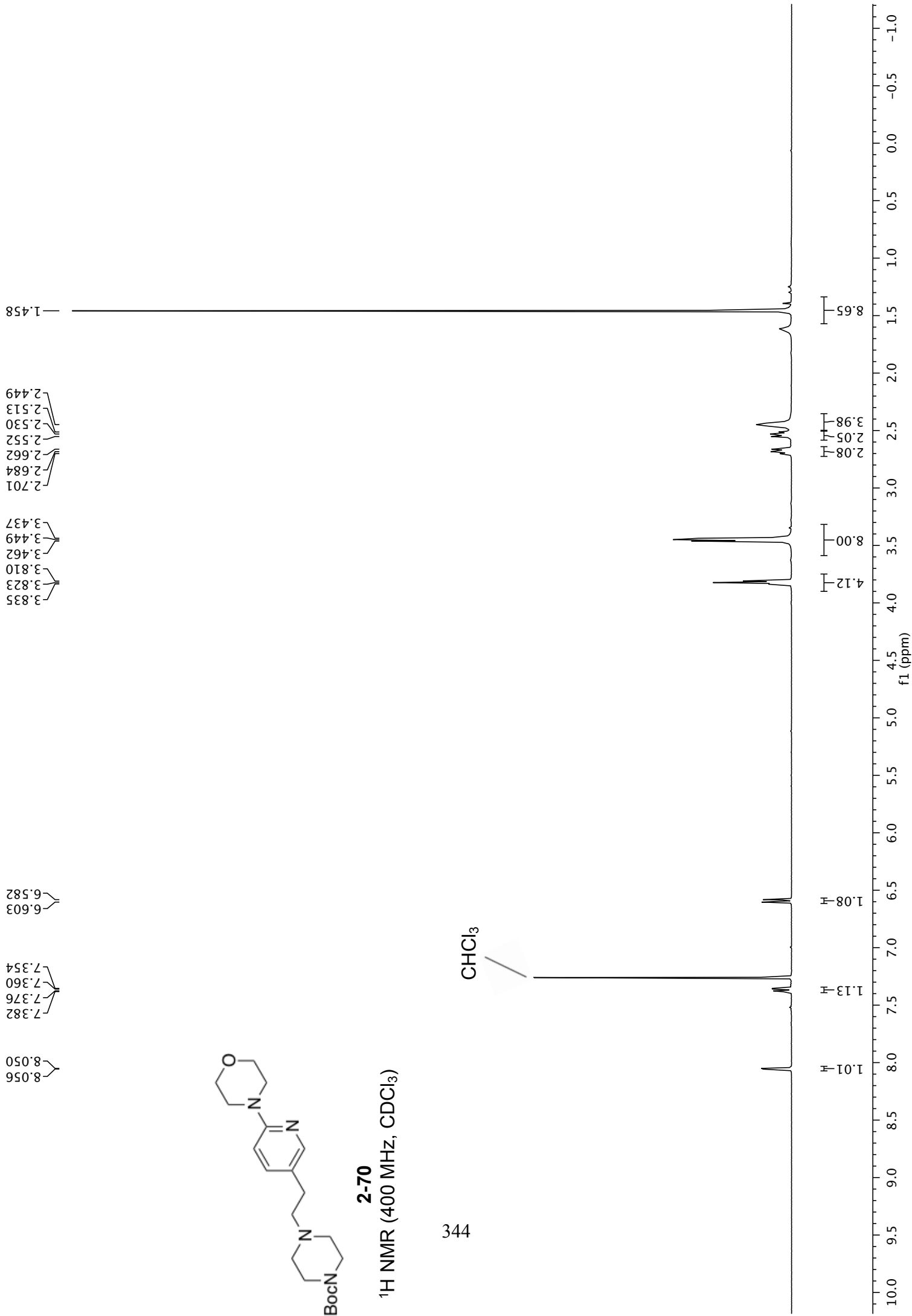


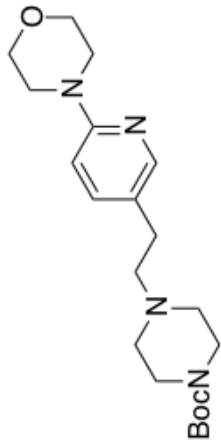


**2-70**

<sup>1</sup>H NMR (400 MHz, CDCl<sub>3</sub>)

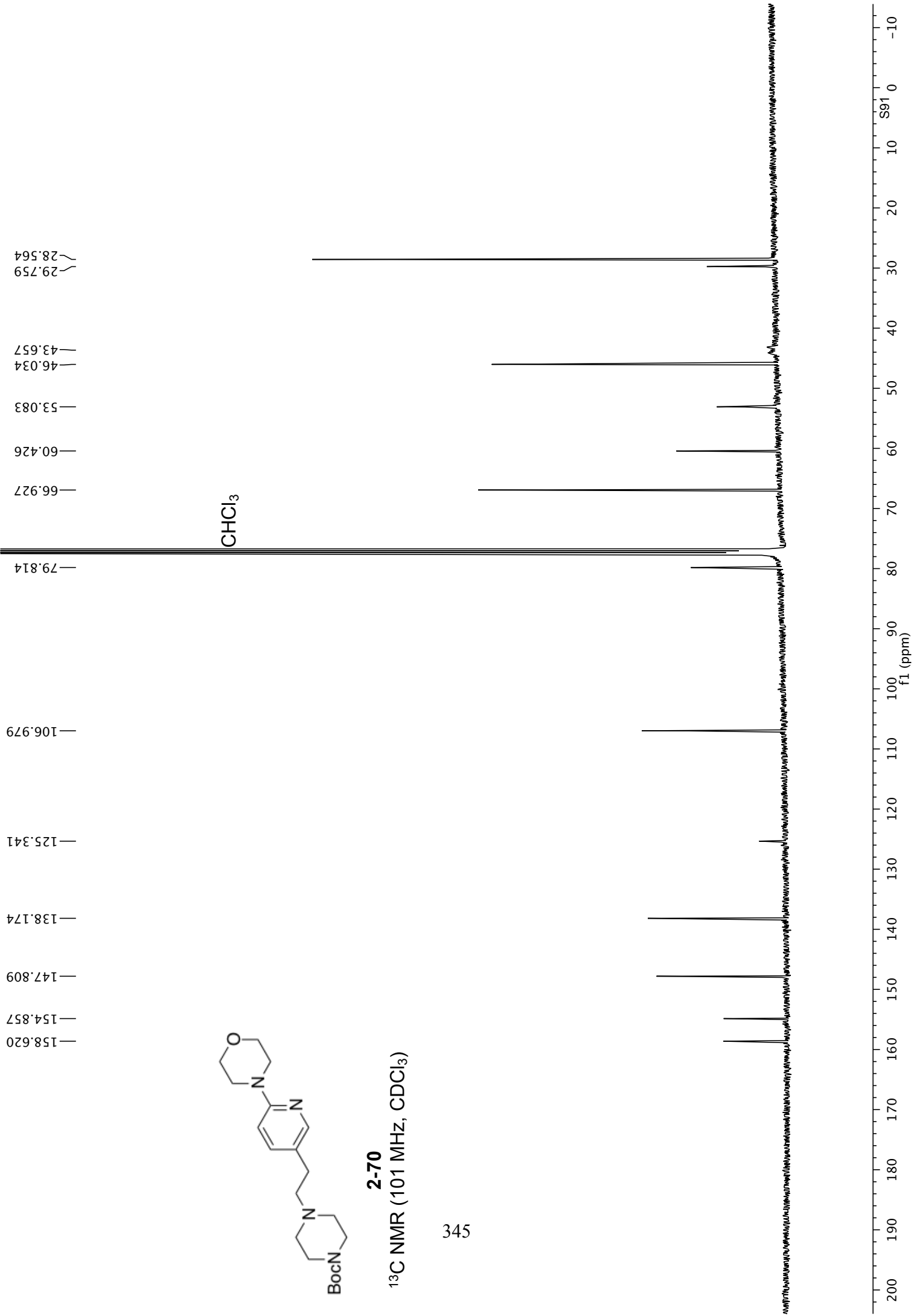
344

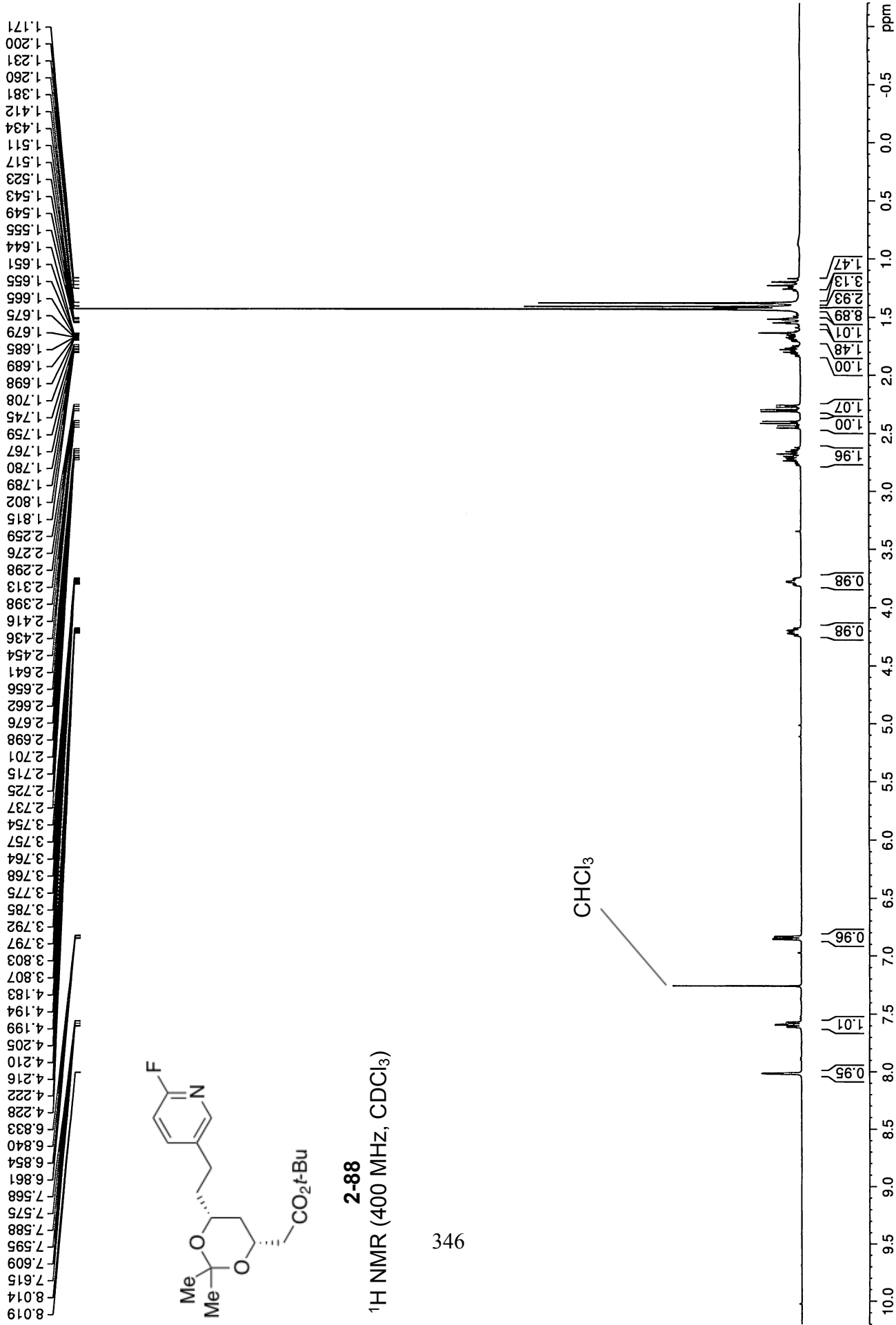


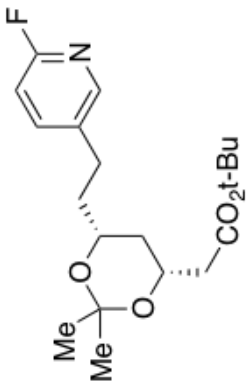


**2-70**

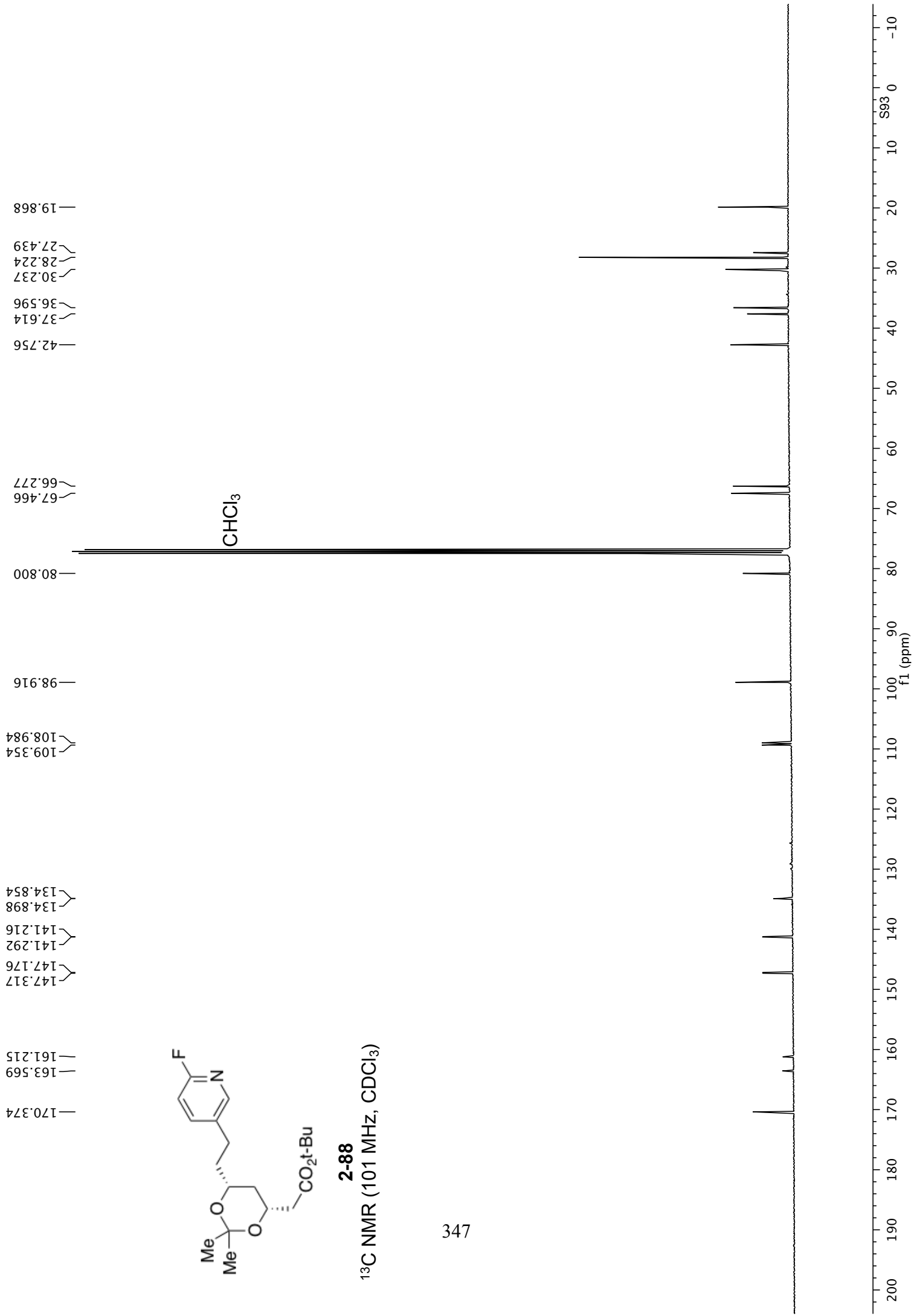
<sup>13</sup>C NMR (101 MHz, CDCl<sub>3</sub>)

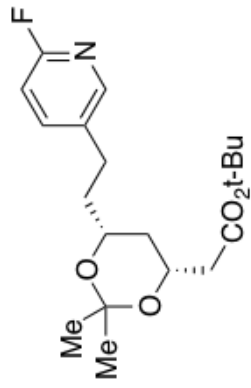






**2-88**  
<sup>13</sup>C NMR (101 MHz, CDCl<sub>3</sub>)





**2-88**

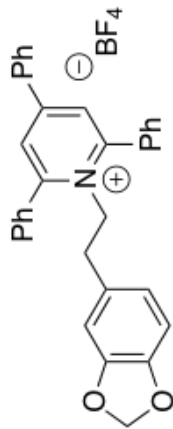
$^{19}\text{F}$  NMR (376 MHz,  $\text{CDCl}_3$ )

— -72.197

348



-40 -45 -50 -55 -60 -65 -70 -75 -80 -85 -90 -95 -100 -105 -110 -115 -120 -125 -130 -135 -140 -145 -150 -155 -160 -165 -170 -175 -180  
f1 (ppm)



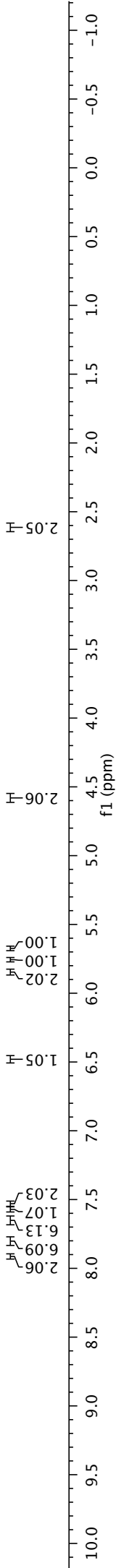
**2-46**

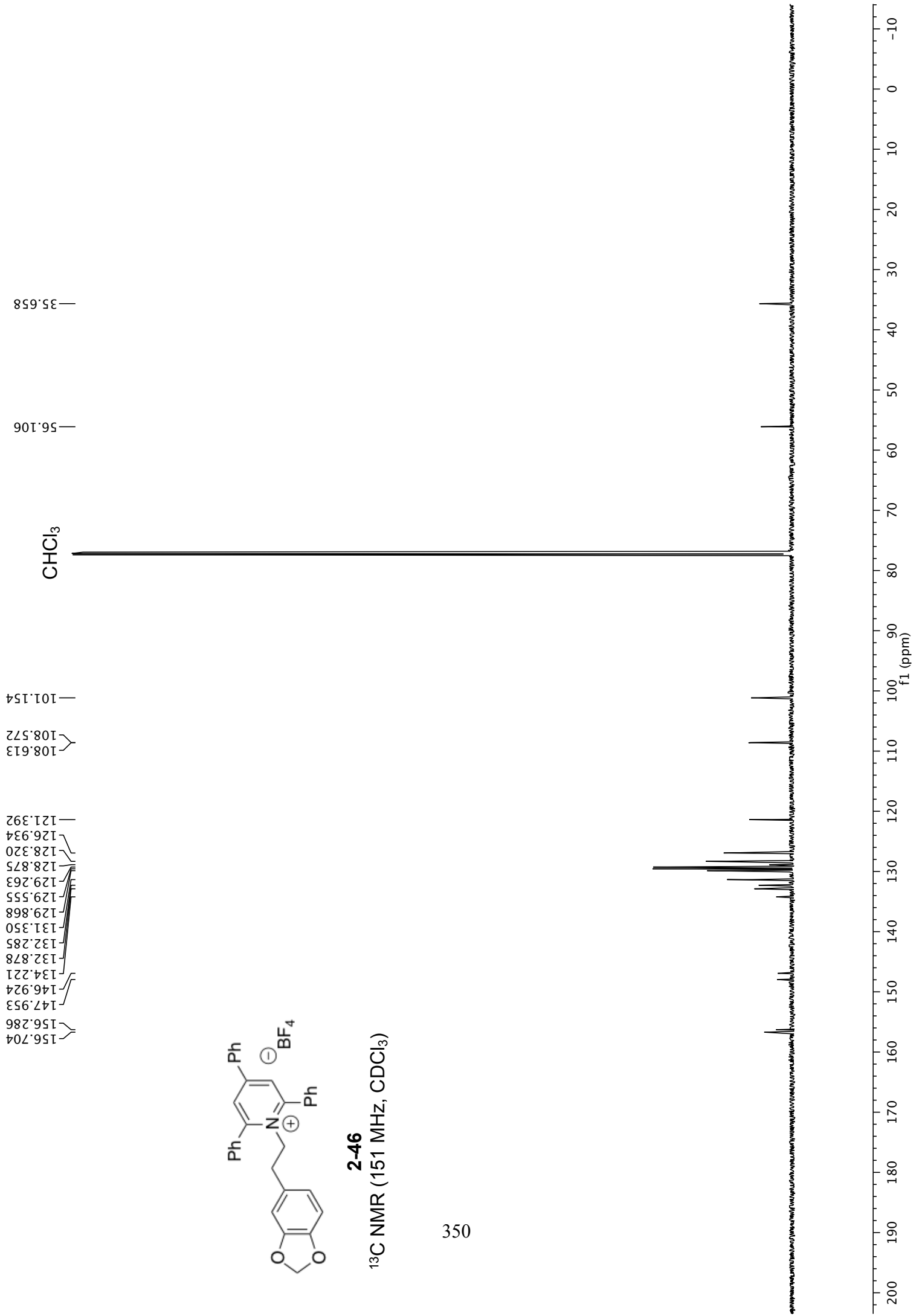
<sup>1</sup>H NMR (600 MHz, CDCl<sub>3</sub>)

7.914, 7.816, 7.805, 7.803, 7.798, 7.785, 7.677, 7.664, 7.654, 7.642, 7.632, 7.627, 7.584, 7.572, 7.560, 7.542, 7.529, 7.517, 6.489, 6.476, 5.847, 5.765, 5.763, 5.752, 5.750, 5.679, 5.677, 4.596, 4.583, 4.569, 2.629, 2.616, 2.602

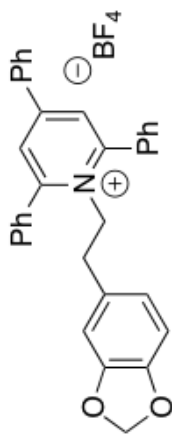
349

CHCl<sub>3</sub>





153.276  
153.329



**2-46**

<sup>19</sup>F NMR (376 MHz, CDCl<sub>3</sub>)

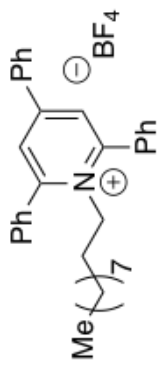
351



-40 -45 -50 -55 -60 -65 -70 -75 -80 -85 -90 -95 -100 -105 -110 -115 -120 -125 -130 -135 -140 -145 -150 -155 -160 -165 -170 -175 -180  
f1 (ppm)

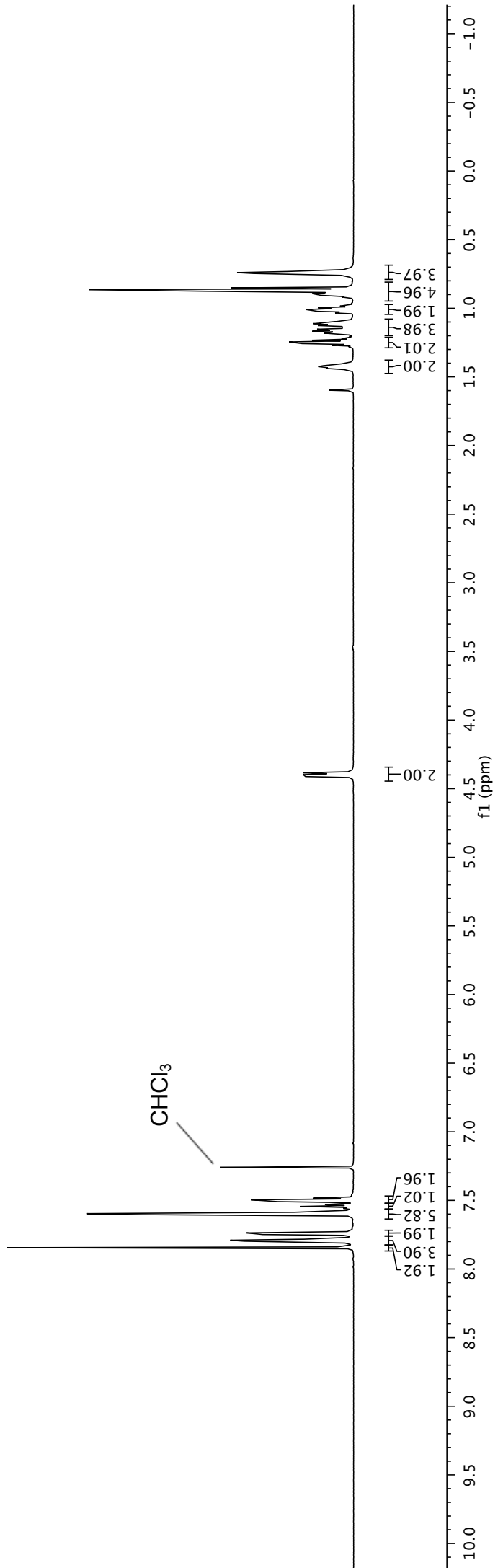
4.412  
4.403  
4.398  
4.384  
4.499  
1.438  
1.430  
1.425  
1.420  
1.411  
1.400  
1.282  
1.270  
1.257  
1.245  
1.233  
1.222  
1.191  
1.180  
1.175  
1.168  
1.165  
1.158  
1.153  
1.143  
1.137  
1.126  
1.114  
1.111  
1.104  
1.099  
1.088  
1.034  
1.023  
1.009  
0.996  
0.985  
0.918  
0.905  
0.893  
0.876  
0.863  
0.851  
0.746  
0.740  
0.734

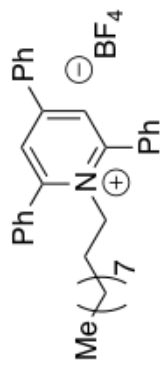
7.845  
7.801  
7.796  
7.790  
7.786  
7.749  
7.737  
7.734  
7.602  
7.596  
7.591  
7.556  
7.548  
7.544  
7.541  
7.532  
7.509  
7.496  
7.484



**2-106**  
<sup>1</sup>H NMR (600 MHz, CDCl<sub>3</sub>)

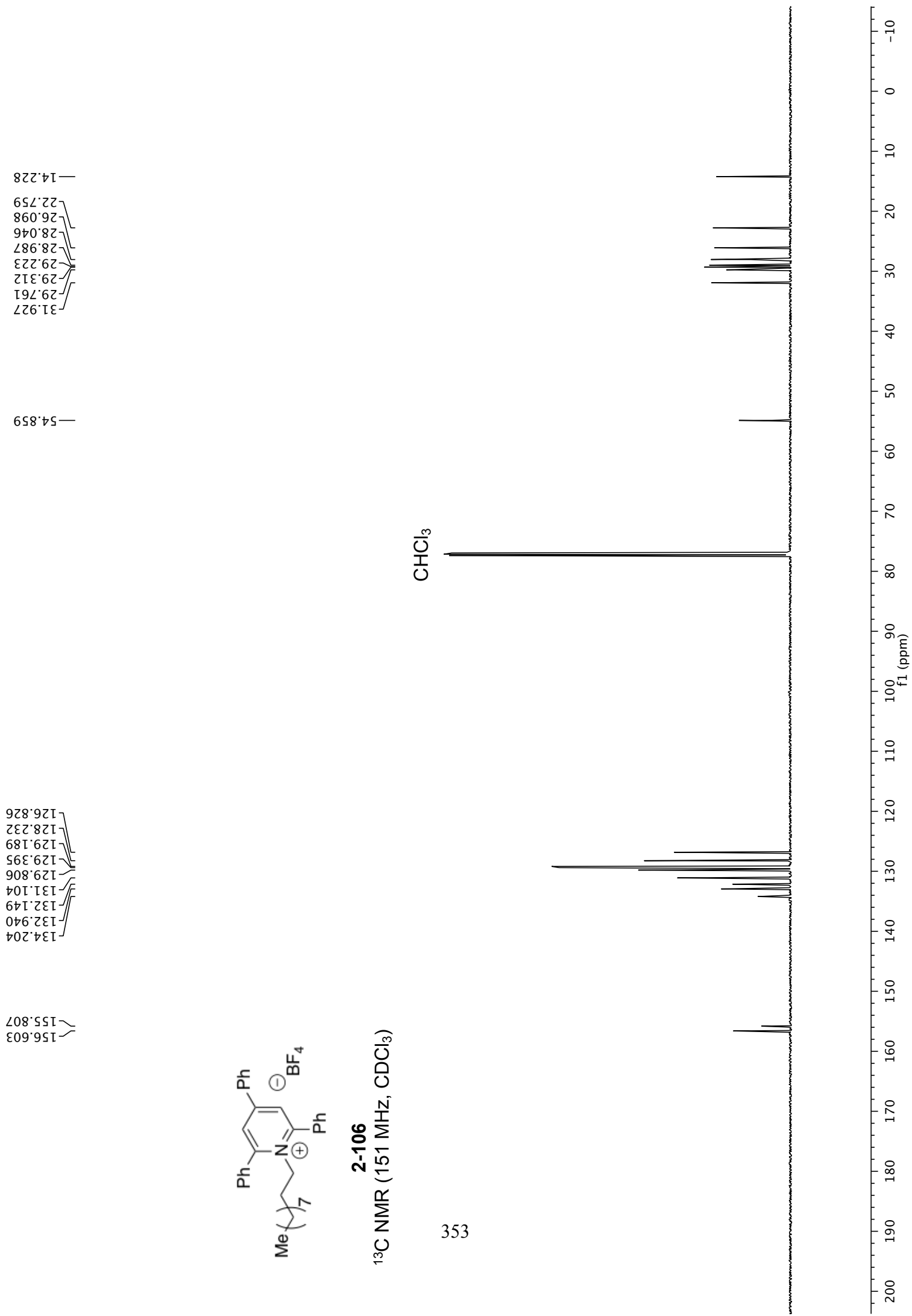
352

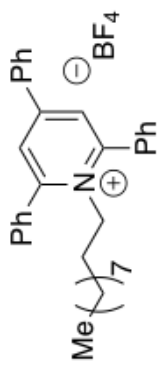




**2-106**  
 $^{13}\text{C}$  NMR (151 MHz,  $\text{CDCl}_3$ )

353



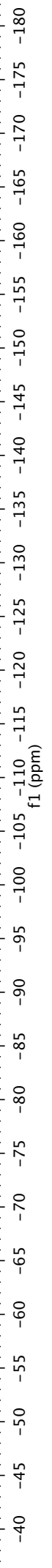


**2-106**

<sup>19</sup>F NMR (376 MHz, CDCl<sub>3</sub>)

-153.401  
-153.454

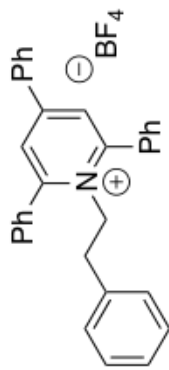
354



2.713  
2.698  
2.693  
2.688  
2.672

4.676  
4.660  
4.655  
4.650  
4.635

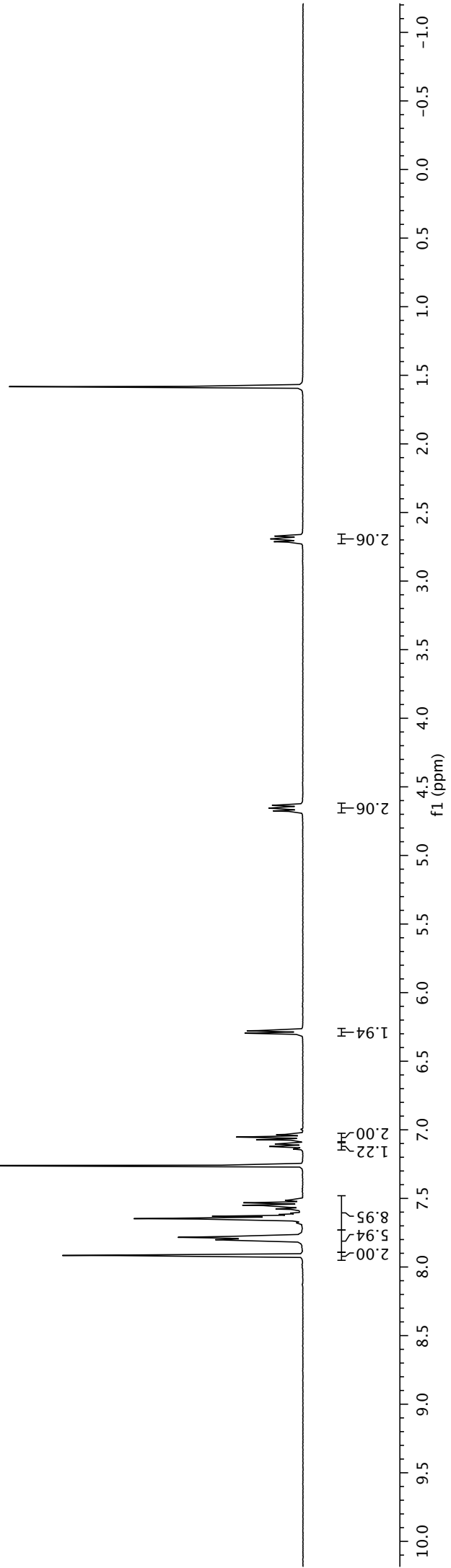
7.916  
7.807  
7.804  
7.801  
7.798  
7.793  
7.788  
7.784  
7.778  
7.658  
7.648  
7.646  
7.640  
7.630  
7.578  
7.561  
7.557  
7.550  
7.547  
7.537  
7.532  
7.470  
7.128  
7.122  
7.116  
7.104  
7.072  
7.053  
7.039  
7.035  
6.296  
6.278  
6.275

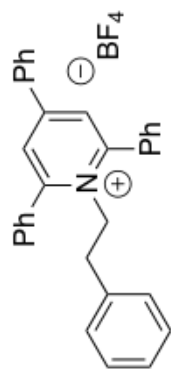


**2-103**  
<sup>1</sup>H NMR (400 MHz, CDCl<sub>3</sub>)

CHCl<sub>3</sub>

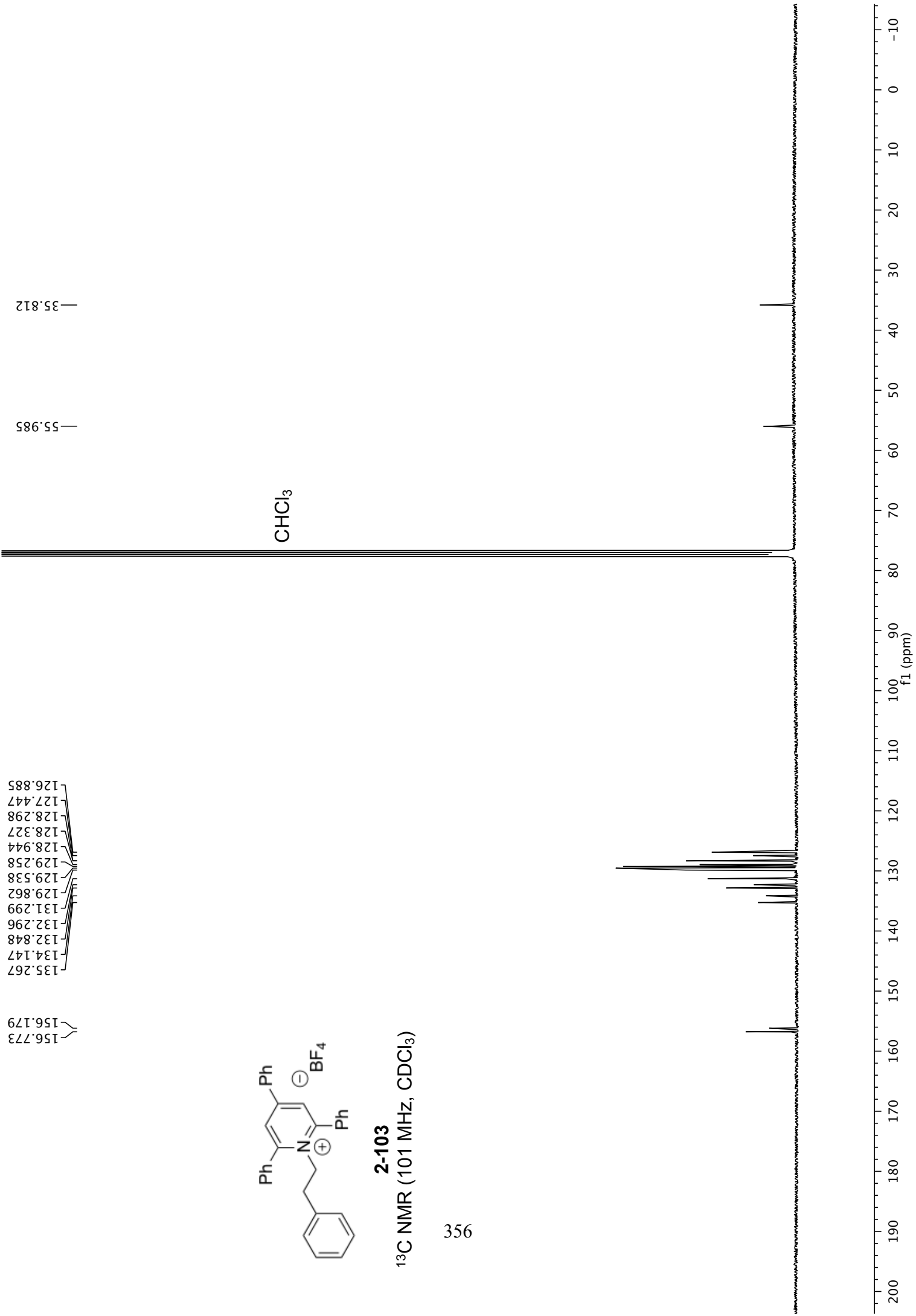
355

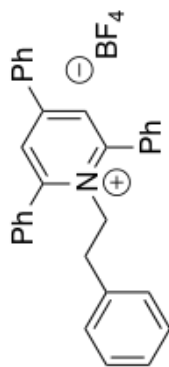




**2-103**

<sup>13</sup>C NMR (101 MHz, CDCl<sub>3</sub>)





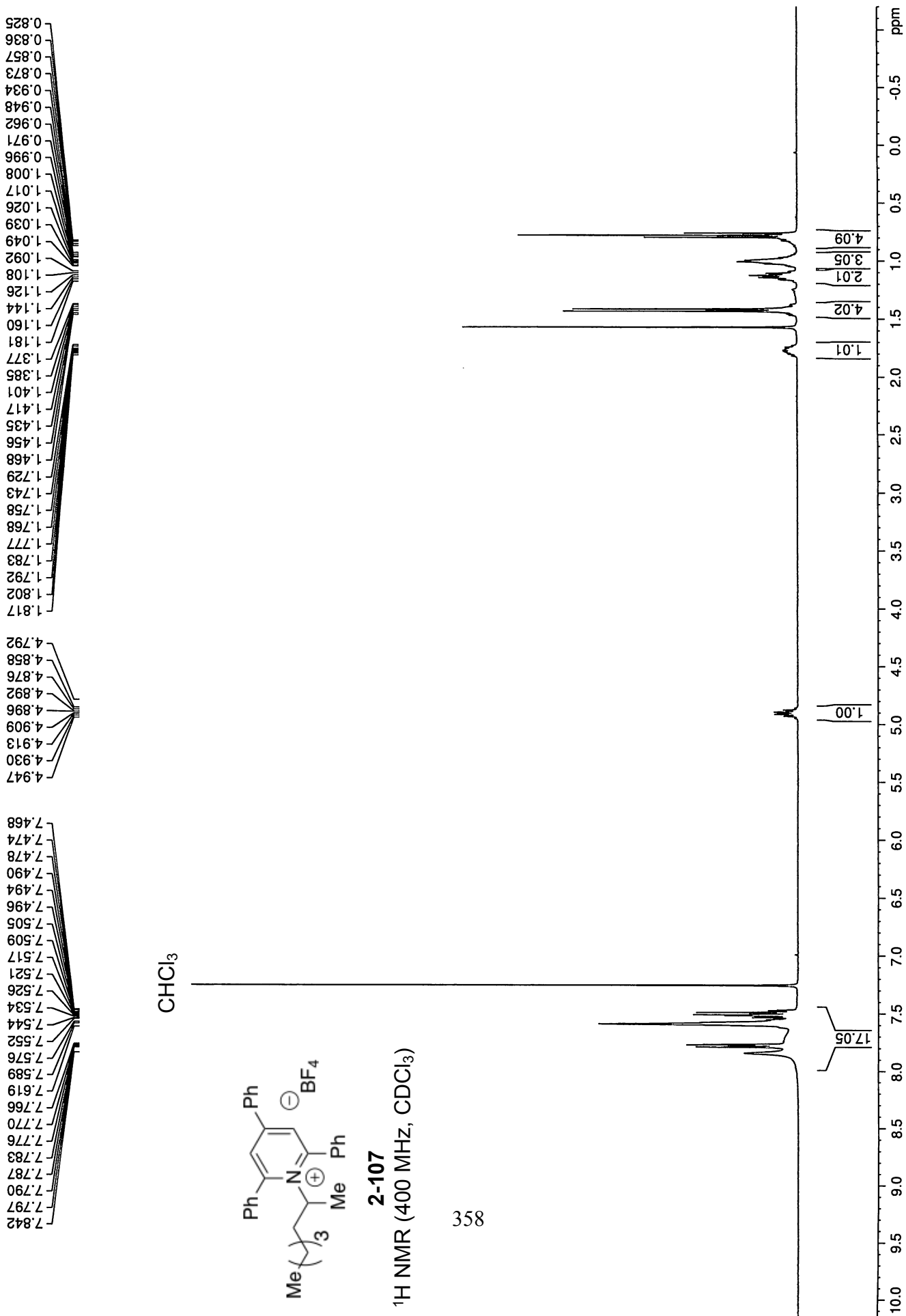
**2-103**

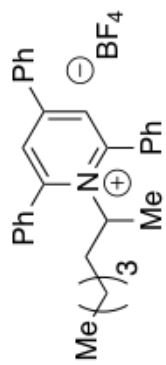
<sup>19</sup>F NMR (376 MHz, CDCl<sub>3</sub>)

357

-153.264  
-153.317

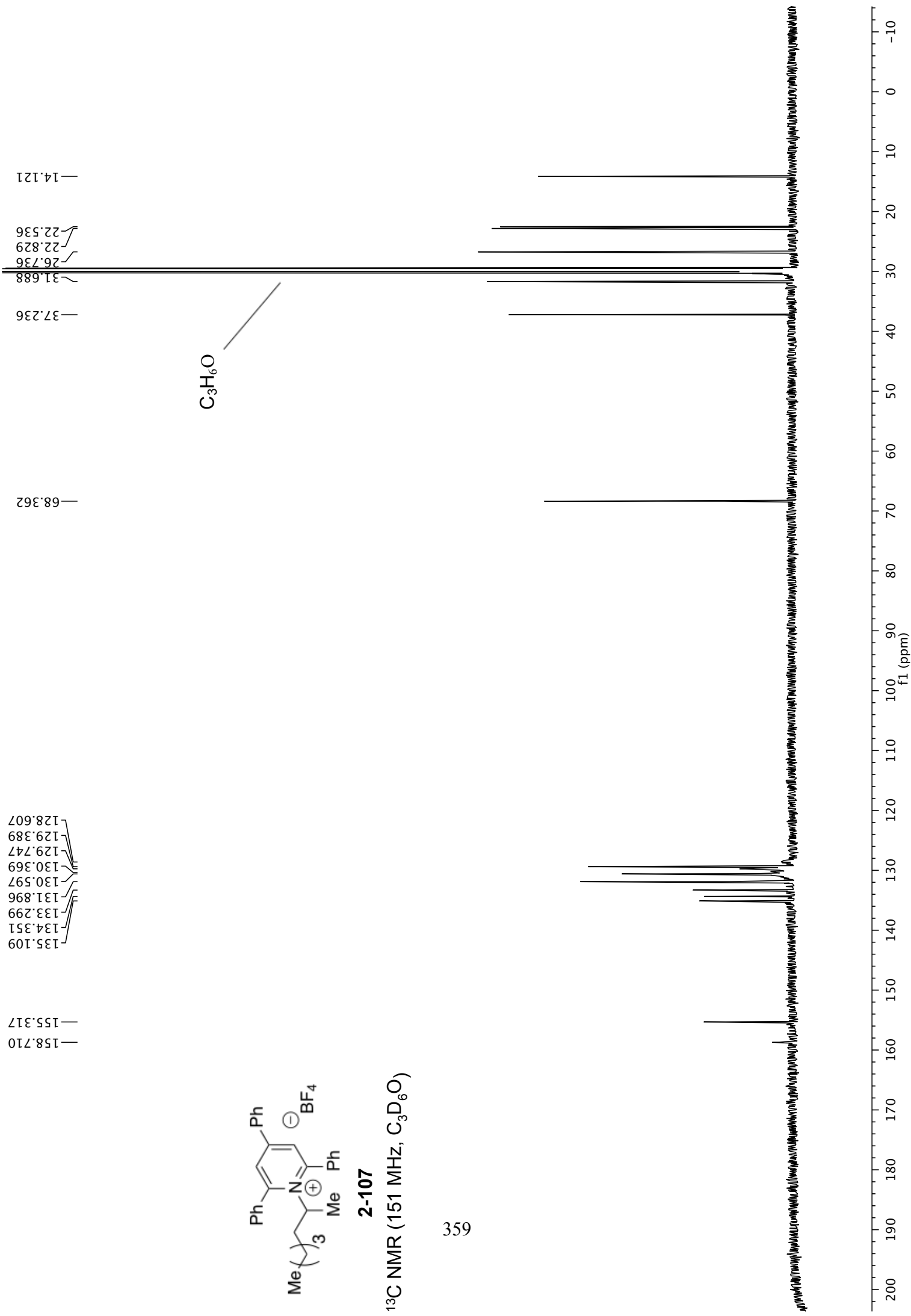
-40 -45 -50 -55 -60 -65 -70 -75 -80 -85 -90 -95 -100 -105 -110 -115 -120 -125 -130 -135 -140 -145 -150 -155 -160 -165 -170 -175 -180  
f1 (ppm)

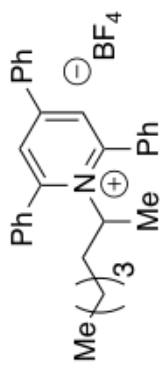




**2-107**

$^{13}\text{C}$  NMR (151 MHz,  $\text{C}_3\text{D}_6\text{O}$ )



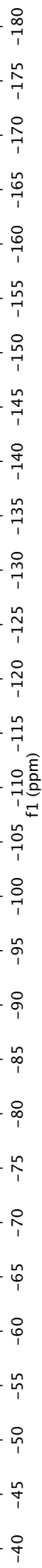


**2-107**

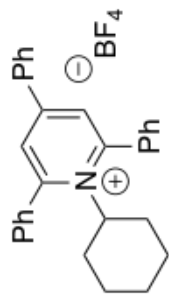
<sup>19</sup>F NMR (565 MHz, CDCl<sub>3</sub>)

360

-153.348  
-153.400

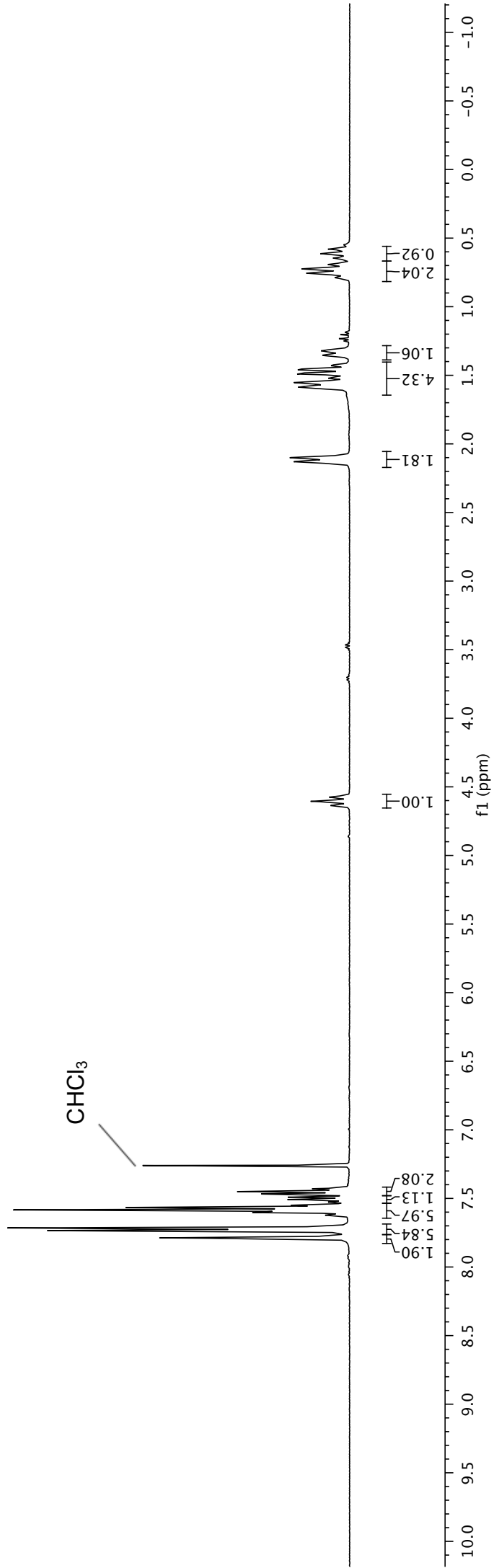


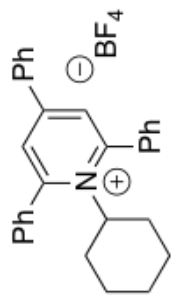
7.789  
7.786  
7.783  
7.746  
7.738  
7.734  
7.729  
7.719  
7.714  
7.626  
7.623  
7.618  
7.616  
7.604  
7.597  
7.592  
7.587  
7.583  
7.566  
7.550  
7.543  
7.528  
7.524  
7.517  
7.508  
7.502  
7.495  
7.492  
7.488  
7.470  
7.468  
7.465  
7.456  
7.451  
7.446  
7.433  
7.429  
7.425  
4.643  
4.636  
4.629  
4.613  
4.605  
4.598  
4.582  
4.575  
4.567  
2.131  
2.101  
1.595  
1.588  
1.580  
1.561  
1.553  
1.545  
1.522  
1.513  
1.492  
1.483  
1.461  
1.453  
1.430  
1.422  
1.354  
1.329  
1.320  
0.788  
0.780  
0.764  
0.756  
0.748  
0.732  
0.724  
0.715  
0.700  
0.692  
0.684  
0.645  
0.637  
0.622  
0.613  
0.604  
0.590  
0.581  
0.571



**2-108**  
**<sup>1</sup>H NMR (400 MHz, CDCl<sub>3</sub>)**

391



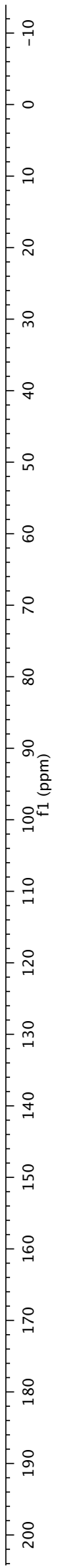


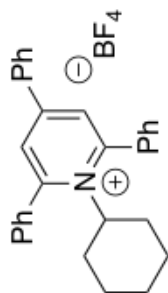
**2-108**

<sup>13</sup>C NMR (101 MHz, CDCl<sub>3</sub>)

157.134  
155.091  
134.154  
134.109  
131.950  
130.931  
129.658  
129.437  
128.888  
128.377  
128.208  
72.012  
33.676  
26.604  
24.744

CHCl<sub>3</sub>





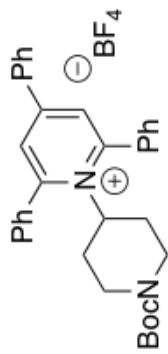
**2-108**

<sup>19</sup>F NMR (376 MHz, CDCl<sub>3</sub>)

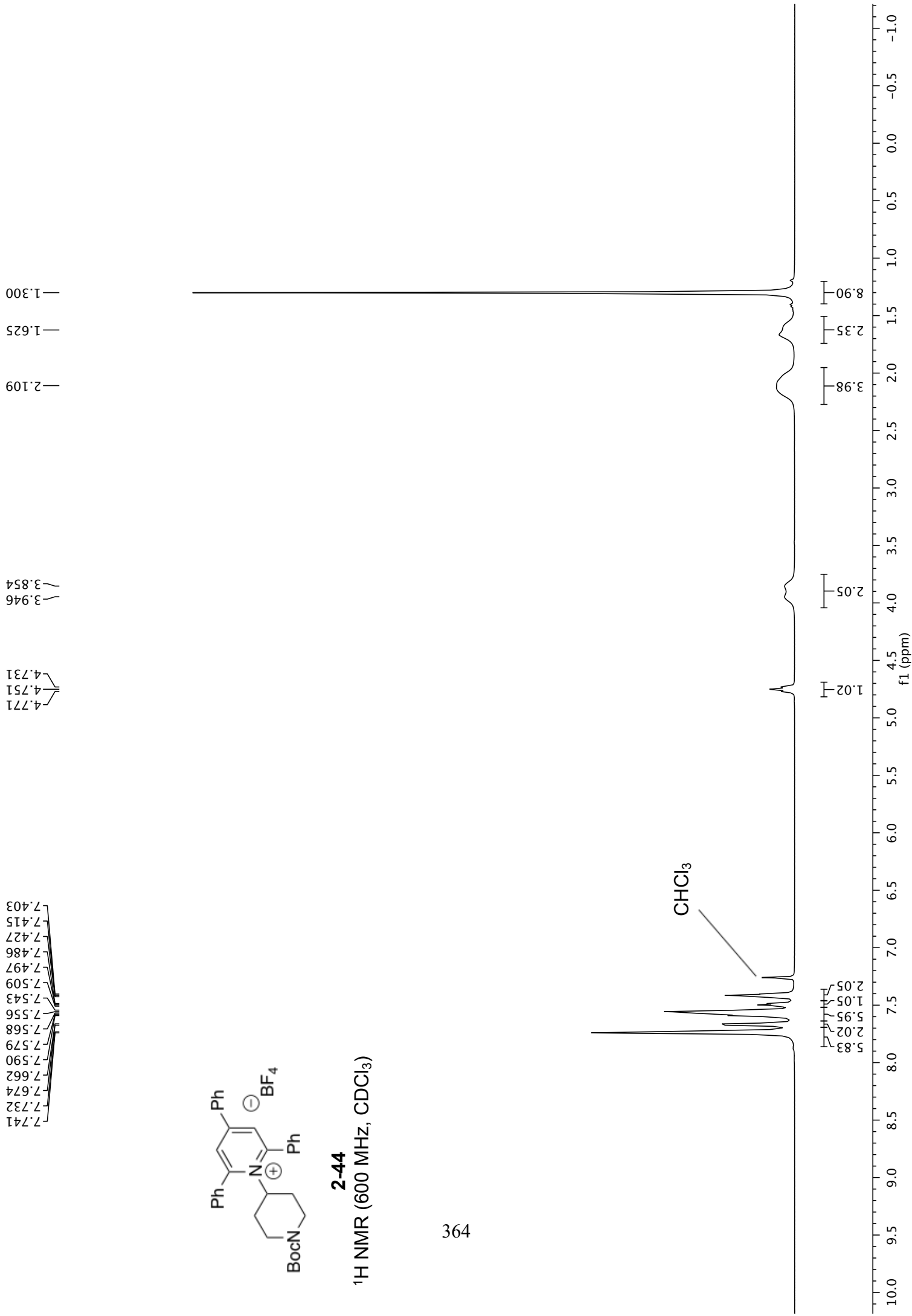
153.358  
153.411

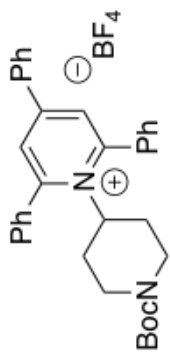
363

-40 -45 -50 -55 -60 -65 -70 -75 -80 -85 -90 -95 -100 -105 -110 -115 -120 -125 -130 -135 -140 -145 -150 -155 -160 -165 -170 -175 -180  
f1 (ppm)



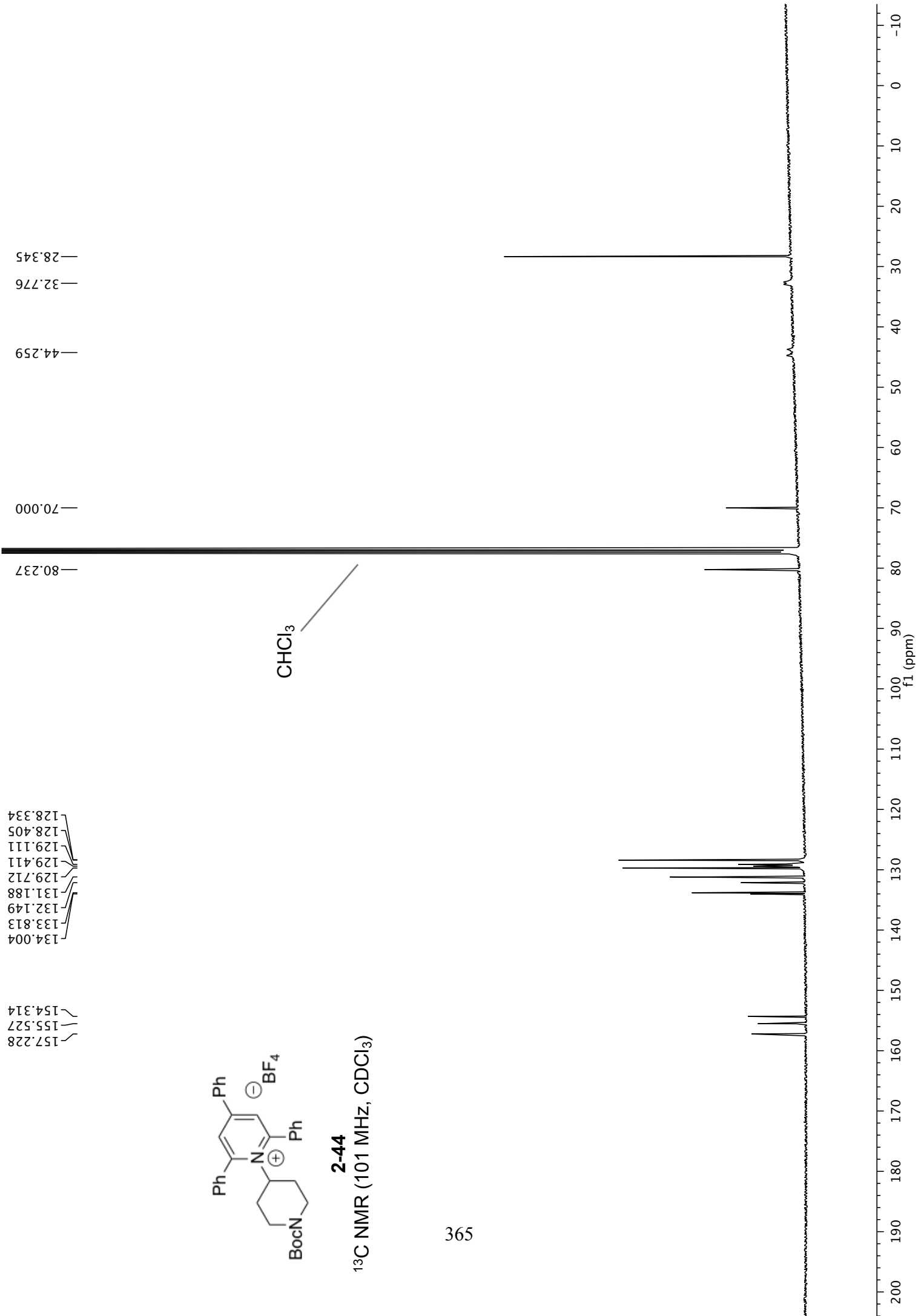
**2-44**  
 $^1\text{H}$  NMR (600 MHz,  $\text{CDCl}_3$ )

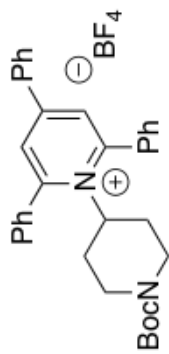




**2-44**

$^{13}\text{C}$  NMR (101 MHz,  $\text{CDCl}_3$ )





**2-44**

<sup>19</sup>F NMR (376 MHz, CDCl<sub>3</sub>)

366

-153.128  
-153.074

-40 -45 -50 -55 -60 -65 -70 -75 -80 -85 -90 -95 -100 -105 -110 -115 -120 -125 -130 -135 -140 -145 -150 -155 -160 -165 -170 -175 -180  
f1 (ppm)

7.826  
7.822  
7.813  
7.721  
7.708  
7.597  
7.593  
7.587  
7.544  
7.532  
7.519  
7.484  
7.471  
7.459

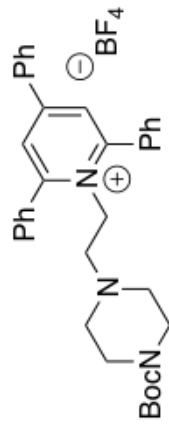
4.627  
4.614  
4.602

3.085  
3.077  
3.069

2.377  
2.365  
2.353

1.762

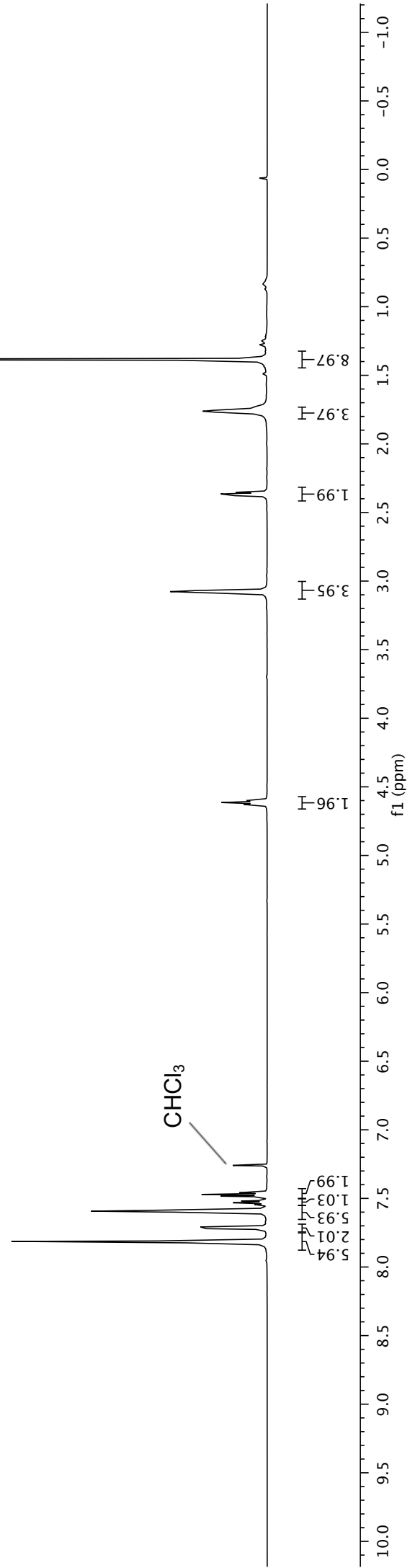
1.385

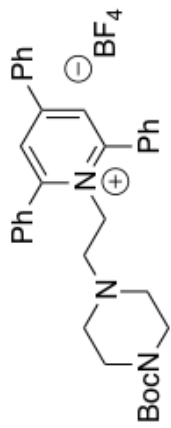


**2-45**

<sup>1</sup>H NMR (600 MHz, CDCl<sub>3</sub>)

367

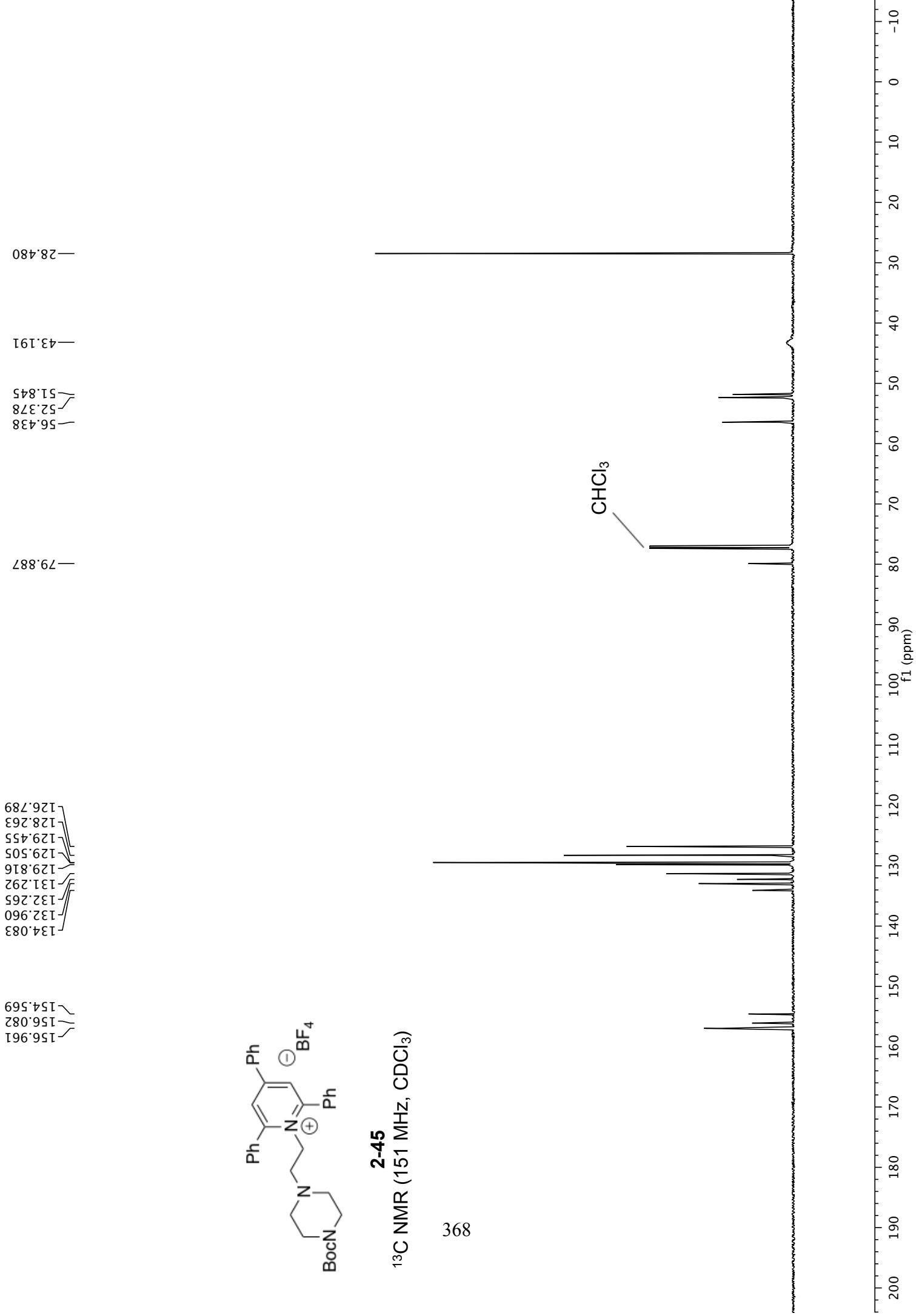


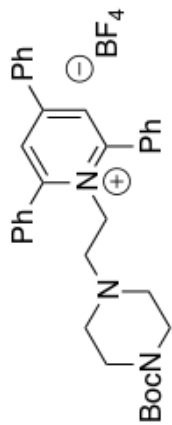


**2-45**

$^{13}\text{C}$  NMR (151 MHz,  $\text{CDCl}_3$ )

368





**2-45**

$^{19}\text{F}$  NMR (565 MHz,  $\text{CDCl}_3$ )

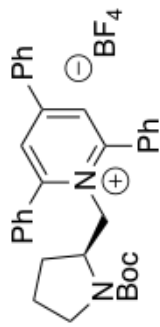
369

152.956  
153.009

-40 -45 -50 -55 -60 -65 -70 -75 -80 -85 -90 -95 -100 -105 -110 -115 -120 -125 -130 -135 -140 -145 -150 -155 -160 -165 -170 -175 -180  
f1 (ppm)

4.820  
4.815  
4.796  
4.791  
4.670  
4.651  
4.627  
3.933  
3.928  
3.915  
3.903  
3.896  
2.932  
2.921  
2.914  
2.903  
2.896  
2.885  
2.679  
2.664  
2.649  
1.534  
1.522  
1.509  
1.497  
1.477  
1.466  
1.315  
1.260  
1.248  
1.240  
1.229  
0.842  
0.830  
0.817  
0.803  
0.788

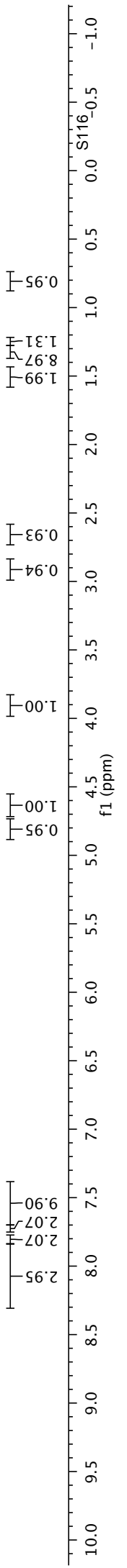
8.046  
7.914  
7.805  
7.731  
7.718  
7.638  
7.627  
7.615  
7.593  
7.581  
7.569  
7.562  
7.550  
7.537  
7.524  
7.513

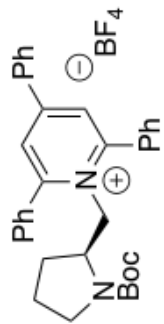


**2-109**  
<sup>1</sup>H NMR (600 MHz, CDCl<sub>3</sub>)

370

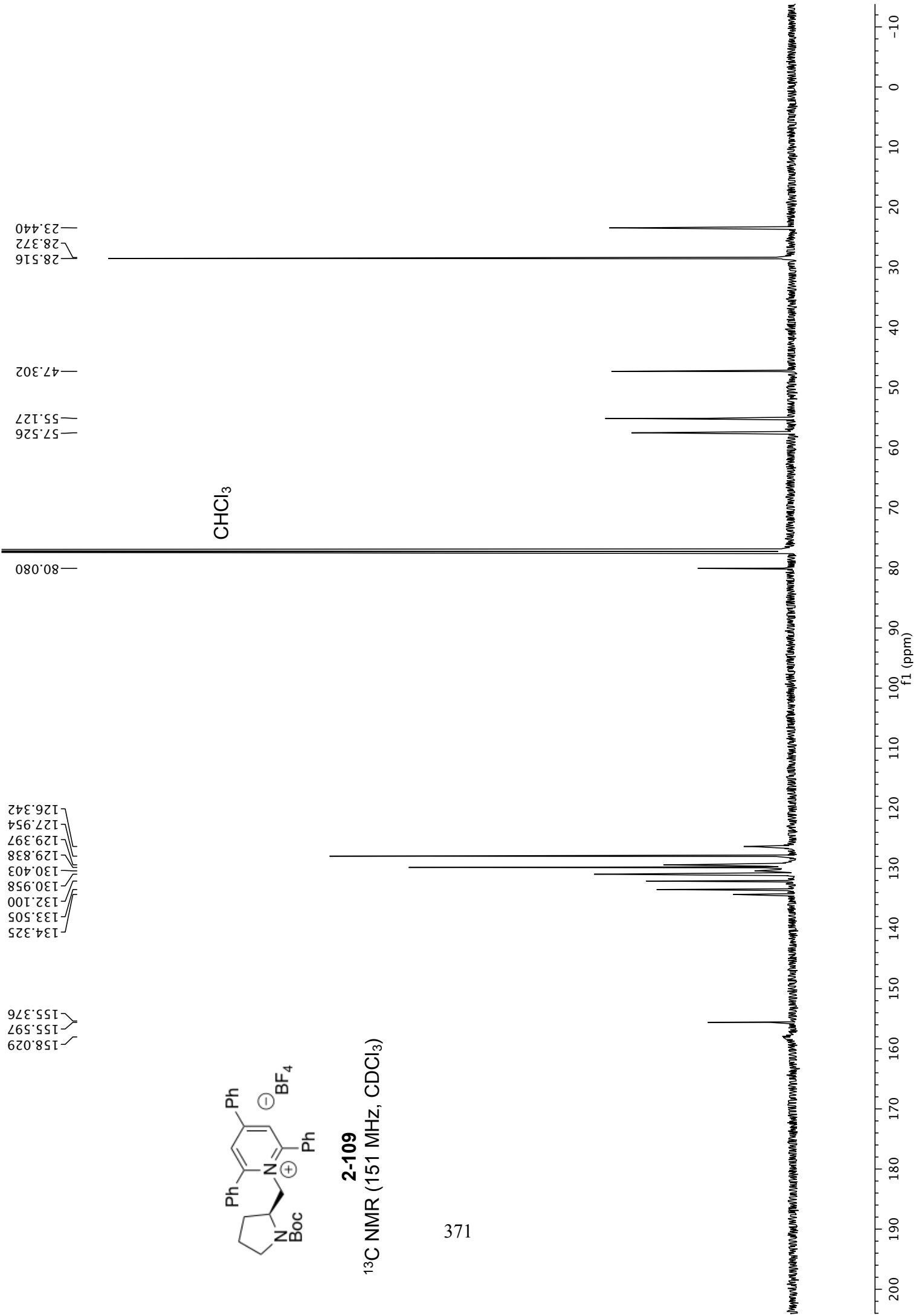
CHCl<sub>3</sub>



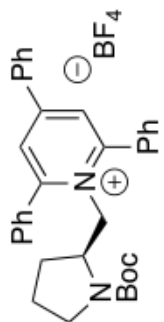


**2-109**

<sup>13</sup>C NMR (151 MHz, CDCl<sub>3</sub>)



153.078  
153.131

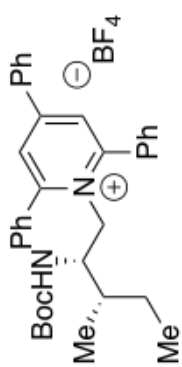


**2-109**

<sup>19</sup>F NMR (565 MHz, CDCl<sub>3</sub>)

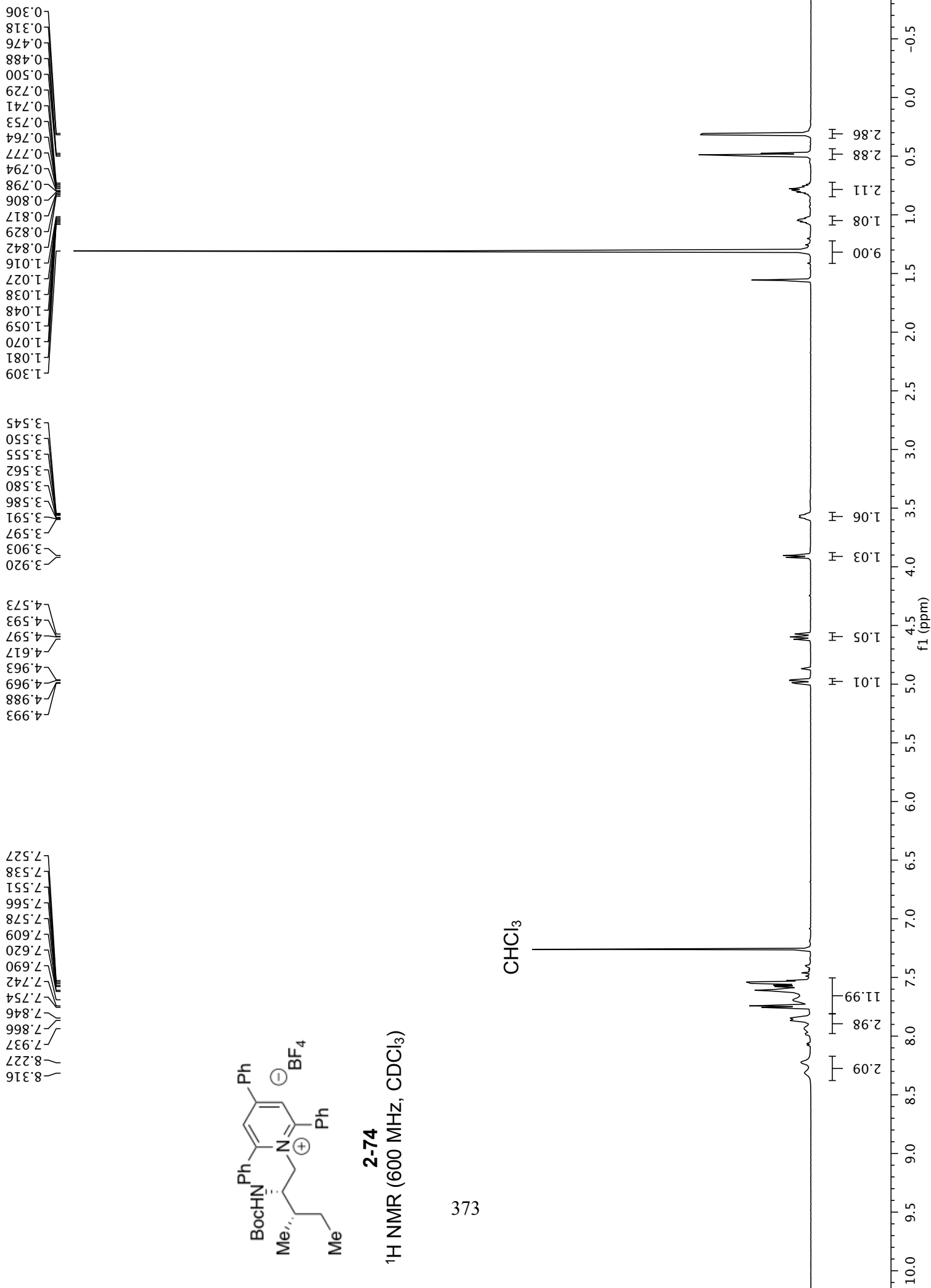
372

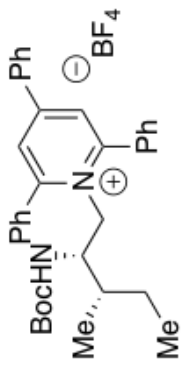
-40 -45 -50 -55 -60 -65 -70 -75 -80 -85 -90 -95 -100 -105 -110 -115 -120 -125 -130 -135 -140 -145 -150 -155 -160 -165 -170 -175 -180  
f1 (ppm)



**2-74**

<sup>1</sup>H NMR (600 MHz, CDCl<sub>3</sub>)





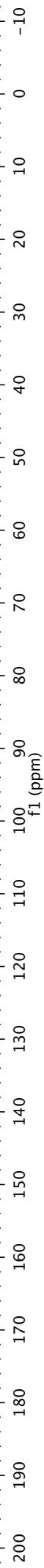
**2-74**

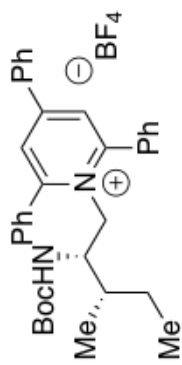
$^{13}\text{C}$  NMR (101 MHz,  $\text{CDCl}_3$ )

— 10.654  
— 14.153  
— 25.191  
— 28.497  
— 37.038  
— 53.485  
— 56.215  
— 80.225

125.982  
126.829  
127.998  
128.932  
129.275  
129.885  
130.193  
130.412  
130.749  
130.749  
131.223  
132.259  
133.098  
133.892  
134.125  
154.978  
155.822  
157.915  
158.310

$\text{CHCl}_3$





**2-74**

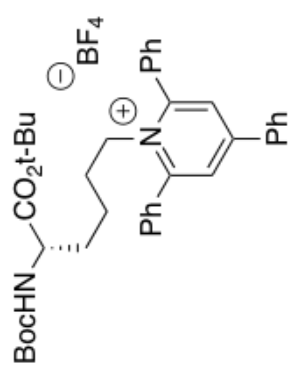
$^{19}\text{F}$  NMR (565 MHz,  $\text{CDCl}_3$ )

375

153.021  
153.073

-40 -45 -50 -55 -60 -65 -70 -75 -80 -85 -90 -95 -100 -105 -110 -115 -120 -125 -130 -135 -140 -145 -150 -155 -160 -165 -170 -175 -180  
f1 (ppm)

7.908, 7.835, 7.829, 7.823, 7.820, 7.802, 7.790, 7.788, 7.658, 7.648, 7.642, 7.640, 7.634, 7.631, 7.618, 7.602, 7.594, 7.590, 7.586, 7.578, 7.559, 7.546, 7.535, 4.847, 4.834, 4.453, 4.440, 4.427, 3.866, 3.855, 3.845, 3.832, 1.537, 1.523, 1.510, 1.498, 1.483, 1.423, 1.402, 1.306, 1.294, 1.284, 1.279, 1.267, 1.103, 1.094, 1.081, 1.072, 1.063, 1.054, 1.041, 0.880, 0.810

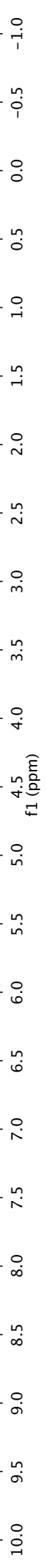


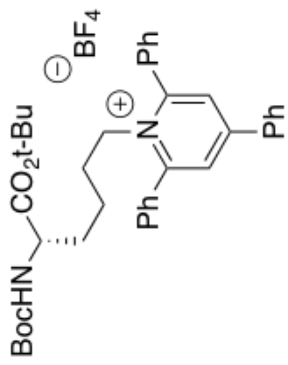
**2-78**  
<sup>1</sup>H NMR (600 MHz, CDCl<sub>3</sub>)

376

CHCl<sub>3</sub>

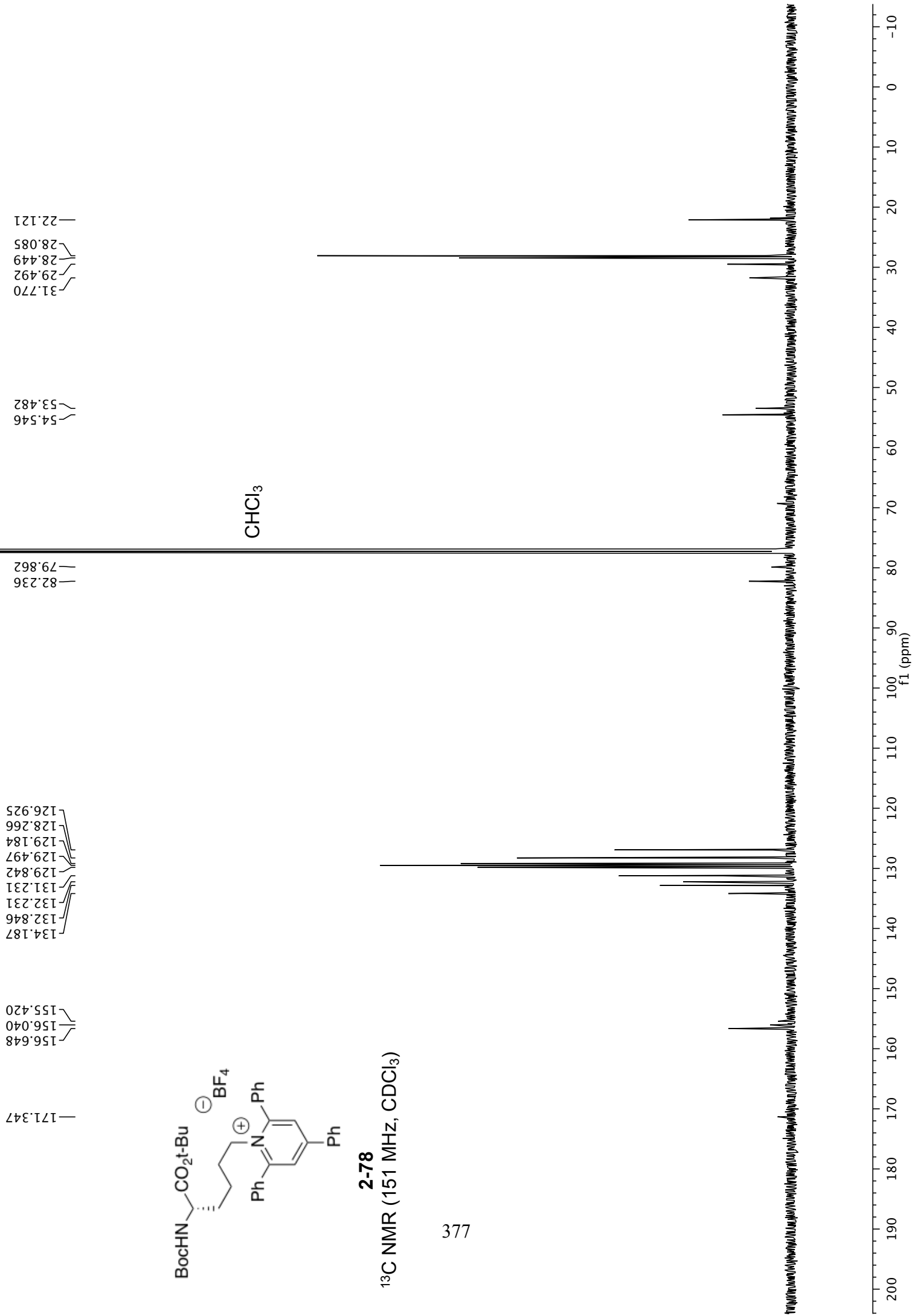
2.09, 2.00, 6.07, 6.04, 1.12, 1.12, 2.26, 1.02, 2.24, 0.99, 2.26, 8.73, 8.81, 1.32, 0.73, 1.12, 2.26

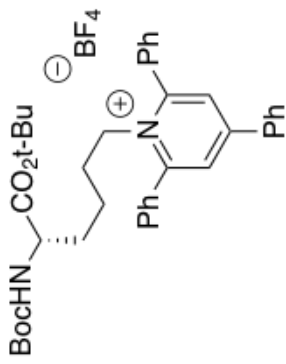




**2-78**

<sup>13</sup>C NMR (151 MHz, CDCl<sub>3</sub>)



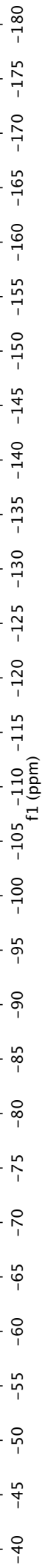


**2-78**

<sup>19</sup>F NMR (376 MHz, CDCl<sub>3</sub>)

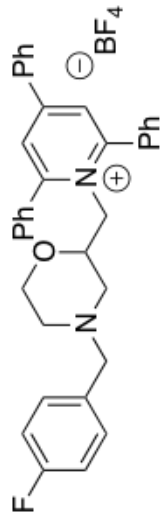
378

-153.302  
-153.355



7.889  
7.822  
7.813  
7.810  
7.805  
7.799  
7.793  
7.789  
7.601  
7.590  
7.584  
7.578  
7.572  
7.568  
7.560  
7.556  
7.547  
7.541  
7.535  
7.525  
7.519  
7.081  
7.076  
7.066  
7.059  
7.051  
7.046  
7.038  
6.973  
6.966  
6.961  
6.950  
6.944  
6.938  
6.928  
6.923  
4.757  
4.746  
4.719  
4.709  
4.585  
4.561  
4.548  
4.523  
3.640  
3.633  
3.617  
3.611  
3.604  
3.317  
3.311  
3.289  
3.283  
3.278  
3.261  
3.255  
3.245  
3.228  
3.220  
3.213  
3.206  
3.197  
3.189  
2.451  
2.446  
2.422  
2.416  
2.103  
2.076  
1.925  
1.917  
1.897  
1.889  
1.869  
1.860  
1.316  
1.293  
1.288  
1.264

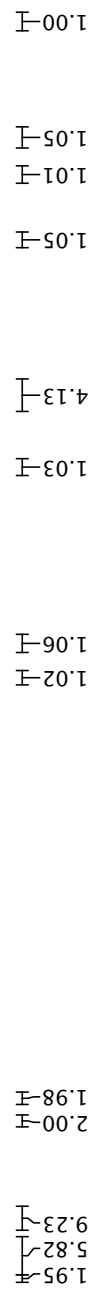
CHCl<sub>3</sub>



2-43

<sup>1</sup>H NMR (400 MHz, CDCl<sub>3</sub>)

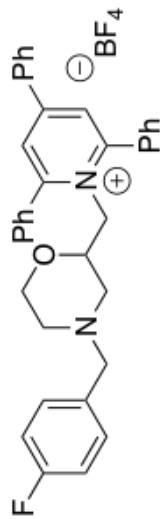
379



10.0  
9.5  
9.0  
8.5  
8.0  
7.5  
7.0  
6.5  
6.0  
5.5  
5.0  
4.5  
4.0  
3.5  
3.0  
2.5  
2.0  
1.5  
1.0  
0.5  
0.0  
-0.5  
-1.0

1.95  
5.82  
9.23  
2.00  
1.98  
1.02  
1.06  
1.03  
4.13  
1.05  
1.01  
1.05  
1.00

f1 (ppm)



**2-43**

$^{13}\text{C}$  NMR (151 MHz,  $\text{CDCl}_3$ )

72.465  
66.604  
61.947  
56.311  
55.642  
52.227

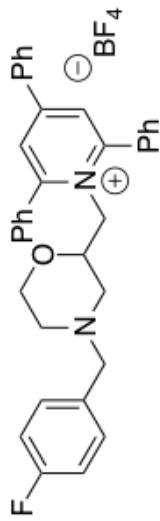
133.979  
133.193  
132.595  
132.383  
131.087  
130.678  
130.626  
129.891  
129.625  
129.307  
128.195  
126.275  
115.320  
115.178

163.046  
161.419  
157.758  
155.748

$\text{CHCl}_3$

380





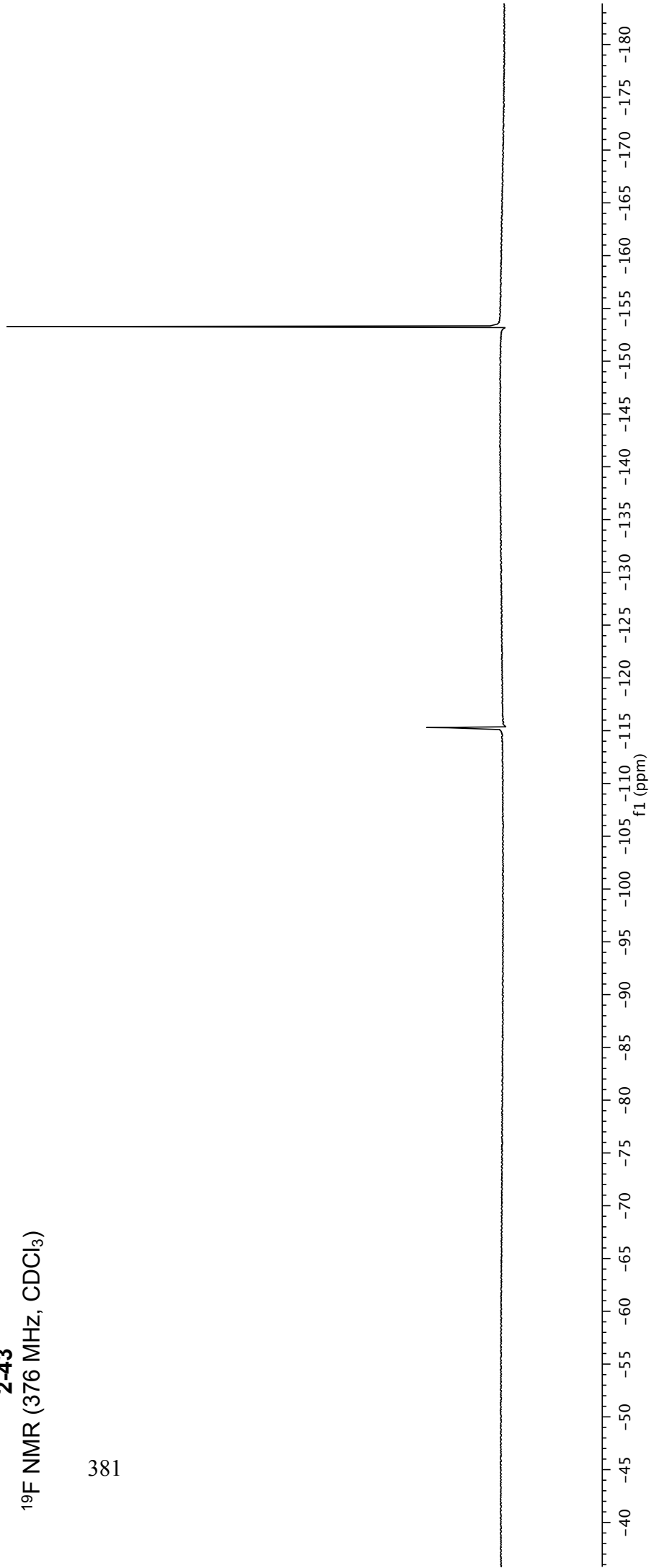
**2-43**

<sup>19</sup>F NMR (376 MHz, CDCl<sub>3</sub>)

381

—153.222  
—153.275

—115.296



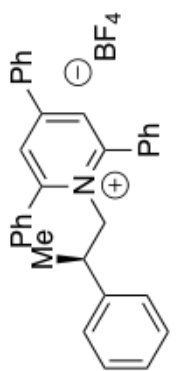
0.83  
0.81

2.75  
2.74  
2.72  
2.72  
2.70  
2.70  
2.68  
2.66

5.04  
5.03  
5.01  
5.00  
4.83  
4.81  
4.80  
4.77

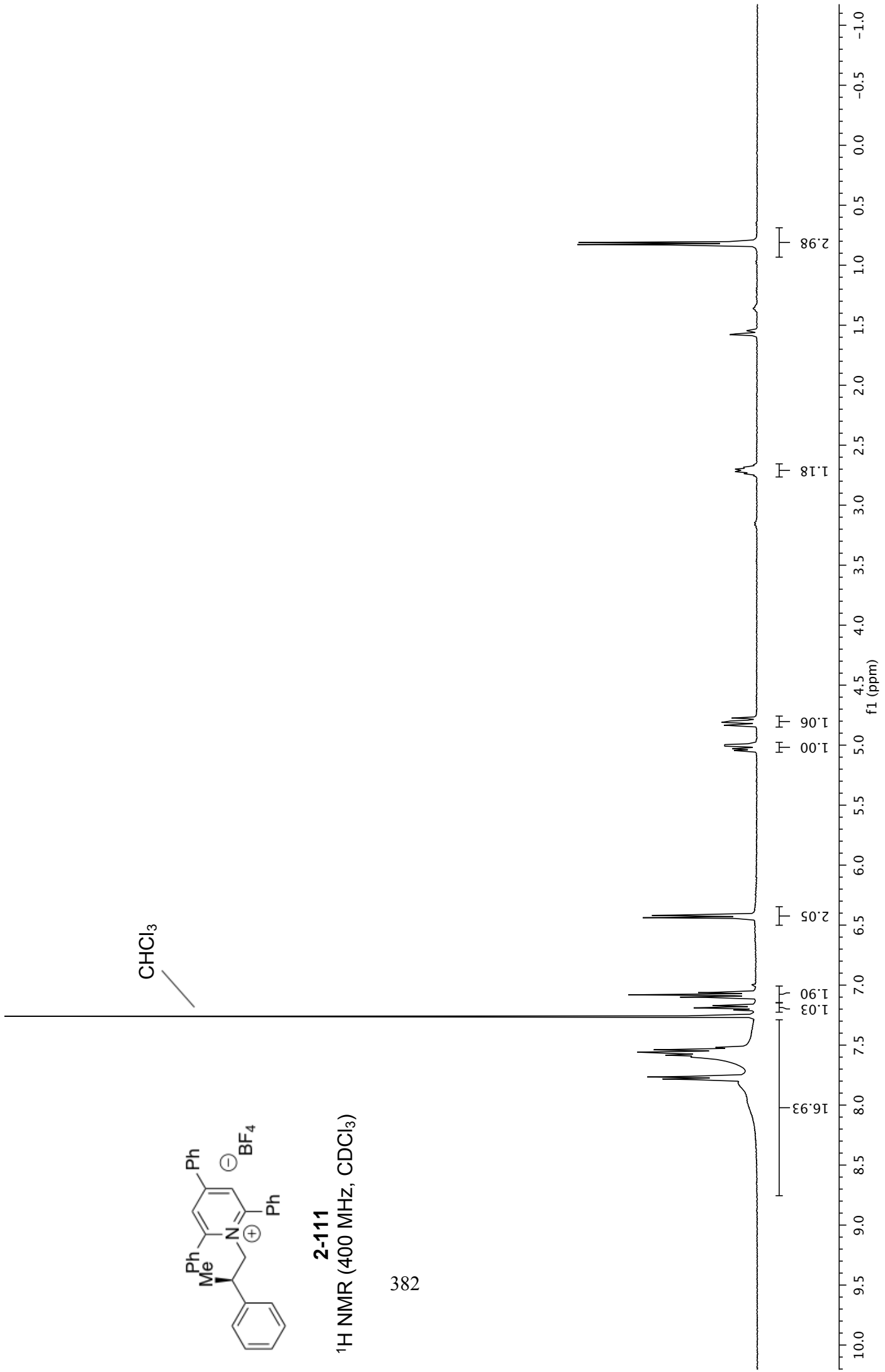
7.97  
7.82  
7.78  
7.77  
7.60  
7.58  
7.57  
7.56  
7.54  
7.52  
7.21  
7.19  
7.17  
7.10  
7.08  
7.06  
6.44  
6.42

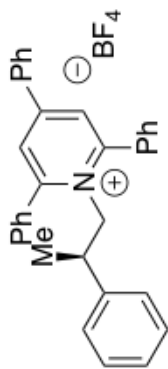
CHCl<sub>3</sub>



**2-111**  
<sup>1</sup>H NMR (400 MHz, CDCl<sub>3</sub>)

382

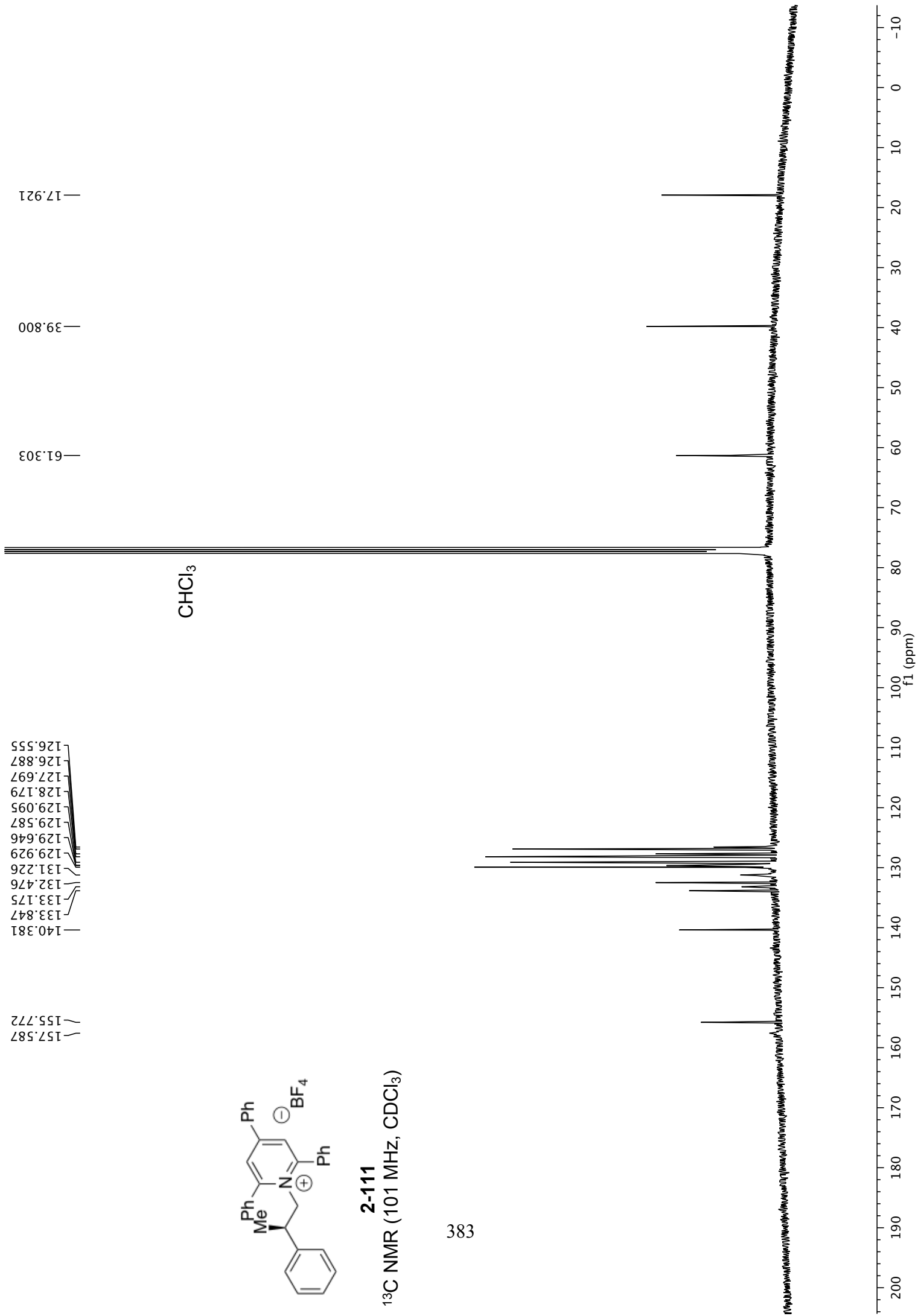


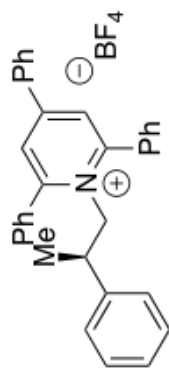


**2-111**

<sup>13</sup>C NMR (101 MHz, CDCl<sub>3</sub>)

383





**2-111**

<sup>19</sup>F NMR (565 MHz, CDCl<sub>3</sub>)

384

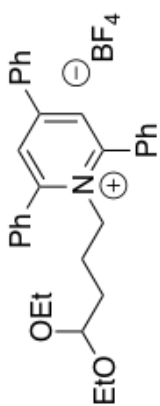
153.127  
153.178

-40 -45 -50 -55 -60 -65 -70 -75 -80 -85 -90 -95 -100 -105 -110 -115 -120 -125 -130 -135 -140 -145 -150 -155 -160 -165 -170 -175 -180

f1 (ppm)

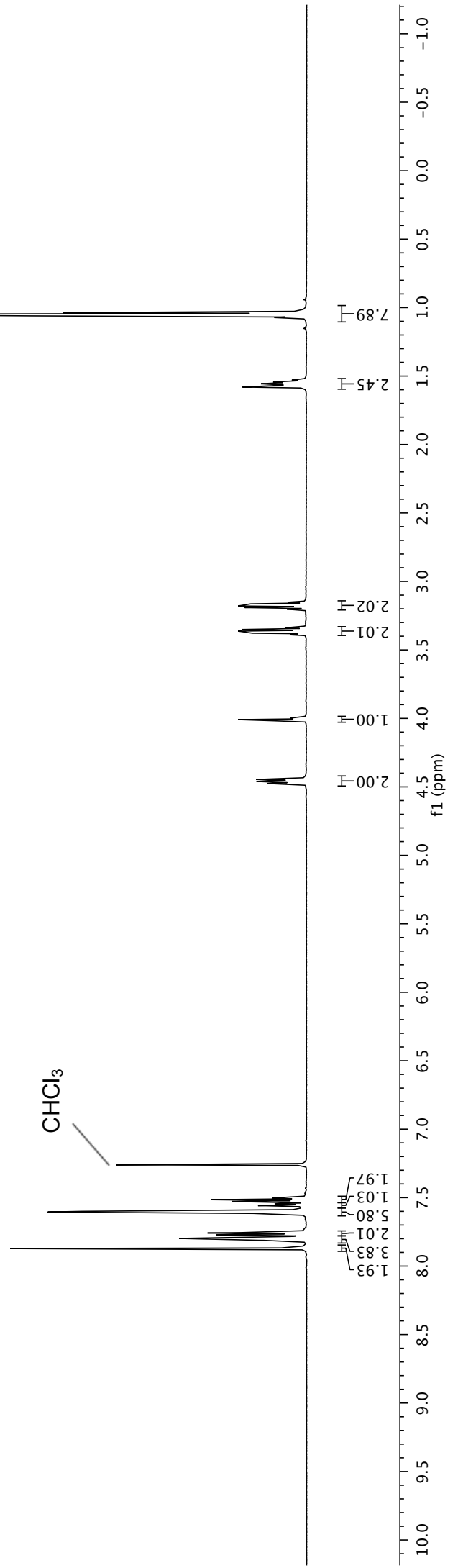
1.037  
1.049  
1.061  
1.072  
1.530  
1.539  
1.544  
1.551  
1.557  
1.562  
1.570  
3.152  
3.164  
3.167  
3.175  
3.179  
3.187  
3.191  
3.203  
3.339  
3.351  
3.354  
3.363  
3.366  
3.374  
3.378  
3.390  
4.000  
4.009  
4.018  
4.446  
4.460  
4.474

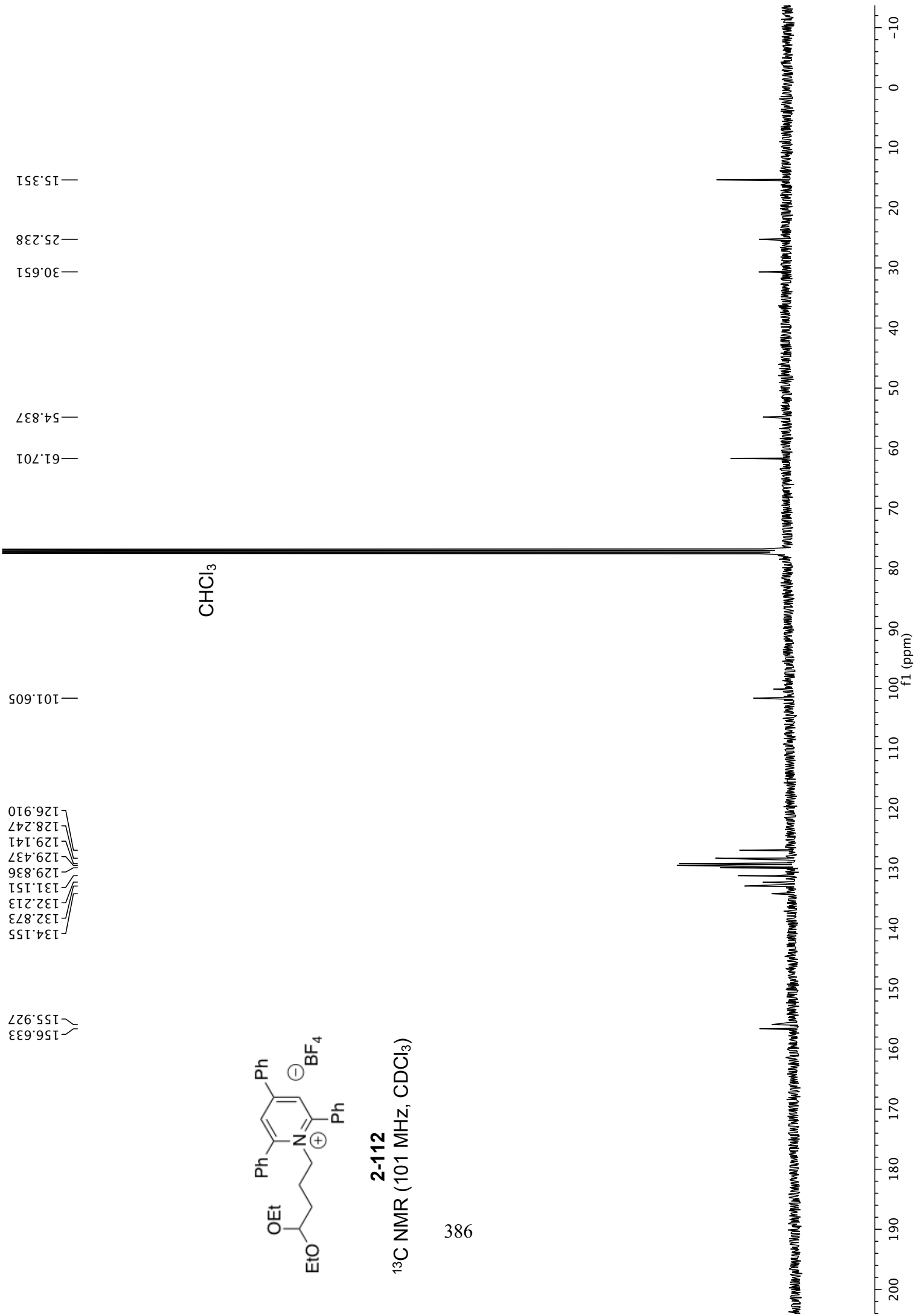
7.260  
7.503  
7.506  
7.515  
7.528  
7.546  
7.555  
7.558  
7.563  
7.571  
7.600  
7.605  
7.610  
7.756  
7.758  
7.770  
7.794  
7.798  
7.804  
7.809  
7.872

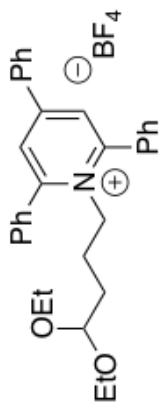


**2-112**  
<sup>1</sup>H NMR (600 MHz, CDCl<sub>3</sub>)

385







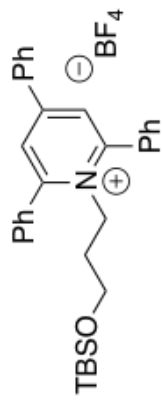
**2-112**

<sup>19</sup>F NMR (376 MHz, CDCl<sub>3</sub>)

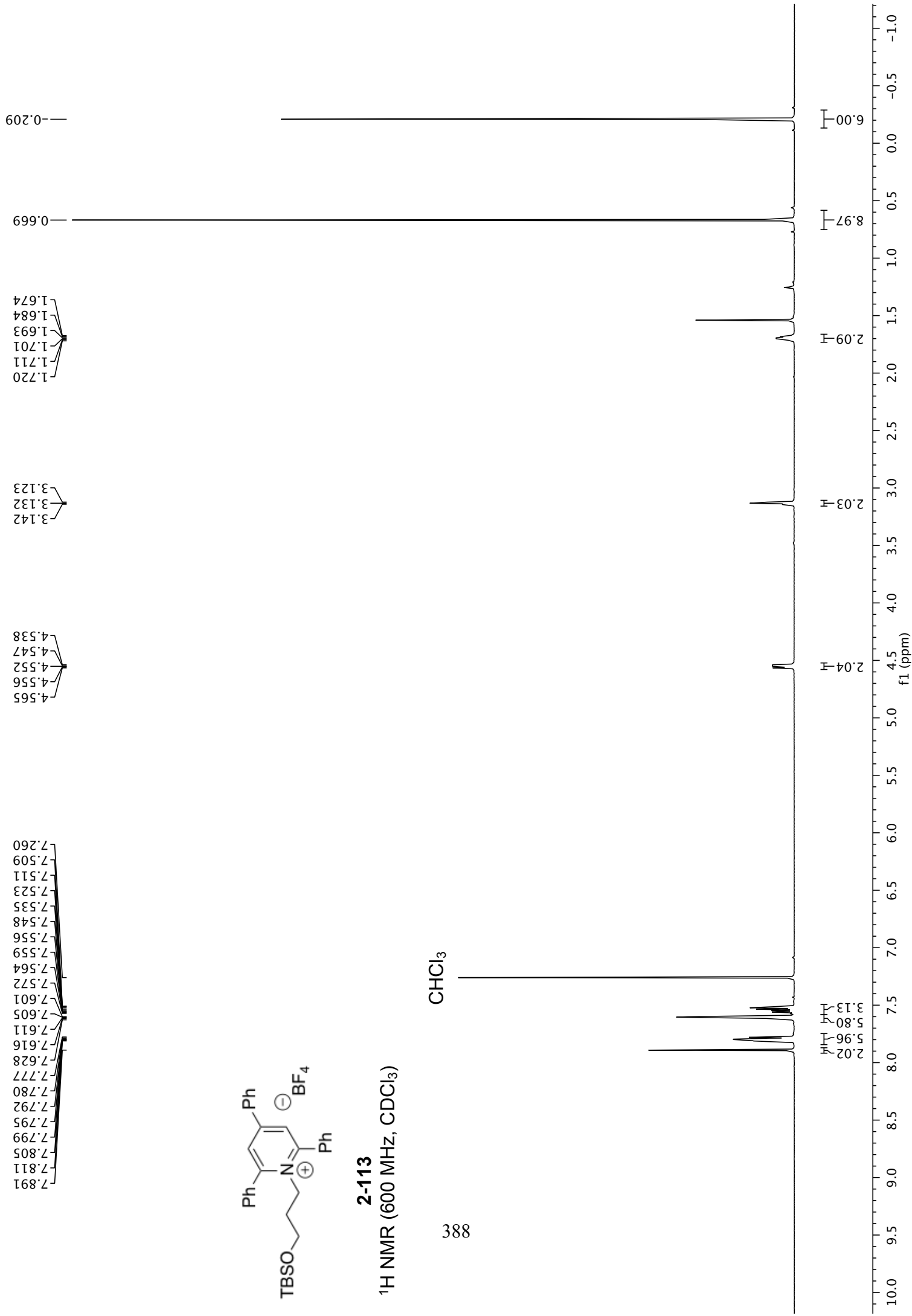
387

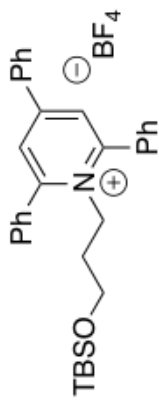
-153.411  
-153.464

-40 -45 -50 -55 -60 -65 -70 -75 -80 -85 -90 -95 -100 -105 -110 -115 -120 -125 -130 -135 -140 -145 -150 -155 -160 -165 -170 -175 -180  
f1 (ppm)

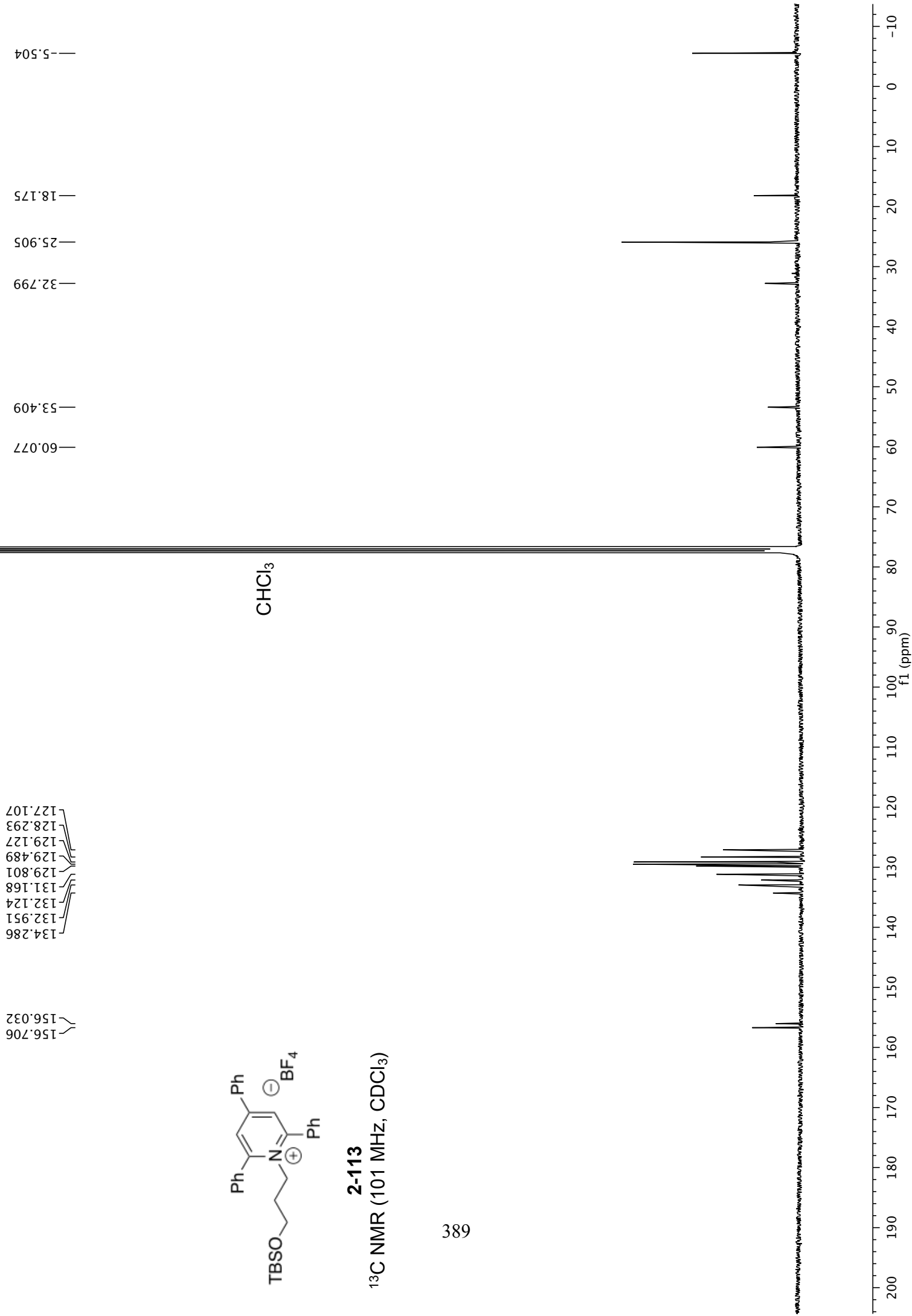


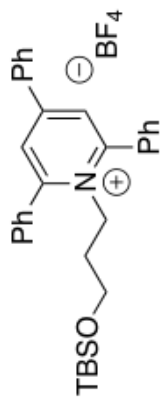
**2-113**  
<sup>1</sup>H NMR (600 MHz, CDCl<sub>3</sub>)





**2-113**  
<sup>13</sup>C NMR (101 MHz, CDCl<sub>3</sub>)





**2-113**

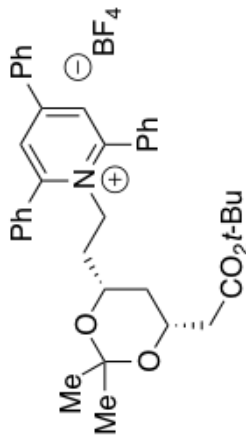
<sup>19</sup>F NMR (376 MHz, CDCl<sub>3</sub>)

390

-153.425  
-153.477

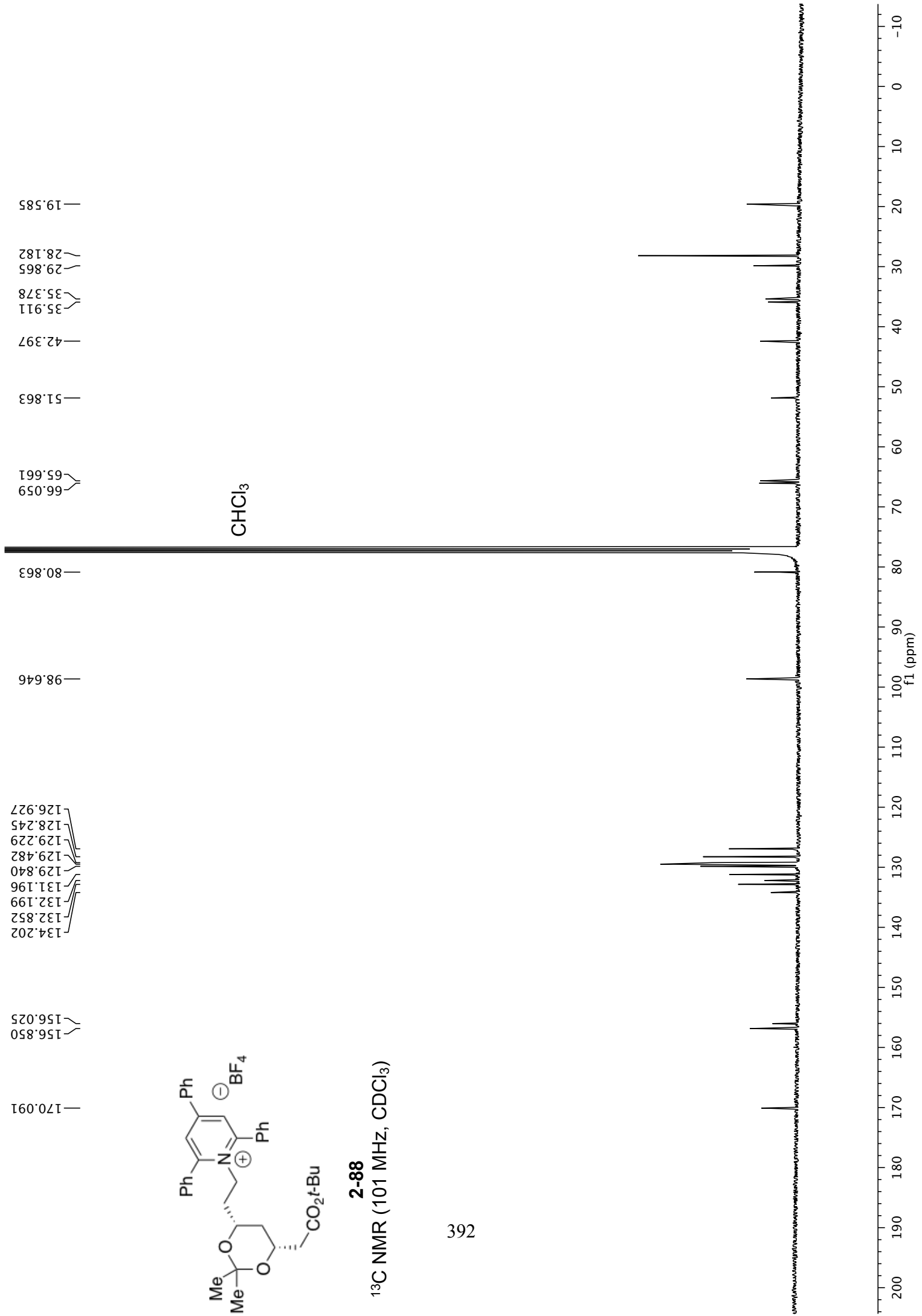
-40 -45 -50 -55 -60 -65 -70 -75 -80 -85 -90 -95 -100 -105 -110 -115 -120 -125 -130 -135 -140 -145 -150 -155 -160 -165 -170 -175 -180  
f1 (ppm)

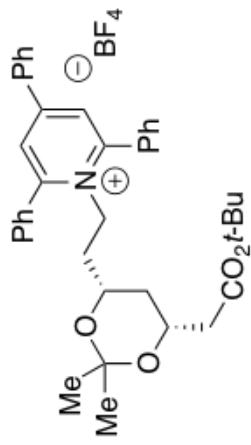




**2-88**

$^{13}\text{C}$  NMR (101 MHz,  $\text{CDCl}_3$ )





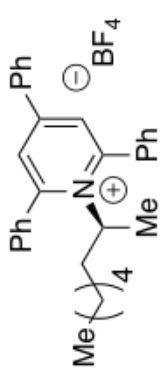
**2-88**

$^{19}\text{F}$  NMR (376 MHz,  $\text{CDCl}_3$ )

393

-153.319  
-153.372

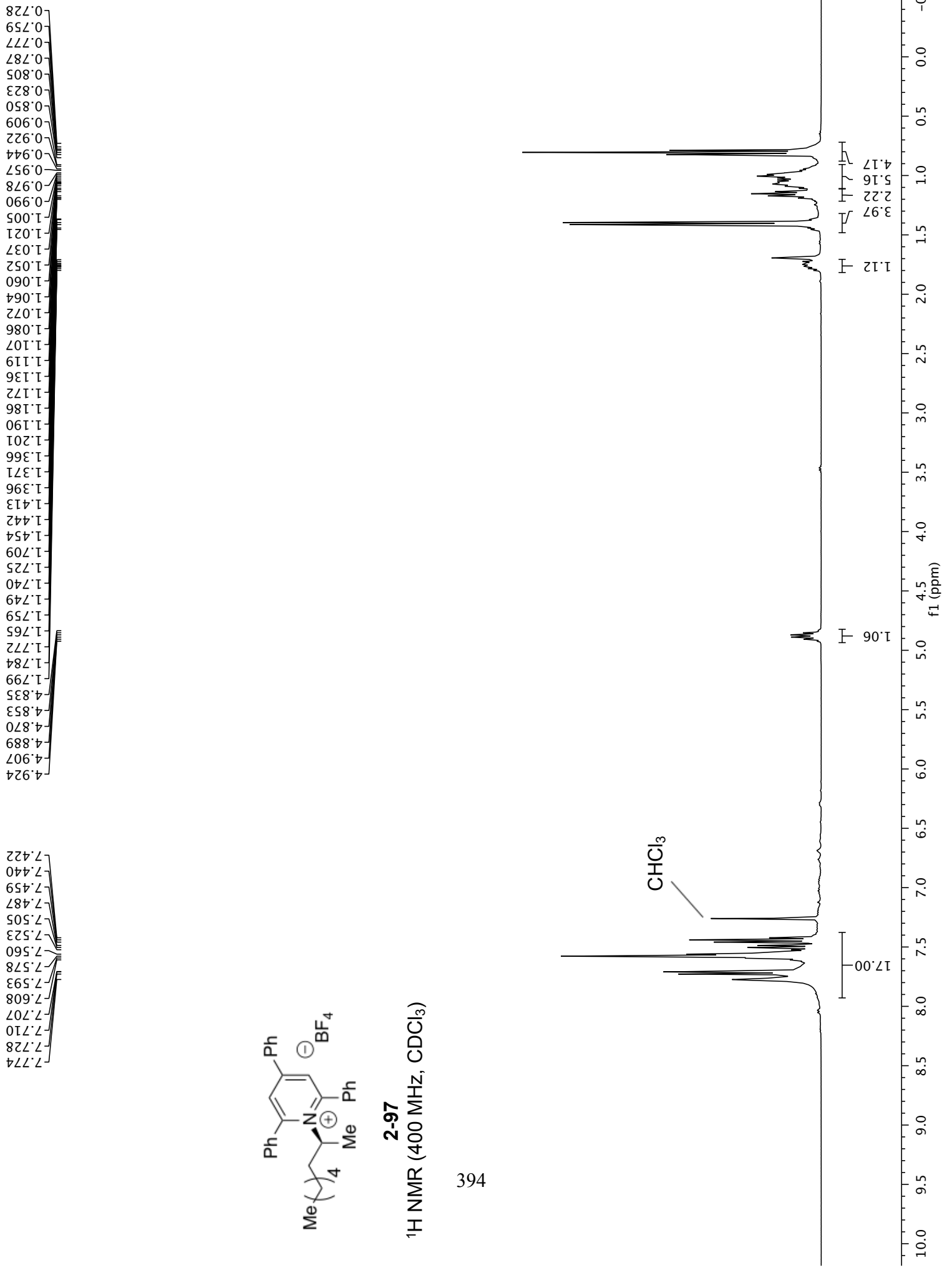
-40 -45 -50 -55 -60 -65 -70 -75 -80 -85 -90 -95 -100 -105 -110 -115 -120 -125 -130 -135 -140 -145 -150 -155 -160 -165 -170 -175 -180  
f1 (ppm)

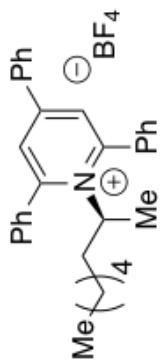


**2-97**

<sup>1</sup>H NMR (400 MHz, CDCl<sub>3</sub>)

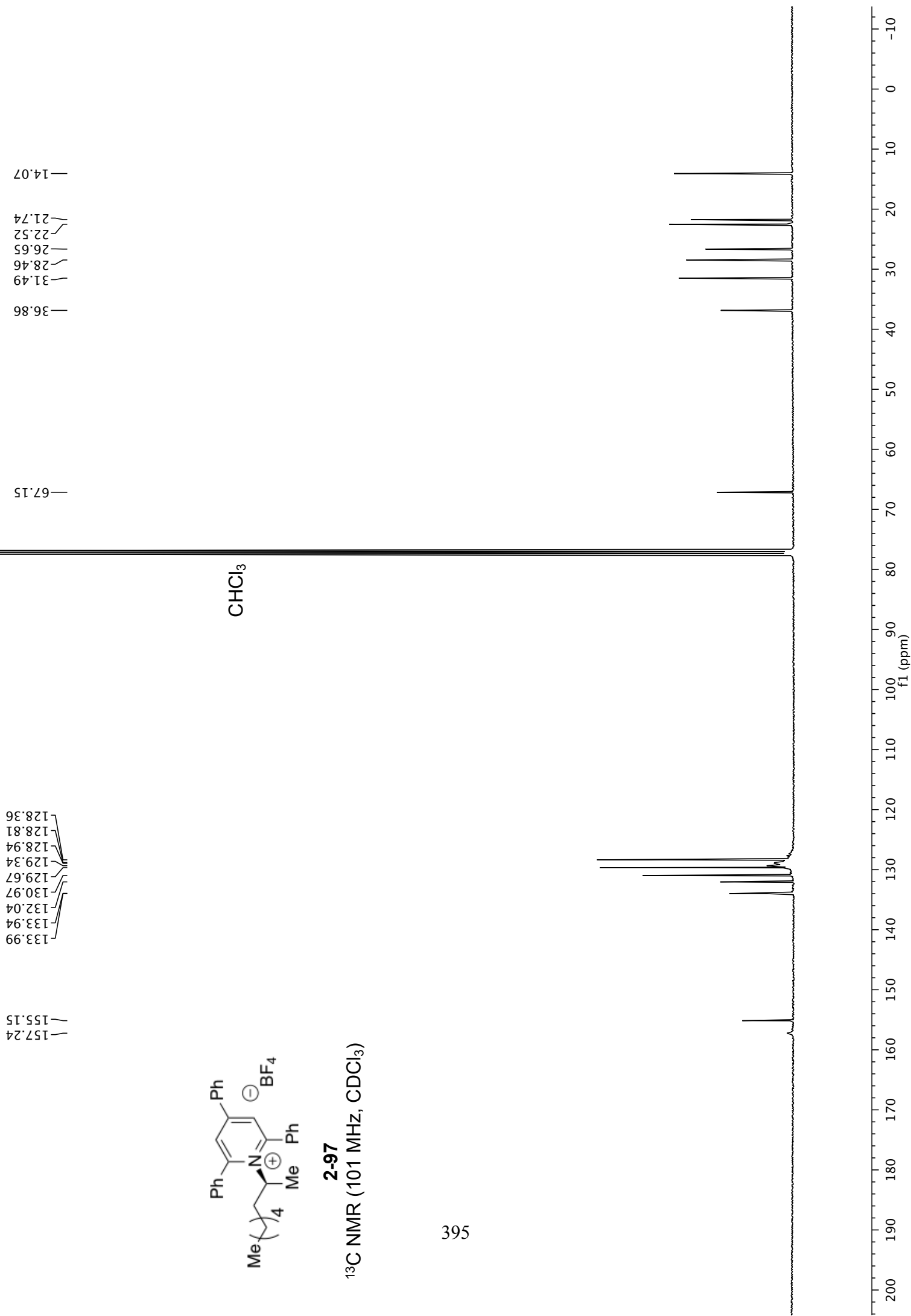
394

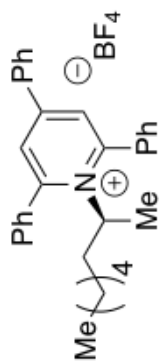




**2-97**

<sup>13</sup>C NMR (101 MHz, CDCl<sub>3</sub>)





**2-97**

<sup>19</sup>F NMR (376 MHz, CDCl<sub>3</sub>)

153.25  
153.31

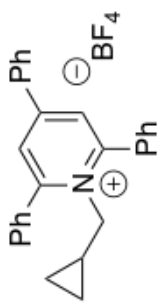
396

-40 -45 -50 -55 -60 -65 -70 -75 -80 -85 -90 -95 -100 -105 -110 -115 -120 -125 -130 -135 -140 -145 -150 -155 -160 -165 -170 -175 -180  
f1 (ppm)

0.711  
0.698  
0.693  
0.691  
0.678  
0.673  
0.669  
0.661  
0.653  
0.649  
0.644  
0.641  
0.629  
0.624  
0.612  
0.294  
0.279  
0.261  
0.259  
0.246  
-0.359  
-0.372  
-0.386  
-0.399

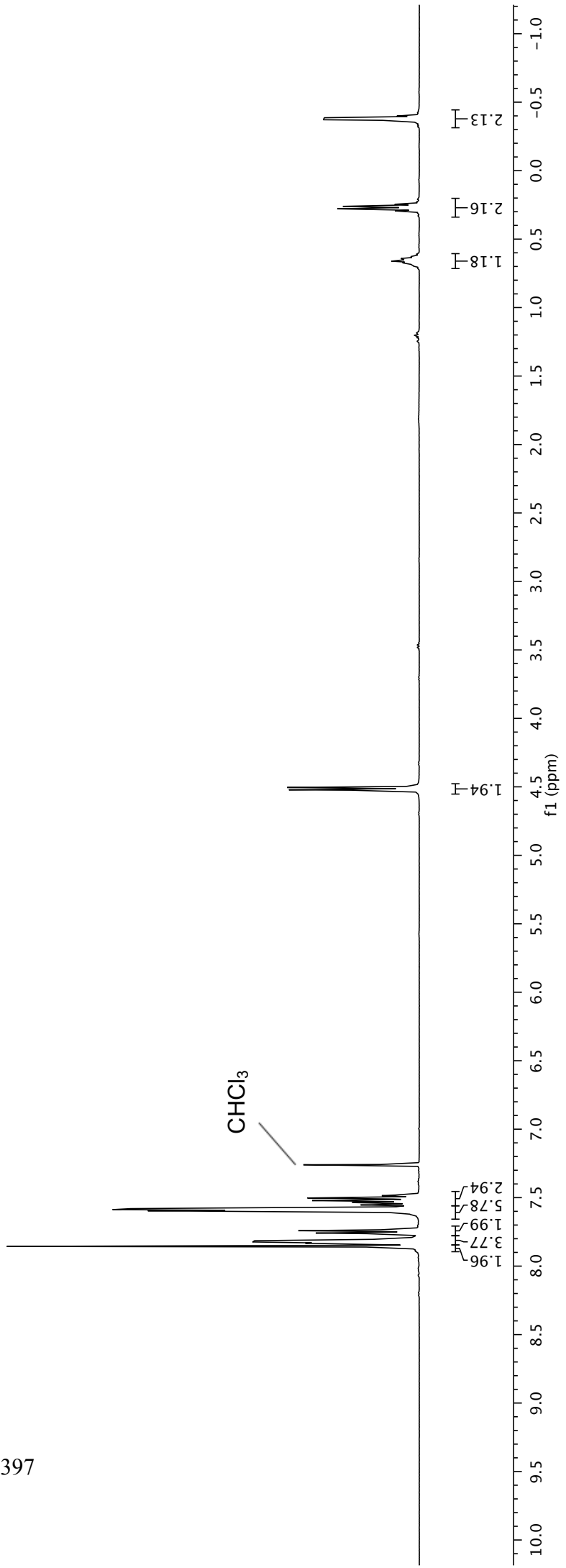
4.522  
4.505

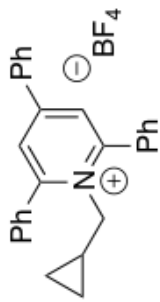
7.856  
7.832  
7.829  
7.824  
7.815  
7.808  
7.759  
7.741  
7.738  
7.596  
7.587  
7.580  
7.553  
7.547  
7.539  
7.536  
7.532  
7.521  
7.503  
7.490  
7.485  
7.481



**2-100**  
<sup>1</sup>H NMR (400 MHz, CDCl<sub>3</sub>)

397





**2-100**

<sup>13</sup>C NMR (101 MHz, CDCl<sub>3</sub>)

133.941  
133.317  
132.298  
131.200  
129.851  
129.538  
129.463  
128.185  
126.763

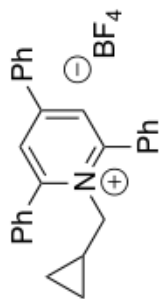
156.951  
155.705

CHCl<sub>3</sub>

10.769  
5.148

59.221





**2-100**

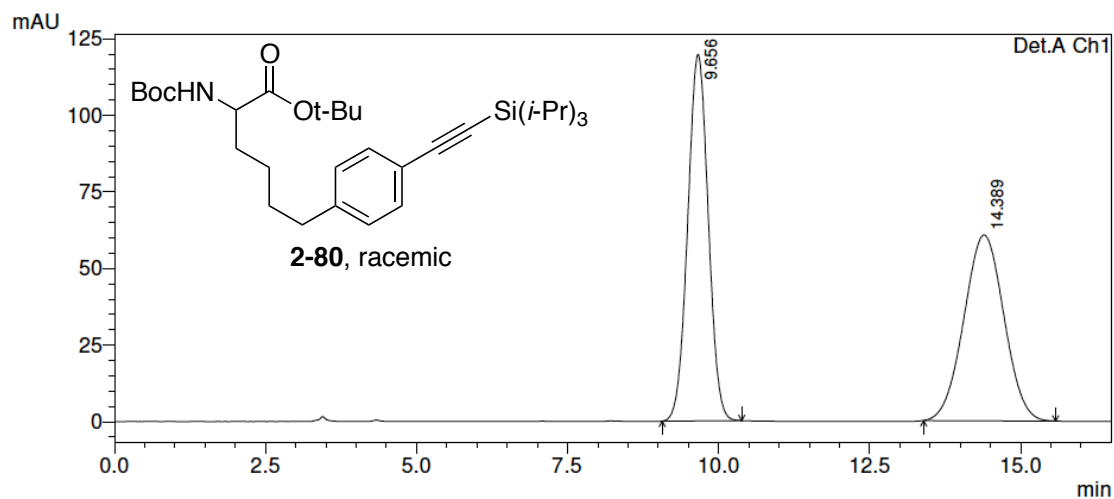
<sup>19</sup>F NMR (376 MHz, CDCl<sub>3</sub>)

-153.232  
-153.286

399

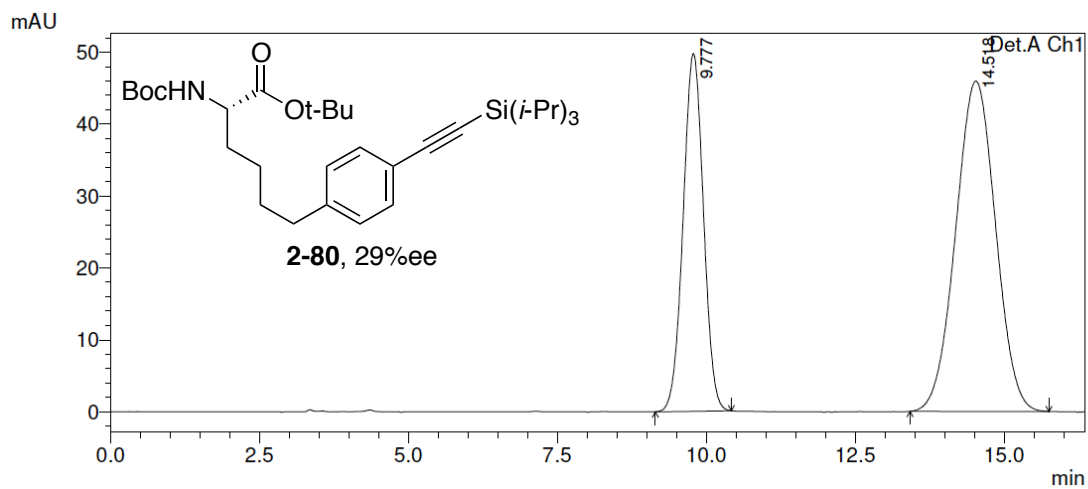
-40 -45 -50 -55 -60 -65 -70 -75 -80 -85 -90 -95 -100 -105 -110 -115 -120 -125 -130 -135 -140 -145 -150 -155 -160 -165 -170 -175 -180  
f1 (ppm)

**Compound 2-80, racemic (254 nm)**



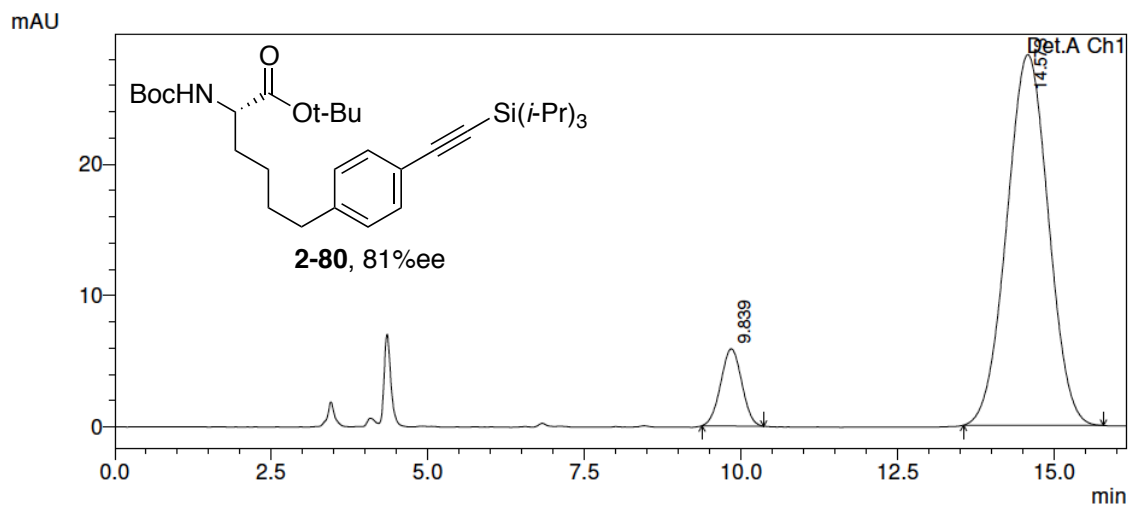
Peak#	Ret. Time	Area	Height	Area %	Height %
1	9.656	2833525	119647	50.307	66.357
2	14.389	2798895	60660	49.693	33.643
Total		5632419	180307	100.000	100.000

**Compound 2-80, 29% ee (254 nm)**



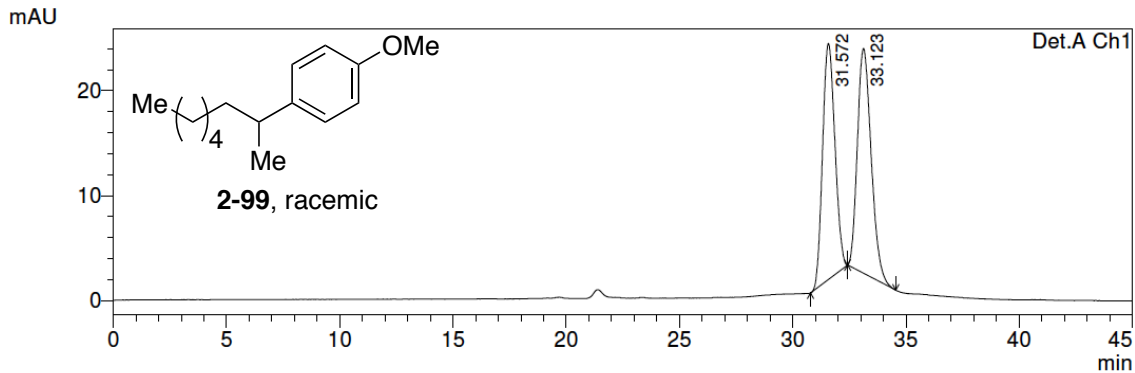
Peak#	Ret. Time	Area	Height	Area %	Height %
1	9.777	1180374	49751	35.522	51.983
2	14.518	2142537	45955	64.478	48.017
Total		3322911	95706	100.000	100.000

**Compound 2-80, 81% ee (254 nm), reaction with 4n (trifluoromethyl)phenol additive**



Peak#	Ret. Time	Area	Height	Area %	Height %
1	9.839	137403	5876	9.510	17.224
2	14.573	1307395	28238	90.490	82.776
Total		1444798	34114	100.000	100.000

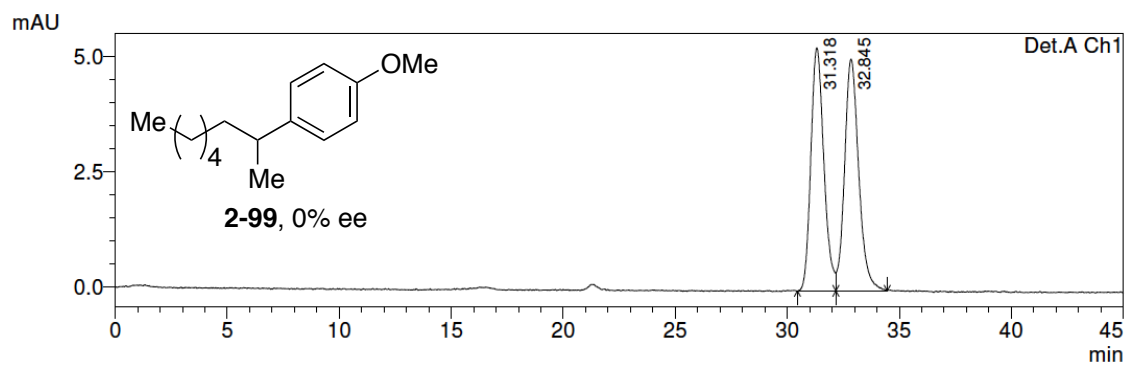
**Compound 2-99, racemic (254 nm)**



Detector A Ch1 254nm

Peak#	Ret. Time	Area	Height	Area %	Height %
1	31.572	850548	22514	48.386	51.255
2	33.123	907290	21411	51.614	48.745
Total		1757837	43925	100.000	100.000

**Compound 2-99, 0% ee (254 nm), from cross-coupling reaction**



Detector A Ch1 254nm

Peak#	Ret. Time	Area	Height	Area %	Height %
1	31.318	212990	5277	49.079	51.202
2	32.845	220984	5029	50.921	48.798
Total		433974	10306	100.000	100.000

**Appendix C**  
**PERMISSION LETTERS**



# RightsLink®

[Home](#)[Create Account](#)[Help](#)**Title:**

Nickel-Catalyzed Borylation of Benzylic Ammonium Salts: Stereospecific Synthesis of Enantioenriched Benzylic Boronates

**Author:**

Corey H. Basch, Kelsey M. Cobb, Mary P. Watson

**Publication:** Organic Letters**Publisher:** American Chemical Society**Date:** Jan 1, 2016

Copyright © 2016, American Chemical Society

[LOGIN](#)

If you're a **copyright.com user**, you can login to RightsLink using your copyright.com credentials. Already a **RightsLink user** or want to [learn more?](#)

## PERMISSION/LICENSE IS GRANTED FOR YOUR ORDER AT NO CHARGE

This type of permission/license, instead of the standard Terms & Conditions, is sent to you because no fee is being charged for your order. Please note the following:

- Permission is granted for your request in both print and electronic formats, and translations.
- If figures and/or tables were requested, they may be adapted or used in part.
- Please print this page for your records and send a copy of it to your publisher/graduate school.
- Appropriate credit for the requested material should be given as follows: "Reprinted (adapted) with permission from (COMPLETE REFERENCE CITATION). Copyright (YEAR) American Chemical Society." Insert appropriate information in place of the capitalized words.
- One-time permission is granted only for the use specified in your request. No additional uses are granted (such as derivative works or other editions). For any other uses, please submit a new request.

[BACK](#)[CLOSE WINDOW](#)

Copyright © 2017 [Copyright Clearance Center, Inc.](#) All Rights Reserved. [Privacy statement.](#) [Terms and Conditions.](#) Comments? We would like to hear from you. E-mail us at [customer@copyright.com](mailto:customer@copyright.com)



# RightsLink®

[Home](#)[Create Account](#)[Help](#)

**Title:** Harnessing Alkyl Amines as Electrophiles for Nickel-Catalyzed Cross Couplings via C–N Bond Activation

**Author:** Corey H. Basch, Jennie Liao, Jianyu Xu, et al

**Publication:** Journal of the American Chemical Society

**Publisher:** American Chemical Society

**Date:** Apr 1, 2017

Copyright © 2017, American Chemical Society

[LOGIN](#)

If you're a **copyright.com user**, you can login to RightsLink using your copyright.com credentials. Already a **RightsLink user** or want to [learn more?](#)

## PERMISSION/LICENSE IS GRANTED FOR YOUR ORDER AT NO CHARGE

This type of permission/license, instead of the standard Terms & Conditions, is sent to you because no fee is being charged for your order. Please note the following:

- Permission is granted for your request in both print and electronic formats, and translations.
- If figures and/or tables were requested, they may be adapted or used in part.
- Please print this page for your records and send a copy of it to your publisher/graduate school.
- Appropriate credit for the requested material should be given as follows: "Reprinted (adapted) with permission from (COMPLETE REFERENCE CITATION). Copyright (YEAR) American Chemical Society." Insert appropriate information in place of the capitalized words.
- One-time permission is granted only for the use specified in your request. No additional uses are granted (such as derivative works or other editions). For any other uses, please submit a new request.

[BACK](#)[CLOSE WINDOW](#)

Copyright © 2017 [Copyright Clearance Center, Inc.](#) All Rights Reserved. [Privacy statement.](#) [Terms and Conditions.](#) Comments? We would like to hear from you. E-mail us at [customer@copyright.com](mailto:customer@copyright.com)